# THE SIXTH BANGALORE BENNY SHILO COURSE IN DEVELOPMENTAL BIOLOGY DEC 17, 2012- DEC 26, 2012

## Teachers


• Amos Arieli (Weizmann Institute of Science, Rehovot. Israel)
• Daniel Greif (Yale University, USA)
• Satyajit Mayor (NCBS-TIFR, Bangalore)
• Maithreyi Narasimha (Tata Institute of Fundamental Research, Mumbai)
• Ze'ev Paroush (Hebrew University, Jerusalem, Israel)
• Erez Raz (University of Muenster, Germany)
• Eyal Schejter ( Weizmann Institute of Science, Rehovot, Israel)
• Ben-Zion Shilo ( Weizmann Institute of Science, Rehovot, Israel)
• K. VijayRaghavan (NCBS-TIFR, Bangalore)
• Talila Volk (Weizmann Institute of Science, Rehovot, Israel)

**LECTURE AND SEMINAR SCHEDULE FOR THE**
**SIXTH BANGALORE BENNY SHILO COURSE IN DEVELOPMENTAL BIOLOGY**
**DEC 17, 2012- DEC 26, 2012**

**ALL ACTIVITIES IN HAAPUS-LH1 except for the 19th Morning 10-15 Talk**

**NOTE- Please find attached research articles and reviews which are linked by page numbers (see right column)**

| DAY | Time | Speaker | Title | Pages |
|---|---|---|---|---|
| | | | | |
| DAY 1 Monday Dec 17 | 8.30 - 9.00 AM | Registration | (Mandatory for course participants) | |
| | 9.00-11.0 AM | K. VijayRaghavan | Introduction to *Drosophila* genetics, methods and questions-I | |
| | 11.0-11.30 AM | Tea Break | | |
| | 11.30-1.0 PM | Benny Shilo | Patterning by gradients in the early Drosophila embryo. | 47-51 |
| | 1.0-2.0 PM | Lunch | | |
| | 2.0-3.30PM | K. VijayRaghavan | Introduction to *Drosophila* genetics, methods and questions-II | |
| | 4.00 – 5.30 PM | - | NCBS ANNUAL WORK SEMINARS (followed by tea) | |
| | 5.30 – 6.30 PM | Benny Shilo | **Egg to Organism-Visualizing the concepts of development** (PUBLIC LECTURE) | |
| | 7.30 PM onwards | - | Dinner followed by<br>(A) General introduction + Q&A<br>(A) Presentation of grant proposal idea | |
| | | | | |
| DAY 2 Tuesday | 9.00 - 11.0 AM | Amos Arieli | Frontiers in Brain Research: A journey into Sensory Perception | |

| | | | | |
|---|---|---|---|---|
| Dec 18 | | | | |
| | 11.0 - 11.30 AM | Tea break | | |
| | 11.30 AM -1.0 PM | Benny Shilo | Morphogen shuttling, and scaling of pattern with size. | 52-64 |
| | 1.0 – 2.0 PM | Lunch | | |
| | 2.00 – 3.30.0 PM | - | Paper preparation (for Journal Club) | |
| | 3.30-4.00 PM | Tea break | | |
| | 4.00-6.00 PM | - | Journal Club with Benny (Multistep molecular mechanism for bone morphogenetic protein extracellular transport in the Drosophila embryo. Sawala A, Sutcliffe C, Ashe HL. Proc Natl Acad Sci U S A. 2012 Jul 10;109(28):11222-7.) | 1-6 |
| | 7.30 PM onwards | - | Dinner followed by General Discussion with Benny and Amos (Are there analogies between developmental biology and brain research?) | |
| | | | | |
| DAY 3 Wednesda Dec 19 | 10.15-11.15 | Mahendra Rao | InStem Frontier Lecture (director of the new NIH intramural Center for Regenerative Medicine.) at Dasheri | |
| | 11.30 AM -1.0 PM | Amos Arieli | Brain and Awareness: Thinking, objectivity and decision making | |
| | 1.0 - 2.00 PM | Lunch | | |
| | 2.00 - 3.30 PM | Ze'ev Paroush | Generating the anteroposterior axis of the *Drosophila* embryo | 139-157 |
| | 3.30 - 4.00 PM | Tea break | | |
| | 4.00 – 6.0 PM | - | Grant proposal preparation | |
| | 7.30 PM onwards | - | Dinner followed by Q&A with Zeév | |
| | | | | |
| | | | | |
| DAY 4 | 9.00 - 11.0 AM | Eyal Schejter | The Cytoskeleton and Establishment of Asymmetry During | 65-75 |

| | | | | |
|---|---|---|---|---|
| Thursday Dec 20 | | | *Drosophila* Oogenesis | |
| | 11.0 - 11.30 AM | Tea break | | |
| | 11.30 AM -12.45 PM | Ze'ev Paroush | From a morphogen gradient to positional information and cell identity | 158-163 |
| | 12.45 - 2.00 PM | Lunch | | |
| | 2.00 - 3.30 PM | Ze'ev Paroush | Negative transcriptional regulation plays a prominent role in Development<br>(Reference- Turki-Judeh W, Courey AJ. Groucho: a corepressor with instructive roles in development. Curr Top Dev Biol. 2012;98:65-96) | ~~** PDF will be added soon~~<br>164 pp |
| | 3.30-4.00 PM | Tea break | | |
| | 4.0-6.0 PM | | Paper preparation | |
| | 6.00 – 7.30 PM | | Paper Discussion with Ze'ev [Löhr U, Chung HR, Beller M, Jäckle H., **Antagonistic action of Bicoid and the repressor Capicua determines the spatial limits of Drosophila head gene expression domains** Proc Natl Acad Sci U S A. 2009 Dec 22;106(51):216 | 7-12 |
| | 7.30 PM onwards | | Dinner followed by discussion with Eyal | |
| | | | | |
| DAY 5 Friday Dec 21 | 10-15-11.15 AM | Daniel Greif | • (SPECIAL SEMINAR) (Greif et al (2012) Radial construction of an arterial wall, Dev Cell) | 127-138 |
| | 11.0 - 11.30 AM | Tea break | | |
| | 11.30 AM-1.0PM | Eyal Schejter | Actin Cables Guide Polarized Secretion in Tubular Organs | 76-87 |
| | 1.0 - 2.00 PM | Lunch | | |
| | 2.00 – 3.15 PM | - | Paper preparation | |
| | 3.15-3.3.0 PM | Tea | | |

| | | | | |
|---|---|---|---|---|
| | 3.30-5.30PM | | Journal Club with Eyal (Growing microtubules push the oocyte nucleus to polarize the **Drosophila** dorsal-ventral axis. Zhao T, Graham OS, Raposo A, **St Johnston D**. Science. 2012 May 25;336(6084):999-1003) | 13-18 |
| | 7.30 PM onwards | | Dinner followed by General Talk<br>"Tracing the lineage and clonal relationships of cells in the mouse: where did these cells come from, how did they get here and to whom are they related?" and Q&A by Daniel Greif | 127-138 |
| | | | | |
| DAY 6<br>Saturday<br>Dec 22 | 9-11.0 AM | Maithreyi Narasimha | Closure and Continuity: the molecular, cellular and physical basis of epithelial fusion during morphogenesis-I | |
| | 11.0-11.30 AM | Tea | | |
| | 11.30-1.0 PM | | (Free for preparing papers, grant proposals etc) | |
| | 1.0-2.0 PM | Lunch | | |
| | 2.0-4.0 PM | Maithreyi Narasimha | Closure and Continuity: the molecular, cellular and physical basis of epithelial fusion during morphogenesis-II | |
| | 6-0-7.30PM | CONCERT | Sitar recital - Kalyanjit Das | |
| | 7.30 PM onwards | Dinner | Free for preparing papers, grant proposals etc | |
| | | | | |
| DAY 7<br>Sunday<br>Dec 23 | FREE | | (Free for preparing papers, grant proposals etc) | |
| | | | | |
| DAY 8<br>Monday<br>Dec 24 | 9-11.0 AM | Erez Raz | Guidance of primordial germ cell migration in zebrafish | 88-94<br>+<br>95-103 |
| | 11.0-11.30 AM | Tea break | | |
| | 11.30-1.0 PM | Talila Volk | Neurogenesis and neuronal pathfinding | 104-117 + |

| | | | | |
|---|---|---|---|---|
| | | | | +<br>118-126 |
| | 1.0-2.0 PM | Lunch | | |
| | 2.0-3.30 PM | | Paper preparation | |
| | 4.00-6.0 PM | | NCBS ANNUAL WORK SEMINARS (followed by tea) | |
| | 6.00 – 7.30 PM | | Journal Club with Erez (Matthews et al (2012) Changes in Ect2 Localization Couple Actomyosin-Dependent Cell Shape Changes to Mitotic Progression, Dev. Cell) | 19-31 |
| | 7.30 PM onwards | | Dinner and Q&A with Erez | |
| | | | | |
| DAY 9<br>Tuesday<br>Dec 25 | 9-11.0 AM | Erez Raz | Molecular and cellular mechanisms controlling primordial germ cell motility | 88-94<br>+<br>95-103 |
| | 11.0-11.30 AM | Tea break | | |
| | 11.30-1.0 PM | Talila Volk | Myogenesis and muscle pathfinding | 104-117 +<br>+<br>118-126 |
| | 1.0-2.0 PM | Lunch | | |
| | 2.0-4.0 PM | | Paper preparation | |
| | 4.00-6.0 PM | Tea | | |
| | 6.00 – 7.30 PM | | Journal Club with Talila [Han et al (2012) Secreted VAPB/ALS8 Major Sperm Protein Domains Modulate Mitochondrial Localization and Morphology via Growth Cone Guidance Receptors, Dev. Cell) | 32-46 |
| | 7.30 PM onwards | | Dinner and Q&A with Talila | |
| | | | | |
| DAY 10<br>Wednesda<br>Dec 26 | 9-11.0 AM | Jitu Mayor | Title: tbc | |
| | 11.0-11.30 AM | Tea break | | |

| | | | | |
|---|---|---|---|---|
| | 11.30-1.0 PM | K. VijayRaghavan | Summary, Evaluation, grant project submission and closing etc | |
| | 1.0 PM onwards | | Depart for airport or railway stations | |

# Multistep molecular mechanism for Bone morphogenetic protein extracellular transport in the *Drosophila* embryo

**Annick Sawala, Catherine Sutcliffe, and Hilary L. Ashe[1]**

Faculty of Life Sciences, University of Manchester, Manchester M13 9PT, United Kingdom

Edited by Gary Struhl, Columbia University College of Physicians and Surgeons, New York, NY, and approved June 8, 2012 (received for review February 16, 2012)

**In the *Drosophila* embryo, formation of a bone morphogenetic protein (BMP) morphogen gradient requires transport of a heterodimer of the BMPs Decapentaplegic (Dpp) and Screw (Scw) in a protein shuttling complex. Although the core components of the shuttling complex—Short Gastrulation (Sog) and Twisted Gastrulation (Tsg)—have been identified, key aspects of this shuttling system remain mechanistically unresolved. Recently, we discovered that the extracellular matrix protein collagen IV is important for BMP gradient formation. Here, we formulate a molecular mechanism of BMP shuttling that is catalyzed by collagen IV. We show that Dpp is the only BMP ligand in *Drosophila* that binds collagen IV. A collagen IV binding–deficient Dpp mutant signals at longer range in vivo, indicating that collagen IV functions to immobilize free Dpp in the embryo. We also provide in vivo evidence that collagen IV functions as a scaffold to promote shuttling complex assembly in a multistep process. After binding of Dpp/Scw and Sog to collagen IV, protein interactions are remodeled, generating an intermediate complex in which Dpp/Scw-Sog is poised for release by Tsg through specific disruption of a collagen IV–Sog interaction. Because all components are evolutionarily conserved, we propose that regulation of BMP shuttling and immobilization through extracellular matrix interactions is widely used, both during development and in tissue homeostasis, to achieve a precise extracellular BMP distribution.**

Bone morphogenetic proteins (BMPs) form a conserved family of signaling proteins with important functions during development and disease. BMP activity is regulated by a large number of extracellular proteins that modulate BMP receptor binding, stability, or distribution (1, 2). The early *Drosophila* embryo serves as an excellent model system to study extracellular mechanisms of BMP regulation, because a gradient of BMP activity specifies cell fates along the dorsoventral axis (3). Although the two BMP ligands, Dpp and Scw, are broadly expressed, a conserved set of extracellular regulators mediate the redistribution of the Dpp/Scw heterodimer to the dorsal midline, where peak signaling occurs (4). In dorsal regions, Dpp and Scw are bound by Sog and Tsg into an inhibitory shuttling complex that is unable to bind to receptors but is capable of moving (5–9). Dpp/Scw is released from the shuttling complex by the protease Tolloid, which cleaves and inactivates Sog (10). If Tolloid cleavage of Sog within the complex occurs in dorsolateral regions near the Sog source, Dpp/Scw is re-bound by Sog/Tsg. Multiple cycles of complex cleavage and reformation can occur, until Tolloid cleaves the complex in dorsalmost regions where the concentration of Sog is low, allowing Dpp/Scw to bind its receptors and activate high levels of signaling (5).

We have shown that the extracellular matrix protein collagen IV is important for BMP gradient formation (11). In embryos mutant for the collagen IV genes *viking* or *Dcg1*, peak signaling is lost and Dpp accumulation at the dorsal midline is reduced. In vitro experiments revealed that the C-terminal NC1 domain of collagen IV can bind to both Dpp and Sog. Based on these and additional findings, we proposed that collagen IV enhances BMP gradient formation by facilitating the assembly of the Dpp/Scw-Sog-Tsg shuttling complex, thereby promoting the long-range movement of BMPs (11). Although this model is supported by recent quantitative modeling of the BMP gradient in the *Drosophila* embryo (12), the molecular mechanism of shuttling complex assembly on collagen IV, and whether it occurs in vivo to regulate BMP distribution, is unknown.

Here, we have mapped the collagen IV binding sites on both Dpp and Sog. Based on these and previous interaction studies, we formulate a multistep, molecular model for the assembly of the Dpp/Scw-Sog-Tsg shuttling complex on collagen IV, which we test in vivo by using a collagen IV binding deficient mutant of Dpp. These experiments also provide in vivo evidence that collagen IV restricts movement of free Dpp ligands. We propose that collagen IV may regulate short- and long-range signaling of BMPs in diverse contexts.

## Results

**Mapping the Collagen IV binding Site in Dpp.** We previously showed that the NC1 domain of the *Drosophila* collagen IV proteins Viking and Dcg1 (named VkgC and Dcg1C, respectively) can directly interact with an HA-tagged form of Dpp (11). Mature Dpp is secreted from *Drosophila* S2 cells in two forms resulting from alternative proprotein cleavage at the S1 or S3 site (13). In GST-pulldown (GST-PD) experiments with bacterially purified GST-VkgC, we found that the larger S1 form binds better to collagen IV than the N-terminally truncated S3 form (Fig. 1 *A* and *B*; compare ratio of S1 to S3 forms in bound vs. input FL fractions). This result suggested that the N-terminus of mature Dpp is important for binding to collagen IV. The S3 site and downstream residues form a highly basic stretch (Fig. 1*A*). Partial or complete deletion of this basic region in Dpp-Δa and Dpp-Δc, respectively, strongly reduced binding of Dpp to collagen IV (Fig. 1*B*), demonstrating that the basic motif is important for its binding to collagen IV. These data also suggest that the observed binding of the S3 form to VkgC (Fig. 1*B*, lane 2) is likely to be due to its dimerization with the S1 form.

**Collagen IV Binding Site Is Not Conserved in Other *Drosophila* BMPs.** We recently determined the *N*-termini of the other two *Drosophila* BMP ligands, Scw and Glass bottom boat (Gbb) (14). Sequence alignment reveals that the Scw and Gbb ligand domains lack the basic stretch found in the S1 form of Dpp (Fig. 2*A*).

Author contributions: A.S. and H.L.A. designed research; A.S. performed research; C.S. contributed new reagents/analytic tools; A.S. and H.L.A. analyzed data; and A.S. and H.L.A. wrote the paper.

The authors declare no conflict of interest.

This article is a PNAS Direct Submission.

Freely available online through the PNAS open access option.

[1]To whom correspondence should be addressed. E-mail: hilary.ashe@manchester.ac.uk.

This article contains supporting information online at www.pnas.org/lookup/suppl/doi:10.1073/pnas.1202781109/-/DCSupplemental.

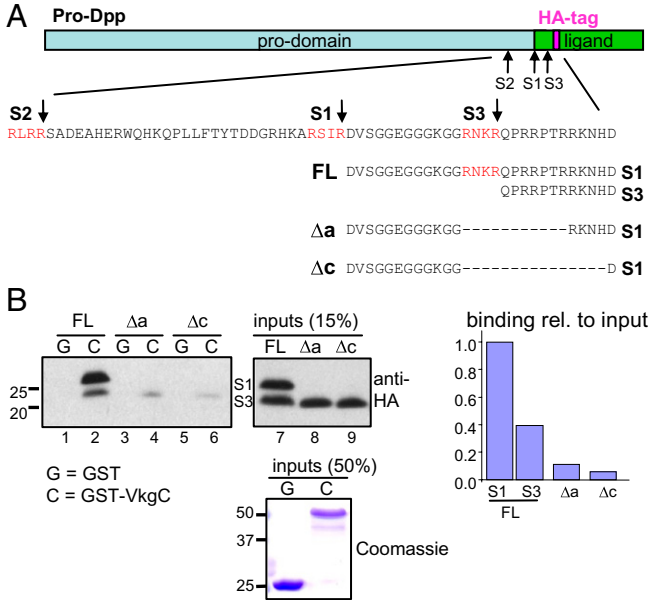


**Fig. 1.** A basic region at the start of Dpp mediates binding to collagen IV. (*A*) Schematic of the Dpp proprotein with the amino acid sequence of Dpp in the region of the furin processing sites (S1, S2, S3) directly upstream of the HA-tagged ligand domain. The sequences of S1/S3 forms of mature wild-type Dpp and the deletion mutants used in *B* are also shown. Note that our S1/S3 site nomenclature, which is consistent with ref. 31, is opposite to that of ref. 13, with our S1 site corresponding to their S3 site. (*B*) GST-PD between GST-VkgC and wild-type or deletion mutants of Dpp-HA. Deletion of the basic region strongly reduces binding to GST-VkgC. FL, full-length.

Consistent with the absence of a basic motif, Scw and Gbb show little or no binding to VkgC (Fig. 2*B*). These results further validate the Dpp basic motif as a collagen IV binding site and show that the only *Drosophila* BMP protein that can interact with the collagen IV NC1 domain is Dpp.

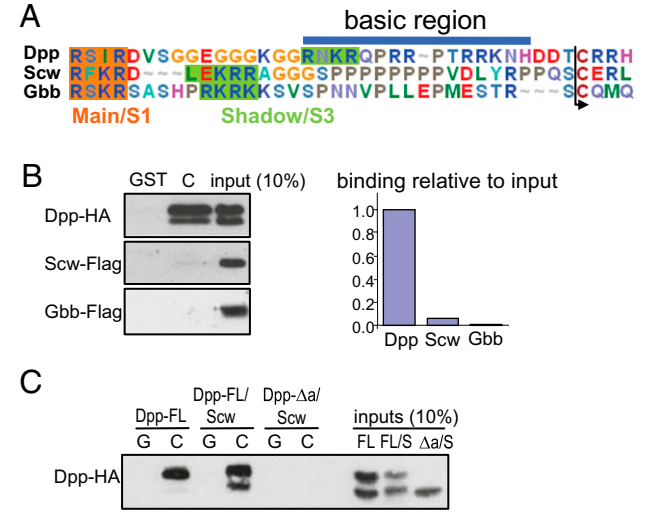


**Fig. 2.** Dpp is the only BMP ligand in *Drosophila* to bind collagen IV. (*A*) Alignment of Dpp, Gbb, and Scw proteins at the N-terminus of the mature ligand domain. Main (S1 for Dpp) and Shadow (S3 for Dpp) processing sites are highlighted. The basic sequence in Dpp required for binding to collagen IV is not conserved in Gbb or Scw. (*B*) GST-PD between GST-VkgC and Dpp-HA, Scw-FLAG, or Gbb-FLAG (*Left*). Scw-FLAG and Gbb-FLAG show very weak binding to GST-VkgC (*Right*). (*C*) GST-PD between GST-VkgC and either Dpp-FL monomer, or Dpp-FL/Scw or Dpp-Δa/Scw heterodimer. Dpp-FL/Scw shows strong binding to VkgC, which depends on the collagen IV binding site in Dpp, because Dpp-Δa/Scw cannot bind to VkgC.

In the early embryo, the Dpp/Scw heterodimer is proposed to be both the most potent signaling species and the best substrate for Sog/Tsg-mediated shuttling to the dorsal midline (9). As shown in Fig. 2*C*, the Dpp/Scw heterodimer displays similar, if not better, binding to VkgC as the Dpp homodimer, again showing relatively more binding of the Dpp S1 form. Consistent with Scw being unable to bind the collagen IV NC1 domain, the collagen IV binding activity of the Dpp/Scw heterodimer is mediated by the basic motif in Dpp, because the DppΔa/Scw heterodimer is unable to interact with VkgC (Fig. 2*C*).

**Mapping the Collagen IV Binding Site in Sog.** We next mapped the collagen IV binding sites on Sog. Sog is a large glycoprotein consisting of four cysteine rich (CR) domains separated by a long "stem" region between CR1 and CR2 (10) (Fig. 3*A*). To identify the regions of Sog important for interaction with the collagen IV NC1 domain, we tested binding of a panel of deletion constructs (Fig. 3 *A* and *B*). Overall, these experiments suggest that (*i*) the CR domains mediate binding to collagen IV in a partially redundant fashion (e.g., compare FL vs. Δ3 vs. Δ4), and (*ii*) the stem region has an inhibitory effect on binding of Sog to collagen IV (compare FL vs. Δ5). We next tested the binding of each CR domain individually. As shown in Fig. 3*C*, CR1 and CR4 bound efficiently to VkgC, whereas no binding was detected for CR2 and CR3. An alignment of the Sog CR domains revealed that both CR1 and CR4 contain basic motifs (named B1, B2, B3, and B4) not found in CR2 or CR3 (Fig. 3*D*). For Sog CR1, mutation of B1 greatly reduced binding to VkgC (Fig. 3*E*). For Sog CR4, B2, B3, or B4 single or double mutants caused a partial loss of binding to VkgC, and the B2/B3/B4 triple mutant further attenuated the interaction (Fig. 3*F*), suggesting that all three basic motifs in CR4 function with partial redundancy in binding collagen IV. Mutation of either B1 or B2/B3/B4 in the context of full-length Sog also partially blocked binding to VkgC, and binding was very weak when basic motifs were mutated in both CR1 and CR4 (Fig. 3*G*).

**Molecular Model for Shuttling Complex Assembly on Collagen IV.** We previously presented evidence that collagen IV enhances BMP transport dorsally and proposed that it acts as a scaffold to enhance shuttling complex formation (11). The identification of the collagen IV binding sites on Sog and Dpp, combined with pre-existing data, allows us to formulate a molecular model for the assembly of the Dpp/Scw-Sog-Tsg shuttling complex on collagen IV. Our previous data showed that the Dpp/Scw heterodimer and Sog together can bind VkgC, but the addition of Tsg releases Dpp/Scw and Sog from collagen IV into the Dpp/Scw-Sog-Tsg shuttling complex (11). Here, we show that the Dpp/Scw heterodimer has only one binding site for collagen IV and that Sog has two binding domains, CR1 and CR4. These findings suggest a probable mechanism of release of Dpp/Scw and Sog from collagen IV into the shuttling complex. The Dpp/Scw heterodimer and Tsg together, but neither of them alone, can release Sog from VkgC (11), suggesting that each—Dpp/Scw and Tsg—competes with one of the two collagen IV binding sites on Sog. In vertebrates, the Dpp ortholog BMP2 and Tsg both bind strongly to CR1 and CR3 (15, 16), whereas the Scw-related protein BMP7 interacts preferentially with CR1 and CR4 (15) (Fig. 4*A*). Because only Scw binds to CR4 with high affinity, we propose that Dpp/Scw interferes with the Sog-CR4/VkgC interaction (via Scw binding to CR4), whereas Tsg competes for binding of collagen IV to Sog-CR1. Furthermore, because neither Sog nor Tsg alone can release Dpp from VkgC (11), we suggest a multistep model for shuttling complex assembly by collagen IV, in which release of Dpp/Scw is coupled to its transfer onto Sog. In the first step, Sog and Dpp/Scw both bind

DEVELOPMENTAL BIOLOGY

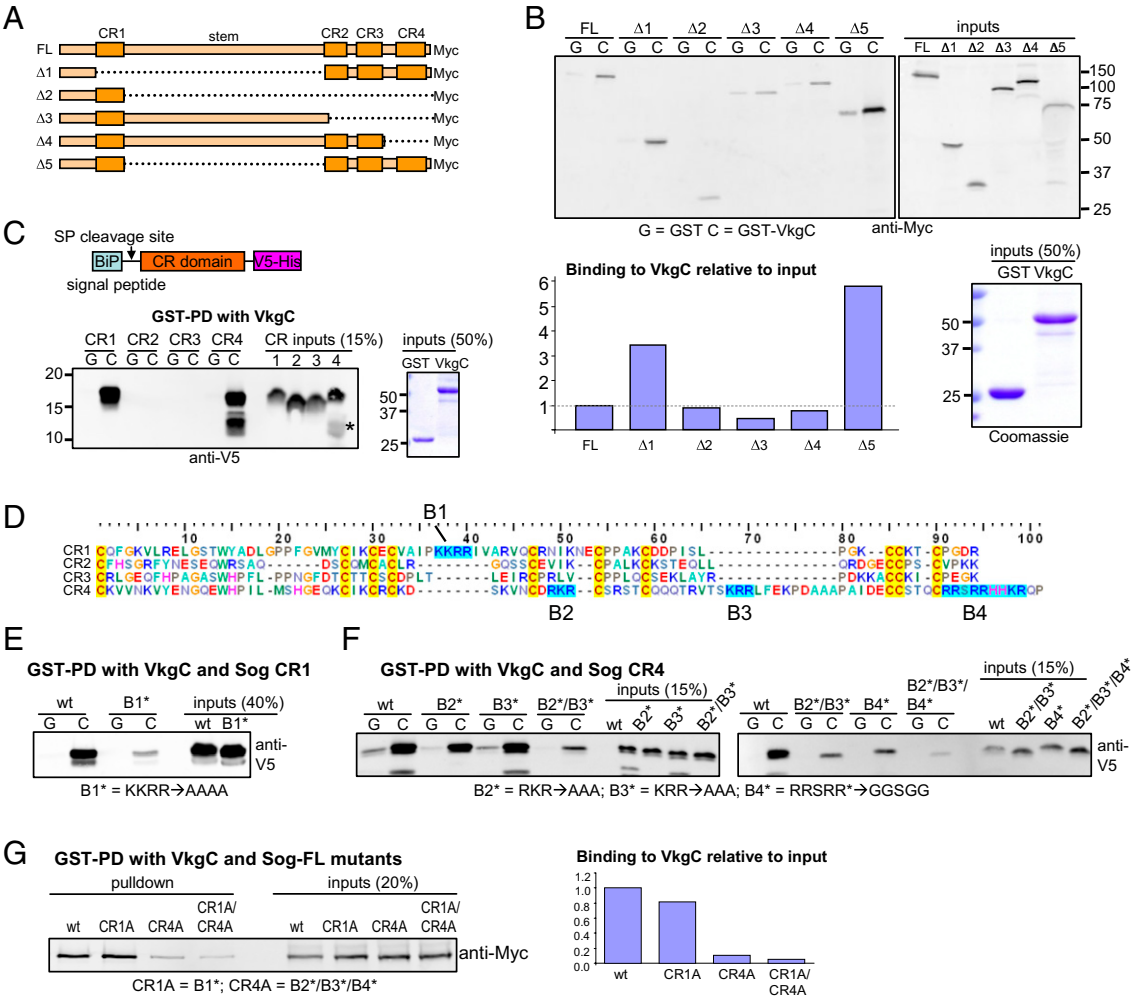


**Fig. 3.** Basic sequences in the CR1 and CR4 domains of Sog mediate binding to collagen IV. (*A*) Domain structure of full-length (FL) Sog and deletion mutants used in *B*. (*B*) GST-PD between GST-VkgC and Myc-tagged Sog deletion mutants. Binding of Sog was quantified as bound protein relative to input levels after subtraction of background binding to GST and normalization to Sog-FL. (*C*) GST-PD between GST-VkgC and individual CR domains of Sog. Only Sog CR1 and CR4 interact with VkgC. CR4 expression results in a degradation product (asterisk). (*D*) Alignment of Sog CR domains reveals basic motifs in CR1 (B1) and CR4 (B2, B3, B4). (*E–G*) Mutation of basic motifs in Sog CR1 (*E*), CR4 (*F*), or full-length Sog (*G*) attenuates binding to GST-VkgC. In panel (*G*) binding was quantified as bound protein relative to input levels, with values of Sog-FL mutants normalized to that of wild-type Sog-FL.

to the NC1 domain of collagen IV within the same NC1 trimer (Fig. 4*B*, step 1). This binding restricts Dpp and Sog diffusion, but it also promotes the transfer of Dpp/Scw onto Sog, through interactions of Dpp with Sog-CR3 and of Scw with Sog-CR4, which leads to disruption of both Dpp/collagen IV and Sog-CR4/collagen IV interactions (Fig. 4*B*, step 2). The resulting Dpp/Scw-Sog complex is bound to collagen IV by the Sog–CR1 interaction only and, therefore, poised for release by Tsg, which outcompetes collagen IV for Sog-CR1 binding (Fig. 4*B*, step 3). Consistent with the formation of a Dpp/Scw-Sog "poised" intermediate on collagen IV, we show that Dpp-Δa/Scw, which lacks the collagen IV binding site, can associate with GST-VkgC in the presence Sog (Fig. 4*C*).

We used the collagen IV binding site mutant of Dpp (Dpp-Δa) to test our model in the context of the early embryo. First, we made use of a system for monitoring Dpp-Δa movement and signaling, based on ectopic expression from a stripe that runs perpendicular to the normal *dpp* expression domain (Fig. 4 *D–F*) (17). Activity of the peak threshold BMP target gene *Race* was visualized, which is normally expressed in a narrow stripe along the dorsal midline (presumptive amnioserosa) (Fig. 4*G*). As shown (7, 17), misexpression of wild-type Dpp under the *even-skipped* stripe 2(st2)-enhancer activates BMP signaling in cells within and outside the stripe, leading to expanded *Race* expression (Fig. 4*H*), consistent with the ability of the Dpp/Scw heterodimer to move long-range in the early embryo. In *st2-dpp-Δa* embryos, *Race* expression is also broadened and extends more posteriorly than in *st2-dpp* embryos (Fig. 4*I*), suggesting that Dpp-Δa can signal normally and may be more mobile than wild-type Dpp. Additionally, evidence is presented that the Δa mutation does not affect Dpp protein levels (Fig. S1).

We next used this expression system to test key aspects of our model of shuttling complex assembly by examining the behavior of Dpp-Δa in *sog*$^-$ and *tsg*$^-$ backgrounds. In both mutants, *Race* expression is lost in the presumptive amnioserosa but expanded in the anterior head region (Fig. 4 *J* and *M*), reflecting the loss of peak signaling and uniform intermediate signaling, due to the loss of dorsal BMP shuttling (6). In our model, collagen IV restricts movement of free Dpp (i.e., when not bound to Sog); thus, one prediction is that Dpp-Δa, unlike wild-type Dpp, can move and signal long range in a *sog*$^-$ background (Fig. 4 *K′* and *L′*). When *st2-dpp-Δa* is expressed in *sog*$^-$ embryos, it induces ectopic *Race* expression outside of its expression domain (Fig. 4*L*),

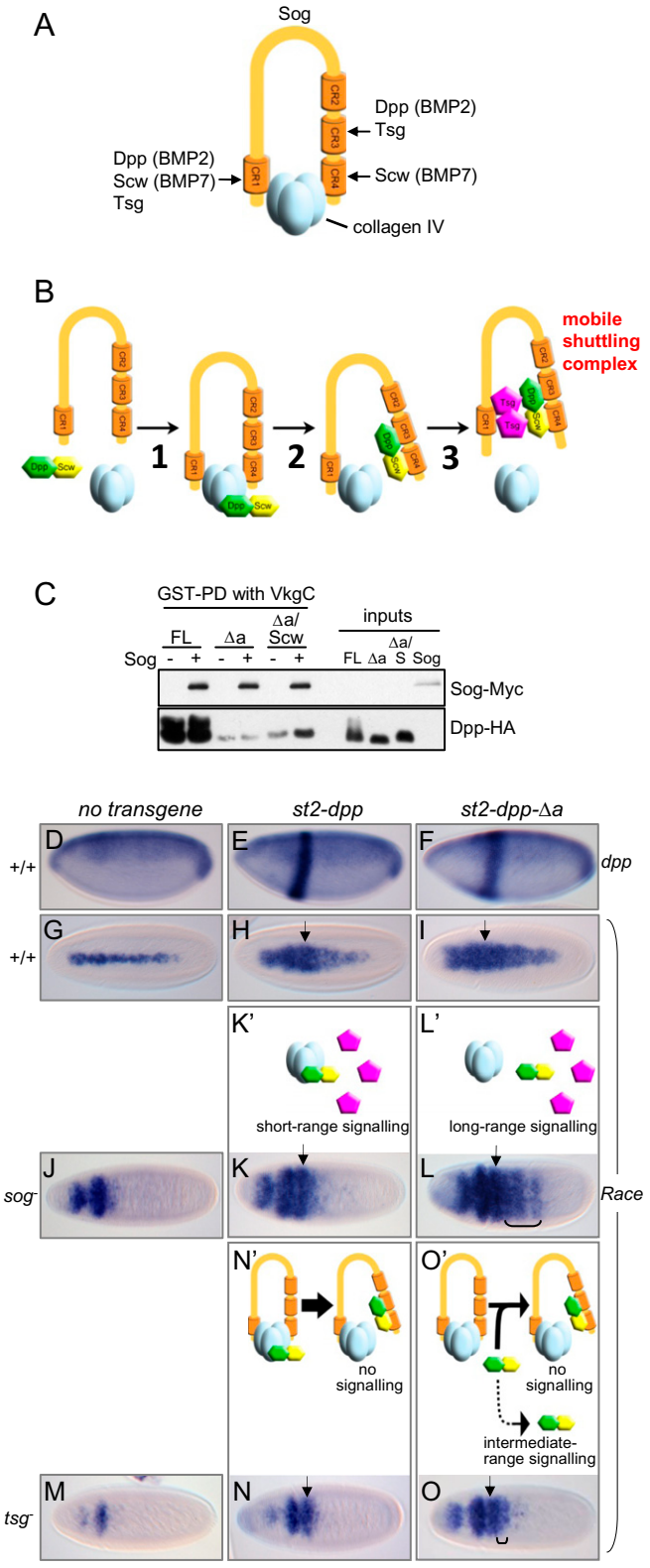


**Fig. 4.** Molecular model for Dpp/Scw-Sog-Tsg shuttling complex assembly on collagen IV. (*A*) Binding domains on Sog for collagen IV (VkgC), Dpp (BMP2), Scw (BMP7), and Tsg. (*B*) Molecular model for BMP shuttling complex assembly on collagen IV. (*C*) GST-PD between GST-VkgC or VkgC-Sog complex and Dpp, Dpp-Δa, or Dpp-Δa/Scw. (*D–O*) RNA in situ hybridizations for *dpp* (*D–F*; lateral views, dorsal up) or the BMP target gene *Race* (*G-O*; dorsal views) in control embryos and those expressing *st2-dpp* or *st2-dpp-Δa* transgenes. Embryos are wild-type (*D–I*), *sog*$^{-}$ (*J–L*) or *tsg*$^{-}$ (*M–O*). Brackets mark ectopic *Race* induction posterior of the st2 expression domain (arrows). Anterior is left in all images. (*K′–O′*) Cartoons depicting Dpp/Scw interactions as predicted by our molecular model. Intermediate-range signaling is attributed to a small number of Dpp/Scw molecules undergoing long-range signaling. Signaling in the st2 domain is at least in part attributed to Dpp homodimers (omitted from cartoons for simplicity).

suggesting that it is capable of long-range movement. This property is in stark contrast to that of ectopically expressed wild-type Dpp, whose effect is restricted to the *st2* expression domain (7) (Fig. 4*K*). A second feature of our model is that Tsg acts to release the Dpp/Scw-Sog complex from collagen IV by disrupting the Sog-collagen IV interaction. Therefore, we predict Dpp-Δa would, in general, be unable to move and signal long range in a *tsg*$^{-}$ background, where most Dpp-Δa/Scw-Sog should remain trapped on collagen IV (Fig. 4*O′*). Indeed, in the absence of Tsg, the effect of Dpp-Δa is largely restricted to its expression stripe (Fig. 4*O*). Finally, our model proposes that collagen IV enhances the association of Dpp/Scw and Sog, implying that formation of the Dpp/Scw-Sog complex should be less efficient for Dpp-Δa. In the *tsg* mutant, where assembly of the Dpp/Scw-Sog complex immobilizes BMPs on collagen IV, we therefore predict that some Dpp-Δa/Scw can move out of its expression stripe, whereas all wild-type Dpp/Scw is trapped by collagen IV-Sog (Fig. 4 *N′* and *O′*). Indeed, compared with wild-type Dpp, which is entirely restricted to its expression domain in *tsg*$^{-}$ embryos (Fig. 4*N*), some Dpp-Δa can activate signaling in cells away from its source. This intermediate-range signaling is observed as *Race* induction in a limited number of cells posterior to the *st2* domain in the majority (~70%) of embryos (Fig. 4*O*). In summary, our in vivo data support three key predictions from our model of shuttling complex assembly.

## Discussion

There is ample experimental and theoretical support for the notion that BMP gradient formation in the early embryo involves the concentration of the most potent signaling species, the Dpp/Scw heterodimer, at the dorsal midline in a process involving Sog and Tsg (4). Here, we present in vivo evidence for a role of collagen IV in two key aspects of this shuttling model, which have remained mechanistically unresolved. First, collagen IV functions to immobilize free Dpp, explaining why Sog and Tsg are needed for Dpp movement. Second, collagen IV acts as a scaffold for assembly of the Dpp/Scw-Sog-Tsg shuttling complex. The advantage to BMP gradient formation of assembling the shuttling complex on collagen IV has been suggested by analysis of organism-scale mathematical models (12). These models reveal that the in vitro binding affinity between BMPs and Sog is too low to account for the rate of shuttling complex formation required in vivo. However, by acting as a scaffold, collagen IV would increase complex formation by locally concentrating Dpp/Scw and Sog. Models with a 10–20% reduction in diffusion rates for Dpp/Scw and Sog and an increased apparent affinity of Dpp/Scw for Sog, show the best fit to in vivo data (12).

Our molecular model of shuttling complex assembly occurs in three steps. The first step involves independent binding of Dpp/Scw and Sog to collagen IV. The ability of Dpp-Δa to signal long range in *sog*$^{-}$ embryos, where wild-type Dpp is trapped in its expression stripe, provides in vivo evidence that the Dpp-collagen IV interaction restricts movement of free Dpp ligands. The result also demonstrates that Sog and Tsg promote long-range movement of Dpp because they release Dpp from collagen IV, and not simply because they prevent Dpp–receptor interactions (8, 18). Restriction of Dpp diffusion by collagen IV may stabilize the gradient by preventing ventral movement of Dpp/Scw after release from Sog/Tsg and promoting Dpp/Scw–receptor inter-

actions at the dorsal midline. It will be interesting, ultimately, to directly visualize Dpp and Dpp-Δa directly in *sog* and *tsg* mutant embryos. Although current methods allow detection of high levels of receptor-bound Dpp (8, 9), there are technical limitations associated with specifically detecting the pools of Dpp that would be informative here, i.e., Dpp/Scw heterodimer within the shuttling complex or Dpp-Δa/Scw diffusing between cells. Our data show that Scw is unable to bind the NC1 domain of collagen IV. This lack of collagen IV-dependent immobilization can explain why Scw, unlike Dpp, is capable of long-range signaling in the absence of Sog (8).

Step 2 of shuttling complex assembly involves remodeling of the protein interactions to generate a poised intermediate. Specifically, step 2 is driven by Scw-mediated disruption of the Sog CR4–collagen IV interaction, so that Dpp/Scw is transferred from collagen IV to the Sog CR3-CR4 domains. Scw displacement of the Sog CR4 domain from collagen IV provides molecular insight as to why Scw is needed for Dpp transport (9). In addition to the binding preference of Sog and Tsg for the Dpp/Scw heterodimer (9), only Scw has a high affinity for the Sog CR4 domain. Therefore, Dpp/Scw can be released from collagen IV into the shuttling complex, whereas the Dpp homodimer remains trapped on collagen IV.

In the final step of our model, Tsg mobilizes the shuttling complex by disrupting the Sog CR1–collagen IV interaction. It has been noted that *tsg* mutants display a more severe reduction in BMP signaling than *sog* and *sog tsg* double mutants (8) (also see *Race* expression in Fig. 4 *J* and *M*). This observation has been attributed to a potential Sog-independent pro-BMP activity of Tsg at the level of receptor binding (8). A second contributing factor is suggested by our model, where Sog and Tsg act at distinct steps to allow formation of the shuttling complex. In *tsg* mutants, Dpp/Scw is loaded onto Sog by collagen IV, but remains locked in this inhibitory poised complex, so that the only BMPs capable of signaling are Dpp and Scw homodimers, which are less potent than the Dpp/Scw heterodimer (9). By contrast, in *sog* or *sog tsg* mutants, Dpp/Scw is not shuttled dorsally but is still capable of signaling locally, adding to signaling by Dpp and Scw homodimers. The weaker level of Dpp/Scw signaling in *tsg* mutants also provides support for our proposed order of steps 2 and 3 in the assembly process, because this order gives rise to the inhibitory intermediate of Dpp/Scw-Sog. Previously it was shown that an N-terminal fragment of Sog, called Supersog, which contains the CR1 domain and a portion of the stem, can partially rescue the loss of peak Dpp/Scw signaling in $tsg^{-}$ embryos (19). Our model suggests that this property of Supersog comes from the ability of its CR1 domain to compete with full-length Sog for binding to collagen IV, thereby releasing Sog-Dpp/Scw, similar to the role of Tsg in shuttling complex assembly. We note that the CR1–collagen IV interaction appears weaker than that of CR4–collagen IV (Fig. 3*G*), which may facilitate release of Dpp/Scw by Tsg or Supersog-like fragments. After Tsg-mediated release from collagen IV, the mobile shuttling complex can diffuse randomly. Upon Tolloid cleavage of Sog, the liberated Dpp/Scw heterodimer rebinds collagen IV, which either promotes receptor binding (11) or a further round of shuttling complex assembly, depending on the local concentration of Sog.

In addition to collagen IV, the basic region in Dpp/BMP2/4 also binds to heparan sulfate proteoglycans (HSPGs), which can either restrict or enhance BMP long-range movement (20, 21). Indeed, we find that an HSPG-binding mutant, Dpp-ΔN, also binds only weakly to collagen IV (Fig. S2), suggesting that the collagen IV- and HSPG-binding sites on Dpp overlap. It will be interesting to test how HSPGs and collagen IV interact to regulate BMP activity in tissues where they are coexpressed, such as the early vertebrate embryo (20). In the early *Drosophila* embryo, the absence of glycosaminoglycan chains (22), which largely mediate binding of HSPG to Dpp (23), make it possible to specifically focus on the Dpp–collagen IV interaction.

A shuttling-based mechanism of BMP transport is also used in a number of other developmental contexts, including the early vertebrate embryo (24), specification of the vertebral field in mice (25), and establishment of the posterior cross-vein territory in the *Drosophila* wing disk (26, 27). Restriction of BMP movement may also be important in other contexts, including several where collagen IV was already shown to regulate a short-range Dpp signal, such as the ovarian stem cell niche and the tip of malpighian tubules (8, 28). The basic collagen IV binding motif is highly conserved among the Dpp/BMP2/4 subfamily (20) and is also found in some other BMPs, including BMP3, consistent with reports that BMP3 and BMP4 can bind collagen IV (11, 29). Overall, these findings support the idea that the collagen IV–BMP interaction is a conserved aspect of extracellular BMP regulation and suggest that the function of collagen IV in both long-range BMP shuttling and local restriction of BMP movement will impact on a number of other contexts in both flies and vertebrates.

## Materials and Methods

**DNA Constructs.** Cu-inducible Scw and Gbb constructs (pMT-Scw-1xFLAG and pMT-Gbb-3xFLAG) (14), Dpp*Δ*N*-HA (21), and pGEX4T1-VkgC (11) have been described. The coding sequences of Dpp-HA (10) and Sog-Myc (19) were inserted into pMT-V5/His-A (Life Technologies) and then modified by PCR to introduce deletions or mutations (details available on request). To express individual Sog CR domains, regions encoding amino acids 95–186 (CR1), 737–814 (CR2), 825–909 (CR3), or 935–1031 (CR4) were cloned into pMT-Bip-V5/His-A (Life Technologies) in frame with the C-terminal V5-His tag. For transgenesis, the Dpp-Δa deletion was introduced into SK-Asc2-Dpp (17) by PCR and transferred as an AscI fragment into the 22FPE vector (30).

**Protein Expression and Purification.** Scw-FLAG, Gbb-FLAG, Dpp-HA, and Sog-Myc proteins were produced in *Drosophila* S2R$^{+}$ cells by effectene-mediated transient transfection followed by Cu-induction as described (14). Sog-CR4 was expressed in S2 cells, because secretion from S2R$^{+}$ cells was inefficient. For Dpp/Scw heterodimers, we cotransfected 3.5 μg of pMT-Dpp-HA and 1.5 μg of pMT-Scw-1xFLAG. Heterodimers were purified from 2 mL of medium by incubation with 50 μL of anti-FLAG M2 matrix (Sigma) according to manufacturer's instructions. GST and GST-VkgC were expressed in *Escherichia coli* BL21 cells and purified on GSH-Sepharose beads (GE Healthcare) (details of purification available on request).

**GST-Pulldown Experiments and Western Blotting.** Equal amounts of GST-fusion proteins bound to GSH beads were incubated with 20–200 μL of Dpp-HA, Scw-FLAG, Sog-Myc, or Sog-CR-domain-V5-His-transfected medium or 100 μL of affinity-purified Scw-FLAG/Dpp-HA complexes in pulldown buffer (20 mM at Tris pH 8.0, 100 mM NaCl, 1 mM EDTA) at 4 °C for 1–2 h. Beads were washed three times in 1 mL of pulldown buffer + 0.1% Nonidet P-40, and eluted in Laemmli buffer. Samples were separated by reducing SDS/PAGE, followed by Western blotting or Coomassie blue staining. Antibodies used were as follows: mouse anti-HA 1:2,000 (Roche), anti-FLAG M2 1:500 (Sigma), anti-Myc 9E10 1:2,000 (Santa Cruz) or anti-Myc 4A6 1:500 (Millipore), and anti-V5 1:2,000 (Abcam).

**Fly Strains.** Flystocks used were $y^{67c23}w^{118}$, $sog^{56}$/*FM7c*, $tsg^{2}$/*FM7c* (both from Bloomington Drosophila Stock Center), *st2-dpp* (17). *st2-dpp-Δa* lines were generated at Bestgene by injecting 22FPE-dppΔa into $y^{1}w^{1118}$ embryos. Transgene expression was activated as described (6).

**Embryo Collection and RNA in Situ Hybridization.** Embryos were collected from crosses of *yw*, $sog^{56}$/*FM7c* or $tsg^{2}$/*FM7c* females to homozygous *st2-dpp* or *st2-dppΔa* males. Embryos were fixed and processed for RNA in situ hybridization with digU-labeled RNA probes by using standard protocols.

**ACKNOWLEDGMENTS.** We thank Abbie Saunders and Mark Ashe for critical reading of the manuscript. This work was supported by Wellcome Trust Studentship 083271/Z/07/Z and Project Grant WT083211AIA, and by the *Drosophila* Core Research Facility at the Faculty of Life Sciences, University of Manchester, established through funds from the University and the Wellcome Trust (087742/Z/08/Z).

1. Little SC, Mullins MC (2006) Extracellular modulation of BMP activity in patterning the dorsoventral axis. *Birth Defects Res C Embryo Today* 78:224–242.
2. Umulis D, O'Connor MB, Blair SS (2009) The extracellular regulation of bone morphogenetic protein signaling. *Development* 136:3715–3728.
3. Ferguson EL, Anderson KV (1992) Decapentaplegic acts as a morphogen to organize dorsal-ventral pattern in the Drosophila embryo. *Cell* 71:451–461.
4. O'Connor MB, Umulis D, Othmer HG, Blair SS (2006) Shaping BMP morphogen gradients in the Drosophila embryo and pupal wing. *Development* 133:183–193.
5. Holley SA, et al. (1996) The Xenopus dorsalizing factor noggin ventralizes Drosophila embryos by preventing DPP from activating its receptor. *Cell* 86:607–617.
6. Ashe HL, Levine M (1999) Local inhibition and long-range enhancement of Dpp signal transduction by Sog. *Nature* 398:427–431.
7. Eldar A, et al. (2002) Robustness of the BMP morphogen gradient in Drosophila embryonic patterning. *Nature* 419:304–308.
8. Wang YC, Ferguson EL (2005) Spatial bistability of Dpp-receptor interactions during Drosophila dorsal-ventral patterning. *Nature* 434:229–234.
9. Shimmi O, Umulis D, Othmer H, O'Connor MB (2005) Facilitated transport of a Dpp/Scw heterodimer by Sog/Tsg leads to robust patterning of the Drosophila blastoderm embryo. *Cell* 120:873–886.
10. Marqués G, et al. (1997) Production of a DPP activity gradient in the early Drosophila embryo through the opposing actions of the SOG and TLD proteins. *Cell* 91:417–426.
11. Wang XM, Harris RE, Bayston LJ, Ashe HL (2008) Type IV collagens regulate BMP signalling in Drosophila. *Nature* 455:72–77.
12. Umulis DM, Shimmi O, O'Connor MB, Othmer HG (2010) Organism-scale modeling of early Drosophila patterning via bone morphogenetic proteins. *Dev Cell* 18:260–274.
13. Künnapuu J, Björkgren I, Shimmi O (2009) The Drosophila DPP signal is produced by cleavage of its proprotein at evolutionary diversified furin-recognition sites. *Proc Natl Acad Sci USA* 106:8501–8506.
14. Fritsch C, et al. (2012) Different requirements for proteolytic processing of bone morphogenetic protein 5/6/7/8 ligands in Drosophila melanogaster. *J Biol Chem* 287:5942–5953.
15. Zhang JL, Huang Y, Qiu LY, Nickel J, Sebald W (2007) von Willebrand factor type C domain-containing proteins regulate bone morphogenetic protein signaling through different recognition mechanisms. *J Biol Chem* 282:20002–20014.
16. Fujisawa T, Huang Y, Sebald W, Zhang J-L (2009) The binding of von Willebrand factor type C domains of Chordin family proteins to BMP-2 and Tsg is mediated by their SD1 subdomain. *Biochem Biophys Res Commun* 385:215–219.
17. Ashe HL, Mannervik M, Levine M (2000) Dpp signaling thresholds in the dorsal ectoderm of the Drosophila embryo. *Development* 127:3305–3312.
18. Mizutani CM, et al. (2005) Formation of the BMP activity gradient in the Drosophila embryo. *Dev Cell* 8:915–924.
19. Yu K, et al. (2000) Processing of the Drosophila Sog protein creates a novel BMP inhibitory activity. *Development* 127:2143–2154.
20. Ohkawara B, Iemura S, ten Dijke P, Ueno N (2002) Action range of BMP is defined by its N-terminal basic amino acid core. *Curr Biol* 12:205–209.
21. Akiyama T, et al. (2008) Dally regulates Dpp morphogen gradient formation by stabilizing Dpp on the cell surface. *Dev Biol* 313:408–419.
22. Bornemann DJ, Park S, Phin S, Warrior R (2008) A translational block to HSPG synthesis permits BMP signaling in the early Drosophila embryo. *Development* 135: 1039–1047.
23. Kirkpatrick CA, et al. (2006) The function of a Drosophila glypican does not depend entirely on heparan sulfate modification. *Dev Biol* 300:570–582.
24. Ben-Zvi D, Shilo BZ, Fainsod A, Barkai N (2008) Scaling of the BMP activation gradient in Xenopus embryos. *Nature* 453:1205–1211.
25. Zakin L, Chang EY, Plouhinec J-L, De Robertis EM (2010) Crossveinless-2 is required for the relocalization of Chordin protein within the vertebral field in mouse embryos. *Dev Biol* 347:204–215.
26. Shimmi O, Ralston A, Blair SS, O'Connor MB (2005) The crossveinless gene encodes a new member of the Twisted gastrulation family of BMP-binding proteins which, with Short gastrulation, promotes BMP signaling in the crossveins of the Drosophila wing. *Dev Biol* 282:70–83.
27. Matsuda S, Shimmi O (2012) Directional transport and active retention of Dpp/BMP create wing vein patterns in Drosophila. *Dev Biol* 366:153–162.
28. Bunt S, et al. (2010) Hemocyte-secreted type IV collagen enhances BMP signaling to guide renal tubule morphogenesis in Drosophila. *Dev Cell* 19:296–306.
29. Paralkar VM, et al. (1990) Interaction of osteogenin, a heparin binding bone morphogenetic protein, with type-IV collagen. *J Biol Chem* 265:17281–17284.
30. Kosman D, Small S (1997) Concentration-dependent patterning by an ectopic expression domain of the Drosophila gap gene knirps. *Development* 124:1343–1354.
31. Sopory S, Kwon S, Wehrli M, Christian JL (2010) Regulation of Dpp activity by tissue-specific cleavage of an upstream site within the prodomain. *Dev Biol* 346:102–112.

# Antagonistic action of Bicoid and the repressor Capicua determines the spatial limits of *Drosophila* head gene expression domains

Ulrike Löhr[a,1], Ho-Ryun Chung[b], Mathias Beller[a], and Herbert Jäckle[a]

[a]Abteilung Molekulare Entwicklungsbiologie, Max-Planck-Institut für biophysikalische Chemie, Am Fassberg 11, 37077 Göttingen, Germany; and [b]Max-Planck-Institut für molekulare Genetik, 14195 Berlin, Germany

Communicated by Walter J. Gehring, University of Basel, Basel, Switzerland, October 20, 2009 (received for review February 24, 2009)

**Bicoid (Bcd) is the anterior determinant in *Drosophila*. Accordingly, loss of Bcd causes loss of head and thorax and their replacement with posterior structures. *bcd* mRNA is maternally deposited at the anterior pole and Bcd forms an anterior-to-posterior (AP) concentration gradient. The expression of a series of zygotic head genes is thought to be differentially regulated by distinct threshold concentrations of the Bcd gradient. Thereby Bcd functions as a morphogen, instructing fields of cells to take on specific fates. Here, we show that spatial limits of anterior genes are also set in the absence of a Bcd gradient and depend on factors of the maternal terminal system. The receptor tyrosine kinase Torso (Tor), a key component of this system, is active in the pole regions of the embryo. Its activity downregulates the maternally deposited repressor Capicua (Cic), leaving high Cic activity in the central regions and decreasingly lower Cic activities toward the poles. We show that the positions of posterior boundaries of Bcd target genes are dependent not only on Bcd, but also on Tor-mediated Cic activity. The results indicate that Cic can mediate repression through distinct binding sites within a Bcd responsive enhancer and that gene activation by Bcd is antagonized by Cic. The activating and repressive effects of Bcd and Cic, respectively, are integrated by the Bcd target gene enhancer. We conclude that the spatial domains of head gene expression are determined by Bcd in concert with Tor-dependent repressors.**

bicoid antagonist | *Drosophila* development | gene regulation | head development | morphogen gradient

Bcd is a homeodomain-containing transcription factor required for head development in *Drosophila* (1, 2). *bcd* mRNA is maternally deposited and localized to the anterior egg pole by its 3′-UTR (3, 4). From there both the mRNA and ultimately the protein form a concentration gradient along the anterior–posterior (AP) axis (5, 6). Interestingly, a change in *bcd* dosage leads to shifts in target gene expression. Reduction by one *bcd* copy leads to an anterior shift of target gene expression boundaries, whereas an additional copy results in a posterior shift (7). Thus, it has been suggested that Bcd functions as a morphogen (8, 9) and that target gene expression depends directly on distinct concentrations of Bcd along the AP axis (7). This concentration-dependent gene activation is thought to be mediated by the affinity of binding sites for Bcd within target genes (10–12). Targets expressed close to the source would contain low affinity binding sites, whereas targets far from the source would contain high affinity sites. Bcd also can activate enhancers via cooperative binding (13, 14).

In addition to Bcd, the terminal system has been shown to affect gene expression in the head region of the embryo. Torso (Tor), a receptor tyrosine kinase, is activated only at the poles (15) from where it signals through the MAP kinase pathway and regulates terminal gene expression by relief of repression (15–18). *capicua* (*cic*) mRNA is maternally deposited in the embryo, resulting in ubiquitous Cic expression. It has been shown that Tor downregulates the DNA binding repressor Cic at the termini by phosphorylation via the activated MAP kinase Rolled (19, 20), resulting in low Cic activity at the termini and high activity in the center of the embryo. Loss of Cic leads to the derepression of head and tail genes and the expansion of these regions at the cost of the trunk and abdomen (19). Also, it has been suggested that Tor activity results in the phosphorylation of Bcd (21) strengthening its morphogenic nature along the AP axis (22, 23). At the anterior pole Tor has been proposed to have an opposite function, i.e., to downregulate Bcd activity, and that this effect causes repression of *hunchback* and *orthodenticle* at the anterior tip (21, 24).

Here we show that uniform expression of Bcd leads to ectopic head gene expression with mirror image polarity at the posterior pole. This effect is dependent on Tor-regulated Cic activity, confirming a major role of the terminal system in the spatial control of Bcd-dependent head gene expression. We found that Cic activity is necessary to determine the spatial limits of head gene expression by repression. These results suggest that this effect of the terminal system is mediated by binding sites located in Bcd responsive enhancers. We conclude that anterior patterning is dependent on the interpretation of activation by Bcd relative to repression by Cic by the enhancers.

## Results

**Uniform Expression of Bcd Causes the Mirror Image Duplications of Target Gene Expression.** To assess the ability of Bcd to activate gene expression independent of its gradient, we used the UASp/Gal4 system (25, 26) to ectopically express *bcd* without its localizing 3′-UTR in the female germline. In embryos that derive from such females, the endogenous Bcd gradient was superimposed with transgene-derived Bcd, resulting in uniform Bcd levels in the posterior half of the embryo (*SI Materials and Methods* and Fig. S1 *A*, *B*, *D*, and *E*). In such embryos, the Bcd target gene *hunchback* (*hb*) (27), which is normally detected in the anterior 50% of the embryo, is ubiquitously expressed (Fig. S2 *A* and *B*). However, Bcd target genes that are normally confined to more anterior regions, such as *cap-n-collar* (*cnc*) (28), *tailless* (*tll*) (29), and *giant* (*gt*) (30) are expressed in distinct but ectopic domains (Fig. 1; see also Figs. S2 *C*, *D*, *G*, and *H* and S3 *A*–*C*). *cnc*, normally expressed only in the anterior region (28) (Fig. 1 *A* and *B*), was also expressed in the posterior of embryos, which contain uniform high levels of Bcd (Fig. 1 *E* and *F*). Similarly, the anterior tip domain of Gt expression (Fig. 1 *A* and *C*) was duplicated in the posterior (Fig. 1 *E* and *G*). Gt expression was also detected in a central, ventrolaterally repressed domain, which resembled the anterior portion of the anterior stripe in wild-type embryos. Finally, the dorsolateral anterior domain of *tll* (Fig. 1 *A* and *D*) was broadly expanded along

Author contributions: U.L., H.-R.C., and H.J. designed research; U.L. and H.-R.C. performed research; M.B. contributed new reagents/analytic tools; U.L., H.-R.C., and M.B. analyzed data; and U.L. and H.J. wrote the paper.

The authors declare no conflict of interest.

Freely available online through the PNAS open access option.

[1]To whom correspondence should be addressed. E-mail: uloehr@gwdg.de.

This article contains supporting information online at www.pnas.org/cgi/content/full/0910225106/DCSupplemental.

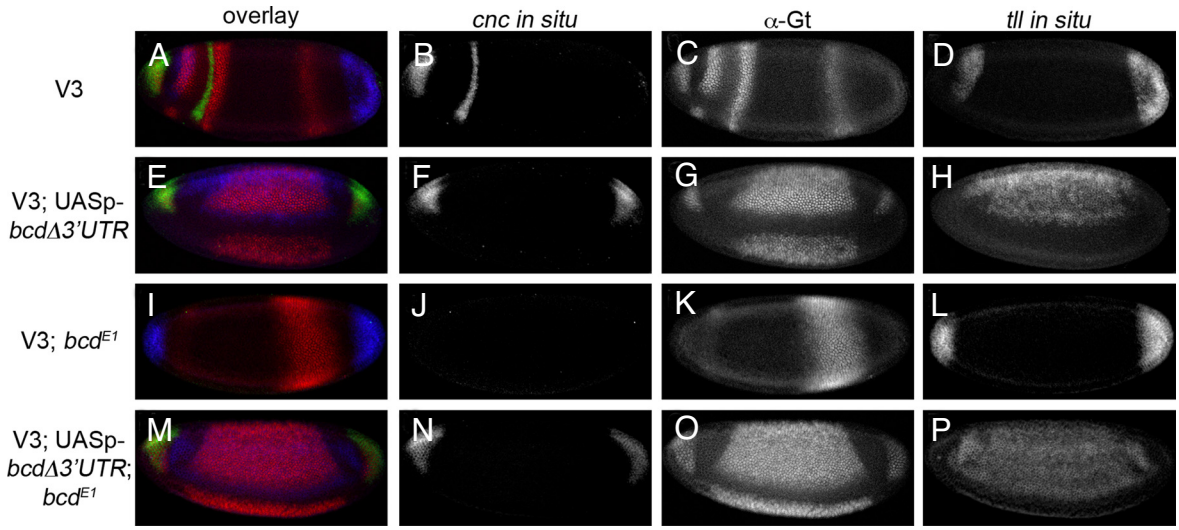


**Fig. 1.** Uniform expression of transgene-derived Bcd in wild-type and $bcd^{E1}$ embryos causes mirror image duplications of anterior expression domains in the posterior region. *cnc* and *tll* mRNAs were detected by fluorescent *in situ* hybridization (green and blue, respectively); Gt was detected by immunohistochemistry (red); *A*, *E*, *I*, and *M* are overlays; *B–D*, *F–H*, *J–L*, and *N–P* are single channel gray scale images; anterior is to the *Left*; dorsal is *Up*. (*A–D*) Expression of *cnc*, Gt, and *tll* in a control embryo (V3). (*A* and *B*) *cnc* is expressed in an anterior cap and a more central collar. (*A* and *C*) Gt is expressed in an anterior tip domain, an anterior double stripe domain, consisting of a discontinuous and a continuous stripe, and a posterior stripe domain. (*A* and *D*) *tll* is expressed in an anterior dorsal-ventral and a posterior cap domain. (*E–H*) Transgene-derived ubiquitous Bcd causes mirror image duplications of anterior patterns in the posterior. (*E* and *F*) The *cnc* cap domain is duplicated at the posterior pole. (*E* and *G*) The tip domain of Gt is also duplicated at the posterior and Gt is expressed centrally as a ventrolaterally repressed stripe. This expression corresponds to the discontinuous anterior stripe. (*E* and *H*) *tll* is expressed in a broad, ventrally repressed domain in the center of the embryo. (*I–L*) Expression of *cnc*, Gt, and *tll* in $bcd^{E1}$ embryos. (*I* and *J*) *cnc* expression is completely absent. (*I* and *K*) Gt is only detected as a broadened posterior stripe. (*I* and *L*) In the anterior *tll* is expressed in a cap, resembling posterior expression. (*M–P*) Uniform Bcd in $bcd^{E1}$ embryos causes mirror image duplications. (*M* and *N*) The anterior cap of *cnc* expression is restored and duplicated in the posterior. (*M* and *O*) Gt tip expression is also restored and duplicated, while a ventrolaterally repressed stripe is expressed in the central regions. (*M* and *P*) *tll* is expressed in a central ventrally repressed domain. Note that the expression patterns observed in *M–P* strongly resemble those observed in *E–H*, showing that the mirror image duplications do not depend on the endogenous Bcd gradient.

the AP axis of the embryo (Fig. 1 *E* and *H*). These findings indicate that the anterior patterns of these three genes were mirrored along an axis, which runs vertically through the anterior *tll* domain, in an area in which it overlaps with the anterior Gt stripe. We confirmed that the ectopic expression domains observed for *cnc* and Gt were indeed mirror image duplications by the use of *lacZ* reporter constructs. The cnc_(+5)-*lacZ* construct recapitulates *cnc* in the wild-type embryos (31) (Fig. S2*E*), while gt_(−6)-*lacZ* recapitulates the *gt* tip expression (31) (Fig. S2*I*). In the presence of unlocalized Bcd both the cnc_(+5) and the gt_(−6) drive *lacZ* expression in distinct domains in the posterior (Fig. S2 *F* and *J*) as was observed for *cnc* and Gt in the presence of unlocalized Bcd. Thus, uniformly expressed Bcd causes an expansion and mirroring of anterior expression domains at the posterior pole (Fig. 1*E*). In fact, the Hox gene *labial* (*lab*) (32), normally expressed in a stripe anterior to the cephalic furrow (33) (Fig. S2*K*), was duplicated in a mirror image fashion in the posterior of embryos (Fig. S2*L*), indicating that these cells have indeed taken on specific anterior identities. Additionaly, we observed that the expression domains of other potential Bcd target genes in the head region, such as those of *knirps* (*kni*) (34), *orthodenticle* (*otd*) (12), *buttonhead* (*btd*) (35), *empty spiracles* (*ems*) (36), and *sloppy-paired* (*slp2*) (37), are duplicated with mirror image polarity in the posterior region in the presence of uniform Bcd (Fig. S3).

To exclude that the endogenous Bcd gradient caused the observed mirror image duplications, we examined the effects of uniform Bcd in embryos lacking endogenous Bcd. In the absence of endogenous Bcd no gradient is detectable in the presence of ectopic unlocalized Bcd, indicating that all nuclei in the embryo receive a similar amount of Bcd (Fig. S1 *C* and *F*). In embryos from females homozygous for the $bcd^{E1}$ loss-of-function allele (2), the anterior domains of *cnc* and Gt are lost and anterior *tll* expression strongly resembles its posterior expression (28–30, 38) (Fig. 1 *I–L*). In such embryos, uniform Bcd caused mirror image expression of head genes indistinguishable from its effect in the presence of endogenous Bcd (compare *E–H* and *M–P* in Fig. 1). *cnc* expression was restored at both poles of the embryos (Fig. 1 *M* and *N*). Thus, endogenous Bcd gradient information cannot be responsible for residual anterior gene expression and their mirror image expression patterns in the posterior. This result shows that although Bcd is necessary to activate head genes such as *cnc*, differential activation of target genes and their spatial order is not dependent on Bcd gradient information. Similar effects have been observed in embryos that express low levels of Bcd uniformly along the entire axis (11, 22, 39).

**Terminal System Activity Is Required for the Mirror Image Duplications of Head Gene Expression Domains.** It has been shown that the maternal terminal system activates anterior target genes by relief of repression (16, 17, 19). One of the main effectors of Tor signaling is Cic, a ubiquitous repressor of anterior and posterior gene expression that is downregulated at the embryonic termini by activated Tor signaling (19). Consequently, Cic and/or other Tor-dependent repressors could antagonize Bcd-dependent gene activation and thereby position posterior boundaries (PBs) of Bcd target genes in the head. As Tor signals at both termini, Cic could also repress Bcd-dependent target genes in embryos which have received uniform levels of Bcd, causing the observed mirror image duplications of anterior expression domains in the posterior region.

In embryos from females homozygous for the $cic^{1}$ loss-of-function allele, the head and tail regions are expanded at the expense of the trunk (19). Consequently, *cnc*, Gt, and *tll* expression is expanded toward the center (19) (Fig. 2 *A–D*), indicating that although their anterior domains were delimited, their PBs were not properly positioned (see below). In $cic^{1}$ embryos uniformly expressing Bcd, *cnc* expression domains appeared at both termini and were connected via a ventrolateral stripe (Fig. 2 *E* and *F*). Gt was also expressed in both pole regions (Fig. 2 *E* and *G*) and *tll* expression

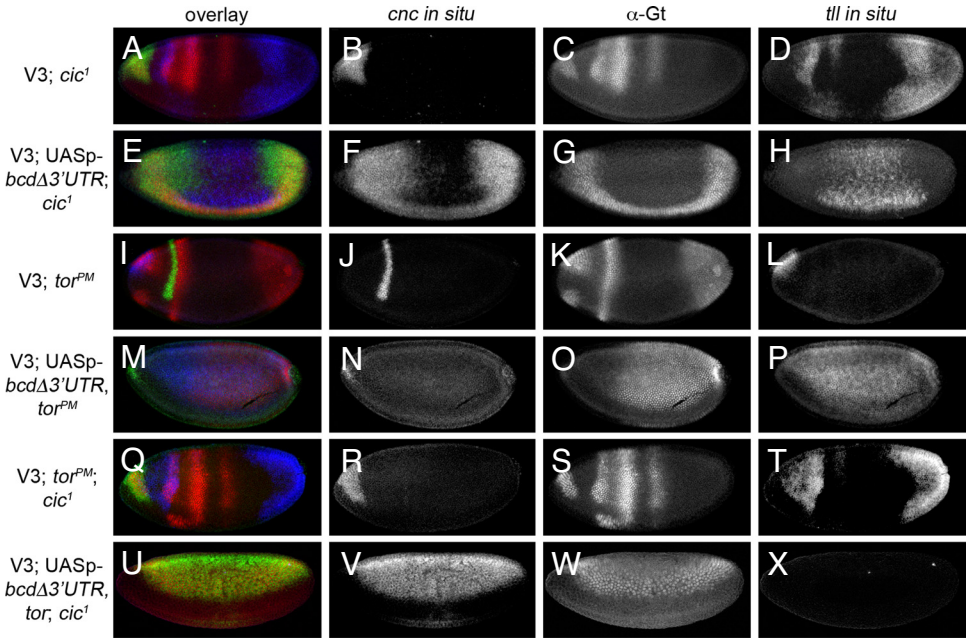


**Fig. 2.** The terminal system components Cic and Tor are required for mirror image duplications in response to uniformly expressed Bcd. Gene expression was visualized as described in Fig. 1. *A*, *E*, *I*, *M*, *Q*, and *U* are overlays of all three channels; *B–D*, *F–H*, *J–L*, *N–P*, *R–T*, and *V–X* are single channel gray scale images; anterior is to the *Left*; dorsal is *Up*. (*A–D*) Expression of *cnc*, Gt, and *tll* in $cic^1$ embryos. (*A* and *B*) The cap domain of *cnc* is expanded toward the center and the collar is missing; compare to Fig. 1*B*. (*A* and *C*) Main domains of Gt expression are formed, but both stripe domains are ventrally repressed. The posterior Gt stripe is shifted toward the center. (*A* and *D*) The anterior and posterior expression domains of *tll* are expanded toward the center. (*E–H*) Ubiquitous Bcd in $cic^1$ embryos causes duplications with minimal patterning information. (*E* and *F*) The cap domain of *cnc* is expanded and duplicated at the posterior, and both caps are connected by a ventrolateral stripe of *cnc* expression. (*E* and *G*) Anterior tip expression of Gt is expanded and duplicated. Both domains are connected by a ventrolateral stripe. (*E* and *H*) *tll* is expressed in the central region but not on the ventral side. This amounts to a duplication of only the anteriormost region with very limited positional information. (*I–L*) Expression of *cnc*, Gt, and *tll* in $tor^{PM}$ embryos. (*I* and *J*) The *cnc* cap domain is absent; the collar is shifted toward the anterior. (*I* and *K*) The anterior tip domain of Gt is absent, the anterior Gt stripe domain is shifted to the anterior pole region and the expanded posterior Gt stripe is shifted to the posterior pole. (*I* and *L*) *tll* expression is absent in the posterior and the anterior dorsal-ventral wedge of expression is shifted to the anterior pole. (*M–P*) Uniformly expressed Bcd in $tor^{PM}$ embryos does not cause duplications, but is unable to activate *cnc*. (*M* and *N*) *cnc* expression is only detected in a few anterior cells, indicating that it is strongly repressed even in the presence of excess Bcd. (*M* and *O*) Anterior tip expression of Gt is not recovered, but a broad ventrolaterally repressed, continuous Gt domain is observed, which most likely corresponds to the anterior discontinuous stripe. (*M* and *P*) *tll* is expressed throughout the embryo and overlaps with Gt expression. Note that *tll* expression is not excluded from the posterior pole. (*Q–T*) Expression of *cnc*, Gt, and *tll* in *tor*; $cic^1$ embryos resembles expression in $cic^1$ embryos (*A–D*). (*Q* and *R*) *cnc* expression at the anterior is restored in these embryos (compare to *I* and *J*) and the collar is missing. (*Q* and *S*) Gt expression strongly resembles Gt expression in $cic^1$ embryos (*A* and *C*) as does *tll* expression (compare *Q* and *T* to *A* and *D*). (*U–X*) Ubiquitous Bcd in *tor*; $cic^1$ embryos does not cause duplications, but continuous expression of the anteriormost targets. (*U* and *V*) *cnc* is expressed from the anterior to the posterior tip in a continuous, ventrally repressed domain. (*U* and *W*) Gt is detected in a ventrolateral stripe spanning the entire embryo, most likely corresponding to an extremely elongated tip domain. (*U* and *X*) *tll* is absent in these embryos. Thus, all cells resemble the anterior tip of a wild-type embryo.

was confined to dorsolateral regions, excluding *cnc*- or Gt-expressing cells (Fig. 2 *E* and *H*). These patterns were distinctly different from those observed upon ubiquitous Bcd expression in wild-type or $bcd^{E1}$ embryos (compare Fig. 2 *E–H* with Fig. 1 *E–H* and *M–P*), indicating that the removal of Cic activity resulted in the expansion of Bcd target gene expression toward the center. However, as minimal anterior patterning was observed at both poles in $cic^1$ embryos expressing uniform Bcd (i.e., *cnc* and Gt expression at both poles separated by *tll* expression), positional information must be provided by additional factors.

To test whether such additional factors are also under the control of the terminal system, we examined the effects of ubiquitous Bcd in embryos lacking Tor activity. Such embryos, derived from $tor^{PM}$ homozygous females, fail to develop head and tail structures (15). Because of ectopic Cic activity in the terminal regions of $tor^{PM}$ embryos (19), the more central expression domains are shifted toward the termini, i.e., *cnc* and Gt expression are lost from the anterior tip and both anterior Gt stripe and *tll* are shifted to the anterior pole (28–30) (Fig. 2 *I–L*). Uniform Bcd expression in $tor^{PM}$ embryos caused no duplications (Fig. 2 *M–P*), but embryos were continuously patterned, i.e., Gt and *tll* were expressed in overlapping, ventrally repressed domains throughout the embryo. However, *cnc*, a marker of anteriormost gene expression, was only weakly restored in some embryos. Thus, in embryos lacking Tor activity, genes normally expressed at the anterior tip of the embryo were repressed despite the presence of Bcd. Thus the entire embryo was continuously patterned, but the anteriormost information (i.e., *cnc* expression) was missing. Corresponding results were reported from embryos containing low uniform levels of Bcd in the absence of *tor* (22).

We next expressed Bcd in embryos devoid of both *tor* and *cic* to observe possible Cic-independent effects of Tor. Overall, expression of target genes in embryos devoid of both *tor* and *cic* (Fig. 2 *Q–T*) was very similar to that in $cic^1$ embryos (19) (Fig. 2 *A–D*). Upon uniform Bcd expression, *cnc* was expressed in a dorsolateral domain along the entire length of the embryo (Fig. 2 *U* and *V*), Gt was expressed in a horizontal stripe of cells (Fig. 2 *U* and *W*), and *tll* expression was undetected (Fig. 2 *U* and *X*). Thus, the anterior pattern was not duplicated, but instead the entire embryo resembled the anterior tip region. In summary, uniformly expressed Bcd can cause anterior gene expression throughout the entire embryo only in the absence of two key components of the terminal system. These results indicate that (*i*) terminal Tor signaling is necessary to establish mirror image duplications in the presence of Bcd in the posterior pole region and (*ii*) Tor does not act in this process through Cic alone. In the presence of uniform Bcd, positional

information can then be provided via Tor-dependent factors, such as Cic, which antagonize activation of Bcd target genes and thus, cause the mirror image duplications.

**Cic Is Required for the Determination of Spatial Limits of Bcd Target Genes.** To assess the Cic requirement for the positioning of PBs of potential Bcd target genes expressed in the embryonic head region, we measured their positions in wild-type and *cic*$^{1}$ mutant embryos. We found that the PBs of the *gt* anterior tip domain as well as the *huckebein* (*hkb*), *kni*, *otd*, *ems*, *slp2*, and *cnc* anterior domains were strongly dependent on Cic activity (summarized in Fig. 3*A*; for RNA expression see Fig. S4). Target genes with PBs posterior to 60% egg length (i.e., the anterior *gt* stripe and *hb*; Fig. S4 *Q*–*T*, anterior pole is 100%, posterior 0%) were not notably affected by the loss of *cic*. These findings suggest that Cic limits Bcd target gene expression strongest, or exclusively, in the presumptive head region. Interestingly, the expression pattern of *gt* appears to contain both a *cic* sensitive (*gt* anterior tip) and insensitive domain (*gt* anterior stripe). Although anterior *gt* stripe expression is not affected in *cic*$^{1}$ embryos, it is clearly shifted to the anterior tip in embryos lacking *tor* (30) (see Fig. 2 *I* and *K*). This observation indicates that Tor-dependent factors other than Cic participate in establishing the PBs of Bcd-responsive genes posterior to 60% egg length. Additionally, our results suggest that repression by Cic antagonizes Bcd activity in the anterior regions of the embryo where Bcd levels are much higher than necessary for target gene activation (39). Conversely, the distinct PBs observed in *cic*$^{1}$ mutants suggest that the Bcd gradient provides some information for the spatial activation of target genes which, however, is not accurate enough to properly pattern the head region of the embryo. It is also possible that additional Tor-dependent factors participate in repression of anterior Bcd targets when Cic is absent.

**Repression by Cic Is Mediated Through the torRE.** Our results show that Tor-dependent repressors such as Cic position the PBs of Bcd targets in the presumptive head region. Does this happen on Bcd-dependent enhancers themselves? It has been shown that human Cic binds to the sequence motif TGAATGAA (40), which is remarkably similar to the Torso-response element (torRE; TCGTCAATGAA) that mediates repression in the *tll* enhancer (16). To identify enhancers that contain both Bcd binding sites and torREs, we screened DNA fragments previously identified as Bcd targets in a chromatin immunoprecipitation assay with subsequent microarray analysis (41) for torREs (Table S1). We identified fragments that bound Bcd and contained torREs in the vicinity of known Bcd targets such as *tll*, *otd*, *ems*, *btd*, and overlapping enhancer modules previously identified in a computational screen as containing both Bcd binding sites and torREs [cnc_+5, btd_head, kni_(−5) and slp2_(−3)] (31). Additionally, we identified fragments overlapping with the enhancer module for the anterior tip expression of *gt* (gt_(−6) (31) and in the vicinity of a number of genes of known [e.g., *homeobrain* (42), *goosecoid* (43) and *Dichaete* (44)] and unknown function (e.g., *CG31670*) with anterior expression domains (Table S1). These observations support our hypothesis that Bcd and Tor-dependent DNA-binding factors share common enhancers and together regulate the spatial limitations of anterior expression domains.

To test whether Cic can indeed repress Bcd-dependent target genes through torREs, we used a minimal Bcd-responsive enhancer containing three Bcd sites (21) ("bcd3T"), and added one ("bcd3T-1torREu") or two ("bcd3T_2torRE") torREs upstream of a *lacZ* reporter gene (Fig. 3*B*). If the posterior expansion of gene expression is dependent on repression by Cic, the addition of torREs should shift the PB of the reporter gene toward the anterior in wild-type embryos and this effect should be lost in *cic*$^{1}$ embryos. As summarized in Fig. 3*C* (Fig. S5 for RNA expression), torRE-dependent shifts were indeed observed, and the extent of the shift was dependent on the number of torREs. Furthermore, the PBs of all *lacZ* reporters were found at around 70% egg length in the absence of Cic, indicating that the repressive effect mediated by the torREs is dependent on Cic. Also, these results indicate that Cic

A

| | wt | | | *cic*$^{1}$ | | |
|---|---|---|---|---|---|---|
| gene | PB average position | stdv | n | PB average position | stdv | n |
| *gt* tip | 88% | 1% | 71 | 83% | 2% | 42 |
| *cnc* | 86% | 2% | 62 | 80% | 2% | 121 |
| *hkb* | 86% | 2% | 96 | 78% | 2% | 140 |
| *kni* | 72% | 2% | 100 | 64% | 3% | 97 |
| *otd* | 69% | 2% | 71 | 66% | 2% | 63 |
| *ems* | 69% | 2% | 116 | 63% | 2% | 122 |
| *slp2* | 68% | 2% | 115 | 61% | 2% | 78 |
| *btd* | 65% | 2% | 82 | 60% | 2% | 107 |
| *gt* stripe | 60% | 2% | 225 | 58% | 2% | 112 |
| *hb* | 50% | 2% | 165 | 49% | 2% | 33 |

B

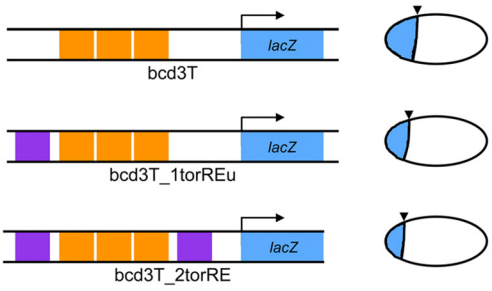


C

| | wt | | | *cic*$^{1}$ | | |
|---|---|---|---|---|---|---|
| *lacZ* reporter | PB average position | stdv | n | PB average position | stdv | n |
| bcd3T | 68% | 3% | 489 | 69% | 3% | 146 |
| bcd3T_1toREu | 72% | 3% | 184 | 70% | 3% | 126 |
| bcd3T_2torRE | 77% | 3% | 464 | 70% | 2% | 255 |

**Fig. 3.** Cic establishes the proper posterior boundaries (PBs) of head genes and can act upon a Bcd-responsive enhancer through torREs. PBs of anterior Bcd-dependent gene expression and reporter genes under control of Bcd-dependent enhancers were analyzed in wild-type (wt) and *cic*$^{1}$ embryos (PB position in % of egg length (EL); anterior tip is 100%, the posterior 0%). (*A*) In *cic*$^{1}$ embryos, the PBs of gene expression domains anterior to 60% EL in wt embryos (i.e., *gt* anterior tip domain, *cnc*, *hkb*, *kni*, *otd*, *ems*, *slp2*, and *btd*) are shifted by around 3–8% toward the posterior, whereas no effect was observed on Bcd target genes whose PBs were located posterior to 60% EL (the *gt* anterior stripe and anterior *hb* expression; see Fig. S4 for RNA expression). Note that the strength of the Cic repression effect declines toward the center of the embryo. (*B*) Schematic representations of minimal enhancers (for sequences see *Materials and Methods*) and expected positions of PBs in a wt background. bcd3T: a minimal *bcd* responsive enhancer containing three Bcd binding sites (orange boxes) was placed upstream of *lacZ* (blue box). bcd3T_1torREu: one torRE (purple box) upstream of the bcd3T. bcd3T_2torRE: torREs on either side of the bcd3T. The most central PB is expected for bcd3T, whereas bcd3t_2torRE should show the most anterior PB (PBs indicated by arrowheads in schematic). The position of the bcd3T_1torREu PB was expected to lie between the two. (*C*) Addition of torREs shifts the PB of the bcd3T toward the anterior. The PB of the bcd3T is located most centrally of the three constructs at 68% EL, whereas that of bcd3T_1torREu is more anterior at 72% EL and that of bcd3T_2torRE is observed at the most anterior position, 77% EL. Unlike the torRE-containing enhancers, bcd3T is not dependent on *cic*. In the absence of *cic* the PBs of all enhancers were measured at around 70% EL (see Fig. S5 for representative stainings). Values are average position in % EL; stdv: standard deviation.

does not act directly on Bcd, as the PB of bcd3T-*lacZ* was independent of Cic. Hence, the spatial limits of Bcd target gene expression can be modified at the level of the enhancer without manipulating the Bcd gradient or Bcd binding sites.

## Discussion

A morphogen should be able to induce the expression of the same target gene in all cells in which it is expressed at the same level (9). When Bcd was uniformly expressed, we found that different Bcd target genes were expressed in spatially distinct domains with mirror image polarity. Thus, Bcd gradient information alone does not delimit the expression domains of target genes in the head region. Removal of *cic* from such embryos caused the duplication of only the anteriormost target gene expression. This residual patterning of the embryo could be the result of Tor functioning independently of Cic. Removal of *tor* from embryos uniformly expressing Bcd in the posterior caused the continuous patterning of the embryo. However, in the absence of Tor, Cic is also active at the anterior pole and thus able to repress for example *cnc* and *gt*. Therefore, to obtain the expected response of target genes to uniform levels of Bcd, both *tor* and *cic* must be removed from the embryo.

It has been shown previously that *tor* is required for the duplication of *otd* at the posterior of embryos that express low levels of ubiquitous Bcd (22). This effect was attributed to the phosphorylation of Bcd by the Tor pathway (21). However, nonphosphorylatable Bcd can rescue the $bcd^{E1}$ phenotype (23), showing that its phosphorylation is not essential for its function. In addition, we observed that Cic activity affects the mirror image duplications in embryos that express uniform levels of Bcd. This result and the observation that Tor mediates the relief of repression of anterior gene expression (16–18) indicate that the posterior duplications are not caused by a direct effect of Tor signaling on Bcd. The appearance of Tor-dependent upregulation of Bcd activity toward the center of the embryo (22, 23) and its downregulation at the anterior tip (21, 24) can be explained by the local downregulation of repressors, such as Cic. Consistently, both the cuticular phenotype and the expression patterns of Bcd target genes in embryos lacking only Cic activity are indistinguishable from those also lacking both Cic and Tor activity (19) (compare *A* and *Q* in Fig. 2). Notably, *cnc* expression, which is lost in $tor^{PM}$ mutants (Fig. 2*I*), is recovered in embryos devoid of both *tor* and *cic* (Fig. 2*Q*). Thus, the anteriormost Bcd target genes are not dependent on Tor-mediated phosphorylation of Bcd. It is likely that Tor downregulates a set of partially redundant repressors at the termini, including Grainyhead, Trithorax-like (16), Tramtrack69 (45), and Female Sterile (1) Homeotic (46), gradually restricting their activities to the central region, which results in Tor-dependent relief of repression (16). The available evidence supports the argument that mirror image duplications that are caused by uniform expression of Bcd are the result of the spatial restriction of repressors by Tor activity as exemplified here for Cic.

It has been previously suggested that repressors regulated by the terminal system are necessary for the proper patterning of the head region of the embryo (17, 39, 47). Our results provide evidence that the Tor-dependent repressor Cic can position PBs of genes that are activated by Bcd. The effect of Cic is strongest on genes expressed at the very anterior and weakens toward the center. This observation is not surprising, as genes whose PBs are found in regions with high Cic activity (such as *hb*) should be less susceptible to repression by Cic or regulated in a different manner. Recently, it has been reported that Bcd levels in the anterior are much higher than needed for target gene activation (39). In fact, we observed that the expression domains of genes, such as *cnc*, indeed expand toward posterior when Cic is absent. Thus, Bcd activates such genes in a broad domain, which becomes restricted by repression through Cic and possibly other Tor-dependent repressors.

The ability of target genes to react to different thresholds of Bcd has been proposed to depend on the affinity of Bcd binding sites within the enhancer (10–12). However, a correlation between binding site affinity and posterior expression boundaries could not be observed in recent computational studies (48, 49). We and others (31) suggest that Bcd responsive enhancer modules such as those of *tll*, *cnc*, *knirps*, *gt*, *otd*, *btd*, and *slp2* contain torREs, originally identified in the *tll* enhancer (16). These sites are similar to the binding sites reported for human Cic (40). Our results demonstrate that the addition of torREs to the bcd3T enhancer caused a Cic-dependent anterior shift of the boundary that corresponds to about one parasegment per added binding site. Thus, such Cic responsive repressor sites have the potential to be important for the precise positioning of the PBs of Bcd activated genes by mediating repression in response to Tor activity.

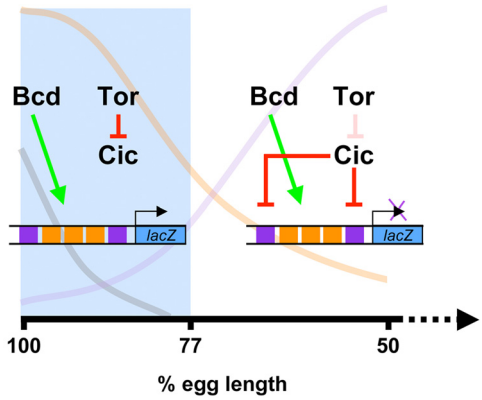


**Fig. 4.** Model of anterior patterning with respect to Bcd and the terminal system. Interactions of the terminal system and Bcd on shared enhancers, exemplified with the bcd3T_2torRE, result in proper positioning of posterior boundaries (PBs). The schematic in the background represents the approximate distribution of Bcd (light orange), Cic (light purple), and Tor (gray) along the anterior half of the embryo. The expression domain of the bcd3T_2torRE is observed from 100 to 77% egg length (EL; blue box). At 100% EL, Tor strongly inhibits activity of Cic and possibly other factors (broad red T-bar), leading to relief of repression of the enhancer. At the same time, Bcd has a strong activating effect on the enhancer (green arrow). At 77% EL the inhibitory effect of Tor is very weak (pink T-bar), so that Cic exerts a strong negative effect on the enhancer (red T-bar), and *lacZ* is no longer expressed at this position. However, we know that Bcd has an activating effect at this position, as it is able to activate the bcd3T construct to 68% EL. Thus, the enhancer is repressed at the position at which the repressive action of Cic outweighs the activating effect of Bcd. We propose that both Bcd activator function and Cic-dependent repression are integrated via the enhancer elements of the target genes, resulting in distinct domains of gene expression. Orange boxes: Bcd binding sites; purple boxes: torRE; blue square: *lacZ* gene. For details on the enhancers see Fig. 3 legend.

Our results suggest a model in which the input from the Bcd gradient alone is not sufficient to determine the spatial limits of target gene expression. Bcd is necessary and sufficient to activate head genes, however, an antagonizing Cic activity gradient regulated by Tor determines their PBs. We propose a mechanism, which integrates information provided by activating Bcd and repressing Cic activities via corresponding binding sites in the target gene enhancers (Fig. 4). At the anterior pole, where Bcd levels are highest, Cic is downregulated by Tor, allowing the activation of anterior genes by Bcd. Further along the AP axis, Tor activity fades (50) and thus, the antagonizing repressor activity of Cic increases. Cic and possibly other Tor-dependent factors can now repress genes controlled by torRE-containing enhancers. Hence, the positions of PBs of anterior genes are determined by activation by Bcd relative to antagonizing repression by Cic on the target gene enhancers.

The dependence of the precise determination of the spatial domains of Bcd target genes on specific Bcd threshold levels has been called into question by this and recent other studies (39). Whereas Ochoa-Espinosa et al. (39) found that Bcd is present at

much higher levels in the anterior of the embryo than necessary for proper gene activation, we have found that Bcd is not able to precisely position the PBs of head genes in the absence of Cic. In summary, we conclude that Bcd is not a "classical morphogen" as initially defined by Wolpert (8), but rather represents the activating component of a maternal "morphogenic network" that includes the terminal system. This network is required to set up both anterior–posterior polarity and to determine the spatial limits of gene expression in the head region of *Drosophila* embryos.

## Materials and Methods

The following mutant alleles were used: $w^{1118}$, for *P*-element transformation and as wild-type reference strain; $bcd^{E1}$ ($bcd^{6}$), $tor^{WK}$ ($tor^{1}$), $tor^{PM}$ ($tor^{4}$), and $cic^{1}$. *bcd* cDNA was cloned into UASp without its 3′-UTR (UASp-*bcdΔ3′UTR*) and expressed with V3-Gal4 (in figures and figure legends referred to as V3) (51) in the female germline. The bcd3T enhancer was cloned with or without torREs into pCaSpeR-hs43-*lacZ* containing *attB* sites. *attB* vectors were injected into embryos from females carrying the $\phi$*C31*-integrase on chromosome IV and an *attP* landing site on chromosome III at 86Fb (line ZH-*attP*-86Fb) (52). Immunohistochemistry and *in situ* hybridizations were conducted using standard methods. See *SI Materials and Methods* for additional information.

**ACKNOWLEDGMENTS.** We thank J. Casanova, E. Wimmer, U. Gaul, and the Bloomington Stock Center for flies; J. Reinitz for antibodies; T. Yakulov and A. Herzig for reagents; A. Ernst, U. Jahns-Meyer, and I. Plischke for generating transgenic flies; A. Ernst, N. Fink, M. Guhlich, and K. Nolde for technical assistance; and S. Small, A. Ochoa-Espinosa, U. Günesdogan, A. Herzig, R. Pflanz, G. Vorbrüggen, U. Schäfer, and all members of the H. Jäckle department for helpful discussions and critical comments. This work was funded by the Max Planck Society.

1. Berleth T, et al. (1988) The role of localization of *bicoid* RNA in organizing the anterior pattern of the *Drosophila* embryo. *EMBO J* 7:1749–1756.
2. Frohnhöfer HG, Nüsslein-Volhard C (1986) Organization of anterior pattern in the *Drosophila* embryo by the maternal gene *bicoid*. *Nature* 324:120–125.
3. St Johnston D, Nüsslein-Volhard C (1992) The origin of pattern and polarity in the *Drosophila* embryo. *Cell* 68:201–219.
4. Macdonald PM, Struhl G (1988) *cis*-acting sequences responsible for anterior localization of *bicoid* mRNA in *Drosophila* embryos. *Nature* 336:595–598.
5. Spirov A, et al. (2009) Formation of the *bicoid* morphogen gradient: An mRNA gradient dictates the protein gradient. *Development* 136:605–614.
6. Driever W, Nüsslein-Volhard C (1988) A gradient of *bicoid* protein in *Drosophila* embryos. *Cell* 54:83–93.
7. Driever W, Nüsslein-Volhard C (1988) The *bicoid* protein determines position in the *Drosophila* embryo in a concentration-dependent manner. *Cell* 54:95–104.
8. Wolpert L (1969) Positional information and the spatial pattern of cellular differentiation. *J Theor Biol* 25:1–47.
9. Gurdon JB, Bourillot PY (2001) Morphogen gradient interpretation. *Nature* 413:797–803.
10. Driever W, Thoma G, Nüsslein-Volhard C (1989) Determination of spatial domains of zygotic gene expression in the *Drosophila* embryo by the affinity of binding sites for the bicoid morphogen. *Nature* 340:363–367.
11. Struhl G, Struhl K, Macdonald PM (1989) The gradient morphogen *bicoid* is a concentration-dependent transcriptional activator. *Cell* 57:1259–1273.
12. Gao Q, Finkelstein R (1998) Targeting gene expression to the head: The *Drosophila* orthodenticle gene is a direct target of the Bicoid morphogen. *Development* 125:4185–4193.
13. Rivera-Pomar R, Lu X, Perrimon N, Taubert H, Jäckle H (1995) Activation of posterior gap gene expression in the *Drosophila* blastoderm. *Nature* 376:253–256.
14. Lebrecht D, et al. (2005) Bicoid cooperative DNA binding is critical for embryonic patterning in *Drosophila*. *Proc Natl Acad Sci USA* 102:13176–13181.
15. Li WX (2005) Functions and mechanisms of receptor tyrosine kinase Torso signaling: Lessons from *Drosophila* embryonic terminal development. *Dev Dyn* 232:656–672.
16. Liaw GJ, et al. (1995) The *torso* response element binds GAGA and NTF-1/Elf-1, and regulates *tailless* by relief of repression. *Genes Dev* 9:3163–3176.
17. Paroush Z, Wainwright SM, Ish-Horowicz D (1997) Torso signalling regulates terminal patterning in *Drosophila* by antagonising Groucho-mediated repression. *Development* 124:3827–3834.
18. Furriols M, Casanova J (2003) In and out of Torso RTK signalling. *EMBO J* 22:1947–1952.
19. Jiménez G, Guichet A, Ephrussi A, Casanova J (2000) Relief of gene repression by Torso RTK signaling: Role of *capicua* in *Drosophila* terminal and dorsoventral patterning. *Genes Dev* 14:224–231.
20. Astigarraga S, et al. (2007) A MAPK docking site is critical for downregulation of Capicua by Torso and EGFR RTK signaling. *EMBO J* 26:668–677.
21. Ronchi E, Treisman J, Dostatni N, Struhl G, Desplan C (1993) Down-regulation of the *Drosophila* morphogen Bicoid by the Torso receptor-mediated signal transduction cascade. *Cell* 74:347–355.
22. Gao Q, Wang Y, Finkelstein R (1996) *Orthodenticle* regulation during embryonic head development in *Drosophila*. *Mech Dev* 56:3–15.
23. Janody F, Sturny R, Catala F, Desplan C, Dostatni N (2000) Phosphorylation of Bicoid on MAP-kinase sites: Contribution to its interaction with the torso pathway. *Development* 127:279–289.
24. Bellaïche Y, Bandyopadhyay R, Desplan C, Dostatni N (1996) Neither the homeodomain nor the activation domain of Bicoid is specifically required for its down-regulation by the Torso receptor tyrosine kinase cascade. *Development* 122:3499–3508.
25. Brand AH, Perrimon N (1993) Targeted gene expression as a means of altering cell fates and generating dominant phenotypes. *Development* 118:401–415.
26. Rørth P (1998) Gal4 in the *Drosophila* female germline. *Mech Dev* 78:113–118.
27. Tautz D (1988) Regulation of the *Drosophila* segmentation gene hunchback by two maternal morphogenetic centres. *Nature* 332:281–284.
28. Mohler J (1993) Genetic regulation of CNC expression in the pharnygeal primordia of *Drosophila* blastoderm embryos. *Roux's Arch Dev Biol* 202:214–223.
29. Pignoni F, Steingrímsson E, Lengyel JA (1992) *bicoid* and the terminal system activate *tailless* expression in the early *Drosophila* embryo. *Development* 115:239–251.
30. Eldon ED, Pirrotta V (1991) Interactions of the *Drosophila* gap gene *giant* with maternal and zygotic pattern-forming genes. *Development* 111:367–378.
31. Schroeder MD, et al. (2004) Transcriptional control in the segmentation gene network of *Drosophila*. *PLoS Biol* 2:E271.
32. Mlodzik M, Fjose A, Gehring WJ (1988) Molecular structure and spatial expression of a homeobox gene from the *labial* region of the *Antennapedia*-complex. *EMBO J* 7:2569–2578.
33. Diederich RJ, Merrill VK, Pultz MA, Kaufman TC (1989) Isolation, structure, and expression of *labial*, a homeotic gene of the *Antennapedia* complex involved in *Drosophila* head development. *Genes Dev* 3:399–414.
34. Rothe M, Wimmer EA, Pankratz MJ, González-Gaitán M, Jäckle H (1994) Identical transacting factor requirement for *knirps* and *knirps-related* gene expression in the anterior but not in the posterior region of the *Drosophila* embryo. *Mech Dev* 46:169–181.
35. Wimmer EA, Simpson-Brose M, Cohen SM, Desplan C, Jäckle H (1995) Trans- and cis-acting requirements for blastodermal expression of the head gap gene *buttonhead*. *Mech Dev* 53:235–245.
36. Hartmann B, Reichert H, Walldorf U (2001) Interaction of gap genes in the *Drosophila* head: *tailless* regulates expression of *empty spiracles* in early embryonic patterning and brain development. *Mech Dev* 109:161–172.
37. Grossniklaus U, Cadigan KM, Gehring WJ (1994) Three maternal coordinate systems cooperate in the patterning of the *Drosophila* head. *Development* 120:3155–3171.
38. Rivera-Pomar R, Jäckle H (1996) From gradients to stripes in *Drosophila* embryogenesis: Filling in the gaps. *Trends Genet* 12:478–483.
39. Ochoa-Espinosa A, Yu D, Tsirigos A, Struffi P, Small S (2009) Anterior-posterior positional information in the absence of a strong Bicoid gradient. *Proc Natl Acad Sci USA* 106:3823–3828.
40. Kawamura-Saito M, et al. (2006) Fusion between CIC and DUX4 up-regulates PEA3 family genes in Ewing-like sarcomas with t(4;19)(q35;q13) translocation. *Hum Mol Genet* 15:2125–2137.
41. Li XY, et al. (2008) Transcription factors bind thousands of active and inactive regions in the *Drosophila* blastoderm. *PLoS Biol* 6:E27.
42. Walldorf U, Kiewe A, Wickert M, Ronshaugen M, McGinnis W (2000) *Homeobrain*, a novel paired-like homeobox gene is expressed in the *Drosophila* brain. *Mech Dev* 96:141–144.
43. Hahn M, Jäckle H (1996) *Drosophila* goosecoid participates in neural development but not in body axis formation. *EMBO J* 15:3077–3084.
44. Russell SR, Sanchez-Soriano N, Wright CR, Ashburner M (1996) The *Dichaete* gene of *Drosophila melanogaster* encodes a SOX-domain protein required for embryonic segmentation. *Development* 122:3669–3676.
45. Chen YJ, Chiang CS, Weng LC, Lengyel JA, Liaw GJ (2002) Tramtrack69 is required for the early repression of *tailless* expression. *Mech Dev* 116:75–83.
46. Florence BL, Faller DV (2008) *Drosophila* Female Sterile (1) Homeotic is a multifunctional transcriptional regulator that is modulated by Ras signaling. *Dev Dyn* 237:554–564.
47. Schaeffer V, Killian D, Desplan C, Wimmer EA (2000) High *bicoid* levels render the terminal system dispensable for *Drosophila* head development. *Development* 127:3993–3999.
48. Ochoa-Espinosa A, et al. (2005) The role of binding site cluster strength in Bicoid-dependent patterning in *Drosophila*. *Proc Natl Acad Sci USA* 102:4960–4965.
49. Segal E, Raveh-Sadka T, Schroeder M, Unnerstall U, Gaul U (2008) Predicting expression patterns from regulatory sequence in *Drosophila* segmentation. *Nature* 451:535–540.
50. Coppey M, Boettiger AN, Berezhkovskii AM, Shvartsman SY (2008) Nuclear trapping shapes the terminal gradient in the *Drosophila* embryo. *Curr Biol* 18:915–919.
51. Häcker U, Perrimon N (1998) *DRhoGEF2* encodes a member of the Dbl family of oncogenes and controls cell shape changes during gastrulation in *Drosophila*. *Genes Dev* 12:274–284.
52. Bischof J, Maeda RK, Hediger M, Karch F, Basler K (2007) An optimized transgenesis system for *Drosophila* using germ-line-specific $\phi$C31 integrases. *Proc Natl Acad Sci USA* 104:3312–3317.


# Growing Microtubules Push the Oocyte Nucleus to Polarize the *Drosophila* Dorsal-Ventral Axis

Tongtong Zhao *et al.*

*Science* **336**, 999 (2012);
DOI: 10.1126/science.1219147



*Science* (print ISSN 0036-8075; online ISSN 1095-9203) is published weekly, except the last week in December, by the American Association for the Advancement of Science, 1200 New York Avenue NW, Washington, DC 20005. 

# Growing Microtubules Push the Oocyte Nucleus to Polarize the *Drosophila* Dorsal-Ventral Axis

Tongtong Zhao,[1] Owen S. Graham,[2] Alexandre Raposo,[1]* Daniel St Johnston[1]†

The *Drosophila* dorsal-ventral (DV) axis is polarized when the oocyte nucleus migrates from the posterior to the anterior margin of the oocyte. Prior work suggested that dynein pulls the nucleus to the anterior side along a polarized microtubule cytoskeleton, but this mechanism has not been tested. By imaging live oocytes, we find that the nucleus migrates with a posterior indentation that correlates with its direction of movement. Furthermore, both nuclear movement and the indentation depend on microtubule polymerization from centrosomes behind the nucleus. Thus, the nucleus is not pulled to the anterior but is pushed by the force exerted by growing microtubules. Nuclear migration and DV axis formation therefore depend on centrosome positioning early in oogenesis and are independent of anterior-posterior axis formation.

The correct positioning of the nucleus is important for several developmental processes, such as cell migration, formation of the neuromuscular junction, and asymmetric cell divisions, whereas nuclear mislocalization is a feature of neurological disorders, such as lissencephaly (*1*). Positioning of the nucleus plays an essential role in *Drosophila* axis formation, because the movement of the nucleus from the posterior of the oocyte to a point at its anterior circumference breaks radial symmetry to polarize the dorsal-ventral (DV) axis (*2*, *3*). At stage 7 of oogenesis, an unknown signal from the posterior follicle cells induces a major reorganization of the oocyte microtubule cytoskeleton. The posterior microtubule organizing center (MTOC) is disassembled, and microtubules are nucleated from the anterior-lateral cortex, resulting in an anterior-posterior (AP) gradient of microtubules that defines the AP axis (*4*). It is believed that dynein subsequently uses this polarized microtubule cytoskeleton to pull the nucleus to the oocyte anterior, making polarization of the DV axis dependent on the prior polarization of the AP axis (*5*–*9*).

**The nucleus is pushed to the anterior by growing microtubules.** To investigate the mechanism

[1]The Gurdon Institute and the Department of Genetics, University of Cambridge, Tennis Court Road, Cambridge CB2 1QN, UK. [2]The Department of Engineering, University of Cambridge, Trumpington Street, Cambridge CB2 1PZ, UK.

*Present address: Instituto Gulbenkian de Ciência, Rua da Quinta Grande, 6, P-2780-156 Oeiras, Portugal.
†To whom correspondence should be addressed. E-mail: d.stjohnston@gurdon.cam.ac.uk

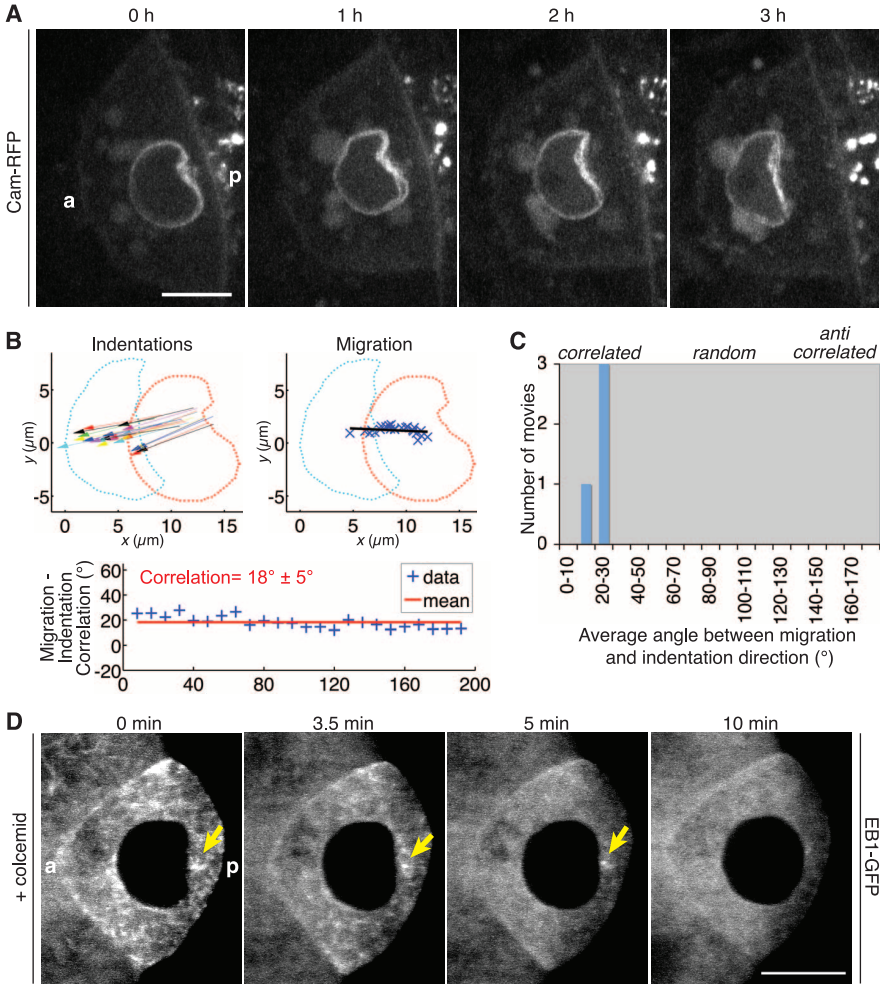


**Fig. 1.** Nuclear migration is driven by a posterior microtubule pushing force. (**A**) Time course of a migrating nucleus. RFP indicates red fluorescent protein. (**B**) Analysis of directions of nuclear indentations during migration (left), direction of overall migration (right), and the correlation between them, expressed as the angle between the directional vectors (bottom) (mean ± SD). Red and cyan dots show the outline of the nucleus at the start and end of migration, respectively; blue ×s show the centroid of the nucleus during migration. (**C**) Mean angle between migration and indentation directions from four migrating nuclei. (**D**) Temporal merges of an EB1-GFP movie of a colcemid-treated egg chamber. Each image is a maximum projection of five time frames (equal to 10 s). Arrow, MTOC. In (A) and (D), a, anterior; p, posterior; scale bars, 10 μm.

of nuclear positioning directly, we imaged the movement of the nucleus in living oocytes. The nucleus migrates at a speed of 4.0 ± 0.7 μm/hour ($n$ = 6) and takes 2 to 3 hours to move across the oocyte (Fig. 1). The trajectory of the nucleus is variable: Sometimes it moves around the cortex of the oocyte directly to an anterior corner, but it often migrates up the center of the oocyte and then turns to move along the anterior cortex (fig. S1 and movie S1), confirming the random nature of this symmetry-breaking event. We observed that all migrating nuclei have large posterior indentations, suggesting that they are being pushed rather than pulled toward the anterior (Fig. 1A and movie S2). This could reflect an intrinsic reorganization of the nuclear architecture or a deformation induced by an external force to the nucleus. In support of the latter view, the direction of the indentation correlates with the direction of migration, suggesting that the same force creates the indentation and moves the nucleus (Fig. 1, B and C). This indentation is not an artifact of long-term imaging in oil, because egg chambers dissected directly into strong fixative have identical indentations (fig. S2).

This idea that the nucleus is pulled to the anterior by dynein has its basis in the finding that mutations in the dynein accessory factors, *Lis1* and *Bic-D*, as well as disruption of the dynactin complex result in mislocalized nuclei at stage 10 (*5*–*9*). This is not compatible with the pushing model of nuclear movement, because motor proteins can only pull their cargoes. We therefore reexamined the role of the dynein complex by imaging the nucleus in *Lis1* mutant egg chambers. *Lis1* mutant oocytes are much smaller than normal because dynein is required for transport from the nurse cells into the oocyte (*6*). Nevertheless, the oocyte nucleus migrates normally with a prominent posterior indentation (movie S3). Thus, dynein is presumably required for the anchoring of the nucleus once it has reached the anterior, rather than for its migration. Consistent with this, the nuclei are only rarely mispositioned in *Lis1* and *Bic-D* mutant oocytes at stage 9 but are mislocalized much more frequently at later stages (fig. S3).

Both actin and microtubule polymerization can generate pushing forces that lead to cellular or organelle deformations (*10*). Two lines of evidence suggest that microtubules are responsible for the nuclear indentation: First, depolymerization of actin with latrunculin A or B does not affect nuclear positioning, whereas the microtubule-depolymerizing drug colcemid induces mislocalized nuclei (*11*). Secondly, several microtubule-associated proteins become enriched on the posterior nuclear envelope during migration, including the dynein light intermediate chain (Dlic), calmodulin (Cam), and the *Drosophila* NuMA homolog mushroom body defect, Mud (fig. S4) (*12*–*14*).

To test the role of microtubules in the formation of the indentation, we added colcemid to living egg chambers expressing the +TIP protein, EB1-GFP (end binding-1–green fluorescent protein), which forms a "comet" on the growing plus ends of microtubules (*15*). Colcemid takes 3.5 min to diffuse into the oocyte, as monitored by a decrease in the number of EB1 comets on growing microtubule plus ends. As soon as microtubule growth starts to decrease, the indentation diminishes in size (Fig. 1D and movie S4). A focus of EB1-GFP persists posterior to the nucleus for several minutes, and, as this dis-

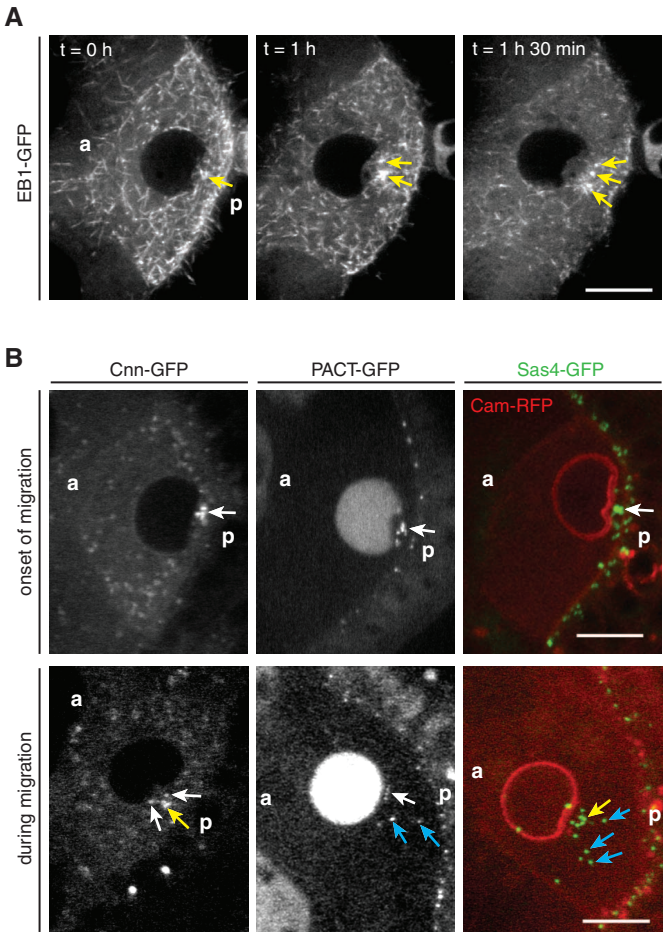


**Fig. 2.** Active centrosomes are localized behind the nuclear indentation. (**A**) Temporal merges (20 time frames, equal to 10 s) of an EB1-GFP movie reveal active MTOCs (arrows) between the nuclear indentation and the posterior oocyte cortex. (**B**) The centriolar markers PACT-GFP and Sas-4-GFP and the PCM marker Cnn-GFP are localized behind the nucleus at the onset of migration (top). During migration, MTOCs can be clustered together (yellow arrows), associated with the nucleus (white arrows), or dispersed in the cytoplasm (blue arrows) (bottom). Scale bars, 10 μm.

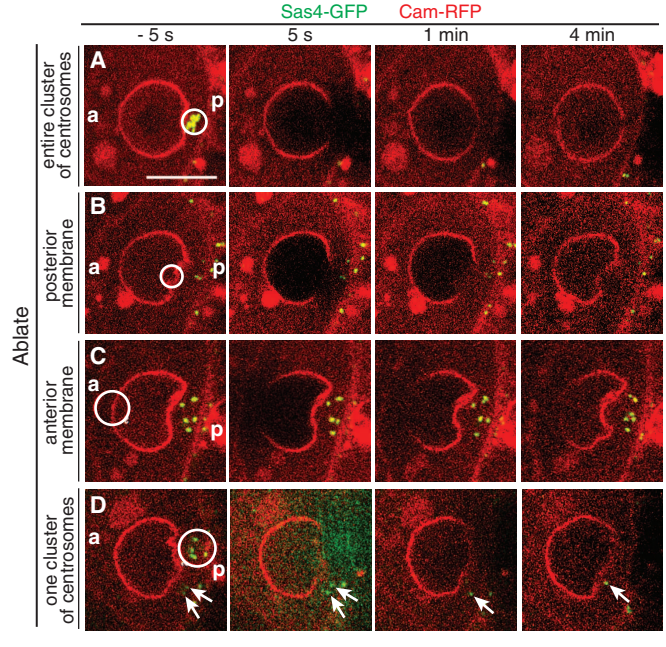


**Fig. 3.** Laser ablation of the centrosomes abolishes the nuclear indentation. (**A** and **D**) Clusters of centrosomes were bleached for 5 s. One to 4 min after ablation, the nuclear indentation facing the ablated centrosomes disappeared. (**B** and **C**) When the nuclear membrane or the anterior of the nucleus was bleached, the indentation was maintained. Circles, area of bleaching; arrows, nonablated, active centrosomes; scale bar, 10 μm.

appears, the nucleus relaxes completely and becomes spherical. Thus, the nuclear indentation depends on microtubule polymerization, and its size is proportional to the number of growing microtubules.

**The nuclear indentation depends on active posterior centrosomes.** Using EB1-GFP to track the growing microtubule plus ends in time-lapse movies of nuclear migration revealed several strong foci of EB1-GFP behind the indentation, with growing microtubules emanating from them in all directions (Fig. 2A and movie S5). This indicates that microtubules are nucleated from MTOCs behind the nucleus. These MTOCs resemble the centrosomes, which migrate from the nurse cells into the oocyte during early oogenesis in a dynein-dependent manner, and localize to the posterior cortex as a result of the initial oocyte polarity (*16*–*20*). Indeed, the centriolar markers Sas4 and PACT, as well as a marker for pericentriolar material (PCM), centrosomin (Cnn) (*21*), localize to the foci behind the nuclear indentation at the onset of migration (Fig. 2B). The centrosomes behave rather dynamically during migration and change reversibly from a dense cluster to a more dispersed distribution (Fig. 2B). Upon completion of nuclear migration, the centrosomes are recruited to the anterior-dorsal cortex of the oocyte, presumably as a consequence of the activation of the dynein-dependent anchoring mechanism that retains the nucleus in this position (fig. S5 and movies S6 and S7). Active centrosomes are therefore positioned behind the nucleus before and during migration.

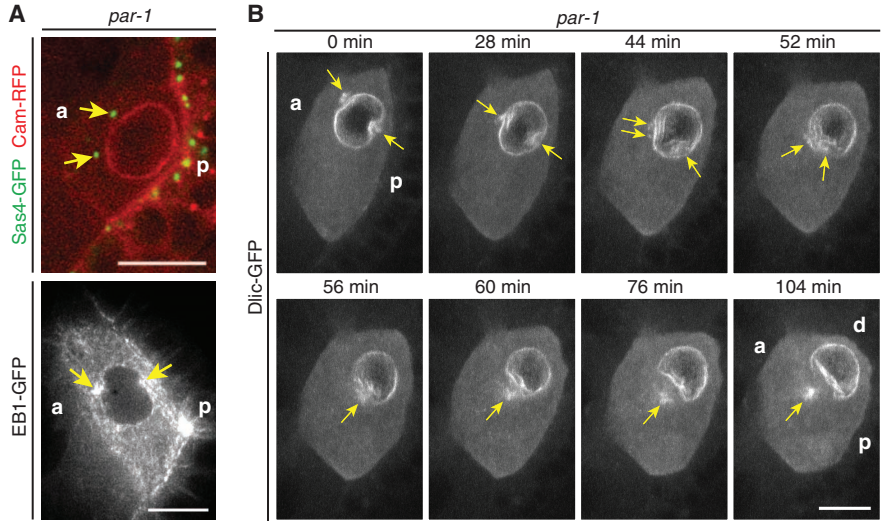


**Fig. 4.** Mispositioned centrosomes induce ectopic nuclear indentations. (**A**) Sas4-GFP (top) and a temporal merge of EB1-GFP (20 frames, equals 10 s) (bottom) reveal active, anterior centrosomes in *par-1*$^{6323}$/*par-1*$^{W3}$ mutants, which induce an anterior indentation in the nucleus. (**B**) Nuclear migration in *par-1*$^{6323}$/*par-1*$^{W3}$ mutants. At the onset of migration, the anterior centrosomes induce an ectopic anterior nuclear indentation. The anterior centrosomes eventually move around the nuclear membrane to cluster with the posterior centrosomes, inducing a broad nuclear indentation and rapid nuclear movement. d, dorsal; arrows, centrosomes; scale bars, 10 μm.

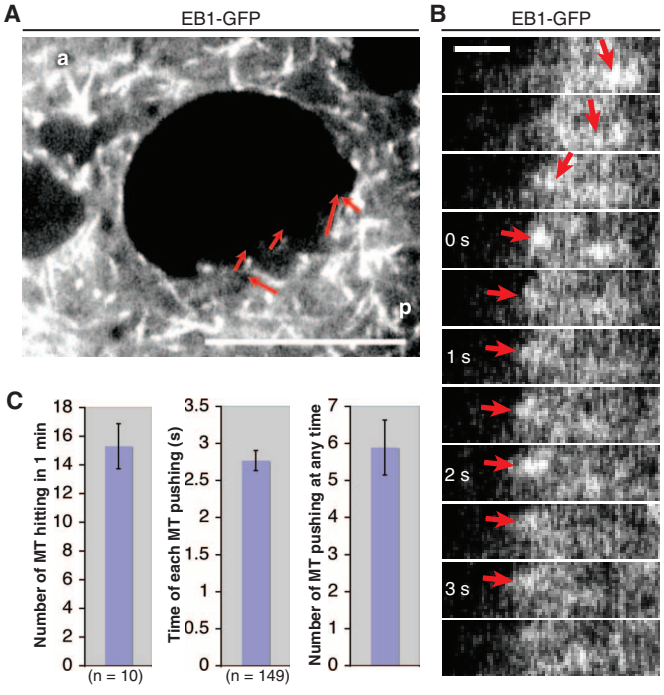


**Fig. 5.** The force of microtubule polymerization is sufficient to move the nucleus. Quantification of the number of microtubules hitting the posterior of the nucleus. (**A**) Temporal merge of 20 frames (equal to 10 s) of an EB1-GFP movie. Red arrows indicate tracked microtubules that hit the nuclear indentation. Scale bar, 10 μm. (**B**) Kymograph of a microtubule that pushes against the nuclear indentation for 3 s; arrows indicate the position of the EB1-GFP comet (plus end of a microtubule). Scale bar, 1 μm. (**C**) Quantification of the number of microtubules hitting the nuclear indentation, the time that each microtubule pushes, and the resulting average number of microtubules that are pushing against the indentation at any given time (error bars, ±SEM).

To test the role of the centrosomes in creating the nuclear indentation, we inactivated them by laser ablation. Upon ablation of the entire cluster of centrosomes, the indentation disappears, and the nucleus becomes spherical within 1 min (Fig. 3A and movie S8). This nuclear relaxation may occur more rapidly, because centrosome ablation causes local bleaching of the nuclear envelope, making it impossible to monitor nuclear shape during the first minute. However, local laser ablation of the nuclear envelope at the site of the indentation has no effect, excluding the possibility that the disappearance of the indentation is a consequence of bleaching of the nuclear membrane (Fig. 3B and movie S9). Furthermore, ablation of the anterior of the nucleus does not affect the indentation, arguing against any pulling force from the anterior (Fig. 3C and movie S10). As described above, centrosomes are sometimes scattered behind the nucleus, causing multiple indentations. Ablating one cluster of centrosomes abolishes only the indentation facing them. The nonablated centrosomes remain active and induce an indentation on the adjacent side of the nucleus (Fig. 3D and movie S11). Thus, the nucleus is not a rigid structure, and the growing microtubules from the centrosomes exert force on the nuclear envelope to induce its deformation.

The centrosomes are dispensable for oogenesis (*22*). We therefore examined nuclear migration in *DSas-4* mutant ovaries that lack centrosomes. Consistent with the previous study, all nuclei migrate to the anterior-dorsal corner ($n = 117$) and show a posterior indentation during migration (fig. S6 and movie S12). GFP-Cnn is still localized in foci behind the nucleus, and EB1-GFP tracks reveal active posterior MTOCs (fig. S6). Thus, acentrosomal MTOCs form in the absence of centrosomes and can provide the pushing force for nuclear migration.

**Nuclear migration is independent of AP axis formation.** As a further test of the idea that the centrosomal microtubules push the nucleus to the anterior, we examined *par-1* hypomorphs, in which some centrosomes fail to migrate to the posterior of the oocyte (*19*). These anterior

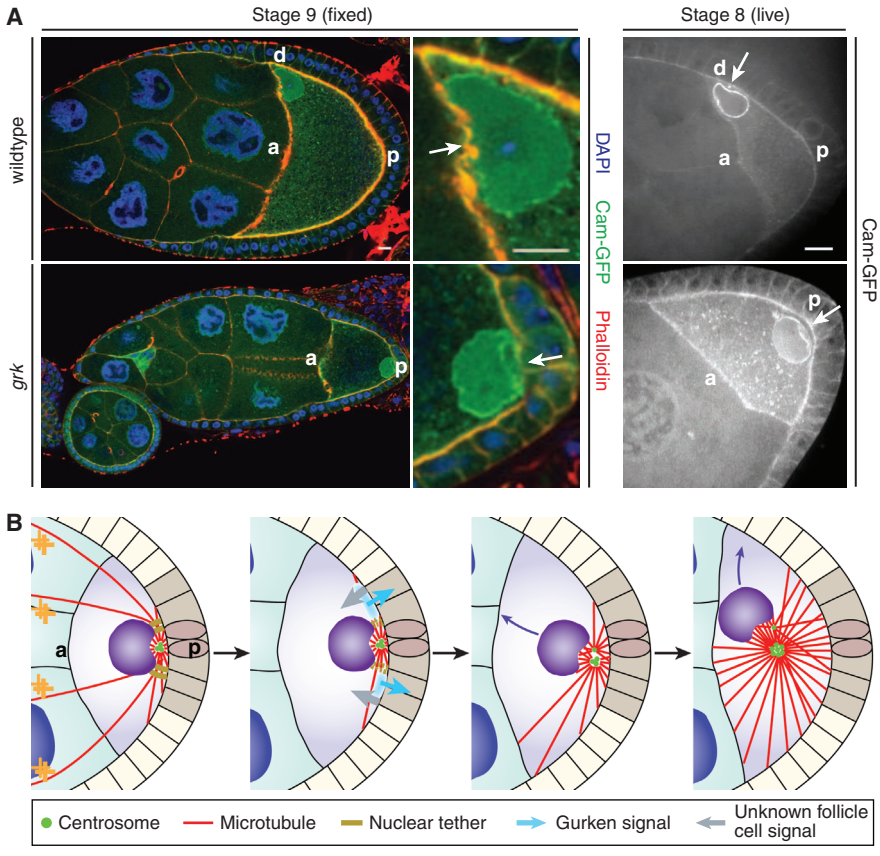


**Fig. 6.** The nucleus is anchored to the posterior before migration. (**A**) The nuclei often fail to migrate in *grk*$^{2B6}$/*grk2*$^{E12}$ mutants but still have prominent posterior indentations (arrows), indicating that they are tethered at the posterior. DAPI, 4′,6-diamidino-2-phenylindole; scale bars, 10 μm. (**B**) A microtubule pushing model for nuclear migration. Before migration, the nucleus is tethered at the posterior with active centrosomes behind it (left). The posterior follicle cell signal induces the release of the nucleus from the tether, and growing microtubules then push the nucleus anteriorly (middle). This movement is essentially random and continues until the oocyte becomes wedged in an anterior corner (right).

centrosomes induce anterior nuclear indentations, leading to dumbbell-shaped nuclei, confirming the role of centrosomal microtubules in pushing the nucleus (Fig. 4A). These ectopic centrosomes eventually fuse with the posterior centrosomes to move the nucleus to the anterior-dorsal corner (Fig. 4B and movie S13). This explains why the nucleus migrates normally in *par-1* mutants even though the AP axis is not polarized (*23*). Consistent with this, the nucleus in wild-type oocytes can migrate to the anterior before the anterior-to-posterior microtubule gradient is established (Fig. 2A and fig. S7).

**Microtubule growth provides sufficient force to move the nucleus.** Another documented example of nuclear positioning by microtubule pushing comes from *Schizosaccharomyces pombe*, where microtubule bundles push against the cell ends to maintain the nucleus in the cell center (*24*). The oocyte nucleus moves a much greater distance, however, and appears to be pushed by the force exerted by single growing microtubules. To test the feasibility of this mechanism, we used Stoke's law ($F = 6\pi\eta r v$) to estimate the drag force ($F$) exerted on the nucleus. Assuming a cytoplasmic viscosity ($\eta$) ≈ 100 Pas (*25*, *26*) and the measured values of the nuclear radius ($r$) ≈ 5 μm and the velocity of migration ($v$) ≈ 4 μm/hour yields a drag force ≈ 10 pN. We expect the actual drag force to be lower, because nuclear migration is so slow (1 nm/s) that the cytoplasmic actin mesh will turn over ahead of the nucleus, decreasing the effective viscosity (*27*, *28*). The longest microtubules can reach ~10 μm between the posterior of the nucleus and the posterior oocyte cortex, resulting in a critical buckling force $F_c \approx 5$ pN (*29*). This value is probably an underestimate, because microtubules embedded within an elastic cytoplasm in vivo have been reported to bear compressive loads 100 times higher than those in vitro (*30*). Each microtubule can therefore generate a pushing force of at least 5 pN. Thus, the force of only two microtubules pushing at any time should be sufficient to move the nucleus to the oocyte anterior.

We measured the number of microtubules pushing the nucleus by using EB1-GFP. In one $z$ plane, 15.3 ± 1.6 (SEM) microtubules hit the nuclear indentation per minute ($n$ = 10, 2 oocytes), and they continued growing and presumably exerting force on the nucleus for 2.77 ± 0.14 s ($n$ = 149) (Fig. 5, A to C, and movie S14). Given the thickness of a confocal section (0.8 μm) and the radius of the indentation [4.3 ± 0.2 μm ($n$ = 10)], an average of 5.9 ± 0.7 microtubules were pushing the nucleus at any given time. Microtubule polymerization can therefore provide sufficient pushing force to drive nuclear migration.

**Nuclear migration is triggered by release from a posterior anchor.** The migration of the nucleus is triggered by an unknown signal from the posterior follicle cells, which could act either by activating the centrosomes or by releasing the nucleus from a posterior tether. To address this question, we examined when the indentation appears during oogenesis. Active centrosomes are already localized behind the nucleus at stage 5 of oogenesis and induce a posterior indentation (fig. S8A). This suggests that the centrosomes continually exert a pushing force on the nucleus, which is tethered to the posterior until it receives a signal for migration. The nucleus remains at the posterior in *gurken* (*grk*) mutants, which block follicle cell signaling to the oocyte (39% penetrance, $n$ = 70) (*2*, *3*). These posterior nuclei still maintain a posterior indentation later in oogenesis (Fig. 6A), suggesting that they fail to migrate because they are not released from the posterior tether (fig. S8B and movie S15). Indeed, microtubules growing from active centrosomes probably always exert a pushing force on the nucleus that must be countered by an opposing pulling force or anchor to keep the nucleus in place. For example, a nuclear indentation is still visible adjacent to the centrosomes after the nucleus is anchored at the anterior (fig. S5A).

Our results lead to a revised model for how the oocyte nucleus moves to break radial symmetry and polarize the *Drosophila* DV axis (Fig. 6B). This model explains the failure to recover mutants that specifically disrupt nuclear migration, because the driving force is provided solely by microtubule polymerization. Furthermore, our results imply that migration is triggered by the release of the nucleus from a posterior anchor,

rather than by microtubule reorganization. Thus, polarization of the DV axis is independent of the formation of the microtubule array that defines the AP axis, as previously proposed.

### References and Notes


1. I. Dupin, S. Etienne-Manneville, *Int. J. Biochem. Cell Biol.* **43**, 1698 (2011).
2. A. González-Reyes, H. Elliott, D. St Johnston, *Nature* **375**, 654 (1995).
3. S. Roth, F. S. Neuman-Silberberg, G. Barcelo, T. Schüpbach, *Cell* **81**, 967 (1995).
4. R. Bastock, D. St Johnston, *Curr. Biol.* **18**, R1082 (2008).
5. A. Swan, B. Suter, *Development* **122**, 3577 (1996).
6. A. Swan, T. Nguyen, B. Suter, *Nat. Cell Biol.* **1**, 444 (1999).
7. Y. Lei, R. Warrior, *Dev. Biol.* **226**, 57 (2000).
8. J. E. Duncan, R. Warrior, *Curr. Biol.* **12**, 1982 (2002).
9. J. Januschke *et al.*, *Curr. Biol.* **12**, 1971 (2002).
10. A. Mogilner, G. Oster, *Curr. Biol.* **13**, R721 (2003).
11. E. A. Koch, R. H. Spitzer, *Cell Tissue Res.* **228**, 21 (1983).
12. Y. C. Lee, J. Wolff, *J. Biol. Chem.* **257**, 6306 (1982).
13. J. R. Kardon, R. D. Vale, *Nat. Rev. Mol. Cell Biol.* **10**, 854 (2009).
14. A. E. Radulescu, D. W. Cleveland, *Trends Cell Biol.* **20**, 214 (2010).
15. Y. Mimori-Kiyosue, N. Shiina, S. Tsukita, *Curr. Biol.* **10**, 865 (2000).
16. A. P. Mahowald, J. M. Strassheim, *J. Cell Biol.* **45**, 306 (1970).
17. N. C. Grieder, M. de Cuevas, A. C. Spradling, *Development* **127**, 4253 (2000).
18. J. Bolívar *et al.*, *Development* **128**, 1889 (2001).
19. J. R. Huynh, J. M. Shulman, R. Benton, D. St Johnston, *Development* **128**, 1201 (2001).
20. P. Fichelson, M. Jagut, S. Lepanse, J. A. Lepesant, J. R. Huynh, *Development* **137**, 815 (2010).
21. N. M. Rusan, G. C. Rogers, *Traffic* **10**, 472 (2009).
22. N. R. Stevens, A. A. Raposo, R. Basto, D. St Johnston, J. W. Raff, *Curr. Biol.* **17**, 1498 (2007).
23. J. M. Shulman, R. Benton, D. St Johnston, *Cell* **101**, 377 (2000).
24. P. T. Tran, L. Marsh, V. Doye, S. Inoué, F. Chang, *J. Cell Biol.* **153**, 397 (2001).
25. A. R. Bausch, W. Möller, E. Sackmann, *Biophys. J.* **76**, 573 (1999).
26. R. M. Hochmuth, *J. Biomech.* **33**, 15 (2000).
27. K. Dahlgaard, A. A. Raposo, T. Niccoli, D. St Johnston, *Dev. Cell* **13**, 539 (2007).
28. N. Watanabe, *Proc. Jpn. Acad. Ser. B* **86**, 62 (2010).
29. M. Dogterom, J. W. Kerssemakers, G. Romet-Lemonne, M. E. Janson, *Curr. Opin. Cell Biol.* **17**, 67 (2005).
30. C. P. Brangwynne *et al.*, *J. Cell Biol.* **173**, 733 (2006).



**Acknowledgments:** We would like to thank J. Raff for providing the Dlic-GFP fly stock and centrosomal markers; H. Nash for providing the Mud antibody; S. Young for help with image analysis; and J. Guck, Y.-C. Oei, and P. K. Trong for help with the force calculations. This work was supported by a Wellcome Trust Principal Research Fellowship to D.St.J., Ph.D. scholarships from the FAZIT Stiftung, the Boehringer Ingelheim Fonds and the Cambridge European Trust to T.Z., the Gulbenkian Ph.D. scholarship of the Fundação para a Ciência e Tecnologia to A.R., and core support from the Wellcome Trust and Cancer Research UK.


### Supplementary Materials

www.sciencemag.org/cgi/content/full/science.1219147/DC1
Materials and Methods
Figs. S1 to S8
References (*31*–*43*)
Movies S1 to S15


16 January 2012; accepted 27 March 2012
Published online 12 April 2012;
10.1126/science.1219147






# Signatures of Majorana Fermions in Hybrid Superconductor-Semiconductor Nanowire Devices


V. Mourik,[1]* K. Zuo,[1]* S. M. Frolov,[1] S. R. Plissard,[2] E. P. A. M. Bakkers,[1,2] L. P. Kouwenhoven[1]†



**Majorana fermions are particles identical to their own antiparticles. They have been theoretically predicted to exist in topological superconductors. Here, we report electrical measurements on indium antimonide nanowires contacted with one normal (gold) and one superconducting (niobium titanium nitride) electrode. Gate voltages vary electron density and define a tunnel barrier between normal and superconducting contacts. In the presence of magnetic fields on the order of 100 millitesla, we observe bound, midgap states at zero bias voltage. These bound states remain fixed to zero bias, even when magnetic fields and gate voltages are changed over considerable ranges. Our observations support the hypothesis of Majorana fermions in nanowires coupled to superconductors.**


All elementary particles have an antiparticle of opposite charge (for example, an electron and a positron); the meeting of a particle with its antiparticle results in the annihilation of both. A special class of particles, called Majorana fermions, are predicted to exist that are identical to their own antiparticle (*1*). They may appear naturally as elementary particles or emerge as charge-neutral and zero-energy quasi-particles in a superconductor (*2*, *3*). Particularly interesting for the realization of qubits in quantum computing are pairs of localized Majoranas separated from each other by a superconducting region in a topological phase (*4*–*11*).

On the basis of earlier and later semiconductor-based proposals (*6*, *7*), Lutchyn *et al.* (*8*) and Oreg *et al.* (*9*) have outlined the necessary ingredients for engineering a nanowire device that should accommodate pairs of Majoranas. The starting point is a one-dimensional (1D) nanowire made of semiconducting material with strong spin-orbit interaction (Fig. 1A). In the presence of a magnetic field $B$ along the axis of the nanowire (i.e., a Zeeman field), a gap is opened at the crossing between the two spin-orbit bands. If the Fermi energy $\mu$ is inside this gap, the degeneracy is twofold, whereas outside the gap it is fourfold. The next ingredient is to connect the semiconducting nanowire to an ordinary s-wave superconductor (Fig. 1A). The proximity of the superconductor induces pairing in the nanowire between electron states of opposite momentum and opposite spins and induces a gap, $\Delta$. Combining this twofold degeneracy with an induced gap creates a topological superconductor (*4*–*11*). The condition for a topological phase is $E_Z > (\Delta^2 + \mu^2)^{1/2}$, with the Zeeman energy $E_Z = g\mu_B B/2$ ($g$ is the Landé $g$ factor, $\mu_B$ is the Bohr magneton). Near the ends of the wire, the electron density is reduced to zero, and subsequently, $\mu$ will drop below the subband energies such that $\mu^2$ becomes large. At the points in space where $E_Z = (\Delta^2 + \mu^2)^{1/2}$, Majoranas arise as zero-energy (i.e., midgap) bound states—one at each end of the wire (*4*, *8*–*11*).

Despite their zero charge and energy, Majoranas can be detected in electrical measurements. Tunneling spectroscopy from a normal conductor into the end of the wire should reveal a state at zero energy (*12*–*14*). Here, we report the observation of such zero-energy peaks and show that they rigidly stick to zero energy while changing $B$ and gate voltages over large ranges. Furthermore, we show that this zero-bias peak (ZBP) is absent if we take out any of the necessary ingredients of the Majorana proposals; that is, the rigid ZBP disappears for zero magnetic field, for a magnetic field parallel to the spin-orbit field, or when we take out the superconductivity.


[1]Kavli Institute of Nanoscience, Delft University of Technology, 2600 GA Delft, Netherlands. [2]Department of Applied Physics, Eindhoven University of Technology, 5600 MB Eindhoven, Netherlands.

*These authors contributed equally to this work.
†To whom correspondence should be addressed. E-mail: l.p.kouwenhoven@tudelft.nl

Developmental Cell
Article

# Changes in Ect2 Localization Couple Actomyosin-Dependent Cell Shape Changes to Mitotic Progression

Helen K. Matthews,[1] Ulysse Delabre,[2,3] Jennifer L. Rohn,[1] Jochen Guck,[2] Patricia Kunda,[1] and Buzz Baum[1,*]
[1]MRC Laboratory for Molecular Cell Biology, University College London, Gower St., London WC1E 6BT, UK
[2]Department of Physics, Cavendish Laboratory, University of Cambridge, J.J. Thomson Avenue, Cambridge CB3 0HE, UK
[3]PCC Curie, Institut Curie/CNRS/Université Paris 6 - UMR 168, 26 rue d'Ulm, 75248 Paris, France
*Correspondence: b.baum@ucl.ac.uk
http://dx.doi.org/10.1016/j.devcel.2012.06.003

## SUMMARY

**As they enter mitosis, animal cells undergo profound actin-dependent changes in shape to become round. Here we identify the Cdk1 substrate, Ect2, as a central regulator of mitotic rounding, thus uncovering a link between the cell-cycle machinery that drives mitotic entry and its accompanying actin remodeling. Ect2 is a RhoGEF that plays a well-established role in formation of the actomyosin contractile ring at mitotic exit, through the local activation of RhoA. We find that Ect2 first becomes active in prophase, when it is exported from the nucleus into the cytoplasm, activating RhoA to induce the formation of a mechanically stiff and rounded metaphase cortex. Then, at anaphase, binding to RacGAP1 at the spindle midzone repositions Ect2 to induce local actomyosin ring formation. Ect2 localization therefore defines the stage-specific changes in actin cortex organization critical for accurate cell division.**

## INTRODUCTION

Cell division requires sequential changes in cell architecture, which are coordinated by a small set of conserved mitotic kinases (Ma and Poon, 2011). Although most recent attention has focused on the changes in microtubule organization that accompany spindle assembly and that drive chromosome segregation, mitotic progression is also accompanied by profound changes in cell shape. These begin at the onset of mitosis as cells detach from the substrate and round up (Cramer and Mitchison, 1997; Harris, 1973); a process that is important for spindle assembly, positioning, and chromosome capture (Carreno et al., 2008; Kunda and Baum, 2009; Kunda et al., 2008). At mitotic exit, cells then elongate and divide in two, before respreading to take up their resting interphase shape once more.

Mitotic rounding requires the loss of substrate adhesion (Dao et al., 2009), together with changes in surface volume ratio and osmotic pressure (Stewart et al., 2011). In addition, the actin cytoskeleton is completely remodeled to generate a rigid and rounded actomyosin cortex (Kunda et al., 2008). Although several actin regulators, including ERM proteins (Carreno et al., 2008; Kunda et al., 2008), myosin II (Maddox and Burridge, 2003), Cofilin, and WDR1 (Fujibuchi et al., 2005), are known to play roles in this process, it is not known how changes in actin organization are coupled to mitotic entry and progression.

Entry into mitosis in mammalian cells is controlled by activation of the mitotic Cdk1/CyclinB complex, through a tightly regulated process that involves multiple feedback loops (Lindqvist et al., 2009). Once active, Cdk1/CyclinB phosphorylates a large number of targets, triggering many of the early events of mitosis including centrosome separation, chromosome condensation, and nuclear envelope breakdown (Gavet and Pines, 2010b). Although some of the key substrates mediating the effects of Cdk1/CyclinB activity on chromatin, the nuclear lamina, and the mitotic spindle have been identified (Blangy et al., 1995; Kimura et al., 1998; Peter et al., 1990), it is not known if changes in Cdk1/CyclinB activity also function to directly alter actin filament organization and dynamics.

Here, we identify a known Cdk1 substrate (Hara et al., 2006; Niiya et al., 2006), Ect2, as a regulator of mitotic rounding. Ect2 is a RhoGEF that was previously shown to be essential for cytokinesis (Tatsumoto et al., 1999), where it activates RhoA to regulate assembly of the actomyosin contractile ring (Chalamalasetty et al., 2006; Nishimura and Yonemura, 2006; Yüce et al., 2005). We show that Ect2 also activates RhoA and its downstream effectors, Rho kinase (ROK), and myosin II, at the onset of mitosis to induce the actomyosin remodeling that drives both mitotic rounding and cortical stiffening. This early function of Ect2 is dependent on its export from the nucleus in prophase, but does not require RacGAP1 (also known as MgcRacGAP) or microtubules, which have been shown to drive the relocalization of Ect2 to the cell equator prior to cytokinesis (Burkard et al., 2009; Petronczki et al., 2007; Somers and Saint, 2003; Wolfe et al., 2009; Yüce et al., 2005). These data show that, through regulated changes in its localization, Ect2 is able to reshape the mitotic cell to drive rounding upon entry into mitosis and cleavage furrow formation at mitotic exit.

## RESULTS

### Rounding Is Initiated at the Start of Mitosis

To better understand the coupling between cell shape changes and mitotic progression, we began by determining the timing of mitotic rounding relative to the other events of mitotic entry. HeLa cells expressing Histone H2B-mRFP and tubulin-GFP

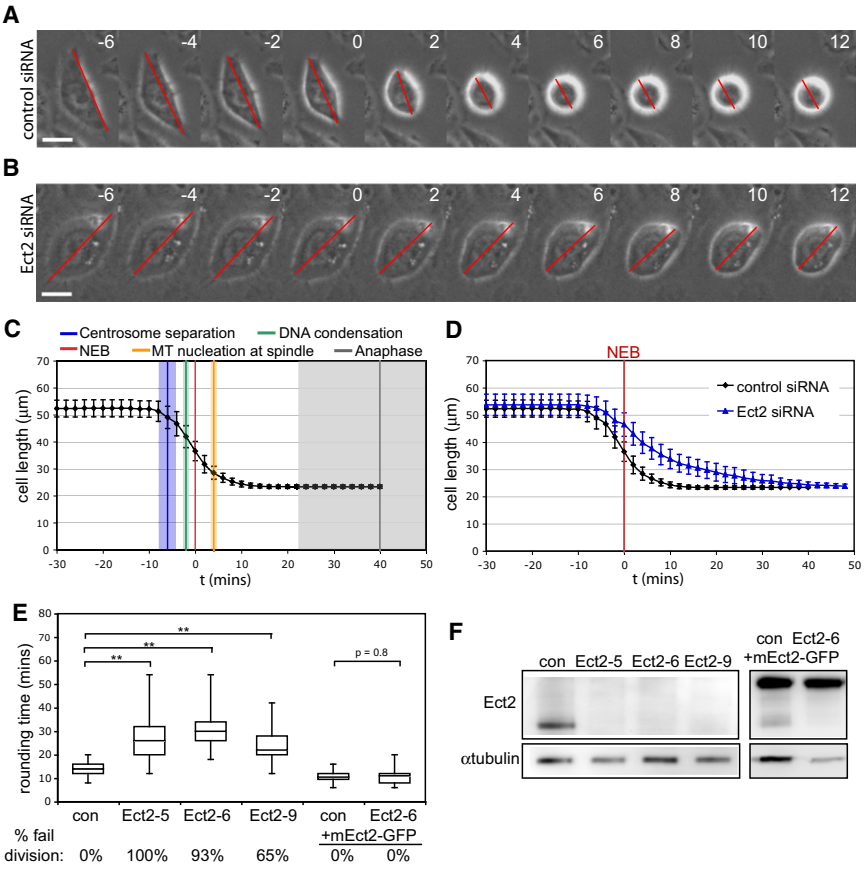


**Figure 1. Ect2 Alters the Dynamics of Mitotic Cell Rounding**

(A and B) Time-lapse phase contrast images of HeLa cells rounding up before mitosis with cell length (Feret's diameter) indicated by red line showing cells treated with (A) control siRNA and (B) Ect2 siRNA. Images taken every 2 min. Scale bar, 20 μm.

(C) Mean length of 22 cells during progression through mitosis, aligned so that time point 0 represents nuclear envelope breakdown (NEB). Error bars denote SD. Colored vertical lines show mean timing of mitotic events with shaded areas showing SD. Mitotic events were visualized using the expression of histone H2B-mRFP (for chromatin condensation and anaphase) and tubulin-GFP (centrosome separation and microtubule nucleation at spindle). NEB was recorded as the time point at which free tubulin-GFP dimers are able to enter the nucleus.

(D) Comparison of rounding in cells treated with control siRNA (n = 20 cells) and Ect2 siRNA (n = 23). Error bars denote SD.

(E) Box plot showing time taken to round up at mitosis for control siRNA (n = 31) compared to three nonoverlapping siRNAs targeting Ect2 (n = 27, 33, and 25) in control HeLa cells, and in HeLa cells expressing mouse Ect2-GFP at endogenous levels (n = 28 cells in each condition). Central line shows median, boxes are quartiles and whiskers show complete range. Cells were imaged 24 hr post-RNAi and only the first division after RNAi treatment was analyzed. The percentage of cells that then go on to fail cytokinesis in each condition is indicated.

(F) Western blot showing knockdown of human Ect2 but not mouse Ect2-GFP (upper band) by three siRNAs targeting Ect2.

See also Figure S1.

(Steigemann et al., 2009) were imaged every 2 min as they progressed through the cell cycle. Cell length (Feret's diameter) was measured (Figure 1A) and used to compare the timing of mitotic rounding with that of centrosome separation, chromosome condensation, nuclear envelope breakdown, and spindle assembly (Figure 1C). Mitotic rounding lasted 13.6 ± 1.8 min, during which time mean HeLa cell length (Picone et al., 2010) was reduced from 53 ± 3 μm to 23.5 ± 1.3 μm. Rounding began in early prophase, before centrosome separation and visible chromatin condensation, around 6 min before nuclear envelope breakdown (Figure 1C). This makes rounding one of the earliest events in mitosis, concordant with the rise in Cdk1 activity during prophase as measured using a FRET probe (Gavet and Pines, 2010b). Since Cdk1/CyclinB is thought to directly control many events of prophase (Gavet and Pines, 2010a), this suggested the possibility that Cdk1/Cyclin B also instigates mitotic rounding. Indeed, Cdk1/Cyclin B has been shown to be sufficient to induce rounding upon injection into interphase cells (Lamb et al., 1990). Thus, in our search for upstream regulators of cell rounding, we focused our attention on established Cdk1 substrates.

## Ect2 Controls the Dynamics of Mitotic Rounding

To identify regulators of mitotic rounding, we carried out an RNAi screen. We used siRNA to silence 60 key actin regulators. Since we aimed to identify genes that couple mitotic progression to changes in cell shape, this set specifically included siRNAs targeting actin regulators previously identified as mitotic kinase substrates in systematic large-scale screens (Beausoleil et al., 2006; Blethrow et al., 2008; Dephoure et al., 2008; Ji et al., 2002). Two days after siRNA treatment, HeLa cells were fixed, stained, and analyzed to identify gene-specific siRNAs that induced reproducible changes in mitotic cell shape and actin organization (for details of screen methodology and list of genes screened, see Supplemental Experimental Procedures and Table S1 available online). This identified a number of siRNAs that affected mitotic cell shape. Unsurprisingly in light of previous work (Fujibuchi et al., 2005), this included two inhibitors of actin filament formation, WDR1 and actin capping protein (Table S1). More significantly for our purposes, the screen also identified a single well-established Cdk1 substrate, Ect2.

To confirm a role for Ect2 in mitotic rounding we turned to time-lapse microscopy. Ect2 loss of function has previously been shown cause cytokinesis failure, leading to the formation of binucleate cells (Tatsumoto et al., 1999). Our analysis therefore focused on the first cell division after Ect2 knockdown (around 24 hr after RNAi treatment) to avoid delays in rounding caused by cells being large and multinucleate. This analysis revealed that Ect2 depleted cells initiate rounding on schedule relative to nuclear envelope breakdown, but round more slowly (mean

rounding time of 31.1 ± 4.3 min, Figures 1B and 1D). The vast majority then went on to fail cytokinesis (Figure 1E). Both phenotypes were replicated using three different nonoverlapping siRNAs (Figure 1E) and the knockdown at 24 hr was verified in each case by western blotting (Figure 1F). Furthermore, as a definitive proof that the phenotype reflects depletion of Ect2 itself, we rescued the RNAi phenotype in HeLa cells using the constitutive expression of mouse Ect2-GFP (Hutchins et al., 2010), which lacks the siRNA binding sequence (Figures 1E and 1F). Finally, this function for Ect2 is not confined to HeLa cells, as a similar phenotype was observed following Ect2 knockdown in RPE1 cells, a diploid nontransformed human cell line, as well as in *Drosophila* S2R+ cells depleted of the fly Ect2 homolog, *pebble* (Prokopenko et al., 1999) (Figure S1). These data lead us to conclude that Ect2 plays a conserved role in mitotic rounding.

## Ect2 Is Required for Assembly of a Stiff Cortical Actin Cytoskeleton at Mitosis

Since the actin cytoskeleton controls mitotic cell shape (Kunda and Baum, 2009), we used confocal time-lapse microscopy to determine whether this role for Ect2 in rounding reflects a role in mitotic actin remodeling. In control cells expressing LifeAct-GFP (Riedl et al., 2008), actin filaments were found to redistribute to form a visible cortex underlying the plasma membrane as cells rounded and increased in height upon entry into mitosis (Figure 2A; Movie S1). This cortical recruitment was clearly perturbed in both live (Figure 2B; Movie S1) and fixed metaphase Ect2 RNAi cells (Figures 2E and 2F). First actin filaments appeared profoundly disorganized in Ect2 RNAi cells (Figure 2E). In addition, Ect2 RNAi cells were considerably flatter than metaphase control cells (Figures 2C and 2D).

This role for Ect2 in mitotic actin cortex assembly would be expected to lead to corresponding changes in mitotic cell mechanics (Kunda et al., 2008). To test whether or not this is the case, we used an ''optical stretcher'' to measure the rigidity of control and Ect2 RNAi cells in mitosis. This phototonic tool consists of two counter-propagating laser beams that are used to trap and exert a stretching force on suspended cells passing through a central microfluidic chamber (Figure 2G) (Guck et al., 2001). The deformation induced by the two beams can then be used to determine a cell's compliance, an inverse measure of its stiffness. Using this system, we first established that, as previously reported (Kunda et al., 2008), mitotic cells are less compliant than interphase cells and that this depends on an intact actin cytoskeleton (Figure S2). Strikingly, however, mitotic Ect2 RNAi cells were significantly more compliant than control cells in mitosis (Figure 2H). Taken together, these data show that Ect2 is essential for the assembly of the normal, rigid, actomyosin-based mitotic cortex.

It has previously been shown that a rigid and rounded actin cortex is essential for spindle assembly in *Drosophila* cells (Carreno et al., 2008; Kunda et al., 2008). In addition, myosin II has been shown to play an important role in centrosome separation (Rosenblatt et al., 2004). Therefore Ect2 depleted HeLa cells might be expected to exhibit spindle defects. We found that while Ect2 RNAi cells were ultimately able to build a bipolar spindle, cells suffered delays in centrosome separation and spindle assembly (Figure S2) similar to those previously observed when myosin activity is compromised (Rosenblatt et al., 2004). In addition, Ect2 RNAi cells exhibited defects in the alignment of chromosomes at the metaphase plate and in their segregation at anaphase, where we frequently observed lagging chromosomes (Figure S2). Furthermore, when we used RNAi mediated depletion of Mad2 to compromise the spindle checkpoint and to accelerate mitotic progression (Jones et al., 2004), the majority of Ect2 depleted cells exhibited catastrophic defects in chromosome segregation (Figure S2), while few defects were seen in Mad2 RNAi control cells. Thus, the Ect2 dependent changes in mitotic actin cytoskeletal organization and cell shape are required to support the timely assembly of a functional bipolar spindle.

## Ect2 Acts Upstream of RhoA and Myosin II to Drive Mitotic Rounding

Ect2 is essential for cytokinesis. It is recruited to the spindle midzone at anaphase through a physical interaction with a component of the centralspindlin complex, RacGAP1 (Somers and Saint, 2003; Yüce et al., 2005), where it induces the local activation of RhoA and actomyosin ring formation (Tatsumoto et al., 1999; Kamijo et al., 2006; Nishimura and Yonemura, 2006). We used small molecule inhibitors and siRNAs to determine which, if any, of these factors function together with Ect2 in mitotic rounding (Figure 3A). Neither treatment with an siRNA against RacGAP1 nor the removal of microtubules with nocodozole affected the rate of rounding. This was the case even though RacGAP1 silencing resulted in a highly penetrant failure in cytokinesis. In contrast, and as expected based on previous work, the inhibition of downstream targets of Ect2, Rho (Maddox and Burridge, 2003), ROK (Meyer et al., 2011), and myosin II (Cramer and Mitchison, 1997) led to a profound delay in mitotic rounding, similar to that seen following Ect2 RNAi (Figure 3B).

To test whether Ect2 is directly responsible for RhoA activation before the onset of anaphase, a RhoA FRET probe was used (Pertz et al., 2006). While RhoA activity was seen at the cortex of control cells in prometaphase (Figure 3C) as previously described (Mali et al., 2010; Yoshizaki et al., 2003), Ect2 silencing resulted in a marked reduction in cortical RhoA activity (Figures 3D and 3E). Since RhoA activates ROK to alter myosin II activity, in part through the phosphorylation of myosin light chain (Amano et al., 1996), we then used an antibody raised against p-myosin II to determine whether Ect2 also influences myosin II activation at the onset of mitosis. In interphase cells, p-myosin II was visible in stress fibers, which were lost along with focal adhesions in early prophase in control and Ect2 RNAi cells (Figure S3). At the same time, p-myosin II was seen accumulating at the retracting margins of control cells as they rounded up (Figure 3F), but was largely absent from Ect2 RNAi cells (Figures 3G and 3H). By contrast, when we examined ERM protein activation using the same approach (Kunda et al., 2008), we observed no differences in ERM phosphorylation between control and Ect2 RNAi cells (Figure S3). Taken together, these data reveal that Ect2 is required at the early stages of mitosis to activate RhoA and Myosin II to drive the actomyosin contraction required for cell rounding. Significantly, however, the upstream regulators of Ect2 activity are distinct from those that are required for contractile ring formation at mitotic exit.

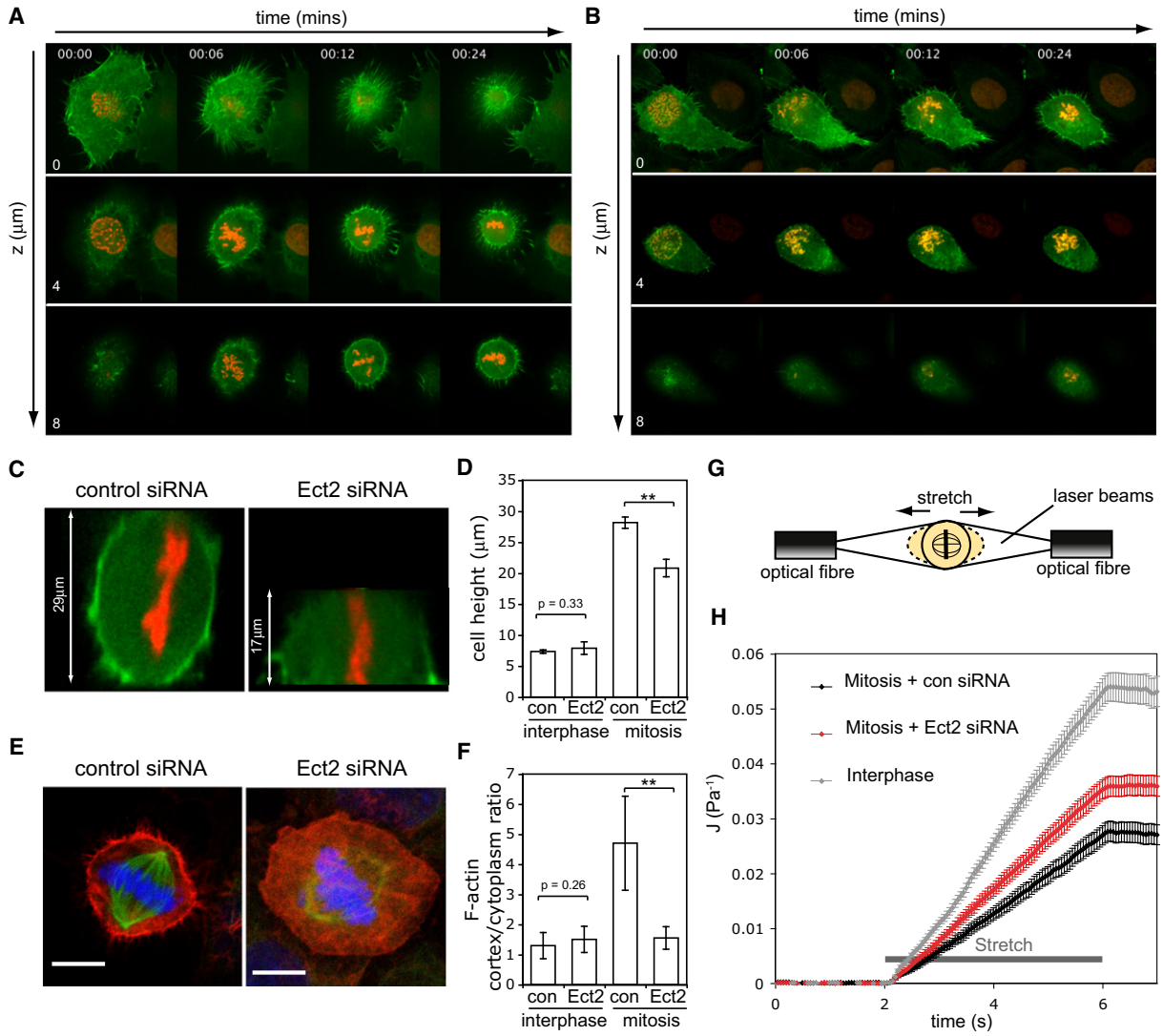


**Figure 2. Ect2 Is Required for the Organization of a Rigid, Cortical Actin Cytoskeleton in Mitosis**

(A and B) Time-lapse confocal images of HeLa cells entering mitosis labeled with LifeAct-GFP and histone H2B-mRFP treated with control siRNA (A) and Ect2 siRNA (B). Time is in minutes. Three different z planes, 4 μm apart are shown. See also Movie S1.

(C) XZ projections of metaphase cells labeled with LifeAct-GFP and histone H2B-mRFP. Confocal Z sections were taken every 200 nm through living cells covering the full height of the cell.

(D) Graph showing the mean height of cells in interphase and metaphase treated with control siRNA or Ect2 siRNA (n = 10–15 cells per condition). Error bars show SD.

(E) Confocal micrographs of fixed metaphase HeLa cells stained to show the actin cytoskeleton in control siRNA and Ect2 siRNA cells. Actin is labeled with phalloidin-TRITC in red, tubulin in green and 4′,6-diamidino-2-phenylindole (DAPI) in blue, scale bars 10 μm.

(F) Quantification of the ratio of cortical/cytoplasmic actin in control and Ect2 RNAi cells in interphase and mitosis. Mean signal intensity in a 3 × 3 pixel box was measured in the actin channel at two locations: 0.5 μm from the cell edge (cortex) and 5 μm from the cell edge (cytoplasm). Four sites per cell were measured and the graph shows the mean values for 15 cells per condition with error bars denoting SD.

(G) Diagram of the optical stretcher set-up used to measure cell compliance.

(H) Graph showing mean compliance J(t) (see Experimental Procedures for detail) over time as cells are subjected to optical stretching for 4 s comparing control siRNA cells in interphase (n = 60 cells) and mitosis (n = 63) and Ect2 siRNA mitotic cells (n = 45). Error bars denote SEM.

See also Figure S2.

## Ect2 Is Phosphorylated throughout Mitosis

How is Ect2 able to control distinct processes at different times in mitosis? Ect2 has previously been shown to be phosphorylated at multiple sites during mitosis, including at several Cdk1 target sites (Hara et al., 2006; Niiya et al., 2006; Su et al., 2011; Yüce et al., 2005). This phosphorylation is required for its GEF activity (Tatsumoto et al., 1999), and has been proposed to regulate changes in Ect2 activity. This led us to examine the phosphorylation status of Ect2 during mitotic progression. Phosphorylated mitotic Ect2 migrates on a gel as a high molecular

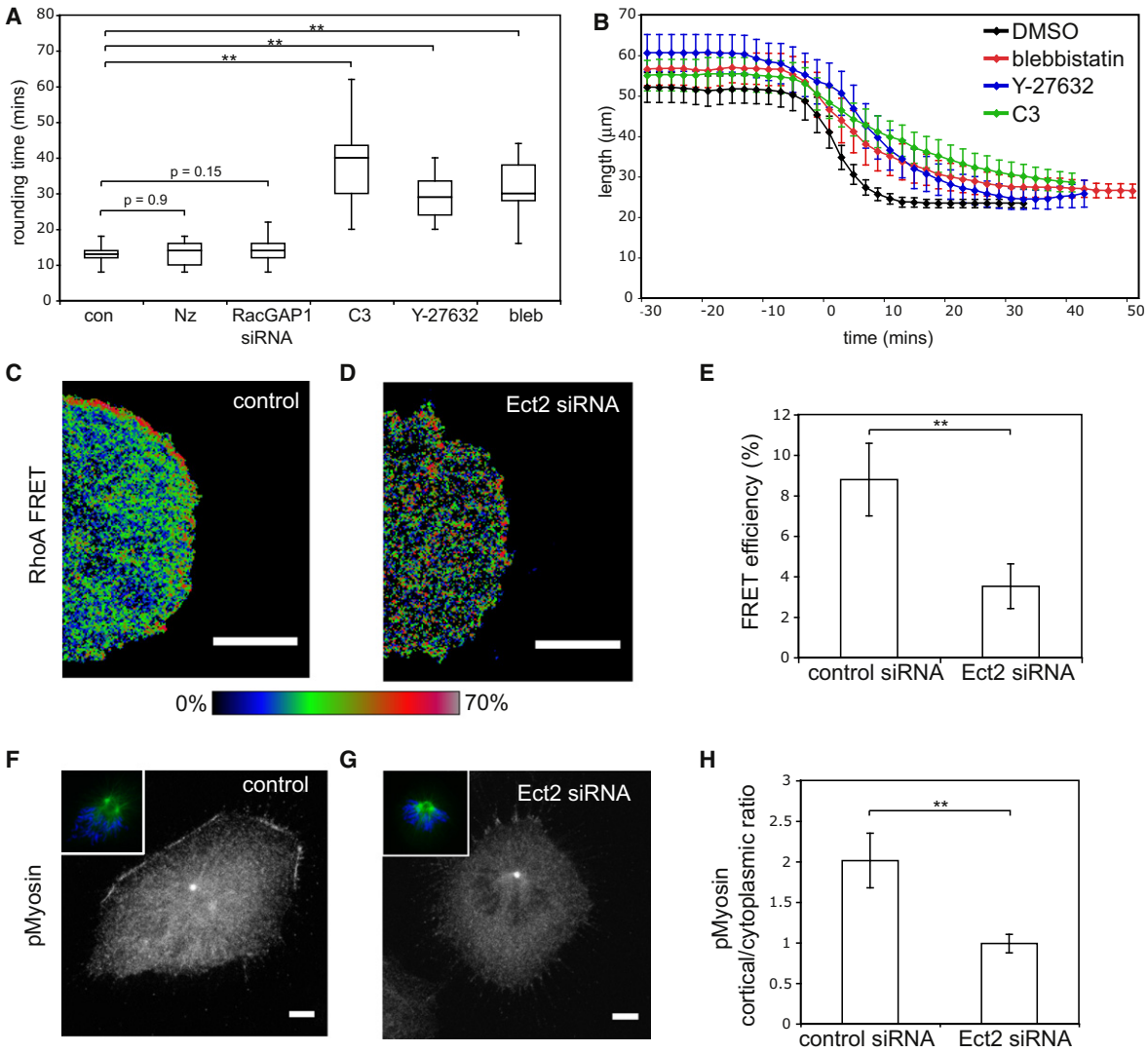


**Figure 3. Ect2 Controls Mitotic Rounding via RhoA, Rho Kinase, and Myosin II**

(A) Box plot comparing rounding times of control cells (n = 22 cells) compared to cells treated with 100 ng/ml nocodozole (Nz) to depolymerize microtubules (n = 16), RacGAP1 siRNA (n = 20), 2 μg/ml C3 transferase to inhibit Rho (n = 22), 50 μM ROK inhibitor Y-27632 (n = 18) and 50 μM blebbistatin to inhibit myosin II (n = 25). Central line shows median, boxes are quartiles, and whiskers show complete range.

(B) Graph showing the cell length through time for conditions in Figure 3A. Error bars denote SD.

(C and D) Pseudo-colored FRET ratio images showing RhoA activity in cells arrested in prometaphase by treatment with 5 μM STLC, comparing a control siRNA cell (C) to an Ect2 siRNA treated cell (D).

(E) Graph showing mean total RhoA FRET efficiency in control siRNA cells (n = 20) and Ect2 siRNA (n = 16) cells. FRET efficiency was calculated using acceptor photo-bleaching (see Experimental Procedures). Error bars denote SD.

(F and G) Representative confocal images of control (F) and Ect2 siRNA (G) prometaphase cells during mitotic rounding stained for phospho-myosin light chain. Insets show tubulin staining and DNA (DAPI stain, blue).

(H) Quantification of the Ect2 siRNA p-myosin II phenotype. The ratio of cortical/cytoplasmic phospho-myosin was calculated by measuring mean signal intensity in a 3 × 3 pixel box at four locations at the cortex of the cell, and four locations 5 μm into the cytoplasm. The graph shows the mean values for 11 cells per condition with error bars denoting SD. Scale bars, 5 μm.

See also Figure S3.

weight band (Tatsumoto et al., 1999) that is rapidly abolished following the inhibition of Cdk1 activity by Roscovitine treatment (Figure 4A). Using this gel mobility shift assay, we analyzed the extent of Ect2 phosphorylation in a synchronized population of cells following their release from a double thymidine block (Figure 4B). Phosphorylated Ect2 first appeared as synchronized cells entered mitosis 11 hr after block release, consistent with this form of the protein having an active role in mitotic rounding. Importantly, Ect2 then remained phosphorylated until 14 hr post-release, by which time the majority of cells had exited mitosis (Figure 4C). A similar time course was observed following release from a metaphase block imposed using nocodozole followed by

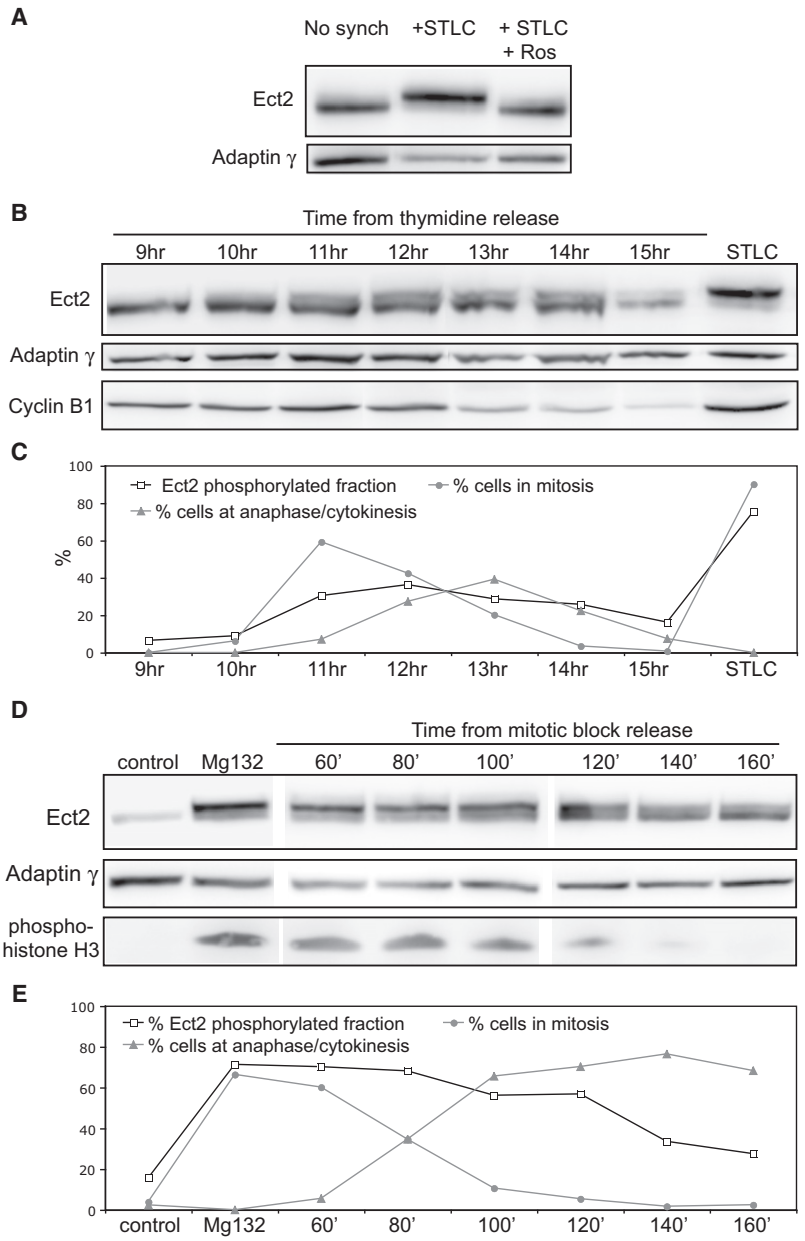


**Figure 4. Ect2 Is Phosphorylated throughout Mitosis**

(A) Gel showing the band shift of Ect2 at mitosis comparing unsynchronized cells (first lane) to cells synchronized at prometaphase by an 18 hr treatment with 5 μM S-trityl-L-cysteine (STLC, second lane). This shift is abolished by addition of 50 μM Roscovitine for 2 hr (third lane), which also reverses cell rounding.

(B) Band shift of Ect2 protein over a time course from 9 to 15 hr after release from double thymidine block. Image shown is representative of all experiments (n = 3).

(C) Quantification of the gel in (B), showing the percentage of Ect2 protein that is phosphorylated and the percentage of cells in mitosis at each time point. The fraction of phosphorylated Ect2 was calculated by normalizing to background and then dividing the band volume for the phospho-species by the total Ect2 band volume. Mitotic stages were determined by visual inspection of the spindle and DNA following fixation and immunostaining with tubulin and DAPI of a sample of cells at each time point (n = 79–221 cells for each time point) "% cells in mitosis" includes cells in prophase, prometaphase, and metaphase.

(D) Phospho-band shift of Ect2 in a synchronized population of cells as they exit mitosis after release from a metaphase arrest. This experiment was repeated twice and the image is representative of both experiments.

(E) Quantification of the gel in D, showing the percentage of Ect2 phosphorylated protein compared to the percentage of cells in mitosis (prophase, prometaphase, and metaphase) and at anaphase/cytokinesis.

MG132 (Figures 4D and 4E). Again, the phospho-shifted form of Ect2 visible in metaphase remained until almost all cells had completed anaphase (Figure 4E). These data show that Ect2 remains phosphorylated throughout mitosis.

## Ect2 Leaves the Nucleus in Early Mitosis

To understand how Ect2 might drive distinct changes in cell shape at the onset and exit of mitosis, we looked at its subcellular distribution during mitotic progression. In fixed cells stained with an Ect2 antibody, endogenous Ect2 was found to localize to the interphase nucleus and nucleolus (Figure 5A). At the onset of mitosis, Ect2 was then localized in the cytoplasm prior to nuclear envelope breakdown, where it remained until it was recruited to the spindle midzone at mitotic exit. We confirmed that this dynamic pattern of immunostaining was specific using Ect2 RNAi cells (Figure S4). Moreover, this localization was recapitulated using live imaging of a HeLa cell line constitutively expressing a BAC-containing mouse Ect2-GFP (Hutchins et al., 2010) (Figures 5B and 5C; Movie S2) and transfected with tubulin-RFP (Kobayashi and Murayama, 2009) as a marker of rounding (Figure 5B), nuclear envelope breakdown (visualized by the exclusion of tubulin from the nucleus; Figure 5C), and spindle morphogenesis. Ect2 could be seen accumulating in the cytoplasm in early prophase, ~6 min before nuclear envelope breakdown and coincident with the onset of mitotic rounding (Figure 5D). In addition, we confirmed that the change in Ect2 localization at prophase was accompanied by the nuclear import of Cyclin B1, which has previously been shown to correlate with an increase in Cdk1 activity (Gavet and Pines, 2010a) and followed shortly after mitotic kinase substrate phosphorylation in the nucleus, which was detected using a phospho-Ser/Thr-Pro antibody (Figure S4). Ect2 contains two Cdk1 consensus sequences in the vicinity of its nuclear localization sequence (NLS). To test whether Cdk1 might act through these sites to regulate Ect2 localization, we generated a phospho-mimetic construct (Ect2-T342D-S366D). This localized to the interphase nucleus (Figure S4), suggesting that phosphorylation at these sites may not be sufficient to induce Ect2 nuclear export. However, this does not rule out the possibility that Cdk1 phosphorylation at other sites could control nuclear release.

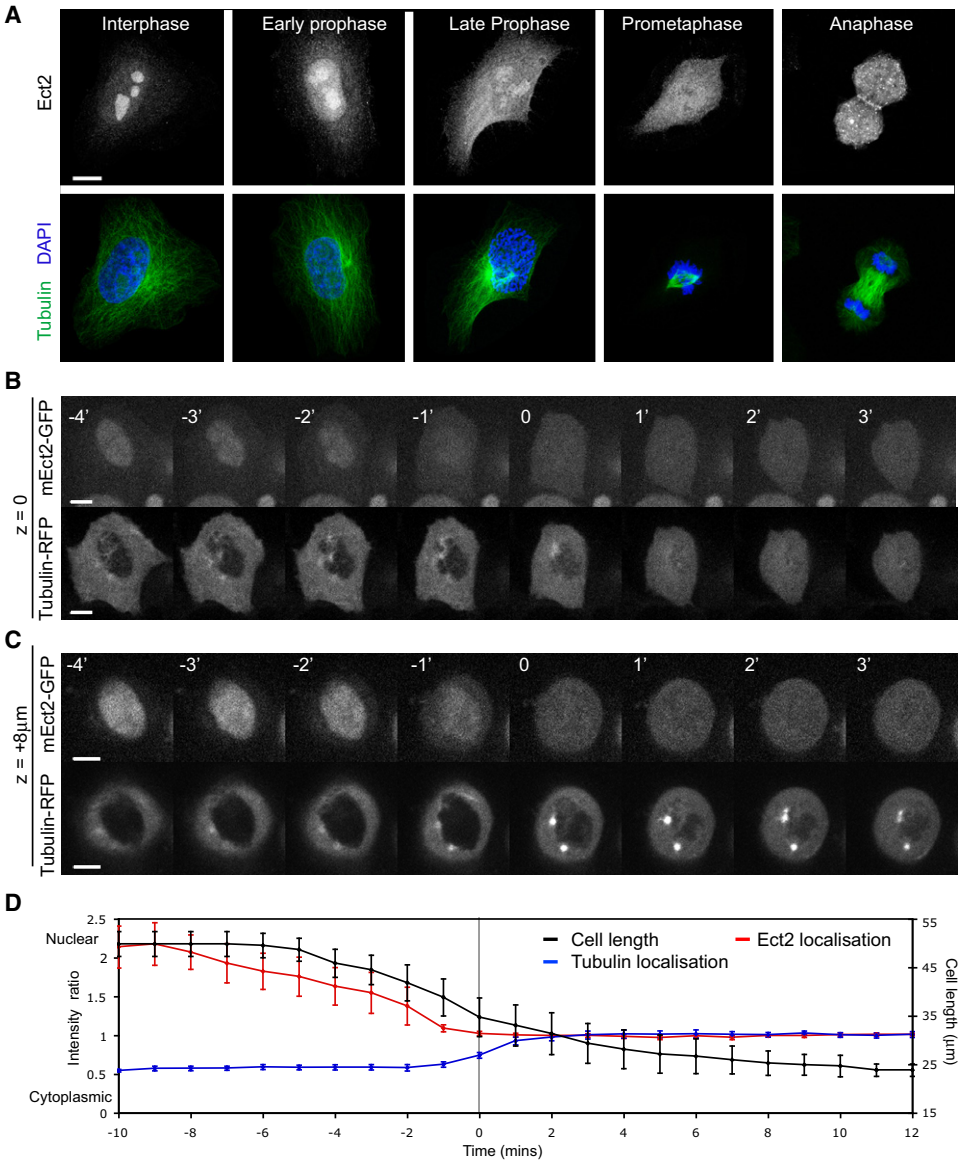


**Figure 5. Ect2 Is Exported from the Nucleus in Early Mitosis**

(A) Confocal micrograph showing Ect2 localization at each stage of mitosis in fixed cells stained with an antibody against Ect2 (upper panel) and tubulin and DAPI to show mitotic stage (lower panel). Scale bar applies to all images, 10 μm.

(B and C) Time-lapse confocal images of a HeLa cell entering mitosis expressing mouse Ect2-GFP (upper panels) and tubulin-RFP (lower panels). Mouse Ect2 is constitutively expressed in a BAC under its endogenous promotor (Hutchins et al., 2010). Two different z planes are shown: the bottom of the cell to show the full extent of the cytoplasm (B), and 8 μm higher (C) at the level of the nucleus. Time is indicated in minutes, with time point 0 being the frame of nuclear envelope breakdown as judged by when tubulin dimers first enter the nucleus. Note increase in Ect2 levels in the cytoplasm before nuclear envelope breakdown in frames −1 and −2. Scale bars, 10 μm.

(D) Quantification of time-lapse images in (B) and (C). Six cells were analyzed and measurements aligned, so that time point 0 represents the frame of nuclear envelope breakdown. Mean signal intensity was measured for Ect2 (red line) and tubulin (blue line) in a 6 × 6 pixel box in the nucleus and cytoplasm and the nuclear/cytoplasmic ratio was plotted. The black line shows mean cell length to give an indication of the onset of mitotic rounding. Error bars denote SD. See also Movie S2. See also Figure S4.

## Mislocalization of Ect2 to the Cytoplasm Is Sufficient to Drive Premature Rounding

Since the recruitment of Ect2 to the spindle midzone triggers actomyosin-dependent furrow formation (Chalamalasetty et al., 2006; Nishimura and Yonemura, 2006; Yüce et al., 2005), we postulated that its relocation from the nucleus to the cytoplasm in prophase could be a key factor in driving mitotic rounding. We utilized several human Ect2 constructs to test this idea (Figure 6A). Mammalian Ect2 protein consists of an N-terminal BRCT repeat domain, which is the site of RacGAP1 binding, a regulatory S domain that harbors NLS sites, and a C-terminal catalytic GEF domain (Miki et al., 1993; Saito et al., 2004; Saito

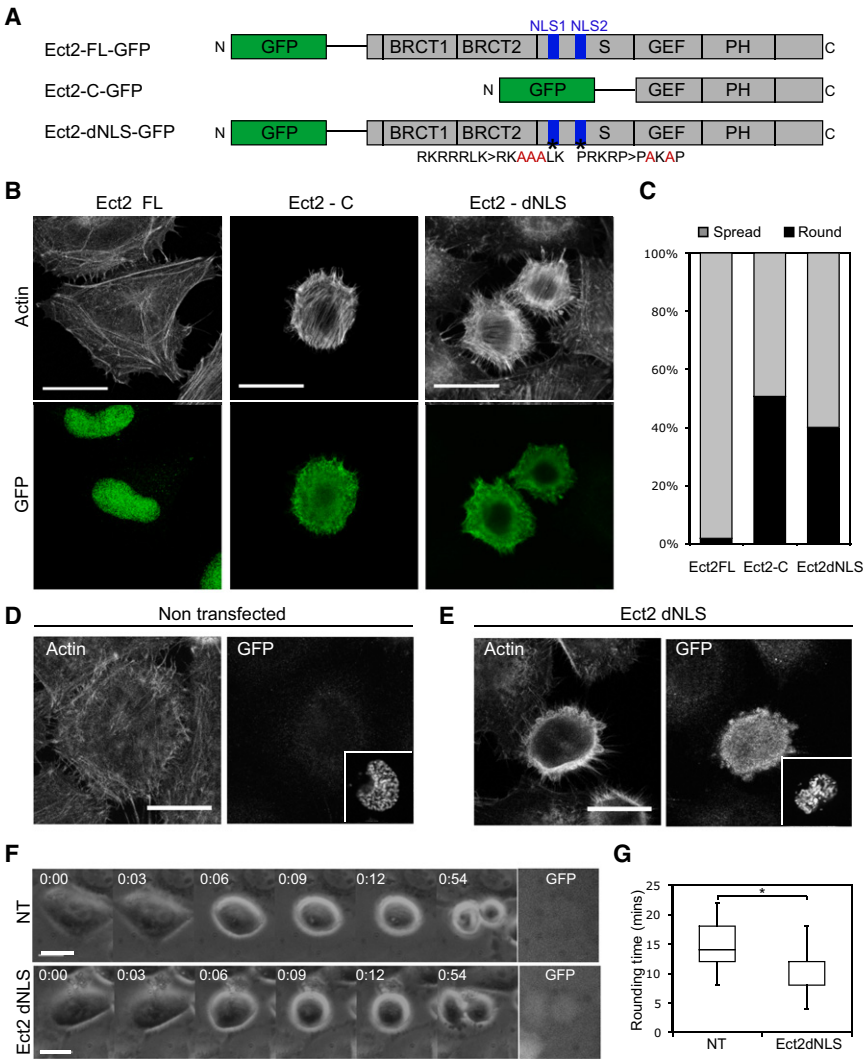


**Figure 6. Cytoplasmic Ect2 Is Sufficient to Induce Cell Rounding**

(A) Three different Ect2 constructs were overexpressed in HeLa cells: Ect2-FL-GFP, Ect2-C-GFP, and Ect2-dNLS-GFP.

(B) Representative confocal micrographs of cells transfected with Ect2-FL, Ect2-C and Ect2-dNLS showing the actin cytoskeleton stained with phalloidin-TRITC (top panel) and Ect2 construct localization (bottom panel). Note the rounded cell morphology in Ect2-C and Ect2-dNLS cells.

(C) Quantification of the percentage of interphase cells displaying the rounded phenotype (n = 80–149 cells).

(D and E) Representative confocal micrographs of cells in prophase showing an a nontransfected cell (D) and a cell transfected with Ect2-dNLS (E). The actin cytoskeleton was visualized by phalloidin staining and an anti-GFP antibody was used to indicate transfected cells. Inset shows the cell nucleus, stained with DAPI, to identify mitotic stage. Note rounded cell morphology in E.

(F) Phase contrast images of a nontransfected (NT) cell and a cell expressing Ect2-dNLS-GFP at low levels rounding up in early mitosis. Transfected cells are indicated by GFP fluorescence in final panel. See also Movie S3.

(G) Box plot comparing the mitotic rounding time of nontransfected cells (n = 21 cells) with those transfected with Ect2-dNLS-GFP (n = 23). To ensure rounding is mitotic rather than apoptotic, only cells that later proceeded to cytokinesis were analyzed. For Ect2-dNLS cells, only cells expressing low levels of the construct that were not already rounded in interphase were analyzed. For box plot, central line shows median, boxes are quartiles, and whiskers show range. For Ect2 dNLS, the median and lower quartile are the same value. Scale bars, 20 μm.

See also Figure S5.

et al., 2003; Yüce et al., 2005). We confirmed first that when overexpressed, full length human Ect2 (Ect2-FL, (Niiya et al., 2006) is confined to the nucleus and does not affect cell morphology (Figure 6B). By contrast, a truncated form of Ect2 (Ect2-C, (Su et al., 2011), which contains the C-terminal catalytic domain but lacks regulatory regions and can act as a constitutively active form (Saito et al., 2004), is localized to the cytoplasm and is able to induce profound changes in interphase cell shape (Figure 6B). Approximately 50% of interphase cells expressing Ect2-C adopt a small, rounded morphology (Figures 6B and 6C; Figure S5). In this they resemble cells in mitosis, with the notable exception that they retain stress fibers, which are normally disassembled in prophase. Thus, the mislocalization of a constitutively active form of Ect2 is sufficient to induce ectopic rounding. As seen for mitotic cells, the interphase rounding induced by ectopic Ect2 is dependent on the activity of ROK and myosin II since it could be reversed by the addition of small molecular inhibitors Y-27632 or blebbistatin (Figure S5).

To test the role of nuclear export in the regulation of Ect2-dependent mitotic rounding, we introduced point mutations in its two NLS sites (Ect2 dNLS), which have been shown to prevent Ect2 nuclear import (Saito et al., 2004). Like Ect2-C, Ect2-dNLS was found to localize to the cytoplasm and to induce ectopic interphase rounding (Figures 6B and 6C). This demonstrates that simply mutating five residues in the NLS sequences is sufficient to induce gross changes in cell morphology. To test whether the timing of Ect2 export from the nucleus contributes to mitotic rounding we then arrested cells expressing low levels of Ect2-dNLS in G2 using the specific Cdk1 inhibitor, RO-3306 (Vassilev et al., 2006) for 14 hr. The inhibitor was washed out to enable cells to synchronously progress into mitosis in the presence or absence of Ect2-dNLS (Figures 6D and 6E). As expected, the presence of low levels of cytoplasmic Ect2-dNLS, just below the threshold required to cause interphase rounding, had a significant effect on the kinetics of rounding. Ect2-dNLS expressing cells already appeared quite spherical in prophase (Figure 6E) and underwent accelerated rounding upon entry into mitosis (Figure 6F and 6G; Movie S3). Thus, the appearance of cytoplasmic Ect2 is rate-limiting for mitotic rounding. Finally, we confirmed that both rounding and cytokinesis require the

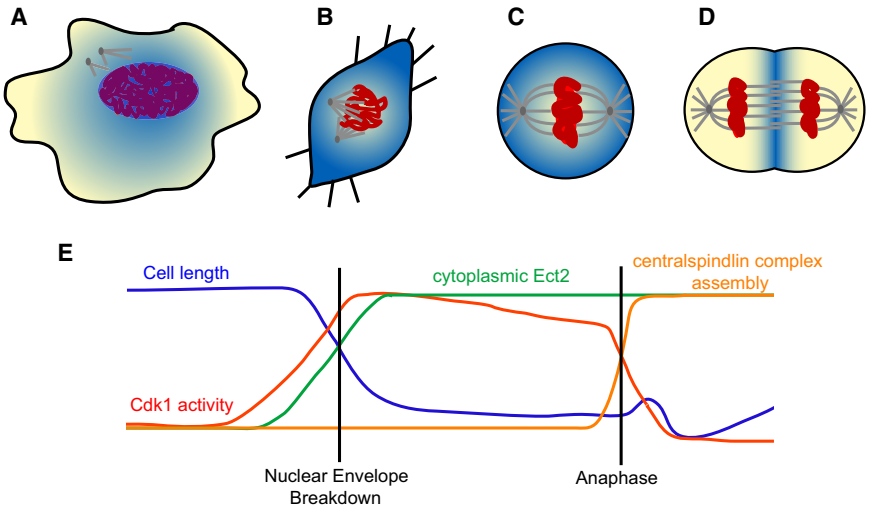


**Figure 7. A Model for Ect2 Function through Mitosis**

(A–D) Dynamic changes in Ect2 localization (shown in blue) control actin remodeling throughout mitosis. (A) Ect2 leaves the nucleus in early prophase. (B) Active Ect2 in the cytoplasm is able to activate RhoA and drive mitotic rounding. (C) Ect2 activation of RhoA results in the formation of a rigid actomyosin cortex that assists metaphase spindle assembly (D). At anaphase, Ect2 is relocalized to the central spindle and removed from the poles, resulting in the redistribution of active RhoA and therefore the contractile actomyosin machinery to drive furrowing in the center of the cell.

(E) Export of active, phosphorylated Ect2 into the cytoplasm at mitotic onset stimulates a decrease in cell length. At anaphase, Ect2 remains active but its location is modulated by binding to RacGAP1 at the spindle midzone, resulting in elongation of the cell, furrowing, and cytokinesis.

GEF activity of Ect2, since a full-length Ect2 construct containing a V566 > D mutation that has shown to be essential for GEF activity (van Impel et al., 2009) was unable to rescue either the failures in rounding or cytokinesis induced by Ect2 siRNA (Figure S5). These data suggest that Ect2 is active throughout mitosis, and that shifts in its localization regulate distinct changes in actomyosin organization and cell shape. These begin with the exit of Ect2 from the nucleus in early prophase, which functions as a key trigger for actomyosin remodeling as cells round up as they enter mitosis.

## DISCUSSION

In this study we identify Ect2 as a critical link between the cell cycle machinery, which triggers numerous events that accompany mitotic entry, and the actin-dependent shape changes that occur in early mitosis. We show that Ect2 is able to induce changes to both cell shape and cortical mechanics in early mitosis through the activation of RhoA and remodeling of the actomyosin cytoskeleton. The timing of mitotic rounding is crucially dependent on the export of Ect2 from the nucleus in prophase, because cells lacking Ect2 fail to undergo timely mitotic rounding, whereas the mislocalization of Ect2 to the cytoplasm is sufficient, at low levels, to increase the speed of mitotic rounding and, at high levels, to induce ectopic mitotic-like rounding in interphase cells.

Together these data allow us to propose a model in which regulated changes in the localization of Ect2 drive stage-specific changes in mitotic cell shape (Figure 7). In prophase, Ect2 is exported from the nucleus and phosphorylated by Cdk1, which allow it to activate RhoA in the cytoplasm to induce the actomyosin reorganization and cell shape changes required for timely bipolar spindle assembly. It is likely that the resulting mechanically rigid metaphase cortex also plays an important role in buffering the spindle from the potentially disruptive influence of external mechanical forces (Kunda and Baum, 2009). At mitotic exit, it has been shown that Ect2 is recruited to the spindle midzone as the result of its binding to a core component of the centralspindlin complex, RacGAP1 (Burkard et al., 2009; Petronczki et al., 2007; Wolfe et al., 2009). There it repositions RhoA activity to control the formation of a circumferential actomyosin band across the center of the anaphase spindle (Chalamalasetty et al., 2006; Nishimura and Yonemura, 2006; Somers and Saint, 2003; Yüce et al., 2005), ensuring the precise segregation of contents between the two daughter cells. Thus, by driving stage-specific changes in the local activation of RhoA and the contractile actomyosin machinery, Ect2 is able to remodel mitotic cell shape; driving rounding in early mitosis and cleavage furrow formation at anaphase. Later, Ect2 is released from the spindle midzone soon after the onset of cytokinesis, leaving RacGAP1 free to catalyze mid-body maturation and abscission (Simon et al., 2008). The bulk of the protein is then degraded by the APC (Liot et al., 2011), while the remainder is reimported into the newly formed nuclei, to restore interphase cell shape. In this way, Ect2 resembles other mitotic proteins that display distinct roles at different times in mitosis, dependent on stage-specific changes in their localization e.g., Plk1 is known to associate with centrosomes at prophase, kinetochores at metaphase and the midzone at anaphase, enabling it to function in centrosome separation, microtubule attachment and cytokinesis respectively (Petronczki et al., 2008).

Ect2 has been shown to be phosphorylated on multiple sites by Cdk1 (Hara et al., 2006; Niiya et al., 2006; Su et al., 2011; Yüce et al., 2005). It is likely that this phosphorylation is required for its function in mitotic rounding, since Ect2 actively remodels the mitotic cortex in early mitosis under conditions of high Cdk1 activity. Previously, one Ect2 Cdk1-dependent phosphorylation site, T342, was shown to inhibit RacGAP1 binding and become dephosphorylated in anaphase (Yüce et al., 2005), leading to the speculation that Cdk1 phosphorylation could inhibit Ect2, functionally coupling the initiation of contractile ring formation to mitotic exit. Our data, however, argue that this is unlikely to be the sole mechanism by which Ect2 is regulated, since we see little change in the global Ect2 phosphorylation level at anaphase and it remains in a hyper-phosphorylated state through until the end of cytokinesis (Figure 4). In line with this, Ect2 phosphorylation has been shown to relieve an auto-inhibitory interaction between the C- and N-terminal domains of the

protein (Hara et al., 2006; Kim et al., 2005) and to be essential for its GEF activity (Tatsumoto et al., 1999). These data suggest that Cdk1 phosphorylation contributes to the activation of Ect2 at anaphase. A recent study identified a role for the C terminus of Ect2 in its recruitment to the membrane at anaphase (Su et al., 2011). This membrane localization was shown to be essential for cytokinesis. Interestingly it was also suggested that this change in localization at anaphase may be triggered by a change in CDK-mediated phosphorylation at T815. It is clear from our analysis, however, that Ect2 is able to activate RhoA at the membrane in metaphase despite its having a largely diffuse cytoplasmic localization. Thus, the dephosphorylation of Ect2 at this site at anaphase likely induces a change in the rates at which Ect2 shuttles between the membrane and cytoplasm, and may function to limit the range of Ect2′s action to allow for polar relaxation (Sedzinski et al., 2011).

If Cdk1-mediated phosphorylation of Ect2 plays a role in the regulation of its activity at both metaphase and anaphase, an important unsolved question is how bulk Ect2 phosphorylation persists following the inactivation of Cdk1/CyclinB at mitotic exit. This may be the result of Plk1-dependent phosphorylation of Ect2 at the midzone (Niiya et al., 2006) or the result of the dynamic regulation of Ect2 dephosphorylation by mitotic phosphatases (Barr et al., 2011; Bouchoux and Uhlmann, 2011). In addition, there may be subtle changes in the set of Ect2 phosphorylation sites that accompany mitotic progression which change the relative potency of Ect2 and/or its specificity to tune its RhoGEF activity to the generation of a rounded cortex during mitotic entry or an actomyosin ring at mitotic exit (Su et al., 2011; Yüce et al., 2005). A comprehensive dissection of the function and dynamics of Ect2 phosphorylation through mitosis however is likely to remain a challenge for some time as it is hampered by the sheer number of sites revealed in both biochemical studies (Hara et al., 2006; Niiya et al., 2006; Yüce et al., 2005) and large-scale screens for mitotic phosphorylation (Beausoleil et al., 2006; Dephoure et al., 2008).

Although Ect2 provides a critical link between mitotic entry and cell rounding, it is clear that other factors are important in the control of mitotic cell shape. These include the loss of substrate adhesion, which is dependent on Rap1 inhibition (Dao et al., 2009) together with changes in osmotic pressure (Stewart et al., 2011). This may explain why Ect2-depleted cells, although suffering from profound defects in actin organization, eventually assume a roughly rounded morphology (Figure 1). Indeed, we observed no defects in the timing of focal adhesion disassembly in Ect2 RNAi cells (Figure S3), suggesting that loss of adhesion may allow cells to decrease in length despite defects in actin organization and myosin contractibility. It is therefore likely that Cdk1/CyclinB and other mitotic kinases directly regulate focal adhesion removal and changes to ion channels in parallel, independently of Ect2, to ensure their coordination. Nevertheless, the involvement of Ect2 in sequential events during mitosis suggests that it is a central organizer of the cortex through mitotic progression. Significant changes to the actomyosin cytoskeleton occur at rounding when actin filaments are rearranged to form a stiff cortical shell (Kunda et al., 2008) and then at cytokinesis when the symmetry is broken by furrowing and polar relaxation (Eggert et al., 2006). Since our data suggest that both processes are controlled by the same molecular "toolbox," downstream of Ect2 and RhoA, one might speculate that they are mechanistically coupled. Thus, the repositioning of Ect2 at anaphase, may serve to loosen the rigid actomyosin cortex at the cell poles, coupling cleavage furrow formation to polar relaxation. In fact, this was long the favored model for cytokinesis, in which polar relaxation was through to precede and to drive furrow formation (Roberts, 1961).

There are several similar parallels in evolution where actin remodeling events required for cytokinesis are initiated before cell division. In the early *Caenorhabditis elegans* embryo, cortical actomyosin flows determine cell polarity before division, in a process that is dependent on Ect2 and RhoA (Motegi and Sugimoto, 2006; Schonegg and Hyman, 2006). Likewise in fission yeast, preparation for cytokinesis begins before anaphase with the formation of actin-nucleating nodes at the onset of mitosis, which later condense to form the contractile ring (Goyal et al., 2011; Pollard and Wu, 2010). Our data suggest that a similar mechanism could operate in mammalian cells, with the events that remodel the actin cortex in preparation for cell division being initiated by Cdk1-dependent Ect2 activity at the onset of mitosis, rather than by Cdk1 inhibition at anaphase.

## EXPERIMENTAL PROCEDURES

### Time-Lapse Microscopy

For live imaging, HeLa stable cell lines expressing LifeAct-GFP/histone2B-mRFP, histone2B-mRFP/tubulin-GFP (Steigemann et al., 2009), Ect2-GFP (hela Kyoto -mEct2-GFP-FLAP (Poser et al., 2008; Hutchins et al., 2010), and a tetracycline-inducible line expressing Cyclin-B1-Venus (Di Fiore and Pines, 2010) were plated on glass-bottomed dishes (MatTek) coated with 10 μg/ml fibronectin (Sigma). For cell length measurements, cells were imaged every 2 min using a Zeiss Axiovert 200M microscope with a 20× objective (numerical aperture, NA 0.4), and images acquired using a Hamamatsu Orca AG camera and Volocity software (Perkin Elmer). Cell length was defined as the furthest distance between two points on the cell perimeter (Feret's Diameter) and measured using Fiji. For filming inhibitor treated cells, inhibitors were dissolved in DMEM + 10% FBS and added one hour prior to commencing filming, except for C3 transferase, which was added 6 hr before filming began. Inhibitors were used at the following concentrations: 100 ng/ml nocodozole (Sigma), 2 μg/ml C3 transferase (Cytoskeleton), 50 μM Y-27632 (Calbiochem), and 50 μM blebbistatin (Sigma). For time-lapse confocal imaging, an UltraView Vox (Perkin Elmer) spinning disc system was used with 60× oil immersion objective (NA 1.4). Images were acquired every 30 s with z slices every 4 μm covering the height of the cell. Single z plane images are shown.

### Immunofluorescence

For immunostaining, cells were plated on fibronectin-coated glass coverslips and fixed with 4% formaldehyde for 20 min, permeablized with 0.2% triton-X in PBS for 5 min, blocked with 5% bovine serum albumin in PBS for 30 min and treated with primary and secondary antibodies for 1 hr at room temperature. Primary antibodies were used at the following dilutions: tubulin 1:400 (DM1A, Sigma-Aldrich), Ect2 1:200 (sc-1005 Santa Cruz), anti-GFP 1:200 (a11122 Molecular Probes), anti-myc 1:500 (9E10 Santa Cruz), phospho-Myosin Light Chain (T18/S19) 1:100 (Cell Signaling Technology 3674), phospho-Ezrin (T567)/ Radixin (T564)/ Moesin (T558) 1:200 (Cell Signaling Technology 3141), phospho-paxillin 1:200 (BD Bioscience 610051), and phospho-Ser/Thr-Pro 1:500 (MPM2, Millipore). Secondary anti-rabbit IgG and anti-mouse IgG antibodies (Molecular Probes) tagged with alexa-fluor 488, 546 or 647 were used at 1:500. TRITC-conjugated phalloidin (Sigma) was used at 0.1 μg/ml and DAPI (Invitrogen) at 1:1000. Immuno-stained cells were mounted with FluorSave (Calbiochem) and imaged on a Leica SPE confocal microscope with a 63× lens (NA 1.3).

### Gel Mobility Shift Assay and Western Blotting

Ect2 bandshift experiments were carried out as previously described (Niiya et al., 2006; Tatsumoto et al., 1999). Unsynchronized cells or cells arrested in mitosis by 5 μM STLC (Sigma) treatment for 18 hr were harvested in Laemmli Buffer (Sigma). Roscovitine (Calbiochem) was used at a concentration of 50 μM for 2 hr. For block and release experiments, cells were synchronized by treatment with 2 mM thymidine (Sigma) for 14 hr, released into fresh medium for 8 hr, followed by a second 14 hr 2 mM thymidine treatment, and then released for 10 hr before harvesting every hour. For mitotic exit, synchronization cells were synchronized at metaphase using the following protocol: 24 hr treatment with 2 mM thymidine, followed by 6 hr release, 4 hr in 100ng/ml nocodozole, and finally 2 hr in 10 μM Mg132. Cells were then released into fresh media and lysed at 20 min intervals. Samples were loaded onto an 8% SDS-PAGE gel before transfer onto an Immobilon-P (Millipore) membrane by western blotting. Membranes were blocked in 5% BSA in TBST for 1 hr, incubated overnight at 4°C with primary antibodies, and for several hours at room temperature with secondary antibodies. Antibodies were used at the following dilutions: Ect2 1:500 (sc-1005 Santa Cruz), Cyclin B1 1:500 (sc-595 Santa Cruz), adaptin γ 1:2000 (BD Biosciences 610386), phospho-histone H3 (S10) 1:4000(Cell Signaling Technology 9706), and tubulin 1:2000 (DM1A, Sigma) and HRP-conjugated secondary antibodies 1:1000 (DAKO). Results were visualized using an ImageQuant LAS4000 system and blots quantified using ImageQuant TL software (GE Healthcare).

### Optical Stretching

Cells were plated at 90% confluency in 25 $cm^2$ flasks for RNAi treatment. Three hours after RNAi treatment, cells were arrested in G2 by addition of 9 μM RO-3306 (Enzo Life Science) for 18 hr, before release from the drug for 90 min and harvest by mitotic shake-off. Interphase cells and multinucleate Ect2 RNAi cells that had already failed cell division were excluded from the analysis by visual inspection of DNA and measurement of cell diameter inside the optical stretcher. The microfluidic optical stretcher (OS) has previously been described in detail (Lincoln et al., 2007). Two counter-propagating near-infrared laser beams ($\gamma$ = 1064 nm), emerging from single-mode optical fibers, are combined in a microfluidic channel to trap (low power p = 0.1 W/fiber) and deform (p = 1.0 W/fiber) single suspended cell by optically induced surface stresses. Cells were introduced into the OS at a concentration of 50 × $10^4$ cells/ml and experiments were done at room temperature (22°C). The mechanical properties of cells were measured by a creep compliance experiment. This test enables a direct comparison between the mechanical properties of cells (Lautenschläger et al., 2009; Wottawah et al., 2005). A cell is first held at low power in the optical trap and then a constant stress is applied to the cell for 4 s (p = 1W). The relative cell deformation, or strain $D(t) = \Delta r(t)/r_o$ (during and after application of the stress) is recorded with phase contrast videomicroscopy. The compliance of the cell, representing a true material property, is defined as $J(t) = D(t)/(\sigma_o F_G)$, which is the strain $D(t)$ normalized by the peak stress applied, $\sigma_o$, and a geometrical factor $F_G$ (Ananthakrishnan et al., 2006; Guck et al., 2001), which accounts for different cell sizes or different refractive indices. The refractive indices of cells were determined by immersion refractometry using BSA solutions as described previously (Guck et al., 2005): $n_{mitotis}$ = 1.3510 ± 0.0096 and $n_{interphase}$ = 1.3563 ± 0.0041.

### FRET Analysis

HeLa cells were transfected with a RhoA YFP-CFP FRET biosensor (Pertz et al., 2006) and 32 hr after transfection 5 μM STLC was added for 15 hr to synchronize cell in mitosis. Cells were then fixed with 4% formaldehyde and imaged using a Leica SP5 scanning confocal system with a 63x oil objective (NA 1.4). FRET efficiency was calculated using acceptor photobleaching as described (Matthews et al., 2008). Briefly, CFP and YFP channels were excited using the 458 nm and 514 nm lasers respectively. Cells were imaged prebleach, then a region consisting of half the cell was bleached for 2 min using the 514 nm laser at maximum power. Postbleach images were then acquired for each channel and the total FRET efficiency ratio for the bleached half of the cell was calculated as $(CFP_{postbleach} - CFP_{prebleach})/CFP_{postbleach}$. An efficiency ratio was also calculated for an equal-seized nonbleached region and subtracted from the bleached region to give the final ratio.

### Statistical Analysis

Graphs were produced and statistical analysis carried out in Microsoft Excel. Bar charts show mean values with error bars representing standard deviation. Box plots show median as line, upper and lower quartiles as box, and range as whiskers. The p values were calculated using the student's t test (two sample equal variance, two-tailed), *p < 0.01, **p < 0.001.

## SUPPLEMENTAL INFORMATION

Supplemental Information includes five figures, one table, Supplemental Experimental Procedures, and three movies and can be found online at http://dx.doi.org/10.1016/j.devcel.2012.06.003.

## ACKNOWLEDGMENTS

We are grateful to Ewa Paluch, Mark Petronczki, and Guillaume Charras for insightful comments on the manuscript and to Jonathan Pines for helpful discussion. We thank Kuan-Chung Su, Mark Petronczki, Toru Miki, Michael Glotzer, Guillaume Charras, and Klaus Hahn for providing plasmids and Andrew Holland, Ina Poser, Tony Hyman, Jan Ellenberg, and Jonathan Pines for cell lines. We also thank Robin Ketteler and Jamie Freeman for help with RNAi screening and Andrew Vaughan and Lauren McLaughlin for their invaluable microscopy expertise. H.K.M.'s and P.K.'s work was supported by Cancer Research UK and by the European FP7 Cancer Pathways project. U.D. acknowledges support from Fondation Pierre-Gilles de Gennes. J.L.R. was supported by the Wellcome Trust and by an EMBO short-term fellowship to join the Ellenberg laboratory (to whom we are grateful). B.B. received support from the Royal Society and Cancer Research UK.

Received: December 7, 2011
Revised: April 4, 2012
Accepted: June 5, 2012
Published online: August 13, 2012

## REFERENCES

Amano, M., Ito, M., Kimura, K., Fukata, Y., Chihara, K., Nakano, T., Matsuura, Y., and Kaibuchi, K. (1996). Phosphorylation and activation of myosin by Rho-associated kinase (Rho-kinase). J. Biol. Chem. *271*, 20246–20249.

Ananthakrishnan, R., Guck, J., Wottawah, F., Schinkinger, S., Lincoln, B., Romeyke, M., Moon, T., and Käs, J. (2006). Quantifying the contribution of actin networks to the elastic strength of fibroblasts. J. Theor. Biol. *242*, 502–516.

Barr, F.A., Elliott, P.R., and Gruneberg, U. (2011). Protein phosphatases and the regulation of mitosis. J. Cell Sci. *124*, 2323–2334.

Beausoleil, S.A., Villén, J., Gerber, S.A., Rush, J., and Gygi, S.P. (2006). A probability-based approach for high-throughput protein phosphorylation analysis and site localization. Nat. Biotechnol. *24*, 1285–1292.

Blangy, A., Lane, H.A., d'Hérin, P., Harper, M., Kress, M., and Nigg, E.A. (1995). Phosphorylation by p34cdc2 regulates spindle association of human Eg5, a kinesin-related motor essential for bipolar spindle formation in vivo. Cell *83*, 1159–1169.

Blethrow, J.D., Glavy, J.S., Morgan, D.O., and Shokat, K.M. (2008). Covalent capture of kinase-specific phosphopeptides reveals Cdk1-cyclin B substrates. Proc. Natl. Acad. Sci. USA *105*, 1442–1447.

Bouchoux, C., and Uhlmann, F. (2011). A quantitative model for ordered Cdk substrate dephosphorylation during mitotic exit. Cell *147*, 803–814.

Burkard, M.E., Maciejowski, J., Rodriguez-Bravo, V., Repka, M., Lowery, D.M., Clauser, K.R., Zhang, C., Shokat, K.M., Carr, S.A., Yaffe, M.B., and Jallepalli, P.V. (2009). Plk1 self-organization and priming phosphorylation of HsCYK-4 at the spindle midzone regulate the onset of division in human cells. PLoS Biol. *7*, e1000111.

Carreno, S., Kouranti, I., Glusman, E.S., Fuller, M.T., Echard, A., and Payre, F. (2008). Moesin and its activating kinase Slik are required for cortical stability and microtubule organization in mitotic cells. J. Cell Biol. *180*, 739–746.

Chalamalasetty, R.B., Hümmer, S., Nigg, E.A., and Silljé, H.H. (2006). Influence of human Ect2 depletion and overexpression on cleavage furrow formation and abscission. J. Cell Sci. *119*, 3008–3019.

Cramer, L.P., and Mitchison, T.J. (1997). Investigation of the mechanism of retraction of the cell margin and rearward flow of nodules during mitotic cell rounding. Mol. Biol. Cell *8*, 109–119.

Dao, V.T., Dupuy, A.G., Gavet, O., Caron, E., and de Gunzburg, J. (2009). Dynamic changes in Rap1 activity are required for cell retraction and spreading during mitosis. J. Cell Sci. *122*, 2996–3004.

Dephoure, N., Zhou, C., Villén, J., Beausoleil, S.A., Bakalarski, C.E., Elledge, S.J., and Gygi, S.P. (2008). A quantitative atlas of mitotic phosphorylation. Proc. Natl. Acad. Sci. USA *105*, 10762–10767.

Di Fiore, B., and Pines, J. (2010). How cyclin A destruction escapes the spindle assembly checkpoint. J. Cell Biol. *190*, 501–509.

Eggert, U.S., Mitchison, T.J., and Field, C.M. (2006). Animal cytokinesis: from parts list to mechanisms. Annu. Rev. Biochem. *75*, 543–566.

Fujibuchi, T., Abe, Y., Takeuchi, T., Imai, Y., Kamei, Y., Murase, R., Ueda, N., Shigemoto, K., Yamamoto, H., and Kito, K. (2005). AIP1/WDR1 supports mitotic cell rounding. Biochem. Biophys. Res. Commun. *327*, 268–275.

Gavet, O., and Pines, J. (2010a). Activation of cyclin B1-Cdk1 synchronizes events in the nucleus and the cytoplasm at mitosis. J. Cell Biol. *189*, 247–259.

Gavet, O., and Pines, J. (2010b). Progressive activation of CyclinB1-Cdk1 coordinates entry to mitosis. Dev. Cell *18*, 533–543.

Goyal, A., Takaine, M., Simanis, V., and Nakano, K. (2011). Dividing the spoils of growth and the cell cycle: The fission yeast as a model for the study of cytokinesis. Cytoskeleton *68*, 69–88.

Guck, J., Ananthakrishnan, R., Mahmood, H., Moon, T.J., Cunningham, C.C., and Käs, J. (2001). The optical stretcher: a novel laser tool to micromanipulate cells. Biophys. J. *81*, 767–784.

Guck, J., Schinkinger, S., Lincoln, B., Wottawah, F., Ebert, S., Romeyke, M., Lenz, D., Erickson, H.M., Ananthakrishnan, R., Mitchell, D., et al. (2005). Optical deformability as an inherent cell marker for testing malignant transformation and metastatic competence. Biophys. J. *88*, 3689–3698.

Hara, T., Abe, M., Inoue, H., Yu, L.R., Veenstra, T.D., Kang, Y.H., Lee, K.S., and Miki, T. (2006). Cytokinesis regulator ECT2 changes its conformation through phosphorylation at Thr-341 in G2/M phase. Oncogene *25*, 566–578.

Harris, A. (1973). Location of cellular adhesions to solid substrata. Dev. Biol. *35*, 97–114.

Hutchins, J.R., Toyoda, Y., Hegemann, B., Poser, I., Heriche, J.K., Sykora, M.M., Augsburg, M., Hudecz, O., Buschhorn, B.A., Bulkescher, J., et al. (2010). Systematic analysis of human protein complexes identifies chromosome segregation proteins. Science *328*, 593–599.

Ji, J.Y., Haghnia, M., Trusty, C., Goldstein, L.S., and Schubiger, G. (2002). A genetic screen for suppressors and enhancers of the Drosophila cdk1-cyclin B identifies maternal factors that regulate microtubule and microfilament stability. Genetics *162*, 1179–1195.

Jones, J.T., Myers, J.W., Ferrell, J.E., and Meyer, T. (2004). Probing the precision of the mitotic clock with a live-cell fluorescent biosensor. Nat. Biotechnol. *22*, 306–312.

Kamijo, K., Ohara, N., Abe, M., Uchimura, T., Hosoya, H., Lee, J.S., and Miki, T. (2006). Dissecting the role of Rho-mediated signaling in contractile ring formation. Mol. Biol. Cell *17*, 43–55.

Kim, J.E., Billadeau, D.D., and Chen, J. (2005). The tandem BRCT domains of Ect2 are required for both negative and positive regulation of Ect2 in cytokinesis. J. Biol. Chem. *280*, 5733–5739.

Kimura, K., Hirano, M., Kobayashi, R., and Hirano, T. (1998). Phosphorylation and activation of 13S condensin by Cdc2 in vitro. Science *282*, 487–490.

Kobayashi, T., and Murayama, T. (2009). Cell cycle-dependent microtubule-based dynamic transport of cytoplasmic dynein in mammalian cells. PLoS ONE *4*, e7827.

Kunda, P., and Baum, B. (2009). The actin cytoskeleton in spindle assembly and positioning. Trends Cell Biol. *19*, 174–179.

Kunda, P., Pelling, A.E., Liu, T., and Baum, B. (2008). Moesin controls cortical rigidity, cell rounding, and spindle morphogenesis during mitosis. Curr. Biol. *18*, 91–101.

Lamb, N.J., Fernandez, A., Watrin, A., Labbé, J.C., and Cavadore, J.C. (1990). Microinjection of p34cdc2 kinase induces marked changes in cell shape, cytoskeletal organization, and chromatin structure in mammalian fibroblasts. Cell *60*, 151–165.

Lautenschläger, F., Paschke, S., Schinkinger, S., Bruel, A., Beil, M., and Guck, J. (2009). The regulatory role of cell mechanics for migration of differentiating myeloid cells. Proc. Natl. Acad. Sci. USA *106*, 15696–15701.

Lincoln, B., Wottawah, F., Schinkinger, S., Ebert, S., and Guck, J. (2007). High-throughput rheological measurements with an optical stretcher. Methods Cell Biol. *83*, 397–423.

Lindqvist, A., Rodríguez-Bravo, V., and Medema, R.H. (2009). The decision to enter mitosis: feedback and redundancy in the mitotic entry network. J. Cell Biol. *185*, 193–202.

Liot, C., Seguin, L., Siret, A., Crouin, C., Schmidt, S., and Bertoglio, J. (2011). APC(cdh1) mediates degradation of the oncogenic Rho-GEF Ect2 after mitosis. PLoS ONE *6*, e23676.

Ma, H.T., and Poon, R.Y. (2011). How protein kinases co-ordinate mitosis in animal cells. Biochem. J. *435*, 17–31.

Maddox, A.S., and Burridge, K. (2003). RhoA is required for cortical retraction and rigidity during mitotic cell rounding. J. Cell Biol. *160*, 255–265.

Mali, P., Wirtz, D., and Searson, P.C. (2010). Interplay of RhoA and motility in the programmed spreading of daughter cells postmitosis. Biophys. J. *99*, 3526–3534.

Matthews, H.K., Marchant, L., Carmona-Fontaine, C., Kuriyama, S., Larraín, J., Holt, M.R., Parsons, M., and Mayor, R. (2008). Directional migration of neural crest cells in vivo is regulated by Syndecan-4/Rac1 and non-canonical Wnt signaling/RhoA. Development *135*, 1771–1780.

Meyer, E.J., Ikmi, A., and Gibson, M.C. (2011). Interkinetic nuclear migration is a broadly conserved feature of cell division in pseudostratified epithelia. Curr. Biol. *21*, 485–491.

Miki, T., Smith, C.L., Long, J.E., Eva, A., and Fleming, T.P. (1993). Oncogene ect2 is related to regulators of small GTP-binding proteins. Nature *362*, 462–465.

Motegi, F., and Sugimoto, A. (2006). Sequential functioning of the ECT-2 RhoGEF, RHO-1 and CDC-42 establishes cell polarity in Caenorhabditis elegans embryos. Nat. Cell Biol. *8*, 978–985.

Niiya, F., Tatsumoto, T., Lee, K.S., and Miki, T. (2006). Phosphorylation of the cytokinesis regulator ECT2 at G2/M phase stimulates association of the mitotic kinase Plk1 and accumulation of GTP-bound RhoA. Oncogene *25*, 827–837.

Nishimura, Y., and Yonemura, S. (2006). Centralspindlin regulates ECT2 and RhoA accumulation at the equatorial cortex during cytokinesis. J. Cell Sci. *119*, 104–114.

Peter, M., Nakagawa, J., Dorée, M., Labbé, J.C., and Nigg, E.A. (1990). In vitro disassembly of the nuclear lamina and M phase-specific phosphorylation of lamins by cdc2 kinase. Cell *61*, 591–602.

Pertz, O., Hodgson, L., Klemke, R.L., and Hahn, K.M. (2006). Spatiotemporal dynamics of RhoA activity in migrating cells. Nature *440*, 1069–1072.

Petronczki, M., Glotzer, M., Kraut, N., and Peters, J.M. (2007). Polo-like kinase 1 triggers the initiation of cytokinesis in human cells by promoting recruitment of the RhoGEF Ect2 to the central spindle. Dev. Cell *12*, 713–725.

Petronczki, M., Lénárt, P., and Peters, J.M. (2008). Polo on the Rise-from Mitotic Entry to Cytokinesis with Plk1. Dev. Cell *14*, 646–659.

Picone, R., Ren, X., Ivanovitch, K.D., Clarke, J.D., McKendry, R.A., and Baum, B. (2010). A polarised population of dynamic microtubules mediates homeostatic length control in animal cells. PLoS Biol. *8*, e1000542.

Pollard, T.D., and Wu, J.Q. (2010). Understanding cytokinesis: lessons from fission yeast. Nature Rev. *11*, 149–155.

Poser, I., Sarov, M., Hutchins, J.R., Hériché, J.K., Toyoda, Y., Pozniakovsky, A., Weigl, D., Nitzsche, A., Hegemann, B., Bird, A.W., et al. (2008). BAC

TransgeneOmics: a high-throughput method for exploration of protein function in mammals. Nature Methods *5*, 409–415.

Prokopenko, S.N., Brumby, A., O'Keefe, L., Prior, L., He, Y., Saint, R., and Bellen, H.J. (1999). A putative exchange factor for Rho1 GTPase is required for initiation of cytokinesis in Drosophila. Genes Dev. *13*, 2301–2314.

Riedl, J., Crevenna, A.H., Kessenbrock, K., Yu, J.H., Neukirchen, D., Bista, M., Bradke, F., Jenne, D., Holak, T.A., Werb, Z., et al. (2008). Lifeact: a versatile marker to visualize F-actin. Nat. Methods *5*, 605–607.

Roberts, H.S. (1961). Mechanisms of cytokinesis: A critical review. Q. Rev. Biol. *36*, 155–177.

Rosenblatt, J., Cramer, L.P., Baum, B., and McGee, K.M. (2004). Myosin II-dependent cortical movement is required for centrosome separation and positioning during mitotic spindle assembly. Cell *117*, 361–372.

Saito, S., Tatsumoto, T., Lorenzi, M.V., Chedid, M., Kapoor, V., Sakata, H., Rubin, J., and Miki, T. (2003). Rho exchange factor ECT2 is induced by growth factors and regulates cytokinesis through the N-terminal cell cycle regulator-related domains. J. Cell. Biochem. *90*, 819–836.

Saito, S., Liu, X.F., Kamijo, K., Raziuddin, R., Tatsumoto, T., Okamoto, I., Chen, X., Lee, C.C., Lorenzi, M.V., Ohara, N., and Miki, T. (2004). Deregulation and mislocalization of the cytokinesis regulator ECT2 activate the Rho signaling pathways leading to malignant transformation. J. Biol. Chem. *279*, 7169–7179.

Schonegg, S., and Hyman, A.A. (2006). CDC-42 and RHO-1 coordinate actomyosin contractility and PAR protein localization during polarity establishment in C. elegans embryos. Development *133*, 3507–3516.

Sedzinski, J., Biro, M., Oswald, A., Tinevez, J.Y., Salbreux, G., and Paluch, E. (2011). Polar actomyosin contractility destabilizes the position of the cytokinetic furrow. Nature *476*, 462–466.

Simon, G.C., Schonteich, E., Wu, C.C., Piekny, A., Ekiert, D., Yu, X., Gould, G.W., Glotzer, M., and Prekeris, R. (2008). Sequential Cyk-4 binding to ECT2 and FIP3 regulates cleavage furrow ingression and abscission during cytokinesis. EMBO J. *27*, 1791–1803.

Somers, W.G., and Saint, R. (2003). A RhoGEF and Rho family GTPase-activating protein complex links the contractile ring to cortical microtubules at the onset of cytokinesis. Dev. Cell *4*, 29–39.

Steigemann, P., Wurzenberger, C., Schmitz, M.H., Held, M., Guizetti, J., Maar, S., and Gerlich, D.W. (2009). Aurora B-mediated abscission checkpoint protects against tetraploidization. Cell *136*, 473–484.

Stewart, M.P., Helenius, J., Toyoda, Y., Ramanathan, S.P., Muller, D.J., and Hyman, A.A. (2011). Hydrostatic pressure and the actomyosin cortex drive mitotic cell rounding. Nature *469*, 226–230.

Su, K.C., Takaki, T., and Petronczki, M. (2011). Targeting of the RhoGEF Ect2 to the equatorial membrane controls cleavage furrow formation during cytokinesis. Dev. Cell *21*, 1104–1115.

Tatsumoto, T., Xie, X., Blumenthal, R., Okamoto, I., and Miki, T. (1999). Human ECT2 is an exchange factor for Rho GTPases, phosphorylated in G2/M phases, and involved in cytokinesis. J. Cell Biol. *147*, 921–928.

van Impel, A., Schumacher, S., Draga, M., Herz, H.M., Grosshans, J., and Müller, H.A. (2009). Regulation of the Rac GTPase pathway by the multifunctional Rho GEF Pebble is essential for mesoderm migration in the Drosophila gastrula. Development *136*, 813–822.

Vassilev, L.T., Tovar, C., Chen, S., Knezevic, D., Zhao, X., Sun, H., Heimbrook, D.C., and Chen, L. (2006). Selective small-molecule inhibitor reveals critical mitotic functions of human CDK1. Proc. Natl. Acad. Sci. USA *103*, 10660–10665.

Wolfe, B.A., Takaki, T., Petronczki, M., and Glotzer, M. (2009). Polo-like kinase 1 directs assembly of the HsCyk-4 RhoGAP/Ect2 RhoGEF complex to initiate cleavage furrow formation. PLoS Biol. *7*, e1000110.

Wottawah, F., Schinkinger, S., Lincoln, B., Ebert, S., Müller, K., Sauer, F., Travis, K., and Guck, J. (2005). Characterizing single suspended cells by optorheology. Acta Biomater. *1*, 263–271.

Yoshizaki, H., Ohba, Y., Kurokawa, K., Itoh, R.E., Nakamura, T., Mochizuki, N., Nagashima, K., and Matsuda, M. (2003). Activity of Rho-family GTPases during cell division as visualized with FRET-based probes. J. Cell Biol. *162*, 223–232.

Yüce, O., Piekny, A., and Glotzer, M. (2005). An ECT2-centralspindlin complex regulates the localization and function of RhoA. J. Cell Biol. *170*, 571–582.

Developmental Cell
Article

# Secreted VAPB/ALS8 Major Sperm Protein Domains Modulate Mitochondrial Localization and Morphology via Growth Cone Guidance Receptors

Sung Min Han,[1] Hiroshi Tsuda,[2,5] Youfeng Yang,[1] Jack Vibbert,[1] Pauline Cottee,[1] Se-Jin Lee,[1] Jessica Winek,[1] Claire Haueter,[3] Hugo J. Bellen,[2,3,4] and Michael A. Miller[1,*]
[1]Department of Cell Biology, University of Alabama School of Medicine, Birmingham, AL 35294, USA
[2]Department of Molecular and Human Genetics
[3]Howard Hughes Medical Institute
[4]Program in Developmental Biology
Baylor College of Medicine, Houston, TX 77030, USA
[5]Present address: Department of Neurology and Neurosurgery, McGill University, Montreal, Quebec H3A 2B4, Canada
*Correspondence: mamiller@uab.edu
DOI 10.1016/j.devcel.2011.12.009

## SUMMARY

**The VAPB/ALS8 major sperm protein domain (vMSP) is implicated in amyotrophic lateral sclerosis and spinal muscular atrophy, yet its function in the nervous system is not well understood. In *Caenorhabditis elegans* and *Drosophila*, the vMSP is cleaved from its transmembrane anchor and secreted in a cell type-specific fashion. We show that vMSPs secreted by neurons act on Lar-like protein-tyrosine phosphatase and Roundabout growth cone guidance receptors expressed in striated muscle. This signaling pathway promotes Arp2/3-dependent actin remodeling and mitochondrial localization to actin-rich muscle I-bands. *C. elegans* VAPB mutants have mitochondrial localization, morphology, mobility, and fission/fusion defects that are suppressed by Lar-like receptor or Arp2/3 inactivation. Hence, growth cone guidance receptor pathways that remodel the actin cytoskeleton have unanticipated effects on mitochondrial dynamics. We propose that neurons secrete vMSPs to promote striated muscle energy production and metabolism, in part through the regulation of mitochondrial localization and function.**

## INTRODUCTION

Mitochondria are obligate endosymbionts that generate ATP for cellular energy through oxidative phosphorylation and play central roles in metabolism, calcium homeostasis, and apoptosis (Parekh, 2003; Suen et al., 2008). They are often distributed nonrandomly in differentiated cells like neurons and muscle, presumably to provide energy to regions high in metabolic demand. In neurons, mitochondria are enriched at synapses (Hollenbeck and Saxton, 2005), whereas in mammalian skeletal muscle, mitochondria are positioned in pairs near the I-bands (Vendelin et al., 2005). Motor proteins that move along microtubules drive mitochondrial transport over long distances (Hollenbeck and Saxton, 2005). However, the actin cytoskeleton can facilitate short-range mitochondrial movement and docking of mitochondria to specific sites (Boldogh and Pon, 2007; Pathak et al., 2010). In chicken sensory neuron cultures, Nerve Growth Factor-conjugated beads promote mitochondrial accumulation and docking by a mechanism dependent on F-actin (Chada and Hollenbeck, 2004). These data raise the possibility that growth factors may affect mitochondrial localization in vivo.

The VAPs (VAMP/synaptobrevin-associated proteins) comprise a highly conserved protein family with an N-terminal MSP (major sperm protein) domain, a coiled-coil motif, and transmembrane-spanning region anchored in endoplasmic reticulum (ER) membranes. The ~120 amino acid MSP domain is named after *C. elegans* MSPs, which function as secreted ligands that induce oocyte maturation and ovarian muscle contraction (Han et al., 2010; Miller et al., 2001). MSPs also have an intracellular cytoskeletal function, but this function is independent of actin and myosin, depends upon MSP polymerization into filaments, and is not conserved in VAPs (Bottino et al., 2002; Han et al., 2010; Lev et al., 2008). VAPs have been implicated in diverse processes, including regulation of lipid transport, ER morphology, and membrane trafficking (Lev et al., 2008). In addition, VAPs and MSPs have a conserved function as a secreted signaling molecule (Tsuda et al., 2008). We have shown that VAP MSP domains (vMSPs) are cleaved from the transmembrane domain and secreted into the extracellular environment, where they bind to Eph receptors (EphRs) and other unidentified receptors (Miller et al., 2003; Tsuda et al., 2008). The secretion mechanism appears to be unconventional and cell type specific.

A P56S mutation in the human VAPB MSP domain causes amyotrophic lateral sclerosis (ALS) and late-onset spinal muscular atrophy (SMA), two neuropathies characterized by progressive muscle atrophy and motor neuron degeneration (Funke et al., 2010; Millecamps et al., 2010; Nishimura et al., 2004). $VAP^{P56S}$ causes VAP ubiquitination, recruitment of wild-type and mutant VAPs to cytoplasmic inclusions (Teuling et al.,

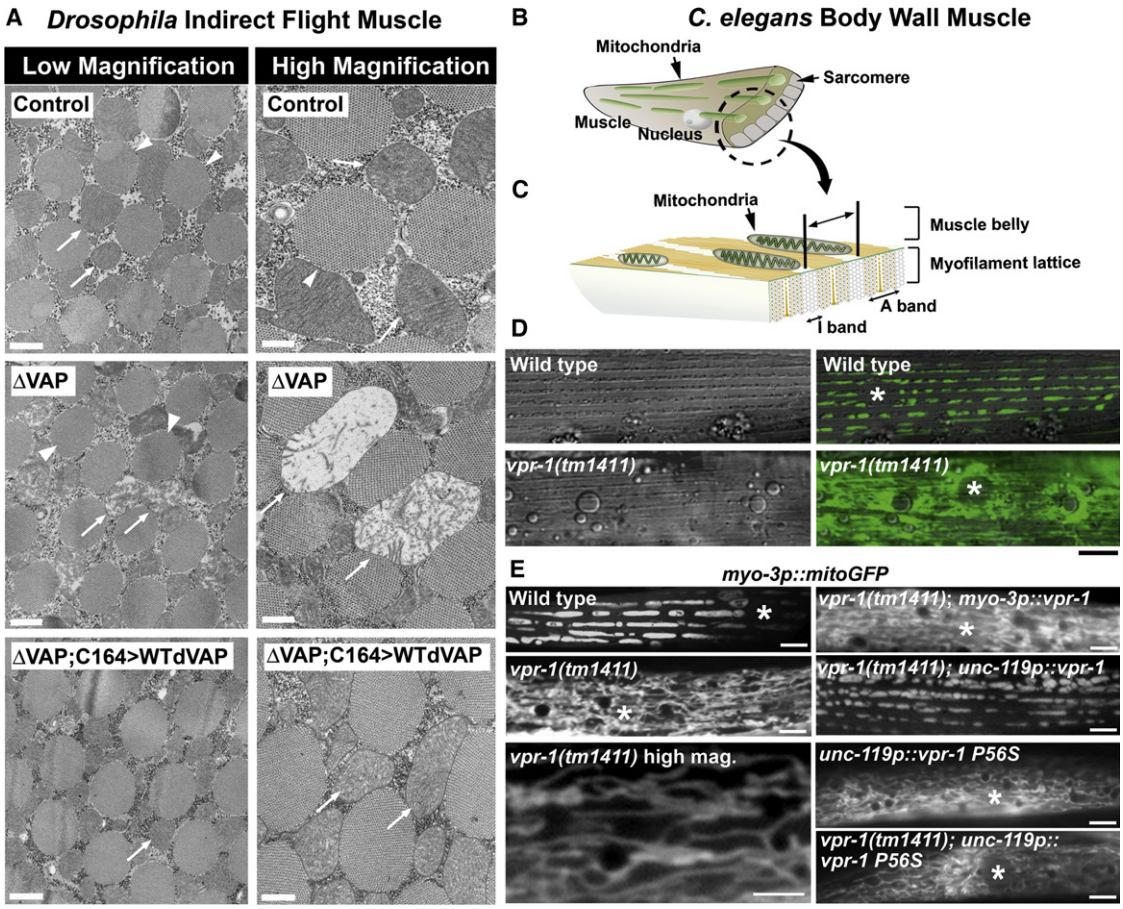


**Figure 1. Neuronal VAPs Modulate Striated Muscle Mitochondrial Morphology in *Drosophila* and *C. elegans***

(A) Transmission electron micrographs of adult IFM (dorsal ventral) in wild-type control and mutant flies. Arrowheads indicate myofibrils and arrows indicate mitochondria. ΔVAP indicates *dvap* null mutant and C164 > WTdVAP indicates wild-type dVAP expression using the neuronal GAL4 driver, C164 GAL4. Low magnification bars, 1.0 μm; high magnification bars, 0.5 μm.

(B and C) *C. elegans* body wall muscle cell diagrams showing mitochondrial arrays (B) and basic myofilament structure (C).

(D) Muscle mitochondria tubules visualized using mitochondrial matrix-targeted GFP (mitoGFP) and dense bodies (small bumps running in parallel) visualized using DIC imaging. Dense bodies occupy the center of the I-band. Quantification is shown in Table S1. Asterisks indicate nucleus. Bar, 5 μm.

(E) Mitochondrial networks in wild-type and mutant body wall muscle. Neuronal expression is driven with the *unc-119* promoter and muscle expression is driven with the *myo-3* promoter. Asterisks indicate nucleus. Bars, 5 μm.

2007; Tsuda et al., 2008), and impaired MSP domain secretion (Tsuda et al., 2008). VAPB levels are reduced in sporadic ALS patients, *sod1* mutant mice, and ALS8 patient motor neurons derived from induced pluripotent stems cells, suggesting that VAPB plays a widespread role in pathogenesis (Anagnostou et al., 2010; Mitne-Neto et al., 2011; Teuling et al., 2007).

Here, we present evidence that MSP domains comprise a conserved ligand class that modulates mitochondrial localization and morphology in muscle and oocytes. Neurons secrete vMSPs to promote mitochondrial docking at actin-rich I-bands of *C. elegans* striated muscle. vMSPs transduce signals through muscle Roundabout and Lar-like receptors that modulate the actin-related protein 2/3 (Arp2/3) complex. VAP loss causes aberrant Lar receptor and Arp2/3 activity that displaces mitochondria from I-bands, influences the fission/fusion balance, and decreases transmembrane potential. We propose that neurons secrete vMSPs to promote mitochondrial localization and function important for energy metabolism in muscles.

## RESULTS

### VAP Loss Causes Muscle Mitochondrial Defects in *Drosophila* and *C. elegans*

We previously documented that neuronal overexpression of dVAP, a *Drosophila* VAPB homolog (Pennetta et al., 2002), caused myofibrillar defects in the indirect flight muscle (IFM) of adult flies (Tsuda et al., 2008). This defect could be suppressed by Eph receptor knockout, suggesting that neurons secrete the dVAP MSP domain. The IFMs are massive and provide most of the energy needed for flight. To test whether VAP loss affects muscle, we examined the IFM in wild-type and *dvap* null mutant flies using transmission electron microscopy (TEM). In wild-type adults, TEM shows that the mitochondria are arranged in columns between the myofibrils (Figure 1A). In contrast, most mitochondria in *dvap* null mutant muscle are small and have abnormal cristae, whereas others are larger and have vacuole-like structures (Figure 1A; 84% of the

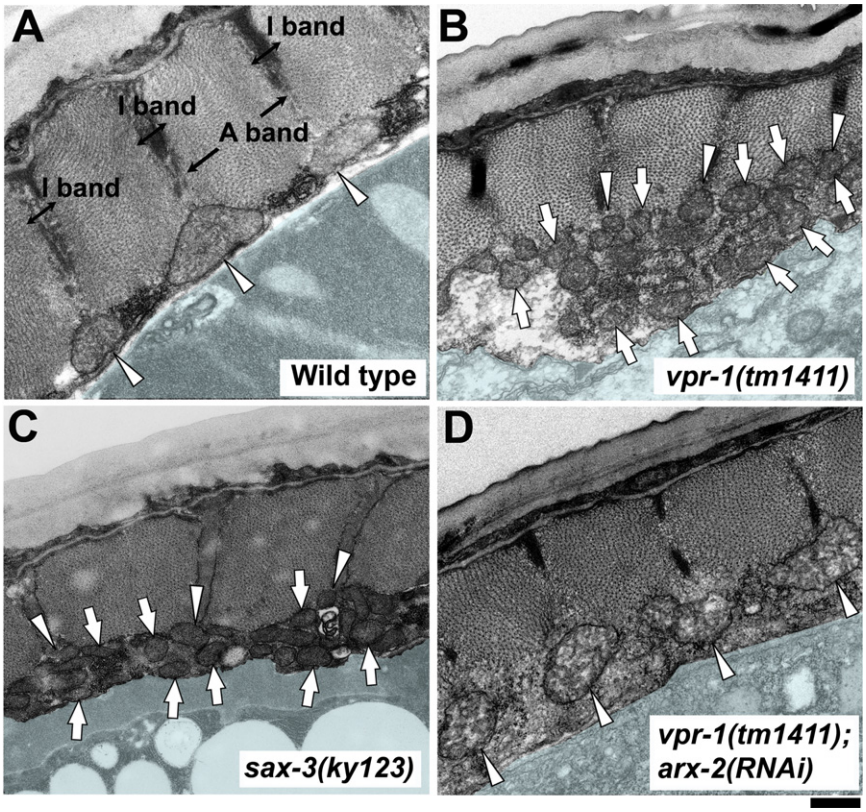


**Figure 2. Transmission Electron Micrographs of Wild-Type and Mutant *C. elegans* Muscle**

(A–D) Adult body wall muscle cross-sections are shown. Arrowheads point to mitochondria with I-band localization, whereas arrows point to mitochondria with abnormal localization. Light blue color demarcates muscle boundary. Bar, 0.5 μm.

mitochondria lack lamellar cristae, whereas 7% are enlarged, lack electron density, and are highly aberrant [n = 123]). The myofibrils, on the other hand, appear similar to control myofibrils. Hence, dVAP loss causes severe mitochondrial morphology defects in adult fly muscles.

Next, we examined adult *C. elegans* body wall muscle to test whether the role of VAPs (*vpr-1* in worms) is evolutionarily conserved. Mitochondria were visualized in live muscle by expressing mitochondrial matrix-targeted GFP (mitoGFP) under control of the *myo-3* muscle promoter, as well as by feeding worms the dyes MitoTracker CMXRos and Rhodamine 6g. In wild-type adults, muscle mitochondria form largely unbranched tubules within the belly (Figures 1B and 1C). 84.7% of these tubules in mitoGFP transgenic worms form linear arrays that are regularly spaced, correlating with the spacing between I-bands (Figures 1C and 1D; Table S1, line 1 available online). Indeed, the mitochondrial arrays overlap with the dense bodies, which occupy the middle of the I-band and appear as small bumps organized in the same orientation as the myofilaments (Figure 1D). Identical results are observed with MitoTracker CMXRos and Rhodamine 6g. Additional support for the association of mitochondria with I-bands comes from muscle TEM cross-sections (Figure 2A).

In contrast to wild-type, mitochondria in *vpr-1(tm1411)* mutants are not arranged in parallel arrays and are rarely associated with dense bodies (Figures 1D and 1E; Table S1, lines 1 and 2). Three-dimensional microscopy indicates that mitochondria form thin and highly branched tubular networks within the muscle belly (Figure 1E). TEM cross-sections confirm that mitochondrial tubules in *vpr-1* mutant muscle are smaller in diameter than controls and mostly displaced from the myofilaments (Figure 2B; Table S1, lines 1 and 2, $p < 0.001$). The muscle belly is expanded, in part due to abnormal actin branching (see below) and mitochondria rarely localize to I-bands. Muscle myofilaments, ER, and motor neuron positions in *vpr-1* mutants appear similar to the wild-type (Figure 2B; data not shown). Moreover, *vpr-1* mutants do not exhibit abnormal muscle ER homeostasis (S.M.H. and M.A.M., unpublished data). We conclude that *vpr-1* is required for formation of tubular and largely unbranched mitochondrial arrays positioned along the I-bands. Collectively, these data indicate that VAP loss in *Drosophila* and *C. elegans* causes specific defects in muscle mitochondrial morphology.

## VAP Mutants Have Interconnected Mitochondrial Networks

The mitochondrial tubules in *vpr-1* mutant muscle appear more fused than tubules in wild-type muscle (Figure 1E). RNAi of the outer membrane fission mediator *drp-1* and the inner membrane fusion mediator EAT-3/OPA1 can be used to shift the fission/fusion balance in mitochondrial networks (Kanazawa et al., 2008; Labrousse et al., 1999). Shifting the balance toward fusion in wild-type animals by *drp-1* RNAi causes the formation of elongated and branched networks similar to those in *vpr-1* mutants, except that the matrix often accumulates in large aggregates (Figure 3A). *drp-1* RNAi in *vpr-1* mutants also causes accumulation of identical aggregates. Shifting the balance toward fission in wild-type and *vpr-1* mutant animals by *eat-3/opa1* RNAi causes mitochondrial fragmentation (Figure 3A). These data suggest that muscle mitochondria in *vpr-1* mutants have low fission/fusion balance.

We tested whether or not the mitochondrial tubules in *vpr-1* mutants are physically connected to each other, consistent with their appearance in confocal axial scans. Fluorescence loss in photobleaching (FLIP) can be used to assess connectivity among muscle mitochondria. Our fluorescence recovery after photobleaching experiments (data not shown) and a previous study demonstrate that mitoGFP rapidly diffuses between contiguous compartments (Labrousse et al., 1999). In FLIP experiments, a mitochondrial tubule is repeatedly photobleached

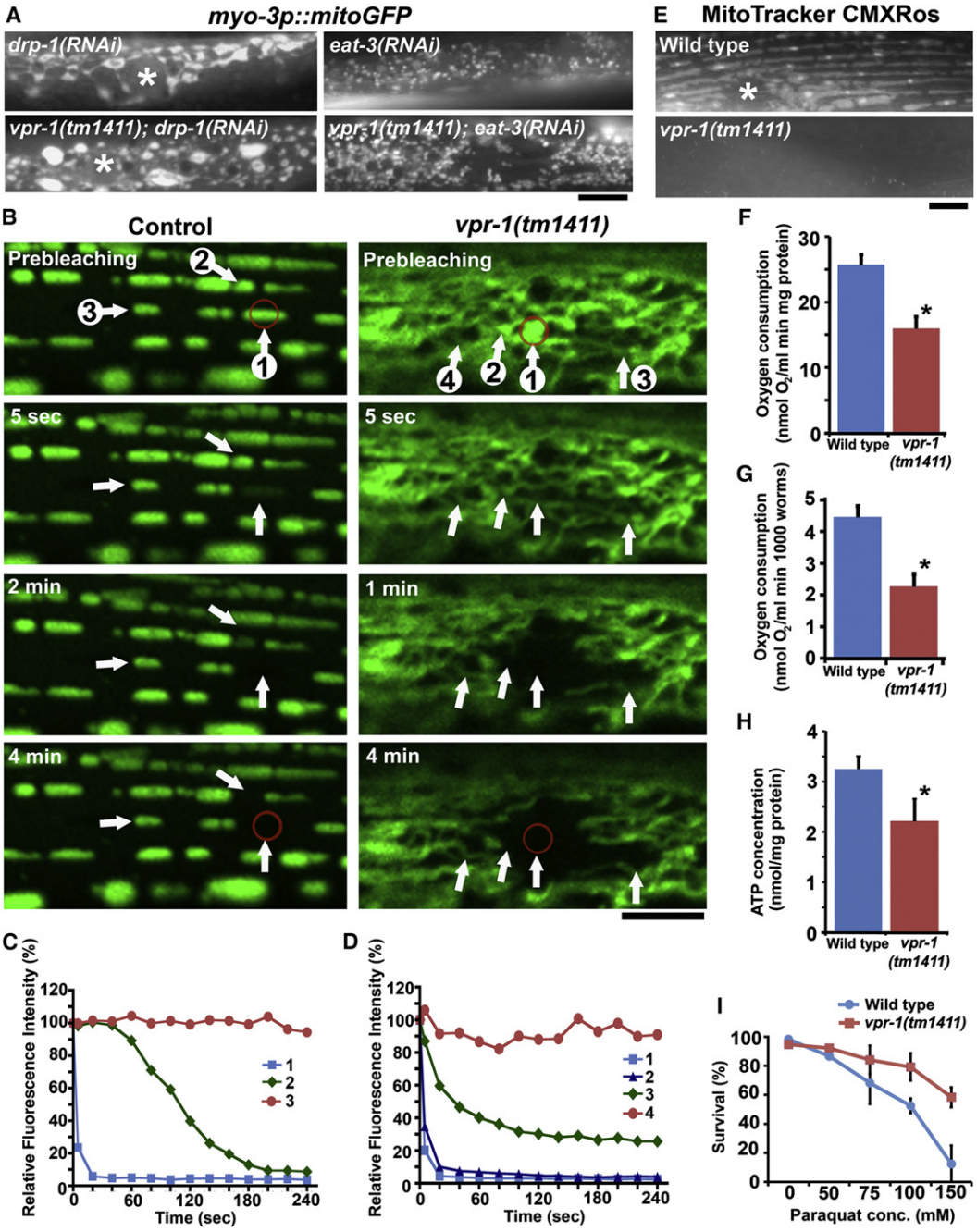


**Figure 3. *vpr-1* Loss Influences Muscle Mitochondrial Connectivity and Function**

(A) Genetic relationships between *vpr-1* and the mitochondrial fission mediator *drp-1* or the fusion mediator *eat-3*. Asterisks indicate nucleus. Bar, 5 μm.

(B) MitoGFP fluorescence loss in photobleaching of wild-type control and *vpr-1* mutant muscle. The red circle indicates the area of laser bleaching. Fluorescence was measured throughout the field after each 5 s cycle. Intensities of numbered spots are shown in (C) and (D). Bar, 5 μm.

(C and D) Quantification of fluorescence intensities in indicated mitochondria (B) of control (C) and *vpr-1* mutant (D) muscles.

(E) MitoTracker CMXRos staining of wild-type and *vpr-1(tm1411)* mutant muscle. Bar, 5 μm.

(F and G) Oxygen consumption rates of wild-type and mutant hermaphrodites. Consumption rates were normalized by protein content (F) or number of worms (G). *$p < 0.001$. Error bars represent SD.

(H) ATP concentration in wild-type and mutant hermaphrodite extracts. *$p < 0.001$ compared to wild-type. Error bars represent SD.

(I) Paraquat sensitivity in wild-type and *vpr-1(tm1411)* hermaphrodites. Error bars represent SD.

every 5 s followed by a scan of the surrounding area. Contiguous mitochondria lose fluorescence during each cycle, as mitoGFP diffuses into the bleached area. Thus, interconnected mitochondrial networks will exhibit rapid reduction in fluorescence outside of the bleached spot. To assess mitochondrial connectivity with FLIP, we used conditions that stabilize mitochondria and prevent

their mobility. FLIP in control muscles causes rapid fluorescence loss in the targeted area, but the vast majority of surrounding mitochondria retain their fluorescence, even after 48 cycles (Figures 3B and 3C). In 5 of 11 experiments, a single neighboring tubule lost fluorescence. The average bleached area in the 11 experiments was 7.8 $\mu m^2$, indicating that individual tubules have limited connectivity in wild-type muscle. In contrast to the wild-type, FLIP in *vpr-1* mutant muscles resulted in rapid loss of fluorescence in the targeted area and numerous surrounding mitochondrial tubules within 20 s of photobleaching initiation (Figures 3B and 3D). The average bleached area in nine experiments was 32.6 $\mu m^2$ ($p < 0.001$ compared to the control). We calculated that each *vpr-1* mutant muscle contains between 20 and 25 contiguous subpopulations of mitochondria, whereas each wild-type muscle contains more than 100 subpopulations (based on an average muscle area of 800 $\mu m^2$). Therefore, mitochondrial networks in *vpr-1* mutant muscle exhibit increased connectivity relative to networks in wild-type muscle. This increase in connectivity may be due to an increase in fusion, reduction in fission, or both.

Mitochondrial dynamics can be observed in live animals using time-lapse fluorescence microscopy. Mitochondria in wild-type muscle appear stably docked at I-bands (Movie S1). Shape changes and fission gradually reduce tubule length over time during imaging. In *vpr-1* mutants, mitochondrial tubules exhibit increased mobility (Movie S2) and occasionally form ring-shaped structures that join other tubules or collapse (Figure S1A; Movie S3). Tubules move at speeds between 0 and 2.0 $\mu m$/min, although only a fraction of tubules are mobile under our conditions. We noticed that fission sites in wild-type muscle are different than sites in *vpr-1* mutant muscle. In the control, fission primarily occurs within elongated tubules (29/29 fission events from eight videos). However, fission rarely occurs within elongated tubules in *vpr-1* mutants (1/12 fission events from eight videos) and instead occurs at connection sites between tubules (Movie S4). We conclude that mitochondria in *vpr-1* mutants are more mobile and have different fission sites relative to mitochondria in wild-type muscle. Taken together, the results support the model that VPR-1 influences the fission/fusion balance.

## VAP Mutants Have Impaired Mitochondrial Function

The abnormal mitochondrial morphology in *vpr-1* mutants raises the possibility that their function is impaired. To evaluate muscle mitochondrial function, we used MitoTracker CMXRos, which concentrates in the mitochondrial matrix depending on transmembrane potential (Pendergrass et al., 2004). MitoTracker accumulation in *vpr-1* mutant muscle mitochondria is reduced compared to accumulation in controls (Figure 3E). We found that *drp-1* RNAi could increase MitoTracker accumulation, suggesting that matrix aggregation caused by DRP-1 loss can partially restore mitochondrial transmembrane potential in *vpr-1* mutants (Figure S1B). Importantly, this MitoTracker accumulation defect can be fully suppressed (see below), indicating that *vpr-1* mutants are not deficient in dye uptake or muscle transport.

Worms with reduced mitochondrial respiration should consume less oxygen and generate less ATP. Indeed, *vpr-1* mutants consume less oxygen than controls, whether the data are normalized to protein content (Figure 3F) or worm number (Figure 3G). ATP concentration in 1-day-old adult *vpr-1* mutants is significantly reduced compared to adult controls (Figure 3H). We previously showed that sperm-derived MSPs promote reactive oxygen species (ROS) production in oocytes (Yang et al., 2010). *vpr-1* mutants are more resistant than the wild-type to paraquat, which generates intracellular ROS that cause a concentration-dependent toxicity depending on endogenous ROS levels (Figure 3I). Hence, *vpr-1* mutants have reduced ROS, which could be due to decreased production or increased breakdown. These independent metabolic assays support the hypothesis that *vpr-1* mutants have altered mitochondrial function.

Inhibition of mitochondrial electron transport chain (ETC) activity causes defects such as sluggish motility, reduced swimming rate in liquid, prolonged defecation cycle, reduced brood size, slow development, and larval arrest (Tsang and Lemire, 2003; Wong et al., 1995a). In particular, muscle-specific ETC inhibition affects motility, brood size, and possibly defecation and development rate (Durieux et al., 2011). Thus, *vpr-1* mutants should exhibit some of these defects if their mitochondria have reduced respiration, as indicated by the metabolic assays. Indeed, *vpr-1* null mutants exhibit sluggish motility, reduced swimming rate (99.7 ± 9.4 thrashes/min for *vpr-1(tm1411)* versus 125.3 ± 11.8 thrashes/min for wild-type; $p < 0.005$), prolonged defecation cycle (59.9 ± 7.2 s for *vpr-1(tm1411)* versus 55.0 ± 7.1 s for wild-type; $p < 0.01$), sterility, and slow development (57.7 ± 3.9 hr for *vpr-1(tm1411)* versus 42 hr for wild-type; $p < 0.001$). We conclude that *vpr-1* mutants have defects consistent with abnormal mitochondrial function in muscle and possibly other cell types.

## Secreted Neuronal vMSPs Modulate Muscle Mitochondrial Position and Morphology

Our previous studies showed that VAP MSP domains are secreted in a cell type-specific fashion (Tsuda et al., 2008). However, VAPs can also have cell autonomous functions. To determine the site(s) where VAPs function, we first examined *Drosophila*. Expressing dVAP in muscle of *dvap* null mutant flies using the *MHC-GAL4* driver causes 100% lethality and does not rescue *dvap* mutant defects. In contrast, expressing dVAP using neuronal drivers, including *C164-GAL4* and *Elav-GAL4*, rescues the lethality (Chai et al., 2008; Tsuda et al., 2008) and nearly 100% of muscle mitochondrial defects associated with *dvap* loss (Figure 1A; data not shown). These data indicate that dVAP functions in a cell nonautonomous fashion, consistent with a signaling role.

Next, we examined the mechanism by which VPR-1 acts on muscle in *C. elegans*. Transgenic GFP reporters driven by upstream *vpr-1* genomic sequence show broad expression in adults, including the ventral nerve cord and body wall muscle (Figure S2), similar to *Drosophila* dVAP. However, *vpr-1* expression in muscles using the *myo-3* promoter or intestine using the *ges-1* promoter does not affect muscle mitochondrial shape or distribution in the mutants (Figure 1E; Figure S1C). In contrast, *vpr-1* expression in neurons with the *unc-119* pan-neuronal promoter rescues mitochondrial morphology, distribution, and I-band position (Figures 1E) in ~30%–40% of muscles, while most remaining muscles exhibit improved phenotypes. The incomplete rescue may be due to transgene expression mosaicism, overexpression, or missing untranslated regulatory

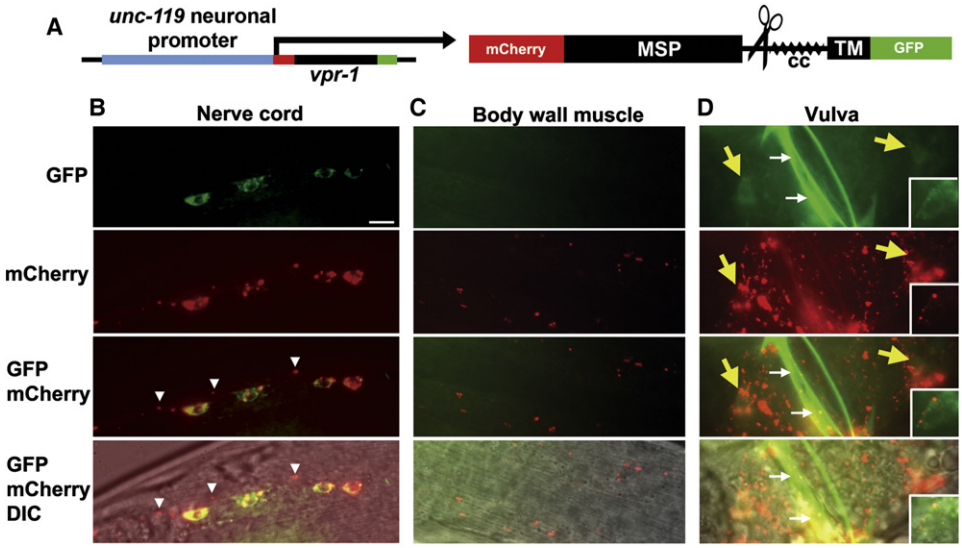


**Figure 4. VAP Cleavage and Secretion in *C. elegans* Neurons**

(A) Diagrams of the mCherry::VPR-1::GFP fusion protein driven specifically in neurons. Scissors show region of cleavage. cc, coiled-coil domain.

(B) Fusion protein expression in nerve cord motor neurons. Arrowheads indicate examples of mCherry/MSP-containing complexes that lack GFP-containing sequences. Bar, 5 μm.

(C) Fusion protein localization outside of neuronal cell bodies.

(D) Fusion protein localization in the vulva region. VC4 and VC5 motor neuron cell bodies (yellow arrows) are in the background (behind the focal plane). Inset shows the HSN motor neuron cell body. Longer mCherry exposure times show mCherry colocalization with GFP in the cytoplasm. The vulva lip exhibits nonspecific autofluorescence seen in nontransgenic controls (white arrows).

sequences, as neuronal expression in flies rescues nearly 100% of mitochondrial defects and neuron-specific VPR-1 inhibition causes mitochondrial defects in nearly all muscle (data not shown and see below). We conclude that VAPs are required in neurons to control muscle mitochondrial position and shape.

The above data are consistent with neurons secreting vMSP domains to regulate muscle mitochondria. To further test this model, we inhibited neuronal vMSP secretion in wild-type worms. The VAP$^{P56S}$ mutation acts as a dominant negative, sequestering wild-type VAP in neuronal aggregates (Ratnaparkhi et al., 2008; Teuling et al., 2007) and preventing secretion of the wild-type protein (Tsuda et al., 2008). Neuronal VPR-1$^{P56S}$ overexpression causes muscle mitochondria to form thin, branched, and abnormally distributed networks within the muscle belly, similar to *vpr-1* null mutants (Figure 1E). When we overexpressed neuronal VPR-1$^{P56S}$ in *vpr-1* null mutants, muscle mitochondria were identical to those seen in nontransgenic *vpr-1* mutant controls. These data confirm that VPR-1$^{P56S}$ acts as a dominant negative and support the model that neurons secrete vMSPs to regulate muscle mitochondria.

*C. elegans*, *Drosophila*, and mammalian VAPs are cleaved between the MSP domain and the transmembrane domain (Gkogkas et al., 2011; Tsuda et al., 2008). Previously, we documented vMSP secretion in *Drosophila* wing disc cells by expressing a dVAP fusion protein with distinct N-terminal and C-terminal tags (Tsuda et al., 2008). Only the N-terminal tag containing the MSP domain was secreted. We used a similar strategy to test whether *C. elegans* neurons secrete the VPR-1 MSP domain. mCherry was fused to the N-terminus of VPR-1 and GFP to the C terminus and this mCherry::VPR-1::GFP fusion protein was expressed in neurons using the *unc-119* promoter (Figure 4A). While partial colocalization of mCherry and GFP was observed in motor neuron cell bodies (and other neuron bodies), mCherry was observed within axons and in the extracellular environment (Figures 4B–4D). GFP does not colocalize with most axonal mCherry, nor does it colocalize with extracellular mCherry, indicating that the VPR-1 fusion protein is cleaved. Secreted mCherry/MSP fragments were observed at the body wall and vulval muscles (Figures 4C and 4D). mCherry also accumulated in the coelomocytes, mesodermal cells that nonspecifically endocytose fluid, and secreted molecules within the body cavity (data not shown) (Fares and Greenwald, 2001). Taken together, these results provide strong evidence that neurons secrete vMSPs.

## An MSP Receptor Screen Identifies SAX-3 Robo and CLR-1 Lar Receptors

An important prediction based on above data is that secreted vMSPs regulate a muscle receptor pathway(s) that transduces signals to mitochondria. vMSPs bind to EphRs and other unidentified receptors (Miller et al., 2003; Tsuda et al., 2008). However, EphR loss in *C. elegans* or *Drosophila* does not influence muscle mitochondria or mitochondria-related phenotypes (data not shown), suggesting that an unknown receptor(s) mediates this signaling mechanism. We previously developed an MSP receptor identification assay based on the ability of recombinant MSP domains conjugated to fluorescein (MSP-FITC) to specifically bind to receptors expressed in oocytes (Miller et al., 2003; Figures S3A and S3B). In the worm gonad, sperm secrete MSPs to induce oocyte maturation (Figure 5A), which involves

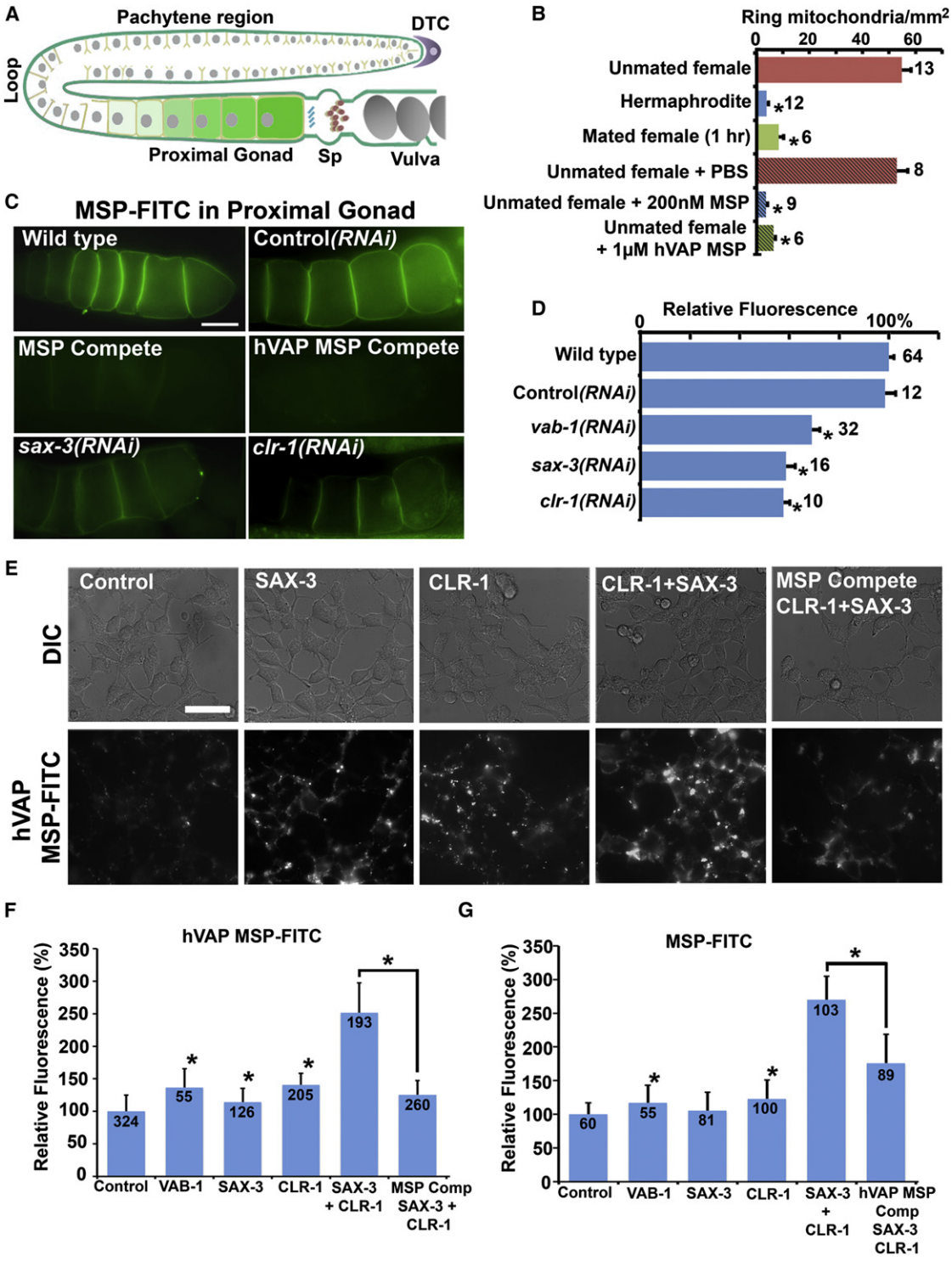


**Figure 5. An MSP Receptor Screen Identifies SAX-3 Robo and CLR-1 Lar-Like Receptors**

(A) Diagram of the *C. elegans* adult gonad. Mitochondrial morphology and MSP domain binding were quantified in oocytes colored green (B–D and Figure S4). DTC, distal tip cell; Sp, spermatheca.

(B) Quantification of ring-shaped mitochondria per $mm^2$ oocyte area in the presence and absence of extracellular MSP domains introduced by mating and microinjection. MSP domains were injected through the vulva into the reproductive tract of unmated females lacking sperm. See Figures S4A–S4D for representative pictures of oocyte mitochondria. *$p < 0.001$ compared to unmated female controls. Error bars represent SEM.

(C) Two hundred nanomolar MSP-FITC binding to oocyte plasma membranes. In the compete panels, a 20-fold molar excess of unlabelled MSP or hVAP MSP was added before the assay. Quantitative data is shown in (D). Proximal is to the right, as shown in (A) (green). Bar, 20 μm.

metabolic changes (Han et al., 2010; Yang et al., 2010). Under conditions where all MSP receptor sites are occupied, MSP-FITC binding to oocytes is reduced by ~35% when the VAB-1 EphR is absent (Miller et al., 2003). The remaining binding is due to unidentified MSP domain receptors. Sperm-derived MSPs and VAP MSP domains bind to identical receptors expressed in oocytes (Miller et al., 2003; Tsuda et al., 2008). We hypothesized that both oocytes and muscle express MSP domain receptors that transduce signals to mitochondria. Support for this hypothesis comes from examining the effects of extracellular MSP addition to oocyte mitochondria. Microinjecting MSPs and human vMSPs into the extracellular spaces of spermless reproductive tracts induces a rapid transition (<15 min) in oocyte mitochondria from ring-shaped to branched, tubular forms (Figures 5A and 5B; Figures S4A–S4D). These shape changes, as well as MSP-induced mitochondrial transport into growing oocytes (Govindan et al., 2009; Wolke et al., 2007), are dependent on *drp-1* (Figures S4E and S4F). Identical shape changes in oocyte mitochondria occur when sperm presence is manipulated through mating (Figure 5B; Figures S4B–S4D). Thus, oocytes likely express MSP receptors that rapidly regulate mitochondrial shape.

To identify MSP domain receptors important for mitochondria, we compared genome-wide DNA microarray data sets of adult hermaphrodites undergoing oogenesis to those undergoing spermatogenesis (Reinke et al., 2004). MSPs bind to oocyte plasma membranes, but not to sperm plasma membranes (Miller et al., 2003). From the top 3000 oogenesis/spermatogenesis-enriched genes, we identified 40 genes that encode cell surface receptors (Table S2). These genes are not specifically expressed in oocytes; many are also expressed in neurons and muscle. We screened RNAi clones corresponding to the 40 predicted receptors to identify clones that cause reduced MSP-FITC binding to oocytes and mitochondrial shape or positioning defects in oocytes and muscle (Table S2). The only RNAi clones that affected both MSP binding and muscle mitochondria corresponded to the SAX-3 Roundabout (Robo) and CLR-1 Lar-like (Lar) receptors (Figures 5C and 5D; Table S2; Kokel et al., 1998; Zallen et al., 1998). Analysis of *clr-1* and *sax-3* mutants confirmed that both receptors are required for MSP-FITC binding and muscle mitochondrial morphology (see below). Previous studies have shown that SAX-3 Robo and CLR-1 Lar are expressed in oocytes, motor neurons, and body wall muscle (Chang et al., 2004; Kohara, 2001; Zallen et al., 1998).

SAX-3 or CLR-1 loss causes a significant reduction in MSP-FITC binding to oocytes, similar to loss of the MSP/ephrin receptor VAB-1 (Figures 5C and 5D). To test whether CLR-1 Lar or SAX-3 Robo expression is sufficient to promote MSP binding, we expressed these receptors alone and in combination in cultured HEK293 cells (Figures 5E–5G). Expressing the VAB-1 EphR in cultured cells confers increased MSP-FITC cell surface binding and rapid internalization in live cells (Miller et al., 2003). We found that CLR-1 Lar expression resulted in the same significantly increased level of MSP-FITC and vMSP-FITC binding as the VAB-1 EphR positive control, whereas Robo expression resulted in a weak increase relative to the negative control (Figures 5E–5G). However, expressing both SAX-3 Robo and CLR-1 Lar together caused a synergistic increase in MSP and vMSP binding, which could be inhibited by incubating cells with an excess of unlabelled MSP (Figures 5E–5G). These data support the model that Robo and Lar function together to promote vMSP binding. Consistent with this idea, SAX-3 and CLR-1 loss synergistically affects human vMSP binding to *C. elegans* oocytes (Figures S3C and S3D). In summary, our screen identified SAX-3 Robo and CLR-1 Lar, perhaps acting via a receptor complex, as candidates for mediating VAP signaling to muscle mitochondria.

## SAX-3 Robo and CLR-1 Lar Function in Muscle to Influence Mitochondria

To specifically evaluate muscle mitochondria in *sax-3* Robo and *clr-1* Lar mutants, we generated *myo-3p::mitoGFP* transgenic lines. *sax-3(ky123)* mutants have incompletely penetrant and variably expressed mitochondrial defects [63.7% of *sax-3(ky123)* muscles affected (n = 55) versus 100% for *vpr-1* mutants [n > 400]). The affected muscles have mitochondrial networks nearly identical to *vpr-1* mutants, including abnormally positioned elongated mitochondria with excess branching (Figure 6A; Table S1, lines 1–3). TEM cross-sections of *sax-3* mutant muscle show that mitochondria are smaller in diameter than controls and mostly displaced from the I-bands, similar to *vpr-1* mutants (Figures 2A–2C). However, the muscle belly is less swollen than *vpr-1* mutants and not all *sax-3* mutant muscles are affected, consistent with the presence of a second vMSP receptor. The *sax-3(ky123)* mutant defects were rescued with a fosmid containing the *sax-3* genomic locus, indicating that the defects are due to loss of SAX-3 Robo (Figure 6A). Temperature shift experiments using the *sax-3(ky200)ts* hypomorphic temperature sensitive (ts) allele indicate that *sax-3* is required postembryonically (Figure 6A). We also tested the gene encoding the Slit ligand for SAX-3 Robo and did not detect mitochondrial defects in *slt-1(eh15)* null mutants (Figure 6A). As *slt-1* is the only Slit homolog present in *C. elegans* (Hao et al., 2001), SAX-3 does not require Slits for regulating muscle mitochondrial morphology. Therefore, *sax-3* Robo influences muscle mitochondrial shape and positioning independent of Slit.

Next, we evaluated metabolic status in *sax-3* Robo mutants. MitoTracker CMXRos staining indicated that *sax-3(ky123)* mutants have a variably expressed transmembrane potential defect (Figure 6B) where the more severe cases resemble

(D) Quantitative MSP-FITC binding data for control and selected RNAi clones (n is to the right of error bars). *p < 0.001 compared to wild-type. Error bars represent SEM.

(E) Two hundred nanomolar human VAP MSP-FITC was incubated with control transfected and receptor transfected HEK293T cells for 30 min, washed three times, and mounted for microscopy. vMSP-FITC was found at the cell surface and in intracellular vesicles of live cells. In the compete panel, a 20-fold molar excess of unlabelled MSP was added before the assay. Bar, 50 μm.

(F) Quantification of human VAP MSP-FITC fluorescence. *p < 0.001 compared to control. Number of cells measured is shown below error bars, which represent SD.

(G) Quantification of MSP-FITC fluorescence. *p < 0.001 compared to control. Number of cells measured is shown below error bars, which represent SD.

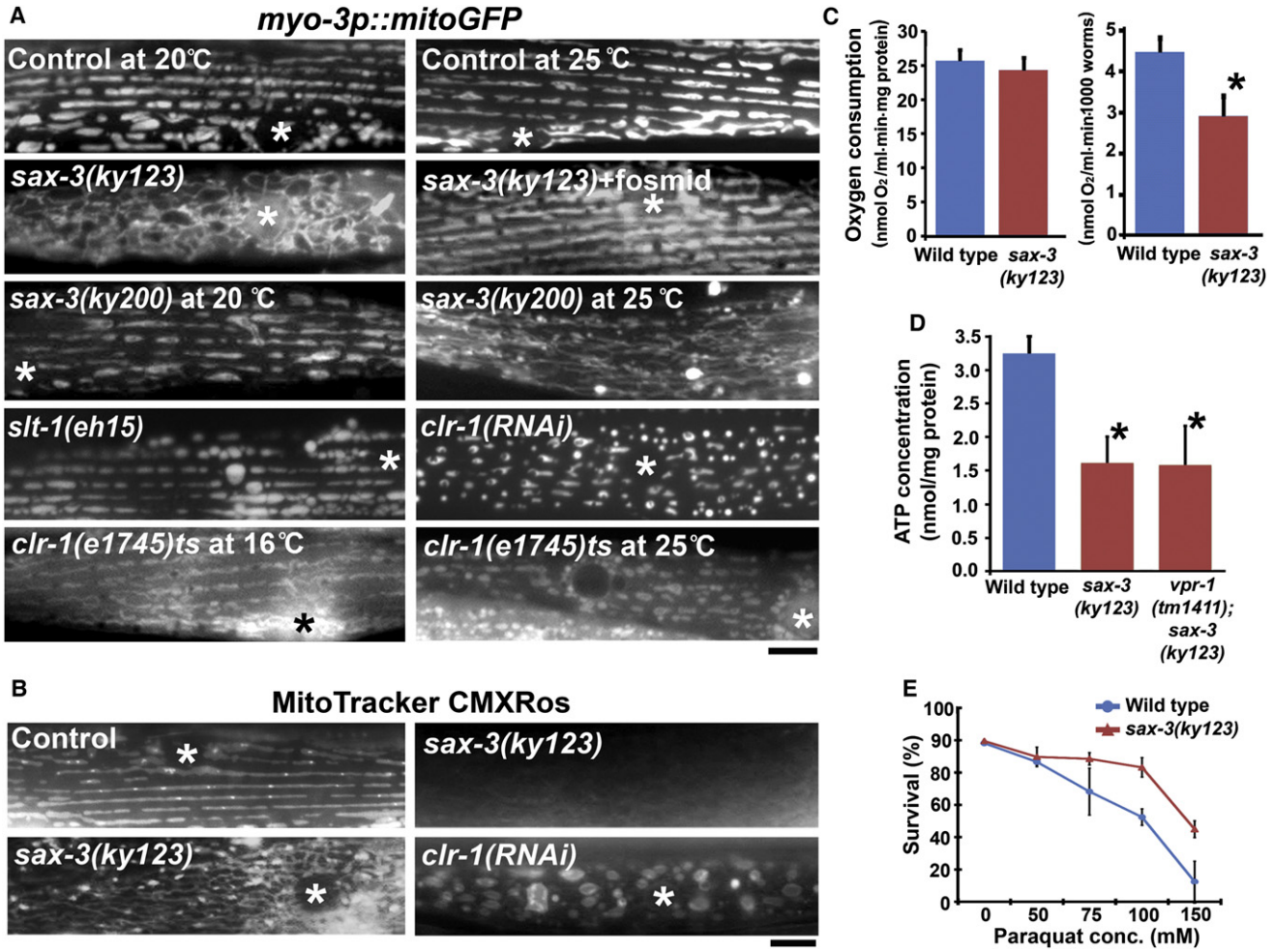


**Figure 6. *sax-3* Robo and *clr-1* Lar-like Receptor Mutant Phenotypes**

(A) Muscle mitochondrial networks in wild-type control and mutant hermaphrodites. Fosmid indicates expression of a transgene containing the *sax-3* genomic locus. *sax-3(ky200)ts* mutants were shifted to the nonpermissive temperature (25°C) at the L1 stage and scored in 1 day adults. *clr-1(e1745)ts* mutants were shifted to the nonpermissive temperature (25°C) in young adults and scored 12 hr later. Asterisks indicate nucleus. Bar, 5 μm.

(B) MitoTracker CMXRos staining of live muscles. Asterisks indicate nucleus. Bar, 5 μm.

(C) Oxygen consumption rates of wild-type and *sax-3* mutant 1-day-old adults. Consumption rates were normalized to protein content (left) or worm number (right). *$p < 0.005$ compared to wild-type. Error bars represent SD.

(D) ATP concentration in wild-type and mutant hermaphrodite extracts. *$p < 0.001$ compared to wild-type. Error bars represent SD.

(E) Paraquat sensitivity in wild-type and *sax-3(ky123)* hermaphrodites. Error bars represent SD.

*vpr-1* mutants. Adult *sax-3* mutants consumed less oxygen than controls, but contained less total protein, so the interpretation depends on the normalization method (Figure 6C). Compared to wild-type controls, *sax-3* mutants had reduced ATP concentration (Figure 6D), increased resistance to paraquat (Figure 6E), and slower growth [53.8 ± 3.6 hr for *sax-3(ky123)* versus 42 hr for wild-type; $p < 0.001$]. These data indicate that *sax-3* mutants have metabolic or mitochondrial defects that are similar to *vpr-1* mutants, but most defects are less severe or occur with reduced frequency.

*sax-3* Robo is expressed in motor neurons and body wall muscle (Chang et al., 2004; Kohara, 2001; Zallen et al., 1998). To test whether *sax-3* functions in muscle, we conducted two experiments. In the first, we expressed SAX-3 specifically in muscle of *sax-3(ky123)* mutants using the *myo-3* promoter. Muscle-specific SAX-3 expression strongly rescued the *sax-3(ky123)* muscle mitochondrial defects (Figure 7A; rescue observed in 27/31 transgenic worms). Next, we specifically depleted SAX-3 in body wall muscle of wild-type worms using an RNAi mosaic strategy (Durieux et al., 2011; Esposito et al., 2007). *sid-1* mutants are defective for systemic RNAi, yet undergo cell autonomous RNAi normally (Winston et al., 2002). We specifically expressed *sax-3* sense and antisense RNAs (creating dsRNA) in *sid-1(pk3321)* muscle and examined their mitochondria. Muscle-specific *sax-3* RNAi caused mitochondrial defects nearly identical to those seen in *sax-3* mutants (Figure 7A). These results indicate that *sax-3* functions cell autonomously in body wall muscle to influence mitochondria.

Our RNAi screen also identified the CLR-1 Lar receptor as a muscle mitochondrial regulator. In *clr-1* RNAi and

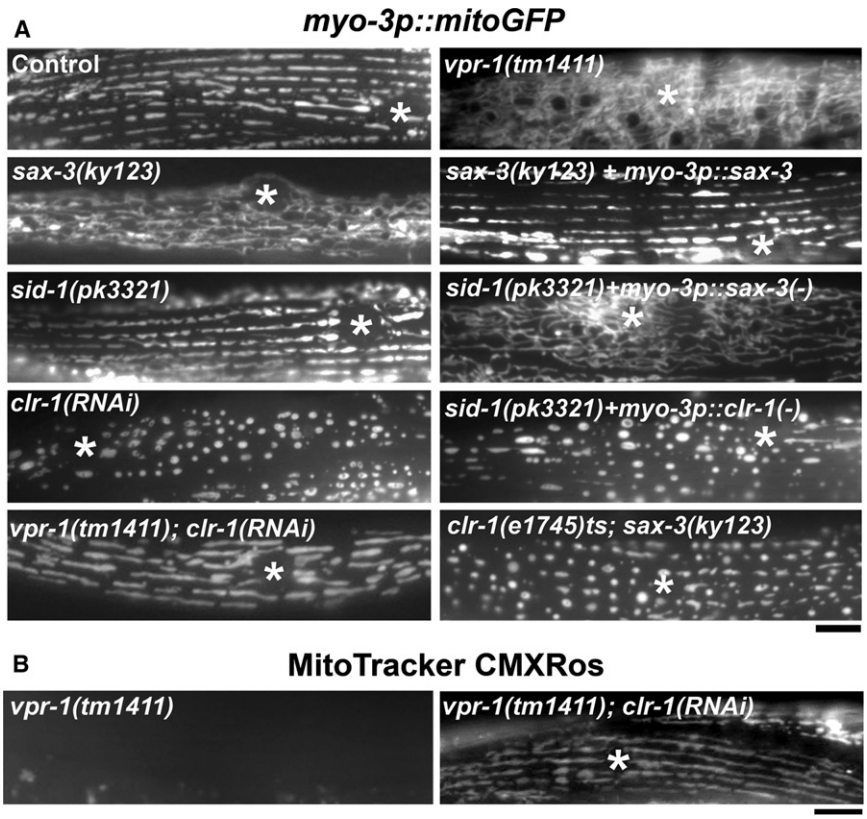


**Figure 7. *sax-3* Robo and *clr-1* Lar Site of Action and Signaling Hierarchy**

(A) Muscle mitochondrial networks in wild-type control and mutant hermaphrodites. The *myo*-3 promoter was used to drive *sax-3* cDNA, *sax-3* antisense/sense RNAi (−), or *clr-1* antisense/sense RNAi (−) expression specifically in body wall muscle. *sid-1(pk3321)* mutants are defective for systemic RNAi, but cell autonomous RNAi occurs normally. *clr-1(e1745)ts; sax-3(ky123)* mutants were scored at the nonpermissive temperature. Unlike mitochondria in *vpr-1(tm1411); clr-1* RNAi mutants, mitochondria in *clr-1(e1745)ts; sax-3(ky123)* mutants fail to elongate on the I-bands. Asterisks indicate nucleus. Bar, 5 μm.

(B) MitoTracker CMXRos staining of live muscles. Asterisks indicate nucleus. Bar, 5 μm.

*clr-1(e1745)ts* mutant adults, most mitochondria are positioned at the I-bands, but tubule length is much shorter than in the wild-type (Figure 6A; Table S1, lines 1 and 4). Despite the abnormal appearance of mitochondria, MitoTracker CMXRos staining did not show decreased transmembrane potential (Figure 6B). *clr-1* is an essential gene required in hypodermal cells for fluid balance and the *e1745* allele is temperature sensitive (Huang and Stern, 2004; Kokel et al., 1998). We conducted temperature shift experiments to assess the temporal requirement of *clr-1* function. At the permissive temperature, *clr-1(e1745)ts* adult muscles contain mostly tubular mitochondria similar to the wild-type. When young adults were shifted to the restrictive temperature for 12 hr, globular mitochondria were observed similar to *clr-1* RNAi animals (Figure 6A). These results demonstrate that CLR-1 Lar is required in adults to maintain mitochondrial elongation on the I-bands. To test whether *clr-1* functions in muscle, we specifically depleted *clr-1* in body wall muscle using the *sid-1* mutant RNAi mosaic strategy. Muscle-specific CLR-1 depletion caused the same mitochondrial defects as those seen in *clr-1* RNAi and *clr-1(e1745)* mutants (Figure 7A). In contrast, hypodermis-specific *clr-1* RNAi caused fluid accumulation, but not muscle mitochondrial defects (data not shown). Taken together, the data indicate that SAX-3 Robo and CLR-1 Lar function in muscle to influence mitochondria.

## VPR-1 and SAX-3 Robo Antagonize CLR-1 Lar Signaling

Our data indicate that SAX-3 Robo and CLR-1 Lar function in muscle, yet their mutant phenotypes are clearly different (Figure 6A). The *sax-3* mutant mitochondrial defects are nearly identical to the *vpr-1* mutant defects. To examine the signaling hierarchy between *vpr-1* and *sax-3*, we compared single and double null mutant strains. TEMs show that mitochondrial shape, including cross-sectional area, and positions in the double mutants are identical to single null *vpr-1* mutants (Table S1, lines 2 and 5, $p > 0.1$; data not shown). In addition, ATP concentration in *vpr-1(tm1411); sax-3(ky123)* double mutants is not significantly different than *sax-3(ky123)* null mutants (Figure 6D). Unfortunately, we were unable to generate mitoGFP transgenic lines in the double mutants. Taken together with the binding data, the results support the model that vMSPs positively regulate SAX-3 Robo.

Robo receptors antagonize Lar receptor signaling during *C. elegans* and *Drosophila* growth cone guidance decisions (Chang et al., 2004; Sun et al., 2000). Consistent with this relationship, the globular mitochondrial morphology in *clr-1* Lar mutants contrasts with the elongated morphology in VAP and Robo mutants (Figures 1E and 6A). To examine the signaling hierarchy, we compared *vpr-1(tm1411); clr-1* RNAi mutants to *vpr-1(tm1441)* mutants using the mitoGFP marker. *clr-1* loss strongly suppresses the muscle mitochondrial defects of *vpr-1* mutants (Figure 7A; Table S1, lines 6 and 2) and muscle mitochondria in *vpr-1(tm1411); clr-1* RNAi mutants are similar in morphology and distribution to mitochondria in wild-type hermaphrodites. Importantly, they are also positioned at muscle I-bands (Table S1, line 6). MitoTracker CMXRos staining and time-lapse imaging indicate that *clr-1* loss suppresses the mitochondrial transmembrane potential and mobility defects of *vpr-1* mutants (Figure 7B and data not shown). Thus, muscle mitochondria in *vpr-1(tm1411); clr-1* RNAi animals are largely normal. This important result indicates that excess CLR-1 activity specifically causes the *vpr-1* mutant muscle mitochondrial defects. Hence, VPR-1 antagonizes Lar signaling in muscle. Moreover, a redundant mechanism must exist that positions mitochondria in the absence of VPR-1 and CLR-1.

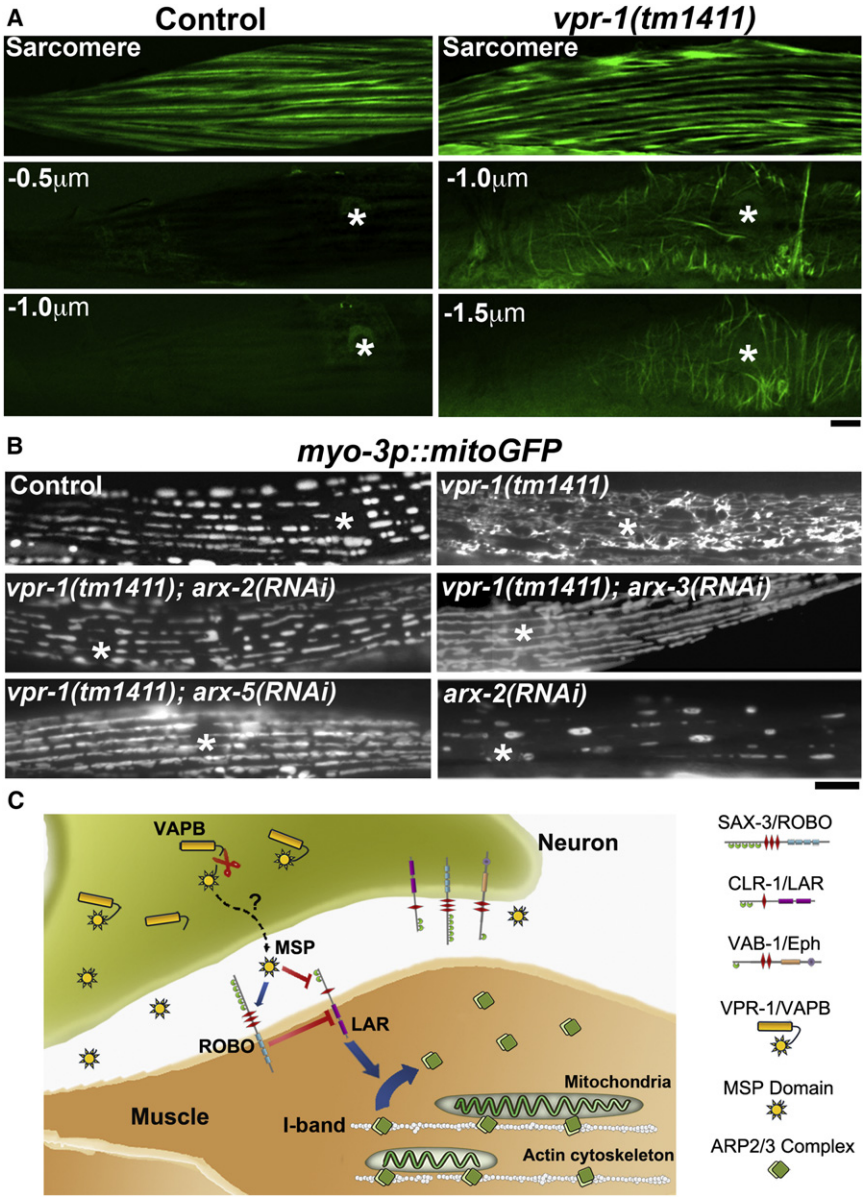


**Figure 8. VAP Regulation of Arp2/3 Complex Activity and Working Model**

(A) Filamentous actin distribution in wild-type and *vpr-1* mutant muscle, observed using muscle-specific expression of the moesin actin binding domain fused to GFP. Deconvolved images from axial scans are shown. Belly panels are shown with distances beneath the sarcomere or myofilaments. Asterisks indicate nucleus. Bar, 5 μm.

(B) Muscle mitochondrial networks in wild-type control and mutant/RNAi hermaphrodites. Asterisks indicate nucleus. Bar, 5 μm.

(C) Working model. See text for details.

The data support the model that SAX-3 Robo helps vMSPs antagonize CLR-1 Lar signaling. To further test this model, we generated *clr-1(e1745)ts; sax-3(ky123)* double mutants that express mitoGFP. The mitochondrial branching and elongation defects caused by *sax-3* loss are suppressed in the double mutant adults (Figure 7A). Furthermore, mitochondria in the double mutants localize correctly to the I-bands. Therefore, VPR-1 and SAX-3 Robo antagonize CLR-1 Lar signaling in muscle to position mitochondria at I-bands. The simplest interpretation is that SAX-3 Robo facilitates vMSP binding to CLR-1 Lar or SAX-3/CLR-1 complexes.

## VAP/Robo/Lar Signaling Modulates the Arp2/3 Complex

Robo and Lar-like growth cone guidance receptors regulate the actin cytoskeleton, which can influence mitochondrial localization, either through direct interactions with F-actin or myosin motors (Boldogh and Pon, 2007; Pathak et al., 2010). To examine actin distribution in body wall muscle, we expressed the filamentous actin binding domain of moesin fused to GFP (Figure 8A). In wild-type muscle, actin was observed in parallel arrays comprising the thin filaments, an I-band component. Little filamentous actin was observed in the muscle belly. While no difference in actin was observed in the sarcomeres of wild-type and *vpr-1* mutant muscle, the latter had extensive actin networks within the muscle belly (Figure 8A). These ectopic actin networks occupy the same position as mitochondria, suggesting that their locations are mechanistically linked. Consistent with this idea, RNAi of genes encoding regulators of the actin cytoskeleton, including known downstream mediators of Robo and Lar receptor signaling, caused muscle mitochondrial defects (Figure S5).

The Arp2/3 complex promotes actin nucleation and branching. Given the branched filament networks in *vpr-1* mutant muscle bellies, we hypothesized that aberrant Arp2/3 activity in the belly displaces mitochondria from I-bands, contributing to the mitochondrial defects. To test this hypothesis, we used RNAi to deplete Arp2/3 complex components in *vpr-1* mutants. *arx-2/arp2*, *arx-3/arp3*, or *arx-5/arp5* RNAi suppresses the mitochondrial morphology and distribution defects of *vpr-1* mutants (Figure 8B). mitoGFP imaging and TEMs of *vpr-1(tm1411); arx-2* RNAi muscle indicate that large mitochondria correctly localize to I-bands (Figure 2D; Table S1, lines 2 and 7). Hence, aberrant Arp2/3 activity causes the VAP mutant mitochondrial defects. The Arp2/3 and CLR-1 Lar suppression data provide unequivocal evidence that these mitochondrial defects are specific and regulatory in nature. Finally, Arp2/3 inactivation in wild-type muscle causes mitochondrial morphology similar to those seen following Lar inactivation (Figure 8B; Table S1, lines 8 and 4). These data support the model that vMSP/Robo/Lar signaling modulates Arp2/3 activity to position mitochondria at I-bands.

## DISCUSSION

EphR, Robo, and Lar-like receptors are called growth cone guidance receptors because of their established roles in regulating the actin cytoskeleton during nervous system development. However, these receptors are also expressed after guidance decisions are made, particularly in the adult central nervous system and muscles (Longo et al., 1993; Zabolotny et al., 2001; Zhang and Goldstein, 1991). Here, we show that Robo and Lar-like receptor pathways act in adults to modulate mitochondrial localization and morphology. Our results and those from previous studies support the following model (Figure 8C). VAP MSP domains are cleaved in the neuron cytoplasm and secreted into the external environment. vMSP interactions with Robo and Lar receptors downregulate Lar signaling to the Arp2/3 complex in muscle, stabilizing mitochondria at the I-bands. In VAP mutants, aberrant Lar and Arp2/3 activity causes ectopic actin filaments in the muscle belly that displace mitochondria from the I-bands, promote mitochondrial mobility, elongation, and branching, and inhibit energy metabolism. We propose that vMSPs restrict Arp2/3 activity to the I-bands, thereby influencing mitochondrial morphology and fission/fusion balance. This neuron-governed mechanism may regulate energy metabolism in response to environmental, nutritional, or developmental cues. Evidence for the model and implications for neurodegenerative diseases are discussed below.

We show that VAPs and sperm-derived MSPs comprise an evolutionarily conserved ligand class that promotes mitochondrial localization and morphology. VAP, Robo, and Lar homologs are present in sponges, animals without neurons and muscles, suggesting that their role in regulating mitochondria is ancestral to their growth cone guidance function (Srivastava et al., 2010). The mechanism by which vMSPs regulate mitochondria appears similar to the mechanism by which Slit repels migrating axons (Chang et al., 2004; Sun et al., 2000). During nervous system development, Slit binding to Robo downregulates Lar receptor signaling that promotes migration. Therefore, Robo acts upstream of Lar. We show that Robo is required for vMSP signaling upstream of Lar. The simplest interpretation of our genetic and binding data is that Robo facilitates vMSP binding to Lar or Robo/Lar complexes, downregulating Lar signaling. However, determining the extent to which high affinity vMSP interactions depend upon receptor complex formation will require further investigation. Given that EphR, Robo, and Lar receptors are broadly expressed throughout the nervous system, it is possible that vMSPs influence mitochondria in neurons. dVAP regulates the presynaptic microtubule cytoskeleton (Pennetta et al., 2002), which controls mitochondrial transport along axons (Hollenbeck and Saxton, 2005). Therefore, neurons may secrete factors like VAPB that regulate mitochondria in muscles and neurons.

The actin cytoskeleton regulates mitochondrial position in *C. elegans* muscle, cultured *Drosophila* and chick neurons, cultured mammalian cells, and yeast (Boldogh and Pon, 2007; Chada and Hollenbeck, 2004; Pathak et al., 2010; Quintero et al., 2009; Starr and Han, 2002). The worm ANC-1 protein is thought to couple actin to mitochondria and *anc-1* mutants have globular muscle mitochondrial morphology similar to *arx-2* RNAi animals (Starr and Han, 2002). We show that vMSPs promote mitochondrial docking at muscle I-bands, actin-enriched sites containing structures analogous to focal adhesions (Lecroisey et al., 2007). CLR-1 Lar and Arp2/3 are required for maintenance or elongation of mitochondrial tubules along I-bands, a process that may facilitate (and/or require) fusion. In *vpr-1* mutants, mitochondria mislocalize to the muscle belly along with ectopic actin filaments and form thin elongated branches with increased mobility, increased fusion/fission balance, and reduced transmembrane potential. Lar or Arp2/3 inactivation suppresses these defects, revealing an unexpected role for the actin cytoskeleton in modulating multiple aspects of mitochondrial biology. Whether Arp2/3 regulates mitochondria directly or indirectly through positioning or docking effects is not clear. The actin cytoskeleton has been shown to influence mitochondrial fission in cultured cells (De Vos et al., 2005; Pathak et al., 2010). vMSP signals are likely regulatory in nature, as a parallel mechanism promotes mitochondrial positioning in the absence of VAP and Arp2/3 function.

Defects in skeletal muscle mitochondria have been implicated in the pathology of ALS (Dupuis et al., 2004; Zhou et al., 2010). In mutant *sod1* transgenic mice, the SOD1 protein aberrantly accumulates in mitochondria (Wong et al., 1995b; Kong and Xu, 1998) and causes skeletal muscle mitochondrial dysfunction that is initiated at the neuromuscular junction (Zhou et al., 2010). Subsarcolemmal aggregates of abnormal mitochondria with low transmembrane potential are found in skeletal muscle of these mice well before the onset of the disease (Zhou et al., 2010). ALS patients with a SOD1 mutation also show a muscle mitochondrial oxidative defect (Corti et al., 2009) and sporadic ALS patients have been documented with muscle mitochondrial respiratory chain dysfunction (Crugnola et al., 2010). Defects in muscle mitochondria may therefore contribute as a primary cause in ALS pathogenesis. Indeed, uncoupling electron transport from ATP synthesis in muscle mitochondria by overexpressing uncoupling protein 1 is sufficient to initiate motor neuron degeneration (Dupuis et al., 2009).

Our results support the hypothesis that secreted vMSPs modulate mitochondrial position through growth cone guidance receptor pathways. It seems likely that this signaling mechanism plays a role in ALS pathogenesis. The VAPB$^{P56S}$ mutation inhibits wild-type and mutant MSP domain secretion (Tsuda et al., 2008). Reducing vMSP secretion might cause abnormal mitochondrial localization, morphology, and function in ALS8 patients. Consistent with this model, low VAP levels in sporadic ALS patients and mouse *sod1* models correlate with widespread mitochondrial abnormalities (Anagnostou et al., 2010; Dupuis et al., 2004, 2008; Teuling et al., 2007; Wong et al., 1995b). Moreover, analyses of data from whole-genome associated studies have discovered that single nucleotide polymorphisms within genes mediating growth cone guidance, including Robo, Lar, and Cdc42 are associated with susceptibility, survival, or onset of ALS (Lesnick et al., 2008). In addition, the discovery that growth cone guidance pathways influence mitochondria may have implications for other neurodegenerative diseases, such as spinal muscular atrophy and Parkinson's disease (Lesnick et al., 2007).

## EXPERIMENTAL PROCEDURES

### Genetics, RNAi, and Plasmids

Bristol N2 is the wild-type *C. elegans* strain. Worms were maintained on NGM plates with NA22 bacteria at 20°C except where indicated otherwise. Strain construction and marker scoring were performed as previously described using PCR and phenotypic analyses (Miller et al., 2003; Tsuda et al., 2008). The *fog-2(q71)* mutation was used to generate male/female strains. RNAi was performed by the feeding method using HT115 bacterial strains (Kamath et al., 2003). Positive clones were sequenced for confirmation. See the Supplemental Experimental Procedures for additional information.

### Staining, Microinjection, and Microscopy

Mitochondria were labeled using MitoTracker CMXRos, Rhodamine 6g, and mito::GFP, which targets the matrix. For MitoTracker CMXRos and Rhodamine 6g staining, dyes were added to seeded NGM plates (Labrousse et al., 1999). Imaging was done without anesthetics on dried 2% agarose pads immediately after mounting. Anesthetics can cause mitochondrial fragmentation. Images were taken using a motorized Zeiss Axioskop 2 with MRM Axiocam Hi-Res digital camera and Perkin Elmer Spinning Disc Nikon TE2000 microscope equipped with an EMCCD C9100-50 camera operated by Velocity 5.3 software. Purified recombinant MSP domains were microinjected into the gonad using a Zeiss Axiovert 200 microscope. Injected animals were mounted for direct observation after a 15 min to 1 hr recovery period.

### Transgenics

To generate transgenic *C. elegans*, plasmids (60 ng/μl) were mixed with pRF4 [*rol-6*] (60 ng/μl) or *myo-3p::mito::GFP* (60 ng/μl) and injected into young adult hermaphrodite gonads. The *myo-3p::mito::GFP* plasmid was generously provided by Dr. van der Bliek. Transgenic lines were selected based on the roller phenotype or GFP expression. Multiple independent transgenic lines were analyzed. Two *vpr-1(tm1411)/hT2; unc-119p::vpr-1* transgenic lines were integrated by gamma irradiation.

### Fluorescence Loss in Photobleaching

Fluorescence loss in photobleaching (FLIP) was achieved with a Perkin Elmer Spinning Disc Nikon TE2000 microscope programmed to cycle between bleaching and scanning every 5 s for 4 min. The fluorescence intensities of indicated areas were analyzed in Volocity software (Perkin Elmer, UK). Animals were immobilized on dried 2% agarose pads under conditions that prevent animal and mitochondrial mobility (i.e., one to three animals per pad). Only muscles with immobile mitochondria were analyzed.

### MSP Binding Assays

MSP-FITC and vMSP-FITC binding assays were conducted as previously described (Miller et al., 2003; Tsuda et al., 2008). Briefly, HEK293T cells were cultured on coverslips in 6-well plates and cells (~50% confluence) were transiently transfected with 2 μg of VAB-1, 3xFLAG::SAX-3, CLR-1::V5, or pcDNA3.2 control plasmids (Miller et al., 2003) using FuGENE HD transfection reagent, according to the manufacturer's instructions (Promega, U.S.A). The 3 × FLAG::SAX-3 construct was generously provided by Dr. Joe Culotti. The CLR-1::V5 construct contained the CLR-1 extracellular and transmembrane domains, but not the phosphatase domains. After 24 hr, cells were incubated with MSP-FITC or vMSP-FITC for 30 min at 23°C and washed three times in 50 ml PBS. Transfected cells were preincubated with a 25-fold molar excess of unlabelled MSP to evaluate specific binding. Fluorescence was measured from linear range exposures using Axiovision software.

### Metabolic Assays

Resistance to paraquat (Ultra Scientific, USA), ATP concentration measurement, oxygen consumption, and MitoTracker CMXRos staining methods are described in Supplemental Experimental Procedures. Oxygen consumption was measured at constant temperature (20°C) using the oxygraph system (Hansatech, UK).

### Transmission Electron Microscopy

TEM was performed as previously described (Tsuda et al., 2008; Whitten and Miller, 2007). Care was taken to ensure that fixation occurred rapidly and cross-sections were orthogonal to muscle myofilaments. Mitochondria do not consistently localize to I-bands near neuromuscular junctions.

## SUPPLEMENTAL INFORMATION

Supplemental Information includes five figures, two tables, Supplemental Experimental Procedures, and four movies and can be found with this article online at doi:10.1016/j.devcel.2011.12.009.

## ACKNOWLEDGMENTS

We thank the *Caenorhabditis* Genetics Center (funded by the NIH Center for Research Resources) for strains, J. Culotti, D. Sherwood, and A. van der Bliek for plasmids, G. Marques and the Yoder lab for help with confocal miscroscopy, and Tim Mahoney, Manish Jaiswal, Hector Sandoval, Vafa Bayat, Chao Tong, and Jennifer Zallen for comments on the manuscript. This work was supported in part by the American Cancer Society (RSG-06-151-01-DDC to M.A.M.), Muscular Dystrophy Association (MDA186119 to M.A.M), ALS Association (to H.T.), and a UAB Clinical Nutrition Center Nutrition or Obesity-Related Pilot Feasibility Studies grant (UAB NORC grant P30DK056336). H.J.B. is an Investigator of the HHMI.

Received: October 4, 2010
Revised: August 24, 2011
Accepted: December 15, 2011
Published online: January 19, 2012

## REFERENCES

Anagnostou, G., Akbar, M.T., Paul, P., Angelinetta, C., Steiner, T.J., and de Belleroche, J. (2010). Vesicle associated membrane protein B (VAPB) is decreased in ALS spinal cord. Neurobiol. Aging *31*, 969–985.

Boldogh, I.R., and Pon, L.A. (2007). Mitochondria on the move. Trends Cell Biol. *17*, 502–510.

Bottino, D., Mogilner, A., Roberts, T., Stewart, M., and Oster, G. (2002). How nematode sperm crawl. J. Cell Sci. *115*, 367–384.

Chada, S.R., and Hollenbeck, P.J. (2004). Nerve growth factor signaling regulates motility and docking of axonal mitochondria. Curr. Biol. *14*, 1272–1276.

Chai, A., Withers, J., Koh, Y.H., Parry, K., Bao, H., Zhang, B., Budnik, V., and Pennetta, G. (2008). hVAPB, the causative gene of a heterogeneous group of motor neuron diseases in humans, is functionally interchangeable with its Drosophila homologue DVAP-33A at the neuromuscular junction. Hum. Mol. Genet. *17*, 266–280.

Chang, C., Yu, T.W., Bargmann, C.I., and Tessier-Lavigne, M. (2004). Inhibition of netrin-mediated axon attraction by a receptor protein tyrosine phosphatase. Science *305*, 103–106.

Corti, S., Donadoni, C., Ronchi, D., Bordoni, A., Fortunato, F., Santoro, D., Del Bo, R., Lucchini, V., Crugnola, V., Papadimitriou, D., et al. (2009). Amyotrophic lateral sclerosis linked to a novel SOD1 mutation with muscle mitochondrial dysfunction. J. Neurol. Sci. *276*, 170–174.

Crugnola, V., Lamperti, C., Lucchini, V., Ronchi, D., Peverelli, L., Prelle, A., Sciacco, M., Bordoni, A., Fassone, E., Fortunato, F., et al. (2010). Mitochondrial respiratory chain dysfunction in muscle from patients with amyotrophic lateral sclerosis. Arch. Neurol. *67*, 849–854.

De Vos, K.J., Allan, V.J., Grierson, A.J., and Sheetz, M.P. (2005). Mitochondrial function and actin regulate dynamin-related protein 1-dependent mitochondrial fission. Curr. Biol. *15*, 678–683.

Dupuis, L., Gonzalez de Aguilar, J.L., Oudart, H., de Tapia, M., Barbeito, L., and Loeffler, J.P. (2004). Mitochondria in amyotrophic lateral sclerosis: a trigger and a target. Neurodegener. Dis. *1*, 245–254.

Dupuis, L., Corcia, P., Fergani, A., Gonzalez De Aguilar, J.L., Bonnefont-Rousselot, D., Bittar, R., Seilhean, D., Hauw, J.J., Lacomblez, L., Loeffler,

J.P., and Meininger, V. (2008). Dyslipidemia is a protective factor in amyotrophic lateral sclerosis. Neurology *70*, 1004–1009.

Dupuis, L., Gonzalez de Aguilar, J.L., Echaniz-Laguna, A., Eschbach, J., Rene, F., Oudart, H., Halter, B., Huze, C., Schaeffer, L., Bouillaud, F., and Loeffler, J.P. (2009). Muscle mitochondrial uncoupling dismantles neuromuscular junction and triggers distal degeneration of motor neurons. PLoS ONE *4*, e5390.

Durieux, J., Wolff, S., and Dillin, A. (2011). The cell-non-autonomous nature of electron transport chain-mediated longevity. Cell *144*, 79–91.

Esposito, G., Di Schiavi, E., Bergamasco, C., and Bazzicalupo, P. (2007). Efficient and cell specific knock-down of gene function in targeted C. elegans neurons. Gene *395*, 170–176.

Fares, H., and Greenwald, I. (2001). Genetic analysis of endocytosis in Caenorhabditis elegans: coelomocyte uptake defective mutants. Genetics *159*, 133–145.

Funke, A.D., Esser, M., Krüttgen, A., Weis, J., Mitne-Neto, M., Lazar, M., Nishimura, A.L., Sperfeld, A.D., Trillenberg, P., Senderek, J., et al. (2010). The p.P56S mutation in the VAPB gene is not due to a single founder: the first European case. Clin. Genet. *77*, 302–303.

Gkogkas, C., Wardrope, C., Hannah, M., and Skehel, P. (2011). The ALS8-associated mutant VAPB(P56S) is resistant to proteolysis in neurons. J. Neurochem. *117*, 286–294.

Govindan, J.A., Nadarajan, S., Kim, S., Starich, T.A., and Greenstein, D. (2009). Somatic cAMP signaling regulates MSP-dependent oocyte growth and meiotic maturation in C. elegans. Development *136*, 2211–2221.

Han, S.M., Cottee, P.A., and Miller, M.A. (2010). Sperm and oocyte communication mechanisms controlling C. elegans fertility. Dev. Dyn. *239*, 1265–1281.

Hao, J.C., Yu, T.W., Fujisawa, K., Culotti, J.G., Gengyo-Ando, K., Mitani, S., Moulder, G., Barstead, R., Tessier-Lavigne, M., and Bargmann, C.I. (2001). C. elegans slit acts in midline, dorsal-ventral, and anterior-posterior guidance via the SAX-3/Robo receptor. Neuron *32*, 25–38.

Hollenbeck, P.J., and Saxton, W.M. (2005). The axonal transport of mitochondria. J. Cell Sci. *118*, 5411–5419.

Huang, P., and Stern, M.J. (2004). FGF signaling functions in the hypodermis to regulate fluid balance in C. elegans. Development *131*, 2595–2604.

Kamath, R.S., Fraser, A.G., Dong, Y., Poulin, G., Durbin, R., Gotta, M., Kanapin, A., Le Bot, N., Moreno, S., Sohrmann, M., et al. (2003). Systematic functional analysis of the Caenorhabditis elegans genome using RNAi. Nature *421*, 231–237.

Kanazawa, T., Zappaterra, M.D., Hasegawa, A., Wright, A.P., Newman-Smith, E.D., Buttle, K.F., McDonald, K., Mannella, C.A., and van der Bliek, A.M. (2008). The C. elegans Opa1 homologue EAT-3 is essential for resistance to free radicals. PLoS Genet. *4*, e1000022.

Kohara, Y. (2001). [Systematic analysis of gene expression of the C. elegans genome]. Tanpakushitsu Kakusan Koso *46* (16, Suppl), 2425–2431.

Kong, J., and Xu, Z. (1998). Massive mitochondrial degeneration in motor neurons triggers the onset of amyotrophic lateral sclerosis in mice expressing a mutant SOD1. J. Neurosci. *18*, 3241–3250.

Kokel, M., Borland, C.Z., DeLong, L., Horvitz, H.R., and Stern, M.J. (1998). clr-1 encodes a receptor tyrosine phosphatase that negatively regulates an FGF receptor signaling pathway in Caenorhabditis elegans. Genes Dev. *12*, 1425–1437.

Labrousse, A.M., Zappaterra, M.D., Rube, D.A., and van der Bliek, A.M. (1999). C. elegans dynamin-related protein DRP-1 controls severing of the mitochondrial outer membrane. Mol. Cell *4*, 815–826.

Lecroisey, C., Ségalat, L., and Gieseler, K. (2007). The C. elegans dense body: anchoring and signaling structure of the muscle. J. Muscle Res. Cell Motil. *28*, 79–87.

Lesnick, T.G., Papapetropoulos, S., Mash, D.C., Ffrench-Mullen, J., Shehadeh, L., de Andrade, M., Henley, J.R., Rocca, W.A., Ahlskog, J.E., and Maraganore, D.M. (2007). A genomic pathway approach to a complex disease: axon guidance and Parkinson disease. PLoS Genet. *3*, e98.

Lesnick, T.G., Sorenson, E.J., Ahlskog, J.E., Henley, J.R., Shehadeh, L., Papapetropoulos, S., and Maraganore, D.M. (2008). Beyond Parkinson disease: amyotrophic lateral sclerosis and the axon guidance pathway. PLoS ONE *3*, e1449.

Lev, S., Ben Halevy, D., Peretti, D., and Dahan, N. (2008). The VAP protein family: from cellular functions to motor neuron disease. Trends Cell Biol. *18*, 282–290.

Longo, F.M., Martignetti, J.A., Le Beau, J.M., Zhang, J.S., Barnes, J.P., and Brosius, J. (1993). Leukocyte common antigen-related receptor-linked tyrosine phosphatase. Regulation of mRNA expression. J. Biol. Chem. *268*, 26503–26511.

Millecamps, S., Salachas, F., Cazeneuve, C., Gordon, P., Bricka, B., Camuzat, A., Guillot-Noel, L., Russaouen, O., Bruneteau, G., Pradat, P.F., et al. (2010). SOD1, ANG, VAPB, TARDBP, and FUS mutations in familial amyotrophic lateral sclerosis: genotype-phenotype correlations. J. Med. Genet. *47*, 554–560.

Miller, M.A., Nguyen, V.Q., Lee, M.H., Kosinski, M., Schedl, T., Caprioli, R.M., and Greenstein, D. (2001). A sperm cytoskeletal protein that signals oocyte meiotic maturation and ovulation. Science *291*, 2144–2147.

Miller, M.A., Ruest, P.J., Kosinski, M., Hanks, S.K., and Greenstein, D. (2003). An Eph receptor sperm-sensing control mechanism for oocyte meiotic maturation in Caenorhabditis elegans. Genes Dev. *17*, 187–200.

Mitne-Neto, M., Machado-Costa, M., Marchetto, M.C., Bengtson, M.H., Joazeiro, C.A., Tsuda, H., Bellen, H.J., Silva, H.C., Oliveira, A.S., Lazar, M., et al. (2011). Downregulation of VAPB expression in motor neurons derived from induced pluripotent stem cells of ALS8 patients. Hum. Mol. Genet. *20*, 3642–3652.

Nishimura, A.L., Mitne-Neto, M., Silva, H.C., Richieri-Costa, A., Middleton, S., Cascio, D., Kok, F., Oliveira, J.R., Gillingwater, T., Webb, J., et al. (2004). A mutation in the vesicle-trafficking protein VAPB causes late-onset spinal muscular atrophy and amyotrophic lateral sclerosis. Am. J. Hum. Genet. *75*, 822–831.

Parekh, A.B. (2003). Mitochondrial regulation of intracellular Ca2+ signaling: more than just simple Ca2+ buffers. News Physiol. Sci. *18*, 252–256.

Pathak, D., Sepp, K.J., and Hollenbeck, P.J. (2010). Evidence that myosin activity opposes microtubule-based axonal transport of mitochondria. J. Neurosci. *30*, 8984–8992.

Pendergrass, W., Wolf, N., and Poot, M. (2004). Efficacy of MitoTracker Green and CMXrosamine to measure changes in mitochondrial membrane potentials in living cells and tissues. Cytometry *A61*, 162–169.

Pennetta, G., Hiesinger, P.R., Fabian-Fine, R., Meinertzhagen, I.A., and Bellen, H.J. (2002). Drosophila VAP-33A directs bouton formation at neuromuscular junctions in a dosage-dependent manner. Neuron *35*, 291–306.

Quintero, O.A., DiVito, M.M., Adikes, R.C., Kortan, M.B., Case, L.B., Lier, A.J., Panaretos, N.S., Slater, S.Q., Rengarajan, M., Feliu, M., and Cheney, R.E. (2009). Human Myo19 is a novel myosin that associates with mitochondria. Curr. Biol. *19*, 2008–2013.

Ratnaparkhi, A., Lawless, G.M., Schweizer, F.E., Golshani, P., and Jackson, G.R. (2008). A Drosophila model of ALS: human ALS-associated mutation in VAP33A suggests a dominant negative mechanism. PLoS ONE *3*, e2334.

Reinke, V., Gil, I.S., Ward, S., and Kazmer, K. (2004). Genome-wide germline-enriched and sex-biased expression profiles in Caenorhabditis elegans. Development *131*, 311–323.

Srivastava, M., Simakov, O., Chapman, J., Fahey, B., Gauthier, M.E., Mitros, T., Richards, G.S., Conaco, C., Dacre, M., Hellsten, U., et al. (2010). The Amphimedon queenslandica genome and the evolution of animal complexity. Nature *466*, 720–726.

Starr, D.A., and Han, M. (2002). Role of ANC-1 in tethering nuclei to the actin cytoskeleton. Science *298*, 406–409.

Suen, D.F., Norris, K.L., and Youle, R.J. (2008). Mitochondrial dynamics and apoptosis. Genes Dev. *22*, 1577–1590.

Sun, Q., Bahri, S., Schmid, A., Chia, W., and Zinn, K. (2000). Receptor tyrosine phosphatases regulate axon guidance across the midline of the Drosophila embryo. Development *127*, 801–812.

Teuling, E., Ahmed, S., Haasdijk, E., Demmers, J., Steinmetz, M.O., Akhmanova, A., Jaarsma, D., and Hoogenraad, C.C. (2007). Motor neuron

disease-associated mutant vesicle-associated membrane protein-associated protein (VAP) B recruits wild-type VAPs into endoplasmic reticulum-derived tubular aggregates. J. Neurosci. *27*, 9801–9815.

Tsang, W.Y., and Lemire, B.D. (2003). The role of mitochondria in the life of the nematode, Caenorhabditis elegans. Biochim. Biophys. Acta *1638*, 91–105.

Tsuda, H., Han, S.M., Yang, Y., Tong, C., Lin, Y.Q., Mohan, K., Haueter, C., Zoghbi, A., Harati, Y., Kwan, J., et al. (2008). The amyotrophic lateral sclerosis 8 protein VAPB is cleaved, secreted, and acts as a ligand for Eph receptors. Cell *133*, 963–977.

Vendelin, M., Béraud, N., Guerrero, K., Andrienko, T., Kuznetsov, A.V., Olivares, J., Kay, L., and Saks, V.A. (2005). Mitochondrial regular arrangement in muscle cells: a "crystal-like" pattern. Am. J. Physiol. Cell Physiol. *288*, C757–C767.

Whitten, S.J., and Miller, M.A. (2007). The role of gap junctions in Caenorhabditis elegans oocyte maturation and fertilization. Dev. Biol. *301*, 432–446.

Winston, W.M., Molodowitch, C., and Hunter, C.P. (2002). Systemic RNAi in C. elegans requires the putative transmembrane protein SID-1. Science *295*, 2456–2459.

Wolke, U., Jezuit, E.A., and Priess, J.R. (2007). Actin-dependent cytoplasmic streaming in C. elegans oogenesis. Development *134*, 2227–2236.

Wong, A., Boutis, P., and Hekimi, S. (1995a). Mutations in the clk-1 gene of Caenorhabditis elegans affect developmental and behavioral timing. Genetics *139*, 1247–1259.

Wong, P.C., Pardo, C.A., Borchelt, D.R., Lee, M.K., Copeland, N.G., Jenkins, N.A., Sisodia, S.S., Cleveland, D.W., and Price, D.L. (1995b). An adverse property of a familial ALS-linked SOD1 mutation causes motor neuron disease characterized by vacuolar degeneration of mitochondria. Neuron *14*, 1105–1116.

Yang, Y., Han, S.M., and Miller, M.A. (2010). MSP hormonal control of the oocyte MAP kinase cascade and reactive oxygen species signaling. Dev. Biol. *342*, 96–107.

Zabolotny, J.M., Kim, Y.B., Peroni, O.D., Kim, J.K., Pani, M.A., Boss, O., Klaman, L.D., Kamatkar, S., Shulman, G.I., Kahn, B.B., and Neel, B.G. (2001). Overexpression of the LAR (leukocyte antigen-related) protein-tyrosine phosphatase in muscle causes insulin resistance. Proc. Natl. Acad. Sci. USA *98*, 5187–5192.

Zallen, J.A., Yi, B.A., and Bargmann, C.I. (1998). The conserved immunoglobulin superfamily member SAX-3/Robo directs multiple aspects of axon guidance in C. elegans. Cell *92*, 217–227.

Zhang, W.R., and Goldstein, B.J. (1991). Identification of skeletal muscle protein-tyrosine phosphatases by amplification of conserved cDNA sequences. Biochem. Biophys. Res. Commun. *178*, 1291–1297.

Zhou, J., Yi, J., Fu, R., Liu, E., Siddique, T., Ríos, E., and Deng, H.X. (2010). Hyperactive intracellular calcium signaling associated with localized mitochondrial defects in skeletal muscle of an animal model of amyotrophic lateral sclerosis. J. Biol. Chem. *285*, 705–712.

internal solution containing 140 mM KCl, 2 mM $MgCl_2$, 10 mM EGTA, 10 mM HEPES at pH 7.2. The external solution was Leibovitz's L-15 (Gibco) containing 136 mM NaCl, 5.8 mM $NaH_2PO_4$, 5.4 mM KCl, 1.3 mM $CaCl_2$, 0.9 mM $MgCl_2$ at pH 7.2. Osmolarity was adjusted to 300 mosM $l^{-1}$. Motility was measured and calibrated using an electro-optical method in which the cell's ciliated pole was imaged through a rectangular slit onto a photodiode[29].

### *In vivo* functional assays

For ABR, DPOAE and CM measurements, mice were anaesthetized with xylazine and ketamine. ABRs and DPOAEs were obtained from one set of animals; CMs from a second set. For ABR, needle electrodes were inserted at vertex and pinna. ABR and CM were evoked with 5-ms tone pips (0.5-ms rise–fall, with a $\cos^2$ envelope, at 35 per s). The response was amplified ( × 10,000), filtered (0.1–3 kHz), and averaged with an A/D board in a PC-based data-acquisition system. Sound level was raised in 5-dB steps from 0 to 90 dB SPL. At each level, 1,024 responses were averaged (with stimulus polarity alternated) after 'artefact rejection'. Threshold was determined by visual inspection. For CM a silver-wire electrode was placed on the round window membrane. Responses to alternating pip polarities were subtracted, and the resultant waveform was digitally high-pass filtered to remove residual uncancelled neural potentials. The DPOAE at $2f_1 - f_2$ was recorded in response to two primary tones: $f_1$ and $f_2$, with $f_2/f_1 = 1.2$ and the $f_2$ level 10 dB lower than the $f_1$ level. Ear-canal sound pressure was amplified and digitally sampled at 4-μs intervals. Fast-Fourier transforms were computed from averaged waveforms of ear-canal sound pressure, and the DPOAE amplitude at $2f_1 - f_2$ and surrounding noise floor were extracted. Iso-response contours were interpolated from plots of amplitude versus sound level, performed in 5-dB steps of $f_1$ level. Threshold is defined as the $f_1$ level required to produce a DPOAE at 0 dB SPL.

Received 29 May; accepted 12 August 2002; doi:10.1038/nature01059.
Published online 28 August 2002.

1. Gold, T. Hearing. II. The physical basis of the action of the cochlea. *Proc. R. Soc. Lond. B* **135,** 492–498 (1948).
2. Dallos, P. & Harris, D. Properties of auditory nerve responses in absence of outer hair cells. *J. Neurophysiol.* **41,** 365–383 (1978).
3. Brown, M. C., Nuttall, A. L. & Masta, R. I. Intracellular recordings from cochlear inner hair cells: effects of stimulation of the crossed olivocochlear efferents. *Science* **222,** 69–72 (1983).
4. Dallos, P. The active cochlea. *J. Neurosci.* **12,** 4575–4585 (1992).
5. Brownell, W. E., Bader, C. R., Bertrand, D. & de Ribaupierre, Y. Evoked mechanical responses of isolated cochlear outer hair cells. *Science* **227,** 194–196 (1985).
6. Kachar, B., Brownell, W. E., Altschuler, R. & Fex, J. Electrokinetic shape changes of cochlear outer hair cells. *Nature* **322,** 365–368 (1986).
7. Ashmore, J. F. A fast motile response in guinea-pig outer hair cells: the cellular basis of the cochlear amplifier. *J. Physiol.* **388,** 323–347 (1987).
8. Ashmore, J. F. *Cochlear Mechanisms* (eds Wilson, J. P. & Kemp, D. T.) 107–116 (Plenum, London, 1989).
9. Santos-Sacchi, J. Reversible inhibition of voltage-dependent outer hair cell motility and capacitance. *J. Neurosci.* **11,** 3096–3110 (1991).
10. Zheng, J. *et al.* Prestin is the motor protein of cochlear outer hair cells. *Nature* **405,** 149–155 (2000).
11. Belyantseva, I. A., Adler, H. J., Curi, R., Frolenkov, G. I. & Kachar, B. Expression and localization of prestin and the sugar transporter GLUT-5 during development of electromotility in cochlear outer hair cells. *J. Neurosci.* **20,** RC116 (2000).
12. Oliver, D. *et al.* Intracellular anions as the voltage sensor of prestin, the outer hair cell motor protein. *Science* **292,** 2340–2343 (2001).
13. Forge, A. Structural features of the lateral walls in mammalian cochlear outer hair cells. *Cell Tissue Res.* **265,** 473–483 (1991).
14. Dallos, P. & Fakler, B. Prestin, a new type of motor protein. *Nature Rev. Mol. Cell Biol.* **3,** 104–111 (2002).
15. Bohne, B. A. & Rabbitt, K. D. Holes in the reticular lamina after noise exposure: implication for continuing damage in the organ of Corti. *Hear. Res.* **11,** 41–53 (1983).
16. Holt, J. R. *et al.* A chemical-genetic strategy implicates myosin-1c in adaptation by hair cells. *Cell* **108,** 371–381 (2002).
17. Kros, C. J. *et al.* Reduced climbing and increased slipping adaptation in cochlear hair cells of mice with Myo7a mutations. *Nature Neurosci.* **5,** 41–47 (2002).
18. Dallos, P. & Wang, C. Y. Bioelectric correlates of kanamycin intoxication. *Audiology* **13,** 277–289 (1974).
19. Kemp, D. T. Stimulated acoustic emissions from within the human auditory system. *J. Acoust. Soc. Am.* **64,** 1386–1391 (1978).
20. Johnstone, B. M., Patuzzi, R. & Yates, G. K. Basilar membrane measurements and the travelling wave. *Hear. Res.* **22,** 147–153 (1986).
21. Ruggero, M. A. & Rich, N. C. Application of a commercially-manufactured Doppler-shift laser velocimeter to the measurement of basilar-membrane vibration. *Hear. Res.* **51,** 215–230 (1991).
22. Sellick, P. M., Patuzzi, R. & Johnstone, B. M. Measurement of basilar membrane motion in the guinea pig using the Mossbauer technique. *J. Acoust. Soc. Am.* **72,** 131–141 (1982).
23. Kiang, N. Y. & Moxon, E. C. Tails of tuning curves of auditory-nerve fibers. *J. Acoust. Soc. Am.* **55,** 620–630 (1974).
24. Ruggero, M. A. Responses to sound of the basilar membrane of the mammalian cochlea. *Curr. Opin. Neurobiol.* **2,** 449–456 (1992).
25. Manley, G. A. Cochlear mechanisms from a phylogenetic viewpoint. *Proc. Natl Acad. Sci. USA* **97,** 11736–11743 (2000).
26. Fettiplace, R., Ricci, A. J. & Hackney, C. M. Clues to the cochlear amplifier from the turtle ear. *Trends Neurosci.* **24,** 169–175 (2001).
27. Hudspeth, A. J. Mechanical amplification of stimuli by hair cells. *Curr. Opin. Neurobiol.* **7,** 480–486 (1997).
28. Ehret, G. *The Auditory Psychobiology of the Mouse* (ed. Willott, J. F.)) 169–200 (Charles Thomas, Springfield, Illinois, 1983).
29. He, D. Z., Evans, B. N. & Dallos, P. First appearance and development of electromotility in neonatal gerbil outer hair cells. *Hear. Res.* **78,** 77–90 (1994).

### Acknowledgements

We thank K. Cullen for technical assistance; T. Curran, B. Fritzsch, C. A. Shera and D. Freeman for comments on the manuscript; and B. Kachar, T. Hasson and P. Gillespie for antibodies. This work is supported in part by NIH grants to M.C.L., Z.Z.H. and J.Z., NIH Cancer Center Support CORE grant, and the American Lebanese Syrian Associated Charities (ALSAC).

### Competing interests statement

The authors declare that they have no competing financial interests.

Correspondence and requests for materials should be addressed to J.Z. (e-mail: jian.zuo@stjude.org).

# Robustness of the BMP morphogen gradient in *Drosophila* embryonic patterning

**Avigdor Eldar*†, Ruslan Dorfman*, Daniel Weiss*†, Hilary Ashe‡, Ben-Zion Shilo* & Naama Barkai*†**

* *Department of Molecular Genetics and* † *Department of Physics of Complex Systems, Weizmann Institute of Science, Rehovot, Israel*
‡ *School of Biological Sciences, University of Manchester, Manchester M13 9PT, UK*

**Developmental patterning relies on morphogen gradients, which generally involve feedback loops to buffer against perturbations caused by fluctuations in gene dosage and expression[1]. Although many gene components involved in such feedback loops have been identified, how they work together to generate a robust pattern remains unclear. Here we study the network of extracellular proteins that patterns the dorsal region of the *Drosophila* embryo by establishing a graded activation of the bone morphogenic protein (BMP) pathway. We find that the BMP activation gradient itself is robust to changes in gene dosage. Computational search for networks that support robustness shows that transport of the BMP class ligands (Scw and Dpp) into the dorsal midline by the BMP inhibitor Sog is the key event in this patterning process. The mechanism underlying robustness relies on the ability to store an excess of signalling molecules in a restricted spatial domain where Sog is largely absent. It requires extensive diffusion of the BMP–Sog complexes, coupled with restricted diffusion of the free ligands. We show experimentally that Dpp is widely diffusible in the presence of Sog but tightly localized in its absence, thus validating a central prediction of our theoretical study.**

Graded activation of the BMP pathway subdivides the dorsal region of *Drosophila* embryos into several distinct domains of gene expression. This graded activation is determined by a well-characterized network of extracellular proteins[2,3], which may diffuse in the perivitelline fluid[4] that surrounds the embryo (Fig. 1a). The patterning network is composed of two BMP class ligands (Scw and Dpp), a BMP inhibitor (Sog), a protease that cleaves Sog (Tld) and an accessory protein (Tsg), all of which are highly conserved in evolution and are used also for patterning the dorso-ventral axis of vertebrate embryos[5]. Previous studies have suggested that patterning of the dorsal region is robust to changes in the concentrations of most of the crucial network components. For example, embryos that contain only one functional allele of *scw*, *sog*, *tld* or *tsg* are viable and do not show any apparent phenotype. Misexpression of *scw* or of *tsg* also renders the corresponding null mutants viable[6–8].

To check whether robustness is achieved at the initial activation gradient, we monitored signalling directly by using antibodies that recognize specifically an activated, phosphorylated intermediate of

  

the BMP pathway (pMad)[9,10]. Prominent graded activation in the dorsal-most eight cell rows was observed for about 1 h, starting roughly 2 h after fertilization at 25 °C (ref. 11 and Fig. 1b). We quantified this activation gradient in heterozygous mutants that were compromised for one of three of the crucial components of the patterning network, Scw, Sog or Tld. Whereas homozygous null mutants that completely lack the normal gene product have a deleterious effect on signalling[11], the heterozygotes, which should produce half the amount of the gene product, were indistinguishable from wild type (Fig. 1c). Similarly, overexpression of the Tld protein uniformly in the embryo did not alter the activation profile (Fig. 1c). The activation profile at 18 °C was the same as that at 25 °C (Fig. 1d). This robustness to temperature variations is marked, considering the wide array of temperature dependencies that are observed in this temperature span. By contrast, the profile of pMad was sensitive to the concentration of Dpp[11] (Fig. 1d). The dosage sensitivity of Dpp is exceptional among morphogens and is singled out as being haploid-insufficient[12].

No apparent transcriptional feedback, which might account for the robustness of dorsal patterning, has been identified so far. Robustness should thus be reflected in the design of interactions in the patterning network. To identify the mechanism underlying robustness, we formulated a general mathematical model of the dorsal patterning network. For simplicity, our initial analysis was restricted to a single BMP class ligand (Scw or Dpp), a BMP inhibitor (Sog) and the protease (Tld). The general model accounted for the formation of the BMP–Sog complex, allowed for the diffusion of Sog, BMP and BMP–Sog, and allowed for the cleavage of Sog by Tld, both when Sog is free and when Sog is associated with BMP. Each reaction was characterized by a different rate constant. The three reaction–diffusion equations that define this model are given in the Methods.

We carried out extensive simulations to identify robust networks. At each simulation, a set of parameters (rate constants and protein

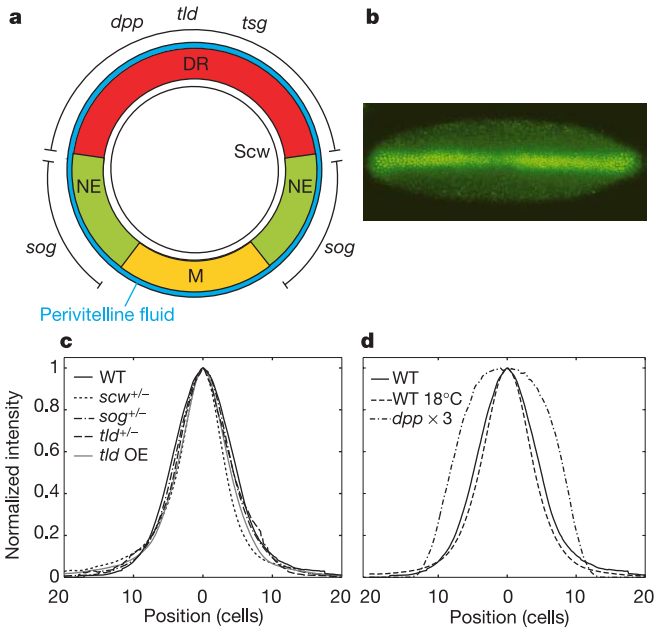


**Figure 1** Robustness of the pMad activation profile. **a**, Cross-section of an early *Drosophila* embryo (~2 h after egg lay) showing the three distinct domains of gene expression. Starting at stage 5, the dorsal domain, which comprises about 50 cells, is subdivided to form the amnioserosa and the dorsal ectoderm. Shown are the genes of the patterning network: Scw and Dpp are two activating BMP class ligands; Sog is an inhibitor of both ligands; Tsg is required for Sog inhibition of Dpp; and Tld is a protease that cleaves Sog. Note that *dpp*, *tld* and *tsg* are expressed only in the dorsal region (DR), whereas expression of *sog* is restricted to the neuroectoderm (NE) and *scw* is expressed by all cells. M, mesoderm. **b**, Activation of the BMP pathway, which induces different cell fates in the dorsal region, visualized by antibodies against pMad. The activation profile is shown in a dorsal view of a wild-type embryo at stage 5. Activation is graded and peaks at the dorsal midline. The pattern of pMad widens at the termini of the embryo, possibly owing to edge effects that modify patterning. Our analysis is focused on the centre of the embryo, where the variability between different embryos is limited (~2 cells). **c**, Normalized activation profile of wild-type embryos (averaged over $n = 11$ embryos) compared with that of three sets of heterozygous mutants containing half the amount of Scw ($n = 23$), Sog ($n = 14$) and Tld ($n = 11$). The activation profile of embryos overexpressing the Tld protein uniformly around the embryo, using the Matα4–Gal4 driver, is also shown ($n = 33$). All embryos were collected at 25 °C. **d**, Activation profiles at 25 °C and 18 °C ($n = 41$). This temperature variation is biologically significant, as development is about two times slower at 18 °C than at 25 °C. Embryos were collected at different times but at the same developmental stage for the two temperatures. Shown also is the activation profile of an embryo carrying three copies of the *dpp* gene.

Box 1
**Mechanism underlying robustness**

We consider an idealized patterning network that consists of a single BMP (Scw for simplicity), Sog and Tld. Robustness will be manifested in the steady-state distribution of Scw. We assume that free Scw does not diffuse and that free Sog is not cleaved. The set of reaction–diffusion equations defining this network is obtained from equations 1–3 (Methods), by setting $D_{BMP} = \alpha_S = k_{-b} = 0$. At steady-state, the system can then be reduced to a single equation:

$$0 = \nabla^2([Scw]^{-1}) - 2l_b^{-2} \quad (1)$$

where $l_b^2 = 2D_S/k_b$, $D_S$ is the diffusion coefficient of Sog and $k_b$ is the binding rate of Sog to Scw. Thus, although free Scw does not diffuse, the system is tuned for providing it with an effective diffusion. Two processes govern this effective diffusion: the shuttling of Scw by Sog from the circumference of the embryo into the dorsal midline, and the degradation of Sog by Tld in the dorsal region. Although both processes depend on the amounts of the respective proteins, those concentrations do not appear in the effective Scw diffusion. The key to this quantitative adjustment is the fact that both processes are mediated by the complex Sog–Scw: only the complex, and not free Scw, can diffuse, and only the complex is subject to degradation by Tld.

The concentrations of the network components, Scw, Sog and Tld could still affect the steady-state activation gradient through the boundary conditions. The solution of equation (1) is given by

$$[Scw(x)] = \frac{l_b^2}{x^2 + \varepsilon^2} \quad (2)$$

where $x = 0$ at the dorsal midline and $\varepsilon$ is an integration coefficient. In general, the value of $\varepsilon$ will depend on most parameters of the system, including the concentrations and the production rates of the network components Scw, Sog and Tld, leading to a nonrobust distribution of Scw. Examining equation (2), however, we note that the only way to accommodate high concentrations of Scw is by placing Scw in a small region surrounding the dorsal midline where Sog is absent, in other words, by setting $\varepsilon$ to 0. Thus, for large enough concentrations of Scw, $\varepsilon$ vanishes and we obtain a robust Scw profile:

$$[Scw(x)] = \frac{l_b^2}{x^2} \quad (3)$$

for every position of $x$ that is far enough from the dorsal midline, in other words, $x \gg \varepsilon$. Indeed, the concentrations of network components have disappeared from this equation of the activation profile, which reflects the robustness of the system. Finally, we note that the same mechanism generates the gradient of the second BMP (Dpp). We assume, however, that Dpp binds Sog only when the latter is bound to Tsg. Thus, the same formalism is applied but with the molecular entities Dpp, Sog–Tsg (instead of Sog) and the complex Dpp–Sog–Tsg (instead of Scw–Sog). The details and precise conditions necessary for robustness are given in the Supplementary Information.

concentrations) was chosen at random and the steady-state activation profile was calculated by solving equations (1) to (3) numerically. A set of three perturbed networks representing heterozygous situations was then generated by reducing the gene dosages of *sog*, *tld* or the BMP class ligand by a factor of two. The steady-state activation profiles defined by those networks were solved numerically and compared with the initial, nonperturbed network. A threshold was defined as a given BMP value (corresponding to the value at a third of the dorsal ectoderm in the nonperturbed network). The extent of network robustness was quantified by measuring the shift in the threshold for all three perturbed networks. Over 66,000 simulations were carried out, with each of the nine parameters allowed to vary over four orders of magnitude.

As expected, in most cases (97.5%) the threshold position in the perturbed networks was shifted by a large extent (>50%; see Fig. 2a). In most of those nonrobust cases, the BMP concentration was roughly uniform throughout the dorsal region (Fig. 2c). By contrast, Sog was distributed in a concentration gradient with its minimum in the dorsal midline, defining a reciprocal gradient of BMP activation. Thus, the key event in this nonrobust patterning mechanism was the establishment of a concentration gradient of Sog, which was governed by diffusion of Sog from its domain of expression outside the dorsal region, coupled with its cleavage by Tld inside the dorsal region. Although such a gradient has been observed[13], it is also compatible with other models (see below).

We identified a small class of networks (198 networks, 0.3%) in which a twofold reduction in the amounts of all three genes resulted in a change of less than 10% in the threshold position (see Fig. 2b). Notably, in all of these robust cases, BMP was redistributed in a sharp concentration gradient that peaked in the dorsal midline (Fig. 2c). In addition, this concentration gradient decreased as a power-low distribution with an exponent $n = 2$, which indicated the uniqueness of the robust solution (Fig. 2d). In these cases, Sog was also distributed in a graded manner in the dorsal region (data not shown). Analysis of the reaction rate constants of the robust networks showed a wide range of possibilities for most parameters. But two restrictions were apparent and defined the robust network design. First, in the robust networks the cleavage of Sog by Tld was facilitated by the formation of the complex Sog–BMP (Fig. 2f). Second, the complex BMP–Sog was broadly diffusible, whereas free BMP was restricted (Fig. 2e).

To identify how robustness is achieved, we considered an idealized network by assuming that free Sog is not cleaved and that free BMP does not diffuse. The steady-state activation profile defined by this network can be solved analytically (Box 1), which reveals the two aspects that are crucial for ensuring robustness. First, the BMP–Sog complex has a central role, by coupling the two processes that establish the activation gradient: BMP diffusion and Sog degradation. This coupling leads to a quantitative buffering of perturbations in gene dosage. Second, restricted diffusion of free BMP enables the system to store excess BMP in a confined spatial domain where Sog is largely absent. Changes in the concentration of BMP

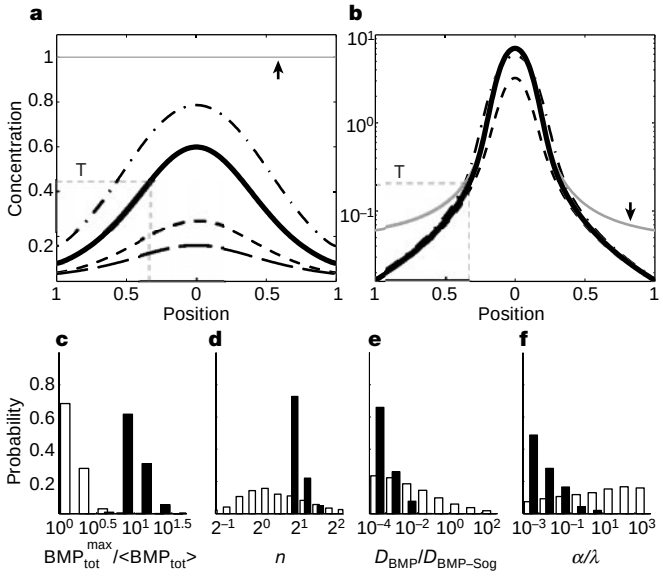


**Figure 2** Patterning mechanism emerges from the features of the robust networks. The general model of the dorsal patterning network was solved numerically for 66,000 different choices of parameters, with each parameter ranging over four orders of magnitude. **a**, A typical, nonrobust network. The profile of free BMP (unbroken curves) is shown for the nonperturbed network and for three perturbed networks representing heterozygotes for *sog*, *tld* and BMP (see Fig. 1c for a key to the lines).The total concentration of BMP (free plus Sog-associated) is indicated by the grey line (arrow). The broken grey line (T) indicates the threshold where robustness was measured. **b**, A typical robust system. **c**–**f**, Statistical distribution of various features in the robust (black) and nonrobust (white) networks. The analysis was restricted to the 22,000 networks that showed at least twofold spatial variation of free BMP concentration. Each feature was calculated for each of the networks, and the histograms were normalized to account for the different numbers of robust (198) and nonrobust (22,000) networks. **c**, The extent of BMP confinement to the dorsal midline was quantified by measuring the ratio between total BMP concentration (free plus Sog-associated) at the centre and its average concentration. In all of the robust cases, a high ratio (>10) was observed. By contrast, the low ratios observed in the nonrobust cases indicated that BMP was distributed approximately uniformly. **d**, The steady-state profile of free BMP was fit to a power-low distribution, $x^{-n}$. Nearly all robust profiles corresponded to $n = 2$, indicating the uniqueness of the robust solution. By contrast, a wide range of exponents were found for the nonrobust solution. The fitting error vanished in the robust cases, but was high in the nonrobust cases (not shown). **e**, Ratio between the diffusion coefficient of free BMP ($D_{BMP}$) and the complex BMP–Sog ($D_{BMP-Sog}$). Note that complex formation significantly enhances BMP diffusion in all robust cases. **f**, Ratio of the degradation rate of free Sog ($\alpha$) to that of BMP-associated Sog ($\lambda$). Note that complex formation greatly enhances Sog degradation in all robust cases.

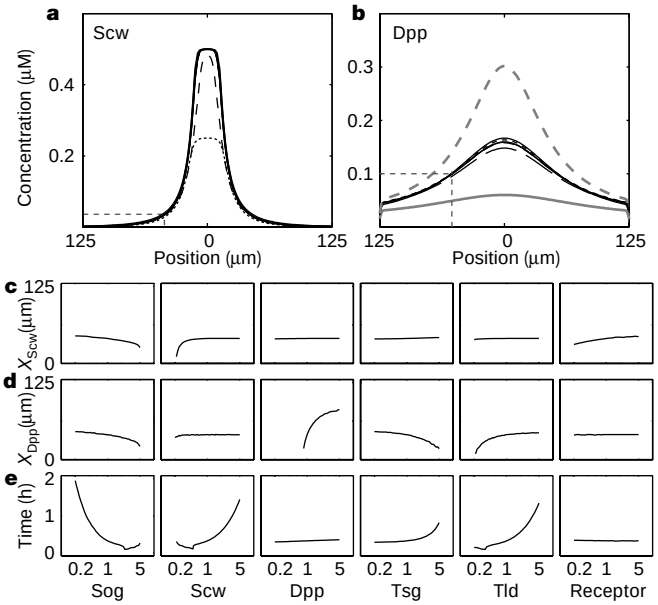


**Figure 3** Properties of the robust model. **a**, **b**, The steady-state concentrations of receptor-bound Scw and Dpp. Six altered systems were obtained from a reference system by reducing to half the amounts of *scw*, *sog*, *tld* (see Fig. 1c for a key to the lines), *dpp* (unbroken grey line), Scw receptor (dotted line), *tsg* (superimposed on the solid line) and by increasing by 50% the amount of *dpp* (grey dashed line). The level and position of the threshold used in **c** and **d** are indicated. **c**, **d**, The positions of the activation thresholds of Scw (**c**) and Dpp (**d**) for a series of altered systems, obtained by changing a single parameter by the indicated fold amount. **e**, Time to reach steady state as a function of the fold change in parameter values. Time is initiated with the onset of ligand production.

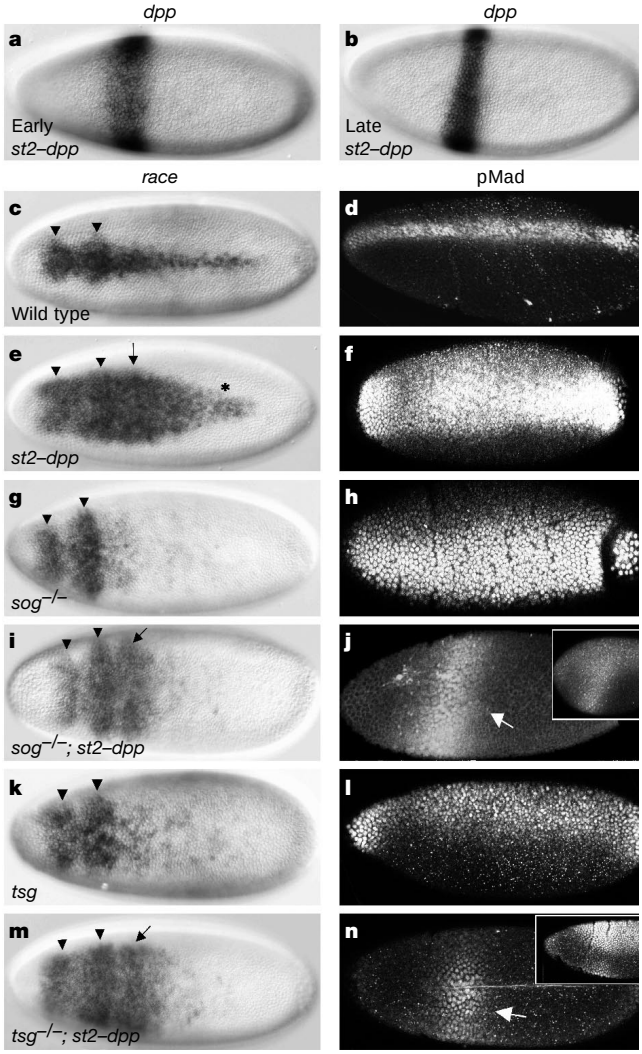


**Figure 4** Dpp diffusion requires Sog and Tsg. Dpp was expressed orthogonal to the dorsoventral axis by the *eve st2* enhancer in a stripe of about 12 cells at early cleavage cycle 14 (**a**), which refines to about 6 cells by late cycle 14 (lateral views, **b**). Note that ectopic amounts of *dpp* were greater than the endogenous transcripts in the dorsal region, which under these exposures were not visible. **c**, Normal pattern of *race* in wild-type embryos. Note the AP bias in the anterior positions (arrowheads). **d**, Normal pattern of pMad in wild-type embryos. **e**, Expression of *st2–dpp* in wild-type embryos leads to an expanded expression of *race*, which forms a wedge shape with its broadest region at the position of *st2–dpp* (arrow) and ranges about 25 cells posteriorly (asterisk). The normal pattern of *race* shows an AP bias at the anterior positions (arrowheads). **f**, *st2–dpp* in wild-type embryos also leads to a broader dorsal distribution of pMad, which extends throughout the AP axis. **g**, In *sog* $^{-/-}$ embryos, the anterior *race* domain expands (arrowheads), whereas posterior expression is diminished and detected only sporadically as a punctate staining. Some expansion of *race* was observed in *sog* $^{+/-}$ embryos, probably due to the higher threshold of *race* induction compared with pMad. **h**, In *sog* $^{-/-}$ embryos, pMad expands in the dorsal domain, but does not reach the ventral domain. **i**, Expression of *st2–dpp* in *sog* $^{-/-}$ embryos leads to a corresponding stripe of *race* of about 10–12 cells (arrow). **j**, *st2–dpp* in *sog* $^{-/-}$ embryos generates a corresponding stripe of pMad (arrow), which extends to the ventral region. The ventral expansion of pMad versus the restricted dorsal expansion of *race* in embryos of the same genotype indicates that a lower threshold of activation can induce pMad even in the ventral domain, which is devoid of endogenous Dpp. Main view is ventral, inset is lateral. **k**, **l**, The patterns of *race* and pMad in *tsg* $^{-/-}$ embryos are similar to *sog* $^{-/-}$ embryos. **m**, **n**, *st2–dpp* in *tsg* $^{-/-}$ generates a corresponding stripe of both *race* and pMad, similar to that observed on expression of *st2–dpp* in *sog* $^{-/-}$ embryos. Main view in **n** is ventral, inset is lateral. Except where stated otherwise, a dorsal view is shown with anterior to the left.

alter the BMP profile close to the dorsal midline but do not change its distribution in most of the dorsal region (Box 1).

We next examined the complete system, comprising Sog, Tld, Tsg, both Scw and Dpp, and their associated receptors (Supplementary Information). Two additional molecular assumptions were required to ensure the robustness of patterning. First, Sog can bind and capture the BMP class ligands even when the latter are associated with their receptors. Second, Dpp can bind Sog only when the latter is bound to Tsg. Indeed, it has been shown that, whereas Sog is sufficient for inhibiting Scw, both Tsg and Sog are required for inhibiting Dpp[6,14,15]. This last assumption implies that Tsg functions to decouple the formation of the Scw gradient from the parallel generation of the Dpp gradient, ensuring that Scw and Dpp are transported to the dorsal midline independently by two distinct molecular entities (Supplementary Information).

The complete model was solved numerically for different choices of rate constants. In particular, we assessed the effect of twofold changes in gene dosage. The steady-state activation profiles can be superimposed, indicating the robustness of the system (Fig. 3a, b). In addition, with the exception of Dpp, the expression of all other crucial network components can be altered by at least an order of magnitude before an effect on the position of a given threshold is observed (Fig. 3c, d). In the model, the lack of robustness to Dpp stems from its insufficient dosage. Note that the time taken to reach steady state is sensitive to these concentrations of protein (Fig. 3e). For the wide range of parameters that we have used, however, the adjustment time does not exceed the patterning time. Flexible adjustment time thus facilitates the buffering of quantitative perturbations.

As discussed above, our analysis identified two principle molecular features that are essential for robust network design: first, free Sog is not cleaved efficiently—an assumption that is supported by the *in vitro* finding that Sog cleavage by Tld requires BMP[6,16]; second, the diffusion of free BMP is restricted. This is the central prediction of our theoretical study, namely, that Scw diffusion requires Sog, whereas Dpp diffusion requires both Sog and Tsg. Although several reports suggest that in wild-type embryos both Dpp and Scw are widely diffusible[6,17], their ability to diffuse in a *sog* or *tsg* mutant background has not been examined as yet.

To monitor the diffusion of Scw or Dpp, we used the *even-skipped* (*eve*) stripe-2 enhancer (*st2*) to misexpress Dpp or Scw in a narrow stripe perpendicular to the normal BMP gradient. In transgenic embryos, *dpp* or *scw* RNA was detected in a stripe just posterior to the cephalic furrow. Initially the stripe was about 12 cells wide at early cleavage cycle 14, but refined rapidly to about 6 cells by late cycle 14 (Fig. 4a, b). The *st2–dpp* and *st2–scw* embryos were viable, despite the high expression of these proteins as compared with their endogenous counterparts.

The activation of the BMP pathway was monitored either by staining for pMad or by following dorsal expression of the target gene *race*, which requires high activation. Scw is a less potent ligand than is Dpp. This experimental setup could not be used to study Scw diffusion properties because expressing *st2–scw* did not alter the pattern of pMad or *race* expression in wild-type or *sog* $^{-/-}$ embryos (data not shown). By contrast, expression of *st2–dpp* led to an expansion of both markers in a region that extends far from the *st2* expression domain, indicating a wide diffusion of Dpp in a wild-type background (compare Fig. 4c, d with 4e, f). Conversely, on expression of *st2–dpp* in *sog* $^{-/-}$ or in *tsg* $^{-/-}$ embryos, both markers were confined to a narrow stripe in the *st2* domain (compare Fig. 4g, h and k, l with 4i, j and m, n, respectively). The width of this stripe was comparable to that of *st2–dpp* expression, ranging from 6 to 12 cells, indicating that Dpp does not diffuse from its domain of expression in the absence of Sog or Tsg. Taken together, these results show that both Sog and Tsg are required for Dpp diffusion, as predicted by the theoretical analysis.

The computation ability of biochemical networks is striking when one considers that they function in a biological environment

where the amounts of the network components fluctuate, the kinetics is stochastic, and sensitive interactions between different computation modules are required. Studies have examined the effect of these properties on cellular computation mechanisms[18–20], and robustness has been proposed to be a 'design principle' of biochemical networks[18,21]. We have shown the applicability of this principle to morphogen gradient patterning during early development. Quantitative analysis can be used to assess rigorously the robustness of different patterning models and to exclude incompatible ones. The remaining, most plausible model points to crucial biological assumptions and serves to postulate the central feedback mechanisms. Applying the same modelling principles to other systems might identify additional 'design principles' that underlie robust patterning by morphogen gradients in development. □

## Methods

### Fly strains

We used the following strains: *screw*[12], *sog*[6], *tolloid*[2], *tolloid*[7], UAS–*tld* (provided by M. O'Connor), Matα4–Gal4 VP16 (provided by D. St. Johnston) and *tsg*$^{XB56}$ (provided by L. Marsh). For altering the number of copies of *dpp*, we used the strain *dpp*$^{1846}$ *sp cn bw/CyO 23P[dpp*$^{+}$*]* (provided by S. Roth), which was crossed to wild-type flies. The mutant chromosomes were maintained over a balancer chromosome. When each strain is crossed to itself, two-thirds of the embryos not showing the null phenotype should be heterozygotes for *scw* and *tld*, and a third for *sog*. The *st2–dpp* strain has been described[17]. We constructed *st2–scw* by inserting a *scw* cDNA fragment into plasmid 22FPE (ref. 22).

### Antibodies and staining

Rabbit antibodies against pMad were kindly provided by P. ten Dijke. Freshly collected embryos were fixed in 7% formaldehyde. The remaining steps of staining were done according to standard procedures. We used Cy2-conjugated secondary antibodies against rabbit IgG (Jackson ImmunoResearch).

### Data analysis

The dorso-ventral activation profile was quantified by using image processing tools written in Matlab. The mean intensity was measured at the middle of the anterior–posterior (AP) axis in a swath that was 20 cells wide in the direction of the AP axis. We then averaged the results over the indicated number of embryos.

### Numerical simulations

For the general patterning model we considered a single BMP, which is denoted here as Scw. The model was defined by the following set of reaction–diffusion equations:

$$\frac{\partial[\mathrm{Sog}]}{\partial t} = D_{\mathrm{S}}\nabla^2[\mathrm{Sog}] - k_{\mathrm{b}}[\mathrm{Sog}][\mathrm{Scw}] + k_{-\mathrm{b}}[\mathrm{Sog–Scw}] - \alpha[\mathrm{Tld}][\mathrm{Sog}] \quad (1)$$

$$\frac{\partial[\mathrm{Scw}]}{\partial t} = D_{\mathrm{BMP}}\nabla^2[\mathrm{Scw}] - k_{\mathrm{b}}[\mathrm{Sog}][\mathrm{Scw}] + \lambda[\mathrm{Tld}][\mathrm{Sog–Scw}] + k_{-\mathrm{b}}[\mathrm{Sog–Scw}] \quad (2)$$

$$\frac{\partial[\mathrm{Sog–Scw}]}{\partial t} = D_{\mathrm{C}}\nabla^2[\mathrm{Sog–Scw}] + k_{\mathrm{b}}[\mathrm{Sog}][\mathrm{Scw}] - k_{-\mathrm{b}}[\mathrm{Sog–Scw}] - \lambda[\mathrm{Tld}] \times[\mathrm{Sog–Scw}] \quad (3)$$

The equations were solved in the region $-1 < x < 1$. The parameters in this model include the diffusion coefficients of Sog, Scw and the complex Scw–Sog, ($D_{\mathrm{S}}$, $D_{\mathrm{BMP}}$ and $D_{\mathrm{C}}$), binding and unbinding of the Scw–Sog complex ($k_{\mathrm{b}}$ and $k_{-\mathrm{b}}$), cleavage of Sog by Tld ($\alpha$ when Sog is free, $\lambda$ when Sog in associated with Scw), a constant flux of Sog on the boundaries ($\eta_{\mathrm{s}}$) and the total Scw concentration ($[\mathrm{Scw}]_{\mathrm{av}}$). $D_{\mathrm{C}}$ is $D_{\mathrm{BMP–Sog}}$ in Fig. 2e. We solved the equations for 66,000 different sets of random parameters. Each parameter was allowed to vary over four orders of magnitude. The parameters defining the centre of this distributions are (in arbitrary units): $D_{\mathrm{S}} = l_1 = [\mathrm{Scw}]_{\mathrm{av}} = 1$, $D_{\mathrm{BMP}} = 0.1$, $D_{\mathrm{C}} = 1$, $k_{\mathrm{b}} = 10$, $k_{-\mathrm{b}} = 1$, $\lambda[\mathrm{Tld}] = 10$, $\alpha[\mathrm{Tld}] = 10$, $\eta_{\mathrm{S}} = 10$. Equations were solved with Matlab. Each run took less than 1 min. The parameters of the systems shown in Fig. 2 are specified in the Supplementary Information.

For the parameters of the full model (Fig. 3), we chose diffusion rates that reflected the rapid *in vivo* patterning time and corresponded to the measured diffusion time in the perivitelline fluid[4]. This measured diffusion coefficient is similar to that of green fluorescent protein (GFP) in water[23]. It is possible that mixing processes in the perivitelline fluid contribute to the equilibration process. For simplicity, we approximate such processes as an effective diffusion. This approximation does not affect our conclusions. No biochemical data restricting the values of the other parameters are available. The parameters of the reference system are within the realistic biochemical range and obey the robustness conditions. The parameter choice is specified and rationalized in detail in the Supplementary Information.

Received 11 April; accepted 27 July 2002; doi:10.1038/nature01061.

1. Freeman, M. Feedback control of intercellular signalling in development. *Nature* **408,** 313–319 (2000).
2. Podos, S. D. & Ferguson, E. L. Morphogen gradients: new insights from DPP. *Trends. Genet.* **15,** 396–402 (1999).
3. Raftery, L. A. & Sutherland, D. J. TGF-β family signal transduction in *Drosophila* development: from Mad to Smads. *Dev. Biol.* **210,** 251–268 (1999).
4. Stein, D., Roth, S., Vogelsang, E. & Nusslein-Volhard, C. The polarity of the dorsoventral axis in the *Drosophila* embryo is defined by an extracellular signal. *Cell* **65,** 725–735 (1991).
5. DeRobertis, E. M. & Sasai, Y. A common plan for dorsoventral patterning in Bilateria. *Nature* **380,** 37–40 (1996).
6. Nguyen, M., Park, S., Marques, G. & Arora, K. Interpretation of a BMP activity gradient in *Drosophila* embryos depends on synergistic signaling by two type I receptors, SAX and TKV. *Cell* **95,** 495–506 (1998).
7. Arora, K., Levine, M. S. & O'Connor, M. B. The screw gene encodes a ubiquitously expressed member of the TGF-β family required for specification of dorsal cell fates in the *Drosophila* embryo. *Genes Dev.* **8,** 2588–2601 (1994).
8. Mason, E. D., Williams, S., Grotendorst, G. R. & Marsh, J. L. Combinatorial signaling by Twisted Gastrulation and Decapentaplegic. *Mech. Dev.* **64,** 61–75 (1997).
9. Persson, U. *et al.* The L45 loop in type I receptors for TGF-β family members is a critical determinant in specifying Smad isoform activation. *FEBS Lett.* **434,** 83–87 (1998).
10. Tanimoto, H., Itoh, S., ten Dijke, P. & Tabata, T. Hedgehog creates a gradient of DPP activity in *Drosophila* wing imaginal discs. *Mol. Cell* **5,** 59–71 (2000).
11. Dorfman, R. & Shilo, B.-Z. Biphasic activation of the BMP pathway in the *Drosophila* embryonic dorsal region. *Development* **128,** 965–972 (2001).
12. Wharton, K. A., Ray, R. P. & Gelbart, W. M. An activity gradient of decapentaplegic is necessary for the specification of dorsal pattern elements in the *Drosophila* embryo. *Development* **117,** 807–822 (1993).
13. Srinivasan, S., Rashka, K. E. & Bier, E. Creation of a Sog morphogen gradient in the *Drosophila* embryo. *Dev. Cell* **2,** 91–101 (2002).
14. Neul, J. L. & Ferguson, E. L. Spatially restricted activation of the SAX receptor by SCW modulates DPP/TKV signaling in *Drosophila* dorsal–ventral patterning. *Cell* **95,** 483–494 (1998).
15. Ross, J. J. *et al.* Twisted gastrulation is a conserved extracellular BMP antagonist. *Nature* **410,** 479–483 (2001).
16. Marques, G. *et al.* Production of a DPP activity gradient in the early *Drosophila* embryo through the opposing actions of the SOG and TLD proteins. *Cell* **91,** 417–426 (1997).
17. Ashe, H. L., Mannervik, M. & Levine, M. Dpp signaling thresholds in the dorsal ectoderm of the *Drosophila* embryo. *Development* **127,** 3305–3312 (2000).
18. Barkai, N. & Leibler, S. Robustness in simple biochemical networks. *Nature* **387,** 913–917 (1997).
19. Barkai, N. & Leibler, S. Circadian clocks limited by noise. *Nature* **403,** 267–268 (2000).
20. von Dassow, G., Meir, E., Munro, E. M. & Odell, G. M. The segment polarity network is a robust developmental module. *Nature* **406,** 188–192 (2000).
21. Hartwell, L. H., Hopfield, J. J., Leibler, S. & Murray, A. W. From molecular to modular biology. *Nature* **402,** C47–C52 (1999).
22. Kosman, D. & Small, S. Concentration-dependent patterning by an ectopic expression domain of the *Drosophila* gap gene *knirps*. *Development* **124,** 1343–1354 (1997).
23. Swaminathan, R., Hoang, C. P. & Verkman, A. S. Photobleaching recovery and anisotropy decay of green fluorescent protein GFP–S65T in solution and cells: cytoplasmic viscosity probed by green fluorescent protein translational and rotational diffusion. *Biophys. J.* **72,** 1900–1907 (1997).

**Supplementary Information** accompanies the paper on *Nature*'s website (http://www.nature.com/nature).

### Acknowledgements

We thank P. ten Dijke for the pMad antibody; L. Marsh, M. O'Connor, S. Roth, D. St. Johnston and the Umea and Bloomington Fly Centers for strains; and S. Leibler and S. Roth for comments and criticism. This work was funded by the Israel Science Foundation (B-Z.S.) and the Israel Science Foundation and the Minerva Foundation (N.B). H.A. is a Lister Institute Research Fellow. B-Z.S. is the incumbent of the Hilda and Cecil Lewis professorial chair in Molecular Genetics. N.B. is the incumbent of the Soretta and Henry Shapiro career development chair.

### Competing interests statement

The authors declare that they have no competing financial interests.

Correspondence and requests for materials should be addressed to N.B. (e-mail: naama.barkai@weizmann.ac.il).

# Molecular basis of seasonal time measurement in *Arabidopsis*

**Marcelo J. Yanovsky & Steve A. Kay**

*The Scripps Research Institute, 10550 N. Torrey Pines Road, La Jolla, California 92037, USA*

**Several organisms have evolved the ability to measure daylength, or photoperiod, allowing them to adjust their development in anticipation of annual seasonal changes. Daylength measurement requires the integration of temporal information, provided by the circadian system, with light/dark discrimination, initiated by specific photoreceptors. Here we demonstrate that in *Arabidopsis* this integration takes place at the level of CONSTANS**

  

# Self-Organized Shuttling: Generating Sharp Dorsoventral Polarity in the Early *Drosophila* Embryo

Michal Haskel-Ittah,[1] Danny Ben-Zvi,[1] Merav Branski-Arieli,[1] Eyal D. Schejter,[1] Ben-Zion Shilo,[1,*] and Naama Barkai[1,*]
[1]Department of Molecular Genetics, Weizmann Institute of Science, Rehovot 76100, Israel
*Correspondence: benny.shilo@weizmann.ac.il (B.-Z.S.), naama.barkai@weizmann.ac.il (N.B.)
http://dx.doi.org/10.1016/j.cell.2012.06.044

## SUMMARY

Morphogen gradients pattern tissues and organs during development. When morphogen production is spatially restricted, diffusion and degradation are sufficient to generate sharp concentration gradients. It is less clear how sharp gradients can arise within the source of a broadly expressed morphogen. A recent solution relies on localized production of an inhibitor outside the domain of morphogen production, which effectively redistributes (shuttles) and concentrates the morphogen within its expression domain. Here, we study how a sharp gradient is established without a localized inhibitor, focusing on early dorsoventral patterning of the *Drosophila* embryo, where an active ligand and its inhibitor are concomitantly generated in a broad ventral domain. Using theory and experiments, we show that a sharp Toll activation gradient is produced through "self-organized shuttling," which dynamically relocalizes inhibitor production to lateral regions, followed by inhibitor-dependent ventral shuttling of the activating ligand Spätzle. Shuttling may represent a general paradigm for patterning early embryos.

## INTRODUCTION

Morphogens are signaling molecules that can induce several cell fates in a concentration-dependent manner (Wolpert, 1989). Gradients of morphogens are instrumental in patterning tissues and organs during the development of multicellular organisms, raising interest in the molecular networks establishing these gradients. In the standard paradigm, a morphogen that is secreted from a localized source establishes a gradient that peaks at the source merely by its diffusion and degradation across the field. Quantitative properties of such gradients are well understood: morphogen spread is defined by the diffusion and degradation rates, and the sensitivity of the gradient to perturbations can be tuned by feedbacks acting on these parameters (Bollenbach et al., 2005; Eldar et al., 2003; Paulsen et al., 2011; Schier, 2009).

Classical examples of morphogen gradients conform to this paradigm, including the Bicoid and Dpp gradients in the *Drosophila* embryo (Driever and Nüsslein-Volhard, 1988a, 1988b; Ephrussi and St Johnston, 2004) and wing imaginal disc (Cadigan, 2002; Lecuit et al., 1996; Nellen et al., 1996), respectively. However, there are also examples where a morphogen is uniformly produced within a wide region, but its graded signaling is confined to a narrow domain that is well within the region of morphogen production. This paradigm is prevalent at early stages of embryogenesis, where broad domains have been defined, but the narrow territory responsible for local production of graded signals has not yet been generated. Quantitative properties of such gradients are less understood. Of particular interest are mechanisms that enable the generation of a sharp gradient and maintain its distribution robust to fluctuations in gene dosages or environmental conditions.

Previously, we analyzed this paradigm of a broadly expressed morphogen in the context of the BMP activation gradient in the early *Drosophila* embryo, which is formed well within the domain in which the activating ligand, Dpp, is expressed (dorsal ~40% of the embryo) (Eldar et al., 2002). Formation of the BMP activation gradient relies on the production of an inhibitor molecule (Sog) in regions flanking the dorsal domain where Dpp is produced. Sog is secreted, diffuses into the dorsal domain, and generates an inhibition gradient. Work by us and others described a novel shuttling mechanism for the formation of this activation gradient: rather than passively inhibiting BMP signaling, the diffusible flux of Sog serves to redistribute the Dpp molecules, concentrating the ligand in the dorsal-most region (Eldar et al., 2002; Mizutani et al., 2005; Shimmi et al., 2005; Wang and Ferguson, 2005).

Theoretical analysis suggested that shuttling provides two advantages: first, it leads to a sharp gradient; second, it enhances the robustness of the gradient to fluctuations in gene dosage (Eldar et al., 2002; Meinhardt and Roth, 2002). The shuttling mechanism is conserved in short-germband insects (van der Zee et al., 2006), and we recently provided evidence that shuttling functions also in the early *Xenopus* embryo, again in generating a BMP activation gradient (Ben-Zvi et al., 2008; Plouhinec et al., 2011). Notably, redistribution of ligand molecules via shuttling does not involve directed transport but depends only on nondirected diffusion.

In the aforementioned example of the BMP activation gradient, expression of an inhibitor outside the patterned domain serves as the key asymmetry cue and is the critical factor in generating a sharp and robust gradient through ligand shuttling.

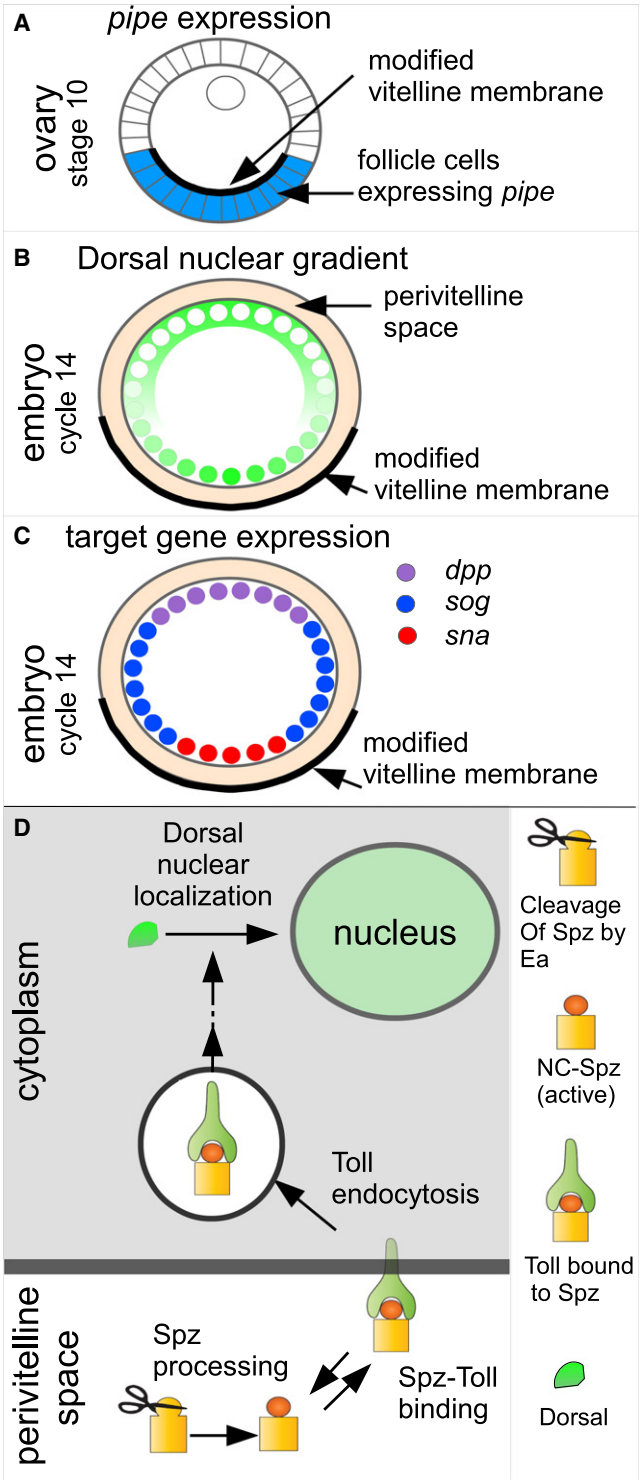


**Figure 1. DV Axis Formation in *Drosophila*: From Ovary to Embryo**

(A) A schematic cross-section of a stage 10 ovary: *pipe* expression (blue) in the follicular epithelium is restricted to a uniform ventral domain occupying 40% of the ventralmost cells. Pipe leads to the modification of the vitelline membrane (black), which surrounds the late oocyte and early embryo.

(B and C) Schematic cross-section of an early embryo. (B) A gradient of nuclear Dl (an NFκB transcription factor) is established peaking in the ventral midline.

(C) Dl regulates the expression of zygotic genes that determine cell fates along the DV axis in the embryo. High nuclear concentration of Dl activates the transcription of *sna* (red, confined to ~20% ventral region), whereas intermediate and low nuclear Dl induce *sog* (blue). *dpp* (purple) is found in cells lacking nuclear Dl.

(D) Ea, a serine protease present in the perivitelline fluid surrounding the embryo is processed and activated in the ~40% ventral region defined by *pipe* expression. Activated Ea cleaves Spz, an NGF-like ligand, to form the ligand NC-Spz. NC-Spz binds Tl receptor and thus triggers the nuclear localization of Dl.

Yet in other cases, such asymmetry may not exist, and gradient formation within the broad expression domain will need to be established without the assistance of external cues. We wished to examine how a sharp gradient is established in these cases and whether similar principles apply.

The transmission of dorsoventral (DV) polarity from the *Drosophila* oocyte to the embryo is a case in point (Moussian and Roth, 2005). During oogenesis, the ventral 40% of the follicle cell layer surrounding the oocyte is patterned by the EGF receptor pathway to express the gene *pipe*, encoding a sulfotransferase (Anderson, 1998; James et al., 2002; Morisato and Anderson, 1995; Peri et al., 2002; Sen et al., 1998; Stein, 1995). Modification by Pipe is thought to activate proteins, which are deposited on the vitelline membrane covering the oocyte and the future embryo (Sen et al., 1998; Zhang et al., 2009; Zhu et al., 2007). Following fertilization, the ventral domain of the vitelline membrane, which was defined by *pipe* expression, guides the subsequent polarity of the embryo by facilitating a proteolytic cascade within the perivitelline space (Figure 1), which culminates in the processing and activation of Spätzle (Spz), a ligand of the Toll (Tl) receptor (Cho et al., 2012; DeLotto and DeLotto, 1998; DeLotto et al., 2001; Dissing et al., 2001; LeMosy et al., 1999; Morisato and Anderson, 1994; Schneider et al., 1994; Weber et al., 2003).

Binding of processed Spz to the Tl receptor on the embryonic plasma membrane activates a signaling pathway within the embryo, whose outcome is the graded nuclear localization of the transcription factor Dorsal (Dl) within embryonic nuclei (Roth et al., 1989; Rushlow et al., 1989; Stathopoulos and Levine, 2002). Notably, this ventral-to-dorsal gradient is generated well within the *pipe* domain. Thus, whereas *pipe* is found uniformly along the ventral 40% of the egg chamber, Dl appears fully nuclear in less than 20% of the circumference and becomes progressively cytoplasmic dorsally. Moreover, gene expression boundaries, such as those defining the expression domains of the high-Dl target genes *twist* (*twi*) and *snail* (*sna*), are also found at the ventral ~20% (Rusch and Levine, 1996; Stathopoulos and Levine, 2002; Zhao et al., 2007). Evidence further suggests that elaboration of the wide *pipe* domain into a narrower gradient of Tl activation involves a self-organization circuit because expanding the *pipe* domain to ~80% of the follicle cells results in a two-peak gradient (Morisato, 2001; Moussian and Roth, 2005; Roth and Schüpbach, 1994). However, how this self-organization is encoded by the molecular machinery remains unknown.

We searched computationally for mechanisms that can generate a sharp and robust gradient within the expression

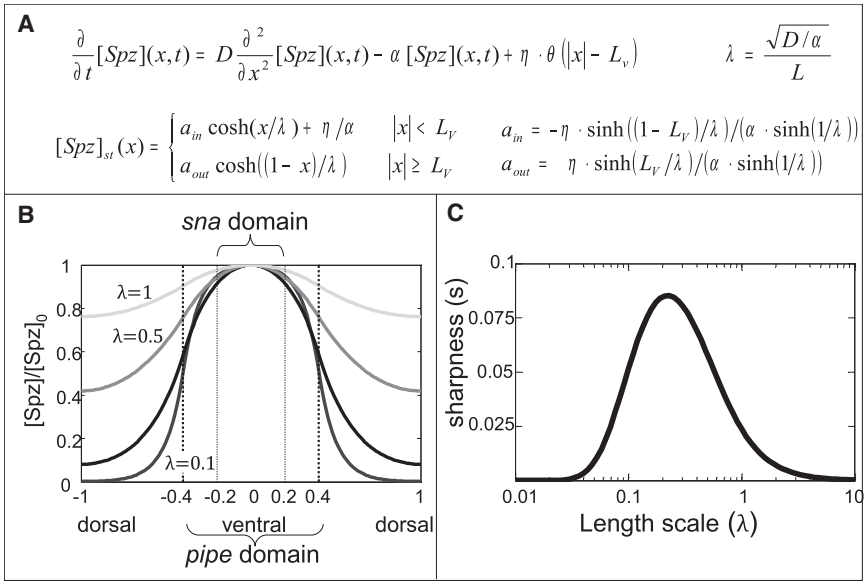


**Figure 2. Morphogen Diffusion Generates a Shallow Gradient within the Source**

(A) The equation defining the naive reaction-diffusion model and its steady-state solution. *[Spz](x,t)* denotes the concentration of Spz in space and time, *D* is the diffusion coefficient, $\alpha$ the Spz degradation rate, and $\eta$ the rate by which Spz is produced, which is restricted to $L_v$, the 40% ventral domain. $\lambda$ is the length scale defining this system. cosh and sinh are the hyperbolic cosine and hyperbolic sine, accordingly.

(B) Steady-state profiles of activated Spz for different values of $\lambda$, as indicated. The profiles are normalized by their maximum value at x = 0. *pipe* and *sna* expression domains are indicated by the broken and solid vertical lines, respectively. x = 0 represents the ventral midline.

(C) The sharpness of Spz profile as a function of $\lambda$. The sharpness is defined as the relative change in concentration between the maximal value (at x = 0) and the value at the *sna* border (x = 0.2).

See also Figure S1.

domain of a broadly produced ligand. We show that a simple model, which relies only on the diffusion of the ligand outside its expression domain, does not suffice. Based on reported properties of the Spz ligand (DeLotto and DeLotto, 1998; DeLotto et al., 2001; Morisato, 2001; Weber et al., 2003), we consider the case where the diffusing morphogen is cleaved to generate an inhibitor that can either inhibit ligand activity or compete for receptor binding. This scenario, however, does not suffice for sharpening the gradient. Rather, we again identify an inhibitor-mediated shuttling mechanism as a way for producing a sharp and robust gradient. Notably, in this case the inhibitor is not produced outside the domain of morphogen expression but, instead, is generated concomitantly with the ligand following its cleavage. Shuttling emerges as a self-organized property of the dynamics, with polar inhibitor production established in a self-consistent manner. Key assumptions of this model are based on known biochemical properties of Spz cleavage (Weber et al., 2007), and we demonstrate the consistency of the mechanism with published genetic experiments, including the observed formation of a double peak when the *pipe* expression domain is expanded. We further provide experimental evidence demonstrating multiple facets of the ligand Spz following cleavage and the capacity to polarize the DV axis according to the flux of the inhibitory Spz prodomain, all consistent with use of shuttling by the early DV patterning network.

## RESULTS

### Computational Model: Searching for a Mechanism that Establishes a Sharp and Robust Morphogen Gradient

We consider a morphogen that is produced in a wide region and examine the gradient of morphogen level that is established within this domain of expression. As a concrete case, we assume the morphogen production domain is restricted to 40% of the embryonic circumference, matching the observed extent of the *pipe* domain where activated Spz is produced (Peri et al., 2002). In addition, the first gene expression boundary is established at 20% circumference, matching the expression boundary of the Dl target gene *sna*. Recent measurements of the Dl gradient have shown that the gradient decays by almost 50% over this 20% spatial range (Kanodia et al., 2009; Liberman et al., 2009; Stathopoulos and Levine, 2002). To rigorously define the steepness of the gradient ("sharpness"), we measure the relative decay from its maximal level, found at x = 0, to its value at the expression boundary, $x = L_V/2$, $L_V$ being the size of the morphogen expression domain, with embryo size normalized to 1.

Spz, the Tl-activating ligand, is uniformly processed by proteolytic cleavage throughout the *pipe* domain. The Spz precursor can be cleaved to generate two entities: the C-terminal domain (C-Spz), which functions as an activating ligand (DeLotto et al., 2001; Weber et al., 2003); and an N-terminal domain (N-Spz), whose overexpression inhibits ventral fates (Morisato, 2001). The mere diffusion of the activated C-Spz away from the domain of morphogen production could produce a gradient within the production domain. However, we noted that such diffusion produced a very shallow gradient (Figures 2A–2C). In fact, analytical analysis confirmed that the maximal sharpness that can be achieved by diffusion of C-Spz out of its domain of expression is 9%, a value that renders the gradient highly sensitive to even small fluctuations in the production or degradation rates of the morphogen, and cannot be used to support robust patterning. Furthermore, extending the model to include nonlinear degradation of Spz did not increase the sharpness of the gradient (Figure S1 available online). Similarly, adding cogeneration of the inhibitory N-Spz and activating C-Spz was not sufficient for producing a sharp gradient (Extended Experimental Procedures).

### A Self-Organized Shuttling Mechanism Produces a Sharp and Robust Gradient

We considered the recently reported observation that following cleavage of the Spz precursor by the serine protease Easter (Ea), the separate C- and N-terminal parts of Spz remain

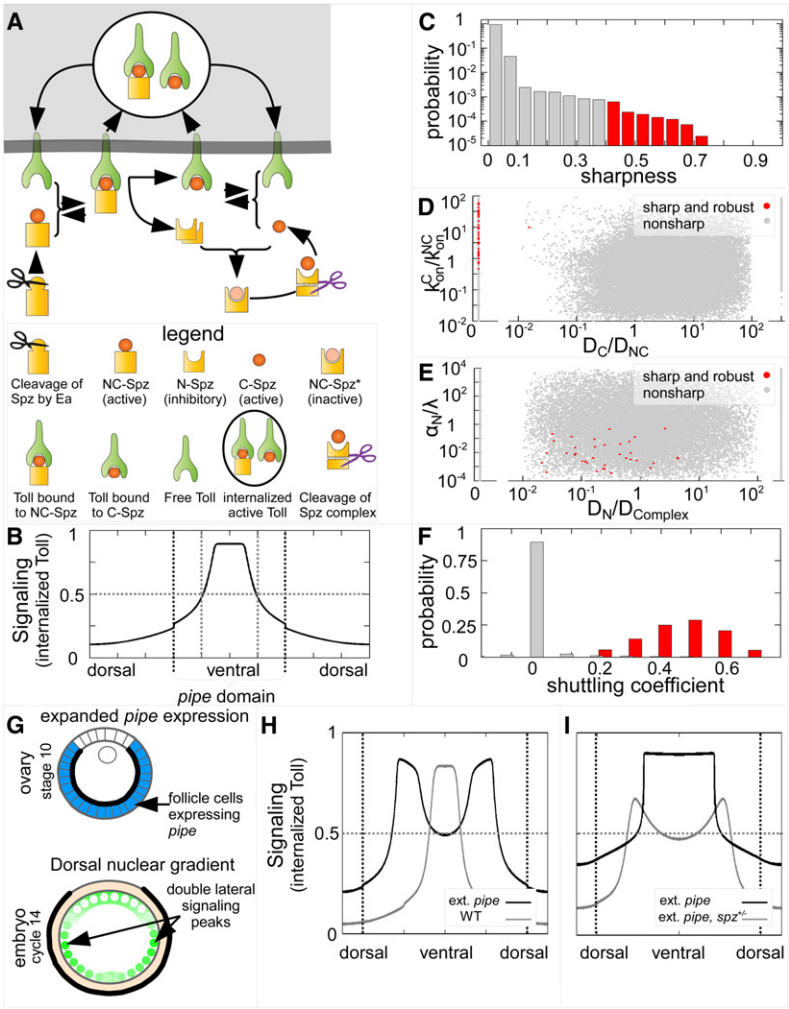


**Figure 3. Formation of a Sharp Gradient by Self-Organized Shuttling**

(A) Molecular model is shown. Cleavage of Spz by Ea produces an active ligand, NC-Spz. Binding of NC-Spz to the receptor Tl may lead to either internalization of the active ligand-receptor complex, or to its dissociation into two inhibitory molecules of N-Spz and an active complex of Tl bound to C-Spz. This complex, in turn, may internalize or dissociate into a free receptor and a free active ligand, C-Spz. C-Spz and N-Spz can bind to form an inert complex, NC-Spz*, which can be cleaved in the *pipe* domain, releasing C-Spz while degrading or inactivating N-Spz. Internalized receptors are the molecular signaling species. Receptors are recycled, whereas internalized ligands are degraded.

(B–F) Numerical screen is shown. A numerical screen was run on the kinetic parameters defining the interactions in (A), allowing also the diffusion and turnover of molecular species, to find parameters that result in sharp and robust signaling profiles (Experimental Procedures).

(B) Particular screen result. A signaling profile (levels of internalized Tl) exhibiting a sharp decrease from the ventral midpoint to the border of *sna* expression (gray vertical dashed lines). *pipe* expression domain is marked with heavy dashed lines. The threshold for *sna* expression is set to half of the maximal signaling level (gray horizontal dashed line).

(C) About one million parameter sets were tested, and only 0.04% were found to be consistent sets, forming a sharp (sharpness >0.4) profile that is robust to parameter perturbations. Over 99% of the solutions had sharpness smaller than 0.1.

(D and E) Consistent parameter sets, in red, were characterized by effectively no diffusion of C-Spz, and faster binding dynamics of C-Spz to Tl than NC-Spz to Tl (D). N-Spz was degraded much faster when in complex with C-Spz, and diffused slower than the inert NC-Spz* complex. Note that almost all consistent parameter sets (red) display no diffusion of C-Spz (E). Gray dots in (D) and (E) represent biologically valid but nonsharp gradients (Extended Experimental Procedures).

(F) Sharp and robust solutions are characterized by shuttling of C-Spz ventrally from its ventro-lateral production domain. Although most solutions displayed almost no shuttling, sharp and robust solutions had a positive shuttling coefficient. To achieve better statistics, a subsequent screen was run to identify over 3,000 parameter sets resulting in shuttling, using parameter characterization in (D) and (E). See Extended Experimental Procedures for definition of the shuttling parameter.

(G) Expanding the *pipe* expression domain to the ventral 80% of the ovary may result in double lateral peaks of Dl nuclear localization in the embryo.

(H) Parameter sets resulting in a sharp and robust gradient (gray) may form a double signaling peak (black) when the *pipe* expression domain is expanded to the ventral 80% of the ovary (ext. *pipe*). Black dashed lines denote the extended *pipe* expression domain; gray dashed line denotes the threshold for *sna* expression.

(I) In accordance with experimental results, some consistent sets display an expanded ventral signaling peak (ext. *pipe*, black). Reducing the *spz* gene dosage reveals the double signaling peak (ext. *pipe*, $spz^{+/-}$, gray). Markings as in (H).

See also Figure S2 and Tables S3 and S4.

associated (Weber et al., 2007). This form of the Spz ligand (NC-Spz) can bind and activate the Tl receptor (Figure 3A). Binding to the Tl receptor is in fact necessary for the final dissociation of the C- and N-terminal parts, generating a free activator (C-Spz) and inhibitor (N-Spz). We reasoned that this property might provide additional regulation of inhibitor production and may sharpen the gradient.

We formulated a mathematical model that accounts for this two-step process of free ligand production. The model allows for the rebinding of the dissociated N- and C-Spz portions to produce an inactive complex (NC-Spz*), and considers the endocytosis of Tl following activation (Lund et al., 2010), which is taken as a measure for signaling. A general analytical solution is not available, and we therefore studied the dynamics of the model using numerical simulations. Specifically, we searched systematically for parameters such as kinetic rate constants and diffusion rates, for which a sharp and robust activation gradient is established.

Although most parameters define a gradient that is rather shallow within the *pipe region* ($x < L_V$), sharp and robust

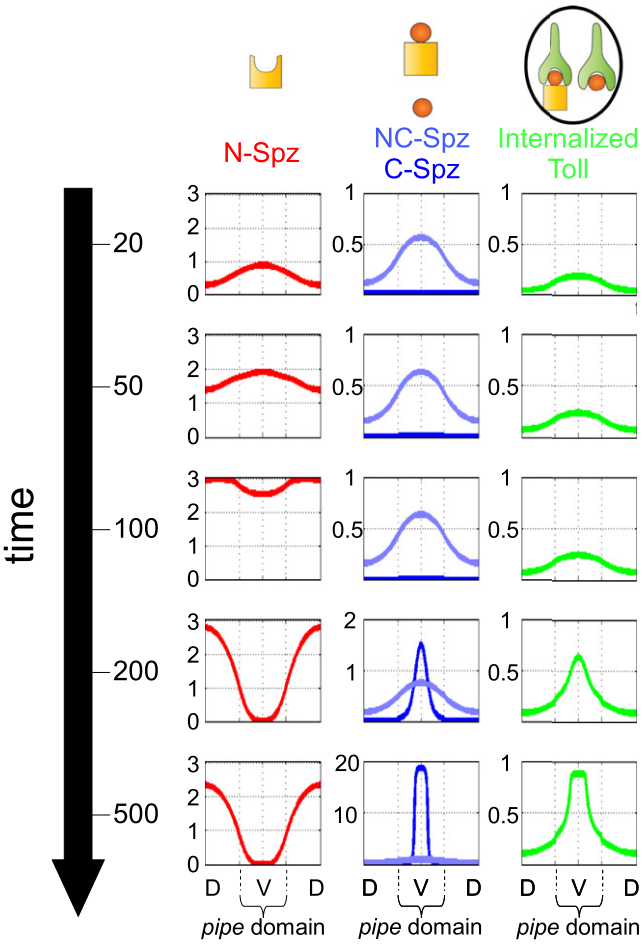


**Figure 4. Dynamics of Gradient Formation Reveals Self-Organized Shuttling**

Shown are the spatial profiles of the inhibitor, N-Spz (red), the active ligands NC-Spz (light blue) and C-Spz (blue), and the internalized Tl levels (green) in time from early (top) to late (bottom). The signaling gradient is initially dominated by NC-Spz, forming a shallow gradient defined by diffusion. N-Spz accumulates following binding of NC-Spz to Tl. Formation of the inert complex with C-Spz and the subsequent degradation of the complex in the ventral domain leads to a dip in N-Spz levels in the lateral domain. A ventral flux of N-Spz facilitates shuttling and leads to the formation of a sharp C-Spz gradient and further polarization of N-Spz gradient. In the ventral domain of the signaling gradient, the internalized receptor, becomes gradually dominated by C-Spz, whereas the dorsal and lateral domains are mostly affected by NC-Spz. Note the change of scale in the middle row. See also Figure S3 and Tables S1, S2, S4, and S5.

gradients did emerge (Figures 3B and 3C). This is in marked contrast to models that considered an immediate, one-step separation between N- and C-Spz following cleavage by Ea, where no sharp gradients could be identified (Extended Experimental Procedures). The sharp solutions were confined to a subset of the parameter space with several characteristics. First, C-Spz did not diffuse freely. Rather it diffused only in association with N-Spz, in either the active (NC-Spz) or inactive (NC-Spz*) complexes. Second, the binding and dissociation kinetics between NC-Spz and the Tl receptor were slower than that of the free C-Spz (Figure 3D; note that in all simulations, the dissociation constant [ratio of on versus off rate] was kept the same, in accordance with experimental results by Weber et al., 2007).

Inactivation of N-Spz is an important additional feature. In all consistent solutions, N-Spz was inactivated mostly while in complex with C-Spz, and this inactivation was biased toward the ventral domain defined by *pipe* expression (Figure 3E). One plausible mechanism may involve a protease that cleaves N-Spz in the NC-Spz* complex, to release active C-Spz. Interestingly, a Pipe-dependent mechanism by which Gastrulation defective (GD) ventrally restricts the processing of Ea by Snake (Snk) was recently reported by Cho et al. (2012). This suggests that the protease that carries out the putative cleavage of the inactive complex could potentially be Ea or Snk.

## The Dynamic Formation of a Sharp Gradient through Self-Organized Shuttling

Examining the consistent solutions that produced a sharp gradient, we noticed that in all cases, the active ligand C-Spz was concentrated toward the ventral midline, $x = 0$. Thus, the sharp gradient was produced not merely by a graded inhibition of a uniformly produced ligand but by the physical translocation of the ligand toward the center from a broad production domain (Figure 3F; Extended Experimental Procedures). As described above, this is the hallmark of a shuttling mechanism (Eldar et al., 2002; Meinhardt and Roth, 2002). Furthermore, several of the biochemical properties characterizing the consistent solutions are defining properties of the canonical shuttling mechanism: low diffusion of the active ligand C-Spz, facilitation of C-Spz movement by binding to the inhibitor N-Spz, and the enhanced degradation of N-Spz when in complex with C-Spz (Figures 3D and 3E).

Identifying the shuttling mechanism here was surprising to us because shuttling of the ligand by its inhibitor is possible only when there is a flux of inhibitor toward the center. Here, however, Spz is processed within the entire *pipe* domain. Moreover, the inhibitor is produced following the binding of the processed ligand (NC-Spz) to the receptor, which is expected to occur primarily throughout the ventral *pipe* expression domain. What then leads to a polarized production of the inhibitor?

Examining the dynamics of gradient formation (Figure 4), we noted that initially, the signaling gradient is dominated by the processed ligand (NC-Spz), whose distribution is determined according to the simple diffusion model. However, binding of NC-Spz to Tl generates N- and C-Spz, mostly in the *pipe* domain. Rebinding of N- and C-Spz generates the inert complex (NC-Spz*) that is subsequently degraded in the *pipe* domain, causing effective degradation of N-Spz in the ventral part of the embryo, whereas C-Spz does not diffuse and is deposited ventrally. Ventral depletion of N-Spz leads to its accumulation laterally, outside the *pipe* domain. The ventral accumulation of C-Spz leads to occupation of the receptors by C-Spz in this domain. NC-Spz therefore binds Tl more laterally, releasing N-Spz in a polarized manner and leading to shuttling (animated in PaperFlick). The gradient can be divided into two regions. The ventralmost part is formed through shuttling and dominated by C-Spz. The sharp profile in this region is characteristic of the shuttling mechanism. The ventro-lateral domain is much flatter

because it is formed through diffusion of NC-Spz and dominated by this ligand. Interestingly, this division of the DV axis and the dynamics of the Dl nuclear gradient were recently observed experimentally by Reeves et al. (2012).

### Reassociation between the Two Parts of Spz

Reassociation between N-Spz and C-Spz plays a crucial role in the model because it provides the means to shuttle C-Spz ventrally. To experimentally demonstrate that N-Spz and C-Spz possess the capacity to physically associate, we made use of two constructs: V5-tagged N-Spz fused C terminally to a transmembrane domain (V5-N-Spz-TM), and a secreted and biologically active signal peptide-C-Spz-GFP fusion protein (SP-C-Spz-GFP) (Figure 5A) (Cho et al., 2010). HeLa cells expressing membrane-anchored V5-N-Spz-TM were incubated with medium secreted by *Drosophila* S2 cells that had been transfected either with SP-C-Spz-GFP, or with a signal peptide-GFP (SP-GFP) fusion protein, that served as a control. Incubation and washes of the medium were carried out under conditions where endocytosis is inhibited, and the subsequent immunohistochemical staining was performed on nonpermeabilized cells, so that only extracellular proteins were detected. A strong GFP signal was displayed on most cells expressing N-Spz-TM and incubated with secreted SP-C-Spz-GFP (75%), but no such signal could be detected following incubation with the control medium (Figures 5B and 5C). These observations imply that, as predicted by the model, N- and C-Spz can readily reassociate.

### The Reassociated N- and C-Spz Complex Is Inactive

A second prediction of the model is that the complex generated by reassociated N- and C-Spz (NC-Spz*) is inactive and is, therefore, functionally distinct from the biologically active NC-Spz, formed immediately after cleavage by Ea. To validate this prediction, we sought to test the activity of the reassociated complex in *Drosophila* embryos. We initially examined alterations in DV fates, following separate overexpression of N- and C-Spz, under control of the maternal driver *nos-Gal4*. Expression of SP-C-Spz-GFP in this manner led to a pronounced lateralizing effect. Although the ventralmost mesodermal fates and their position were not significantly altered, the expression domain of the lateral marker *intermediate neuroblasts defective* (*ind*) expanded considerably, to cover the entire dorsal side of the embryo, whereas dorsal fates, normally marked by expression of *dpp*, were strongly diminished. In contrast, expression of N-Spz by the same driver did not give rise to any detectable phenotype at the level of altered gene expression or cuticle patterns, and the embryos were viable.

A marked inhibitory effect of N-Spz was detected, however, following coexpression with SP-C-Spz-GFP. The expanded *ind* expression induced by SP-C-Spz-GFP was no longer apparent, and dorsal *dpp* expression was restored (Figures 5D–5L). These observations imply formation of a functionally distinct, reassociated complex between N- and C-Spz, which interferes with the capacity of C-Spz to activate the Tl signaling pathway. They further suggest that binding to C-Spz can account for the previously reported inhibitory activity of N-Spz when injected into early embryos (Morisato, 2001).

Interestingly, in the ventral region, coexpression of N- and C-Spz in this manner had an attenuating effect, such that the endogenous expression of ventro-lateral genes such as *ind* was abolished, and expression of the ventral marker *sna* became narrower. Because this effect was not observed upon expression of N-Spz alone (where the wild-type pattern was maintained), it represents an outcome of the reassociated N- and C-Spz complex. We hypothesize that this results from some interaction with other signaling processes that function in the ventral region, for example through interaction of the NC-Spz* with the Ea protease processing Spz, or by the formation of higher-order complexes between the N-Spz and C-Spz that inhibit Tl activation.

### Self-Organized Shuttling Accounts for Axis Duplication

As an additional test of the model, we examined whether it can account for the observation that increasing the *pipe* expression domain from its endogenous 40% to 80% of the ventral region results in a pattern duplication: the monotonous single-peak gradient observed in wild-type is replaced by a two-peak profile in a significant portion of the embryos (Figure 3G) (Morisato, 2001; Moussian and Roth, 2005; Roth and Schüpbach, 1994). Indeed, we could readily identify parameters for which extending the region of Spz processing in the model leads to axis duplication (Figure 3I).

Notably, the resulting ventral minimum between the two peaks is rather shallow and may be close to the threshold value for *twi* and *sna* expression. This can explain why only half of the embryos showed axis duplication, whereas the rest showed an expanded *twi* expression domain (Morisato, 2001). Small differences in system parameters between different embryos can result in one embryo exhibiting a single, extended peak, and the other two peaks. The model can also explain the observation that reduction in *spz* gene dosage increases the fraction of embryos with two *twi* expression domains, in cases where the *pipe* expression domain was expanded (Morisato, 2001) (Figure 3H).

A simple explanation accounts for formation of the two peaks: shuttling is not sufficiently effective in concentrating the ligand at the midline but only to shift it from the edges of the *pipe* domain. As a result, the ligand is not concentrated toward the ventralmost regions, and signaling is below maximal levels.

### The Phenotype of Uniform *pipe* Is Consistent with Self-Organized Shuttling

The double peak observed when the *pipe* domain is extended to 80% of the embryo was lost when *pipe* was expressed uniformly throughout the embryo (Sen et al., 1998). This is a surprising observation that presents a challenge to self-organized mechanisms that rely on the spontaneous breaking of symmetry, such as those described by a Turing mechanism (Turing, 1952). We asked if self-organized shuttling can account for this observation as well. Indeed, we find that when uniform cleavage of the Spz precursor is imposed on the model, no pattern is observed within the typical patterning time. Instead, the inability to concentrate the ligand toward the midline of the embryo predicts a uniform, intermediate level of signaling (Figures 6A and 6B; note that this symmetry can be broken, leading to a double-peak solution

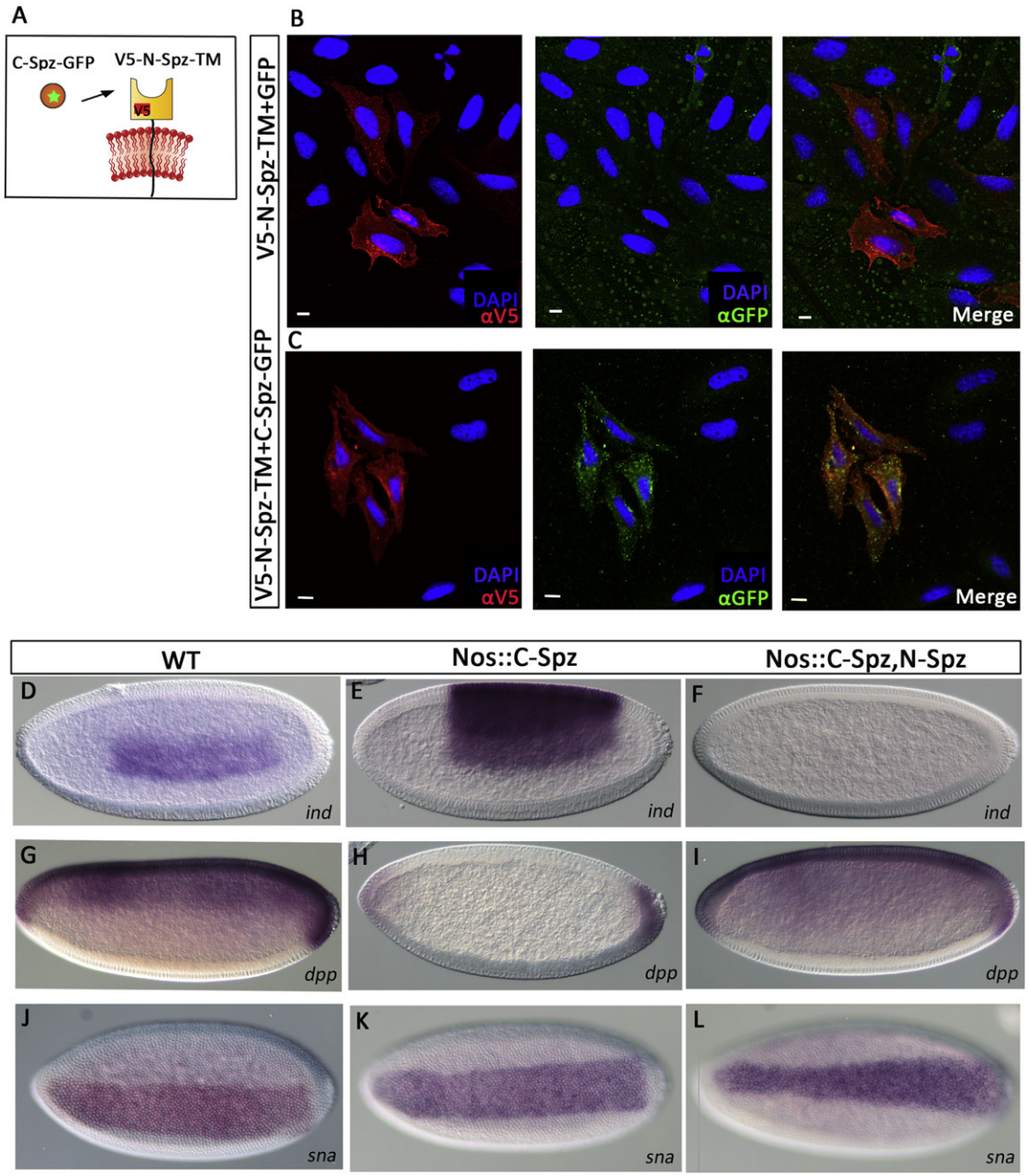


**Figure 5. N-Spz and C-Spz Can Rebind and Create an Inactive Complex**

(A) Schematic drawing of the experimental procedure: a membrane-anchored construct of N-Spz tagged with V5 was expressed in cells, and secreted C-Spz tagged with GFP was added to the medium.

(B) Secreted GFP (green) does not bind cells that are transfected with membrane-anchored N-Spz (red). Scale bars, 10 μm.

(C) C-Spz GFP (green) is attached specifically to cells that are transfected with membrane-anchored N-Spz (red). Scale bars, 10 μm.

(D, G, and J) RNA in situ hybridization to wild-type embryos with a probe to *ind*, *dpp*, and *sna*, respectively.

(E, H, and K) In embryos expressing *UAS-C-Spz* by *nos:Gal4* (E) *ind* expression is broader, (H) *dpp* expression is absent, and (K) *sna* expression is unaltered, indicating an elevation in Tl signaling in the dorsal region.

(F, I, and L) In embryos expressing *UAS-C-Spz* and *UAS-N-Spz* using *nos:Gal4*, (F) *ind* expression is absent, (I) *dpp* reappears, and (L) *sna* is mildly narrower, indicating an abolishment of the effects of ectopic C-Spz.

Anterior is oriented toward the left, and dorsal is up in (D)–(L).

Cell

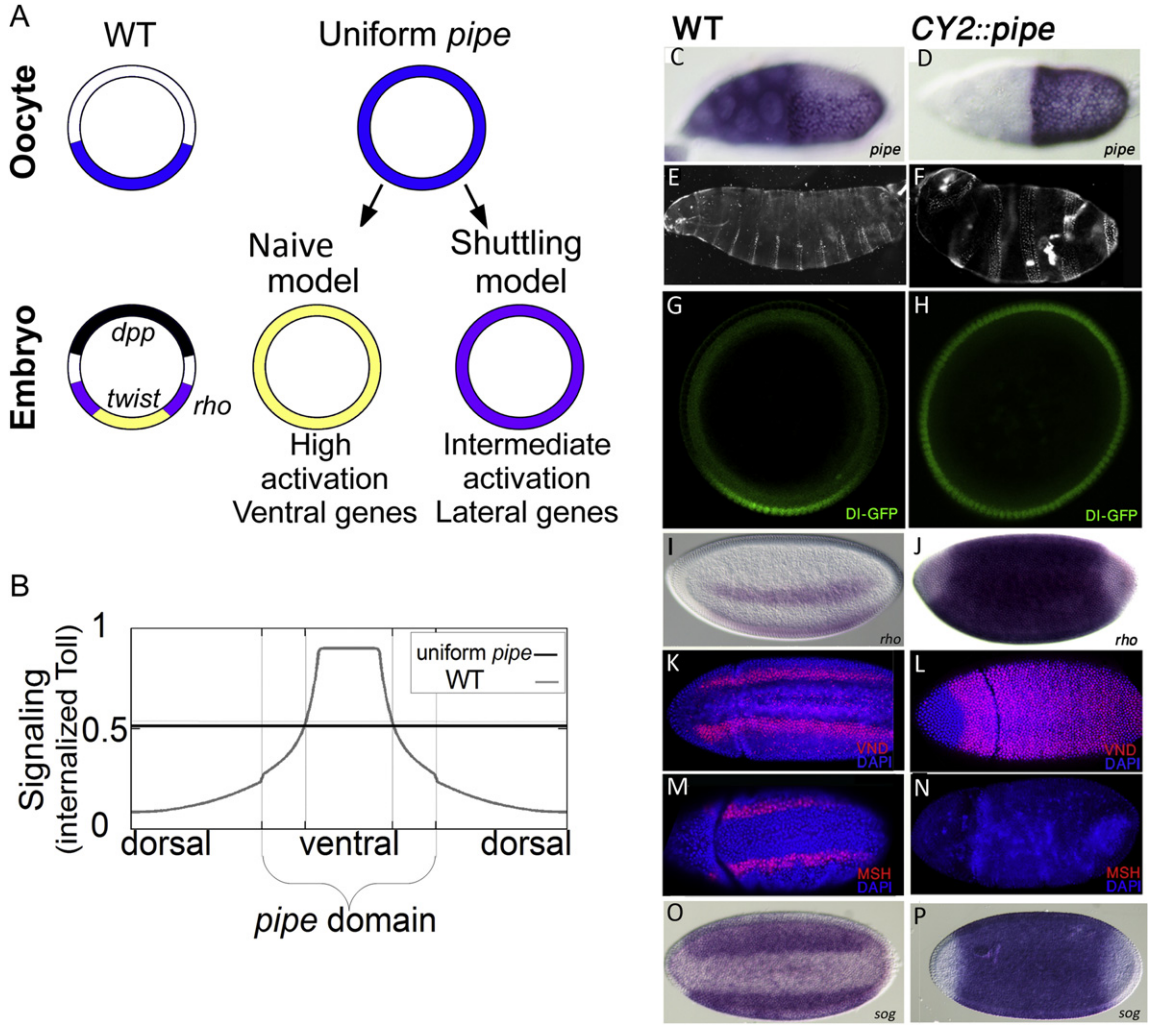


**Figure 6. Uniform Expression of *pipe* Leads to Lateralization of the Embryo**

(A) Predicted phenotype upon uniform *pipe* expression: naive models predict maximal Tl receptor activation leading to uniform *twi* and *sna* expression. In contrast the shuttling model predicts medium activation because the ligand is not concentrated ventrally, leading to lateral fates and the expression of ventro-lateral genes as *rho*.

(B) A uniform profile of activated Tl obtained upon uniform expression of *pipe.* The black curve is the numerical solution obtained when *pipe* is taken to be uniformly expressed in the follicular epithelium, and the gray curve is the profile of Tl activation obtained for the same parameters in the wild-type case. *sna* expression threshold is indicated by the dashed gray horizontal line.

(C–P) Experimental results supporting the shuttling model.

(C) Stage 10 ovary of a wild-type female stained by an RNA probe for *pipe*. *pipe* is expressed in the ventral 40% of the follicular epithelium.

(D) Stage 10 ovary of a *cy2:Gal4; UAS-pipe* female stained by the same probe. *pipe* is expressed uniformly in all the follicular epithelium. Note that WT *pipe* in situ detects also nurse cell staining because of the longer exposure, compared to the exposure time in the uniform *pipe* case (approximately six times longer). (E, G, I, K, M, and O) Progeny of WT females. (F, H, J, L, N, and P) Progeny of *cy2:Gal4; UAS-pipe* females.

(E) Lateral view of larval cuticle: stripes of ventral denticles are formed along the AP axis in the ventro-lateral region.

(F) Larval cuticles show the formation of rings of ventral denticle material, indicating acquisition of ventro-lateral fate throughout the DV axis.

(G and H) GFP staining of Dl-GFP in early stage 4 embryos laid by WT (G) and *cy2:Gal4; UAS-pipe* (H) females. In the WT case a gradient of nuclear Dl is observed with a peak in the ventral region. In the uniform *pipe* case, nuclear Dl is distributed uniformly in the nuclei, at an intermediate level corresponding to lateral fates.

(I and J) *rho* expression pattern in a stage 5 embryo laid by WT (I) and *cy2:Gal4; UAS-pipe* (J) females. In the WT case, *rho* is expressed in ventro-lateral stripes (the image was taken from a ventro-lateral view). In the uniform *pipe* case, *rho* displays a uniform expression along the DV axis (the image was taken from a lateral view).

(K and L) Ventral view of Vnd protein staining of early embryos laid by WT (K) and *cy2:Gal4; UAS-pipe* (L) females. Normally, Vnd is expressed in ventro-lateral stripes, but in the uniform *pipe* case, it is expressed uniformly throughout the embryo.

(M and N) Ventral view of Msh staining of early embryos laid by WT (M) and *cy2:GAL4; UAS-pipe* (N) females. In the WT case Msh is expressed in two lateral stripes, located dorsally to the Vnd stripes. In the uniform *pipe* case, Msh is not expressed at all.

(O and P) The expansion of ventro-lateral fates, following uniform expression of *pipe* in females, is also reflected by the expansion of the WT lateral *sog* expression domain (O) to the entire circumference of the embryo (P). These stainings reveal that the embryos laid by *cy2:Gal4; UAS-pipe* females acquire a ventro-lateral fate corresponding to the Vnd expression domain, throughout the DV axis.

See also Table S5.

following a delay that is significantly longer than the time in which the pattern is generated; data not shown).

This prediction of intermediate-level signaling in embryos following uniform expression of *pipe* during oogenesis is in fact a unique signature of shuttling, which requires the concentration of ligands in order to achieve maximal signaling levels. In contrast, mechanisms that rely only on the diffusion and degradation of C-Spz, and perhaps its inhibition by a coproduced inhibitor, naturally lead to a uniform, maximal level of activation throughout the embryo, when *pipe* is uniformly expressed.

Thus, our model predicts that uniform expression of *pipe* will lateralize, rather than ventralize, the embryos. Previous reports indicated that this is indeed the case. Embryos laid by females that express *pipe* uniformly in follicle cells lose any mark of polarity along the DV axis. Ventral gastrulation movements appear everywhere, and the larval cuticles show the formation of rings of denticle material, indicating lateralization of the progeny embryos (Sen et al., 1998).

To better define the precise degree of these fate shifts, we expressed *pipe* uniformly in follicle cells and followed both the expression of target genes and the nuclear localization of Dl in the embryo (Figures 6C–6P). The *rhomboid* (*rho*), *short gastrulation* (*sog*), and *ventral nervous system defective* (*vnd*) genes, which are normally expressed in the lateral neuroectoderm (Bier et al., 1990) or at a restricted domain within the neuroectoderm (Chu et al., 1998; McDonald et al., 1998), respectively, are seen throughout the circumference when *pipe* is uniform. A transgenic Dorsal-GFP (Dl-GFP), which faithfully recapitulates distribution of the Dl protein (DeLotto et al., 2007), shows a nuclear localization throughout the circumference at intermediate levels matching those of nuclei at the lateral region of wild-type embryos (Figures 6G and 6H). Together, these results indicate intermediate levels of Tl pathway activation throughout the embryo, consistent with the shuttling mechanism: despite the uniform activation of Spz resulting from ubiquitous *pipe* expression, maximal levels of Tl activation cannot be obtained in the absence of asymmetries and shuttling.

### The Flux of N-Spz Dictates Mesoderm Position

The essence of the shuttling model is the redistribution of the active ligand by a shuttling molecule (N-Spz in this case), whose effective production domain flanks the morphogenic field. Upon association with the ligand, the shuttling molecule inhibits signaling. However, association provides the driving force for shuttling because the diffusion flux directs the release and concentration of the ligand in the region furthest from the region in which the shuttling molecule is produced. This distribution allows the shuttling molecule to function as an inhibitor of signaling close to the source that produces the shuttling molecule and as a facilitator of signaling furthest away from it.

To locally produce N-Spz, we capitalized on the fact that binding of NC-Spz to Tl promotes the dissociation between N- and C-Spz (Weber et al., 2007). A full-length Tl construct tagged C terminally with the Myc antigen was expressed at the anterior end of the embryo using the *Hsp83* maternal promoter and the *bcd* 3′ UTR. Staining for the Myc tag showed a highly restricted anterior localization (Figures 7A and S4), consistent with the limited diffusion capacity of Tl, even prior to cellularization (Huang et al., 1997).

Lateralized embryos display a uniform, intermediate level of Dl protein in all nuclei (Figure 7B). Expression of Toll-Myc (Tl-Myc) at the anterior end of such embryos alters the uniform nuclear distribution of Dl, affecting it in three major ways. First, high nuclear Dl levels are sometimes induced in the anterior region where Tl-Myc is expressed (Figure 7C). This local effect is likely to result from excess anterior expression of Tl and does not bear on our model. Second, the levels of nuclear Dl are diminished up to about half embryo length from the anterior pole, reflecting the shorter-range nonautonomous effect of releasing high levels of N-Spz, which can sequester and inactivate C-Spz (Figure 7D). Finally, the levels of nuclear Dl appear elevated toward the posterior pole, consistent with long-range facilitation of ligand release (Figure 7D).

To ascertain whether the shift to a nonuniform distribution of nuclear Dl following anterior Tl expression is reflected in the expression patterns of high nuclear Dl target genes, we monitored the *sna* mRNA pattern in lateralized embryos. A significant increase in the proportion of lateralized embryos expressing *sna*, following anteriorly localized expression of Tl-Myc, was indeed observed: from ~81% of lateralized embryos that did not express *sna* at all (Figure 7E) to ~59% *sna*-expressing embryos. In particular, 30% of the anterior-Tl-expressing embryos displayed a prominent posterior *sna* stripe (Figure 7G). Only 6% of embryos derived from females expressing *pipe* uniformly, but not anterior Tl, display this pattern (Figure 7F), a feature that can be attributed to rare, spontaneous symmetry breaking, which is in fact predicted by the model. Taken together, the changes in the patterns of Dl nuclear localization and *sna* gene expression upon anteriorly localized expression of Tl-Myc suggest that a flux of N-Spz can generate maximal signaling levels at the position that is furthest from its source.

Thus, ectopic expression of Tl at the anterior-most region establishes a signaling gradient along the anterior-posterior axis. This supports the main prediction of the shuttling mechanism: namely, the capacity of N-Spz to act as a nonautonomous short-range inhibitor and long-range activator of signaling.

## DISCUSSION

### A Self-Organized Shuttling Mechanism

By its nature, diffusion tends to homogenize concentration differences and is, therefore, not ideal for refining a wide expression domain into narrower gradients. Indeed, passive diffusion of a morphogen away from its source is insufficient for producing a sharp gradient within the source itself, as we demonstrated here. Yet, during early development, pattern often has to be established within a wide domain in which the morphogen is expressed.

We describe a self-organized shuttling mechanism that establishes a robust and sharp gradient of morphogen concentration within a broad domain of morphogen production in the early *Drosophila* embryo. This mechanism relies only on diffusion but necessitates an additional inhibitor molecule, which binds the morphogen and facilitates its diffusion. We and others have previously characterized the shuttling mechanism in the context

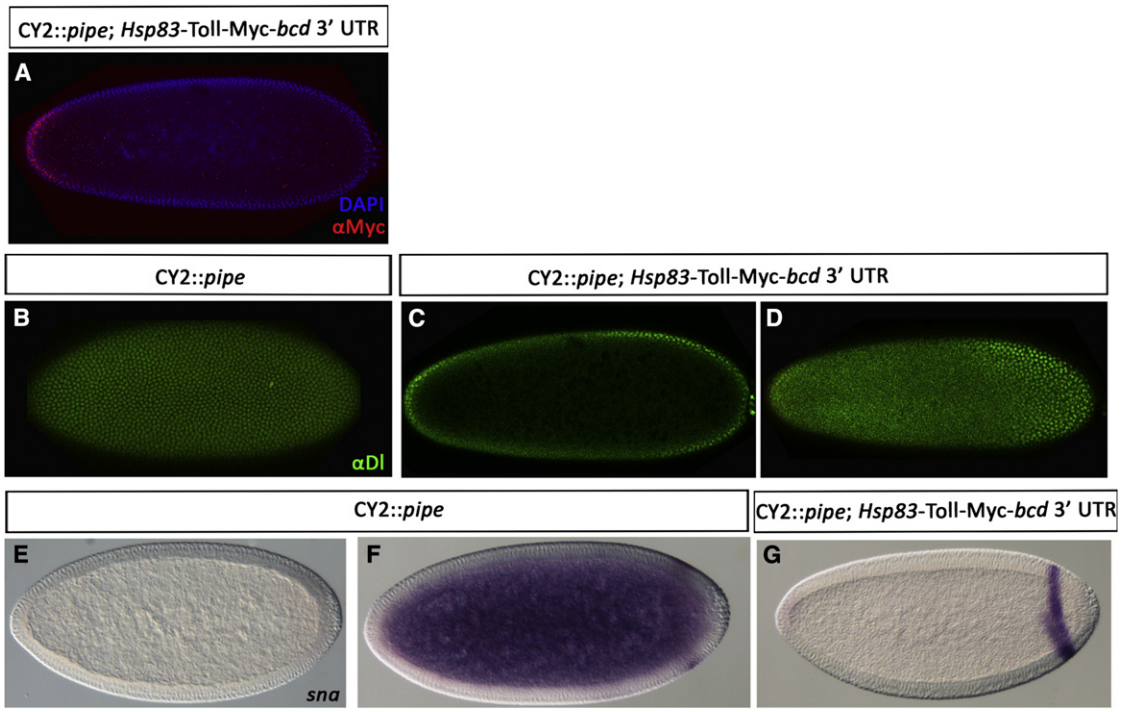


**Figure 7. Anterior Tl Overexpression Leads to Short-Range Inhibition and Long-Range Activation of Dl along the AP Axis**

(A) High levels of anterior Tl expression were obtained by *Hsp83* promoter and *bcd* 3′ UTR. Tl-Myc is localized to the anterior pole.

(B) Embryos laid by females expressing uniform *pipe* show uniform intermediate levels of nuclear Dl.

(C and D) Uniform *pipe* embryos that overexpress Tl at the anterior pole show short-range inhibition, indicated by low levels of nuclear Dl at the anterior region, and long-range activation, indicated by high levels at the posterior pole. High nuclear Dl at the anterior Tl overexpression domain reflects a cell-autonomous effect. Panels represent different focal planes of the same embryo.

(E) Of uniform *pipe* embryos, 81% does not express the ventral gene *sna*.

(F) Of uniform *pipe* embryos, 6% expresses *sna* in a weak posterior stripe (n = 115).

(G) Of uniform *pipe* embryos that overexpress Tl at the anterior pole, 59% expresses *sna* (n = 96), and half of them expresses *sna* in a posterior stripe. Expression of *sna* at the posterior pole indicates long-range activation, consistent with posterior shuttling of C-Spz by the anterior source of N-Spz. Anterior is oriented toward the left, and dorsal is up.

See also Figure S4.

of a patterning event taking place later in embryogenesis—the formation of the embryonic BMP activation gradient (Eldar et al., 2002; Matsuda and Shimmi, 2012; Meinhardt and Roth, 2002; Mizutani et al., 2005; Shimmi et al., 2005; Wang and Ferguson, 2005). In this context, however, the key asymmetry is provided by a prepattern that allows for asymmetric secretion of the inhibitor Sog, outside the domain being patterned, to drive the process. Such asymmetry, however, is not available to the earlier patterning system, the initial establishment of DV polarity, where the inhibitor is coproduced during morphogen processing. Our main finding is that such asymmetry is also established here, through a self-organized mechanism.

## Versatile Activities of the Spz Prodomain

Self-organization is made possible by the remarkable structural and functional versatility of the N- and C-terminal domains of Spz following its cleavage by the protease Ea, and their capacity to generate an active complex, as well as an inactive complex following reassociation. Spz encodes a secreted protein that contains a signal peptide, an N-terminal prodomain, and a cysteine-rich C-terminal domain that mediates binding to the Tl receptor. An Ea cleavage site separates between these two domains. Spz is secreted as a dimer and facilitates the corresponding dimerization of Tl upon binding. However, the N terminus appears to be much more than an inhibitory prodomain. Upon cleavage by Ea the conformation of Spz is altered such that the C terminus is now exposed to bind Tl, while a noncovalent association with the N terminus is maintained. Binding to Tl releases the N-terminal region of Spz. Our model also requires the dissociation constant between Tl and C-Spz to be relatively high, allowing for release of some of the C-Spz molecules.

A central prediction of the model is that N-Spz and C-Spz can reassociate following their initial separation, and we verified this prediction experimentally. There are biological precedents for reassociation between the active ligand and its prodomain that have important physiological consequences: the BMP family ligands Myostatin and GDF11 are expressed as a proligand. In both cases, cleavage is followed by reassociation of the N-terminal prodomain with the C-terminal dimer, maintaining the ligand in a latent form. Subsequent cleavage of the prodomain by the Tolloid metalloprotease activates the latent ligand (Ge et al., 2005; Wolfman et al., 2003).

We have further demonstrated that reassociation of the N- and C-terminal domains of Spz produces a distinct form that cannot activate Tl. This diversity of Spz-based molecules thus allows the implementation of a shuttling mechanism during the early phase of development, despite the limited number of players, because each of the Spz forms plays a different role in the process. Interestingly, a distinct role for the N-terminal region of the protease Gd was recently reported. Following cleavage of this fragment, it binds the vitelline membrane in the domain defined by expression of *pipe*, and facilitates the processing of Ea by Snk (Cho et al., 2012).

The capacity of N- and C-Spz to reassociate and form an inert complex constitutes the shuttling pair. In analogy to shuttling of Dpp in the dorsal ectoderm, N-Spz fulfills an equivalent role to Sog. Indeed, we can dictate the polarity of the DV axis in lateralized embryos simply by generating a local source for producing higher levels of N-Spz that will lead to a flux, and direct the expression of mesodermal genes at the opposite pole.

In conclusion, by combining computational and experimental analyses of the Spz/Tl pathway, we demonstrate that a sharp and robust patterning gradient can be generated within a uniform region, through a mechanism we term self-organized shuttling. This mechanism relies on diverse interactions between the ligand and its prodomain, leading to a dynamic and predictable distribution of the active ligand. Although the initial shuttling models were restricted to BMP family ligands in several organisms, the current work extends the concept to another signaling pathway involving Spz and Tl. Shuttling mechanisms that generate sharp gradients are essential in the early embryo, where the spatial refinement of gene expression is minimal, and the initial patterning that takes place, prior to the onset of zygotic gene expression, cannot rely on transcriptional networks.

## EXPERIMENTAL PROCEDURES

### Fly Strains

The following lines were used: *UAS-pipeST2* (Sen et al., 1998), Dl-GFP (DeLotto et al., 2007), *UAS-C-Spz-GFP* inserted on a chromosome that contains a deficiency that covers *Tl* (Cho et al., 2010). *UAS–N–Spz* contains the Spz signal peptide (aa 1-29), followed by a triple V5 tag, and N-Spz (aa 30-147). It was inserted into an AttB UASp plasmid and targeted in flies into the attP40 site. *Hsp83-Tl-Myc-bcd* flies were prepared from a construct that was generated by inserting *Hsp83* promoter upstream to Tl-Myc (from T. Ip) into a pAttB plasmid. Transgenic lines were inserted into the attP40 site.

### In Situ Hybridization

Probes for *ind*, *sna*, *dpp*, *sog*, and *rho* were prepared using Roche PCR Dig Probe Synthesis Kit. A probe for *pipe* was prepared using digoxigenin-labeled antisense RNA. Fixation, hybridization, and detection were as previously described by Melen et al. (2005).

### DNA Constructs

N-Spz was prepared by GeneScript from a sequence of Spz signal peptide (Spz amino acids 1–29) followed by triple V5 tag, N-spz (Spz amino acids 30–147), Egfr TM domain (EGFR amino acids 803–856), followed by an HA tag. Signal peptide-C-Spz tagged with GFP (Cho et al., 2010), and Signal peptide-GFP (Schlesinger et al., 2004).

### Cell Culture

HeLa cells were transfected with a DNA construct containing CMV promoter-V5-N-Spz-TM, using jutPEI (from Polyplus). S2 cells were transfected with DNA using ESCORT IV transfection reagent. Expression of *UAS-C-Spz-GFP* was achieved by cotransfection with an *actin-GAL4* plasmid. Medium of C-Spz-GFP-expressing cells was changed to fresh medium w/o serum after 1 day, collected after 2 days, and added to HeLa cells with 0.1% azide. Following 45 min incubation at 37°C, cells were washed three times with PBS and fixed at 4% FA. Antibodies used included anti-V5 (mouse, 1:800; Invitrogen) and anti-GFP (chicken, 1:1,000; Abcam).

### Cuticle Preparation

Embryos were dechorionated using 6% sodium hypochlorite, and the vitelline membrane was removed using methanol (together with Heptan). Embryos were incubated in Hoyer's solution overnight at 67°C and viewed by dark-field microscopy.

### Embryo Immunohistochemistry

Embryos were processed and stained as described by Ben-Yaacov et al. (2001). Primary antibodies and dilutions used in this study include anti-Vnd and anti-Msh (rat, 1:500; a gift from Z. Paroush), anti-GFP (chicken, 1:1000; Abcam), anti-Myc (mouse, 1:100; Santa-Cruz Biotechnology), and anti-Dl (mouse,1:25; Developmental Studies Hybridoma Bank). Secondary Cy2, Cy3 (Jackson ImmunoResearch), or Alexa 488, Alexa 555 (Molecular Probes) conjugated antibodies against the relevant species were used.

Cross-sections were generated using a tungsten needle on stained embryos. Images were obtained using a Zeiss LSM710 confocal system.

### Numerical Screen

The following eight equations were solved systematically using MATLAB:

$$(a)\ \frac{\partial[NCSpz]}{\partial t} = D_{NC}\nabla^2[NCSpz] + \eta(x) - K_{On}[Tl][NCSpz] + K_{Off}[NCSpz - Tl] - \alpha_{NC}[NCSpz];\ \eta(x) = \eta_0\theta(L_V - |x|)$$

$$(b)\ \frac{\partial[CSpz]}{\partial t} = D_C\nabla^2[CSpz] - k_{bind}[NSpz][CSpz] + \lambda[NCSpz^*] - k_{on,C}[Tl][CSpz] + k_{off,C}[CSpz - Tl] + k_{split}[NCSpz - Tl] - \alpha_C[CSpz]$$

$$(c)\ \frac{\partial[NSpz]}{\partial t} = D_N\nabla^2[NSpz] - k_{bind}[NSpz][CSpz] + 2k_{split}[NCSpz - Tl] - \alpha_N[NSpz]$$

$$(d)\ \frac{\partial[NCSpz^*]}{\partial t} = D_{NC^*}\nabla^2[NCSpz^*] + k_{bind}[NSpz][CSpz] - \lambda[NCSpz^*]$$

$$(e)\ \frac{\partial[CSpz - Tl]}{\partial t} = k_{on,C}[Tl][CSpz] - k_{off,C}[CSpz - Tl] + k_{split}[NCSpz - Tl] - k_{end}[CSpz - Tl]$$

$$(f)\ \frac{\partial[NCSpz - Tl]}{\partial t} = K_{On}[Tl][NCSpz] - (K_{Off} + k_{split} + k_{end})[NCSpz - Tl]$$

$$(g)\ \frac{\partial[Tl_{end}]}{\partial t} = k_{end}([NCSpz - Tl] + [CSpz - Tl]) - k_{rec}[Tl_{end}]$$

$$(h)\ T^{tot} = [Tl] + [CSpz - Tl] + [NCSpz - Tl] + [Tl_{end}]$$

A total of 12 parameters were allowed to vary over several orders of magnitude, resulting in a 12-dimensional parameter space that was assayed statistically. For each such parameter set, we solved the equations in a region $-1 < x < 1$, with Spz processing occurring at $-0.4 < x < 0.4$ domain. Zero flux was assumed in the boundaries. Consistent sets were those that result in a monotonous gradient along the DV axis in which signaling in the ventral midline is at least 50% of the maximum, decreases at least by 40% from the ventral midline to $x = 0.2$, and by at least 75% to $x = 0.8$. Robustness was assessed by perturbing the production and degradation rates of all components and measuring the positions where four thresholds were met, resulting in five expression domains. A set was considered robust and consistent if at least 67% of the perturbed sets did not display a large change in expression domains, and were also consistent. See Extended Experimental Procedures, for more details of the screen.

## SUPPLEMENTAL INFORMATION

Supplemental Information includes Extended Experimental Procedures, four figures, and five tables and can be found with this article online at http://dx.doi.org/10.1016/j.cell.2012.06.044.

## ACKNOWLEDGMENTS

We thank R. DeLotto, T. Ip, Z. Paroush, and D. Stein for reagents; Y. Gilad, A. Rubinstein, and I. Koren for technical help; T. Volk for insightful suggestions; and Orit Bechar, Tali Wiesel, and Itzchak Reuven for their dedicated graphic design and animation work. We thank members of our groups for fruitful discussions. D.B.-Z. is supported by the Adams Fellowship Program of the Israeli Academy of Sciences and Humanities. This work was supported by the European Research Council, Israel Science Foundation, Minerva, and the Helen and Martin Kimmel Award for Innovative Investigations to N.B., who is the incumbent of the Lorna Greenberg Scherzer Professorial Chair, and the Minerva Foundation to B.-Z.S., who is an incumbent of the Hilda and Cecil Lewis Professorial Chair in Molecular Genetics.

Received: October 20, 2010
Revised: February 28, 2012
Accepted: June 19, 2012
Published: August 30, 2012

## REFERENCES

Anderson, K.V. (1998). Pinning down positional information: dorsal-ventral polarity in the *Drosophila* embryo. Cell *95*, 439–442.

Ben-Yaacov, S., Le Borgne, R., Abramson, I., Schweisguth, F., and Schejter, E.D. (2001). Wasp, the *Drosophila* Wiskott-Aldrich syndrome gene homologue, is required for cell fate decisions mediated by Notch signaling. J. Cell Biol. *152*, 1–13.

Ben-Zvi, D., Shilo, B.Z., Fainsod, A., and Barkai, N. (2008). Scaling of the BMP activation gradient in *Xenopus* embryos. Nature *453*, 1205–1211.

Bier, E., Jan, L.Y., and Jan, Y.N. (1990). rhomboid, a gene required for dorsoventral axis establishment and peripheral nervous system development in *Drosophila melanogaster*. Genes Dev. *4*, 190–203.

Bollenbach, T., Kruse, K., Pantazis, P., Gonzalez-Gaitan, M., and Julicher, F. (2005). Robust formation of morphogen gradients. Phys. Rev. Lett. *94*, 18103.

Cadigan, K.M. (2002). Regulating morphogen gradients in the *Drosophila* wing. Semin. Cell Dev. Biol. *13*, 83–90.

Cho, Y.S., Stevens, L.M., and Stein, D. (2010). Pipe-dependent ventral processing of Easter by Snake is the defining step in *Drosophila* embryo DV axis formation. Curr. Biol. *20*, 1133–1137.

Cho, Y.S., Stevens, L.M., Sieverman, K.J., Nguyen, J., and Stein, D. (2012). A ventrally localized protease in the *Drosophila* egg controls embryo dorsoventral polarity. Curr. Biol. *22*, 1013–1018.

Chu, H., Parras, C., White, K., and Jiménez, F. (1998). Formation and specification of ventral neuroblasts is controlled by vnd in *Drosophila* neurogenesis. Genes Dev. *12*, 3613–3624.

DeLotto, R., DeLotto, Y., Steward, R., and Lippincott-Schwartz, J. (2007). Nucleocytoplasmic shuttling mediates the dynamic maintenance of nuclear Dorsal levels during *Drosophila* embryogenesis. Development *134*, 4233–4241.

DeLotto, Y., and DeLotto, R. (1998). Proteolytic processing of the *Drosophila* Spätzle protein by easter generates a dimeric NGF-like molecule with ventralising activity. Mech. Dev. *72*, 141–148.

DeLotto, Y., Smith, C., and DeLotto, R. (2001). Multiple isoforms of the *Drosophila* Spätzle protein are encoded by alternatively spliced maternal mRNAs in the precellular blastoderm embryo. Mol. Gen. Genet. *264*, 643–652.

Driever, W., and Nüsslein-Volhard, C. (1988a). The bicoid protein determines position in the *Drosophila* embryo in a concentration-dependent manner. Cell *54*, 95–104.

Driever, W., and Nüsslein-Volhard, C. (1988b). A gradient of bicoid protein in *Drosophila* embryos. Cell *54*, 83–93.

Eldar, A., Dorfman, R., Weiss, D., Ashe, H., Shilo, B.Z., and Barkai, N. (2002). Robustness of the BMP morphogen gradient in *Drosophila* embryonic patterning. Nature *419*, 304–308.

Eldar, A., Rosin, D., Shilo, B.Z., and Barkai, N. (2003). Self-enhanced ligand degradation underlies robustness of morphogen gradients. Dev. Cell *5*, 635–646.

Ephrussi, A., and St Johnston, D. (2004). Seeing is believing: the bicoid morphogen gradient matures. Cell *116*, 143–152.

Ge, G., Hopkins, D.R., Ho, W.B., and Greenspan, D.S. (2005). GDF11 forms a bone morphogenetic protein 1-activated latent complex that can modulate nerve growth factor-induced differentiation of PC12 cells. Mol. Cell. Biol. *25*, 5846–5858.

Huang, A.M., Rusch, J., and Levine, M. (1997). An anteroposterior Dorsal gradient in the *Drosophila* embryo. Genes Dev. *11*, 1963–1973.

James, K.E., Dorman, J.B., and Berg, C.A. (2002). Mosaic analyses reveal the function of *Drosophila* Ras in embryonic dorsoventral patterning and dorsal follicle cell morphogenesis. Development *129*, 2209–2222.

Kanodia, J.S., Rikhy, R., Kim, Y., Lund, V.K., DeLotto, R., Lippincott-Schwartz, J., and Shvartsman, S.Y. (2009). Dynamics of the Dorsal morphogen gradient. Proc. Natl. Acad. Sci. USA *106*, 21707–21712.

Lecuit, T., Brook, W.J., Ng, M., Calleja, M., Sun, H., and Cohen, S.M. (1996). Two distinct mechanisms for long-range patterning by Decapentaplegic in the *Drosophila* wing. Nature *381*, 387–393.

LeMosy, E.K., Hong, C.C., and Hashimoto, C. (1999). Signal transduction by a protease cascade. Trends Cell Biol. *9*, 102–107.

Liberman, L.M., Reeves, G.T., and Stathopoulos, A. (2009). Quantitative imaging of the Dorsal nuclear gradient reveals limitations to threshold-dependent patterning in *Drosophila*. Proc. Natl. Acad. Sci. USA *106*, 22317–22322.

Lund, V.K., DeLotto, Y., and DeLotto, R. (2010). Endocytosis is required for Toll signaling and shaping of the Dorsal/NF-kappaB morphogen gradient during *Drosophila* embryogenesis. Proc. Natl. Acad. Sci. USA *107*, 18028–18033.

Matsuda, S., and Shimmi, O. (2012). Directional transport and active retention of Dpp/BMP create wing vein patterns in *Drosophila*. Dev. Biol. *366*, 153–162.

McDonald, J.A., Holbrook, S., Isshiki, T., Weiss, J., Doe, C.Q., and Mellerick, D.M. (1998). Dorsoventral patterning in the *Drosophila* central nervous system: the vnd homeobox gene specifies ventral column identity. Genes Dev. *12*, 3603–3612.

Meinhardt, H., and Roth, S. (2002). Developmental biology: sharp peaks from shallow sources. Nature *419*, 261–262.

Melen, G.J., Levy, S., Barkai, N., and Shilo, B.Z. (2005). Threshold responses to morphogen gradients by zero-order ultrasensitivity. Mol. Syst. Biol., 1:2005.0028.

Mizutani, C.M., Nie, Q., Wan, F.Y., Zhang, Y.T., Vilmos, P., Sousa-Neves, R., Bier, E., Marsh, J.L., and Lander, A.D. (2005). Formation of the BMP activity gradient in the *Drosophila* embryo. Dev. Cell *8*, 915–924.

Morisato, D. (2001). Spätzle regulates the shape of the Dorsal gradient in the *Drosophila* embryo. Development *128*, 2309–2319.

Morisato, D., and Anderson, K.V. (1994). The Spätzle gene encodes a component of the extracellular singnaling pathway establishing the dorso-ventral pattern of the *Drosophila* embryo. Cell *76*, 677–688.

Morisato, D., and Anderson, K.V. (1995). Signaling pathways that establish the dorsal-ventral pattern of the *Drosophila* embryo. Annu. Rev. Genet. *29*, 371–399.

Moussian, B., and Roth, S. (2005). Dorsoventral axis formation in the *Drosophila* embryo—shaping and transducing a morphogen gradient. Curr. Biol. *15*, R887–R899.

Nellen, D., Burke, R., Struhl, G., and Basler, K. (1996). Direct and long-range action of a DPP morphogen gradient. Cell *85*, 357–368.

Paulsen, M., Legewie, S., Eils, R., Karaulanov, E., and Niehrs, C. (2011). Negative feedback in the bone morphogenetic protein 4 (BMP4) synexpression

group governs its dynamic signaling range and canalizes development. Proc. Natl. Acad. Sci. USA *108*, 10202–10207.

Peri, F., Technau, M., and Roth, S. (2002). Mechanisms of Gurken-dependent pipe regulation and the robustness of dorsoventral patterning in *Drosophila*. Development *129*, 2965–2975.

Plouhinec, J.L., Zakin, L., and De Robertis, E.M. (2011). Systems control of BMP morphogen flow in vertebrate embryos. Curr. Opin. Genet. Dev. *21*, 696–703.

Reeves, G.T., Trisnadi, N., Truong, T.V., Nahmad, M., Katz, S., and Stathopoulos, A. (2012). Dorsal-ventral gene expression in the *Drosophila* embryo reflects the dynamics and precision of the dorsal nuclear gradient. Dev. Cell *22*, 544–557.

Roth, S., and Schüpbach, T. (1994). The relationship between ovarian and embryonic dorsoventral patterning in *Drosophila*. Development *120*, 2245–2257.

Roth, S., Stein, D., and Nüsslein-Volhard, C. (1989). A gradient of nuclear localization of the dorsal protein determines dorsoventral pattern in the *Drosophila* embryo. Cell *59*, 1189–1202.

Rusch, J., and Levine, M. (1996). Threshold responses to the dorsal regulatory gradient and the subdivision of primary tissue territories in the *Drosophila* embryo. Curr. Opin. Genet. Dev. *6*, 416–423.

Rushlow, C.A., Han, K., Manley, J.L., and Levine, M. (1989). The graded distribution of the dorsal morphogen is initiated by selective nuclear transport in *Drosophila*. Cell *59*, 1165–1177.

Schier, A.F. (2009). Nodal morphogens. Cold Spring Harb. Perspect. Biol. *1*, a003459.

Schlesinger, A., Kiger, A., Perrimon, N., and Shilo, B.Z. (2004). Small wing PLCgamma is required for ER retention of cleaved Spitz during eye development in *Drosophila*. Dev. Cell *7*, 535–545.

Schneider, D.S., Jin, Y., Morisato, D., and Anderson, K.V. (1994). A processed form of Spätzle protein defines dorso-ventral polarity in the *Drosophila* embryo. Development *120*, 1243–1250.

Sen, J., Goltz, J.S., Stevens, L., and Stein, D. (1998). Spatially restricted expression of pipe in the *Drosophila* egg chamber defines embryonic dorsal-ventral polarity. Cell *95*, 471–481.

Shimmi, O., Umulis, D., Othmer, H., and O'Connor, M.B. (2005). Facilitated transport of a Dpp/Scw heterodimer by Sog/Tsg leads to robust patterning of the *Drosophila* blastoderm embryo. Cell *120*, 873–886.

Stathopoulos, A., and Levine, M. (2002). Linear signaling in the Toll-Dorsal pathway of *Drosophila*: activated Pelle kinase specifies all threshold outputs of gene expression while the bHLH protein Twist specifies a subset. Development *129*, 3411–3419.

Stein, D. (1995). Pattern formation: the link between ovary and embryo. Curr. Biol. *5*, 1360–1363.

Turing, A.M. (1952). The chemical basis of morphogenesis. Philos. Trans. R. Soc. Lond. B Biol. Sci. *237*, 37–72.

van der Zee, M., Stockhammer, O., von Levetzow, C., Nunes da Fonseca, R., and Roth, S. (2006). Sog/Chordin is required for ventral-to-dorsal Dpp/BMP transport and head formation in a short germ insect. Proc. Natl. Acad. Sci. USA *103*, 16307–16312.

Wang, Y.C., and Ferguson, E.L. (2005). Spatial bistability of Dpp-receptor interactions during *Drosophila* dorsal-ventral patterning. Nature *434*, 229–234.

Weber, A.N., Tauszig-Delamasure, S., Hoffmann, J.A., Lelièvre, E., Gascan, H., Ray, K.P., Morse, M.A., Imler, J.L., and Gay, N.J. (2003). Binding of the *Drosophila* cytokine Spätzle to Toll is direct and establishes signaling. Nat. Immunol. *4*, 794–800.

Weber, A.N., Gangloff, M., Moncrieffe, M.C., Hyvert, Y., Imler, J.L., and Gay, N.J. (2007). Role of the Spatzle Pro-domain in the generation of an active toll receptor ligand. J. Biol. Chem. *282*, 13522–13531.

Wolfman, N.M., McPherron, A.C., Pappano, W.N., Davies, M.V., Song, K., Tomkinson, K.N., Wright, J.F., Zhao, L., Sebald, S.M., Greenspan, D.S., and Lee, S.J. (2003). Activation of latent myostatin by the BMP-1/tolloid family of metalloproteinases. Proc. Natl. Acad. Sci. USA *100*, 15842–15846.

Wolpert, L. (1989). Positional information revisited. Development Suppl. *107*, 3–12.

Zhang, Z., Stevens, L.M., and Stein, D. (2009). Sulfation of eggshell components by Pipe defines dorsal-ventral polarity in the *Drosophila* embryo. Curr. Biol. *19*, 1200–1205.

Zhao, G., Wheeler, S.R., and Skeath, J.B. (2007). Genetic control of dorsoventral patterning and neuroblast specification in the *Drosophila* central nervous system. Int. J. Dev. Biol. *51*, 107–115.

Zhu, X., Stevens, L.M., and Stein, D. (2007). Synthesis of the sulfate donor PAPS in either the *Drosophila* germline or somatic follicle cells can support embryonic dorsal-ventral axis formation. Development *134*, 1465–1469.

Development 136, 2493-2503 (2009) doi:10.1242/dev.032391

# Lighting up mRNA localization in *Drosophila* oogenesis

**Agata N. Becalska and Elizabeth R. Gavis***

The asymmetric localization of four maternal mRNAs – *gurken*, *bicoid*, *oskar* and *nanos* – in the *Drosophila* oocyte is essential for the development of the embryonic body axes. Fluorescent imaging methods are now being used to visualize these mRNAs in living tissue, allowing dynamic analysis of their behaviors throughout the process of localization. This review summarizes recent findings from such studies that provide new insight into the elaborate cellular mechanisms that are used to transport mRNAs to different regions of the oocyte and to maintain their localized distributions during oogenesis.

## Introduction

mRNA localization has emerged as an important mechanism for generating asymmetric protein distributions that promote morphological and functional cell polarization during development. A recent in situ hybridization screen uncovered over 1500 transcripts with distinct subcellular localizations in early *Drosophila* embryos, hinting at diverse roles for mRNA localization in regulating cell physiology (Lécuyer et al., 2007). In contrast to direct protein targeting, mRNA localization provides an effective way in which to create high local protein concentrations, as each transcript can be translated many times. The coupling of translational activity to mRNA localization prevents premature or ectopic protein synthesis that might be deleterious to the cell. In addition, an existing pool of localized mRNA allows for precise temporal control of local protein synthesis in response to external stimuli.

The first localized mRNAs were discovered in ascidian eggs over 20 years ago (Jeffery et al., 1983), and localized transcripts have since been found in many other cell types, including fibroblasts and neurons, as well as in plant cells and fungi (see Box 1). mRNA localization is particularly important during early development, when many organisms rely on proteins synthesized from maternal mRNAs to guide development until the onset of zygotic transcription. As these mRNAs are present in the egg at fertilization, when and where their protein products are expressed must be regulated post-transcriptionally. Accordingly, numerous maternal mRNAs have been shown to be asymmetrically localized in oocytes and eggs from a broad spectrum of organisms, including echinoderms, ascidians, insects, amphibians and fish (Kloc and Etkin, 2005; Palacios and St Johnston, 2001). These mRNAs direct the local synthesis of proteins essential for embryonic germ layer specification, axis formation and germline determination.

Although ascidian and *Xenopus* eggs provided the first model systems for studying localized transcripts, the *Drosophila* oocyte has become a major workhorse for both functional and mechanistic analysis of mRNA localization owing to the availability of powerful genetic and transgenic tools. Intensive analysis of four mRNAs, *gurken* (*grk*), *bicoid* (*bcd*), *oskar* (*osk*) and *nanos* (*nos*), whose localizations to different regions of the oocyte are essential to specify the anteroposterior (AP) and dorsoventral (DV) body axes of the *Drosophila* embryo, has provided insight into the role of mRNA localization in setting up developmental asymmetries, as well as into the mechanisms that mediate mRNA localization.

Localization is a multistep process that requires recognition of cis-acting sequences – localization signals – within mRNAs by localization factors, packaging of these RNA-protein complexes (designated hereafter as RNPs) into transport particles, trafficking of these particles within the cytoplasm and, finally, anchoring of mRNAs at their target destination. RNP assembly may begin in the nucleus, with subsequent remodeling occurring in the cytoplasm to recruit additional factors that confer specificity to the transport process. In many cases, mechanisms that maintain translational silencing during transport particle formation and transit are superimposed. We refer the reader to recent reviews for detailed coverage of these molecular events (Gavis et al., 2007; Kugler and Lasko, 2009; Lewis and Mowry, 2007).

Much of the framework for modeling mRNA localization pathways derives from invaluable biochemical, genetic and histological studies. However, these approaches provide only static snapshots of a continuous event. In this review, we discuss how the application of powerful new imaging technologies to the analysis of *grk*, *bcd*, *osk* and *nos* mRNAs in *Drosophila* oocytes has provided a window into the highly dynamic features of mRNA trafficking by visualizing the movements of RNP particles and the paths that they follow. We summarize recent findings that reveal unanticipated complexities in transport and anchoring mechanisms and in their cellular requirements.

## Role of mRNA localization in the establishment of embryonic body axes

Axial polarity of the *Drosophila* embryo arises from asymmetries set up during oogenesis by a series of mRNA localization events (Fig. 1; see Box 2 for an overview of *Drosophila* oogenesis). Establishment of both the AP and DV axes depends on signaling from the oocyte to subsets of follicle cells via Grk, a transforming growth factor α-like ligand (González-Reyes et al., 1995; Neuman-Silberberg and Schüpbach, 1993). To achieve this, *grk* mRNA is localized first to the posterior of the oocyte, where Grk signaling to the overlying follicle cells triggers a reorganization of the oocyte cytoskeleton. This enables the subsequent localization of *bcd* and *osk* mRNAs to the anterior and posterior poles of the oocyte, respectively, and the dorsal anterior localization of *grk* itself (González-Reyes et al., 1995). There, Grk signaling initiates a cascade of events that will ultimately generate the embryonic DV axis.

Osk protein, translated upon posterior localization of *osk* mRNA, initiates the assembly of the germ plasm, a specialized cytoplasm that is maintained at the posterior pole into embryogenesis and contains determinants, including *nos* mRNA, that are necessary for germline and abdominal development (Lehmann and Nusslein-Volhard, 1986). *nos* mRNA accumulates at the posterior of the oocyte only at late stages of oogenesis, and this accumulation is dependent on Osk and germ plasm assembly (Wang et al., 1994). Although *nos* is translated upon its posterior localization, Nos protein has no known function in

Department of Molecular Biology, Princeton University, Princeton, NJ 08544, USA.

*Author for correspondence (e-mail: gavis@princeton.edu)

**Box 1. Key examples of localized mRNAs**

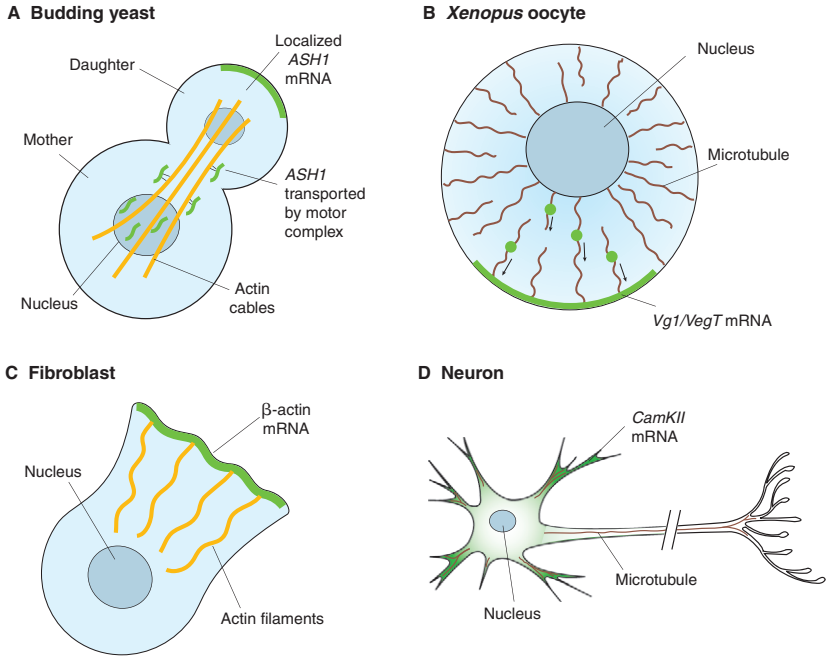


In budding yeast, localization of *ASH1* mRNA to the bud tip by myosin-mediated transport on actin cables (see A in figure) targets Ash1p to the daughter cell, where it is required to repress mating type switching (reviewed by Gonsalvez et al., 2005). Thus, mating type switching occurs only in the mother cell, thereby ensuring that both yeast mating types are present in the population. Germ layer specification in *Xenopus* embryos relies on localized mRNAs, including *Vg1* and *VegT* (reviewed by King et al., 2005) (see B in figure), which are transported to the vegetal pole of the oocyte by kinesin motors and anchored to the cortex by an actin-dependent mechanism. After fertilization, *Vg1* and *VegT* RNAs are inherited by the embryonic vegetal cells, where Vg1 protein, a TGFβ homolog, participates in mesoderm specification, while VegT, a transcription factor, regulates endoderm specification and mesoderm induction. mRNA localization plays an important role in the polarization of somatic cells, such as fibroblasts and neurons (see C,D in figure). Localization of β-actin mRNA to the leading edge of migrating fibroblasts provides a high local concentration of actin monomers that drives assembly of the actin filaments needed for forward movement. Similarly, β-actin mRNA localization to growth cones in developing axons promotes the motility required for axon guidance (reviewed by Condeelis and Singer, 2005). Dendritic localization of RNAs like calcium/calmodulin-dependent protein kinase IIα (CaMKIIα) mRNA in hippocampal neurons facilitates a rapid response to synaptic activity in the form of local protein translation and contributes to learning and memory-related synaptic plasticity (reviewed by Martin et al., 2000).

the oocyte (Forrest et al., 2004). Similarly, Bcd, whose synthesis is repressed during oogenesis, functions only after fertilization (Driever and Nüsslein-Volhard, 1988). Localization of these mRNAs during oogenesis, however, endows the newly fertilized embryo with sources for the production of opposing protein gradients that establish the AP body axis. Bcd, acting both as a transcriptional activator and a translational repressor, determines the head and thoracic regions, while Nos, a translational repressor, determines the abdomen (reviewed by Thompson et al., 2007). In addition, localized *nos* mRNA is incorporated into the germ cells as they form at the posterior of the embryo, supplying the Nos protein that is necessary for germline development (Gavis et al., 2008).

Genetic manipulations that disrupt localization or cause the mislocalization of *grk*, *bcd*, *osk* or *nos* during oogenesis provide compelling evidence that the specific subcellular distributions of these mRNAs are essential for their function in axial and germline development. For example, mutations that abolish *osk* or *nos* localization produce embryos that lack an abdomen (Ephrussi et al., 1991; Wang et al., 1994). These embryos also exhibit the respective defects in germ cell formation and function that are characteristic of *osk* and *nos* mutants (Ephrussi and Lehmann, 1991; Gavis et al., 2008). Conversely, the targeting of *osk* or *nos* to both poles of the oocyte results in embryos in which the anterior structures are replaced by mirror image duplications of posterior structures (Ephrussi and Lehmann, 1992; Gavis and Lehmann, 1992). Similarly, failure to localize *grk* mRNA leads to DV polarity defects (Neuman-Silberberg and Schüpbach, 1993). The ability to test the significance of mRNA localization to developmental gene function has been a major contribution of the *Drosophila* system.

## Live fluorescent visualization methods

In situ hybridization experiments have elucidated mRNA localization patterns and, combined with genetic, cell biological and biochemical manipulations, have been used to demonstrate that the mRNA localization process requires cis-acting signals, trans-acting factors, and cytoskeletal components. However, in situ hybridization can only detect the steady state accumulation of mRNAs. Thus, to understand how mRNAs travel to their destinations and to investigate the roles played by localization factors and cytoskeletal elements in executing this process, we need to be able to visualize mRNA localization as it occurs in real time. A further challenge in the analysis of *Drosophila* oocyte mRNAs arises from the increasing impenetrability of oocytes to molecular probes as the vitelline membrane and egg shell are laid

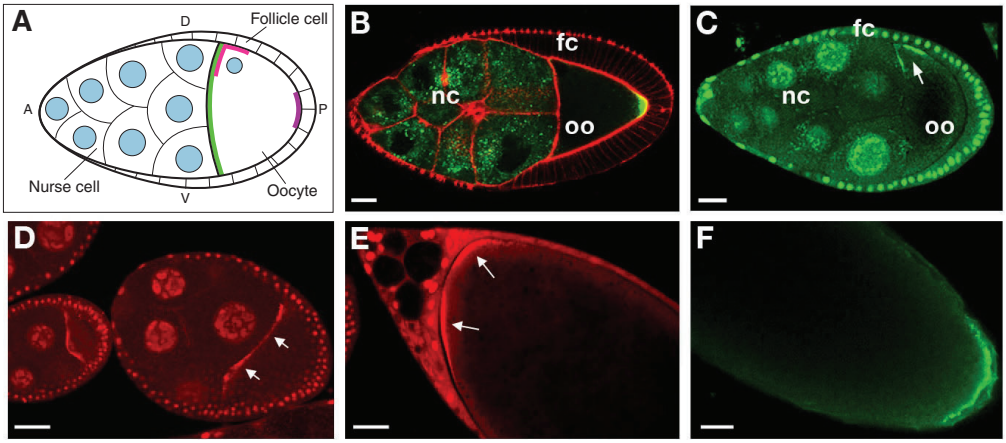


**Fig. 1. Localized distributions of *grk*, *bcd*, *osk* and *nos* mRNAs.** (**A**) Schematic showing *grk* (pink), *bcd* (green) and *osk* (purple) mRNA localization in mid-oogenesis (stage 9). *nos* mRNA is not yet localized at this stage. The anteroposterior (AP) and dorsoventral (DV) axes are indicated. (**B**) GFP-Stau (green), as proxy for *osk* mRNA, at the posterior pole of the oocyte (oo) during mid-oogenesis. GFP-Stau is also detected in the nurse cell (nc) cytoplasm. The actin cytoskeleton is highlighted in red with phalloidin. fc, follicle cells. Orientation is the same as in A. (**C-F**) Visualization of endogenous mRNAs using the MS2 system: (C) *grk* and (D) *bcd* during mid-oogenesis; (E) *bcd* and (F) *nos* in late oocytes. Owing to the promoter used, the MCP-GFP and MCP-RFP fusion proteins are expressed in both the nurse cells and follicle cells, whereas the MS2-tagged mRNAs are produced only in the nurse cells. MCP-GFP/RFP that is not bound to mRNA enters both the nurse cell and follicle cell nuclei. Scale bars: 20 μm. Image in B was modified, with permission, from Huynh et al. (Huynh et al., 2004); image in C was modified, with permission, from Jaramillo et al. (Jaramillo et al., 2008); images in D and E are reproduced, with permission, from Weil et al. (Weil et al., 2006). Image in F is courtesy of K. Sinsimer (Princeton University, Princeton, NJ, USA). *bcd*, *bicoid*; *grk*, *gurken*; GFP, green fluorescent protein; MCP, MS2 coat protein; *nos*, *nanos*; *osk*, *oskar*; RFP, red fluorescent protein.

down. The difficulty of detecting localization patterns at later stages of oogenesis by in situ hybridization left events that occur during this sizeable temporal window largely unexplored. The development of live-imaging methods using fluorescently tagged RNAs and proteins has recently overcome these limitations to the analysis of mRNA localization dynamics. At lower resolution, time-lapse imaging has provided integrated spatiotemporal information about RNA distributions during the course of oogenesis. Imaging at higher spatial and temporal resolution has permitted detailed characterization of the kinetics and paths of individual RNA particles. The application of techniques like fluorescence recovery after photobleaching (FRAP) and fluorescence loss in photobleaching (FLIP) has further facilitated a dynamic analysis of localization events. These methods assess the mobility of fluorescent molecules, by monitoring either the restoration of fluorescence to a photobleached area of a cell caused by the movement of fluorescently labeled molecules from surrounding unbleached regions (FRAP) or the depletion of fluorescently labeled molecules from an unbleached region after repetitive photobleaching of an adjacent area (FLIP).

Visualization of RNA localization in living cells was first accomplished in oligodendrocytes by injection of *in vitro* transcribed myelin basic protein RNA labeled with fluorescein (Aigner et al., 1993). Similarly, injection of fluorescently labeled transcripts has been a successful strategy for investigating the localization of *grk* and *bcd* RNAs in *Drosophila* oocytes, with the relatively large size of the egg chamber making it possible to perform injections into both the nurse cells and oocyte (Cha et al., 2001; Clark et al., 2007; Delanoue et al., 2007; MacDougall et al., 2003; Mische et al., 2007) (Fig. 2A). The ability to control the site and time at which the fluorescent RNA is introduced enables the investigator to perform pulse-chase type experiments, making this method particularly advantageous for the dissection of multi-step RNA localization pathways. Although caution must be taken to discern artifacts that result from damage to the egg chamber during injection, a more difficult issue to address is whether the behavior of RNA injected directly into the cytoplasm recapitulates the behavior of native mRNA that has first been processed in the nucleus. Additionally, the benefit of being able to introduce large quantities of RNA that facilitate detection must be weighed against the possibility that the introduction of nonphysiological amounts of exogenous RNA could result in its aggregation or could saturate the localization machinery.

The recent development of genetically encoded fluorescent tagging methods has enabled the direct visualization of endogenous transcripts (Fig. 2B). Pioneered in yeast for *ASH1* mRNA (Bertrand et al., 1998), this approach involves tethering a fluorescent protein, such as green or red fluorescent protein (GFP or RFP) to mRNA. This is usually accomplished by fusing GFP (or another fluorescent protein) to the bacteriophage MS2 coat protein (MCP) and, in parallel, inserting multiple stem-loop binding sites for the coat protein into the transcript of interest (Fig. 2B). When the MCP-GFP fusion protein and MS2-tagged RNA are co-expressed, binding of the MCP domain to its cognate stem-loops generates fluorescently tagged mRNA in vivo. The system was adapted for transgenic use in *Drosophila* to investigate *nos* mRNA localization in late oocytes (Forrest and Gavis, 2003), and has been subsequently applied to *grk, bcd* and *osk* (Jaramillo et al., 2008; Weil et al., 2006; Zimyanin et al., 2008) (Fig. 1C-F), as well as to several neuronal mRNAs (Ashraf et al., 2006; Brechbiel and Gavis, 2008; Estes et al., 2008). A major strength of this system is the production of fluorescent transcripts, at or near physiological levels, that have been subject to endogenous processing steps. The method has been particularly advantageous in the *Drosophila* ovary, where localization pathways are often active over many hours and at developmental stages that are not readily penetrated by other detection methods. Moreover, the analysis of steady-state localization afforded by this method provides a complement to the investigation of transient events following RNA

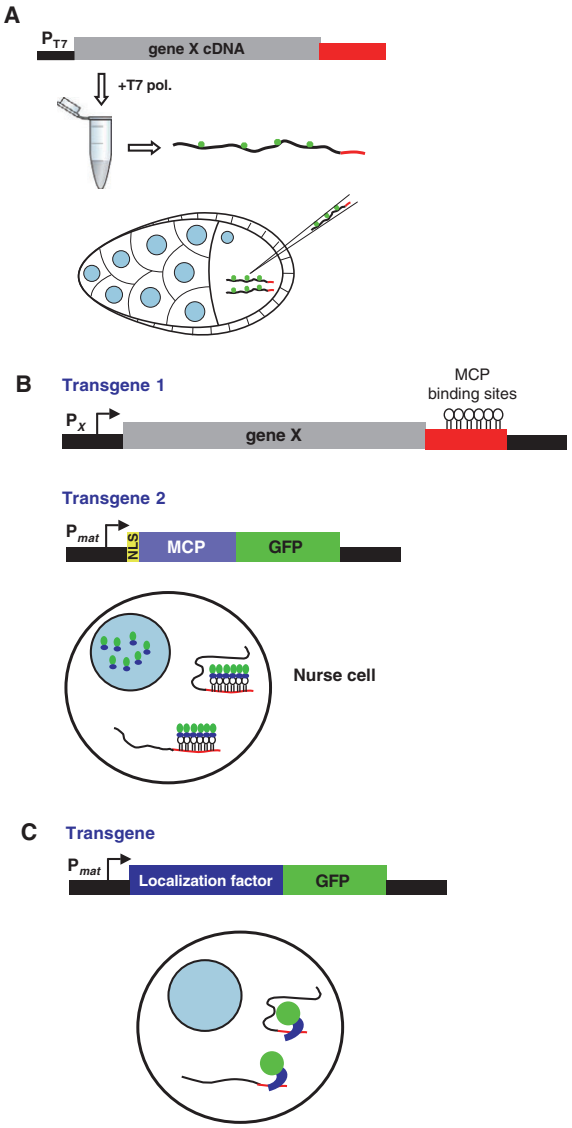


**Fig. 2. Fluorescent labeling methods.** (**A**) A construct designed for in vitro transcription of the gene of interest from a bacteriophage promoter (T7 in this example), with the coding region shown in gray and the 3′UTR containing the RNA localization signal in red. Transcription of this construct by T7 polymerase in the presence of a fluorophore-coupled nucleotide produces fluorescently labeled RNA for injection into cultured egg chambers. RNA can be injected directly into the oocyte as illustrated or into the nurse cells. (**B**) In vivo labeling of endogenous mRNA by the MS2 system. This strategy requires two components: a transgene (transgene 1) that encodes the target RNA with an insertion of tandem copies of the stem-loop binding site for the bacteriophage MS2 coat protein (MCP), shown here in the 3′ UTR, usually under the control of its own promoter ($P_x$); and a transgene (transgene 2) that encodes a fluorescent protein fused to MCP (GFP is shown here) under the control of a maternally active promoter ($P_{mat}$). Transgenic fly lines for each component are crossed together to generate females that express both the tagged RNA and the MCP-GFP protein in their ovarian nurse cells. When the two transgenes are thus coexpressed, the binding of MCP to its recognition motif labels the RNA with GFP. The nuclear localization signal (NLS) in the MCP-GFP fusion protein retains excess unbound protein in the nucleus, reducing cytoplasmic background. Fluorescently labeled mRNA enters the oocyte from the nurse cells (not shown). (**C**) Transgenic expression of GFP-tagged localization factors. A transgene encoding a localization factor fused to a fluorescent protein (e.g. GFP) under the control of its own or a maternally active promoter. Expression of the transgene in the nurse cells of transgenic females will result in production of the fusion protein in the nurse cells. Colocalization of the fusion protein with the target RNA could occur in the nurse cells or oocyte (not shown), through direct RNA-protein interaction (as shown) or through their co-assembly into a larger RNP.

injection and has been essential for the dissection of anchoring mechanisms. Of potential concern with this approach, however, is the possibility that the inserted MS2 stem-loops will destabilize a transcript or impair its ability to interact with localization factors. Moreover, binding of the transcript by multiple copies of MCP-GFP could compromise transport particle assembly or function. Comparison of RNA distributions achieved using this method with those detected by in situ hybridization, together with genetic rescue experiments, is therefore essential to confirm that the tagged transcripts faithfully reproduce the behavior of the native mRNA.

In an alternative approach to the direct detection of mRNA in vivo, GFP-tagged localization factors have been used as proxies for their target mRNAs (Fig. 2C). Because it relies on the identification of appropriate factors and a prior knowledge of coordinated mRNA-protein transport, this method is less widely applicable. In addition, a single localization factor might provide only a partial readout of an mRNA's travels if its association with the RNP is limited to particular steps in the localization pathway. Moreover, as individual localization factors are increasingly implicated in the transport of multiple different mRNAs, sometimes to different locations, discriminating which of the fluorescent RNPs contain the mRNA of interest could be difficult. Nonetheless, the need for only a single transgene and the ease of detecting the tagged protein have made two such protein fusions, GFP-Exu and GFP-Stau, choice tools for monitoring the transport of *bcd* and *osk* mRNAs (Mische et al., 2007; Theurkauf and Hazelrigg, 1998; Zimyanin et al., 2008) (Fig. 1B). Genetic requirements for Exuperentia (Exu) and Staufen (Stau) function in *bcd* and *osk* mRNA localization, together with colocalization studies, have implicated Exu and Stau as components of *bcd* and *osk* RNPs (reviewed by Kugler and Lasko, 2009; St Johnston, 2005). However, whether Exu is specific for *bcd* or can also contribute to *osk* RNPs is not yet clear. Because Stau functions in *osk* localization during midoogenesis and in *bcd* localization only at late stages of oogenesis, GFP-Stau can serve as an independent proxy for each mRNA in the oocyte.

## RNA localization dynamics in *Drosophila* oogenesis

Recent analyses of RNA localization dynamics during *Drosophila* oogenesis, made possible by new imaging technologies, have led to revised models for the localization of four key mRNAs. Below, we discuss findings from these studies that have provided new insights into the mechanisms that mediate the transport of these mRNAs from the ovarian nurse cells into the oocyte, their localization within the oocyte, and their anchoring at targeted regions of the oocyte cortex.

### Transport from nurse cells to oocyte

Maternal mRNAs, proteins and even organelles produced in the ovarian nurse cells must be transferred into the oocyte for the production of the egg and early embryo. Until stage 10 of oogenesis,

when the nurse cells contract and extrude or 'dump' their contents into the oocyte, the transport of cargoes from the nurse cells to the oocyte is continuous and selective. This intercellular transport occurs via the ring canals that connect the nurse cells to the oocyte and to each other (Box 2). During the first half of oogenesis, microtubules that extend from a microtubule-organizing center (MTOC) at the posterior of the oocyte through the ring canals into the nurse cells could provide a direct route to the oocyte (Theurkauf et al., 1992). However, this microtubule 'highway' is decommissioned at stage 7, when Grk-dependent signaling events between the oocyte and overlying follicle cells trigger the disassembly of the posterior MTOC and the reorganization of the microtubule cytoskeleton. Live-imaging studies of *bcd* and *grk,* using injected fluorescent transcripts or GFP-Exu as a localization factor proxy for *bcd* mRNA, have shed light on the mechanism of nurse cell-to-oocyte transport at mid-stages of oogenesis, as well as on its cytoskeletal basis (Cha et al., 2001; Clark et al., 2007; Mische et al., 2007; Theurkauf and Hazelrigg, 1998).

In the nurse cells, injected *bcd* and *grk* transcripts and GFP-Exu each form particles that move rapidly and on linear tracks toward ring canals at the nurse cell-oocyte boundary, where they accumulate (Cha et al., 2001; Clark et al., 2007; Mische et al., 2007; Theurkauf and Hazelrigg, 1998) (see Movie 2 in the supplementary material; Fig. 3A). During stages 8-9, microtubules appear to be concentrated at these ring canals in arrays that project into the nurse cell cytoplasm, suggesting a possible path for mRNA transport. Indeed, treatment of oocytes with microtubule-depolymerizing drugs prevents the directional movement of GFP-Exu, and of *bcd* and *grk* RNA. To test whether the observed motility reflects active transport, Mische et al. and Clark et al. compromised dynein function genetically (Mische et al., 2007; Clark et al., 2007). The resulting decrease in motility of both GFP-Exu and *grk* RNA particles in nurse cells indicates that oocyte-destined mRNAs share a common dynein-dependent transport pathway for translocation to the ring canals. How RNA particles encounter the ring canal-associated microtubules is not yet clear. In addition to directed movement, GFP-Exu particles exhibit randomly oriented microtubule-dependent movement throughout the nurse cell cytoplasm (Mische et al., 2007; Theurkauf and Hazelrigg, 1998). These particles could therefore encounter ring canal-associated microtubules through a microtubule-dependent random walk. By contrast, particles of injected *grk* RNA distant from the ring canals appear to follow cytoplasmic flows (Clark et al., 2007). Random movements caused by these flows might facilitate chance encounters with ring canal-associated microtubules.

GFP-Exu and *grk* particles that accumulate at the ring canal subsequently pass through into the oocyte. Movement through the ring canals is slower than movement towards them, however, suggesting that transport to and through the ring canals may occur by two distinct mechanisms. Intriguingly, the size and shape of GFP-Exu particles change as they enter the oocyte (Mische et al., 2007). This might reflect a remodeling of the RNP to exchange localization factors required in the nurse cells for oocyte-specific factors or to sort co-transported mRNAs that are destined for different locations within the oocyte. The formation of a *bcd*-Exu RNP in the nurse cells is not required for transport of injected *bcd* RNA to the oocyte, but is essential for the anterior localization of *bcd* in the oocyte (see below) (Cha et al., 2001). Thus, it is an intriguing possibility that Exu coordinates a remodeling event that triggers the recognition of *bcd*-containing particles by the oocyte transport machinery.

**Box 2. *Drosophila* oogenesis**

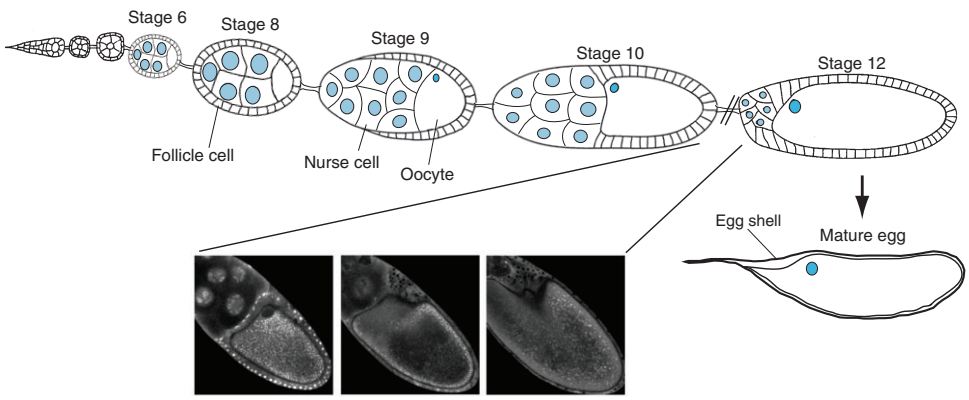


The *Drosophila* ovary is composed of 14-16 ovarioles, each of which contains a series of developing egg chambers (reviewed by Spradling, 1993) (see figure). Each egg chamber is composed of an oocyte and its 15 sister nurse cells, which comprise a 16-cell cyst, surrounded by a somatic follicular epithelium. The germ cell cyst arises from a stem cell-derived cystoblast that undergoes four synchronous divisions. Incomplete cytokinesis during these divisions leaves the 16 cells interconnected by actin-rich cytoplasmic bridges referred to as ring canals. One of these cells differentiates as the oocyte and enters meiosis, while the remainder become polyploid nurse cells.

The egg chamber develops through 14 morphologically distinct stages to give rise to a mature oocyte. Throughout oogenesis, the nurse cells produce maternal RNAs, proteins and organelles that are delivered to the developing oocyte via the ring canals. This supply of maternal factors by the nurse cells is critical to development of the oocyte and the future embryo as the oocyte nucleus is largely transcriptionally quiescent. At the end of stage 10, when the nurse cell cluster and the oocyte are similar in volume, the nurse cells contract to extrude or 'dump' their contents into the oocyte and are subsequently eliminated by apoptosis (see inset in figure). Vigorous streaming of the oocyte cytoplasm (ooplasmic streaming), which accompanies nurse cell dumping, mixes the incoming nurse cell cytoplasm with the ooplasm (see Movie 1 in the supplementary material). The follicle cells, which migrate to enclose the oocyte, secrete both the vitelline membrane and the chorion or egg shell to protect the maturing egg.

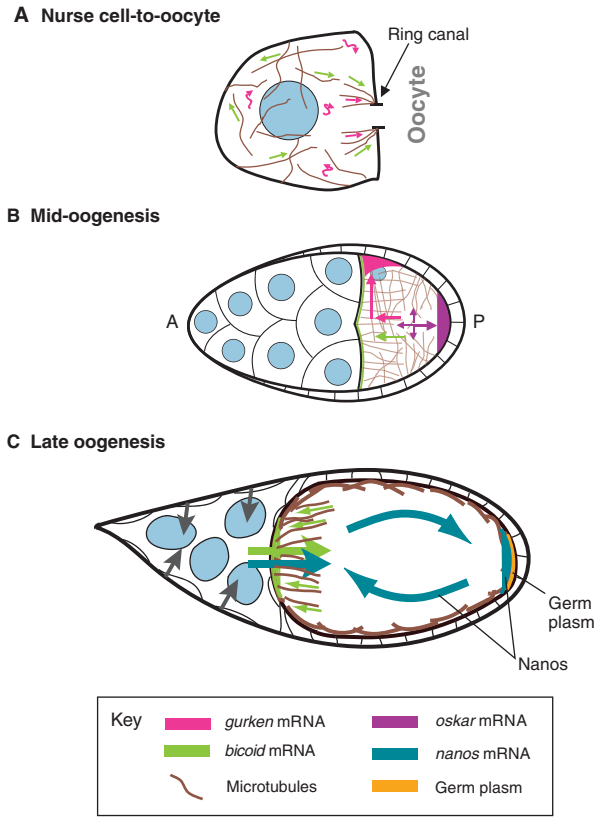


**Fig. 3. Models for mRNA localization.** In all panels, microtubules are shown in brown, nurse cell and follicle cell nuclei in blue. (**A**) Movements of *grk* and *bcd* mRNAs within the nurse cells during mid-oogenesis. Straight arrows indicate directed movement on microtubules, squiggly arrows indicate movement of *grk* with cytoplasmic flows. (**B**) Microtubule-dependent transport of *grk*, *bcd* and *osk* mRNAs within the oocyte during mid-oogenesis. The oocyte nucleus is shown in gray. Colored arrows show the directions of RNA movements. (**C**) Localization of *bcd* and *nos* at late stages of oogenesis. Contraction of the nurse cells for dumping is indicated by gray arrows pointing inward; entry of *bcd* and *nos* into the oocyte is indicated by large straight arrows. Small green arrows depict transport of *bcd* on anterior microtubules, curved dark green arrows depict diffusion of *nos* facilitated by ooplasmic streaming.

## Transport during mid-oogenesis

After entering the oocyte, mRNAs must be translocated to specific cortical regions. Because RNPs enter the oocyte at its anterior end, anterior localization could occur simply by them being 'captured' through interactions with cytoskeletal or membrane proteins at the anterior cortex. By contrast, posterior localization requires that RNPs traverse distances of 50 μm or more. The anterior localization of *bcd* and the posterior localization of *osk* mRNA are both disrupted by the treatment of egg chambers with microtubule-depolymerizing drugs (Pokrywka and Stephenson, 1991; Pokrywka and Stephenson, 1995). These early experiments, which were performed using in situ hybridization to detect end-stage localization, could not distinguish whether microtubules act directly or indirectly. Nonetheless, they suggested that the oocyte possesses microtubule-based machinery for the delivery of mRNAs to different cortical destinations.

Reorganization of the oocyte microtubule cytoskeleton during mid-oogenesis results in an apparent AP gradient of microtubules (Theurkauf et al., 1992). A longstanding model proposed that these microtubules are polarized along the AP axis, with minus ends nucleated at the anterior cortex and plus ends projected towards the posterior. Accordingly, whether an RNP particle is transported to the anterior or posterior pole would depend on whether it associates with dynein or kinesin motor proteins. This model is based on a number of observations. First, partial microtubule depolymerization leaves short microtubules associated with the anterior cortex (Theurkauf et al., 1992). Because microtubules depolymerize from the plus end, this result suggests that microtubules are nucleated at the anterior cortex. Furthermore, a fusion between the motor domain of kinesin and β-galactosidase (kinesin-β-gal) that localizes to the plus ends of microtubules in neurons (Giniger et al., 1993) accumulates at the posterior of mid-stage oocytes (Clark et al., 1994). Consistent with the proposed polarity of the microtubule cytoskeleton, genetic studies subsequently implicated the plus-end-directed motor kinesin I in the localization of *osk* mRNA to the posterior pole (Brendza et al., 2000) and the minus-end-directed motor dynein in the localization of *bcd* mRNA to the anterior (Duncan and Warrior, 2002; Januschke et al., 2002).

This simple model was first called into question by the live-imaging studies of Cha et al. (Cha et al., 2001), who compared the behavior of fluorescent *bcd* RNA transported to the oocyte following its injection into nurse cells with the behavior of *bcd* RNA injected directly into the oocyte. Whereas *bcd* transcripts injected into the nurse cells accumulate specifically at the anterior oocyte cortex, those injected directly into the oocyte accumulate at the nearest cortex and this nonpolarized transport depends on Exu and microtubules. Subsequent work by Mische et al. (Mische et al., 2007) showed that the nonpolarized cortical transport of *bcd* RNA injected into the oocyte is mediated by dynein. The ability of the injected RNA to be transported by dynein to any part of the cortex suggests that microtubule minus ends are not restricted to the anterior cortex and that microtubule organization alone is not sufficient to dictate asymmetric RNA localization. Further support for this conclusion comes from high-resolution imaging of *bcd* RNP particles formed after injection of *bcd* RNA directly into the oocyte. These particles move with linear trajectories but in random directions near the oocyte anterior (Mische et al., 2007).

How then is *bcd* directed to the anterior cortex? Fluorescent *bcd* RNA does accumulate selectively at the anterior cortex if it is injected first into nurse cells, then withdrawn and injected into a naïve oocyte (Cha et al., 2001). By contrast, localization occurs in a nonpolar manner if *bcd* is injected first into nurse cells from *exu* mutant egg chambers. This result places a prior requirement for Exu in the nurse cells for the subsequent localization of *bcd* mRNA in the oocyte. Thus, although Exu present in the oocyte is sufficient for the nonpolar localization of injected *bcd* RNA, the Exu-dependent assembly of *bcd* RNPs in the nurse cells is crucial for targeting to the anterior cortex. Components of this RNP might promote dynein-mediated transport on a select subpopulation of microtubules nucleated from the anterior cortex or might prevent transport on microtubules nucleated at the lateral cortex (Cha et al., 2002) (Fig. 3B). Distinguishing which, if either, of these scenarios is correct will be facilitated by the analysis of genetically encoded fluorescent *bcd* mRNA. Intriguingly, a recent analysis of *Vg1* mRNA transport in *Xenopus* oocytes suggests that kinesin-bound *Vg1* RNPs may use a distinct subpopulation of microtubules that has the plus ends oriented towards the vegetal cortex (Messitt et al., 2008).

A different way to achieve net polarized transport during mid-oogenesis has come to light from a dynamic analysis of *osk* localization (Zimyanin et al., 2008). This study tracked the movement of *osk* RNP particles during midstages of oogenesis by using either the MS2 system to label *osk* mRNA directly with GFP or by using GFP-Stau as a proxy for *osk* transport particles. Live imaging revealed rapid, directed movements of both GFP-Stau and *osk* RNP particles throughout the oocyte, consistent with kinesin-dependent transport (see Movie 3 in the supplementary material). Surprisingly, however, *osk* particles move with similar average velocities in all directions, showing only a slight posterior bias. As the velocity of all rapidly moving *osk* particles, regardless of their direction and position in the oocyte, is decreased in kinesin I mutants with reduced motor speed but not in dynein mutants, it is unlikely that differential transport by opposing motor proteins leads to the observed bias. Rather, Zimyanin et al. (Zimyanin et al., 2008) proposed that kinesin transports *osk* on randomly oriented microtubules, but that a slight polarization in oocyte microtubule organization leads to a small excess of posteriorly directed transport events (Fig. 3B). Over the relatively long period that *osk* is being localized (6-10 hours), this weak bias could suffice to greatly enrich *osk* mRNA at the posterior of the oocyte. Importantly, the interpretation of microtubule orientation based on the behavior of *osk* RNPs fits the existing data. Assuming a slight posterior bias of microtubule plus ends, plus-end markers, such as kinesin–β-gal, would be expected to accumulate at the oocyte posterior by a biased random walk, similarly to *osk*. In addition, the observed accumulation of injected *bcd* RNA at the nearest cortex (Cha et al., 2002) and the dynein-dependent movement of *bcd* RNA particles in multiple directions (Mische et al., 2007) is consistent with a largely random distribution of minus ends.

Intriguingly, the posterior bias in *osk* movement is reversed in mutants for several *osk* localization factors, including *Tropomyosin II* (*TmII*; *Tm1* – FlyBase), *barentsz* (*btz*) and *mago nashi* (*mago*). Previous in situ hybridization experiments have shown that these mutants accumulate *osk* mRNA at the anterior of the oocyte, instead of at the posterior as in wild-type oocytes (Erdélyi et al., 1995; Newmark and Boswell, 1994; van Eeden et al., 2001). A plausible explanation is that these factors are required to uncouple *osk* RNP particles from the dynein motors that mediate nurse cell-to-oocyte transport so that they can associate with kinesin in the oocyte, although aberrant microtubule organization could be a contributing factor in *mago* mutant egg chambers (Micklem et al., 1997).

During mid-oogenesis, *grk* mRNA displays a spatiotemporally dynamic distribution that first became evident from in situ hybridization experiments. In early oocytes, *grk* accumulates at the posterior pole; following microtubule reorganization, *grk* accumulates transiently along the anterior oocyte cortex, then becomes restricted to the dorsal anterior region during stages 8-9 (see Fig. 1) (Neuman-Silberberg and Schüpbach, 1993). To distinguish whether these distributions arise by distinct localization mechanisms or whether they are interdependent, MacDougall et al. (MacDougall et al., 2003) tracked individual RNP particles formed after the injection of fluorescent *grk* RNA into oocytes. By varying the site of injection and the time at which particles were imaged after injection, they showed that *grk* particles follow two distinct paths in sequence, the first directed toward the anterior cortex and the second directed dorsally along the anterior cortex (Fig. 3B). Both steps can be inhibited by microtubule depolymerization and injection of anti-dynein heavy chain (dhc) antibodies that block dynein function (MacDougall et al., 2003). Further evidence for dynein-dependent transport of *grk* RNA on microtubules is provided by high-resolution ultrastructural studies that combine in situ hybridization and immunoelectron microscopy (ISH-EM). This method detects clusters of injected *grk* transcripts assembled in nonmembranous electron dense structures that probably represent transport particles (Delanoue et al., 2007). Most of these particles reside within 100 nm of the nearest microtubule and colocalize with dynein, consistent with *grk* transport particles in transit.

Whether *grk* and *bcd* transcripts are transported to the anterior cortex on the same set of microtubules is not known. However, the complex trajectory followed by *grk* RNP particles indicates that, unlike *bcd*, they must be able to recognize two different microtubule subpopulations. Several studies have reported evidence for a network of microtubules associated with the dorsally located oocyte nucleus that might mediate transport of *grk* from the anterior cortex to its dorsal anterior position (Januschke et al., 2006; MacDougall et al., 2003). Presumably, components specific to *grk* or *bcd* RNPs regulate the choice of microtubules by their associated dynein motors, possibly by recognizing chemical modifications or microtubule-associated proteins (MAPS) that are present on different subsets of microtubules. The *grk* mRNA localization factor Squid (Sqd) is a candidate for such a specificity factor. In situ hybridization to *grk* mRNA first showed that *grk* accumulates at the oocyte anterior but does not shift anterodorsally in *sqd* mutants (Neuman-Silberberg and Schüpbach, 1993). Subsequently, MacDougall et al. (MacDougall et al., 2003) found reduced dorsal anteriorly directed movement and increased ventrally directed movement of injected *grk* particles in *sqd* mutant egg chambers. This effect on the directionality of *grk* RNP particles implicates Sqd in selective microtubule utilization.

### Localization during late stages of oogenesis

The fluorescent tagging of endogenous mRNA using the MS2 system has been instrumental in the investigation of mRNA localization during late stages of oogenesis, when molecular probes have limited access to the egg because of the presence of the vitelline membrane and the egg shell. The use of genetically encoded fluorescent *nos* and *bcd* mRNAs led to the discovery of two mechanistically distinct, late-acting localization pathways that operate simultaneously at late stages of oogenesis to position these RNAs at opposite poles of the oocyte (Forrest and Gavis, 2003; Weil et al., 2006; Weil et al., 2008).

*nos* represents a class of mRNAs, including *cyclin B*, *germ cell-less* and *polar granule component*, that is deposited in the oocyte by nurse cell dumping and localizes to the posterior late in oogenesis (Dalby and Glover, 1992; Jongens et al., 1992; Nakamura et al., 1996; Wang et al., 1994). Time-lapse imaging of endogenous fluorescent *nos* mRNA showed a steady accumulation of *nos* at the posterior pole of the oocyte following the onset of nurse cell dumping (Forrest and Gavis, 2003). At the posterior, *nos* colocalizes with the germ plasm component Vasa (Vas) in large particles, consistent with the known genetic requirement for germ plasm in *nos* localization. In contrast to the localization of *grk*, *bcd* and *osk* mRNA during mid-oogenesis, the posterior localization of *nos* is reduced but not abolished by complete depolymerization of the microtubule cytoskeleton, providing evidence against microtubule-dependent transport. The reduction in *nos* localization, however, points to the role of another microtubule-dependent process called ooplasmic streaming. Immediately prior to nurse cell dumping, oocyte microtubules reorganize to form parallel arrays beneath the oocyte cortex. These cortical microtubules mediate a vigorous kinesin-dependent flow of oocyte cytoplasm that mixes the incoming contents of the nurse cells with the ooplasm (Gutzeit and Koppa, 1982; Palacios and St Johnston, 2002; Theurkauf, 1994) (see Movie 1 in the supplementary material). Because microtubule

depolymerization blocks ooplasmic streaming but not nurse cell dumping, the effect on *nos* localization supports a model whereby *nos* RNPs diffuse throughout the oocyte but become trapped at the posterior by association with the germ plasm (Fig. 3C). Ooplasmic streaming thus enhances localization by facilitating encounters between *nos* RNPs and the germ plasm (Forrest and Gavis, 2003). Supporting this model, high-resolution imaging of fluorescent *nos* mRNA has subsequently detected individual *nos* mRNA particles moving in concert with yolk granules during ooplasmic streaming, consistent with passive transport (Weil et al., 2008) (see Movie 4 in the supplementary material).

Time-lapse imaging of genetically encoded fluorescent *bcd* mRNA during the transition from mid to late stages of oogenesis showed that *bcd* continues to accumulate at the anterior during nurse cell dumping. This late localization actually accounts for the majority of *bcd* mRNA that is present at the anterior of the embryo (Weil et al., 2006). Differing genetic requirements suggest that the initial and late phases of *bcd* localization use mechanistically distinct pathways. Mutations in *stau* and *swallow* (*swa*) selectively disrupt the late phase of *bcd* localization, and particles containing both *bcd* mRNA and Stau are detected only at these stages (St Johnston et al., 1989; Weil et al., 2006; Weil et al., 2008). Although *exu* is essential for *bcd* localization during both mid and late oogenesis, Exu phosphorylation is selectively required during the initial period (Riechmann and Ephrussi, 2004). Differences in *bcd* RNP assembly and composition might adapt *bcd* to the cellular machinery operating at different stages.

In contrast to *nos*, transport of *bcd* mRNA is both microtubule and dynein dependent. Live imaging of the microtubule marker Tau-GFP revealed a subpopulation of microtubules that project from the anterior cortex, distinct from the cortical microtubules that drive ooplasmic streaming (Fig. 3C). By co-visualizing microtubules labeled with Tau-GFP together with fluorescent *bcd* mRNA, Weil et al. (Weil et al., 2008) demonstrated directly that *bcd* RNP particles travel on these microtubule tracks (see Movie 5 in the supplementary material). The anterior microtubules are probably nucleated by a MTOC formed at the anterior cortex at the onset of nurse cell dumping (Schnorrer et al., 2002), suggesting that a specific reorganization of microtubules at the anterior cortex is responsible for maintaining an anterior transport pathway, while the majority of microtubules are reorganized for ooplasmic streaming. Surprisingly, Weil et al. (Weil et al., 2006) found that localization of *bcd* mRNA during nurse cell dumping can also be disrupted by actin depolymerization. This actin dependence proved to be indirect, however, because of a role for cortical actin in anchoring the anterior microtubules (Fig. 4A).

The finding that maximal *bcd* mRNA accumulation occurs after nurse cell dumping suggests that other mRNAs localized during mid-oogenesis could continue to be localized at late stages. Although endogenous *osk* mRNA has not yet been examined, injected *osk* transcripts accumulate at the posterior of late oocytes, facilitated by ooplasmic streaming (Glotzer et al., 1997). Thus, molecular asymmetries established through the polarized transport of mRNAs during mid-oogenesis might be maintained and reinforced by the subsequent localization of additional transcripts provided to the oocyte during nurse cell dumping.

## Anchoring of mRNAs at the oocyte cortex

The effectiveness of a localization pathway depends on the ability to maintain transcripts at the target destination. The term ‘anchoring’ is commonly used to describe this end point of localization, implying a stable association of mRNA with a component of the cellular architecture. For mRNAs like *osk* and *nos*, anchoring is requisite for translation (Gavis and Lehmann, 1994; Markussen et al., 1995; Rongo et al., 1995). Transport and anchoring phases of localization pathways have been difficult to separate by traditional static imaging methods that visualize cumulative events. By permitting the investigation of the steady-state behavior of RNAs at the oocyte cortex, live-imaging methods have revealed an unexpected diversity of mechanisms for maintaining transcript localization.

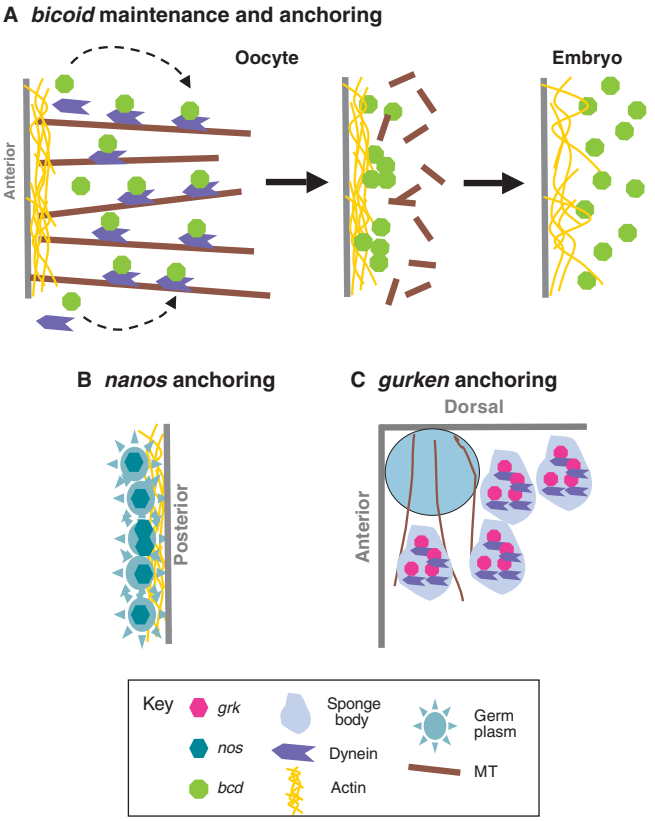


**Fig. 4. Maintenance of localized mRNAs.** (**A**) Maintenance of *bcd* mRNA at the anterior cortex of late oocytes by continual active transport on microtubules (MT), transition to a static actin-dependent anchoring mechanism at the end of oogenesis, and release from the tight cortical anchor at fertilization. (**B**) Stable, actin-dependent anchoring of *nos* mRNA and germ plasm (including *osk*) in late oocytes. (**C**) Dynein-dependent anchoring of *grk* mRNA in sponge bodies during mid-oogenesis. The oocyte nucleus is depicted as a blue circle.

Live imaging of both GFP-tagged *nos* mRNA and Vas-GFP has provided evidence for the retention of posteriorly localized mRNAs via actin-dependent anchoring of the germ plasm (Fig. 4B). Following treatment of late oocytes with cytochalasin D to depolymerize actin filaments, *nos* mRNA and Vas-GFP that have previously accumulated at the posterior cortex are released coincidently and swept away by the force of ooplasmic streaming (Forrest and Gavis, 2003). The dependence of *nos* localization on the germ plasm and the coincident release of *nos* and Vas suggests that *nos* mRNA is anchored to the cortical actin cytoskeleton via its association with the germ plasm. FRAP experiments, in which RFP-tagged *nos* RNA at the posterior cortex of a late (stage 13) oocyte was irreversibly photobleached, showed no fluorescence recovery by exchange with unbleached RFP-tagged *nos* mRNA from the nearby cytoplasm, confirming that this cortical association is highly stable (Weil et al., 2006).

An actin-dependent posterior anchoring system could be established through a feedback loop that initiates with *osk* mRNA localization itself. Upon localization to the posterior during mid-

oogenesis, *osk* mRNA is translated to produce two protein isoforms, Long Osk and Short Osk (Markussen et al., 1995; Rongo et al., 1995). Long Osk is required in turn to maintain *osk* mRNA and Short Osk localization at the posterior, whereas Short Osk recruits Vas and other germ plasm components (Breitwieser et al., 1996; Vanzo and Ephrussi, 2002). Both isoforms appear to be involved in the organization of long F-actin projections at the posterior cortex (Vanzo et al., 2007). Whether this actin organization is required for the posterior anchoring of *osk* is not known, but a role for actin is consistent with the partial release of *osk* mRNA from the posterior cortex observed after the treatment of egg chambers with actin-depolymerizing drugs (Cha et al., 2002). An interplay between actin, *osk* mRNA, germ plasm, and *nos* mRNA anchoring is further supported by the ability of mutations in the cortical actin binding protein Moesin to cause the delocalization *osk* mRNA, Vas protein and *nos* mRNA, along with detachment of F-actin from the posterior cortex (Jankovics et al., 2002; Polesello et al., 2002).

In contrast to posteriorly localized mRNAs, *bcd* mRNA retention at the anterior of the oocyte requires microtubules. By performing in situ hybridization on paraffin sections, Pokrykwa and Stephenson (Pokrykwa and Stephenson, 1991) found that treatment of stage 10 egg chambers with microtubule-depolymerizing drugs disrupts *bcd* localization. A role for microtubules in maintaining anterior *bcd* mRNA localization during stages 10-12 was confirmed by live-imaging experiments, which showed that *bcd* RNP particles detach from the anterior cortex upon treatment of cultured oocytes with microtubule-depolymerizing drugs (Weil et al., 2006). Surprisingly, however, microtubules do not serve to anchor *bcd* to the anterior cortex. Rather, FRAP and FLIP analysis revealed that the association of *bcd* mRNA with the anterior cortex is dynamic, even after nurse cell dumping and ooplasmic streaming are complete and *bcd* accumulation appears maximal. High-resolution imaging during this time period showed dynein-dependent translocation of *bcd* particles, with the majority directed towards or along the anterior cortex (Weil et al., 2006; Weil et al., 2008) (see Movie 4 in the supplementary material). Together, these results indicate that *bcd* mRNA does not become stably anchored during these stages and that steady-state localization requires continual active transport (Fig. 4A).

The ability to monitor the behavior of *bcd* particles as oogenesis progresses towards fertilization has uncovered additional temporal complexity in the *bcd* mRNA localization pathway. Such a temporal analysis of *bcd* mRNA particle dynamics revealed that *bcd* mRNA shifts from continuous active transport to stable actin-dependent anchoring at the end of oogenesis, with *bcd* RNPs coalescing in large foci in association with the cortical actin cytoskeleton (Weil et al., 2008) (Fig. 4A). Furthermore, through a combination of in vitro manipulations and mutational analysis, Weil et al. (Weil et al., 2008) showed that calcium signaling events that occur prior to fertilization trigger the dissipation of these foci throughout the anterior of the egg, probably through an effect on the actin cytoskeleton (Fig. 4A). Intriguingly, a similar mechanism appears to release *Xenopus Vg1* mRNA from its actin tether during fertilization (Yisraeli et al., 1990). Although it is unclear why a stable anchoring system is not established until late in oogenesis, the transition to actin-dependent anchoring could ensure the integrity of *bcd* mRNA localization, like that of *nos*, during periods when eggs are held dormant in the female prior to fertilization.

Like *bcd*, *grk* mRNA also undergoes a shift from dynamic maintenance to stable cortical association, but in this case the transition coincides with the shift from anterior to dorsal anterior *grk* localization. FRAP experiments performed on both injected and endogenous fluorescent *grk* RNA showed fluorescence recovery of *grk* at the anterior cortex of the oocyte, but not at its dorsal anterior position (Delanoue et al., 2007; Jaramillo et al., 2008). Thus, *grk* mRNA is statically anchored only after it becomes dorsally restricted and not during its transient localization at the anterior cortex. Surprisingly, however, dorsal anterior anchoring of *grk* is compromised by the injection of antibodies to dhc (Delanoue et al., 2007). To further investigate this dynein-dependent anchoring mechanism, Delanoue et al. (Delanoue et al., 2007) turned to ISH-EM. By this method, injected and endogenous *grk* transcripts are detected, together with dynein heavy chain and Sqd, at the dorsal anterior region in large cytoplasmic structures that resemble previously described sponge bodies (Fig. 4C). Hypomorphic mutations in *dhc* disrupt these sponge bodies and cause the dispersal of *grk* RNA. Dynein therefore plays two biochemically distinct roles in *grk* localization: first as a motor for transport and then as an anchor via an as yet unknown function in sponge body integrity. Sponge bodies form in *sqd* mutants, but when *grk* RNA is injected into the mutant oocytes, it fails to enter the sponge bodies and remains in transport particles (Delanoue et al., 2007). Inhibition of Sqd function by antibodies causes the detachment of anchored *grk* RNA; ultrastructural analysis showed that *grk* resides in transport particles rather than in sponge bodies when Sqd is inhibited. This accumulation of transport particles outside of the sponge bodies suggests an additional role for Sqd in the remodeling of transport particles to anchoring complexes following their transport to the dorsal anterior corner.

## Conclusions

The ability to visualize mRNA localization events in real time and to monitor the behavior of RNA particles at high temporal and spatial resolution has advanced and expanded our understanding of the cellular mechanisms used to transport mRNAs to different destinations and to maintain their localized distributions. Live-imaging studies have also provided new insight into the functional organization of the oocyte cytoskeleton and its use by mRNA transport machinery.

Detailed dynamic analysis has revealed intriguing similarities, as well as differences, in behavior among localized mRNAs. The use of a common dynein-mediated transport pathway in nurse cells raises the possibility that oocyte-destined mRNAs like *grk*, *bcd* and *osk* might be packaged together into the same nurse cell transport particle. Remodeling of these particles upon their arrival in the oocyte would then segregate different component mRNAs into distinct oocyte transport particles coupled to the appropriate motors for translocation within the oocyte. Such a co-transport model can be tested either by co-injection of RNAs labeled with different fluorophores or by using different RNA stemloop and cognate protein pairs to label two different endogenous transcripts simultaneously. Co-transport of different mRNAs to the yeast bud tip has recently been observed using the latter method (Lange et al., 2008).

In another direction, co-visualization of fluorescently labeled mRNAs and proteins will provide insight into the temporal regulation of RNP assembly and the remodeling events that alter the composition of RNP particles at different stages of the localization process. Given the growing number of localization factors reported to regulate multiple mRNAs, determining how these proteins contribute to the localization of each target mRNA will be facilitated by the ability to follow differentially labeled mRNA-protein pairs. For example, Stau coassembles with *osk* mRNA transport particles during mid-oogenesis and with *bcd* particles in late oocytes and in

early embryos, consistent with the genetic requirements for *stau* in *osk* and *bcd* mRNA localization at these stages (Weil et al., 2006; Weil et al., 2008; Zimyanin et al., 2008).

One remaining gap in our knowledge stems from the inability to follow the entire path of an individual RNP particle en route to its destination, owing to the tendency of particles to move out of the plane of focus and to the photobleaching that occurs during long periods of imaging at high resolution. The continuing generation of brighter and more photostable fluorophores together with the development of new microscopes that allow rapid imaging in four dimensions hold the promise for another great leap forward.

**Acknowledgements**

We thank Jack Lee and Amanda Norvell for comments on the manuscript. Our work was supported by a grant from the National Institutes of Health to E.R.G. and by an NSERC postgraduate fellowship to A.N.B. Deposited in PMC for release after 12 months.

**Supplementary material**

Supplementary material for this article is available at http://dev.biologists.org/cgi/content/full/136/15/2493/DC1

**References**

**Aigner, K., Avossa, D., Morgan, F., Hill, S. J., Barry, C., Barbarese, E. and Carson, J. H.** (1993). Transport and localization of exogenous myelin basic protein mRNA microinjected into oligodendrocytes. *J. Cell Biol.* **123**, 431-441.

**Ashraf, S. I., McLoon, A. L., Sclarsic, S. M. and Kunes, S.** (2006). Synaptic protein synthesis associated with memory is regulated by the RISC pathway in *Drosophila*. *Cell* **124**, 191-205.

**Bertrand, E., Chartrand, P., Schaefer, M., Shenoy, S. M., Singer, R. H. and Long, R. M.** (1998). Localization of ASH1 mRNA particles in living yeast. *Mol. Cell* **2**, 437-445.

**Brechbiel, J. L. and Gavis, E. R.** (2008). Spatial regulation of *nanos* is required for its function in dendrite morphogenesis. *Curr. Biol.* **18**, 745-750.

**Breitwieser, W., Markussen, F. H., Horstmann, H. and Ephrussi, A.** (1996). Oskar protein interaction with Vasa represents an essential step in polar granule assembly. *Genes Dev.* **10**, 2179-2188.

**Brendza, R. P., Serbus, L. R., Duffy, J. B. and Saxton, W. M.** (2000). A function for kinesin I in the posterior transport of *oskar* mRNA and Staufen protein. *Science* **289**, 2120-2122.

**Cha, B. J., Koppetsch, B. S. and Theurkauf, W. E.** (2001). *In vivo* analysis of *Drosophila bicoid* mRNA localization reveals a novel microtubule-dependent axis specification pathway. *Cell* **106**, 35-46.

**Cha, B. J., Serbus, L. R., Koppetsch, B. S. and Theurkauf, W. E.** (2002). Kinesin I-dependent cortical exclusion restricts pole plasm to the oocyte posterior. *Nat. Cell Biol.* **4**, 592-598.

**Clark, A., Meignin, C. and Davis, I.** (2007). A Dynein-dependent shortcut rapidly delivers axis determination transcripts into the *Drosophila* oocyte. *Development* **134**, 1955-1965.

**Clark, I., Giniger, E., Ruohola-Baker, H., Jan, L. Y. and Jan, Y. N.** (1994). Transient posterior localization of a kinesin fusion protein reflects anteroposterior polarity of the *Drosophila* oocyte. *Curr. Biol.* **4**, 289-300.

**Condeelis, J. and Singer, R. H.** (2005). How and why does beta-actin mRNA target? *Biol. Cell* **97**, 97-110.

**Dalby, B. and Glover, D. M.** (1992). 3′ non-translated sequences in *Drosophila* cyclin B transcripts direct posterior pole accumulation late in oogenesis and peri-nuclear association in syncytial embryos. *Development* **115**, 989-997.

**Delanoue, R., Herpers, B., Soetaert, J., Davis, I. and Rabouille, C.** (2007). *Drosophila* Squid/hnRNP helps Dynein switch from a *gurken* mRNA transport motor to an ultrastructural static anchor in sponge bodies. *Dev. Cell* **13**, 523-538.

**Driever, W. and Nüsslein-Volhard, C.** (1988). A gradient of bicoid protein in *Drosophila* embryos. *Cell* **54**, 83-93.

**Duncan, J. E. and Warrior, R.** (2002). The cytoplasmic Dynein and Kinesin motors have interdependent roles in patterning the *Drosophila* oocyte. *Curr. Biol.* **12**, 1982-1991.

**Ephrussi, A. and Lehmann, R.** (1992). Induction of germ cell formation by *oskar*. *Nature* **358**, 387-392.

**Ephrussi, A., Dickinson, L. K. and Lehmann, R.** (1991). *osk*ar organizes the germ plasm and directs localization of the posterior determinant *nano*s. *Cell* **66**, 37-50.

**Erdélyi, M., Michon, A. M., Guichet, A., Glotzer, J. B. and Ephrussi, A.** (1995). Requirement for *Drosophila* cytoplasmic tropomyosin in *oskar* mRNA localization. *Nature* **377**, 524-527.

**Estes, P. S., O'Shea, M., Clasen, S. and Zarnescu, D. C.** (2008). Fragile X protein controls the efficacy of mRNA transport in *Drosophila* neurons. *Mol. Cell Neurosci.* **39**, 170-179.

**Forrest, K. M. and Gavis, E. R.** (2003). Live imaging of endogenous mRNA reveals a diffusion and entrapment mechanism for *nanos* mRNA localization in *Drosophila*. *Curr. Biol.* **13**, 1159-1168.

**Forrest, K. M., Clark, I. E., Jain, R. A. and Gavis, E. R.** (2004). Temporal complexity within a translational control element in the *nanos* mRNA. *Development* **131**, 5849-5857.

**Gavis, E. R. and Lehmann, R.** (1992). Localization of *nano*s RNA controls embryonic polarity. *Cell* **71**, 301-313.

**Gavis, E. R. and Lehmann, R.** (1994). Translational regulation of *nanos* by RNA localization. *Nature* **369**, 315-318.

**Gavis, E. R., Singer, R. H. and Hüttelmaier, S.** (2007). Localized translation through messenger RNA localization. In *Translational Control in Biology and Medicine* (ed. J. W. B. Hershey, M. B. Mathews and N. Sonenberg), pp. 687-717. Cold Spring Harbor, NY: Cold Spring Harbor Laboratory Press.

**Gavis, E. R., Chatterjee, S., Ford, N. R. and Wolff, L. J.** (2008). Dispensability of *nanos* mRNA localization for abdominal patterning but not for germ cell development. *Mech. Dev.* **125**, 81-90.

**Giniger, E., Jan, L. Y. and Jan, Y. N.** (1993). Specifying the path of the intersegmental nerve of the *Drosophila* embryo: a role for Delta and Notch. *Development* **117**, 431-440.

**Glotzer, J. B., Saffrich, R., Glotzer, M. and Ephrussi, A.** (1997). Cytoplasmic flows localize injected *oskar* RNA in *Drosophila* oocytes. *Curr. Biol.* **7**, 326-337.

**Gonsalvez, G. B., Urbinati, C. R. and Long, R. M.** (2005). RNA localization in yeast: moving towards a mechanism. *Biol. Cell* **97**, 75-86.

**González-Reyes, A., Elliot, H. and St Johnston, D.** (1995). Polarization of both major body axes in *Drosophila* by *gurken-torpedo* signalling. *Nature* **375**, 654-658.

**Gutzeit, H. O. and Koppa, R.** (1982). Time-lapse film analysis of cytoplasmic streaming during late oogenesis of *Drosophila*. *J. Embryol. Exp. Morphol.* **67**, 101-111.

**Huynh, J. R., Munro, T. P., Smith-Litière, K., Lepesant, J. A. and St Johnston, D.** (2004). The Drosophila hnRNPA/B homolog, Hrp48, is specifically required for a distinct step in *osk* mRNA localization. *Dev. Cell* **6**, 625-635.

**Jankovics, F., Sinka, R., Lukacsovich, T. and Erdelyi, M.** (2002). MOESIN crosslinks actin and cell membrane in *Drosophila* oocytes and is required for OSKAR anchoring. *Curr. Biol.* **12**, 2060-2065.

**Januschke, J., Gervais, L., Dass, S., Kaltschmidt, J. A., Lopez-Schier, H., St Johnston, D., Brand, A. H., Roth, S. and Guichet, A.** (2002). Polar transport in the *Drosophila* oocyte requires Dynein and Kinesin I cooperation. *Curr. Biol.* **12**, 1971-1981.

**Januschke, J., Gervais, L., Gillet, L., Keryer, G., Bornens, M. and Guichet, A.** (2006). The centrosome-nucleus complex and microtubule organization in the *Drosophila* oocyte. *Development* **133**, 129-139.

**Jaramillo, A. M., Weil, T. T., Goodhouse, J., Gavis, E. R. and Schupbach, T.** (2008). The dynamics of fluorescently labeled endogenous *gurken* mRNA in *Drosophila*. *J. Cell Sci.* **121**, 887-894.

**Jeffery, W. R., Tomlinson, C. R. and Brodeur, R. D.** (1983). Localization of actin messenger RNA during early ascidian development. *Dev. Biol.* **99**, 408-417.

**Jongens, T. A., Hay, B., Jan, L. Y. and Jan, Y. N.** (1992). The *germ cell-less* gene product: a posteriorly localized component necessary for germ cell development in *Drosophila*. *Cell* **70**, 569-584.

**King, M. L., Messitt, T. J. and Mowry, K. L.** (2005). Putting RNAs in the right place at the right time: RNA localization in the frog oocyte. *Biol. Cell* **97**, 19-33.

**Kloc, M. and Etkin, L. D.** (2005). RNA localization mechanisms in oocytes. *J. Cell Sci.* **118**, 269-282.

**Kugler, J. M. and Lasko, P.** (2009). Localization, anchoring and translational control of *oskar*, *gurken*, *bicoid* and *nanos* mRNA during *Drosophila* oogenesis. *Fly* **3**, 1-14.

**Lange, S., Katayama, Y., Schmid, M., Burkacky, O., Brauchle, C., Lamb, D. C. and Jansen, R. P.** (2008). Simultaneous transport of different localized mRNA species revealed by live-cell imaging. *Traffic* **9**, 1256-1267.

**Lécuyer, E., Yoshida, H., Parthasarathy, N., Alm, C., Babak, T., Cerovina, T., Hughes, T. R., Tomancak, P. and Krause, H. M.** (2007). Global analysis of mRNA localization reveals a prominent role in organizing cellular architecture and function. *Cell* **131**, 174-187.

**Lehmann, R. and Nusslein-Volhard, C.** (1986). Abdominal segmentation, pole cell formation, and embryonic polarity require the localized activity of *oskar*, a maternal gene in *Drosophila*. *Cell* **47**, 141-152.

**Lewis, R. A. and Mowry, K. L.** (2007). Ribonucleoprotein remodeling during RNA localization. *Differentiation* **75**, 507-518.

**MacDougall, N., Clark, A., MacDougall, E. and Davis, I.** (2003). *Drosophila gurken* (TGFalpha) mRNA localizes as particles that move within the oocyte in two dynein-dependent steps. *Dev. Cell* **4**, 307-319.

**Markussen, F. H., Michon, A. M., Breitwieser, W. and Ephrussi, A.** (1995). Translational control of *oskar* generates Short OSK, the isoform that induces pole plasm assembly. *Development* **121**, 3723-3732.

**Martin, K. C., Barad, M. and Kandel, E. R.** (2000). Local protein synthesis and its role in synapse-specific plasticity. *Curr. Opin. Neurobiol.* **10**, 587-592.

**Messitt, T. J., Gagnon, J. A., Kreiling, J. A., Pratt, C. A., Yoon, Y. J. and Mowry, K. L.** (2008). Multiple kinesin motors coordinate cytoplasmic RNA transport on a subpopulation of microtubules in *Xenopus* oocytes. *Dev. Cell* **15**, 426-436.

**Micklem, D. R., Dasgupta, R., Elliot, H., Gergely, F., Davidson, C., Brand, A., González-Reyes, A. and St Johnston, D.** (1997). The *mago nashi* gene is required for the polarisation of the oocyte and the formation of perpendicular axes in *Drosophila*. *Curr. Biol.* **7**, 468-478.

**Mische, S., Li, M., Serr, M. and Hays, T. S.** (2007). Direct observation of regulated ribonucleoprotein transport across the nurse cell/oocyte boundary. *Mol. Biol. Cell* **18**, 2254-2263.

**Nakamura, A., Amikura, R., Mukai, M., Kobayashi, S. and Lasko, P.** (1996). Requirement for a noncoding RNA in *Drosophila* polar granules for germ cell establishment. *Science* **274**, 2075-2079.

**Neuman-Silberberg, F. S. and Schüpbach, T.** (1993). The *Drosophila* dorsoventral patterning gene *gurken* produces a dorsally localized RNA and encodes a TGFa-like protein. *Cell* **75**, 165-174.

**Newmark, P. A. and Boswell, R. E.** (1994). The *mago nashi* locus encodes an essential product required for germ plasm assembly in *Drosophila*. *Development* **120**, 1303-1313.

**Palacios, I. M. and St Johnston, D.** (2001). Getting the message across: the intracellular localization of mRNAs in higher eukaryotes. *Annu. Rev. Cell Dev. Biol.* **17**, 569-614.

**Palacios, I. M. and St Johnston, D.** (2002). *Kinesin light chain*-independent function of the *Kinesin heavy chain* in cytoplasmic streaming and posterior localisation in the *Drosophila* oocyte. *Development* **129**, 5473-5485.

**Pokrywka, N. J. and Stephenson, E. C.** (1991). Microtubules mediate the localization of *bicoid* RNA during *Drosophila* oogenesis. *Development* **113**, 55-66.

**Pokrywka, N. J. and Stephenson, E. C.** (1995). Microtubules are a general component of mRNA localization systems in *Drosophila* oocytes. *Dev. Biol.* **167**, 363-370.

**Polesello, C., Delon, I., Valenti, P., Ferrer, P. and Payre, F.** (2002). Dmoesin controls actin-based cell shape and polarity during *Drosophila melanogaster* oogenesis. *Nat. Cell Biol.* **4**, 782-789.

**Riechmann, V. and Ephrussi, A.** (2004). Par-1 regulates *bicoid* mRNA localisation by phosphorylating Exuperantia. *Development* **131**, 5897-5907.

**Rongo, C., Gavis, E. R. and Lehmann, R.** (1995). Localization of *oskar* RNA regulates *oskar* translation and requires Oskar protein. *Development* **121**, 2737-2746.

**Schnorrer, F., Luschnig, S., Koch, I. and Nusslein-Volhard, C.** (2002). *Gamma-Tubulin37C* and *gamma-tubulin ring complex protein 75* are essential for *bicoid* RNA localization during *Drosophila* oogenesis. *Dev. Cell* **3**, 685-696.

**Spradling, A. C.** (1993). Developmental genetics of oogenesis. In *The Development of Drosophila Melanogaster*, vol. I (ed. M. Bate and A. Martinez Arias), pp. 1-70. Cold Spring Harbor, NY: Cold Spring Harbor Press.

**St Johnston, D.** (2005). Moving messages: the intracellular localization of mRNAs. *Nat. Rev. Mol. Cell Biol.* **6**, 363-375.

**St Johnston, D., Driever, W., Berleth, T., Richstein, S. and Nüsslein-Volhard, C.** (1989). Multiple steps in the localization of *bicoid* RNA to the anterior pole of the *Drosophila* oocyte. *Development Suppl.* **107**, 13-19.

**Theurkauf, W. E.** (1994). Premature microtubule-dependent cytoplasmic streaming in *cappuccino* and *spire* mutant oocytes. *Science* **265**, 2093-2096.

**Theurkauf, W. E. and Hazelrigg, T. I.** (1998). *In vivo* analyses of cytoplasmic transport and cytoskeletal organization during *Drosophila* oogenesis: characterization of a multi-step anterior localization pathway. *Development* **125**, 3655-3666.

**Theurkauf, W. E., Smiley, S., Wong, M. L. and Alberts, B. M.** (1992). Reorganization of the cytoskeleton during *Drosophila* oogenesis: implications for axis specification and intercellular transport. *Development* **115**, 923-936.

**Thompson, B., Wickens, M. and Kimble, J.** (2007). Translational control in development. In *Translational Control in Biology and Medicine* (ed. J. W. B. Hershey, M. B. Mathews and N. Sonenberg), pp. 507-544. Cold Spring Harbor, NY: Cold Spring Harbor Laboratory Press.

**van Eeden, F. J., Palacios, I. M., Petronczki, M., Weston, M. J. and St Johnston, D.** (2001). Barentsz is essential for the posterior localization of *oskar* mRNA and colocalizes with it to the posterior pole. *J. Cell Biol.* **154**, 511-523.

**Vanzo, N. F. and Ephrussi, A.** (2002). Oskar anchoring restricts pole plasm formation to the posterior of the *Drosophila* oocyte. *Development* **129**, 3705-3714.

**Vanzo, N., Oprins, A., Xanthakis, D., Ephrussi, A. and Rabouille, C.** (2007). Stimulation of endocytosis and actin dynamics by Oskar polarizes the *Drosophila* oocyte. *Dev. Cell* **12**, 543-555.

**Wang, C., Dickinson, L. K. and Lehmann, R.** (1994). Genetics of *nanos* localization in *Drosophila. Dev. Dyn.* **199**, 103-115.

**Weil, T. T., Forrest, K. M. and Gavis, E. R.** (2006). Localization of *bicoid* mRNA in late oocytes is maintained by continual active transport. *Dev. Cell* **11**, 251-262.

**Weil, T. T., Parton, R., Davis, I. and Gavis, E. R.** (2008). Changes in *bicoid* mRNA anchoring highlight conserved mechanisms during the oocyte-to-embryo transition *Curr. Biol.* **18**, 1055-1061.

**Yisraeli, J. K., Sokol, S. and Melton, D. A.** (1990). A two-step model for the localization of maternal mRNA in *Xenopus* oocytes: Involvement of microtubules and microfilaments in the translocation and anchoring of Vg1 mRNA. *Development* **108**, 289-298.

**Zimyanin, V. L., Belaya, K., Pecreaux, J., Gilchrist, M. J., Clark, A., Davis, I. and St Johnston, D.** (2008). *In vivo* imaging of *oskar* mRNA transport reveals the mechanism of posterior localization. *Cell* **134**, 843-853.

Developmental Cell
Article

# Apical Secretion in Epithelial Tubes of the *Drosophila* Embryo Is Directed by the Formin-Family Protein Diaphanous

R'ada Massarwa,[1] Eyal D. Schejter,[1] and Ben-Zion Shilo[1,*]
[1]Department of Molecular Genetics, Weizmann Institute of Science, Rehovot 76100, Israel
*Correspondence: benny.shilo@weizmann.ac.il
DOI 10.1016/j.devcel.2009.04.010

## SUMMARY

**Apical localization of filamentous actin (F-actin) is a common feature of epithelial tubes in multicellular organisms. However, its origins and function are not known. We demonstrate that the Diaphanous (Dia)/Formin actin-nucleating factor is required for generation of apical F-actin in diverse types of epithelial tubes in the *Drosophila* embryo. Dia itself is apically localized both at the RNA and protein levels, and apical localization of its activators, including Rho1 and two guanine exchange factor proteins (RhoGEFs), contributes to its activity. In the absence of apical actin polymerization, apical-basal polarity and microtubule organization of tubular epithelial cells remain intact; however, secretion through the apical surface to the lumen of tubular organs is blocked. Apical secretion also requires the Myosin V (MyoV) motor, implying that secretory vesicles are targeted to the apical membrane by MyoV-based transport, along polarized actin filaments nucleated by Dia. This mechanism allows efficient utilization of the entire apical membrane for secretion.**

## INTRODUCTION

Tubular epithelial networks are an essential component of the body plan in all multicellular organisms. Branched tubular structures evolved to transfer solutes, hormones, nutrients, waste products, and air between tissues, thereby facilitating growth of the organism. Several features are common to all tubular structures, despite their distinct functions. The tube cells are highly polarized, such that the protein and lipid composition of the apical membrane facing the lumen is distinct from the basolateral domain that is attached to the extracellular matrix. The epithelial cells comprising the tube wall form junctions that are essential for maintaining tube integrity, and provide a seal preventing leakage of substances from the lumen to the basolateral surface, and vice versa (Bryant and Mostov, 2008; Hogan and Kolodziej, 2002; O'Brien et al., 2002).

Several mechanisms have been shown to generate polarity in epithelial tubes. In cases where the tubes are derived by invagination of polarized ectodermal cells (e.g., during formation of the *Drosophila* tracheal system or salivary glands, or the vertebrate lung), the original polarity is maintained during the formation and elaboration of the tube (Kerman et al., 2006; Lubarsky and Krasnow, 2003). Alternatively, cell clusters that are not yet polarized generate a lumen, as cells in the center of the cluster acquire apical-basal polarity (e.g., in the mammary gland and early pancreas bud) (Hogan and Kolodziej, 2002). Finally, polarized lumens may even be formed within a single cell. In the terminal cells of the *Drosophila* trachea, or in the excretory cell of *Caenorhabditis elegans*, coalescence and fusion of apical vesicles leads to the formation of a continuous, polarized, intracellular tube (Buechner et al., 1999; Ghabrial et al., 2003).

Generation and maintenance of the polarized tube structure, requires distinct trafficking mechanisms of secretory vesicles that will supply the different components to each membrane domain. Regulated apical secretion was shown to be responsible for stereotyped tube diameter expansion in the *Drosophila* trachea (Beitel and Krasnow, 2000; Hemphala et al., 2003) and salivary glands (Myat and Andrew, 2002). When the general secretory machinery was compromised by mutations in the COPII or COPI complexes, defects in luminal secretion of a variety of proteins were observed in the *Drosophila* tracheal system (Devine et al., 2005; Jayaram et al., 2008; Tsarouhas et al., 2007). Since many epithelial tubes are actively involved in secretion of substances to the lumen, efficient vectorial trafficking of secretory vesicles to the apical surface is essential, not only for generating and maintaining the tube, but also for carrying out the physiological function of the organ.

Tubular epithelial networks display considerable diversity in size and architecture, and secrete distinct components to the lumen. Yet the similarity in cellular epithelial organization raises the possibility that common mechanisms may be involved in apical secretion. One unifying feature that was identified is the concentration of filamentous actin (F-actin) at the apical surface of the cells comprising the tube. Such organization of actin was observed in cells forming the trachea of *Drosophila*, and in mammalian Madin-Darby canine kidney (MDCK) cells that are induced to form tubes in culture (O'Brien et al., 2002; Tsarouhas et al., 2007). This dense organization of actin is distinct from the actin that is typically associated with adherens junctions, as it is present under the entire apical surface. The nucleation machinery responsible for apical F-actin (commonly termed "the terminal web"), as well as its functional role, have not been well explored. It has been suggested that the terminal web contributes to the elastic properties of the cells lining the lumen. Dynamic alterations in the structure of the terminal web were observed upon stimulated secretion (e.g., in the lacrimal gland),

raising the possibility that it may either impede or facilitate regulated secretion to the lumen (Jerdeva et al., 2005; Wu et al., 2006).

In this work, we demonstrate that apical F-actin in epithelial tubes of the *Drosophila* embryo is generated by the Diaphanous (Dia)/Formin actin-nucleating factor. Formins constitute a diverse family of proteins found in all eukaryotes. They regulate nucleation of linear actin filaments, which give rise to protruding filipodia or intracellular actin filaments. Formins are involved in diverse cellular processes, including cytokinesis, cell migration utilizing filipodia, focal adhesions, polarized cell growth, stabilization of adherens junctions (Homem and Peifer, 2008), and microtubule stabilization (reviewed by Faix and Grosse [2006]). Dia-family formins are autoinhibited through intramolecular interactions. Upon binding to GTP-bound Rho GTPases, the Dia molecule assumes an open conformation and dimerizes. The Formin-homology domain 2 within the protein initiates actin filament assembly, and remains associated with the fast-growing barbed end, allowing rapid insertion of monomeric actin, while protecting the end from capping proteins (reviewed by Goode and Eck [2007]).

We show that the Dia-induced apical actin nucleation mechanism is common to several tubular structures, including the tracheal network, salivary glands, hindgut, and Malpighian tubules. In the absence of Dia, while the overall polarity of the cells and microtubule organization remains intact, apical F-actin is not formed. A complete block of secretion via the apical surface to the tube lumen is coupled to the loss of apical F-actin in all tubular organs examined, while proteins that are secreted to the lumen via septate junctions are not affected. Our data suggest that the apical restriction of Dia nucleating activity is a consequence of apical localization of the Dia-activating machinery, Rho1, and associated guanine exchange factors (GEFs), as well as of Dia itself. We further show that apical secretion requires the Myosin V (MyoV) motor protein, implying that secretory vesicles are targeted to the apical, lumen-facing membrane by MyoV-based transport along polarized actin filaments nucleated by Dia. This mechanism allows efficient utilization of the entire apical membrane for secretion, and appears to be general for distinct types of tubes, differing in their diameter, luminal composition, and physiological role.

## RESULTS

### Apical Filamentous Actin in Embryonic Tubular Networks Is Generated by Dia

We explored the distribution of F-actin in tubular structures of the *Drosophila* embryo using tissue-specific expression of the GFP-tagged F-actin binding domain of Moesin (Chihara et al., 2003), and observed a common apical localization. In the tracheal system, apical F-actin is first observed at stage 13 at the apical side of the cells forming the dorsal trunk. As the smaller tracheal tubes organize and form a lumen, F-actin appears (Figures 1A and 1C). F-actin was also detected apically in the hindgut, salivary glands, Malpighian tubules, and proventriculus (Figures 1B and 1D–1G).

To identify the molecular machinery responsible for formation of the apical layer of microfilaments in these tubular organs, we interfered with the function of several prominent F-actin nucleating systems. To study the requirement for Dia in this context, we examined both embryos homozygous for a strong loss-of-function allele of *dia* (where maternally provided *dia* transcripts allow the embryos to proceed normally through the first stages of embryogenesis, where Dia is required for other processes [Homem and Peifer, 2008]), as well as embryos in which *dia* RNAi constructs were expressed in tubular structures, using appropriate Gal4 drivers. Under both strategies, we observed loss of apical F-actin in the trachea, while residual F-actin in the adherens junctions was maintained (Figures 1H, 1J, 1M, and 1N). Maintenance of intact adherens junctions in the absence of Dia was also observed by the presence of Armadillo (Arm), and the electron-dense structures observed at the junctions in transmission electron microscopy (Figures 1I–1L). In contrast, inactivation of another actin-nucleation factor, the Arp2/3 complex, had no effect. Specifically, coexpression in the trachea of RNAi constructs for the *Sop2* and *Arp3* genes, encoding subunits of the Arp2/3 complex, did not alter the apical F-actin localization pattern (Figure 1O). When expressed in muscles, the same RNAi constructs phenocopied the Arp2/3 mutant phenotype (Massarwa et al., 2007), demonstrating their biological potency (Figures 1P–1Q). Similar results were obtained in the hindgut and salivary glands (see Figure S1 available online). These results demonstrate that Dia is essential for the formation of the apical F-actin web in the cells comprising the various tubes, and is likely to be the primary actin nucleator operating in this context.

To rule out the possibility that the absence of apical F-actin is a secondary consequence of disruptions to epithelial cell polarity, we monitored the localization pattern of different polarity markers in the *dia* mutant background. These markers included Crumbs (Crb), which localizes to the apical membrane, DE-Cadherin and Arm, which concentrate at adherens junctions, and Discs large (Dlg), which localizes to septate junctions (Figures 2A–2D). All markers exhibited normal localization in the tracheal tubes of *dia* mutant embryos (Figures 2E–2H), indicating that cell polarity is maintained. A similar conservation of cell polarity was observed in the hindgut and salivary glands of *dia*-mutant embryos (Figure S2).

Another hallmark of cell polarity, which impinges on targeted intracellular trafficking, is the organization of microtubules. The polarity of microtubules in *Drosophila* cells can be examined by Nod-lacZ, a microtubule minus-end-directed reporter (Clark et al., 1997). We find that Nod-lacZ is localized to the apical side of all embryonic epithelial tubes. Staining of microtubules by antibodies directed against β-tubulin demonstrates that Nod-lacZ is concentrated at the apical end of the domain harboring microtubules, indicating that microtubule polarization remained intact in the absence of Dia (Figures 2I and 2J; Figure S2). Taken together, these observations demonstrate that crucial aspects of epithelial cell polarity, including distinct membrane domains and microtubule organization, remain fully intact when Dia function is disrupted. The observed loss of apical F-actin in this background is thus likely to be a direct result of impaired Dia-nucleating activity.

### Dia mRNA and Protein Are Apically Localized

The apical concentration of F-actin generated by Dia prompted us to examine the basis for the apical focus of Dia activity. Dia displays a widespread and dynamic expression pattern during early and mid-stages of embryogenesis (data not shown).

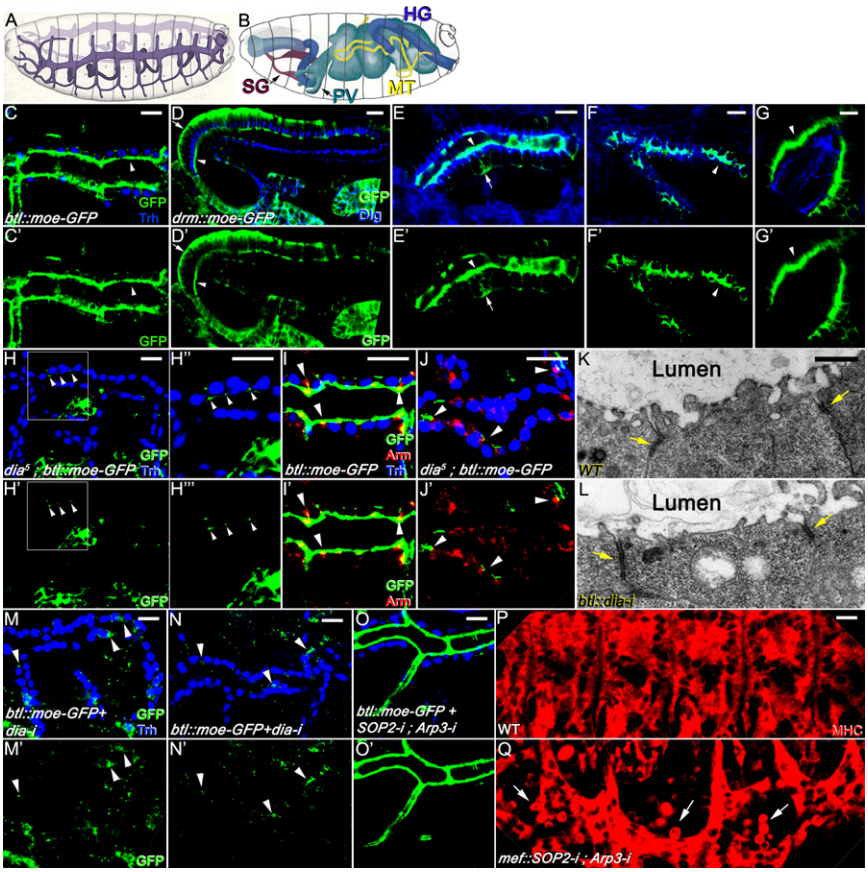


**Figure 1. Apical F-Actin in Tubular Epithelia Is Formed by Dia/Formin**

(A) Scheme of embryo at stage 14 showing the branched tracheal network comprised of polarized unicellular tubes that are interconnected.

(B) Scheme of a stage 16 embryo, showing the diverse tubular organs, including the hindgut (HG), salivary glands (SG), malpighian tubules (MT), and proventriculus (PV) (Hartenstein, 1993). In all subsequent panels, F-actin is marked by localization of Moe-GFP (green), which was expressed in the trachea by *btl-Gal4*, and in the hindgut, salivary glands, malpighian tubules, and proventriculus by *drm-Gal4*. In (C)–(G), arrowheads and arrows mark apical and basal surfaces, respectively.

(C) Dorsal trunk of trachea. Tracheal nuclei marked by Trachealess (Trh; blue).

(D) Hindgut: cell borders marked by Dlg (blue); F-actin shows both apical and basal concentrations.

(E) Salivary gland: Dlg, blue.

(F) Malpighian tubules: Dlg, blue.

(G) Proventriculus: Dlg, blue. This organ is comprised of two epithelial layers, where actin is observed on the apical side of the outer layer.

(H) In $dia^5$ zygotic mutant embryos, apical F-actin disappears, and is retained only in the adherens junctions (arrowheads).

(I and J) The position of Arm (red) in the adherens junctions in $dia^5$ mutants is comparable to wild-type, and colocalizes with the residual F-actin (arrowheads).

(K and L) Transmission electron microscopy analysis of a stage 15 embryo shows that, following expression of *dia* RNAi (VDRC20518) in the trachea, adherens junctions in the dorsal trunk are maintained, and are detected by electron-dense material (arrows). Scale bar, 0.5 μm.

(M and N) Loss of apical F-actin was also obtained following expression of RNAi for *dia* by *btl-Gal4* by using two nonoverlapping constructs (NIG1768R-1 or VDRC20518, respectively). Arrowheads show residual F-actin in adherens junctions. Scale bars, 10 μm.

(O) No alteration in apical F-actin in the trachea was observed following expression of RNAi constructs directed against the genes encoding Sop2 and Arp3 subunits of the Arp2/3 complex (VDRC42172, VDRC35260) by *btl-Gal4*. Scale bar, 10 μm.

(P and Q) Expression of the *Sop2* and *Arp3* RNAi constructs in muscles by *mef2-Gal4* mimicked the Arp2/3 muscle fusion phenotype (arrows), confirming their biological potency. (C′)–(J′) and (M′)–(O′) show only the F-actin (green) channel. Scale bar, 10 μm.

Scale bars, 10 μm (C–J).

However, from embryonic stage 14 and onward, *dia* mRNA is found predominantly within cells that form tubular structures, including the trachea, hindgut, salivary glands, Malpighian tubules, and the outer layer of the proventriculus (Figures 3A and 3B). Moreover, within each of these epithelial structures, the mRNA is tightly concentrated at the apical side (Figures 3C–3G). The apical localization of *dia* mRNA is mirrored at the protein level. Staining with anti-Dia antibodies shows that Dia protein persists in most tissues even during advanced stages of embryogenesis. At these stages, Dia protein exhibits a polarized apical localization specifically within the tubular structures, similar to *dia* mRNA, while a uniform distribution is observed in the other tissues (Figures 3H–3L). The activity of the *dia* RNAi construct could be demonstrated by disappearance of Dia protein in tissues where it was induced (Figure 3M).

To examine the mechanism for apical localization of *dia* mRNA and protein, we expressed a *dia-GFP* construct in which the 3′ untranslated region (UTR) was removed (Homem and Peifer, 2008). This mRNA, monitored in situ by a *GFP* probe, loses its apical localization (Figure 3N), demonstrating that the 3′UTR contains sequences required for apical targeting. However, the Dia-GFP protein remained apically localized, as determined by the GFP label (Figures 3O and 3P). Thus, a distinct apical targeting mechanism for the Dia protein, operating only within tubular epithelial cells, is sufficient for localization, even when the mRNA is uniformly distributed within these cells.

## Dia Is Required for Secretion to the Lumen of Tubular Organs

A central feature of tubular epithelial cells is their ability to secrete proteins to the tube lumen. We followed the distribution of several proteins normally secreted into tubular lumens to determine whether secretion was affected by loss of Dia and apical F-actin. Antibodies to the 2A12 antigen and to other secreted proteins normally detect secretion to the lumen of the trachea beginning at stage 13 of embryogenesis (Tsarouhas et al., 2007). The 2A12 antigen was absent from the lumen of the trachea in *dia* mutant embryos and following *dia* RNAi expression, and only traces could occasionally be detected within the cells comprising the smaller tubes (Figures 4A–4C).

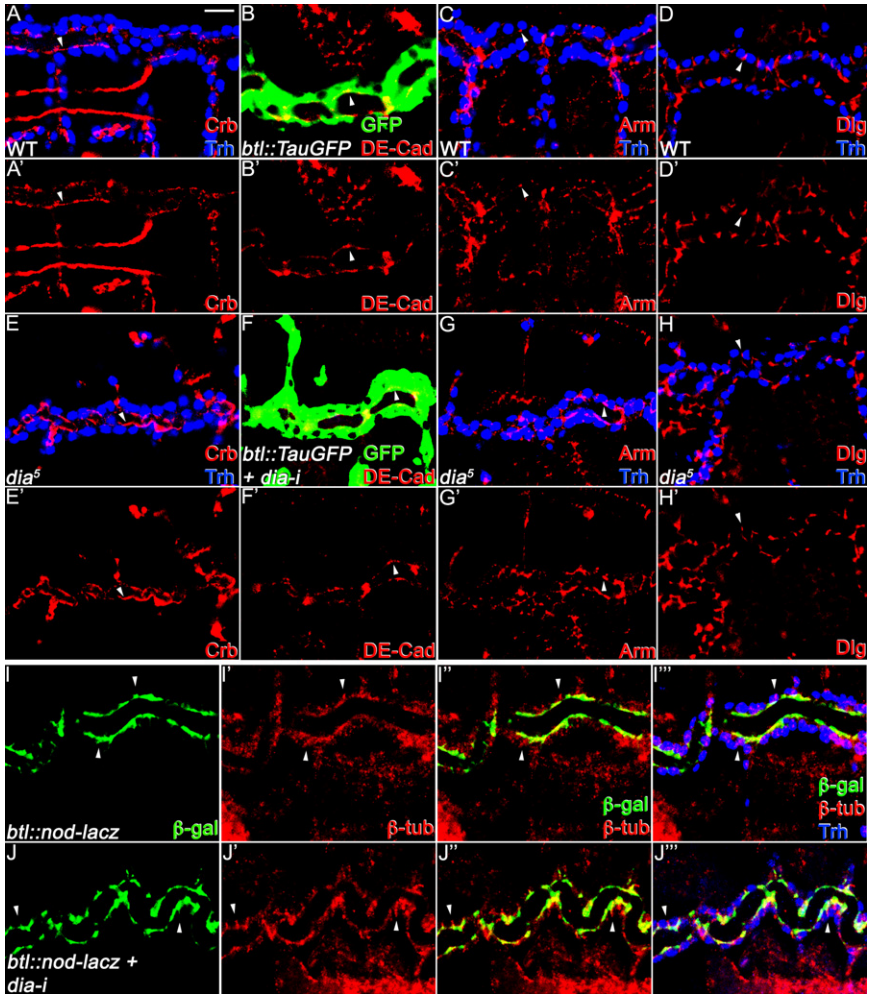


**Figure 2. Cell Polarity Is Maintained in *dia* Mutants**

The position of polarity and junctional markers (red, arrowheads) was examined in the tracheal dorsal trunk with respect to the position of the tracheal nuclei, marked by Trh (blue).

(A–D) Wild-type embryos showing the positions of the apical membrane protein, Crb, the adherens junctions marked by DE-Cad or Arm, and the septate junctions marked by Dlg. Scale bar, 10 μm.

(E–H) In *dia*$^{5}$ mutants, although the dorsal trunk is less regular, the markers maintain their normal positions.

(I–J‴) The apical position (arrowheads) of microtubule-minus ends and microtubules was determined with Nod-lacZ (green) and anti-β-tubulin (red), respectively, in wild-type embryos and following expression of *dia* RNAi VDRC20518.

The 2A12 antigen that failed to be secreted did not accumulate within the tracheal cells. To ascertain that the defect was indeed in secretion and not in synthesis of the 2A12 protein, we blocked trafficking to the lysosome by expressing an RNAi construct for *deep orange* (*dor*) (Sriram et al., 2003). When expressed alone in the trachea, accumulation of 2A12 in the lumen is normal and, in addition, some apical intracellular accumulation is also observed. When both *dor* and *dia* RNAi constructs were expressed, no secretion of 2A12 to the lumen was observed due to the absence of Dia, but apical accumulation within the tracheal cells was detected (Figures 4D and 4E). Accumulation of 2A12 antigen within the tracheal cells was also observed when a *dia* mutant was combined with a *sar1* mutant (encoding a subunit of the CopII trafficking complex), as a consequence of an early block in the secretory pathway ((Tsarouhas et al., 2007) and Figure S3). We can conclude that the 2A12 antigen is properly synthesized in the *dia* mutant background, but is rapidly targeted to degradation when a late step in secretion fails.

Another protein secreted by several tubular structures is the ZP-domain protein Piopio (Pio) (Figures 4F, 4K, and 4N and Jazwinska et al. [2003]). This protein contains a signal peptide and transmembrane domain, where the extracellular domain is constitutively cleaved upon maturation. Secreted Pio was shown to form a matrix within the lumen, together with the ZP-domain protein, Dumpy, generating a scaffold to support the migration of cells within the tube as they rearrange their positions and intercellular junctions (Jazwinska et al., 2003). In *dia* mutants, secretion of Pio is blocked in the trachea, hindgut, and salivary glands (Figures 4G, 4H, 4L, 4M, 4O, and 4P). Again, the Pio protein that failed to be secreted did not accumulate within the cells. Labeling of the tracheal cytoplasm of *dia* mutant embryos demonstrates discontinuities in the dorsal branches (Figures 4I and 4J and Figure S4F), resembling the *pio* mutant phenotype (Jazwinska et al., 2003). We also tested secretion of the ANF-GFP protein in the trachea (Tsarouhas et al., 2007), and observed loss of secretion in the absence of Dia (Figure S4). Thus, Dia appears to be required for apical secretion of multiple proteins.

The terminal cells of the trachea form a unique type of intracellular lumen (Ghabrial et al., 2003), which can be detected by antibodies directed against proteins, such as 2A12. The formation of this internal lumen is different from the lumens of the primary and secondary branches, where cells secrete material to the apical extracelullar space. While the cellular extensions of the terminal cells can be detected in *dia* mutant embryos, they do not contain the 2A12 antigen (Figure S4F), indicating that Dia is also required for the intracellular targeting of proteins toward the coalescing vesicles, that form the lumen of terminal cells.

## Dia Is Required for Secretion of a Distinct Class of Vesicles

Proper localization of Crb to the apical membrane of tracheal tubes in *dia* mutants while protein secretion to the lumen is blocked suggests that multiple routes are employed in trafficking protein cargo to the apical surface in these cells. Verm and Serp, chitin-modifying enzymes that are deposited in the tracheal lumen, were previously shown to require septate junctions for

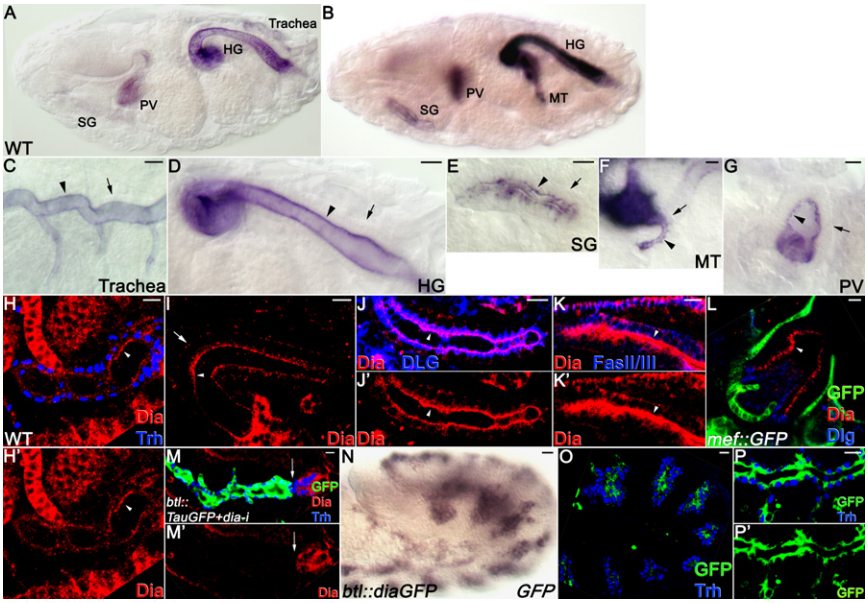


**Figure 3. *dia* mRNA and Protein Are Apically Localized in Diverse Tubular Organs**

(A and B) Starting at embryonic stage 14, *dia* mRNA begins to be detected predominantly in tubular organs, and this pattern becomes more prominent by stages 15 (A) and 16 (B).

(C–G) Within each one of the tubular organs, including trachea, hindgut, salivary glands, Malpighian tubules, and proventriculus, respectively, *dia* mRNA is localized to the apical side facing the tube lumen. In these and subsequent panels, arrowheads and arrows mark apical and basal surfaces, respectively. Scale bars, 10 μm.

(H–L) Staining the same tissues with anti-Dia demonstrates apical localization of the Dia protein. In contrast to the mRNA, protein generated at earlier stages perdures in other tissues, where it exhibits a nonpolarized distribution. Cell borders are marked in the salivary gland by Dlg (blue), and in Malpighian tubules by Fas II and III (blue). In (L), the muscle lining the outer layer of the proventriculus is marked with *mef2*-Gal4::*UAS-GFP*. Arrowheads and arrows mark apical and basal surfaces, respectively. Scale bars, 10 μm.

(M) Disappearance of Dia protein in the tracheal cells where *dia* RNAi (VDRC20518) is expressed, but not in the adjacent posterior spiracle cells (arrow). Scale bar, 10 μm.

(N) In embryos carrying *btl-Gal4*::*UAS-dia-GFP*, the localization of the ectopic transcript is followed by a probe for *GFP*, and shows a uniform distribution within the tracheal cells starting at stage 12. This indicates that the 3′UTR, which is lacking in the construct, is essential for apical localization of the *dia* transcript. Scale bar, 10 μm.

(O and P) The ectopic Dia-GFP protein was followed by staining for GFP (green), and shows a normal apical localization with respect to the tracheal nuclei (Trh, blue) at stages 12 and 15, respectively. Thus, an independent mechanism for apical localization of the Dia protein is utilized, even when the mRNA is not properly distributed. Scale bars, 10 μm.

their secretion. Compromising the structure of the septate junctions leads to failure to secrete these proteins to the lumen, while the secretion of 2A12 and Pio is unaffected (Luschnig et al., 2006; Wang et al., 2006). When we examined the secretion of the Verm and Serp proteins in a *dia* mutant background, we observed normal secretion (Figures 4Q–4S; Figures S3 and S4). This strengthens previous findings that the chitin-modifying enzymes are secreted by a distinct class of vesicles, which is not targeted apically. Dia is apparently required only for secretion of proteins that are packaged in apically secreted vesicles. The specific effect of *dia* mutants on secretion of a distinct class of vesicles, rather than a global effect on vesicle trafficking, was also ascertained by demonstrating a normal distribution of endoplasmic reticulum, Golgi, and recycling endosome markers (Figure S5), and normal endocytosis of Verm from the tracheal lumen at stage 17 (Figures 4T and 4U).

## Dia Is Activated Apically by Rho1 and Two Rho-GEFs

Activation of Dia-type Formins is commonly triggered by Rho and associated Rho-GEFs (Goode and Eck, 2007). We wanted to examine the localization and activity of these proteins, in the context of secretion by epithelial tube cells. The Rho1 protein shows an apical localization in tracheal tubes (Figure 5A). Furthermore, expression of PKNG58AeGFP, a GFP sensor for active Rho1 (Simoes et al., 2006), demonstrates that activation is apically restricted (Figure 5B). The Rho1 sensor can function as a Rho1-dominant negative, and its expression indeed leads to loss of 2A12 antigen secretion (Figure 5B). A similar effect is observed following expression of either Rho1 RNAi or dominant-negative constructs (Figures 5C and 5D), demonstrating the central role of Rho1 as a critical regulator of Dia. Since Rho1 is tethered to the membrane, its apical localization is particularly important in guiding polarized synthesis of F-actin by Dia. Thus, Dia will generate polarized actin cables, the barbed ends of which are embedded within the apical membrane.

The two Rho-GEFs, Gef2 and Gef64C, were previously shown to trigger Rho1 (Simoes et al., 2006). Both Gef2 and Gef64C display an apical protein localization in tracheal cells (Figures 5E and 5F). The apical localization of the pair of Rho-GEFs and Rho1 was also demonstrated in other tubular organs (Figure S6). When the level of Gef2 in the trachea was compromised by using a mutant background (Figure 5H), or by expression of an RNAi construct (Figure 6B), a block in secretion of 2A12 to the tracheal lumen was observed. Similar results were obtained in the *Gef64C* mutant background (Figure 5I), or following expression of *Gef64C* RNAi (Figure 6C), indicating that both Rho-GEFs are essential for apical secretion. Removal of one copy of either *Gef* gene has no effect (Figure S7). However, a strong block in secretion was observed in embryos that are transheterozygous for mutations in the two Rho-GEFs, (Figure 5J), suggesting that apical secretion requires a cumulative level of the two Rho-GEF proteins above a critical threshold. When present at sufficiently high levels, either GEF can drive 2A12 secretion, as demonstrated by the ability of Gef64C overexpression to rescue *Gef2* mutant or *Gef2* RNAi-expressing embryos (Figure S7). Markers of cell polarity display a normal

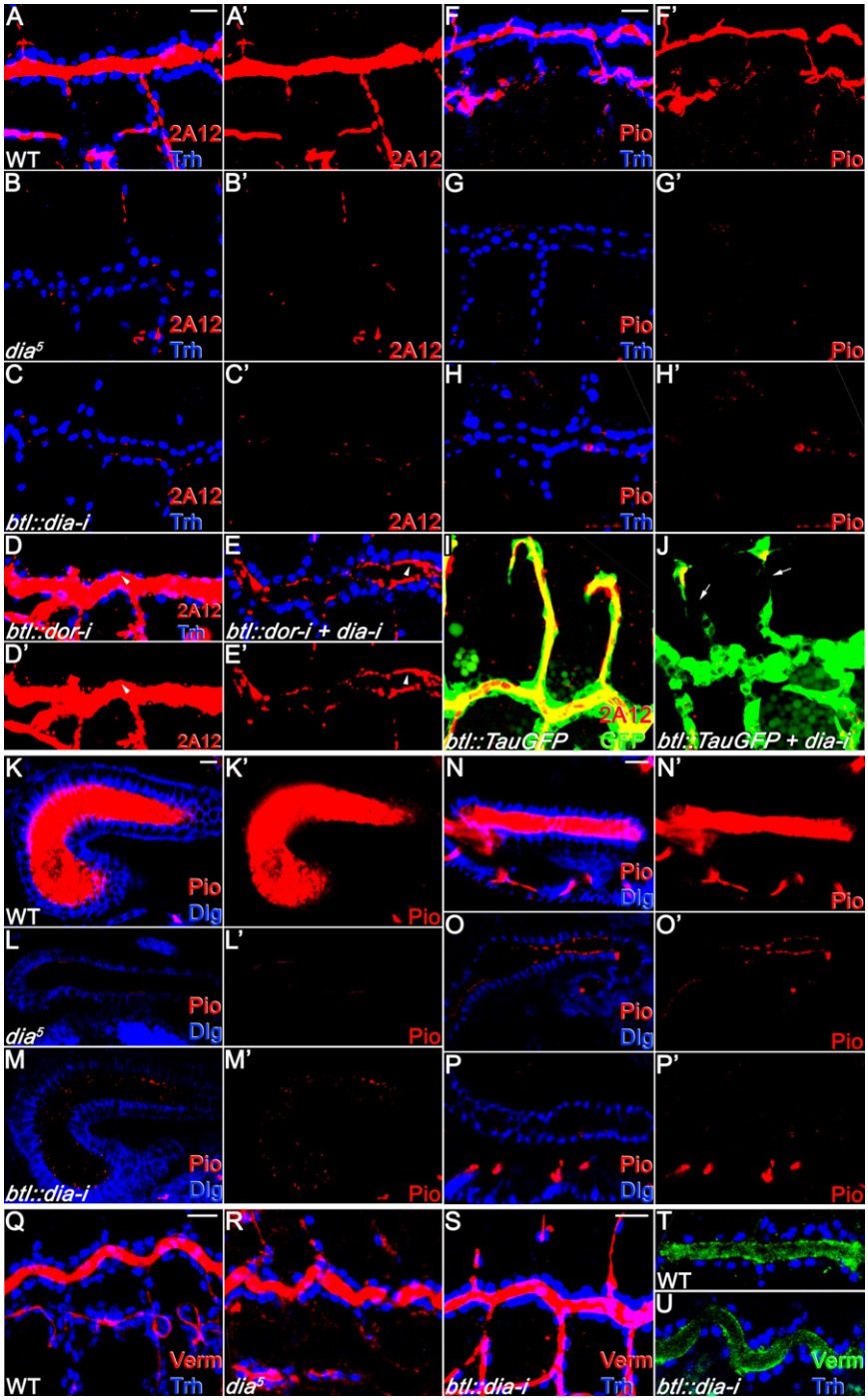


**Figure 4. Dia Is Required for Apical Secretion to the Lumen**

(A) In wild-type embryos, the 2A12 antigen (red) is secreted to the lumen of all tracheal tubes. Scale bar, 10 μm.

(B and C) In *dia*$^{5}$ mutant embryos, or *btl-Gal4* embryos expressing the VDRC20518 *dia* RNAi, the antigen is not deposited in the lumen, and does not accumulate within the tracheal cells. Occasionally, small patches of nonsecreted protein can be detected.

(D) Following expression of *dor* RNAi VDRC33734 in the trachea, secretion of 2A12 to the lumen is maintained, but accumulation of some antigen within the tracheal cells, apical to the nuclei, is observed (arrowhead).

(E) Upon coexpression of *dor* and *dia* RNAi, secretion of 2A12 to the lumen is blocked, but apical accumulation within the cells is detected (arrowhead).

(F) In wild-type embryos, the Pio ZP protein (red) is secreted to the tracheal lumen. Scale bar, 10 μm.

(G and H) No secretion or intracellular accumulation of Pio was detected in the two *dia* loss-of-function backgrounds tested above.

(I and J) Failure to secrete Pio in the absence of Dia leads to a tracheal phenotype reminiscent of *pio* mutant embryos (i.e., disruption of the junctions connecting the dorsal-branch cells [arrows]).

(K) Pio is normally secreted to the lumen of other tubular organs, which allows for examination of the requirement for Dia in additional tissues. In a wild-type embryo at stage 16, the hindgut lumen is filled with the Pio protein (cell junctions are marked by Dlg [blue]). Scale bar, 10 μm.

(L and M) In a *dia* mutant or in *drm-Gal4* embryos driving VDRC20518 *dia* RNAi, secretion of Pio is blocked and the protein does not accumulate within the cells.

(N) Wild-type embryo showing secretion of Pio (red) to the salivary gland lumen. Dlg-blue.

(O and P) In mutant *dia* embryos of the genotypes noted above, only marginal secretion of Pio to the lumen was observed.

(Q) Verm protein (red) is secreted to the tracheal lumen through the septate junctions (Trh, blue). Scale bar, 10 μm.

(R and S) In *dia*$^{5}$ mutant embryos or following expression of VDRC20518 *dia* RNAi in the trachea by *btl-Gal4*, secretion of Verm was not impaired, indicating that Dia is required only for secretion through the apical membrane. Scale bar, 10 μm.

(T and U) Endocytosis of Verm (green) from the tracheal lumen at stage 17 is also normal following *dia* RNAi expression.

Prime panels display staining of only 2A12 or Pio.

distribution in *Rho1*, *Gef2*, or *Gef64C* RNAi-expressing embryos (Figure S8), as in *dia* mutants.

We also wanted to test whether compromising the activity of Rho-GEFs or Rho1 gives rise to defects in the immediate output of Dia activity, namely, the nucleation of apical F-actin. When RNAi constructs for *Gef2*, *Gef64C*, or *Rho1* were expressed in the trachea, hindgut, or salivary glands, loss of apical F-actin was observed concomitant with defects in secretion (Figure 6). These results strengthen the causal link between Dia-mediated actin polymerization and apical secretion.

## Dia Activation Determines the Onset of Secretion

We used Rho1$^{V14}$, an activated form of Rho1, to validate the functional hierarchy between the Rho-GEFs, Rho1 and Dia, in tracheal cells. No defects in tracheal development or secretion were observed following expression of Rho$^{V14}$ in wild-type embryos (Figure 5L), likely due to the restricted apical localization of the protein. Expression of the same construct rescued the secretion defect in *Gef2*- or *Gef64C*-RNAi-expressing embryos (Figure 5M and data not shown), but failed to do so in *dia*-RNAi-expressing embryos (Figure 5N), thus demonstrating

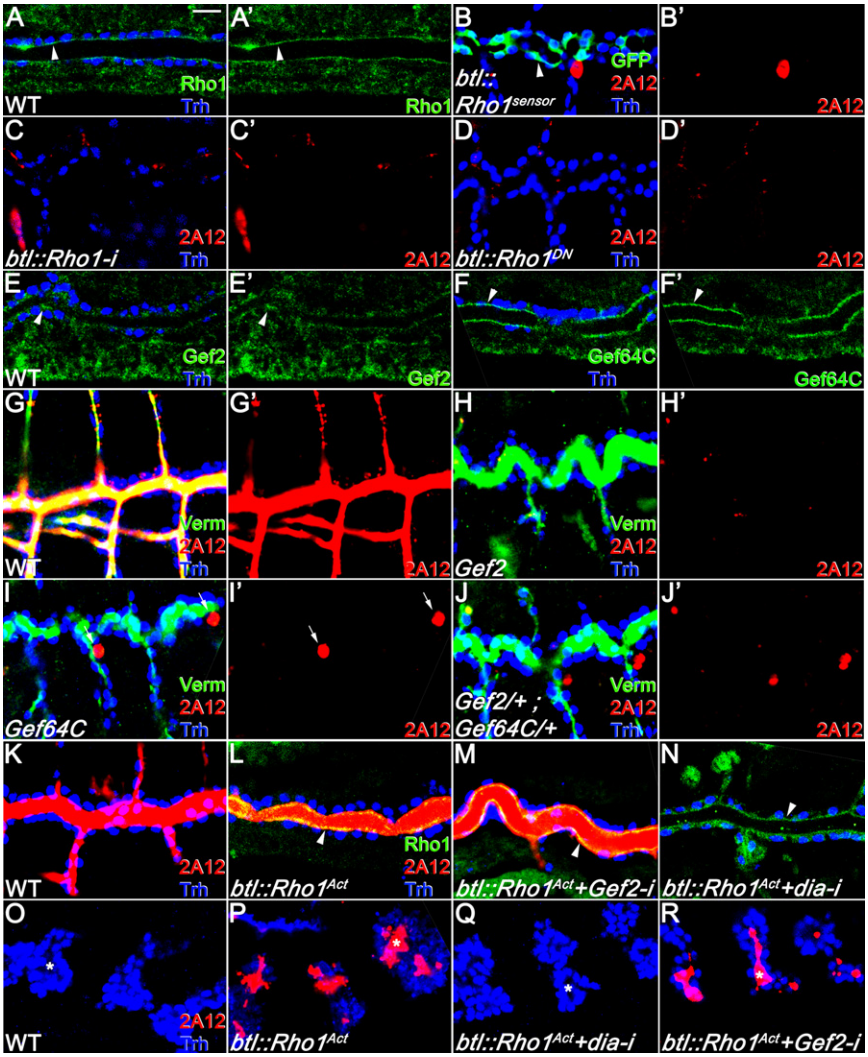


**Figure 5. Rho1 and Rho-GEFs Are Apically Localized and Trigger Dia**

(A) Rho1 (green) is apically localized in tubular structures of the trachea. Note that, in the adjacent, nontubular tissues, the protein is not polarized. Arrowheads mark apical surfaces. Scale bar, 10 μm.

(B) The active Rho sensor, PKNG58-eGFP (green), localizes apically following expression in trachea with *btl-Gal4*. Since the sensor functions as a dominant negative for Rho1, secretion of 2A12 (red) was blocked. Arrowhead marks apical surfaces.

(C and D) Expression of a *Rho1* RNAi VDRC12734 or $Rho1^{N19}$, a Rho1 dominant-negative construct, also blocked 2A12 secretion.

(E) Gef2 (green) is apically localized in the tracheal dorsal branch (Trh, blue). Arrowheads mark apical surfaces.

(F) Gef64C (green) is apically localized in the trachea. Arrowheads mark apical surfaces.

(G) Secretion was followed by 2A12 (red) and Verm (green). In a wild-type embryo, both accumulate in the lumen; (G′) shows only 2A12.

(H) In a *Gef2* mutant embryo, Verm was normally secreted, but no secretion of 2A12 was detected ([H′]2A12 channel).

(I) A similar result was observed in *Gef64C* mutant embryos. The clusters of 2A12 staining mark the cells of the spiracular branch, which accumulate the protein intracellularly at stage 16 (arrows).

(J) In a transheterozygous embryo of the genotype $Gef2^{-}$/+; $Gef64C^{-}$/+, no secretion of 2A12 was observed. This indicates that the two Rho-GEF proteins have similar functions, but must accumulate to a critical level in order to trigger Rho1.

(K) Wild-type (2A12, red; Trh, blue).

(L) Activated Rho1 was expressed by *btl-Gal4*. When monitored in the trachea at stage 15, the ectopic protein (expressed at higher levels than the endogenous Rho1) shows normal apical localization (Rho1, green; Trh, blue; 2A12, red). Arrowheads mark apical surfaces.

(M) Similar expression of activated Rho1 in a *Gef2* RNAi NIG9635R-3 background shows rescue of 2A12 secretion (red), indicating that activated Rho1 can bypass activation by Rho-GEFs. Arrowheads mark apical surfaces.

(N) Similar expression of activated Rho1 in a VDRC20518 *dia* RNAi background shows normal apical localization of Rho1, but no rescue of 2A12 secretion (red). Arrowheads mark apical surfaces.

(O) Tracheal pits of wild-type embryos at stage 12 do not show accumulation or secretion of 2A12 (red; Trh, blue). Asterisk indicates apical position.

(P) When embryos of the genotype in (L) were followed at stage 11/12, premature secretion of 2A12 antigen to the lumen was detected. Asterisk indicates apical position.

(Q) This premature secretion depends on the activity of Dia, since it was not observed in a *dia* VDRC20518 RNAi mutant background. The results suggest that the schedule of Dia activation is determined by a threshold for activation of Rho1 by GEFs. Asterisk indicates apical position.

(R) Premature secretion by activated Rho1 does not depend on GEFs, and was observed in a *Gef2* NIG9635R-3 RNAi background. Asterisk indicates apical position.

the expected functional epistatic relationship between the three proteins.

Apical secretion of proteins, like 2A12 and Pio, in the trachea is temporally regulated and is observed long after the lumen of the tracheal pits is formed at stage 11, suggesting a regulatory switch for onset of secretion. The high sensitivity of the system to the levels of the two Rho-GEFs that activate Rho1, suggests that activation of Rho1 may provide such a trigger. To test this notion, we examined the effects of activated Rho1 at earlier stages of tracheal development. Secretion was initiated at early stages of tracheal formation, and could be readily detected already at stage 12 (Figure 5P). This premature apical secretion is dependent on activation of Dia, since no secretion was observed when activated Rho1 was expressed in the presence of RNAi for *dia* (Figure 5Q). Conversely, activated Rho1 continued to trigger premature secretion in *Gef2*- or *Gef64C*-RNAi-expressing embryos (Figure 5R and data not shown). These results suggest that, normally, the machinery for apical localization of the critical components is already operational at early stages of tube morphogenesis, but that the activation of Dia takes place only at a subsequent phase.

We wanted to examine if the mechanism of apical localization of Rho-GEFs, Rho1 and Dia, is dependent on, or facilitated by, the apical actin cables formed by Dia. When the localization of

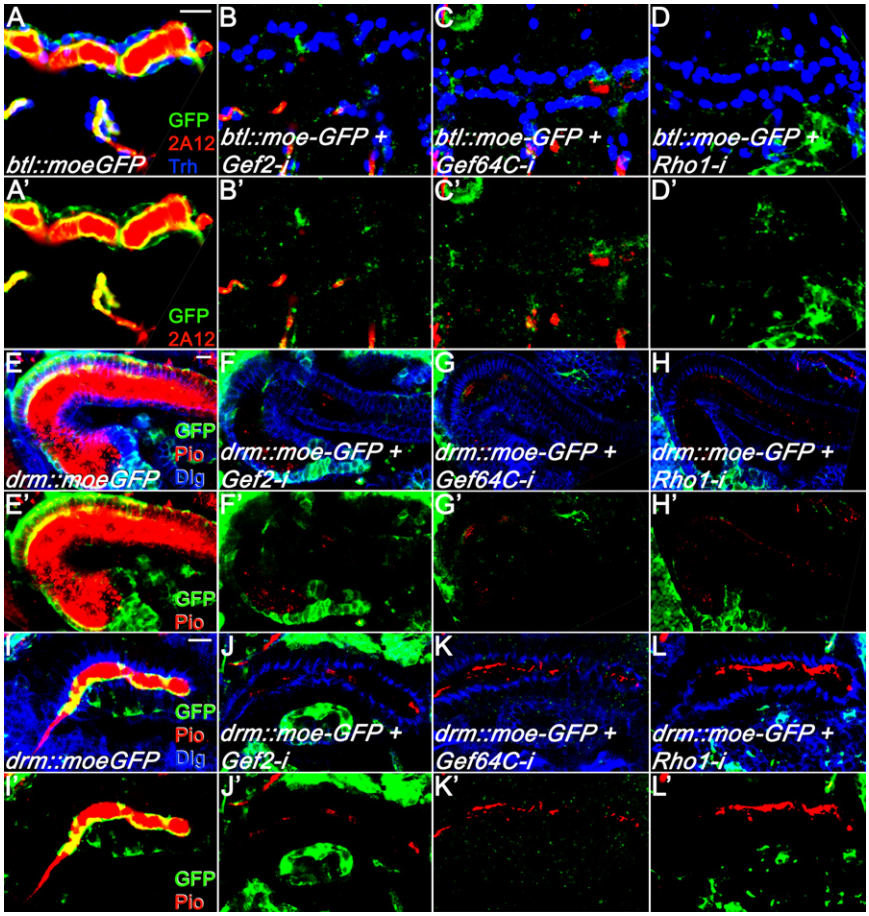


**Figure 6. Rho-GEFs and Rho1 Are Required for the Formation of Apical F-Actin in Tubular Structures**

F-actin was followed by Moe-GFP (green) to test if GEFs and Rho1 affect apical secretion through the formation of apical F-actin.

(A–D) 2A12 is secreted to the lumen of wild-type trachea, and apical F-actin is detected. When RNAi constructs for Gef2, Gef64C, or Rho1 were expressed by *btl-Gal4*, apical F-actin disappeared in parallel to the block in 2A12 secretion (Trh, blue; 2A12, red). Scale bar, 10 μm.

(E–H) In a wild-type embryo, Pio is secreted to the hindgut lumen and F-actin is detected both apically and basally. Expression of the above RNAi constructs by *drm-Gal4* abolished Pio secretion and accumulation of F-actin (Dlg, blue; Pio, red). Scale bar, 10 μm.

(I–L) In a wild-type embryo, Pio is secreted to the salivary gland lumen and F-actin is apically localized. Expression of the above RNAi constructs by *drm-Gal4* significantly reduced Pio secretion and abolished apical F-actin accumulation (Dlg, blue; Pio, red).

Gef2, Gef64C, or Rho1 was examined in a *dia*-RNAi background, it was comparable to the normal distribution (Figure S6). Furthermore, Dia retains its normal apical distribution in a *Rho1*-RNAi background (Figure S6). Thus, the apical localization of the upstream Dia regulators, and of Dia itself, is independent of Dia activity.

### MyoV Transports Cargo Vesicles Apically on Actin Cables

The simultaneous disruption of apical actin organization and apically directed secretion in *dia* mutants suggests that the Dia-nucleated actin filaments serve as tracks for polarized secretion. The actin-based MyoV motors have been linked to polarized secretion in a variety of biological systems (Reck-Peterson et al., 2000). A single homolog (*myoV*) is found in *Drosophila* (Bonafe and Sellers, 1998; MacIver et al., 1998). To assess its role in tubular organ secretion, we specifically inactivated *myoV* in the tracheal system, hindgut, and salivary gland with two independent RNAi constructs or a dominant-negative MyoV construct (Li et al., 2007). While secretion of 2A12 and Pio was abolished in these organs, the apical distribution of F-actin was not perturbed (Figures 7A–7J). MyoV protein is detected in a punctate distribution, and is eliminated from the tracheal cells following expression of an RNAi construct by *btl-Gal4*. In the trachea of *myoV* mutant embryos that develop to late stages, absence of 2A12 secretion, but normal Verm secretion, is detected. Finally, localization of MyoV is not altered in *dia* mutants and vice versa, and cell polarity markers are normal in embryos expressing *myoV* RNAi in the trachea (Figure S9).

The functional connection between MyoV and the Dia pathway was demonstrated by the ability to block premature secretion in the trachea, which was induced by activated Rho1 or constitutively activated Dia (Somogyi and Rorth, 2004) following coexpression of a *myoV* RNAi construct (Figures 7K–7N). These observations are consistent with a scenario whereby MyoV acts as a motor for trafficking secreted vesicles apically along actin cables generated by Dia.

## DISCUSSION

Apical localization of F-actin is a general feature of tubular epithelial structures. It was observed in mammalian MDCK cells forming tubes in three-dimensional cell culture (O'Brien et al., 2002), in the cytoplasm underlying the apical membrane facing the lumen in mammalian secretory organs, such as the lacrimal gland (Jerdeva et al., 2005), and in the different epithelial tubes of the *Drosophila* embryo (Tsarouhas et al., 2007) (Figure 1; Figure S1). The lower level of gene duplication in *Drosophila*, and the ability to follow the consequences of targeted gene inactivation in the tubular structures, allowed us to identify the mechanism responsible for nucleating the actin terminal web at the apical side of epithelial tube cells. We demonstrate that Dia, which is known to promote the formation of linear actin filaments, is responsible for producing this actin network in *Drosophila* embryonic tubular structures. Despite differences in the diameter and function of the different tubular organs, the polarized apical actin cables formed by Dia appear to have a common role in trafficking secretory vesicles to the apical tube surface.

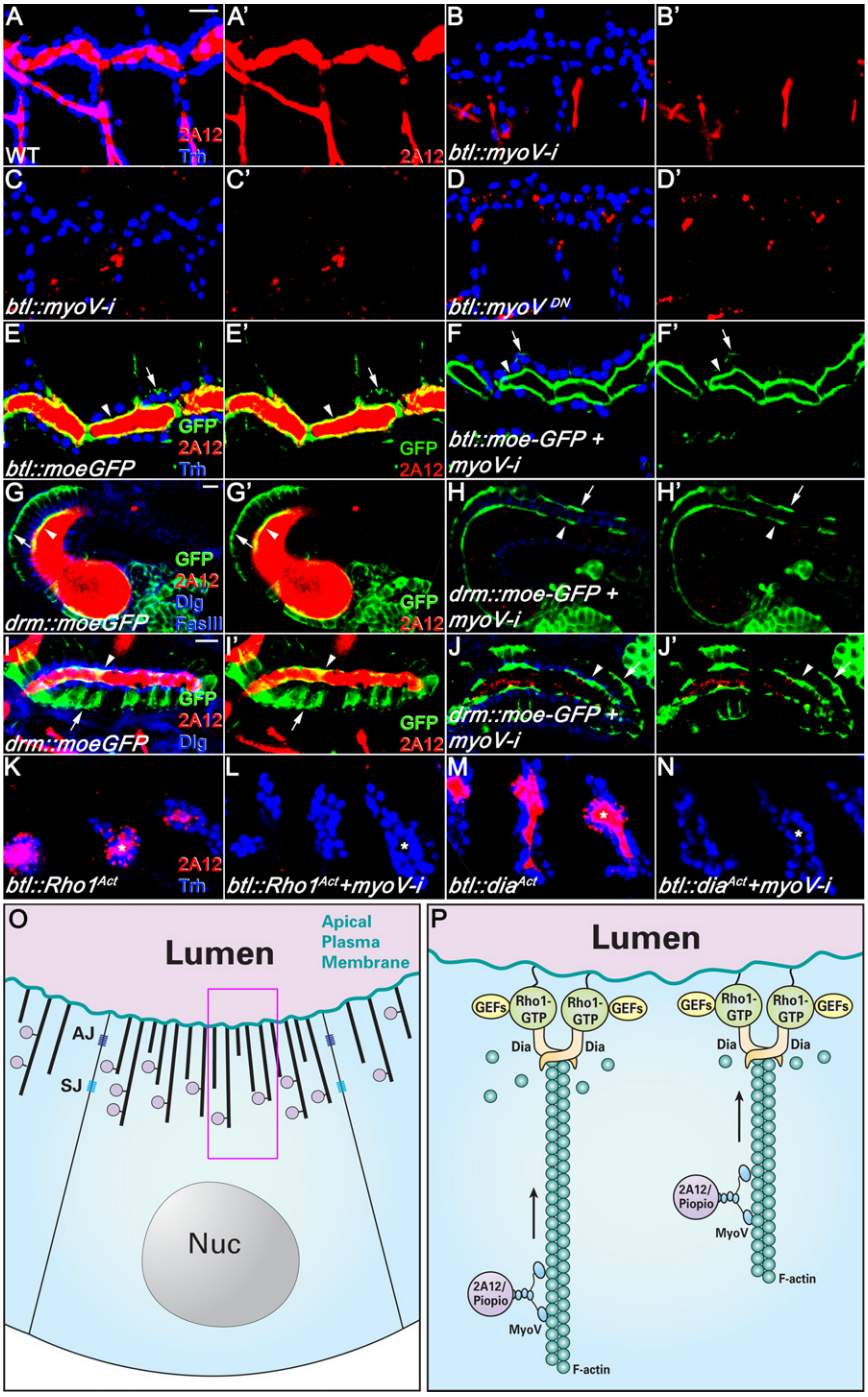


**Figure 7. MyoV Is Required for Apical Secretion in Tubular Structures**

(A–D) Secretion of 2A12 (red, Trh-blue) in the trachea of wild-type embryos (A) was compared to *btl-Gal4* embryos expressing *myoV* RNAi VDRC44291 (B), *myoV* RNAi (Li et al., 2007) (C), or a MyoV dominant-negative construct (D), are shown; 2A12 secretion to the lumen was blocked in all cases where MyoV activity was compromised; (A′)–(D′) show only the red channel. Scale bar, 10 μm.

(E and F) When Moe-GFP (green) was expressed in the trachea of wild-type or *myoV* RNAi VDRC44292 embryos, the apical F-actin was retained in the mutant; (E′) and (F′) show only green and red channels.

(G and H) The same experiments were carried out in the hindgut (Dlg, blue; Pio, red); (G′) and (H′) show only green and red channels. In a wild-type embryo, Pio is secreted to the hindgut lumen and F-actin is localized both apically and basally. When *myoV* RNAi was expressed by *drm-Gal4*, Pio was not secreted, but F-actin was retained. Scale bar, 10 μm.

(I and J) Similarly, the secretion of Pio and F-actin were monitored in the salivary glands, giving comparable results to the other tissues; (I′) and (J′) show only green and red channels. Arrowheads and arrows show apical and basal surfaces, respectively, in (E)–(H). Scale bar, 10 μm.

(K–N) Expression of activated Rho1 in the trachea leads to premature secretion of 2A12 (red) at stage 12, which is blocked by coexpression of *myoV* RNAi (VDRC44291) (L). Similar results were obtained following expression of activated Dia alone (M), or in combination with *myoV* RNAi (N). Asterisks show apical positions.

(O and P) Model for apical secretion in tubular structures. In diverse tubular structures, the single epithelial cell layer is highly polarized. Polarity is maintained by the adherens junction (AJ) and septate junction (SJ), forming tight barriers. Apical localization of the Dia activators (Rho-GEFs and Rho1), and Dia itself, promote the formation of polarized actin cables emanating from the apical membrane, with their barbed ends facing the membrane. This allows efficient trafficking by MyoV motors of a specific class of secretory vesicles toward the apical membrane. It is possible that, prior to loading of the vesicles onto MyoV motors and actin cables, they reach the general vicinity of the apical domain by microtubule-based mechanisms. (P) Magnified view of boxed area in (O).

While the role of Dia in promoting apical secretion spans the entire duration of tracheal morphogenesis, two other Formin-homology proteins act at very specific junctions of *Drosophila* tracheal morphogenesis. Formin 3 participates in the generation of a continuous dorsal trunk tube by promoting vesicular trafficking in the fusion cells of each metamer, perpendicular to the tube lumen (Tanaka et al., 2004). Another Formin domain protein, DAAM, promotes the organization of F-actin in rings around the circumference of the tracheal tube, at the final stages of tracheal morphogenesis (Matusek et al., 2006).

It is likely that each of the three Formin domain proteins is regulated by distinct activators that are concentrated at different sites. The localized activation of Formin 3 may eventually lead to polarized vesicle movement, similar to Dia, but toward a different membrane. The activation of DAAM may be necessary for the localized synthesis of F-actin, which will modify the contours of the apical membrane, and thus define the shape of chitin layered on top. The function of Dia stands out, since it is required throughout tracheal development, and is also involved in morphogenesis of other tubular organs.

### Multiple Tiers of Apical Localization Restrict Dia Activity to the Apical Surface

The mechanism of localized activation of Dia operates after apical-basal polarity of the cells has been established. Thus, we did not observe any defects in overall polarity in *dia* mutant embryos (Figure 2; Figure S2). It seems that the steps upstream to Dia activation utilize the existing polarity at multiple tiers in order to trigger Dia at a highly restricted position. The two Rho-GEF proteins, Gef2 and Gef64C, exhibit a tight apical localization in the cells forming the tubes. The single Rho1 protein, which is downstream to the Rho-GEFs, is again tightly localized to the apical surface in tubular structures (Figure 5). Binding of Rho1 to Dia leads to an opening of the autoinhibited form of Dia and to the formation of a Dia dimer representing the active form (Goode and Eck, 2007). Since GTP-bound Rho1 is the immediate activator of Dia, it is particularly important that Rho1 be embedded in the apical membrane, to ensure spatially restricted nucleation of actin polymerization. In *C. elegans*, a GEF and a Rho protein were shown to be essential for the development of the lumen of the excretory cell (Suzuki et al., 2001). It will be interesting to determine if a Dia-family protein is subsequently activated to promote secretion.

Dia is also apically localized, both at the mRNA and protein levels (Figure 3). Elimination of the *dia* 3′UTR demonstrated a persistence of apical protein localization, even when mRNA localization was lost, suggesting that there are two parallel and independent mechanisms for apical localization. The multiple tiers of apical localization assure that activated Dia will be highly restricted to the apical surface.

It is interesting to note that, while Gef2, Gef64C, Rho1, and Dia proteins are broadly expressed, partially due to maternal contribution of mRNA, they exhibit apical localization only in the tubular structures (Figures 3 and 5). This raises the possibility that genes that are specifically expressed in the tubular organs contribute to the apical localization. Alternatively, apical localization may rely directly on the specific phospholipid composition of the apical tube membranes. It will be interesting to determine if a common mechanism is responsible for the apical localization of the different proteins in the pathway, and if this mechanism relies on components that are restricted to the tubular organs.

The cellular machinery which dictates the apical localization of Rho-GEFs/Rho1/Dia appears to be in place early on. For example, expression of Dia-GFP in the trachea demonstrated apical localization of the protein already at the stage when the tracheal pits are formed (Figure 3P). Yet, generation of the polarized actin cables by Dia, and their utilization for secretion, takes place at a later stage, and follows a stereotypic temporal order in the different tracheal branches. What triggers activation of Dia, following the apical localization of the different components? We have demonstrated that both Gef2 and Gef64C are required to trigger Rho1, which activates Dia. While the activity of the two Rho-GEFs is similar, both have to accumulate to a critical level in order to activate the system (Figures 5H–5J). Thus, no secretion takes place when either of them is missing, or when each of them is present at half dose. The delay in activation of Dia and in secretion, may be explained by the time required to accumulate sufficient levels of Rho-GEF proteins. When the system was "short circuited" by expression of activated Rho1, which was properly localized to the apical surface, Dia-dependent apical secretion was observed already at early stages of tracheal pit formation (Figures 5P and 5Q).

### Cargo Vesicles Are Transported Apically on Actin Cables by MyoV

Our results identify *Drosophila* MyoV as a primary motor for apical trafficking of secretory vesicles along the polarized, Dia-nucleated actin cables in tubular organs. When the activity of MyoV was compromised in the tubular epithelia, apical secretion of cargos requiring Dia-generated actin cables was abolished. On the other hand, since MyoV operates downstream to Dia, the actin cables themselves remained intact (Figure 7). An analogous role for MyoV has been recently demonstrated during trafficking of Rhodopsins to photoreceptor rhabdomers (Li et al., 2007). The functional link between the Dia pathway and MyoV was demonstrated by the ability of *myoV* RNAi to suppress constitutively activated Rho1 or Dia phenotypes (Figures 7L and 7N). These results further support the direct link between Dia and apical secretion. A model describing the mechanism of Dia-regulated apical secretion in tubular organs is presented in Figures 7O and 7P.

The polarized actin network formed via the nucleating activity of Dia can account for the final phase of secretory vesicle transport to the apical plasma membrane. Class V myosins, such as MyoV, are known to be involved in transfer of vesicles from microtubules to cortical actin networks (Desnos et al., 2007), suggesting that polarized microtubule arrays may promote the long-range trafficking of the secretory vesicles from their sites of formation to the cell cortex. Consistent with this scenario, we have demonstrated a polarized arrangement of microtubules in tube epithelial cells, the minus ends of which are in close proximity to the apical membrane, which remains intact in the absence of Dia (Figure 2; Figure S2). The universality of this system is highlighted by similarities to polarized secretion in budding yeast, where Myo2p-mediated transport of secretory vesicles into the bud utilizes Dia-generated actin bundles as tracks, in order to deposit the compounds for polarized cell growth (Faix and Grosse, 2006).

### Actin Cables Promote the Apical Secretion of a Distinct Class of Vesicles

When early steps in the secretory pathway are compromised by reducing the activity of the COPII or COPI complexes, accumulation of cargo is observed within the cells and reduced amounts are detected in the lumen (Devine et al., 2005; Jayaram et al., 2008; Tsarouhas et al., 2007). Since these manipulations block an early and global process of secretion, all cargo vesicles are affected (Tsarouhas et al., 2007). However, after exit from the Golgi, it appears that distinct classes of vesicles are generated, each containing a different set of cargos, and trafficked by a distinct mechanism. One class of vesicles contains chitin-modifying enzymes (such as Verm or Serp), and is targeted to the septate junctions. When the structure of the septate junctions was compromised, these proteins failed to be secreted (Luschnig et al., 2006; Wang et al., 2006). Another class of vesicles may contain transmembrane proteins that are deposited in the apical membrane, such as Crb.

Our study now uncovers a third class of cargo vesicles. Several distinct cargos that are secreted to the apical lumen rely on Dia for

their secretion. These cargos include the 2A12 antigen, Pio, and the artificial rat ANF-GFP construct. In the absence of Dia, these proteins failed to be secreted to the lumen, but also did not accumulate within the epithelial tube cells (Figure 4; Figure S4). We believe that when secretion is disrupted, the vesicles are efficiently targeted for lysosomal degradation, since a block of lysosomal targeting facilitated intracellular accumulation of vesicles that failed to be secreted (Figure 4E). Inability to secrete Pio resulted in tracheal defects that were similar to *pio* mutant embryos. Additional defects of *dia* pathway mutant embryos, such as highly convoluted tracheal branches (compare Figures 2I and 2J), may stem from the absence of additional, yet unknown, proteins in the lumen. The mechanisms underlying the incorporation of distinct cargos into different secretory vesicles, as well as the recognition of each vesicle type by different motors and trafficking scaffolds, remain unknown.

In conclusion, this work has uncovered a universal mechanism, which operates in very different types of tubular epithelial structures in *Drosophila*. The conserved feature of an apical F-actin network in tubular epithelia of diverse multicellular organisms, and the high degree of conservation of the different components generating and utilizing these actin structures, strongly suggests that this polarized secretion mechanism is broadly used across phyla. The ability to generate polarized actin cables that initiate at the apical membrane provides an efficient route for trafficking vesicles by MyoV, leading to their fusion with the apical membrane and secretion. It is likely that different pathological situations manifested in aberrant formation of epithelial structures, or their utilization for secretion once the tubular organ is formed, represent defects in different components of this pathway. For example, it was shown that mutations in MyoVa in humans disrupt actin-based melanosome transport in epidermal melanocytes (Pastural et al., 1997).

## EXPERIMENTAL PROCEDURES

### Fly Strains

UAS-RNAi lines were as follows: *dia* (VDRC20518, NIG1768R-1), *Sop2* (VDRC42172), *Arp3* (VDRC35260), *dor* (VDRC33733, 33734), *Gef2* (NIG9635R-3), *Gef64C* (VDRC47121), *Rho1* (VDRC12734), *myoV* (VDRC44291, VDRC44292, RNAi flies from D. Ready [Li et al., 2007]). Other UAS lines include: *UAS-moe-GFP* (Chihara et al., 2003); *UAS-nod-lacZ* (Clark et al., 1997); *UAS-dia-GFP* (Homem and Peifer, 2008); *UAS-Dia CA* (activated) (Somogyi and Rorth, 2004); *UAS-serp-GFP* and *UAS-anf-GFP* (Tsarouhas et al., 2007); UAS-Rab11$^{SN}$ (dominant negative, provided by M. Gonzalez-Gaitan); *UAS-PKNG58eGFP* (active Rho1 sensor [Simoes et al., 2006]); *UAS-Rho1$^{N19}$* (DN); *UAS-Rho1$^{V14}$* (activated); *UAS-myoV-CT-GFP* (DN [Li et al., 2007]).

Mutants were as follows: *dia$^{5}$*, *Gef2$^{l(2)04291}$*, and *Gef64C$^{29}$*, PDI-GFP (Bobinnec et al., 2003), *myoV$^{Q1052st}$* (Li et al., 2007). *sar1$^{EP3575\Delta 28}$* (Tsarouhas et al., 2007) and *dar23$^{11\text{-}3\text{-}63}$* (Ye et al., 2007) represent different alleles of *sar1* and were used in a transheterozygous combination. Drivers were *btl-Gal4*, *drm-Gal4*, and *mef2-Gal4*.

The phenotypes observed following expression of RNAi constructs or in zygotic mutant backgrounds were highly consistent, but showed some variability, possibly due to fluctuation in the level of RNAi expression or the maternal mRNA contribution, respectively.

### Probes and Antibodies

Dig-labeled DNA probes for *dia* (nucleotide positions 12–676 or 2518–3228 in the coding region) and *GFP* (encompassing the entire coding region) were used for RNA in situ hybridization according to Melen et al. (2005). Antbodies include: Trh (rat 1:100), anti-GFP (chicken 1:500; Abcam); Crb, Arm, Dlg, Fas II, and Fas III (mouse 1:100; DSHB), DE-Cad (rat 1:100; DSHB), Dia-rabbit 1:250 (Grosshans et al., 2005), 2A12 (mouse IgM 1:5; DSHB), Pio-rabbit 1:100 (Jazwinska et al., 2003), Verm-guinea pig 1:200 (Wang et al., 2006), β-tubulin (mouse 1:500; Sigma), Golgi (dGMAP, rabbit 1:500; C. Rabouille), Rab11 (rabbit 1:50; M. Gonzalez-Gaitan), Gef2-rabbit 1:1000 (Grosshans et al., 2005), Gef64C-mouse 1:50 (Bashaw et al., 2001), Rho1-mouse 1:50 (Magie et al., 2002). Cy2, -3, and -5 secondary antibodies and biotin-conjugated goat-anti mouse IgM (for 2A12 antigen) were purchased from Jackson ImmunoResearch and diluted 1:200. For detection of IgM antibodies, streptavidin-HRP and TSA kit (Perkin-Elmer), followed by Cy-conjugated streptavidin, were used.

Standard fixation and staining procedures were followed. To detect Dia, GEFs, and Rho1, heat fixation was used: embryos were collected and bleached in a nylon mesh, immersed in 5 ml boiling 0.7% NaCl and 0.04% Triton X-100 for 10 s, and vortexed briefly. Cold solution (20 ml) was quickly added, and embryos chilled on ice before devitellinization in heptane/methanol. EM procedure was carried out according to (Massarwa et al., 2007).

## SUPPLEMENTAL DATA

Supplemental Data include nine figures and can be found with this article online at http://www.cell.com/developmental-cell/supplemental/S1534-5807(09)00172-5/.

## ACKNOWLEDGMENTS

We thank the following scientists and organizations for generously providing fly strains and antibodies: M. Affolter, Y. Bobinnec, M. Gonzalez-Gaitan, J. Grösshans, S. Hayashi, A. Jacinto, Y. Jan, M. Peifer, C. Rabouille, D. Ready, P. Rorth, C. Samakovlis, Vienna *Drosophila* RNAi Center, National Institute of Genetics (Japan), the Developmental Studies Hybridoma Bank, and the Bloomington *Drosophila* stock center. We thank S. Yogev for helpful discussions. The work was funded by grants from the Israel Science Foundations (to E.D.S. and B.-Z.S.) and Nissim Foundation (B.-Z.S.). B.-Z.S. is an incumbent of the Hilda and Cecil Lewis chair for Molecular Genetics.

Received: December 10, 2008
Revised: March 15, 2009
Accepted: April 21, 2009
Published: June 15, 2009

## REFERENCES

Bashaw, G.J., Hu, H., Nobes, C.D., and Goodman, C.S. (2001). A novel Dbl family RhoGEF promotes Rho-dependent axon attraction to the central nervous system midline in *Drosophila* and overcomes Robo repulsion. J. Cell Biol. *155*, 1117–1122.

Beitel, G.J., and Krasnow, M.A. (2000). Genetic control of epithelial tube size in the *Drosophila* tracheal system. Development *127*, 3271–3282.

Bobinnec, Y., Marcaillou, C., Morin, X., and Debec, A. (2003). Dynamics of the endoplasmic reticulum during early development of *Drosophila* melanogaster. Cell Motil. Cytoskeleton *54*, 217–225.

Bonafe, N., and Sellers, J.R. (1998). Molecular characterization of myosin V from *Drosophila* melanogaster. J. Muscle Res. Cell Motil. *19*, 129–141.

Bryant, D.M., and Mostov, K.E. (2008). From cells to organs: building polarized tissue. Nat. Rev. Mol. Cell Biol. *9*, 887–901.

Buechner, M., Hall, D.H., Bhatt, H., and Hedgecock, E.M. (1999). Cystic canal mutants in *Caenorhabditis elegans* are defective in the apical membrane domain of the renal (excretory) cell. Dev. Biol. *214*, 227–241.

Chihara, T., Kato, K., Taniguchi, M., Ng, J., and Hayashi, S. (2003). Rac promotes epithelial cell rearrangement during tracheal tubulogenesis in *Drosophila*. Development *130*, 1419–1428.

Clark, I.E., Jan, L.Y., and Jan, Y.N. (1997). Reciprocal localization of Nod and kinesin fusion proteins indicates microtubule polarity in the *Drosophila* oocyte, epithelium, neuron and muscle. Development *124*, 461–470.

Desnos, C., Huet, S., and Darchen, F. (2007). 'Should I stay or should I go?': myosin V function in organelle trafficking. Biol. Cell *99*, 411–423.

Devine, W.P., Lubarsky, B., Shaw, K., Luschnig, S., Messina, L., and Krasnow, M.A. (2005). Requirement for chitin biosynthesis in epithelial tube morphogenesis. Proc. Natl. Acad. Sci. USA *102*, 17014–17019.

Faix, J., and Grosse, R. (2006). Staying in shape with formins. Dev. Cell *10*, 693–706.

Ghabrial, A., Luschnig, S., Metzstein, M.M., and Krasnow, M.A. (2003). Branching morphogenesis of the *Drosophila* tracheal system. Annu. Rev. Cell Dev. Biol. *19*, 623–647.

Goode, B.L., and Eck, M.J. (2007). Mechanism and function of formins in the control of actin assembly. Annu. Rev. Biochem. *76*, 593–627.

Grosshans, J., Wenzl, C., Herz, H.M., Bartoszewski, S., Schnorrer, F., Vogt, N., Schwarz, H., and Muller, H.A. (2005). RhoGEF2 and the formin Dia control the formation of the furrow canal by directed actin assembly during *Drosophila* cellularisation. Development *132*, 1009–1020.

Hartenstein, V. (1993). Atlas of *Drosophila Development* (Cold Spring Harbor, NY: Cold Spring Harbor Laboratory Press).

Hemphala, J., Uv, A., Cantera, R., Bray, S., and Samakovlis, C. (2003). Grainy head controls apical membrane growth and tube elongation in response to Branchless/FGF signalling. Development *130*, 249–258.

Hogan, B.L., and Kolodziej, P.A. (2002). Organogenesis: molecular mechanisms of tubulogenesis. Nat. Rev. Genet. *3*, 513–523.

Homem, C.C., and Peifer, M. (2008). Diaphanous regulates myosin and adherens junctions to control cell contractility and protrusive behavior during morphogenesis. Development *135*, 1005–1018.

Jayaram, S.A., Senti, K.A., Tiklova, K., Tsarouhas, V., Hemphala, J., and Samakovlis, C. (2008). COPI vesicle transport is a common requirement for tube expansion in *Drosophila*. PLoS ONE *3*, e1964. 10.1371/journal.pone.0001964.

Jazwinska, A., Ribeiro, C., and Affolter, M. (2003). Epithelial tube morphogenesis during *Drosophila* tracheal development requires Piopio, a luminal ZP protein. Nat. Cell Biol. *5*, 895–901.

Jerdeva, G.V., Wu, K., Yarber, F.A., Rhodes, C.J., Kalman, D., Schechter, J.E., and Hamm-Alvarez, S.F. (2005). Actin and non-muscle myosin II facilitate apical exocytosis of tear proteins in rabbit lacrimal acinar epithelial cells. J. Cell Sci. *118*, 4797–4812.

Kerman, B.E., Cheshire, A.M., and Andrew, D.J. (2006). From fate to function: the *Drosophila* trachea and salivary gland as models for tubulogenesis. Differentiation *74*, 326–348.

Li, B.X., Satoh, A.K., and Ready, D.F. (2007). Myosin V, Rab11, and dRip11 direct apical secretion and cellular morphogenesis in developing *Drosophila* photoreceptors. J. Cell Biol. *177*, 659–669.

Lubarsky, B., and Krasnow, M.A. (2003). Tube morphogenesis: making and shaping biological tubes. Cell *112*, 19–28.

Luschnig, S., Batz, T., Armbruster, K., and Krasnow, M.A. (2006). serpentine and vermiform encode matrix proteins with chitin binding and deacetylation domains that limit tracheal tube length in *Drosophila*. Curr. Biol. *16*, 186–194.

MacIver, B., McCormack, A., Slee, R., and Bownes, M. (1998). Identification of an essential gene encoding a class-V unconventional myosin in *Drosophila melanogaster*. Eur. J. Biochem. *257*, 529–537.

Magie, C.R., Pinto-Santini, D., and Parkhurst, S.M. (2002). Rho1 interacts with p120ctn and alpha-catenin, and regulates cadherin-based adherens junction components in *Drosophila*. Development *129*, 3771–3782.

Massarwa, R., Carmon, S., Shilo, B.Z., and Schejter, E.D. (2007). WIP/WASp-based actin-polymerization machinery is essential for myoblast fusion in *Drosophila*. Dev. Cell *12*, 557–569.

Matusek, T., Djiane, A., Jankovics, F., Brunner, D., Mlodzik, M., and Mihaly, J. (2006). The *Drosophila* formin DAAM regulates the tracheal cuticle pattern through organizing the actin cytoskeleton. Development *133*, 957–966.

Melen, G.J., Levy, S., Barkai, N., and Shilo, B.Z. (2005). Threshold responses to morphogen gradients by zero-order ultrasensitivity. Mol. Syst. Biol. *1*, 2005.0028. 10.1038/msb4100036.

Myat, M.M., and Andrew, D.J. (2002). Epithelial tube morphology is determined by the polarized growth and delivery of apical membrane. Cell *111*, 879–891.

O'Brien, L.E., Zegers, M.M., and Mostov, K.E. (2002). Opinion: building epithelial architecture: insights from three-dimensional culture models. Nat. Rev. Mol. Cell Biol. *3*, 531–537.

Pastural, E., Barrat, F.J., Dufourcq-Lagelouse, R., Certain, S., Sanal, O., Jabado, N., Seger, R., Griscelli, C., Fischer, A., and de Saint Basile, G. (1997). Griscelli disease maps to chromosome 15q21 and is associated with mutations in the myosin-Va gene. Nat. Genet. *16*, 289–292.

Reck-Peterson, S.L., Provance, D.W., Jr., Mooseker, M.S., and Mercer, J.A. (2000). Class V myosins. Biochim. Biophys. Acta *1496*, 36–51.

Simoes, S., Denholm, B., Azevedo, D., Sotillos, S., Martin, P., Skaer, H., Hombria, J.C., and Jacinto, A. (2006). Compartmentalisation of Rho regulators directs cell invagination during tissue morphogenesis. Development *133*, 4257–4267.

Somogyi, K., and Rorth, P. (2004). Evidence for tension-based regulation of *Drosophila* MAL and SRF during invasive cell migration. Dev. Cell *7*, 85–93.

Sriram, V., Krishnan, K.S., and Mayor, S. (2003). deep-orange and carnation define distinct stages in late endosomal biogenesis in *Drosophila melanogaster*. J. Cell Biol. *161*, 593–607.

Suzuki, N., Buechner, M., Nishiwaki, K., Hall, D.H., Nakanishi, H., Takai, Y., Hisamoto, N., and Matsumoto, K. (2001). A putative GDP-GTP exchange factor is required for development of the excretory cell in *Caenorhabditis elegans*. EMBO Rep. *2*, 530–535.

Tanaka, H., Takasu, E., Aigaki, T., Kato, K., Hayashi, S., and Nose, A. (2004). Formin3 is required for assembly of the F-actin structure that mediates tracheal fusion in *Drosophila*. Dev. Biol. *274*, 413–425.

Tsarouhas, V., Senti, K.A., Jayaram, S.A., Tiklova, K., Hemphala, J., Adler, J., and Samakovlis, C. (2007). Sequential pulses of apical epithelial secretion and endocytosis drive airway maturation in *Drosophila*. Dev. Cell *13*, 214–225.

Wang, S., Jayaram, S.A., Hemphala, J., Senti, K.A., Tsarouhas, V., Jin, H., and Samakovlis, C. (2006). Septate-junction-dependent luminal deposition of chitin deacetylases restricts tube elongation in the *Drosophila* trachea. Curr. Biol. *16*, 180–185.

Wu, K., Jerdeva, G.V., da Costa, S.R., Sou, E., Schechter, J.E., and Hamm-Alvarez, S.F. (2006). Molecular mechanisms of lacrimal acinar secretory vesicle exocytosis. Exp. Eye Res. *83*, 84–96.

Ye, B., Zhang, Y., Song, W., Younger, S.H., Jan, L.Y., and Jan, Y.N. (2007). Growing dendrites and axons differ in their reliance on the secretory pathway. Cell *130*, 717–729.

Available online at www.sciencedirect.com
ScienceDirect
Current Opinion in Cell Biology
ELSEVIER

# The nuts and bolts of germ-cell migration

Katsiaryna Tarbashevich and Erez Raz

In many species, primordial germ cells (PGCs) migrate from the position where they are specified to the site where the gonad develops, where they differentiate into sperm and egg. Germ cells thus serve as an excellent model for studying cell migration in the context of the live organism. In recent years, a number of cues directing the migration of the cells towards their target were identified and some of the relevant molecules and biochemical pathways were revealed. In this review we present those results, focusing on 'cell mechanics' of the process including cell adhesion, traction generation and cell polarization.

**Address**
Institute of Cell Biology, Center for Molecular Biology of Inflammation, Von-Esmarch-Str. 56, 48149, Münster University, 48147 Münster, Germany

Corresponding author: Raz, Erez (erez.raz@uni-muenster.de)

**Current Opinion in Cell Biology** 2010, **22**:715–721

This review comes from a themed issue on
Cell differentiation
Edited by Mark Van Doren

Available online 13th October 2010

0955-0674/$ – see front matter


**DOI** 10.1016/j.ceb.2010.09.005

## Introduction

Primordial germ cells (PGCs) are specified early in development at a position that is distant from the gonad, where they differentiate into gametes, sperm and egg. Hence, the cells have to migrate through the complex environment of a developing embryo to reach the region of the developing gonad. The mechanisms facilitating the motility and controlling the directed migration of these cells are relevant for a wide range of processes in normal development and disease, thus keeping PGCs as a focus of scientific interest for decades. These studies, performed primarily in *Drosophila*, zebrafish and mouse have unfolded the basic mechanisms controlling PGC guidance and motility and revealed that barring a number of differences, the principal characteristics of PGC migration appear to be conserved among different organisms; immediately following their specification, PGCs of *Drosophila* and zebrafish exhibit a simple round morphology and are non-motile [1•,2,3•]. Subsequently, the germ cells polarize and actively migrate at a stage corresponding to the time of zygotic transcription initiation [3•,4]. Similarly, using electron microscopy analysis mouse PGCs were shown to be stationary and round before assuming a motile behavior [5]. In the mouse, the initiation of PGC migration appears to rely on paracrine cues from surrounding somatic and extra-embryonic tissues [2,6], while the role of the somatic environment remains unclear in the case of PGC motility in *Drosophila* and zebrafish embryos. Zebrafish PGCs isolated from embryos at migratory stages show normal motility when transplanted into embryos of premigratory stages, suggesting that the early somatic environment is permissive for PGC migration [3•]. However, a putative role for the soma in inducing the transition to cell motility has not been ruled out in both organisms.

Following this initial stage of PGC development, repulsive and attractive cues provided by the environment can bias the inherent motility of the germ cells, culminating in directed migration of the cells towards their targets [7–10]. As the mechanisms controlling germ-cell migration in different organisms have been recently described in a comprehensive review by Richardson and Lehmann [11••], we will focus here on the 'mechanics' of PGC migration and on intracellular signaling controlling germ-cell motility.

## Migration challenges

Migrating germ cells have to overcome several hurdles. First, the migration takes place along and through tissues that undergo extensive morphogenetic movements themselves and has to be completed relatively quickly. Inability to reach their target early enough in embryonic development carries the risk of becoming 'locked' within a differentiated environment that presents barriers that are more difficult or impossible to penetrate and lacks the factors essential for germ-cell survival [1•,12•,13,14•,15•]. In spite of the crowded and complex cellular environment through which germ cells migrate, they can exhibit relatively high migration speeds *in vivo* of up to 140 μm/h [16–18], a speed range comparable to that of cancer cells that face similar challenges (e.g. about 120 μm/h for breast cancer cells migrating individually *in vivo* [19]). Interestingly, in a manner similar to that of metastatic tumor cells, zebrafish germ cells meet the requirement for high speed and flexibility in migrating through the complex environment by generating blebs, a special type of cellular protrusions [20,21].

A related challenge the germ cells encounter is the necessity to generate traction force that would allow them to actively migrate in a context of their cellular environment. This task is complicated by the fact that the germ

cells migrate through diverse cellular environments and tissues with which they have to physically interact. The solution employed by germ cells in different organisms is to make use of the ubiquitously expressed cell–cell adhesion molecule E-cadherin. Indeed, proper control of E-cadherin function was shown to be essential for the process of germ-cell migration both in vertebrates and *Drosophila* [22–25,26••]. Significantly, as will be further discussed below, regulation of E-cadherin levels was shown to be important also for cancer-cell metastasis and invasive cell migration during normal development (e.g. [27,28]).

Last, following the acquisition of basic motility, cell migration has to be directed by cues in the environment, enabling the cells to reach their targets. Whereas ligands, receptors and second messengers involved in biasing the direction of the motility are well known, less is known about the precise molecular cascade that polarizes the cells in the correct direction.

## Get in shape

In essence, cell migration includes protrusion formation in the direction of the migration and pulling the back of the cell that together result in forward movement. Consequently, migrating cells are easily recognizable by dynamic cell-shape alterations as compared to their immotile neighbors. Two major strategies for producing cellular protrusions have been described. The more extensively studied type is the lamellipodium, where polymerization of actin filaments provides the physical force pushing the plasma membrane in the direction of migration [29]. However, an increasing number of recent reports suggest blebs as an additional mechanism for protrusion formation that can support invasive cell migration *in vivo* [30]. Blebs are defined as membrane inflation driven by hydrostatic pressure and cytoplasmic streaming [31•,32]. The formation of the bleb initiates with a separation of the plasma membrane from the actin cortex at a given site and is powered by subsequent flow of cytoplasm that further expands the protrusion. Persistent formation of such protrusions in a specific direction, coupled with attachment of the cell front to the environment and retraction of the back, result in a net forward displacement. Considering that bleb-based motility presumably requires less energy [33], and that blebs form relatively fast, while easily adapting to the shape of the environment, it constitutes a useful strategy for rapid cell motility in the 3-dimentional environment of the embryo.

A formation of a protrusion at the cell front is key to directional migration. In the case of the lamellipodium, enhanced actin turnover at the front of the cell leads to polarized protrusion at this aspect of the cell. Two models were suggested for directing blebs to the cell front, both relying on localized myosin activity at the cell cortex. Increased myosin-based contractility at the cell front could result in elevated local pressure that separates the membrane from the cortex at this location, thereby nucleating a bleb that expands in response to further cytoplasm streaming [34,35]. Alternatively, the localization of the bleb to the cell front is dictated by local reduction of the adhesion between the membrane and the cell cortex as a result of contractility-induced breaks in the actomyosin cortex [31•]. Last, nucleation of blebs could result from asymmetric distribution of cortex–membrane linker molecules that define a region of weakened membrane–cortex adhesion where a bleb is more likely to form [20,31•,36,37].

Thus, bleb-based motility is characterized by separation between the membrane and the cell cortex and lack of polymerized actin in the forming protrusion. These features were clearly demonstrated in an *in vitro* setting for migrating tumor cells (M2 melanoma, neuroblastoma and Walker carcinoma cells) [20,38,39]. Such a demonstration poses a greater challenge in *in vivo* contexts where the accessibility of the embryo and the optical properties of the tissue limit the spatial and temporal resolution of the imaging. It is for that reason that the properties of the leading edge were not directly examined for mouse germ cells, while the germ cells of *Drosophila* appear to form bleb-like protrusions, at least during some stages of their migration. Specifically, fixed *Drosophila* germ cells exhibit thinning of the cortical actin at the base of the protrusion that itself appears to be devoid of polymerized actin [1•]. Employing other methods such as single-plane illumination microscope (SPIM) having higher temporal resolution for live imaging of germ-cell migration might solve the question of the precise cellular mechanism governing protrusion formation in mouse and Drosophila [40]. Unlike in mouse and *Drosophila*, the translucent nature of the zebrafish embryo and the relatively superficial location of the migrating cells allowed this issue to be examined using relatively simple microscopy. The investigation revealed that zebrafish germ cells utilize predominantly blebs in their forward movement [41]. The polarized formation of blebs at the cell front correlated with elevation of calcium, a second messenger that could induce bleb formation when introduced at ectopic locations [41]. The site of bleb formation is further characterized by activation of the small RhoGTPases RhoA and Rac1 [26••]. Importantly, whereas guidance cues direct the polarity and migration of the cells, in the absence of such cues, zebrafish germ cells do polarize and migrate albeit, non directionally [9]. An interesting question that arises in this context concerns the mechanisms responsible for the directional cue-independent polarization of blebbing activity and migration. Proteins that could participate in establishing the apparent polarity with respect to bleb formation include structural components of the actomyosin cortex, and regulators of its contractility (e.g. kinases activating myosin contraction), proteins and lipids involved in facilitating membrane–

cortex binding (e.g. ERM (Ezrin, Radixin, Moesin) proteins and regulators of their activity) and G-protein coupled receptors. For example, a possible scenario is that G-protein coupled receptors stochastically activate phospholipase C (PLC), which in turn would reduce PIP2 levels in the membrane. Local hydrolysis of PIP2 could decrease the adhesion between the membrane and underlying cytoskeleton, trigger IP3-dependent cofilin-triggered actin polymerization at the cell front and elevation in Calcium levels that could enhance myosin contraction [42–44] thereby establishing a leading edge. Indeed, whereas a detailed understanding of germ-cell polarization is still lacking, some of the molecular components listed above have been shown to play a role in germ-cell motility, for example the G-protein coupled receptor Tre-1 of *Drosophila* [25,45], lipids that could affect the activation of G-protein coupled receptors [46] and the lipid composition of the cell membrane [47].

## Love thy neighbor

Whereas the generation of protrusions is crucial for cell motility, the actual translocation of the cell mass forward requires interactions with the environment. The interactions of a migrating cell with its surrounding includes pushing against structures in the environment, squeezing within confined spaces, adhesion to the extracellular matrix (ECM) or to neighboring cells [48–50]. In mouse, several types of collagen, fibronectin and tentactin-C are expressed along the germ-cell migration route [51,52], consistent with the idea that ECM components play a role in germ-cell migration [53]. Indeed, β1-integrin was shown to be expressed by mouse germ cells and to be important for their *in vivo* migration to genital ridges [54]. However, mouse germ cells were capable of migrating *in vitro* in the absence of somatic cells or any defined matrix support, suggesting that at least some steps of their migration could be ECM independent [55]. *Drosophila* germ cells lacking β-integrin can reach their target [1•,56], suggesting that despite indications that the basement membrane component laminin might play a role in germ-cell migration [1•,56], integrin–ECM interactions appear dispensable. Similar to these results, interfering with PGC–ECM interactions in zebrafish did not affect the ability of the cells to reach their target [26••]. It remains to be determined whether despite the fact that the cells can reach the gonad independently of the ECM, their migration is affected as manifested in altered speed, morphology or other dynamic parameters. Together, these results suggest that the interaction with the ECM probably plays a relatively minor role in facilitating germ-cell motility. An important clue concerning the molecular basis for interaction between germ cells and their environment stems from the observation that isolated *Drosophila* and zebrafish germ cells tend to adhere to one another [1•,26••], raising the possibility that cell–cell interaction plays a role in the generation of traction force. An attractive candidate for mediating cell–cell adhesion is E-cadherin, a molecule that is ubiquitously expressed in the embryo and could thus promote the interaction of germ cells with cells of different tissues. Indeed, E-cadherin was shown to be involved in germ-cell migration in different organisms; in *Drosophila* and zebrafish for example, E-cadherin expression level decreases just before the cells become motile, suggesting that tight control of cell–cell adhesion level is required for migration [3•,24,25]. In mouse, E-cadherin is necessary for PGC migration out of the hindgut [22,23], while in *Drosophila*, DE-Cadherin facilitates PGC polarization and is important for gonad coalescence at later stages [24,25]. In zebrafish, E-cadherin appears to supports PGC motility during the entire migratory phase such that alteration of its activity leads to strong inhibition of germ-cell locomotion [3•,26••]. Interestingly, reduction of E-cadherin activity is sufficient to promote tumor cell metastasis and is correlated with poor prognosis [57–59]; similar to the events at the initiation of germ-cell migration, E-cadherin activity is reduced to allow cancer cells to leave their tissue of origin. However, unlike E-cadherin essential role during germ-cell migration, tumor cells appear to invade tissues also in an E-cadherin independent fashion. In the context of normal development, homophilic cell–cell adhesion was shown to play an important role, for example in *Drosophila* where E-cadherin functions to promote the migration of border cells on the surface of the nurse cells during oogenesis [28,60,61]. The mechanisms by which E-cadherin contributes to cell motility were investigated in zebrafish PGCs. There, as a result of enhanced Rac1 and RhoA activity at the cell front, actin belts are generated that undergo retrograde flow. The binding of E-cadherin to these actin structures within the cell and to external E-cadherin on neighboring cells, allows traction forces to be established [26••]. This course of events is reminiscent of the scenario described for N-cadherin-mediated neuronal growth cone migration, where N-cadherin and intracellular actin flow are mechanically coupled [62]. Several interesting questions remain to be explored regarding the model implicating cell–cell adhesion in promoting germ-cell migration; the precise control over the level of E-cadherin expression that is essential for proper migration is not known and specifically, whether it involves transcription regulation (e.g. [63,64]) or operates at the posttranscriptional level (e.g. [65]). Also, as constituents of forward movement, migrating cells need not only to adhere to the neighboring cells but periodically to detach their back; an interesting open question is thus whether the activity of E-cadherin is polarized, such that the cell front exhibits enhanced adhesion as compared with the retracting back.

## Seek guidance

The polarization, formation of protrusions and generation of traction represent inherent properties of germ cells and are the basis for their motility. This inherent motility is biased to become directional migration upon integration

of signals from the environment, thus enabling efficient arrival of germ cells at the gonad.

The migration of PGCs, therefore, serves as a model for guided migration during normal development, with relevance for medical conditions such as cancer and inflammation, where directed cell migration plays a critical role. The metastatic destination of breast cancer cells for example, was suggested to be controlled by directed migration of the tumor cells towards target tissues expressing the chemokine CXCL12 [66]. Similarly, the directional cues for germ cells define regions that either attract or repel the migrating cells, thereby guiding them towards intermediate and final migration targets. A number of different types of cues can modify the migration path of germ cells; these include protein ligands for different receptors (bone morphogenetic factor receptor, chemokine and the kit receptor tyrosine kinase. Reviewed in [11••]), lipid signaling molecules [67] and molecules that assume their attractant function following specific post-translational modifications [68].

Despite the identification of this array of guidance cues, little is known concerning the precise mechanism by which they direct cell migration. A conceivable possibility is that polarized activation of the receptor leads to a local enhancement of the basal motility pathway, thus converting random migration into a directed one (Figure 1).

**Figure 1**

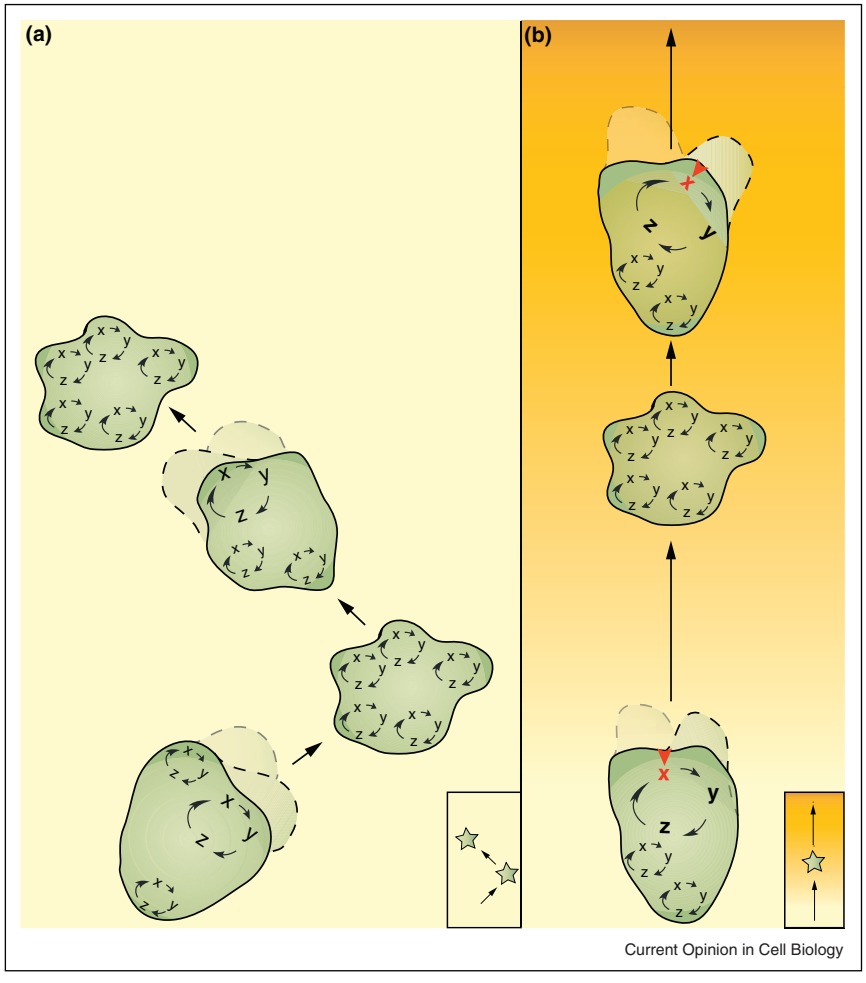


Hypothetical model for basic and guided motility based on zebrafish PGCs. The motility of the germ cells could be supported by positive feedback loops. In such circuits, elements x, y, z represent relevant molecules involved in adhesion, myosin activation, membrane–cytoskeleton interaction, small Rho GTPases activation, and so on. In the absence of a chemotactic gradient **(a)** stochastic, chemotactic-signal independent increased activation of such a loop at a certain position would result in protrusion formation at that location. If effective adhesion and formation of additional blebs is more likely to happen in a region where a bleb formed before (e.g. due reduced adhesion between the newly formed cortex with the newly expanded membrane of the bleb), a leading edge could be established, resulting in migration in a certain direction. Such periods of active migration are interrupted by de-polarization (tumbling), re-sensing of the environment and re-acquisition of the polarity in the random direction. In the presence of a guidance-cue gradient **(b)**, persistent feedback loops are more likely to be generated at the site of higher receptor activation (red arrowhead), that corresponds to the aspect of the cell exposed to higher chemoattractant level.

Indeed, triggering the relevant guidance receptors by ligand binding (e.g. in the case of the c-Kit, CXCR4 or Tre-1) was shown to result in activation of signaling transduction pathways involving PI3K, Rac1, RhoA, ERK, Calcium, PLC and MAPK. These molecules that serve as constituents of the motility machinery and acquisition of cell polarity also function in the context of directed migration. For example, the activity of PI3K is necessary for proper migration of mouse and zebrafish PGCs [47,55], as are RhoA and Rac1 signaling for polarization and locomotion of *Drosophila* and zebrafish PGCs [26••,45] and elevated Calcium levels at the leading edge of migrating zebrafish germ cells [41]. According to this view, stochastic cell-autonomous polarization and motility circuits result in non-directional migration, whereas receptor activation acts on the same signaling pathways, while providing dominant spatial information; this spatial information localizes the activation of pathway components that in turn establish a persistent leading edge, thus steering the cells to migrate along a vector dictated by the distribution of the guidance cue (Figure 1).

## Acknowledgements

We thank Michal Reichman-Fried for comments on the manuscript. We are supported by funds from the German Research Foundation (DFG), the Max Planck Society (MPG) and the Medical Faculty of the University of Münster.

## References and recommended reading

Papers of particular interest, published within the period of review, have been highlighted as:

- • of special interest
- •• of outstanding interest

1. • Jaglarz MK, Howard KR: **The active migration of Drosophila primordial germ cells**. *Development* 1995, **121**:3495-3503.
This paper combines electon microscopy, immunohistochemisry and mutational analysis to thoroughly describe stages of *Drosophila* PGC migration, with particular emphasis on the transendodermal migration phase. Of special interest is the characterization of PGC shape and cytoskeleton rearrangements correlated to their migratory behaviour at different developmental stages.

2. Saitou M, Barton SC, Surani MA: **A molecular programme for the specification of germ cell fate in mice**. *Nature* 2002, **418**:293-300.

3. • Blaser H, Eisenbeiss S, Neumann M, Reichman-Fried M, Thisse B, Thisse C, Raz E: **Transition from non-motile behaviour to directed migration during early PGC development in zebrafish**. *J Cell Sci* 2005, **118**:4027-4038.
The study describes the early development of zebrafish PGCs *in vivo* in the context of live embryos from their specification to the acquisition of cellular motility. The work characterizes three phases of Zebrafish PGC maturation focusing on changes of cell morphology, ability to migrate and responsiveness to CXCL12a.

4. Van Doren M, Williamson A, Lehmann R: **Regulation of zygotic gene expression in Drosophila primordial germ cells**. *Curr Biol* 1998, **8**:243-246.

5. Clark JM, Eddy EM: **Fine structural observations on the origin and associations of primordial germ cells of the mouse**. *Dev Biol* 1975, **47**:136-155.

6. Wylie C: **Germ cells**. *Cell* 1999, **96**:165-174.

7. Zhang N, Zhang J, Purcell KJ, Cheng Y, Howard K: **The Drosophila protein Wunen epels migrating germ cells**. *Nature* 1997, **385**:64-67.

8. Van Doren M, Broihier HT, Moore LA, Lehmann R: **HMG-CoA reductase guides migrating primordial germ cells [see comments]**. *Nature* 1998, **396**:466-469.

9. Doitsidou M, Reichman-Fried M, Stebler J, Koprunner M, Dorries J, Meyer D, Esguerra CV, Leung T, Raz E: **Guidance of primordial germ cell migration by the chemokine SDF-1**. *Cell* 2002, **111**:647-659.

10. Molyneaux K, Zinszner H, Kunwar P, Schaible K, Stebler J, Sunshine M, O'Brien W, Raz E, Littman D, Wylie C *et al.*: **The chemokine SDF1/CXCL12 and its receptor CXCR4 regulate mouse germ cell migration and survival**. *Development* 2003, **130**:4279-4286.

11. •• Richardson BE, Lehmann R: **Mechanisms guiding primordial germ cell migration: strategies from different organisms**. *Nat Rev Mol Cell Biol* 2010, **11**:37-49.
This comprehensive review describes the molecular mechanisms governing PGC migration, with a detailed description of the process in the mouse, Zebrafish and the *Drosophila* models.

12. • Weidinger G, Wolke U, Koprunner M, Klinger M, Raz E: **Identification of tissues and patterning events required for distinct steps in early migration of zebrafish primordial germ cells**. *Development* 1999, **126**:5295-5307.
This work provides a detailed analysis of PGC migration during the first 24 h of Zebrafish embryonic development, defining six distinct steps of migration towards the gonad. Analysis of the migration process in mutant embryos revealing a role for specific somatic tissues in supporting proper PGC migration and arrival at the gonad.

13. Anderson R, Copeland TK, Scholer H, Heasman J, Wylie C: **The onset of germ cell migration in the mouse embryo**. *Mech Dev* 2000, **91**:61-68.

14. • Ewen KA, Koopman P: **Mouse germ cell development: from specification to sex determination**. *Mol Cell Endocrinol* 2010, **323**:76-93.
A very detailed review describing the key events of PGC ontogeny in the mouse model.

15. • Moore LA, Broihier HT, Van Doren M, Lunsford LB, Lehmann R: **Identification of genes controlling germ cell migration and embryonic gonad formation in Drosophila**. *Development* 1998, **125**:667-678.
This paper reports on a large-scale mutagenesis screen for genes controlling germ-cell migration in *Drosophila*. This effort led to the identification of sets of genes responsible for distinct steps of PGC migration in this model organism.

16. Molyneaux KA, Stallock J, Schaible K, Wylie C: **Time-lapse analysis of living mouse germ cell migration**. *Dev Biol* 2001, **240**:488-498.

17. Sano H, Renault AD, Lehmann R: **Control of lateral migration and germ cell elimination by the Drosophila melanogaster lipid phosphate phosphatases Wunen and Wunen 2**. *J Cell Biol* 2005, **171**:675-683.

18. Reichman-Fried M, Minina S, Raz E: **Autonomous modes of behavior in primordial germ cell migration**. *Dev Cell* 2004, **6**:589-596.

19. Giampieri S, Manning C, Hooper S, Jones L, Hill CS, Sahai E: **Localized and reversible TGFbeta signalling switches breast cancer cells from cohesive to single cell motility**. *Nat Cell Biol* 2009, **11**:1287-1296.

20. Cunningham CC, Gorlin JB, Kwiatkowski DJ, Hartwig JH, Janmey PA, Byers HR, Stossel TP: **Actin-binding protein requirement for cortical stability and efficient locomotion**. *Science* 1992, **255**:325-327.

21. Sahai E, Marshall CJ: **Differing modes of tumour cell invasion have distinct requirements for Rho/ROCK signalling and extracellular proteolysis**. *Nat Cell Biol* 2003, **5**:711-719.

22. Bendel-Stenzel MR, Gomperts M, Anderson R, Heasman J, Wylie C: **The role of cadherins during primordial germ cell migration and early gonad formation in the mouse**. *Mech Dev* 2000, **91**:143-152.

23. Di Carlo A, De Felici M: **A role for E-cadherin in mouse primordial germ cell development**. *Dev Biol* 2000, **226**:209-219.

24. Jenkins AB, McCaffery JM, Van Doren M: **Drosophila E-cadherin is essential for proper germ cell-soma interaction during gonad morphogenesis**. *Development* 2003, **130**:4417-4426.

25. Kunwar PS, Sano H, Renault AD, Barbosa V, Fuse N, Lehmann R: **Tre1 GPCR initiates germ cell transepithelial migration by regulating Drosophila melanogaster E-cadherin**. *J Cell Biol* 2008, **183**:157-168.

26. •• Kardash E, Reichman-Fried M, Maitre JL, Boldajipour B, Papusheva E, Messerschmidt EM, Heisenberg CP, Raz E: **A role for Rho GTPases and cell–cell adhesion in single-cell motility in vivo**. *Nat Cell Biol* 2010, **12**:47-53 sup pp. 41-11.
Recent work defining the mechanisms responsible for PGC motility in the zebrafish. The paper shows how the activation of RhoA and Rac1 at the leading edge of zebrafish PGCs and E-cadherin-mediated cell–cell adhesion facilitate the generation of traction force and cell migration.

27. Naora H, Montell DJ: **Ovarian cancer metastasis: integrating insights from disparate model organisms**. *Nat Rev Cancer* 2005, **5**:355-366.

28. Pacquelet A, Rorth P: **Regulatory mechanisms required for DE-cadherin function in cell migration and other types of adhesion**. *J Cell Biol* 2005, **170**:803-812.

29. Pollard TD, Borisy GG: **Cellular motility driven by assembly and disassembly of actin filaments**. *Cell* 2003, **112**:453-465.

30. Friedl P, Wolf K: **Plasticity of cell migration: a multiscale tuning model**. *J Cell Biol* 2010, **188**:11-19.

31. • Charras G, Paluch E: **Blebs lead the way: how to migrate without lamellipodia**. *Nat Rev Mol Cell Biol* 2008, **9**:730-736.
This review presents the knowledge concerning the mechanics of bleb formation and bleb-driven migration and suggests mechanisms by which blebs contribute to cell polarization and motility.

32. Charras GT, Coughlin M, Mitchison TJ, Mahadevan L: **Life and times of a cellular bleb**. *Biophys J* 2008, **94**:1836-1853.

33. Bereiter-Hahn J, Luck M, Miebach T, Stelzer HK, Voth M: **Spreading of trypsinized cells: cytoskeletal dynamics and energy requirements**. *J Cell Sci* 1990, **96(Part 1)**:171-188.

34. Charras GT, Yarrow JC, Horton MA, Mahadevan L, Mitchison TJ: **Non-equilibration of hydrostatic pressure in blebbing cells**. *Nature* 2005, **435**:365-369.

35. Mitchison TJ, Charras GT, Mahadevan L: **Implications of a poroelastic cytoplasm for the dynamics of animal cell shape**. *Semin Cell Dev Biol* 2008, **19**:215-223.

36. Cunningham CC: **Actin polymerization and intracellular solvent flow in cell surface blebbing**. *J Cell Biol* 1995, **129**:1589-1599.

37. Keller H, Eggli P: **Protrusive activity, cytoplasmic compartmentalization, and restriction rings in locomoting blebbing Walker carcinosarcoma cells are related to detachment of cortical actin from the plasma membrane**. *Cell Motil Cytoskeleton* 1998, **41**:181-193.

38. Hagmann J, Burger MM, Dagan D: **Regulation of plasma membrane blebbing by the cytoskeleton**. *J Cell Biochem* 1999, **73**:488-499.

39. Keller H, Rentsch P, Hagmann J: **Differences in cortical actin structure and dynamics document that different types of blebs are formed by distinct mechanisms**. *Exp Cell Res* 2002, **277**:161-172.

40. Engelbrecht CJ, Stelzer EH: **Resolution enhancement in a light-sheet-based microscope (SPIM)**. *Opt Lett* 2006, **31**:1477-1479.

41. Blaser H, Reichman-Fried M, Castanon I, Dumstrei K, Marlow FL, Kawakami K, Solnica-Krezel L, Heisenberg CP, Raz E: **Migration of zebrafish primordial germ cells: a role for myosin contraction and cytoplasmic flow**. *Dev Cell* 2006, **11**:613-627.

42. van Rheenen J, Song X, van Roosmalen W, Cammer M, Chen X, Desmarais V, Yip SC, Backer JM, Eddy RJ, Condeelis JS: **EGF-induced PIP2 hydrolysis releases and activates cofilin locally in carcinoma cells**. *J Cell Biol* 2007, **179**:1247-1259.

43. Barret C, Roy C, Montcourrier P, Mangeat P, Niggli V: **Mutagenesis of the phosphatidylinositol 4,5-bisphosphate (PIP(2)) binding site in the NH(2)-terminal domain of ezrin correlates with its altered cellular distribution**. *J Cell Biol* 2000, **151**:1067-1080.

44. Raucher D, Stauffer T, Chen W, Shen K, Guo S, York JD, Sheetz MP, Meyer T: **Phosphatidylinositol 4,5-bisphosphate functions as a second messenger that regulates cytoskeleton-plasma membrane adhesion**. *Cell* 2000, **100**:221-228.

45. Kunwar PS, Starz-Gaiano M, Bainton RJ, Heberlein U, Lehmann R: **Tre1 a G protein-coupled receptor directs transepithelial migration of Drosophila germ cells**. *PLoS Biol* 2003, **1**:E80.

46. Pilquil C, Ling ZC, Singh I, Buri K, Zhang QX, Brindley DN: **Co-ordinate regulation of growth factor receptors and lipid phosphate phosphatase-1 controls cell activation by exogenous lysophosphatidate**. *Biochem Soc Trans* 2001, **29**:825-830.

47. Dumstrei K, Mennecke R, Raz E: **Signaling pathways controlling primordial germ cell migration in Zebrafish**. *J Cell Sci* 2004, **117**:4787-4795.

48. Malawista SE, de Boisfleury Chevance A, Boxer LA: **Random locomotion and chemotaxis of human blood polymorphonuclear leukocytes from a patient with leukocyte adhesion deficiency-1: normal displacement in close quarters via chimneying**. *Cell Motil Cytoskeleton* 2000, **46**:183-189.

49. Wolf K, Mazo I, Leung H, Engelke K, von Andrian UH, Deryugina EI, Strongin AY, Brocker EB, Friedl P: **Compensation mechanism in tumor cell migration: mesenchymal-amoeboid transition after blocking of pericellular proteolysis**. *J Cell Biol* 2003, **160**:267-277.

50. Lammermann T, Bader BL, Monkley SJ, Worbs T, Wedlich-Soldner R, Hirsch K, Keller M, Forster R, Critchley DR, Fassler R *et al.*: **Rapid leukocyte migration by integrin-independent flowing and squeezing**. *Nature* 2008, **453**:51-55.

51. Garcia-Castro M, Anderson R, Heasman J, Wylie C: **Interactions between germ cells and extracellular matrix glycoproteins during migration and gonad assembly in the mouse embryo**. *J Cell Biol* 1997, **138**:471-480.

52. Soto-Suazo M, San Martin S, Zorn TM: **Collagen and tenascin-C expression along the migration pathway of mouse primordial germ cells**. *Histochem Cell Biol* 2004, **121**:149-153.

53. Bendel-Stenzel M, Anderson R, Heasman J, Wylie C: **The origin and migration of primordial germ cells in the mouse [In Process Citation]**. *Semin Cell Dev Biol* 1998, **9**:393-400.

54. Anderson R, Fassler R, Georges-Labouesse E, Hynes R, Bader B, Kreidberg J, Schaible K, Heasman J, Wylie C: **Mouse primordial germ cells lacking beta1 integrins enter the germline but fail to migrate normally to the gonads**. *Development* 1999, **126**:1655-1664.

55. Farini D, La Sala G, Tedesco M, De Felici M: **Chemoattractant action and molecular signaling pathways of Kit ligand on mouse primordial germ cells**. *Dev Biol* 2007, **306**:572-583.

56. Devenport D, Brown NH: **Morphogenesis in the absence of integrins: mutation of both Drosophila beta subunits prevents midgut migration**. *Development* 2004, **131**:5405-5415.

57. Cavallaro U, Christofori G: **Cell adhesion and signalling by cadherins and Ig-CAMs in cancer**. *Nat Rev Cancer* 2004, **4**:118-132.

58. Lehembre F, Yilmaz M, Wicki A, Schomber T, Strittmatter K, Ziegler D, Kren A, Went P, Derksen PW, Berns A *et al.*: **NCAM-induced focal adhesion assembly: a functional switch upon loss of E-cadherin**. *EMBO J* 2008, **27**:2603-2615.

59. Onder TT, Gupta PB, Mani SA, Yang J, Lander ES, Weinberg RA: **Loss of E-cadherin promotes metastasis via multiple downstream transcriptional pathways**. *Cancer Res* 2008, **68**:3645-3654.

60. Niewiadomska P, Godt D, Tepass U: **DE-Cadherin is required for intercellular motility during Drosophila oogenesis**. *J Cell Biol* 1999, **144**:533-547.

61. Pinheiro EM, Montell DJ: **Requirement for Par-6 and Bazooka in Drosophila border cell migration**. *Development* 2004, **131**:5243-5251.

62. Bard L, Boscher C, Lambert M, Mege RM, Choquet D, Thoumine O: **A molecular clutch between the actin flow and N-cadherin adhesions drives growth cone migration**. *J Neurosci* 2008, **28**:5879-5890.

63. Cano A, Perez-Moreno MA, Rodrigo I, Locascio A, Blanco MJ, del Barrio MG, Portillo F, Nieto MA: **The transcription factor snail controls epithelial–mesenchymal transitions by repressing E-cadherin expression**. *Nat Cell Biol* 2000, **2**:76-83.

64. Peinado H, Olmeda D, Cano A: **Snail Zeb and bHLH factors in tumour progression: an alliance against the epithelial phenotype?** *Nat Rev Cancer* 2007, **7**:415-428.

65. Fujita Y, Krause G, Scheffner M, Zechner D, Leddy HE, Behrens J, Sommer T, Birchmeier W: **Hakai, a c-Cbl-like protein, ubiquitinates and induces endocytosis of the E-cadherin complex**. *Nat Cell Biol* 2002, **4**:222-231.

66. Muller A, Homey B, Soto H, Ge N, Catron D, Buchanan ME, McClanahan T, Murphy E, Yuan W, Wagner SN *et al.*: **Involvement of chemokine receptors in breast cancer metastasis**. *Nature* 2001, **410**:50-56.

67. Renault AD, Sigal YJ, Morris AJ, Lehmann R: **Soma-germ line competition for lipid phosphate uptake regulates germ cell migration and survival**. *Science* 2004, **305**: 1963-1966.

68. Santos AC, Lehmann R: **Isoprenoids control germ cell migration downstream of HMGCoA reductase**. *Dev Cell* 2004, **6**:283-293.

Developmental Cell
Short Article

# Identification and Regulation of a Molecular Module for Bleb-Based Cell Motility

Mehdi Goudarzi,[1,6] Torsten U. Banisch,[1,6] Mehrpouya B. Mobin,[1] Nicola Maghelli,[2] Katsiaryna Tarbashevich,[1] Ina Strate,[3] Jana van den Berg,[1] Heiko Blaser,[4] Sabine Bandemer,[1] Ewa Paluch,[2,5] Jeroen Bakkers,[3] Iva M. Tolić-Nørrelykke,[2] and Erez Raz[1,*]

[1]Institute of Cell Biology, Center of Molecular Biology of Inflammation, University of Münster, Von-Esmarch-Strasse 56, D-48149 Münster, Germany
[2]Max Planck Institute of Molecular Cell Biology and Genetics, D-01307 Dresden, Germany
[3]Hubrecht Institute, KNAW and University Medical Center Utrecht, 3584 CT Utrecht, The Netherlands
[4]Max Planck Institute for Biophysical Chemistry, Am Fassberg 11, D-37077 Göttingen, Germany
[5]International Institute of Molecular and Cell Biology, Warsaw 02-109, Poland
[6]These authors contributed equally to this work
*Correspondence: erez.raz@uni-muenster.de
DOI 10.1016/j.devcel.2012.05.007

## SUMMARY

**Single-cell migration is a key process in development, homeostasis, and disease. Nevertheless, the control over basic cellular mechanisms directing cells into motile behavior in vivo is largely unknown. Here, we report on the identification of a minimal set of parameters the regulation of which confers proper morphology and cell motility. Zebrafish primordial germ cells rendered immotile by knockdown of Dead end, a negative regulator of miRNA function, were used as a platform for identifying processes restoring motility. We have defined myosin contractility, cell adhesion, and cortex properties as factors whose proper regulation is sufficient for restoring cell migration of this cell type. Tight control over the level of these cellular features, achieved through a balance between miRNA-430 function and the action of the RNA-binding protein Dead end, effectively transforms immotile primordial germ cells into polarized cells that actively migrate relative to cells in their environment.**

## INTRODUCTION

Cell migration is a critical process that is involved in gastrulation, the generation of organs, and in the maintenance and function of the organs. This process is also key to normal and abnormal immune responses and constitutes the basis for a range of pathological conditions (Borregaard, 2010; Friedl and Gilmour, 2009; Richardson and Lehmann, 2010; Rørth, 2009; Roussos et al., 2011; Solnica-Krezel, 2005). A fundamental issue in cell migration concerns the actual acquisition of cell motility, the ability of cells to change their position relative to neighboring cells. Determining the mechanisms controlling cell motility would thus contribute to the understanding of a range of events in normal development, homeostasis, and disease.

A useful model for studying single-cell migration in vivo is that of primordial germ cells (PGCs) in early zebrafish embryos (Raz, 2004). The signal guiding zebrafish PGCs toward their target, the chemokine Cxcl12a, and the mechanisms controlling its distribution have been identified (Boldajipour et al., 2008; Doitsidou et al., 2002). Furthermore, the processes contributing to cell motility have been extensively studied. These studies showed that zebrafish PGCs generate protrusions in the form of actin-free cellular extensions powered by hydrostatic pressure (Blaser et al., 2006), while generation of traction that allows the cells to move with respect to neighboring cells requires the function of the cell-cell adhesion molecule E-cadherin (Kardash et al., 2010). Whereas those processes appear to be important for efficient PGC migration, it is not clear whether they are sufficient for promoting cell motility. Furthermore, the understanding of the molecular mechanisms regulating these cellular features is currently lacking.

A protein whose function is especially important in this context is the RNA-binding protein Dead end (Dnd) (Weidinger et al., 2003). This protein was found to function, at least in part, by counteracting the action of microRNAs (miRNAs), facilitating the stabilization and translation of specific mRNAs (Kedde et al., 2007). Interestingly, Dnd was shown to be essential for PGC motility, as cells knocked down for its activity display striking morphological defects, such that they fail to generate protrusions and to migrate (Weidinger et al., 2003). These immotile PGCs thus constitute an attractive platform for defining the fundamental processes controlling the acquisition of cell motility in vivo.

In this work, we show that the morphology and the motility of the germ cells rely on the proper regulation of contractility, as well as of cell adhesion and on the control over cortex-membrane interaction. Specifically, we demonstrate that cells lacking Dnd exhibit reduced contractile activity on one hand and elevated levels of Annexin A5b, a scaffold calcium- and phospholipid-binding protein that could control membrane-cortex interaction on the other. In addition, in the absence of Dnd, expression levels of the transcriptional repressor Zeb1 are reduced, resulting in elevated levels of the cell adhesion molecule E-cadherin. Consistent with the idea that contractility, adhesion level, and cortex-membrane interaction constitute key elements in the cellular motility program, manipulation of these determinants was sufficient to direct cells toward motile

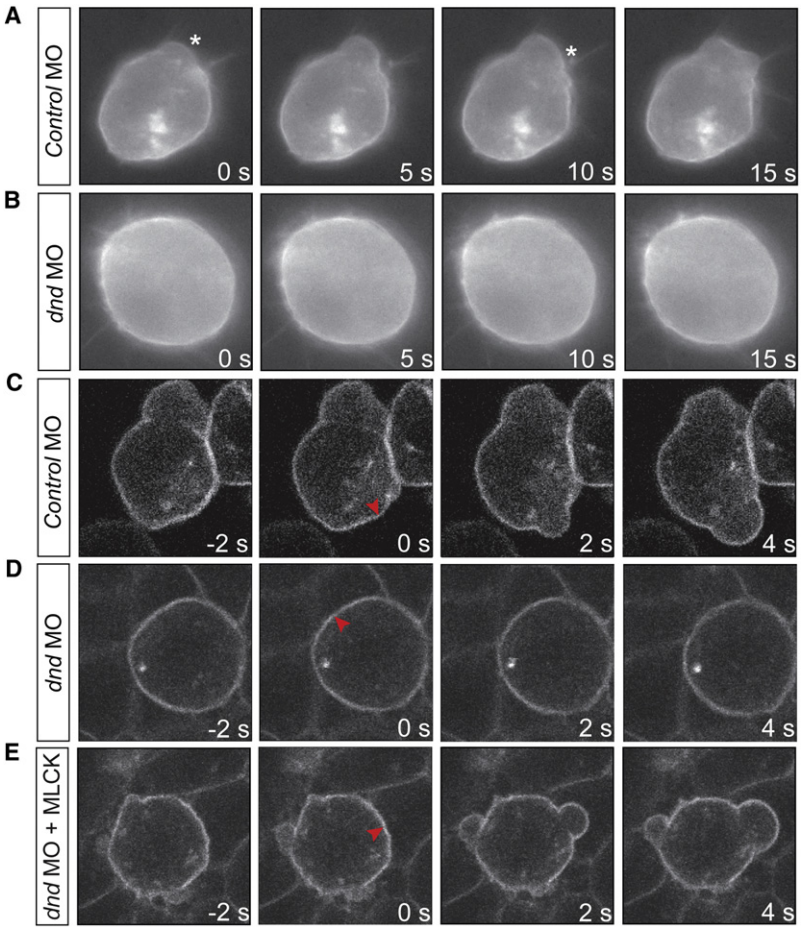


**Figure 1. Lack of Bleb Formation in PGCs Knocked Down for Dnd Is Correlated with Reduced Contractility**

(A) Control germ cells form blebs in the direction of migration. Asterisks mark bleb initiation.

(B) Lack of blebs in cells depleted for the Dnd protein.

(C) Cortex ablation induces blebs in control cells.

(D) Lack of bleb induction by a similar manipulation in cells knocked down for Dnd.

(E) MLCK restores bleb formation in response to cortex ablation.

Red arrowheads indicate the ablation point. See also Movies S1 and S2.

behavior. Specifically, enhancing the contractility in PGCs knocked down for Dnd, coupled to controlling the level of cell-cell adhesion and cortex properties, results in a striking recovery of protrusion generation and migration. Together, these findings define a set of cellular events that in concert potentiate single-cell motility in vivo and uncover the molecular mechanisms controlling them, namely, a balance between miRNA function and the action of a cell-specific RNA-binding protein.

## RESULTS AND DISCUSSION

### The Generation of Hydrostatic Pressure-Powered Protrusions in PGCs Depends on Dnd Function

During their migration, zebrafish PGCs dynamically generate cellular protrusions (Figure 1A; Movie S1, left section, available online) (Blaser et al., 2006). This cellular behavior depends on the function of the RNA-binding protein Dnd, as cells lacking it exhibit simple, round morphology and are immotile (Figure 1B and Movie S1, right section) (Weidinger et al., 2003).

Previous analysis of the protrusions generated by PGCs revealed that they are powered by hydrostatic pressure that pushes the membrane away from the actin cortex of the cell (Blaser et al., 2006). These protrusions, termed blebs, are produced by a range of other cell types (reviewed in Fackler and Grosse, 2008) and are nucleated at a point around the cell perimeter, where the interaction between the cell membrane and the cortex is reduced. At this position, local detachment of the membrane from the cell cortex occurs, followed by cytoplasmic flow-driven inflation, powered by intracellular pressure (Charras and Paluch, 2008). Indeed, similar to results obtained in vitro (Tinevez et al., 2009), using two-photon laser ablation to generate local damage to the cortex of PGCs in the context of the live embryo, we could effectively induce the formation of a bleb at the ablation point (Figure 1C and Movie S2, first section, 24 successful bleb inductions in 27 trials in 20 cells). Remarkably, a similar treatment of PGCs knocked down for Dnd function never resulted in bleb formation (Figure 1D and Movie S2, second section, no bleb induction in 48 attempts in 29 cells). Increasing the laser power resulted in a complete rupture of the cell (Movie S2, second section). These results are consistent with the idea that unlike wild-type cells, where intracellular pressure inflates the bleb, Dnd-depleted cells do not produce sufficient pressure for pushing the membrane away from the damaged cortex. Indeed, the simple round morphology of the Dnd knocked down PGCs is highly reminiscent of that observed in cells in which myosin contractility is inhibited (Blaser et al., 2006). To test this supposition, we introduced myosin light chain kinase (MLCK, referred to as MYLKa in zebrafish) into these cells, effectively restoring their ability to form blebs, in particular in response to laser-mediated damage to the cortex (Figure 1E and Movie S2, third section, induction of blebs in 24 out of 29 trials in 18 cells). Along these lines, overexpression of ROCK2a or RhoA, other activators of myosin contractility led to similar results (data not shown). Together, these experiments show that increasing myosin contractility, a feature connected to enhanced intracellular pressure (Charras et al., 2005; Sedzinski et al., 2011), is sufficient for restoring bleb formation in PGCs depleted of Dnd function. These observations are consistent with the notion that contractility-dependent hydrostatic pressure is at the basis of the characteristic morphology of wild-type motile PGCs. PGCs thus offer a useful model for exploring the genetic regulation over cellular hydrostatic pressure, a process of general importance in the control of cell shape and behavior (Charras et al., 2005; Stewart et al., 2011).

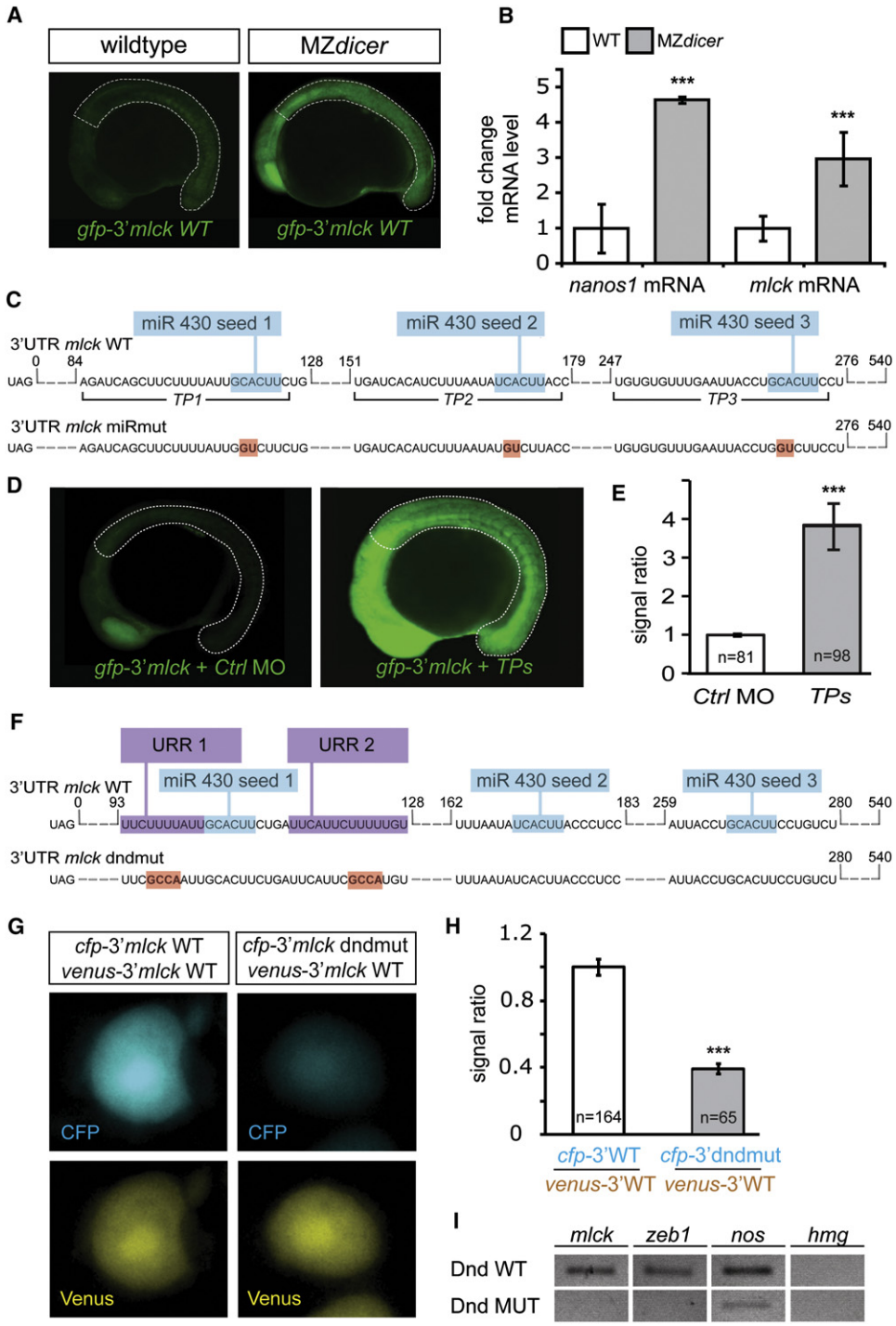


**Figure 2. Control of MLCK Expression by microRNAs and Dnd Protein**

(A) Lack of miRNAs in MZ*dicer* embryos results in higher GFP signal from a reporter containing the 3′ UTR of *mlck,* measured at 16 hpf within the dotted line marked areas (for quantitation, see Figure S1B).

(B) qPCR analysis comparing the endogenous levels of *mlck* and *nanos* mRNAs in wild-type and MZ*dicer* embryos.

(C) The 3′ UTR of *mlck* contains seed sequences for miR-430 (blue). Binding sites for target protector (TP) morpholinos that mask the miRNA seeds (*TP1-3*) are indicated and point mutations disrupting the seeds are labeled in red.

(D) Application of TPs increases GFP expression from the reporter RNA as compared to embryos treated with control morpholinos.

(E) Quantitative representation of the results of the experiment in (D), depicting the GFP signal level within the dotted line in (D) normalized to that of a coinjected mCherry control.

(F) The 3′ UTR of *mlck* contains two putative URR sites for Dnd binding (violet) adjacent to miR-430 seed sequences (blue). Mutations introduced are marked in red.

## MicroRNAs Control MLCK Expression Levels

As the Dnd protein was shown to counteract miRNA function (Kedde et al., 2007), we set out to examine the possibility that the level of proteins controlling myosin contractility is regulated by miRNAs and Dnd.

We found that whereas *rhoA* lacks canonical seed sequences indicative of miRNA regulation, such elements are found in the 3′ untranslated regions (UTRs) of *rock2a* and *mlck.* To determine whether these mRNAs are subjected to miRNA regulation, we employed RNA reporters containing the green fluorescent protein (GFP) open reading frame (ORF) fused to the 3′ UTR of the *mlck* or *rock2a* RNA (or to that of the *nanos* RNA as an miRNA-responsive control) and injected it into 1-cell stage wild-type or MZ*dicer* mutant embryos that are devoid of mature miRNAs (Giraldez et al., 2005). Quantitative pixel-intensity analysis revealed dramatically elevated GFP level in somatic cells of 16 hr postfertilization (hpf) MZ*dicer* embryos as compared to wild-type control embryos in the case of *mlck*, but not for *rock2a* (Figures 2A, S1A, and S1B; data not shown). Thus, as previously shown for the *nanos* 3′ UTR (Mishima et al., 2006), the 3′ UTR of *mlck* could potentially confer negative regulation on the translation of linked ORFs through the action of miRNAs. Consistently, quantitative PCR (qPCR) performed on RNA extracted from MZ*dicer* and wild-type embryos revealed highly significant elevation in the endogenous levels of both *mlck* and *nanos* in embryos lacking mature miRNAs (Figure 2B). Interestingly, whereas *cis*-elements located within the *mlck* 3′ UTR lead to a reduction in *mlck* RNA levels and repressed GFP expression in somatic cells, the *mlck* 3′ UTR-containing RNA directed strong GFP expression to the PGCs (Figure S1C, inset).

Indeed, we found that *mlck* RNA possesses miRNA-430 binding sites in its 3′ UTR (Figure 2C), prompting us to assess the role of this miRNA in controlling MLCK level and in acquiring proper cell morphology and attaining motility. We analyzed the function of the three seed sequences for miR-430 (Figure 2C, blue boxes) by introducing point mutations within the seed sequences (Figure 2C, red boxes), or by application of "target protector" morpholinos (TP) (Figure 2C, *TP1*, *TP2*, *TP3*) (Choi et al., 2007). Both manipulations led to a strong increase in GFP expression, similar to that observed in MZ*dicer* embryos (Figures 2D, 2E, and S1C–1F). These results further substantiate the notion that *mlck* RNA is inhibited by miR-430 in the soma of zebrafish embryos.

## Binding of Dnd to *mlck* mRNA Alleviates miRNA-Mediated Repression in Primordial Germ Cells

The results presented above indicate that MLCK expression and thus MLCK-dependent contractility is repressed in somatic cells by miRNAs. However, in the PGCs this repression was not effective (Figure S1C, inset), suggesting that miRNA activity on the 3′ UTR of *mlck* is alleviated in these cells. An attractive candidate to counteract the action of miRNAs in the PGCs is the Dnd protein that exerts such an effect on other RNAs like those encoding for Nanos and Tdrd7 (Kedde et al., 2007), proteins that are essential for germline development (Lehmann and Nüsslein-Volhard, 1991).

Indeed, Dnd function in the PGCs was essential for the expression of a fluorescent reporter whose ORF was fused to the wild-type 3′ UTR of the *mlck* RNA (Figures S1G and S1H). Importantly, the function of Dnd was dispensable when a miR-mutated *mlck* 3′ UTR was examined (Figures S1G and S1H). These findings suggest that Dnd counteracts the miR-430-mediated repression over *mlck* 3′ UTR in PGCs, explaining at least in part the enhanced contractility and dynamic cell-shape changes required for the motility of these cells. In agreement with this assertion, is the presence of Uridine-rich regions (URRs) within the 3′ UTR of *mlck,* sequences with which Dnd was shown to interact (Kedde et al., 2007) and which reside in close proximity to miRNA seed 1 (Figure 2F, violet boxes). As shown in Figures 2G and 2H, mutating these URRs resulted in a dramatic reduction in the level of the CFP reporter (CFP whose ORF was fused to this 3′ UTR). Consistent with such a direct role for Dnd in controlling the function of *mlck* RNA, we could demonstrate a specific interaction of Dnd with *mlck* RNA (Figures 2I and S1I). Together, these findings suggest that Dnd counteracts miR-430-mediated repression in PGCs by binding to URRs located within the *mlck* 3′ UTR, thereby controlling the cellular features relevant for bleb-associated motility. Increasing MLCK level in Dnd knocked-down cells restores bleb formation, but not motility. We therefore sought to identify additional molecules the function of which, in concert with that of MLCK would support active migration of the cells.

## Regulation of Cell Adhesion by Dnd-Mediated Control of Zeb1 Expression

In addition to actomyosin contractility, the motility of zebrafish PGCs requires proper regulation of adhesion to surrounding cells through E-cadherin (Kardash et al., 2010). Interestingly, PGCs knocked down for Dnd, show elevated levels of E-cadherin, relative to those detected in migrating wild-type PGCs at the same developmental stage (Blaser et al., 2005). In addition, a slight reduction in E-cadherin level in wild-type PGCs precedes the acquisition of motility and is thought to allow the detachment of PGCs from neighboring cells, while maintaining sufficient level of the molecule compatible with the generation of traction (Blaser et al., 2005). In other cell types, E-cadherin was shown to be regulated at the transcriptional level as well as at the level of protein activity and localization (Ahn et al., 2011; Jeanes et al., 2008; Málaga-Trillo et al., 2009; Ulrich et al., 2005).

(G) Mutating the URRs in *mlck* 3′ UTR results in reduced CFP expression in the PGCs as compared to the control wild-type 3′ UTR. The coinjected RNA (*venus-3′mlck* WT) served as a control.

(H) Quantitative representation of the normalized signal intensity in the experiment presented in (G).

(I) Immunoprecipitation of Dnd protein followed by RT-PCR for bound RNAs showing binding of Dnd to *mlck* and *zeb1* compared to that of a Dnd version impaired for RNA binding (Dnd.MUT; Y104C, Slanchev et al., 2009). Amplification of *nanos* and *hmg* transcripts served as control.

n signifies the number of PGCs examined in (H) or the number of embryos analyzed in (E). Error bars depict the SEM and the ***$p < 0.001$, calculated using two-tailed, unpaired t test.

See also Figure S1.

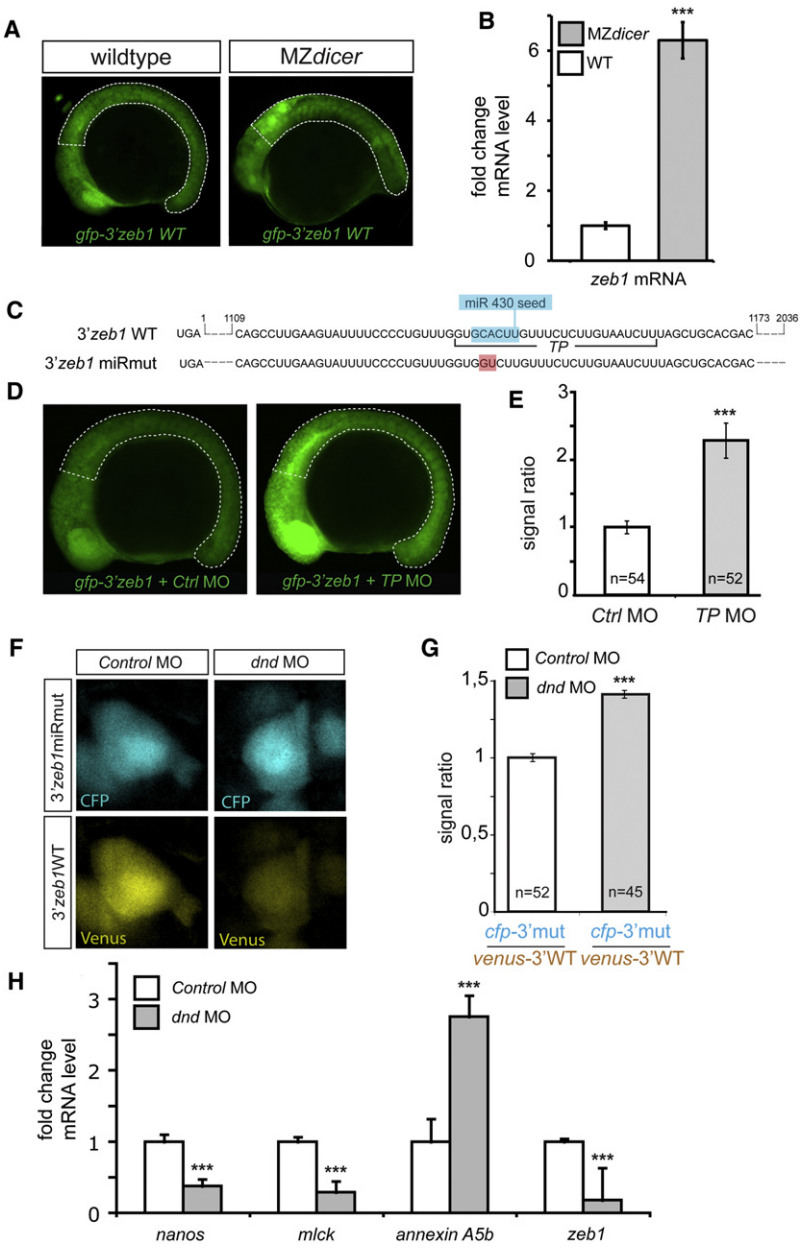


**Figure 3. Control of ZEB1 and Annexin A5b Expression by miRNAs and Dnd**

(A) Lack of miRNAs in MZ*dicer* embryos results in higher GFP signal from a reporter containing the 3′ UTR of *zeb1*, measured at 16 hpf from the line marked areas (Figure S2A).

(B) qPCR analysis comparing the endogenous levels of *zeb1* mRNA in MZ*dicer* and wild-type embryos.

(C) The 3′ UTR of *zeb1* contains a seed sequence of miR-430 (blue). Binding site for the target protector (TP) morpholino masking the miRNA seed (*TP*) is indicated and the point mutation disrupting the seed is labeled in red.

(D) Application of TPs increases GFP expression from the reporter RNA as compared to embryos treated with control morpholinos.

(E) Quantitative representation of the results of the experiment in (D) measured within the area marked by the dotted lines in (D), depicting the GFP signal level normalized to that of a coinjected mCherry control.

(F) Expression of the Venus protein from RNA containing the wild-type *zeb1* 3′ UTR is reduced in *dnd* MO treated PGCs as compared to that from an RNA reporter mutated for miRNA binding (*cfp-3′zeb1 miRmut*).

(G) Quantitative representation of the results in (F).

(H) qPCR analysis of endogenous *annexin* A5b, *nanos*, *mlck*, and *zeb1* mRNA in PGCs isolated from Dnd knocked-down embryos compared to control morpholino-injected animals.

n is the number of embryos analyzed in (E) or the number of PGCs examined in (G). Error bars depict the SEM and ***$p < 0.001$, calculated using two-tailed, unpaired t test. See also Figure S2.

A plausible candidate for controlling E-cadherin expression in the PGCs is the transcriptional repressor Zeb1 (also named ZFHX1), which was shown to function in controlling epithelial-to-mesenchymal transition (Peinado et al., 2007). Relevant for this study, it was shown that Zeb1 expression is regulated by miRNAs in various cell types (Brabletz and Brabletz, 2010). We examined the miRNA regulation of Zeb1 expression in zebrafish by monitoring wild-type and MZ*dicer* embryos for 1. The fluorescent intensity of a GFP reporter construct containing *zeb1* 3′ UTR and 2. The endogenous *zeb1* mRNA level. Indeed, both parameters reveal that miRNAs interfere with Zeb1 expression, as a significant increase in GFP and *zeb1* mRNA level was observed in embryos lacking mature miRNAs (Figures 3A, 3B, and S2A). Consistent with these results, is the presence of a miR-430 binding site in the *zeb1* 3′ UTR (Figure 3C, blue box). To determine the relevance of this seed sequence for miRNA regulation, we examined the activity of reporter constructs in which the seed was mutated (Figure 3C, red box), or blocked by TP morpholinos (Figure 3C, *TP*). Both manipulations resulted in a strong increase in GFP level from the reporter construct (Figures 3D, 3E, and S2B), proving that miR-430 family members target *zeb1* 3′ UTR.

The miRNA-mediated regulation of Zeb1 in somatic cells could account for the higher level of E-cadherin detected in these cells, as compared to that observed in motile PGCs. We sought to determine whether in analogy to the control over contractility, Dnd protein is involved in controlling E-cadherin level in PGCs by regulating the expression levels of its repressor, Zeb1. In agreement with this notion, we found that the expression level of the reporter protein, whose ORF was fused to the 3′ UTR of *zeb1*, depended on Dnd expression in the PGCs (Venus in Figures 3F and 3G). Furthermore, the role of Dnd here is to counteract the action of miRNAs on the 3′ UTR of *zeb1*, since mutating the miR-430 seed rendered the reporter RNA insensitive to the lack of Dnd (CFP in Figures 3F and 3G). These results can be explained by the binding of Dnd protein to *zeb1* mRNA, as demonstrated in Figures 2I and S1I. Together, these findings suggest that Dnd functions in the PGCs to inhibit microRNA function on the mRNA encoding the transcriptional repressor Zeb1. This action of Dnd could in turn

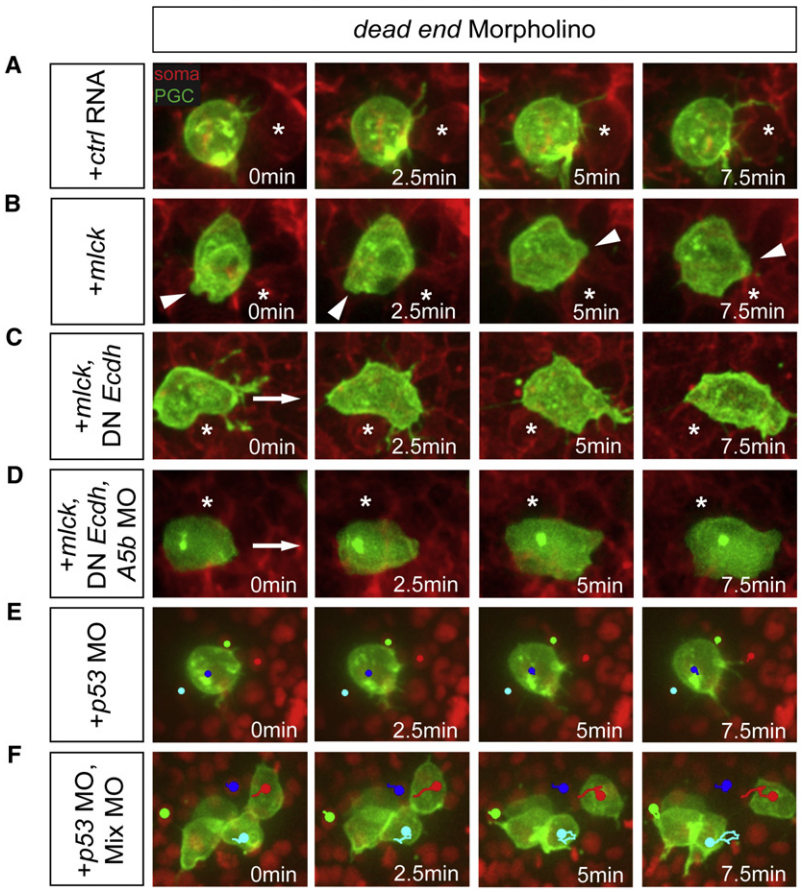


**Figure 4. Motility Reprogramming of PGCs and Somatic Cells**

(A) *dnd* MO treated PGCs (green) are immotile with respect to somatic cells (red).

(B) Bleb formation in immotile *dnd* MO treated PGCs overexpressing MLCK.

(C) Motility of *dnd* MO-treated PGCs expressing MLCK and a dominant-negative E-cadherin.

(D) Enhanced motility of *dnd* MO-treated PGCs knocked down for Annexin A5b in addition to the manipulation in (C).

(E and F) Dnd-depleted PGCs treated with p53 morpholino (E). Tracking a nucleus of such a round PGC (blue track) reveals no movement relative to somatic cells (light blue, green, and red). Such cells treated with a morpholino mixture (F), show active migration (red and light blue tracks for PGCs, green and blue for somatic cells) and cell shape changes.

Asterisks mark a stationary reference point in the soma. Arrowheads point at bleb formation positions. Arrows indicate direction of movement.

See also Figure S3 and Movies S4 and S5.

reduce the level of E-cadherin in the PGCs, thereby promoting their motility. Accordingly, overexpression of Zeb1 resulted in overall lower E-cadherin protein levels in zebrafish embryos (Figure S2C). These results thus suggest that Dnd functions in regulating the adhesion level of the PGCs to cells in their environment, thereby promoting their motility by protecting *zeb1* mRNA from miR-430-mediated inhibition.

## Downregulation of Annexin A5b Allows Bleb Formation in *dnd*-Morpholino-Treated PGCs

Annexins (ANXs) constitute a family of calcium- and phospholipid-binding proteins that have been implicated in a wide spectrum of cellular processes (Gerke and Moss, 2002; Rescher and Gerke, 2004). Included in these processes, Annexins are thought to control membrane to cortex attachment (Babiychuk et al., 1999; Bouter et al., 2011), a parameter considered to negatively regulate bleb formation (Diz-Muñoz et al., 2010; Lorentzen et al., 2011). Consistently, a dramatic increase in the mRNA encoding for Annexin A5b is observed in Dnd morphant PGCs, cells that do not bleb (Figure 3H). The increase in *annexin* A5b RNA levels in *dnd* morpholino-treated PGCs could be indirect and presumably miRNA independent. Irrespective of the mode by which Dnd controls Annexin A5b expression, we examined whether this scaffold protein could contribute to the lack of blebs in immotile Dnd knocked-down cells. Interestingly, downregulation of Annexin A5b in Dnd morphant embryos effectively restored bleb formation in PGCs (Figures S3A and S3B; Movie S3). Collectively, these results suggest that Annexin A5b-dependent cortex properties contribute to the Dnd knockdown phenotype and thus constitutes one of the components responsible for the rounded shape of these cells and their inability to move.

## Reprogramming Bleb-Based Single-Cell Motility of PGCs

We have identified three key cellular properties that are differentially controlled in somatic and germ cells and showed that they are required for the acquisition of proper cellular morphology and motility. The importance of regulating these features in somatic cells is revealed by the fact that relieving *mlck* RNA from miRNA regulation (Figures S2D and S2E), overexpression of Zeb1 (Muraoka et al., 2000) and morpholino-mediated knockdown of Annexin A5b (Figure S2F) lead to defects in gastrulation. In the germ cells, manipulations of hydrostatic pressure, cell-cell adhesion, and cortex-membrane interaction affected the morphology of Dnd knocked-down cells, but individually were insufficient to restore motility. As cell movement involves the integration of several physical cellular properties, we next examined whether a combination of these could restore the motility of PGCs compromised for Dnd function.

In wild-type PGCs, Dnd enhances contractility by counteracting miR-430 action on *mlck* RNA. Indeed, increasing the contractility by reintroducing MLCK, effectively restored bleb formation in Dnd knocked-down cells that nevertheless, remained immotile (Figures 4A and 4B; Movie S4 first and second section). Further, by regulating Zeb1 level, Dnd also acts to reduce cell-cell adhesion to a level compatible with single-cell motility in the embryo. Last, Dnd function is important for controlling the cell cortex properties by maintaining low levels of Annexin A5b. In this case too, Dnd knocked-down PGCs in which the level of Annexin A5b was lowered exhibit dynamic alteration in cell morphology and formation of blebs, but remain immotile (Figure S3B; Movie S3).

These results thus correlate three cellular features, namely, myosin-mediated contractility, cell adhesion, and cell cortex-membrane interaction, with the ability to acquire proper cellular morphology and motility. We next investigated whether the combination of these components is sufficient for conferring single-cell motility in PGCs knocked down for Dnd function. As a first step, we examined the effect of reducing cell adhesion combined with increased contractility in PGCs knocked down for Dnd. To this end, we expressed moderate levels of MLCK (lower than those restoring bleb formation), as well as of a dominant-negative form of E-cadherin (EcdhΔEC1-2) in the PGCs, and observed a modest rescue of the Dnd phenotype; similar to the example shown in Figure 4C and Movie S4, third section, out of 60 cells examined in 30 embryos, over 80% of Dnd knocked-down cells that otherwise exhibited simple static morphology and were completely immotile showed polarization and limited movement relative to their neighbors. Moreover, providing such partially rescued PGCs with morpholino against *annexin* A5b, further enhanced their protrusive activity (by 2.6-fold, and by 1.7-fold when only blebs formed at the direction of cell movement were considered), as well as their motility relative to neighboring somatic cells (Figure 4D; Movie S4, fourth section).

The results presented above demonstrate that modulating three cellular parameters by a combination of RNAs and antisense oligonucleotides is sufficient for transforming immotile cells into cells that actively migrate. Subsequently, we sought to perform reprogramming of cellular motility by altering the activity of a small set of transcripts endogenously expressed in the PGCs. For this purpose, we used a mixture of target protectors that counteract the miR-430 function on *mlck* and *zeb1* RNAs (*mlck* TP1;2;3 and *zeb1* TP) and morpholinos inhibiting the translation of *annexin* A5b (*annexin* A5b MO). In addition, we included morpholinos inhibiting p53 translation in the mixture to inhibit cell death resulting from loss of RNAs such as *nanos* in PGCs lacking Dnd function (Robu et al., 2007), thus allowing us to focus on the role of Dnd in PGC motility (Figure 4E). Remarkably, out of 60 PGCs treated in this way in 25 different embryos, over 80% showed protrusive behavior and 40% actively migrated (Figures 4E and 4F; Movie S5, first and second section). Despite the dramatic reversion of the Dnd motility phenotype, the migration of the rescued PGCs that lack the expression of proteins responsible for PGC identity was slower than that wild-type cells exhibit, prohibiting them from effectively reaching their target. Germ cells differ from somatic cells with respect to the regulation over actin-based structures relevant for migration, in their ability to respond to specific guidance cues and the modes of cell adhesion that govern their motility. Interestingly, despite these differences, employing the "PGC-motility module" on somatic cells resulted in enhanced cell-shape changes and protrusive activity, while actual motility was not observed (Figures S3C and S3D; Movie S5, third and fourth sections). The lack of full migration of somatic cells provided with the PGC-motility module highlights the relevance of the initial state of the cell with respect to this property. This phenomenon is analogous to that observed in reprogramming cell fate, where the initial cellular state determines the response of cells to the relevant manipulations (Hanna et al., 2010).

In conclusion, we have demonstrated that a proper regulation of three biophysical parameters is sufficient to reverse the immotile state of PGCs lacking Dnd. Intriguingly, these parameters were sufficient to induce cell-shape changes and protrusive activity, characteristic of motile single cells, also in cells that normally do not show this behavior. The identification of this set of requirements for single-cell motility is relevant for processes in normal development when cells delaminate from their tissue of origin, as well as in disease conditions (Baum et al., 2008; Clay and Halloran, 2011). For example, gene expression profiles of cancer cells revealed upregulation of RNAs encoding for proteins controlling contractility, coinciding with downregulation of genes controlling cell adhesion and membrane to cortex attachment (e.g., microarray profile GDS2545 in Yu et al., 2004, GDS2618 in Kreike et al., 2006, and GDS1965 in Hoek et al., 2004). Studying the biophysical aspects governing PGC motility and the regulation of these cellular properties is thus likely to shed light on a range of processes where single-cell migration is involved.

## EXPERIMENTAL PROCEDURES

### Zebrafish Strains

Zebrafish (*Danio rerio*) of the AB background and transgenic fish carrying the *Tol-kop-egfp-f-nanos* -3′ UTR transgene (Blaser et al., 2005) were used as wild-type fish. MZ*dicer* mutant embryos (Giraldez et al., 2005) were used to examine the effect of lack of mature miRNAs. The zebrafish were handled according to the law of the state of North Rhine-Westphalia, supervised by the veterinarian office of the city Münster.

### RNA Expression Constructs and Injections

Capped sense mRNA was synthesized using the mMessageMachine kit (Ambion). One and a half to 2 nanoliters were microinjected into the yolk of 1-cell stage embryos, unless stated otherwise.

The zebrafish ORF and 3′ UTR of *mlck* (NM_001105682) and *zeb1* (NM_131709) were amplified from zebrafish cDNA and cloned into expression vectors.

To direct protein expression to the germ cells, the ORFs were fused to *nanos* 3′ UTR, or to their own 3′ UTR to mimic the endogenous protein expression. A list of constructs is provided in the Supplemental Experimental Procedures.

### Cortex Ablation Experiments

Ablation experiments were performed using a setup described before (Maghelli and Tolić-Nørrelykke, 2008) on PGCs of 7–8 hpf embryos. Defined circular region of interest centered immediately internal to the membrane was ablated.

### Pixel Intensity Measurements

Ratio of mGFP/mCherry and Venus/SECFP were performed as previously described (Kedde et al., 2007).

### Motility Induction

Embryos were injected with 600 pg of *control* or *dnd* MO together with 400 pg of *mlck.mlck*3′UTRmiRmut1;2;3 or PA-*gfp.globin*3′ UTR as control to demonstrate bleb formation in *dnd*-morpholino-treated PGCs. For manipulation of MLCK and E-cadherin, 400 pg of DN *EcdhΔEC1-2.nanos* 3′ UTR and 400 pg *mlck.mlck*3′UTR miRmut1;2;3, or 800 pg of a control RNA (PA-*gfp*.globin3′UTR) were used. PGCs membranes were labeled with enhanced green fluorescent protein (EGFP) and all cells membranes were labeled with mCherry (Figures 4A–4D).

Manipulation of MLCK, E-cadherin, and Annexin A5b levels was performed by injecting 800 pg of *mlck* TP1, *zeb1* TP, 400 pg of *mlck* TP2 and TP3, 800 pg of *annexin* A5b MO1 or MO2, and 2 ng of *p53* MO into embryos knocked down for Dnd. Membrane of PGCs labeled with EGFP and all nuclei were labeled with H2B-mCherry (Figures 4E and 4F). The effect of this mixture

without p53 morpholino on somatic cell behavior (Figures S3C and S3D) was examined by injecting half of the above amounts into one of the four central cells of the 16-cell stage embryos whose cell membranes was labeled with EGFP.

## SUPPLEMENTAL INFORMATION

Supplemental Information includes three figures, Supplemental Experimental Procedures, and five movies and can be found with this article online at doi:10.1016/j.devcel.2012.05.007.

## ACKNOWLEDGMENTS

This work was supported by grants from the DFG, ERC, and HFSP to E.R. and funds from the Max-Planck Society to E.R. and I.M.T.-N. The Polish Ministry of Science and Higher Education supported E.P. We thank Michal Reichman-Fried for critical comments on the manuscript and Anne Albers, Esther-Maria Messerschmidt, Ursula Jordan, and Ines Sandbote for technical support.

Received: November 16, 2011
Revised: April 21, 2012
Accepted: May 10, 2012
Published online: June 14, 2012

## REFERENCES

Ahn, S.M., Cha, J.Y., Kim, J., Kim, D., Trang, H.T., Kim, Y.M., Cho, Y.H., Park, D., and Hong, S. (2011). Smad3 regulates E-cadherin via miRNA-200 pathway. Oncogene. Published online October 24, 2011. 10.1038/onc.2011.484.

Babiychuk, E.B., Palstra, R.J., Schaller, J., Kämpfer, U., and Draeger, A. (1999). Annexin VI participates in the formation of a reversible, membrane-cytoskeleton complex in smooth muscle cells. J. Biol. Chem. *274*, 35191–35195.

Baum, B., Settleman, J., and Quinlan, M.P. (2008). Transitions between epithelial and mesenchymal states in development and disease. Semin. Cell Dev. Biol. *19*, 294–308.

Blaser, H., Eisenbeiss, S., Neumann, M., Reichman-Fried, M., Thisse, B., Thisse, C., and Raz, E. (2005). Transition from non-motile behaviour to directed migration during early PGC development in zebrafish. J. Cell Sci. *118*, 4027–4038.

Blaser, H., Reichman-Fried, M., Castanon, I., Dumstrei, K., Marlow, F.L., Kawakami, K., Solnica-Krezel, L., Heisenberg, C.P., and Raz, E. (2006). Migration of zebrafish primordial germ cells: a role for myosin contraction and cytoplasmic flow. Dev. Cell *11*, 613–627.

Boldajipour, B., Mahabaleshwar, H., Kardash, E., Reichman-Fried, M., Blaser, H., Minina, S., Wilson, D., Xu, Q., and Raz, E. (2008). Control of chemokine-guided cell migration by ligand sequestration. Cell *132*, 463–473.

Borregaard, N. (2010). Neutrophils, from marrow to microbes. Immunity *33*, 657–670.

Bouter, A., Gounou, C., Bérat, R., Tan, S., Gallois, B., Granier, T., d'Estaintot, B.L., Pöschl, E., Brachvogel, B., and Brisson, A.R. (2011). Annexin-A5 assembled into two-dimensional arrays promotes cell membrane repair. Nat. Commun. *2*, 270.

Brabletz, S., and Brabletz, T. (2010). The ZEB/miR-200 feedback loop—a motor of cellular plasticity in development and cancer? EMBO Rep. *11*, 670–677.

Charras, G., and Paluch, E. (2008). Blebs lead the way: how to migrate without lamellipodia. Nat. Rev. Mol. Cell Biol. *9*, 730–736.

Charras, G.T., Yarrow, J.C., Horton, M.A., Mahadevan, L., and Mitchison, T.J. (2005). Non-equilibration of hydrostatic pressure in blebbing cells. Nature *435*, 365–369.

Choi, W.Y., Giraldez, A.J., and Schier, A.F. (2007). Target protectors reveal dampening and balancing of Nodal agonist and antagonist by miR-430. Science *318*, 271–274.

Clay, M.R., and Halloran, M.C. (2011). Regulation of cell adhesions and motility during initiation of neural crest migration. Curr. Opin. Neurobiol. *21*, 17–22.

Diz-Muñoz, A., Krieg, M., Bergert, M., Ibarlucea-Benitez, I., Muller, D.J., Paluch, E., and Heisenberg, C.P. (2010). Control of directed cell migration in vivo by membrane-to-cortex attachment. PLoS Biol. *8*, e1000544.

Doitsidou, M., Reichman-Fried, M., Stebler, J., Köprunner, M., Dörries, J., Meyer, D., Esguerra, C.V., Leung, T., and Raz, E. (2002). Guidance of primordial germ cell migration by the chemokine SDF-1. Cell *111*, 647–659.

Fackler, O.T., and Grosse, R. (2008). Cell motility through plasma membrane blebbing. J. Cell Biol. *181*, 879–884.

Friedl, P., and Gilmour, D. (2009). Collective cell migration in morphogenesis, regeneration and cancer. Nat. Rev. Mol. Cell Biol. *10*, 445–457.

Gerke, V., and Moss, S.E. (2002). Annexins: from structure to function. Physiol. Rev. *82*, 331–371.

Giraldez, A.J., Cinalli, R.M., Glasner, M.E., Enright, A.J., Thomson, J.M., Baskerville, S., Hammond, S.M., Bartel, D.P., and Schier, A.F. (2005). MicroRNAs regulate brain morphogenesis in zebrafish. Science *308*, 833–838.

Hanna, J.H., Saha, K., and Jaenisch, R. (2010). Pluripotency and cellular reprogramming: facts, hypotheses, unresolved issues. Cell *143*, 508–525.

Hoek, K., Rimm, D.L., Williams, K.R., Zhao, H., Ariyan, S., Lin, A., Kluger, H.M., Berger, A.J., Cheng, E., Trombetta, E.S., et al. (2004). Expression profiling reveals novel pathways in the transformation of melanocytes to melanomas. Cancer Res. *64*, 5270–5282.

Jeanes, A., Gottardi, C.J., and Yap, A.S. (2008). Cadherins and cancer: how does cadherin dysfunction promote tumor progression? Oncogene *27*, 6920–6929.

Kardash, E., Reichman-Fried, M., Maitre, J.L., Boldajipour, B., Papusheva, E., Messerschmidt, E.M., Heisenberg, C.P., and Raz, E. (2010). A role for Rho GTPases and cell-cell adhesion in single-cell motility in vivo. Nat. Cell Biol. *12*, 47–53, suppl. 1–11.

Kedde, M., Strasser, M.J., Boldajipour, B., Oude Vrielink, J.A., Slanchev, K., le Sage, C., Nagel, R., Voorhoeve, P.M., van Duijse, J., Ørom, U.A., et al. (2007). RNA-binding protein Dnd1 inhibits microRNA access to target mRNA. Cell *131*, 1273–1286.

Kreike, B., Halfwerk, H., Kristel, P., Glas, A., Peterse, H., Bartelink, H., and van de Vijver, M.J. (2006). Gene expression profiles of primary breast carcinomas from patients at high risk for local recurrence after breast-conserving therapy. Clin. Cancer Res. *12*, 5705–5712.

Lehmann, R., and Nüsslein-Volhard, C. (1991). The maternal gene nanos has a central role in posterior pattern formation of the Drosophila embryo. Development *112*, 679–691.

Lorentzen, A., Bamber, J., Sadok, A., Elson-Schwab, I., and Marshall, C.J. (2011). An ezrin-rich, rigid uropod-like structure directs movement of amoeboid blebbing cells. J. Cell Sci. *124*, 1256–1267.

Maghelli, N., and Tolić-Nørrelykke, I.M. (2008). Versatile laser-based cell manipulator. J. Biophotonics *1*, 299–309.

Málaga-Trillo, E., Solis, G.P., Schrock, Y., Geiss, C., Luncz, L., Thomanetz, V., and Stuermer, C.A. (2009). Regulation of embryonic cell adhesion by the prion protein. PLoS Biol. *7*, e55.

Mishima, Y., Giraldez, A.J., Takeda, Y., Fujiwara, T., Sakamoto, H., Schier, A.F., and Inoue, K. (2006). Differential regulation of germline mRNAs in soma and germ cells by zebrafish miR-430. Curr. Biol. *16*, 2135–2142.

Muraoka, O., Ichikawa, H., Shi, H., Okumura, S., Taira, E., Higuchi, H., Hirano, T., Hibi, M., and Miki, N. (2000). Kheper, a novel ZFH/deltaEF1 family member, regulates the development of the neuroectoderm of zebrafish (Danio rerio). Dev. Biol. *228*, 29–40.

Peinado, H., Olmeda, D., and Cano, A. (2007). Snail, Zeb and bHLH factors in tumour progression: an alliance against the epithelial phenotype? Nat. Rev. Cancer *7*, 415–428.

Raz, E. (2004). Guidance of primordial germ cell migration. Curr. Opin. Cell Biol. *16*, 169–173.

Rescher, U., and Gerke, V. (2004). Annexins—unique membrane binding proteins with diverse functions. J. Cell Sci. *117*, 2631–2639.

Richardson, B.E., and Lehmann, R. (2010). Mechanisms guiding primordial germ cell migration: strategies from different organisms. Nat. Rev. Mol. Cell Biol. *11*, 37–49.

Robu, M.E., Larson, J.D., Nasevicius, A., Beiraghi, S., Brenner, C., Farber, S.A., and Ekker, S.C. (2007). p53 activation by knockdown technologies. PLoS Genet. *3*, e78.

Rørth, P. (2009). Collective cell migration. Annu. Rev. Cell Dev. Biol. *25*, 407–429.

Roussos, E.T., Condeelis, J.S., and Patsialou, A. (2011). Chemotaxis in cancer. Nat. Rev. *11*, 573–587.

Sedzinski, J., Biro, M., Oswald, A., Tinevez, J.Y., Salbreux, G., and Paluch, E. (2011). Polar actomyosin contractility destabilizes the position of the cytokinetic furrow. Nature *476*, 462–466.

Slanchev, K., Stebler, J., Goudarzi, M., Cojocaru, V., Weidinger, G., and Raz, E. (2009). Control of Dead end localization and activity—implications for the function of the protein in antagonizing miRNA function. Mech. Dev. *126*, 270–277.

Solnica-Krezel, L. (2005). Conserved patterns of cell movements during vertebrate gastrulation. Curr. Biol. *15*, R213–R228.

Stewart, M.P., Helenius, J., Toyoda, Y., Ramanathan, S.P., Muller, D.J., and Hyman, A.A. (2011). Hydrostatic pressure and the actomyosin cortex drive mitotic cell rounding. Nature *469*, 226–230.

Tinevez, J.Y., Schulze, U., Salbreux, G., Roensch, J., Joanny, J.F., and Paluch, E. (2009). Role of cortical tension in bleb growth. Proc. Natl. Acad. Sci. USA *106*, 18581–18586.

Ulrich, F., Krieg, M., Schötz, E.M., Link, V., Castanon, I., Schnabel, V., Taubenberger, A., Mueller, D., Puech, P.H., and Heisenberg, C.P. (2005). Wnt11 functions in gastrulation by controlling cell cohesion through Rab5c and E-cadherin. Dev. Cell *9*, 555–564.

Weidinger, G., Stebler, J., Slanchev, K., Dumstrei, K., Wise, C., Lovell-Badge, R., Thisse, C., Thisse, B., and Raz, E. (2003). *dead end*, a novel vertebrate germ plasm component, is required for zebrafish primordial germ cell migration and survival. Curr. Biol. *13*, 1429–1434.

Yu, Y.P., Landsittel, D., Jing, L., Nelson, J., Ren, B., Liu, L., McDonald, C., Thomas, R., Dhir, R., Finkelstein, S., et al. (2004). Gene expression alterations in prostate cancer predicting tumor aggression and preceding development of malignancy. J. Clin. Oncol. *22*, 2790–2799.

Development 137, 1939-1952 (2010) doi:10.1242/dev.044511


# Moving away from the midline: new developments for Slit and Robo

**Athena R. Ypsilanti[1,2,3], Yvrick Zagar[1,2,3] and Alain Chédotal[1,2,3,*]**

## Summary

In most tissues, the precise control of cell migration and cell-cell interaction is of paramount importance to the development of a functional structure. Several families of secreted molecules have been implicated in regulating these aspects of development, including the Slits and their Robo receptors. These proteins have well described roles in axon guidance but by influencing cell polarity and adhesion, they participate in many developmental processes in diverse cell types. We review recent progress in understanding both the molecular mechanisms that modulate Slit/Robo expression and their functions in neural and non-neural tissue.

**Key words: Axon guidance, Cell migration, Cell-cell interaction**

## Introduction

In most organisms, the central nervous system (CNS) develops along a bilateral axis of symmetry located at the midline (Placzek and Briscoe, 2005). During development, the ventral midline or floor plate acts as an organiser through the secretion of diffusible proteins (Placzek and Briscoe, 2005; Gore et al., 2008), which control the growth of axons and dendrites and the migration of neurons across the midline. In the forebrain, glial or neuronal cells delineate the midline (see Glossary, Box 1) and also control axon guidance. For more than two decades, many developmental neurobiologists have tried to understand the mechanisms that control midline crossing in the CNS and to answer some key questions. Firstly, how are commissural axons (see Glossary, Box 1) attracted to the midline and how do their growth cones (see Glossary, Box1) receive and integrate the multiple and contrasting signals released by midline cells? Secondly, what are the molecular and signalling changes that enable commissural axons to leave the midline and often to switch to a longitudinal growth mode? All midline-derived axon guidance factors are expressed at other locations in many developing and mature tissues, where they control a wide range of biological processes.

Roundabout receptors (Robo) and their Slit ligands form one of the most crucial ligand-receptor pairings among the axon guidance molecules. Robos were identified in *Drosophila* in a mutant screen for genes that control the midline crossing of commissural axons (Kidd et al., 1998; Seeger et al., 1993). Similarly, Slit was discovered in *Drosophila* as a protein secreted by midline glia (Rothberg et al., 1988; Rothberg et al., 1990). Homologues of both proteins have since been discovered in many species (for a review, see Chédotal, 2007). However, the Slit/Robo couple not only functions in axon guidance but also in a variety of developmental

[1]INSERM, U968, Paris F-75012, France. [2]UPMC Univ Paris 06, UMR_S 968, Institut de la Vision, 17 rue Moreau, Paris F-75012, France. [3]CNRS, UMR_7210, Paris F-75012, France.

*Author for correspondence (alain.chedotal@inserm.fr)

**Box 1. Glossary**

**Choroid plexus** Specialised ependymal cells located inside the ventricles of the brain that secrete cerebrospinal fluid.

**Commissural axons** Axons with cell bodies (somata) located on one side of the central nervous system (CNS) that project axons across the midline to contact target cells on the opposite side.

**Growth cone** A specialised bulbous enlargement at the end of growing axons that is characterised by dynamic filamentous extensions, known as filopodia. They sense the environment and respond to adhesion and guidance molecules.

**Inferior olive (IO)** A characteristic olive-shaped nucleus of the medulla oblongata (a region of the brainstem located above the spinal cord) involved in motor learning. Neurons of the IO project to Purkinje cells in the cerebellar cortex. The terminal axonal arborisation of IO axons is called a climbing fibre.

**Midline** An imaginary line that runs along the longitudinal axis of the CNS and delineates the axis of symmetry. In the midbrain, hindbrain and spinal cord, the ventral midline is called the floor plate and the dorsal midline, the roof plate.

**Mossy fibers** Axons originating from several hindbrain and spinal cord nuclei that synapse onto granule cell dendrites in the cerebellar cortex.

**Myotopic map** A particular type of topographic map in which muscle fibers project to neurons of the peripheral nervous system in an ordered manner to create a structured projection pattern.

**Netrin/Dcc** Netrins are axon guidance proteins best known for their role in the development of commissural tracts. Deleted in colorectal cancer (Dcc) is a transmembrane receptor for netrin 1 that mediates its chemoattractive action.

**Neuroblast** A neuronal progenitor cell that originates in the subventricular zone and that migrates along the rostral migratory stream towards the olfactory bulb, where it differentiates into olfactory interneurons.

**Olfactory bulb** An anterior protrusion of the brain to which olfactory and vomeronasal sensory neurons project, and from which the olfactory tract originates.

**Overlay assay** A technique in which immobilised proteins or cells are incubated with a protein of interest that is labelled to identify binding sites and measure binding affinity.

**Pontine nucleus (PN) neurons** A major source of mossy fiber axons. The cell bodies of PN neurons are located in the basilar pons, a structure of the ventral midbrain.

**Radial migration** A type of neuronal migration during which neurons migrate perpendicular to the brain surface and follow radial glia processes.

**Septum** A region of the forebrain comprising several nuclei that have afferent and cholinergic efferent connections with various forebrain and brainstem areas. It secretes Slit proteins, which might contribute to repelling neuroblasts towards the olfactory bulb.

**Subventricular zone** A brain structure located along the walls of the lateral ventricles. It is one of two regions in the adult mammalian brain where neurogenesis occurs.

**Tangential migration** A type of migration during which neurons migrate parallel to the surface of and independently of radial glia.

processes outside of the midline and the CNS. As such, it is insightful to explore the roles of Slit/Robo in different systems and to contrast their modes of action. Moreover, in this review, we delve into some of the mechanisms of Robo regulation and signalling that vary tremendously from one region to another. Although we focus on recent findings discovered in vertebrates, we also mention relevant studies in invertebrates where appropriate.

## Robo and Slit structure

Robo receptors belong to the immunoglobulin (Ig) superfamily of cell adhesion molecules (CAMs) and, as with other IgCAMs, they can mediate homophilic and heterophilic interactions (Hivert et al., 2002). In most vertebrates, there are three Robo receptors expressed in brain cells (Chédotal, 2007). In zebrafish and mammals, a fourth Robo receptor, Robo4, is expressed by endothelial cells and functions in angiogenesis (Bedell et al., 2005; Jones et al., 2008); this receptor will not be discussed further here. The standard/archetypical Robo receptor contains five Ig motifs, three fibronectin type III domains and four conserved cytoplasmic domains, expressed in different combinations within the Robo receptor family (Fig. 1).

All Robo receptors can be alternatively spliced to generate various isoforms. Alternative splicing in the 5′ coding sequence can generate two distinct receptor isoforms, A and B, which differ at their N-terminal end. Type A isoforms are longer (16-40 residues) than type B isoforms (Camurri et al., 2005; Kidd et al., 1998; Sundaresan et al., 1998; Yue et al., 2006). In the case of Robo3, alternative splicing by the retention or excision of one intron in the 3′ coding sequence generates two isoforms that differ in their C-terminal domain, with Robo3.1 being longer than Robo3.2 (Chen et al., 2008a). For more information on the structure of Robo receptors, we refer readers to a recent review by Chédotal (Chédotal, 2007).

Slits are the principal ligands for the Robo receptors (Kidd et al., 1999). Slit was originally discovered in *Drosophila* (Rothberg et al., 1988; Rothberg et al., 1990), and its homologues have since been discovered in several species, including worms, teleosts and mammals (Chédotal, 2007). In mammals, there are three Slit genes, all of which are expressed in the nervous system and in most organs (Marillat et al., 2002). Slits are secreted glycoproteins that possess the following general structure: an N-terminal signal peptide, four domains (D1-D4) containing leucine-rich repeats (LRR), several EGF-like sequences, a laminin-G domain and a C-terminal cysteine-rich knot (see Fig. 1). Slits can be cleaved to yield a short C-terminus fragment of unknown function and a long N-terminus fragment that is active and mediates binding to Robos (Nguyen Ba-Charvet et al., 2001; Wang et al., 1999).

Analysis of the Slit LRR regions has demonstrated that *Drosophila* Robo receptors bind to a common site located within the D2 region of Slit (Howitt et al., 2004). Moreover, Robos bind

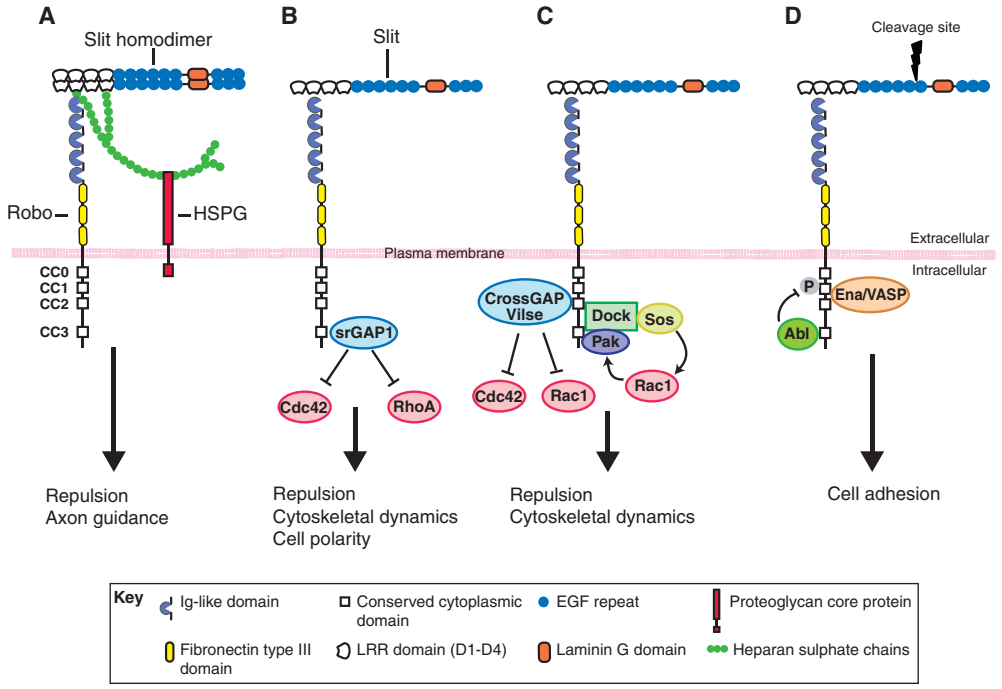


**Fig. 1. Slit-Robo signalling.** A schematic of Slit-Robo signalling. (**A**) Slits bind to the immunoglobulin (Ig) 1 domain of Robo receptors through its second (D2) domain, which contains leucine-rich repeats (LRRs). Heparan sulphate proteoglycans (HSPGs) such as syndecan (Sdc), which consist of a proteoglycan core protein and heparan sulphate (HS) chains, are co-receptors for Robo and Slit. HSPGs stabilise Robo and Slit binding by forming ternary complexes with the Ig1 domain of Robo receptors and the D2 domain of Slit through their HS polymers. (**B**) The Rho GTPases and their regulators (GAPs and GEFs) are key components of the Slit-Robo signalling pathway. In the presence of Slit, Slit-RoboGAP1 (srGAP1) binds to the CC3 domain of Robo and inactivates RhoA and Cdc42. These effector proteins are able to mediate, among other outcomes, repulsion, control of cytoskeletal dynamics and cell polarity. (**C**) In the presence of Slit, Vilse/CrossGAP can also bind to the CC2 domain of Robo and inhibit Rac1 and Cdc42. Rac1 is also activated by the recruitment of the GEF protein Son of sevenless (Sos) via the adaptor protein Dreadlocks (Dock), which binds to the CC2-3 domain of Robo. This activates the downstream target of Rac1 and p21-activated kinase (Pak), which also binds to Robo CC2-3 domains. These downstream signalling partners of Robo control repulsion and cytoskeletal dynamics. (**D**) The tyrosine kinase Abelson (Abl) binds Robo CC3 domain and antagonises Robo signalling through phosphorylation of the CC1 domain and mediates cell adhesion. Enabled (Ena) a substrate of Abl also binds Robo CC1 and CC2 domains. The slit cleavage site is also shown.

to Slits through their Ig1 and Ig2 domains (Liu et al., 2004). The resolution of the structure of a minimal Slit-Robo complex revealed that the Ig1 domain of Robo1 is bound by the concave face of Slit-D2, and that the binding residues of the Slit LRR2 domain are highly conserved among all Slits across species, as are those of the Robo Ig1 domain (Morlot et al., 2007). This conservation could explain the promiscuous binding of Slit ligands to Robo receptors that has been previously described using overlay assays (see Glossary, Box 1) (Brose et al., 1999; Sabatier et al., 2004). Although Slit does not always bind to Robo as a dimer, heparan sulphate proteoglycans (HSPGs) have been shown to stabilise the Slit homodimer through the interaction of heparan sulphates (HSs) with the D4 domain of Slit, which furthermore seems to potentiate Slit activity (Seiradake et al., 2009).

However, Slit is not the only ligand for Robo and vice versa. In *Caenorhabditis elegans*, SLT-1/Slit also binds to the EVA-1 transmembrane protein that has homologues in mammals (Fujisawa et al., 2007). Likewise, biochemical and genetic data demonstrate that an interaction occurs between the LRR tendon-specific protein (LRT) and Robo, highlighting a mechanism by which LRT can modulate Robo-Slit interactions and influence muscle cell migration (Wayburn and Volk, 2009). Moreover, as we discuss below, several studies have identified HSPGs as co-receptors for Slits that are necessary for Slit-Robo signalling (Hu, 2001; Steigemann et al., 2004). Recent structural analysis has revealed that Slit/Robo form a ternary complex with a heparin/HS that stabilises and strengthens the Slit-Robo interaction (Fukuhara et al., 2008; Hussain et al., 2006). And, as mentioned above, structural studies have also shown that the Slit D4 region binds HS and promotes Slit homodimerisation (Seiradake et al., 2009).

## A ménage à trois with heparan sulphates

HSPGs are proteoglycan core proteins attached to HS chains, which are either membrane bound, like syndecans (Sdc) and glypicans, or secreted, like perlecan and agrin. Modifications of the heparan polymers by epimerisation or sulphation generate many distinct HS isoforms. HSPGs have a dual role: as regulators of cell adhesion, as they can bind to other components in the extracellular space; and as signalling molecules, because they can act as co-receptors (Johnson et al., 2006; Lee and Chien, 2004; Van Vactor et al., 2006).

HSPGs have been implicated in Slit/Robo signalling in various studies over the years. For example, the enzymatic removal of HS along the optic tract of developing *Xenopus* embryos induces guidance defects in retinal axons (Walz et al., 1997). HSPG removal also decreases the affinity of Slit2 for Robo and abolishes the repulsive activity of Slit2 on rat olfactory axons in vitro (Hu, 2001). Slit2 also binds to glypican 1 (Ronca et al., 2001). In addition, when heparan sulphates are disrupted, Slit2 fails to repel *Xenopus* retinal axons (Piper et al., 2006). In zebrafish, dopaminergic axons are surrounded by HS, and their removal enhances the mis-positioning of this longitudinal tract in *Robo2/astray* mutants (Kastenhuber et al., 2009). In addition, the ablation of exostosin 1 (*Ext1*), which encodes a glycosyltransferase involved in HSPG synthesis, induces defects at the mouse optic chiasm, which resemble those observed in *Slit1/Slit2* double-knockout mice (Inatani et al., 2003; Plump et al., 2002). Furthermore, Slit and Ext1 have been shown genetically to interact (Inatani et al., 2003). In *Drosophila*, the transmembrane HSPG Sdc interacts with Robo and Slit, and contributes to the Slit-dependent repulsion of axons at the CNS midline (Johnson et al., 2004; Steigemann et al., 2004). The extracellular domain of Sdc can be proteolytically cleaved and shed as a soluble proteoglycan (Fitzgerald et al., 2000), which is necessary and sufficient to mediate Slit signalling in target cells (Chanana et al., 2009). The enzymatic modification of HS is also important for Slit activity, and *O*-sulphation of glypican 1 significantly potentiates Slit2 binding in human embryonic kidney 293 cells (Ronca et al., 2001). Recent genetic data in *C. elegans* strongly suggest that HS *O*-sulphation of LON-2/glypican regulates motor axon guidance, probably by modulating SLT-1/Slit binding to EVA-1, and its interaction with SAX-3/Robo (Bulow et al., 2008; Fujisawa et al., 2007). So far, HSPGs have been shown to mostly affect the functions of Slit/Robo in axon guidance. As discussed in the following sections, other molecules also interact with Robos and Slits and their downstream effectors to influence cell migration.

## Slit and Robo in cell migration

### Repulsion and cell polarity

In most developing tissues, cells migrate in a precise direction, following stereotyped pathways under the influence of repulsive and attractive factors. In vertebrates, two main types of neuronal migration have been described: radial migration (see Glossary, Box 1) and tangential migration (see Glossary, Box 1). As discussed below, Slit/Robo repulsion influences tangential migration in several systems (Andrews et al., 2008; Metin et al., 2008).

Slit/Robo function in tangential neuronal migration was first shown in the mouse forebrain, where Slit1 and Slit2, secreted from the choroid plexus and septum (see Glossary, Box 1), repel neuroblasts (see Glossary, Box 1) derived from the subventricular zone (see Glossary, Box 1), thus guiding them towards the olfactory bulb (see Glossary, Box 1) (Hu, 1999; Nguyen-Ba-Charvet et al., 2004; Sawamoto et al., 2006; Wu et al., 1999).

Slit/Robo repulsion also orchestrates tangential migration in the mouse hindbrain. Hindbrain precerebellar nuclei (see Glossary, Box 1) contain neurons that project to the cerebellum. These neurons are born in the dorsal edges of the neuroepithelium that lines the fourth ventricle (the so-called rhombic lip) and migrate tangentially towards the floor plate under the attractive action of netrin 1 (see Fig. 2) (Bloch-Gallego et al., 1999; Marcos et al., 2009; Sotelo and Chédotal, 2005; Yee et al., 1999). Axons that originate from neurons of the inferior olive (IO; see Glossary, Box 1), the climbing fibers, synapse onto Purkinje cells. All other hindbrain precerebellar neurons, from the pontine nucleus (PN; see Glossary, Box 1), the lateral reticular nucleus (LRN) and the external cuneatus nucleus (ECN), project mossy fibers (see Glossary, Box 1) that synapse onto granule cell dendrites. All hindbrain precerebellar neurons migrate towards the floor plate, but whereas the cell bodies of LRN and ECN neurons cross it, the soma of IO neurons (IONs) and of most PN neurons stop at the midline and only their axons cross the midline (see Fig. 2D).

Migrating precerebellar neurons express all Robo receptors (except Robo4) (Marillat et al., 2002; Marillat et al., 2004; Di Meglio et al., 2008; Geisen et al., 2008). Slits are expressed in the floor plate, the rhombic lip and in several cranial motor nuclei, such as the facial nucleus (Geisen et al., 2008; Gilthorpe et al., 2002; Hammond et al., 2005). In vitro assays had previously shown that Slits can repel migrating precerebellar neurons (Causeret et al., 2002; Causeret et al., 2004; Gilthorpe et al., 2002). Recent studies of Slit and Robo mutant mice have confirmed that Slit/Robo signalling controls the migration of precerebellar neurons in vivo.

In *Robo1/Robo2* double knockouts and to a lesser extent in *Slit1/Slit2* double knockouts, a significant proportion of the somata of IONs do not stop at the floor plate but migrate to the

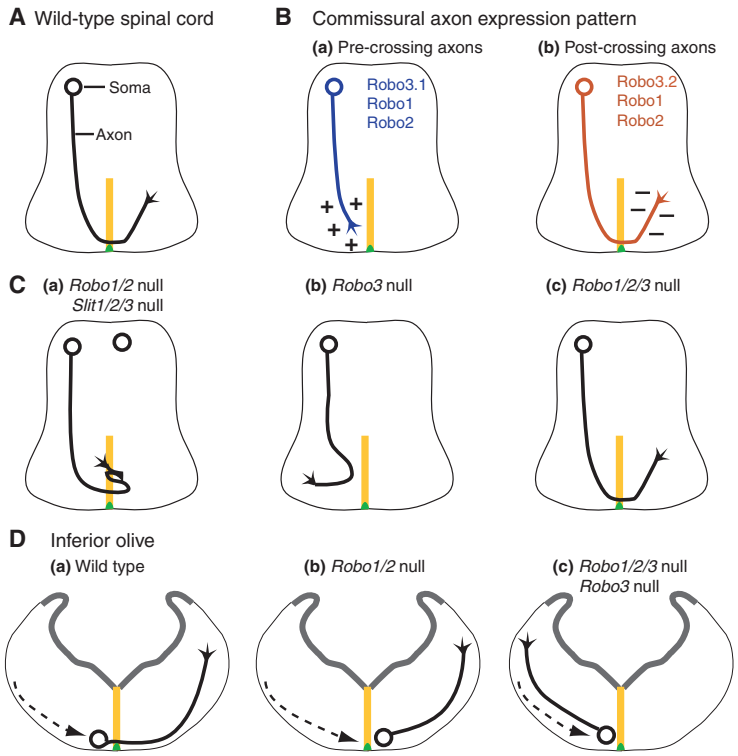


**Fig. 2. Role and mechanism of Slit/Robo action in mouse commissural axons.** Schematics of cross sections of the mouse embryonic spinal cord (A-C) and hindbrain (D), showing the midline (yellow) and floor plate (green). In these schematics, the dorsal region is facing up. (**A**) Commissural axon (black) in the mouse spinal cord of a wild-type adult mouse. (**B**) Spinal commissural axons (blue) grow towards the floor plate (green) under the attractive action (+) of netrin 1 and Shh. (**a**) Before crossing the midline, these axons express Robo1, Robo2 and Robo3.1; Robo3.1 blocks the repulsive activity of Slit. (**b**) After midline crossing, the axons (red) express Robo3.2, a second isoform of Robo3, in place of Robo3.1, which cooperates with Robo1 and Robo2 to repel axons (–) away from the midline. (**C**) Commissural axons in *Slit* and *Robo* knockouts. (**a**) In *Slit* triple and *Robo1/Robo2* double-knockout mice, axons stall at the floor plate and make targeting errors. (**b**) In *Robo3* knockout mice, they are prematurely repelled and fail to cross. (**c**) In *Robo1/Robo2/Robo3* triple knockouts, crossing is restored. (**D**) Development of inferior olive (IO) neurons in the hindbrain of Robo knockouts. (**a**) In wild-type mice, IO neurons migrate from the rhombic lip dorsally (where the arrow begins) towards the midline. Their axons cross the midline but their somata do not. (**b**) In *Robo1/Robo2* double knockouts, IO neurons initially migrate as in wild-type mice but many IO neurons fail to stop prior to reaching the midline and migrate across the midline. (**c**) In *Robo3* knockout mice, both IO neurons and their axons fail to cross the midline, as in the spinal cord. However, unlike in the spinal cord, IO axon midline crossing is not restored in *Robo* triple-knockout mice, indicating that Robo3 does not modulate Robo-dependent repulsion in these neurons.

contralateral side (Fig. 2D). Thus, in these mice the olivary projection is bilateral and not exclusively contralateral, as in wild-type mice. These findings are in agreement with Slit/Robo having a gate-keeper role at the midline, selecting neurons and axons that are allowed to cross it. Interestingly, the migration of PN neurons is also perturbed in these mutants but in a different way. Upon leaving the rhombic lip, PN neurons migrate rostrally across several rhombomeres in a compact stream before turning ventrally towards the midline (Geisen et al., 2008). In *Robo1/Robo2* and *Slit1/Slit2* double knockouts, the stream of PN neurons splits and many neurons prematurely migrate towards the floor plate (Geisen et al., 2008). In this system, the major source of Slit1 and Slit2 seems to be the facial nuclei, rather than the floor plate (Geisen et al., 2008).

At a subcellular level, novel data suggest that Slits control neuronal migration by influencing cell polarity. Calcium ($Ca^{2+}$) signalling and Rho GTPases are known to modulate the radial migration of cortical neurons and cerebellar granule cells (Gomez and Zheng, 2006; Komuro and Rakic, 1996). In granule cell/radial glia co-cultures, the focal application of Slit2 to one pole of the migrating neuron induces an elevation of intracellular $Ca^{2+}$ concentration (Xu et al., 2004), accompanied by a reversal of the direction of migration. Although the signalling pathway activated by Slit2 during repolarisation is still obscure, Slit2 controls the orientation of tangentially migrating rat cerebellar granule cells by inducing a local burst of $Ca^{2+}$ in their leading process and soma. This $Ca^{2+}$ burst redistributes active RhoA from the front of the migrating granule cell to the opposite side, and reverses the direction of migration (see below) (Guan et al., 2007). The forward movement of migrating cells also correlates with the positioning of the centrosome or microtubule organising center (MTOC) at the rostral pole of the cell (Higginbotham and Gleeson, 2007). In migrating mouse SVZ neuroblasts in vitro, a Slit gradient influences cell polarity by controlling the positioning of the centrosome (Higginbotham et al., 2006). In a breast cancer cell line, Slit also seems to primarily act upon cell motility by influencing centrosome movement and cell polarity (Yuasa-Kawada et al., 2009a). Slits also regulate the polarity of murine retinal ganglion cell (RGC) axons (Thompson et al., 2006). During development, axons extend from RGC neurons in a highly polarised fashion, projecting radially towards the optic disc. In *Slit1/Slit2* double-knockout mice, as well as in *Robo2* knockout mice, the initial polarity of RGC axons is abnormal with many axons forming loops in the retina (Thompson et al., 2009; Thompson et al., 2006).

## Cytoskeletal dynamics

The cytoplasmic domains of Robo receptors do not possess autonomous catalytic activities and they must therefore interact with different signalling molecules to exert their specific effects, such as controlling cytoskeletal rearrangements (for reviews, see Chédotal, 2007; O'Donnell et al., 2009). Robo signalling is mediated by a range of secondary molecules and/or co-receptors, such as the netrin 1 receptor Dcc, which binds to the Robo1 CC1 domain (Stein and Tessier-Lavigne, 2001) (see Box 2).

Small GTPases of the Rho family (Heasman and Ridley, 2008), such as RhoA, Rac1 and Cdc42, are key regulators of actin cytoskeletal dynamics. These proteins switch from an inactive GDP-bound state to an active GTP-bound state and are regulated by the GTPase-activating proteins (GAPs) and the guanine nucleotide-exchange factors (GEFs). Downstream of Robo receptors, GAP proteins, such as CrossGAP/Vilse (Hu et al., 2005; Lundstrom et al., 2004) and Slit-RoboGAPs (srGAPs), control cytoskeletal dynamics (Wong et al., 2001), as do GEF proteins like

**Box 2. The netrin/Dcc axon guidance signalling pathway**

Netrins are a family of extracellular guidance molecules that share sequence homology with laminin and that control axon guidance and cell migration. Netrin is also involved in other functional roles, such as tissue morphogenesis, vascular development, cancer and cell survival (Rajasekharan and Kennedy, 2009). In vertebrates, the netrins consist of three secreted proteins, netrin 1, netrin 3 and netrin 4, and two glycosylphosphatidylinositol (GPI)-anchored membrane proteins, netrin G1 and netrin G2 (Cirulli and Yebra, 2007). The secreted netrins can function as either a chemoattractant or a chemorepellent. This dual activity is dependent upon the presence of distinct receptors, cell types and cellular context. Netrin 1 produces attractive effects via receptors of the deleted in colorectal cancer (Dcc) family, which includes the vertebrate-associated receptors Dcc and neogenin (Keino-Masu et al., 1996), the *C. elegans* receptor UNC-40 (Chan et al., 1996) and the Frazzled protein of *Drosophila* (Kolodziej et al., 1996). Netrin 1 mediates repulsive effects through UNC-5 receptors alone or in combination with Dcc (Hong et al., 1999; Keleman and Dickson, 2001). Recently, the Down syndrome cell adhesion molecule (Dscam) has been also identified as a netrin 1 receptor (Ly et al., 2008). Netrins signal via several different transduction pathways, including the small GTPases and various kinases [such as mitogen-activated protein kinase (MAPK), focal adhesion kinase (FAK), Src family kinase and phosphatidylinositol 3-kinase (PI3K)], and also through calcium, cyclic nucleotides, transcription factors, nuclear factor of activated T-cells (NFAT), and Elk1, which contributes to the reorganisation of the cytoskeleton (Barallobre et al., 2005). Although the mechanism remains unclear, Netrin/Dcc activity can also be influenced by the Slit/Robo signalling pathway through the direct interaction of their intracellular domains, which results in the inhibition of netrin attraction (Stein and Tessier-Lavigne, 2001).

Son of sevenless (Sos) (Yang and Bashaw, 2006) (see Fig. 1). Slit-Robo GAP1, 2 and 3 (srGAP1, 2 and 3) were identified in a yeast two-hybrid screen for binding partners of the CC3 domain of Robo1 (Wong et al., 2001). These proteins contain a GAP domain, a SH3 domain (which binds the proline-rich region of Robo1) and a Fes/CIP4 (FCH) homology domain (Wong et al., 2001; Li et al., 2006). SrGAPs are widely expressed in the mouse nervous system (Bacon et al., 2009; Endris et al., 2002; Guerrier et al., 2009; Madura et al., 2004; Waltereit et al., 2008; Yao et al., 2008), and bind to WASP/WAVE proteins, which are involved in actin reorganisation (Soderling et al., 2007; Wong et al., 2001). SrGAP1 mediates the repulsive effect of Slit on migrating subventricular zone-derived neural progenitors, through its GAP domain, by inactivating Cdc42 and RhoA but not Rac1 (Wong et al., 2001). By contrast, SrGAP3 (also known as MEGAP and WRP), mutations in which have been associated with severe mental retardation in humans (Endris et al., 2002) (see also Hamdan et al., 2009), regulates Rac activity and plays a role in neuronal morphogenesis, synaptic plasticity and cell migration (Endris et al., 2002; Soderling et al., 2002; Soderling et al., 2007; Yang et al., 2006). A recent study showed that srGAP2, through its F-BAR (Fes-Cip4–Bin/Amphiphysin/Rsv) domain, is a key regulator of neuronal migration (Guerrier et al., 2009). SrGAP2 promotes neurite extension and branching during mouse cortical development in vivo by generating outward protrusions of the neuronal membrane, thereby inhibiting neuronal migration as observed in vitro in cortical slices. However, it will be important to determine to what extent srGAP functions are associated with Slit/Robo signalling.

## Regulation of cell adhesion

Increasing and recent evidence suggests that Slit and Robo are important regulators of cell adhesion, especially during migration.

Neural crest cells (NCCs) and placodal cells delaminating from the neural tube and epibranchial ectoderm, respectively, migrate along precise pathways in the embryo to generate a variety of structures, such as sensory ganglia and parts of the cardiovascular system (Shiau et al., 2008; Stoller and Epstein, 2005). It had been reported that Slits influence the motility and patterning of NCCs, through a classic repulsive mechanism (De Bellard et al., 2003). Therefore, Slit2 appears to prevent Robo1-expressing trunk NCCs from entering the gut region (De Bellard et al., 2003) and might repel them from the dorsal part of the embryo (Jia et al., 2005). Robo1/Slit2 signalling could also control the migration of cardiac NCCs, as suggested by the fact that Robo1 is expressed in the NCC lineage and by the fact that Slit2 is selectively downregulated in mice deficient for the T-box transcription factor Tbx1. Slit is also downregulated in *Gbx2* (gastrulation brain homeobox 2) knockout mice, and both Tbx1 and Gbx2 control cardiac NCC migration during fourth pharyngeal arch artery formation (Calmont et al., 2009). Some cranial ganglia, such as the trigeminal ganglion, have a mixed origin, containing both placodal cells and NCCs. It was recently shown that during gangliogenesis cross talk occurs between these two cell populations, and that Slit1, secreted by NCCs, promotes the aggregation of Robo2-expressing placodal cells (Shiau et al., 2008). Interestingly, Robo2 function involves the calcium-dependent cell-adhesion molecule N-cadherin, which is also expressed by placodal cells (Shiau and Bronner-Fraser, 2009). N-cadherin is expressed at the surface of placodal cells, and the aggregation of these cells increases upon Slit1 binding to Robo2, although the exact molecular mechanism is unknown (Shiau and Bronner-Fraser, 2009). A similar process could participate in the development of several neuronal cell types, including precerebellar neurons and cerebellar granule cells, which express Robo2, and the migration of which requires N-cadherin (Rieger et al., 2009; Taniguchi et al., 2006).

In vitro studies had previously linked Slit/Robo signalling to N-cadherin and cell adhesion (Rhee et al., 2007; Rhee et al., 2002). These studies reported that the activation of Robo2 by Slit triggers the formation of a quaternary complex, consisting of Robo, Abelson tyrosine kinase (Abl), Cables (a Cdk5 and Abl substrate) and N-cadherin, which leads to the phosphorylation and detachment of β-catenin from N-cadherin to result in the inhibition of cell adhesion. In breast cancer cells, Slit2 overexpression increases proteasomal degradation of β-catenin, but also seems to facilitate/promote its association with E-cadherin (Prasad et al., 2008). Although these studies link Slit/Robo signalling to cell adhesion, this can cause either inhibition or enhancement of cell adhesion depending on the system, and, possibly, on the presence of co-receptors.

An anti-adhesive activity of Slit/Robo signalling has also been reported to function during cardiac tube formation in *Drosophila* (Qian et al., 2005; Santiago-Martinez et al., 2006). In this system, the cardiac lumen forms after the preferential attachment of the dorsal and ventral edges of pairs of cardioblasts, which are aligned in two symmetrical rows along the dorsal midline. It was previously shown that the migration and alignment of cardiac cells is regulated by Slit/Robo repulsion (Qian et al., 2005; Santiago-Martinez et al., 2006; Zmojdzian et al., 2008). More importantly, the lack of contact between the membrane of bilateral pairs of cardioblasts at the lumenal surface involves Slit/Robo signalling,

which, via an autocrine or paracrine action, leads to the selected inhibition of E-cadherin adhesion in this central/luminal domain (Medioni et al., 2008; Santiago-Martinez et al., 2008). In vertebrates, Slit/Robo function was also proposed to contribute to the development of the cardiovascular system (Calmont et al., 2009; Liu et al., 2003), although it is still unknown whether this involves a classic, repulsive, mechanism or cadherin-dependent cell adhesion.

Although, Robo receptors share many structural features and molecular partners, mounting evidence suggests that distinct Robo receptors exert some unique functions. Vertebrate Robo3 provides the best example.

## Vertebrate Robo3: the black sheep of the Robo family?

Vertebrate Robo3 differs from other Robo receptors for several reasons. First, Robo3 shows greater structural heterogeneity; it possesses at least four splice variants and possibly a secreted form (Chen et al., 2008b; Yuan et al., 1999), and in mammals it lacks the CC1 domain (Yuan et al., 1999). Second, mammalian Robo3 has only been detected in the nervous system (Barber et al., 2009; Jen et al., 2004; Marillat et al., 2004; Sabatier et al., 2004). Third, its ability to bind Slits is debated (Camurri et al., 2005; Mambetisaeva et al., 2005), and there is to date no biological response associated with the direct binding of Slit to Robo3. Last, although it primarily controls axon guidance at the midline, Robo3 function is unusual when compared with the functions of the other Robos (Fig. 2).

In the developing spinal cord and hindbrain, Robo3 is expressed at high levels on commissural axons until they have crossed the floor plate (Marillat et al., 2004; Sabatier et al., 2004; Tamada et al., 2008). In *Robo3* knockout mice, most commissural axons fail to cross the midline and neuronal migration across the floor plate is prevented (Marillat et al., 2004; Sabatier et al., 2004; Tamada et al., 2008) (see Fig. 2C). These findings have led to a model in which, before midline crossing, the presence of Robo3 in commissural axons interferes with Slit/Robo repulsion, allowing commissural axons and neurons to progress towards the ventral midline under the action of chemoattractants, such as netrin 1 (Fig. 2A-C). After crossing, Robo3 expression is downregulated, allowing the activation of Robo1 and Robo2 by Slit, which triggers axon repulsion. This model is further supported by the fact that there is axon stalling and errors at the midline in Slit and Robo mutants (Chen et al., 2008b; Long et al., 2004). In addition, crossing is 'partially' restored for commissural axons of the spinal cord in *Robo1/Robo3* double knockouts and in *Robo1/Robo2/Robo3* triple knockouts (Chen et al., 2008b; Sabatier et al., 2004). Likewise, the migration of LRN neurons across the midline is also rescued when Robo1 and Robo2 are deleted in a *Robo3* null background (Di Meglio et al., 2008). Interestingly, in spinal cord commissural axons, two splice variants of Robo3, Robo3.1 and Robo3.2, have opposite actions on commissural axons (Chen et al., 2008b). Robo3.1 is expressed before crossing and seems to inhibit Robo1/Robo2 repulsion, whereas Robo3.2 is expressed after midline crossing and appears to cooperate with Robo1 and Robo2 to repel commissural axons away from the floor plate (see Fig. 2A). However, the mechanism by which Robo3 blocks Slit/Robo signalling is still unknown (Chen et al., 2008b; Sabatier et al., 2004). In addition, the axons of IONs are still unable to cross the midline in *Robo1/Robo2/Robo3* triple knockouts (Di Meglio et al., 2008), indicating that in this system Robo3 functions independently of other Robos (Fig. 2). An alternative model supports a chemoattractive function for Robo3 in commissural axons rather than an anti-repulsive activity (Sabatier et al., 2004); in this model, in the absence of Robo3, commissural axons would fail to be attracted to the floor plate.

Although it is expressed in the forebrain, the function of Robo3 in this region remains mysterious as the main forebrain commissures develop normally in mice and humans deficient for *Robo3* (Haller et al., 2008; Jen et al., 2004; Marillat et al., 2004; Renier et al., 2010). To date, the only evidence that Robo3 possesses any function in this region comes from a study of cortical interneuron migration (Barber et al., 2009). In *Robo3* null mice, but not in *Robo1* or *Robo2* nulls, fewer cortical interneurons are present in the marginal zone of the early cortex, a region in which Slit1 and Slit3 are strongly expressed, indicating that the absence of Robo3 decreases Slit repulsion and allows some neurons to enter the marginal zone. By contrast, forebrain commissures are disorganised in *Slit1/Slit2* and *Robo1/Robo2* simple and double knockouts (Andrews et al., 2006; Bagri et al., 2002; Lopez-Bendito et al., 2007). This suggests that, in mammals, Robo3-independent molecular mechanisms regulate Slit/Robo function, at least in some commissural axons.

Whatever its mechanism of action is, Robo3 deficiency has some profound effects on motor and sensory motor behaviours in mice, zebrafish and humans (Amoiridis et al., 2006; Burgess et al., 2009; Jen, 2008; Jen et al., 2004; Renier et al., 2010). Humans suffering from a rare autosomal recessive disease named 'horizontal gaze palsy with progressive scoliosis' (or HGPPS) carry mutations in *ROBO3*. In HGPPS patients, both the descending corticospinal tract motor projections and the ascending lemniscal sensory projections are abnormally uncrossed (Haller et al., 2008; Jen, 2008). In addition, patients are unable to perform conjugate lateral eye movements (Jen, 2008). Likewise, *robo3/twitch twice* double-mutant zebrafish have defects in eye movements and balance (Burgess et al., 2009). *Robo3* null mice die shortly after birth, precluding behavioural studies. However, recently, a unique genetic tool designed to probe the function of selected hindbrain commissures was generated by crossing a novel *Robo3* conditional-knockout line with transgenic mice expressing Cre recombinase in specific subsets of hindbrain commissural neurons (Renier et al., 2010). In Robo3-deficient lines, commissural axons project ipsilaterally, and this is associated with profound motor, sensory and sensory-motor deficits.

Apart from controlling commissural axon guidance and cell migration, there is evidence that Robo/Slit signalling also controls later aspects of axonal development, as we discuss below.

## A role in axonal targeting

Once they have reached their terminal territory, axons have to find their target cells and form synaptic contacts. In most neuronal systems, axons do not project randomly on target cells but follow a precise spatial pattern that often reflects their respective origins in the brain, and defines so-called topographic maps.

A role for Slits and Robos in axonal targeting has best been described in the mouse olfactory system (Cho et al., 2009). Briefly, in the principal olfactory system, olfactory sensory neurons (OSNs) extend from the olfactory epithelium to the olfactory bulb (OB) where they connect with the major OB output neurons, mitral cells and tufted cells. A distinct feature of the mammalian olfactory system is that all OSNs that express the same odorant receptor converge within each OB on a single glomerulus (Ressler, 1994; Vassar, 1994). In many mammals, an accessory olfactory system exists, which plays an important role in pheromone sensing and

social behaviour (Dulac and Wagner, 2006). In this system, vomeronasal sensory neurons (VSN) of the vomeronasal organ (VNO), project to glomeruli located in the accessory olfactory bulb (AOB). VSNs project in a topographical manner. As such, VSNs that originate in the apical and basal regions of the VNO, project to the anterior and posterior portions of the AOB, respectively (Dulac and Wagner, 2006) (Fig. 3). Slits and Robos have been implicated in controlling the proper targeting of axons in both olfactory systems.

Slits are expressed in a gradient in the AOB, with high expression in the anterior region and low expression posteriorly (Knoll et al., 2003). In addition, Slit1 controls the targeting of basal VSN axons, which show abnormal extension into the anterior AOB in *Slit1* knockouts (Cloutier et al., 2004) (Fig. 3B). Basal VSN axons are also misrouted in *Slit1/Slit2* double-heterozygous mice, but not in *Slit3* knockouts, thus establishing a role for Slit2, in addition to Slit1, in the proper targeting of VSN axons to the AOB (Prince et al., 2009). Although VSNs express both Robo1 and Robo2 receptors, only Robo2 appears to be essential for maintaining proper segregation of VSN axons in the AOB. Indeed, when Robo2 is specifically deleted from VSNs, some of the basal VSN neurons are misrouted into the anterior AOB, indicating that Slit1 function is primarily mediated by Robo2 (Prince et al., 2009).

In mice, OSNs from the dorsomedial epithelium project to dorsally located glomeruli in the OB, and OSNs from the ventrolateral region of the olfactory epithelium (OE) extend to glomeruli more ventrally in the OB (Miyamichi et al., 2005) (Fig. 3C). Robo2 has a graded expression profile in the OE, with highest levels in the dorsomedial region (Cho et al., 2007). In *Robo2* and *Slit1* knockout mice, a subset of OSN axons that normally segregate in a glomerulus located in the dorsal region of the OB form a glomerulus in the ventral region, which indicates that Robo2 and Slit1 are necessary for the proper targeting of OSN axons to their appropriate location within the OB (Cho et al., 2007). In *robo2* mutant zebrafish, glomerular spatial arrangements in the main olfactory system are also impaired (Miyasaka et al., 2005). The mistargeting of OSN axons is even more obvious in *Robo1/Robo2* and *Slit1/Slit2* double-null mice, in which OSNs that express the same odorant receptors project on to multiple glomeruli (Nguyen-Ba-Charvet et al., 2008) (Fig. 3C). Interestingly, Slits and Robos also act on other aspects of the development of the olfactory system, in controlling the migration of OB interneurons (see references above) and in the pathfinding of the axons of OB output neurons (Fouquet et al., 2007; Nguyen-Ba-Charvet et al., 2002).

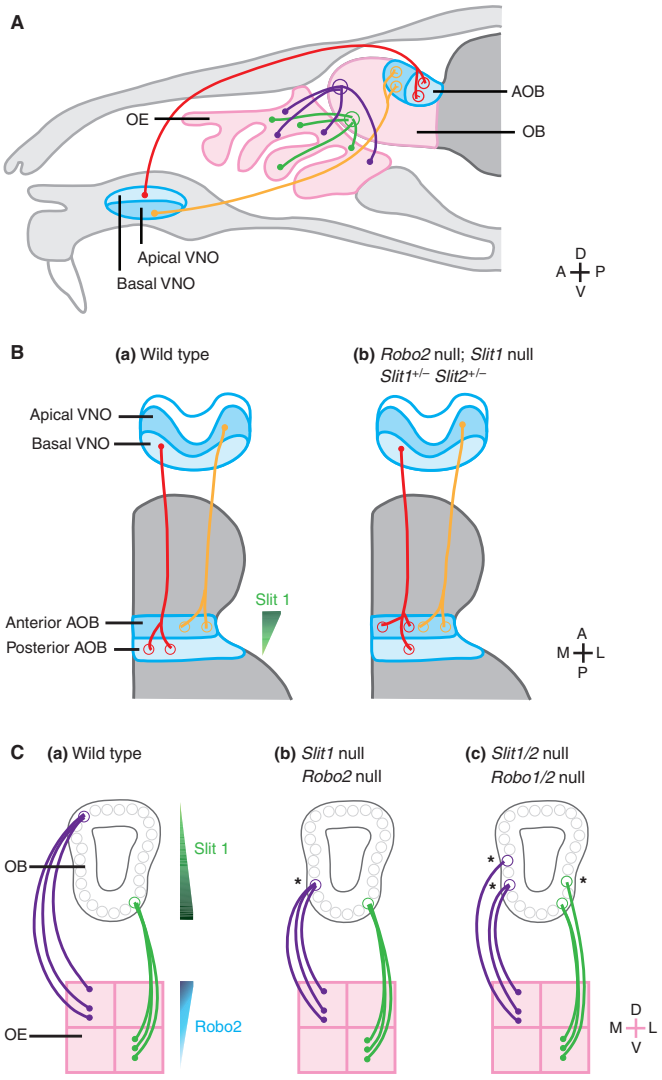


**Fig. 3. The main and accessory olfactory systems in wild-type and *Slit/Robo* knockout mice.** (**A**) A sagittal section through a rodent head, depicting the types of axonal segregation that occur in the main and vomeronasal olfactory systems. In the main olfactory system [shown in pink, consisting of the olfactory bulb (OB) and olfactory epithelium (OE)], olfactory sensory neurons (OSNs) located in the OE that express the same olfactory receptors (ORs, depicted here in purple and green) project to specific glomeruli in the OB. In the accessory olfactory system (shown in blue), vomeronasal sensory neurons (VSNs) located in the apical vomeronasal organ (VNO) (depicted in orange) project to the anterior portion of the accessory olfactory bulb (AOB), and those located in the basal VNO (depicted in red) project to the posterior AOB. (**B**) Depiction of the VNO and the AOB in the horizontal plane. In the AOB, there is a Slit1 (and Slit3) gradient, with high levels in the anterior AOB and lower levels in the posterior AOB. (**a**) In wild-type mice, Robo2-expressing VSNs (depicted here in red and orange) from the basal and apical VNO project to the posterior and anterior AOB, respectively. (**b**) In *Robo2* knockout mice, *Slit1* knockout mice and *Slit1/Slit2* double heterozygous mice, basal VSNs misproject to glomeruli located in the posterior AOB. (**C**) A coronal depiction of the main olfactory system. OSNs (purple and green) from the OE (depicted as a pink box) project to glomeruli (shown as pale grey circles) located within the olfactory bulb. (**a**) In wild type, a Robo2 gradient exists in the main olfactory system, with highest levels in the dorsomedial OE. A Slit1 gradient also exists in the OB, with high levels ventrally and lower levels dorsally. OSNs that express the same OR and that are located in the dorsomedial OE normally project to glomeruli in the dorsal OB. (**b**) In *Robo2* and *Slit1* knockout mice, certain dorsal OSNs project aberrantly to a ventrally located glomerulus (highlighted with an asterisk). (**c**) In *Robo1/Robo2* and *Slit1/Slit2* knockout mice, dorsal and ventral OSNs expressing the same receptor aberrantly project to multiple glomeruli (highlighted with asterisks). A, anterior; D, dorsal; l, lateral; M, medial; P, posterior; V, ventral.

Interestingly, in *Drosophila*, two recent papers have uncovered a similar role for Slit/Robo outside of the nervous system, in the development of a myotopic map (see Glossary, Box 1), in which leg motoneuron dendrites are targeted to their respective muscle field by the combinatorial signalling of Slit/Robo and netrin 1/Frazzled (Brierley et al., 2009; Mauss et al., 2009). It is unclear whether Slit/Robo play a similar role in the targeting of motoneuron dendrites in vertebrates.

## Molecular mechanisms regulating Slit/Robo function

Migrating cells and growing axons often change direction during their journey, and the repertoire of receptors they express at their surface is tightly controlled by the environmental factors they encounter. Accordingly, during mouse development, the expression of Robo receptors is known to be precisely regulated in time and space. By contrast, Slits appear to be expressed in a more stable way in the embryo. Below, we review some of the ways in which transcriptional regulation, receptor transport to the membrane and alternative splicing control the expression of Robo receptors.

### Transcriptional regulation

The transcriptional regulation of Robo receptor expression at the midline contributes to the modulation of axon guidance decisions. The molecular mechanisms that underpin this regulation have remained elusive, but recent studies have identified some of the transcription factors involved.

In *Drosophila,* the protein Midline, which belongs to the T-box family of transcription factors (Stennard and Harvey, 2005), controls the transcription of Robo and Slit along the midline of the central and peripheral nervous systems (Liu et al., 2009). Interestingly, Midline has orthologues in other species, such as Tbx20 in the mouse (Liu et al., 2009). Moreover, this transcription factor is evolutionarily conserved from flies to humans, suggesting that its transcriptional regulation of Robos and Slits is a conserved mechanism (Takeuchi et al., 2005). Accordingly, both *Tbx20* and *Slit1/Slit2* knockout mice have defects in the development of hindbrain motoneurons (Hammond et al., 2005; Song et al., 2006). In the mouse, Tbx1 regulates a second transcription factor, Gbx2, which functions in hindbrain and pharyngeal arch artery (PAA) development (Calmont et al., 2009). In further support of this, the expression of Slit2 and Robo1 is downregulated in the pharyngeal region of *Tbx1* and *Gbx2* null mouse mutants (Calmont et al., 2009). This suggests that these transcription factors directly regulate Slit2 and Robo1 expression, and that Slits and Robos play a role in controlling PAA development.

In the case of Robo3, several transcription factors that could control its expression have been identified. Robo3 was discovered as a gene that is upregulated in retinoblastoma (*Rb*)-deficient mice (Yuan et al., 1999). It was later confirmed that Rb represses *Robo3* promoter activity in vitro but also that Pax2 activates *Robo3* transcription by binding to Rb and thereby inhibiting its repressor function on *Robo3* (Yuan et al., 2002).

*Robo3* expression is also upregulated in a subset of mammillary neurons of the hypothalamus of mouse embryos deficient for the basic helix-loop-helix (bHLH) transcription factors Sim1 and Sim2 (Marion et al., 2005). Interestingly, mammillary axons are rerouted toward the midline in *Sim1/Sim2* null mice, possibly because of abnormal Robo3 expression (Marion et al., 2005).

Different combinations of transcription factors from the LIM homeodomain (LIM-HD) family have been found to confer subtype identity to neurons in which they are expressed; they are also able to control the migration of these neurons (Avraham et al., 2009; Polleux et al., 2007). In the dorsal spinal cord of the mouse, a subset of interneurons, the dI1 neurons, express the two LIM-HD transcription factors, Lhx2 and Lhx9. However, the level of expression of these two factors differs between dI1 interneurons that project ipsilaterally and those that project contralaterally (Wilson et al., 2008). The commissural contingent expresses higher levels of Lhx2 and lower levels of Lhx9 than does the ipsilateral group. In *Lhx2*/*Lhx9* double-null mutants, the fate of dI1 interneurons is not affected, but commissural dI1 neurons fail to express *Robo3*, and, as a result, their axons do not project across the floor plate. In gel shift assays, Lhx2 directly interacts with consensus LIM binding sites in *Robo3*, which indicates that LIM-HD proteins are activators of *Robo3* transcription (Wilson et al., 2008).

The *Hox* genes encode homeodomain-containing transcription factors that control the patterning of the body axis, as well as neuronal specification and connectivity (Dasen et al., 2008). They are highly expressed in the hindbrain in a rhombomere-specific code (Kiecker and Lumsden, 2005). The analysis of pontine neuron development in *Hoxa2* and *Hoxb2* null mice has revealed that their migration is perturbed and that cohorts of neurons abandon the main stream prematurely (Geisen et al., 2008). This phenotype is highly reminiscent of the defects observed in *Robo1/Robo2*, *Slit1/Slit2* and *Robo2/Slit2* double-null mice. This result together with the presence of Hox binding sites in the *Robo2* locus, suggests that Robo genes could be direct targets of Hox transcription factors. This hypothesis is further supported by chromatin immunoprecipitation experiments and the downregulation of *Robo2* expression in *Hoxa2/Hoxb2*-deficient pontine neurons (Geisen et al., 2008). The presence of Hox binding sites in the *Drosophila Robo2* gene suggests that Hox transcription factors might control Robo gene expression in many species and tissues (Kraut and Zinn, 2004).

### Robo receptor transport regulation

In the ventral nerve cord of *Drosophila*, Robo-expressing commissural axons are repelled by Slits secreted at the midline. As pre-crossing commissural axons grow towards the midline, Robo is negatively regulated by the transmembrane protein Commissureless (Comm), which diverts Robo to the endosomes for degradation (Keleman et al., 2002). Upon entering the midline, an unknown mechanism diminishes Comm expression, resulting in increased amounts of Robo at the membrane and, consequently, in the axon being repelled from the midline to prevent it from re-crossing (Keleman et al., 2005). Comm expression can also be regulated in other ways. For instance, a recent study has revealed that Frazzled/Dcc (Fra), in addition to being a receptor for Netrin, can also influence the expression of *comm* mRNA (Yang et al., 2009). In this context, Frazzled concurrently regulates the attraction of commissural axons in response to Netrin and the silencing of repulsive cues by negatively regulating the presence of Robo at the membrane via *comm* expression. This latter function occurs independently of the presence of Netrin. Moreover, other data obtained in *Drosophila* show that the RNA-binding protein Elav (embryonic lethal, abnormal vision) interacts with Robo and Slit in a dose-dependent manner and regulates *comm* mRNA (Simionato et al., 2007).

As a Comm homologue has not been found in vertebrates, it was not clear until recently whether receptor sorting also contributed to the regulation of Robo expression in vertebrates. However, new yeast two-hybrid experiments have identified the ubiquitin-specific protease 33 (Usp33) as a Robo1 partner and have provided in vitro

and in vivo evidence that these two proteins interact (Yuasa-Kawada et al., 2009a; Yuasa-Kawada et al., 2009b). The role of ubiquitin-mediated modification in regulating protein stability and function has been well established (Hershko and Ciechanover, 1998). Upon examining the effect of Usp33 interaction with Robo, it was demonstrated that this de-ubiquitylating enzyme is required for the Slit-responsiveness of commissural neurons and of breast cancer cells (Yuasa-Kawada et al., 2009a; Yuasa-Kawada et al., 2009b). Usp33 mediates both of these functions by either preventing Robo1 from being targeted for degradation or by facilitating its endosomal recycling.

### Slit/Robo and netrin 1/Dcc inter-regulation

Slit/Robo and netrin 1/Dcc (see Box 2) are key components in midline crossing, and there is increasing evidence that their signalling pathways are intertwined and regulate one another at different level. As mentioned above, netrin 1 attracts commissural axons at the midline upon binding to Dcc, whereas Slit repels them after binding Robo1 or Robo2 (Fig. 4A). A genetic study in *Drosophila* using Robo/Dcc chimeras demonstrated that in commissural axons the cytosolic domains of these receptors are the effectors of their attractive or repulsive responses (Bashaw and Goodman, 1999). Moreover, in the presence of Slit, Robo1 binds to Dcc to silence netrin 1 attraction (Stein and Tessier-Lavigne, 2001). Whether Dcc can interact directly with the other Robo receptors to modulate attraction or repulsion is currently unknown. In addition, experiments in *C. elegans* have shown that UNC-40/Dcc participates in SLT-1/SAX-3 signalling in a netrin-independent manner and that this modulation involves UNC-34/Ena. It had been previously shown that UNC-40/Dcc potentiates the netrin 1 repulsion mediated by the receptor UNC-5 (Colavita and Culotti, 1998; Hedgecock et al., 1990; Hong et al., 1999). In

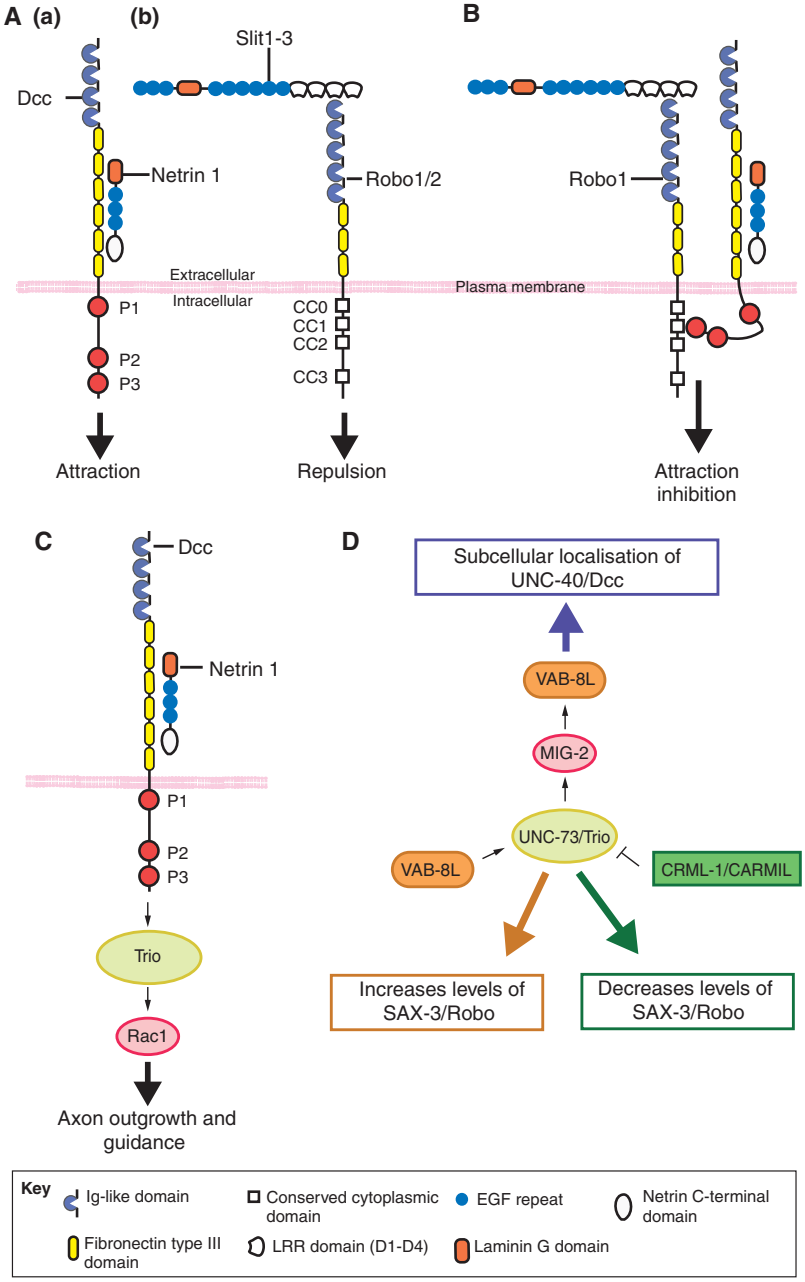


**Fig. 4. Netrin/Dcc and Slit/Robo pathway interactions.** Schematic of the interactions between Netrin/Dcc and Slit/Robo pathways. (**A**, **a**) At the midline, netrin 1 attracts commissural axons through Dcc. (**b**) Conversely, Slit mediates commissural axon repulsion upon binding to Robo1 or Robo2. (**B**) In the presence of Slit and netrin 1, the intracellular domains of Dcc (P3) and Robo1 (CC1) interact, silencing netrin 1 attraction. (**C**) Trio is a GEF that is required during netrin/Dcc signalling to activate Rac1 in mice. (**D**) In *C. elegans*, UNC-73/Trio modulates both UNC-40/Dcc and SAX-3/Robo signalling pathways. UNC-73/Trio targets the Rho GTPase MIG-2 and the kinesin-like protein VAB-8L, which then act as upstream regulators of UNC-40/Dcc to specify its subcellular localisation. However, VAB-8L and CRML-1/CARMIL actively and negatively regulate UNC-73/Trio to induce the up- and downregulation, respectively, of SAX-3/Robo levels at the membrane.

mouse neurons, netrin 1 binding to Dcc induces Rac1 activation in the presence of the RhoGEF Trio protein (Briancon-Marjollet et al., 2008) (Fig. 4C). Moreover, in *C. elegans*, UNC-73, a homologue of Trio, modulates netrin and Slit signalling. Indeed, UNC-73/Trio influences UNC-40/Dcc subcellular localisation by acting through MIG-2, a Rho GTPase, and VAB-8L, a kinesin-like protein (Levy-Strumpf and Culotti, 2007) (Fig. 4D). Likewise, genetic evidence suggests that VAB-8L modulates UNC-73/Trio, which then increases SAX-3/Robo levels at the membrane (Watari-Goshima et al., 2007) (Fig. 4D). By contrast, recent work indicates that UNC-73/Trio can also be negatively regulated by the CRML-1/CARMIL (Capping, Arp2/3, Myosin I Linker) protein. This decreases the levels of SAX-3/Robo at the membrane (Vanderzalm et al., 2009) (Fig. 4D).

Finally, although the effect of netrins and Slits are diametrically opposed, they act together to specify the lateral positioning of dopaminergic axons in the diencephalon (Kastenhuber et al., 2009). In this system, attraction mediated by Dcc/netrin 1 appears to be counterbalanced by Slit/Robo2 signalling (Kastenhuber et al., 2009). Similarly, Robo and Frazzled are required cell autonomously in motoneurons for the appropriate targeting of their neurites to their respective muscle fields; this action is controlled by the combinatorial and opposing actions of Robo and Frazzled (Brierley et al., 2009; Mauss et al., 2009).

## Conclusion

As illustrated here, the range of biological functions that involve the Slits and Robos is much broader than was originally thought. Thus, a major question in this field concerns how different Slits are able to mediate their disparate actions. Slits have been shown to bind with similar affinity to all of the Robo receptors using evolutionarily conserved binding residues (Brose et al., 1999; Morlot et al., 2007). However, in different systems, Slits mediate differing effects; for instance OSN axonal targeting is modulated by Slit1 and Slit2, but not by Slit3 (Prince et al., 2009). It will therefore be important to identify the molecules, such as co-receptors, that mediate such ligand specificity.

Another remaining enigma is how increasing or decreasing levels of Robo receptors and/or different combinations of Robo receptors mediate varying effects within a given cell or between neighbouring cells.

In *Drosophila*, a combinatorial Robo code specifies the lateral position of longitudinal axons; in this system, the expression of only one Robo receptor (Robo1) specifies a medial positioning of these axons, whereas expression of all three Robo receptors drives axons laterally. By contrast, the expression of Robo1 and Robo3 causes an intermediate positioning (Rajagopalan et al., 2000; Simpson et al., 2000). One possible interpretation of these results is that the higher the levels are of Robo receptors at the surface of longitudinal axons, the more these axons will respond to the repulsive effect of Slits that are present at the midline. Similarly, there are phenotypical differences between *Robo1* null and hypomorphic mutant mice, which indicate that different levels of Robo receptors at the membrane within the same cell mediate subtly different effects (Andrews et al., 2006; Lopez-Bendito et al., 2007).

However, more recent studies suggest that, in *Drosophila*, the lateral position of longitudinal axons is not determined by a particular combination of Robo proteins [the so-called 'Robo code' (Rajagopalan et al., 2000; Simpson et al., 2000)], but is rather driven by differential Robo gene expression (Evans et al., 2010; Spitzweck et al., 2010). The different responses of Robos to Slits would reflect intrinsic structural differences in the extracellular Ig domains of Robos. For instance, Robo2 Ig1 and Ig3 domains specify lateral positioning of axons, the Ig2 domain promotes midline crossing and the Robo1 cytoplasmic domain prevents midline crossing (Spitzweck et al., 2010). There are also cases in which the identity of the Robo receptors or of their combination could be the determining factor in the type of response generated. This could for instance contribute to specifying the position of longitudinal axons in the *Drosophila* nerve cord. Likewise, in the mouse spinal cord, Robo2 rather than Robo1, controls the positioning of a longitudinal axonal tract, the lateral funiculus (Long et al., 2004). Moreover, chick commissural axons that prematurely misexpress Robo2 fail to enter the floor plate and preferentially adopt a longitudinal phenotype (Reeber et al., 2008). Finally, in the *Drosophila* tergotrochanteral motoneuron (TTMn), the dendrites of which contact the giant fiber, the overexpression of Robo repels TTMn dendrites from the midline. By contrast, the overexpression of Robo2 or Robo3 at the surface of TTMn dendrites has no noticeable effect (Godenschwege et al., 2002). Further studies need to be conducted on Robo receptor subtypes to elucidate the specificity of each isoform in mediating particular effects in different systems.

Research into the signalling mechanisms of Slit/Robo needs to advance in order to resolve these outstanding questions. Such advances will require adopting a cross-disciplinary approach for studying Slits and Robos in order to integrate information from such disparate fields as CNS and heart development, and immune cell migration and tumourigenesis.

**Acknowledgements**

Y.Z. is supported by Agence nationale de la recherché (ANR), A.R.Y. is supported by Natural Sciences and Engineering Research Council of Canada (NSERC) and Ecole des neurosciences de Paris (ENP). A.C. is supported by the Fondation pour la Recherche médicale (Programme équipe FRM) and ANR.

**Competing interests statement**

The authors declare no competing financial interests.

**References**

**Amoiridis, G., Tzagournissakis, M., Christodoulou, P., Karampekios, S., Latsoudis, H., Panou, T., Simos, P. and Plaitakis, A.** (2006). Patients with horizontal gaze palsy and progressive scoliosis due to ROBO3 E319K mutation have both uncrossed and crossed central nervous system pathways and perform normally on neuropsychological testing. *J. Neurol. Neurosurg. Psychiatry* **77**, 1047-1053.

**Andrews, W., Liapi, A., Plachez, C., Camurri, L., Zhang, J., Mori, S., Murakami, F., Parnavelas, J. G., Sundaresan, V. and Richards, L. J.** (2006). Robo1 regulates the development of major axon tracts and interneuron migration in the forebrain. *Development* **133**, 2243-2252.

**Andrews, W., Barber, M., Hernadez-Miranda, L. R., Xian, J., Rakic, S., Sundaresan, V., Rabbitts, T. H., Pannell, R., Rabbitts, P., Thompson, H. et al.** (2008). The role of Slit-Robo signaling in the generation, migration and morphological differentiation of cortical interneurons. *Dev. Biol.* **313**, 648-658.

**Avraham, O., Hadas, Y., Vald, L., Zisman, S., Schejter, A., Visel, A. and Klar, A.** (2009). Transcriptional control of axonal guidance and sorting in dorsal interneurons by the Lim-HD proteins Lhx9 and Lhx1. *Neural Dev.* **4**, 21.

**Bacon, C., Endris, V. and Rappold, G.** (2009). Dynamic expression of the Slit-Robo GTPase activating protein genes during development of the murine nervous system. *J. Comp. Neurol.* **513**, 224-236.

**Bagri, A., Marin, O., Plump, A. S., Mak, J., Pleasure, S. J., Rubenstein, J. L. and Tessier-Lavigne, M.** (2002). Slit proteins prevent midline crossing and determine the dorsoventral position of major axonal pathways in the mammalian forebrain. *Neuron* **33**, 233-248.

**Barallobre, M. J., Pascual, M., Del Rio, J. A. and Soriano, E.** (2005). The Netrin family of guidance factors: emphasis on Netrin-1 signalling. *Brain Res. Brain Res. Rev.* **49**, 22-47.

**Barber, M., Di Meglio, T., Andrews, W. D., Hernandez-Miranda, L. R., Murakami, F., Chédotal, A. and Parnavelas, J. G.** (2009). The Role of Robo3 in the development of cortical interneurons. *Cereb. Cortex* **19**, i22-i31.

**Bashaw, G. J. and Goodman, C. S.** (1999). Chimeric axon guidance receptors: the cytoplasmic domains of slit and netrin receptors specify attraction versus repulsion. *Cell* **97**, 917-926.

**Bedell, V. M., Yeo, S. Y., Park, K. W., Chung, J., Seth, P., Shivalingappa, V., Zhao, J., Obara, T., Sukhatme, V. P., Drummond, I. A. et al.** (2005). roundabout4 is essential for angiogenesis in vivo. *Proc. Natl. Acad. Sci. USA* **102**, 6373-6378.

**Bloch-Gallego, E., Ezan, F., Tessier-Lavigne, M. and Sotelo, C.** (1999). Floor plate and netrin-1 are involved in the migration and survival of inferior olivary neurons. *J. Neurosci.* **19**, 4407-4420.

**Briancon-Marjollet, A., Ghogha, A., Nawabi, H., Triki, I., Auziol, C., Fromont, S., Piche, C., Enslen, H., Chebli, K., Cloutier, J. F. et al.** (2008). Trio mediates netrin-1-induced Rac1 activation in axon outgrowth and guidance. *Mol. Cell. Biol.* **28**, 2314-2323.

**Brierley, D. J., Blanc, E., Reddy, O. V., Vijayraghavan, K. and Williams, D. W.** (2009). Dendritic targeting in the leg neuropil of Drosophila: the role of midline signalling molecules in generating a myotopic map. *PLoS Biol.* **7**, e1000199.

**Brose, K., Bland, K. S., Wang, K. H., Arnott, D., Henzel, W., Goodman, C. S., Tessier-Lavigne, M. and Kidd, T.** (1999). Slit proteins bind Robo receptors and have an evolutionarily conserved role in repulsive axon guidance. *Cell* **96**, 795-806.

**Bulow, H. E., Tjoe, N., Townley, R. A., Didiano, D., van Kuppevelt, T. H. and Hobert, O.** (2008). Extracellular sugar modifications provide instructive and cell-specific information for axon-guidance choices. *Curr. Biol.* **18**, 1978-1985.

**Burgess, H. A., Johnson, S. L. and Granato, M.** (2009). Unidirectional startle responses and disrupted left-right co-ordination of motor behaviors in robo3 mutant zebrafish. *Genes Brain Behav.* **8**, 500-511.

**Calmont, A., Ivins, S., Van Bueren, K. L., Papangeli, I., Kyriakopoulou, V., Andrews, W. D., Martin, J. F., Moon, A. M., Illingworth, E. A., Basson, M. A. et al.** (2009). Tbx1 controls cardiac neural crest cell migration during arch artery development by regulating Gbx2 expression in the pharyngeal ectoderm. *Development* **136**, 3173-3183.

**Camurri, L., Mambetisaeva, E., Davies, D., Parnavelas, J., Sundaresan, V. and Andrews, W.** (2005). Evidence for the existence of two Robo3 isoforms with divergent biochemical properties. *Mol. Cell Neurosci.* **30**, 485-493.

**Causeret, F., Danne, F., Ezan, F., Sotelo, C. and Bloch-Gallego, E.** (2002). Slit antagonizes netrin-1 attractive effects during the migration of inferior olivary neurons. *Dev. Biol.* **246**, 429-440.

**Causeret, F., Hidalgo-Sanchez, M., Fort, P., Backer, S., Popoff, M. R., Gauthier-Rouviere, C. and Bloch-Gallego, E.** (2004). Distinct roles of Rac1/Cdc42 and Rho/Rock for axon outgrowth and nucleokinesis of precerebellar neurons toward netrin 1. *Development* **131**, 2841-2852.

**Chan, S. S., Zheng, H., Su, M. W., Wilk, R., Killeen, M. T., Hedgecock, E. M. and Culotti, J. G.** (1996). UNC-40, a C. elegans homolog of DCC (Deleted in Colorectal Cancer), is required in motile cells responding to UNC-6 netrin cues. *Cell* **87**, 187-195.

**Chanana, B., Steigemann, P., Jackle, H. and Vorbruggen, G.** (2009). Reception of Slit requires only the chondroitin-sulphate-modified extracellular domain of Syndecan at the target cell surface. *Proc. Natl. Acad. Sci. USA* **106**, 11984-11988.

**Chédotal, A.** (2007). Slits and their receptors. *Adv. Exp. Med. Biol.* **621**, 65-80.

**Chen, B., Wang, S. S., Hattox, A. M., Rayburn, H., Nelson, S. B. and McConnell, S. K.** (2008a). The Fezf2-Ctip2 genetic pathway regulates the fate choice of subcortical projection neurons in the developing cerebral cortex. *Proc. Natl. Acad. Sci. USA* **105**, 11382-11387.

**Chen, Z., Gore, B. B., Long, H., Ma, L. and Tessier-Lavigne, M.** (2008b). Alternative splicing of the Robo3 axon guidance receptor governs the midline switch from attraction to repulsion. *Neuron* **58**, 325-332.

**Cho, J. H., Lepine, M., Andrews, W., Parnavelas, J. and Cloutier, J. F.** (2007). Requirement for Slit-1 and Robo-2 in zonal segregation of olfactory sensory neuron axons in the main olfactory bulb. *J. Neurosci.* **27**, 9094-9104.

**Cho, J. H., Prince, J. E. and Cloutier, J. F.** (2009). Axon guidance events in the wiring of the mammalian olfactory system. *Mol. Neurobiol.* **39**, 1-9.

**Cirulli, V. and Yebra, M.** (2007). Netrins: beyond the brain. *Nat. Rev. Mol. Cell Biol.* **8**, 296-306.

**Cloutier, J. F., Sahay, A., Chang, E. C., Tessier-Lavigne, M., Dulac, C., Kolodkin, A. L. and Ginty, D. D.** (2004). Differential requirements for semaphorin 3F and Slit-1 in axonal targeting, fasciculation, and segregation of olfactory sensory neuron projections. *J. Neurosci.* **24**, 9087-9096.

**Colavita, A. and Culotti, J. G.** (1998). Suppressors of ectopic UNC-5 growth cone steering identify eight genes involved in axon guidance in Caenorhabditis elegans. *Dev. Biol.* **194**, 72-85.

**Dasen, J. S., De Camilli, A., Wang, B., Tucker, P. W. and Jessell, T. M.** (2008). Hox repertoires for motor neuron diversity and connectivity gated by a single accessory factor, FoxP1. *Cell* **134**, 304-316.

**De Bellard, M. E., Rao, Y. and Bronner-Fraser, M.** (2003). Dual function of Slit2 in repulsion and enhanced migration of trunk, but not vagal, neural crest cells. *J. Cell Biol.* **162**, 269-279.

**Di Meglio, T., Nguyen-Ba-Charvet, K. T., Tessier-Lavigne, M., Sotelo, C. and Chédotal, A.** (2008). Molecular mechanisms controlling midline crossing by precerebellar neurons. *J. Neurosci.* **28**, 6285-6294.

**Dulac, C. and Wagner, S.** (2006). Genetic analysis of brain circuits underlying pheromone signaling. *Annu. Rev. Genet.* **40**, 449-467.

**Endris, V., Wogatzky, B., Leimer, U., Bartsch, D., Zatyka, M., Latif, F., Maher, E. R., Tariverdian, G., Kirsch, S., Karch, D. et al.** (2002). The novel Rho-GTPase activating gene MEGAP/ srGAP3 has a putative role in severe mental retardation. *Proc. Natl. Acad. Sci. USA* **99**, 11754-11759.

**Evans, T. A. and Bashaw, G. J.** (2010). Functional diversity of robo receptor immunoglobulin domains promotes distinct axon guidance decisions. *Curr. Biol.* **20**, 567-572.

**Fitzgerald, M. L., Wang, Z., Park, P. W., Murphy, G. and Bernfield, M.** (2000). Shedding of syndecan-1 and -4 ectodomains is regulated by multiple signaling pathways and mediated by a TIMP-3-sensitive metalloproteinase. *J. Cell Biol.* **148**, 811-824.

**Fouquet, C., Di Meglio, T., Ma, L., Kawasaki, T., Long, H., Hirata, T., Tessier-Lavigne, M., Chédotal, A. and Nguyen-Ba-Charvet, K. T.** (2007). Robo1 and robo2 control the development of the lateral olfactory tract. *J. Neurosci.* **27**, 3037-3045.

**Fujisawa, K., Wrana, J. L. and Culotti, J. G.** (2007). The slit receptor EVA-1 coactivates a SAX-3/Robo mediated guidance signal in C. elegans. *Science* **317**, 1934-1938.

**Fukuhara, N., Howitt, J. A., Hussain, S. A. and Hohenester, E.** (2008). Structural and functional analysis of slit and heparin binding to immunoglobulin-like domains 1 and 2 of Drosophila Robo. *J. Biol. Chem.* **283**, 16226-16234.

**Geisen, M. J., Di Meglio, T., Pasqualetti, M., Ducret, S., Brunet, J. F., Chédotal, A. and Rijli, F. M.** (2008). Hox paralog group 2 genes control the migration of mouse pontine neurons through slit-robo signaling. *PLoS Biol.* **6**, e142.

**Gilthorpe, J. D., Papantoniou, E. K., Chédotal, A., Lumsden, A. and Wingate, R. J.** (2002). The migration of cerebellar rhombic lip derivatives. *Development* **129**, 4719-4728.

**Godenschwege, T. A., Simpson, J. H., Shan, X., Bashaw, G. J., Goodman, C. S. and Murphey, R. K.** (2002). Ectopic expression in the giant fiber system of Drosophila reveals distinct roles for roundabout (Robo), Robo2, and Robo3 in dendritic guidance and synaptic connectivity. *J. Neurosci.* **22**, 3117-3129.

**Gomez, T. M. and Zheng, J. Q.** (2006). The molecular basis for calcium-dependent axon pathfinding. *Nat. Rev. Neurosci.* **7**, 115-125.

**Gore, B. B., Wong, K. G. and Tessier-Lavigne, M.** (2008). Stem cell factor functions as an outgrowth-promoting factor to enable axon exit from the midline intermediate target. *Neuron* **57**, 501-510.

**Guan, C. B., Xu, H. T., Jin, M., Yuan, X. B. and Poo, M. M.** (2007). Long-range Ca2+ signaling from growth cone to soma mediates reversal of neuronal migration induced by slit-2. *Cell* **129**, 385-395.

**Guerrier, S., Coutinho-Budd, J., Sassa, T., Gresset, A., Jordan, N. V., Chen, K., Jin, W. L., Frost, A. and Polleux, F.** (2009). The F-BAR domain of srGAP2 induces membrane protrusions required for neuronal migration and morphogenesis. *Cell* **138**, 990-1004.

**Haller, S., Wetzel, S. G. and Lutschg, J.** (2008). Functional MRI, DTI and neurophysiology in horizontal gaze palsy with progressive scoliosis. *Neuroradiology* **50**, 453-459.

**Hamdan, F. F., Gauthier, J., Pellerin, S., Dobrzeniecka, S., Marineau, C., Fombonne, E., Mottron, L., Lafreniere, R. G., Drapeau, P., Lacaille, J. C. et al.** (2009). No association between SRGAP3/MEGAP haploinsufficiency and mental retardation. *Arch Neurol.* **66**, 675-676.

**Hammond, R., Vivancos, V., Naeem, A., Chilton, J., Mambetisaeva, E., Andrews, W., Sundaresan, V. and Guthrie, S.** (2005). Slit-mediated repulsion is a key regulator of motor axon pathfinding in the hindbrain. *Development* **132**, 4483-4495.

**Heasman, S. J. and Ridley, A. J.** (2008). Mammalian Rho GTPases: new insights into their functions from in vivo studies. *Nat. Rev. Mol. Cell Biol.* **9**, 690-701.

**Hedgecock, E. M., Culotti, J. G. and Hall, D. H.** (1990). The unc-5, unc-6, and unc-40 genes guide circumferential migrations of pioneer axons and mesodermal cells on the epidermis in C. elegans. *Neuron* **4**, 61-85.

**Hershko, A. and Ciechanover, A.** (1998). The ubiquitin system. *Annu. Rev. Biochem.* **67**, 425-479.

**Higginbotham, H. R. and Gleeson, J. G.** (2007). The centrosome in neuronal development. *Trends Neurosci.* **30**, 276-283.

**Higginbotham, H., Tanaka, T., Brinkman, B. C. and Gleeson, J. G.** (2006). GSK3beta and PKCzeta function in centrosome localization and process stabilization during Slit-mediated neuronal repolarization. *Mol. Cell Neurosci.* **32**, 118-132.

**Hivert, B., Liu, Z., Chuang, C. Y., Doherty, P. and Sundaresan, V.** (2002). Robo1 and Robo2 are homophilic binding molecules that promote axonal growth. *Mol. Cell. Neurosci.* **21**, 534-545.

**Hong, K., Hinck, L., Nishiyama, M., Poo, M. M., Tessier-Lavigne, M. and Stein, E.** (1999). A ligand-gated association between cytoplasmic domains of UNC5 and DCC family receptors converts netrin-induced growth cone attraction to repulsion. *Cell* **97**, 927-941.

**Howitt, J. A., Clout, N. J. and Hohenester, E.** (2004). Binding site for Robo receptors revealed by dissection of the leucine-rich repeat region of Slit. *EMBO J.* **23**, 4406-4412.

**Hu, H.** (1999). Chemorepulsion of neuronal migration by Slit2 in the developing mammalian forebrain. *Neuron* **23**, 703-711.

**Hu, H.** (2001). Cell-surface heparan sulfate is involved in the repulsive guidance activities of Slit2 protein. *Nat. Neurosci.* **4**, 695-701.
**Hu, H., Li, M., Labrador, J. P., McEwen, J., Lai, E. C., Goodman, C. S. and Bashaw, G. J.** (2005). Cross GTPase-activating protein (CrossGAP)/Vilse links the Roundabout receptor to Rac to regulate midline repulsion. *Proc. Natl. Acad. Sci. USA* **102**, 4613-4618.
**Hussain, S. A., Piper, M., Fukuhara, N., Strochlic, L., Cho, G., Howitt, J. A., Ahmed, Y., Powell, A. K., Turnbull, J. E., Holt, C. E. et al.** (2006). A molecular mechanism for the heparan sulfate dependence of slit-robo signaling. *J. Biol. Chem.* **281**, 39693-39698.
**Inatani, M., Irie, F., Plump, A. S., Tessier-Lavigne, M. and Yamaguchi, Y.** (2003). Mammalian brain morphogenesis and midline axon guidance require heparan sulfate. *Science* **302**, 1044-1046.
**Jen, J. C.** (2008). Effects of failure of development of crossing brainstem pathways on ocular motor control. *Prog. Brain Res.* **171**, 137-141.
**Jen, J. C., Chan, W. M., Bosley, T. M., Wan, J., Carr, J. R., Rub, U., Shattuck, D., Salamon, G., Kudo, L. C., Ou, J. et al.** (2004). Mutations in a human ROBO gene disrupt hindbrain axon pathway crossing and morphogenesis. *Science* **304**, 1509-1513.
**Jia, L., Cheng, L. and Raper, J.** (2005). Slit/Robo signaling is necessary to confine early neural crest cells to the ventral migratory pathway in the trunk. *Dev. Biol.* **282**, 411-421.
**Johnson, K. G., Ghose, A., Epstein, E., Lincecum, J., O'Connor, M. B. and Van Vactor, D.** (2004). Axonal heparan sulfate proteoglycans regulate the distribution and efficiency of the repellent slit during midline axon guidance. *Curr. Biol.* **14**, 499-504.
**Johnson, K. G., Tenney, A. P., Ghose, A., Duckworth, A. M., Higashi, M. E., Parfitt, K., Marcu, O., Heslip, T. R., Marsh, J. L., Schwarz, T. L. et al.** (2006). The HSPGs Syndecan and Dallylike bind the receptor phosphatase LAR and exert distinct effects on synaptic development. *Neuron* **49**, 517-531.
**Jones, C. A., London, N. R., Chen, H., Park, K. W., Sauvaget, D., Stockton, R. A., Wythe, J. D., Suh, W., Larrieu-Lahargue, F., Mukouyama, Y. S. et al.** (2008). Robo4 stabilizes the vascular network by inhibiting pathologic angiogenesis and endothelial hyperpermeability. *Nat. Med.* **14**, 448-453.
**Kastenhuber, E., Kern, U., Bonkowsky, J. L., Chien, C. B., Driever, W. and Schweitzer, J.** (2009). Netrin-DCC, Robo-Slit, and heparan sulfate proteoglycans coordinate lateral positioning of longitudinal dopaminergic diencephalospinal axons. *J. Neurosci.* **29**, 8914-8926.
**Keino-Masu, K., Masu, M., Hinck, L., Leonardo, E. D., Chan, S. S., Culotti, J. G. and Tessier-Lavigne, M.** (1996). Deleted in Colorectal Cancer (DCC) encodes a netrin receptor. *Cell* **87**, 175-185.
**Keleman, K. and Dickson, B. J.** (2001). Short- and long-range repulsion by the Drosophila Unc5 netrin receptor. *Neuron* **32**, 605-617.
**Keleman, K., Rajagopalan, S., Cleppien, D., Teis, D., Paiha, K., Huber, L. A., Technau, G. M. and Dickson, B. J.** (2002). Comm sorts robo to control axon guidance at the Drosophila midline. *Cell* **110**, 415-427.
**Keleman, K., Ribeiro, C. and Dickson, B. J.** (2005). Comm function in commissural axon guidance: cell-autonomous sorting of Robo in vivo. *Nat. Neurosci.* **8**, 156-163.
**Kennedy, T. E., Serafini, T., de la Torre, J. R. and Tessier-Lavigne, M.** (1994). Netrins are diffusible chemotropic factors for commissural axons in the embryonic spinal cord. *Cell* **78**, 425-435.
**Kidd, T., Brose, K., Mitchell, K. J., Fetter, R. D., Tessier-Lavigne, M., Goodman, C. S. and Tear, G.** (1998). Roundabout controls axon crossing of the CNS midline and defines a novel subfamily of evolutionarily conserved guidance receptors. *Cell* **92**, 205-215.
**Kidd, T., Bland, K. S. and Goodman, C. S.** (1999). Slit is the midline repellent for the robo receptor in Drosophila. *Cell* **96**, 785-794.
**Kiecker, C. and Lumsden, A.** (2005). Compartments and their boundaries in vertebrate brain development. *Nat. Rev. Neurosci.* **6**, 553-564.
**Knoll, B., Schmidt, H., Andrews, W., Guthrie, S., Pini, A., Sundaresan, V. and Drescher, U.** (2003). On the topographic targeting of basal vomeronasal axons through Slit-mediated chemorepulsion. *Development* **130**, 5073-5082.
**Kolodziej, P. A., Timpe, L. C., Mitchell, K. J., Fried, S. R., Goodman, C. S., Jan, L. Y. and Jan, Y. N.** (1996). Frazzled encodes a Drosophila member of the DCC immunoglobulin subfamily and is required for CNS and motor axon guidance. *Cell* **87**, 197-204.
**Komuro, H. and Rakic, P.** (1996). Intracellular $Ca^{2+}$ fluctuations modulate the rate of neuronal migration. *Neuron* **17**, 275-285.
**Kraut, R. and Zinn, K.** (2004). Roundabout 2 regulates migration of sensory neurons by signaling in trans. *Curr. Biol.* **14**, 1319-1329.
**Lee, J. S. and Chien, C. B.** (2004). When sugars guide axons: insights from heparan sulphate proteoglycan mutants. *Nat. Rev. Genet.* **5**, 923-935.
**Levy-Strumpf, N. and Culotti, J. G.** (2007). VAB-8, UNC-73 and MIG-2 regulate axon polarity and cell migration functions of UNC-40 in C. elegans. *Nat. Neurosci.* **10**, 161-168.
**Li, X., Chen, Y., Liu, Y., Gao, J., Gao, F., Bartlam, M., Wu, J. Y. and Rao, Z.** (2006). Structural basis of Robo proline-rich motif recognition by the srGAP1 Src homology 3 domain in the Slit-Robo signaling pathway. *J. Biol. Chem.* **281**, 28430-28437.
**Liu, J., Zhang, L., Wang, D., Shen, H., Jiang, M., Mei, P., Hayden, P. S., Sedor, J. R. and Hu, H.** (2003). Congenital diaphragmatic hernia, kidney agenesis and cardiac defects associated with Slit3-deficiency in mice. *Mech. Dev.* **120**, 1059-1070.
**Liu, Q. X., Hiramoto, M., Ueda, H., Gojobori, T., Hiromi, Y. and Hirose, S.** (2009). Midline governs axon pathfinding by coordinating expression of two major guidance systems. *Genes Dev.* **23**, 1165-1170.
**Liu, Z., Patel, K., Schmidt, H., Andrews, W., Pini, A. and Sundaresan, V.** (2004). Extracellular Ig domains 1 and 2 of Robo are important for ligand (Slit) binding. *Mol. Cell Neurosci.* **26**, 232-240.
**Long, H., Sabatier, C., Ma, L., Plump, A., Yuan, W., Ornitz, D. M., Tamada, A., Murakami, F., Goodman, C. S. and Tessier-Lavigne, M.** (2004). Conserved roles for Slit and Robo proteins in midline commissural axon guidance. *Neuron* **42**, 213-223.
**Lopez-Bendito, G., Flames, N., Ma, L., Fouquet, C., Di Meglio, T., Chédotal, A., Tessier-Lavigne, M. and Marin, O.** (2007). Robo1 and Robo2 cooperate to control the guidance of major axonal tracts in the mammalian forebrain. *J. Neurosci.* **27**, 3395-3407.
**Lundstrom, A., Gallio, M., Englund, C., Steneberg, P., Hemphala, J., Aspenstrom, P., Keleman, K., Falileeva, L., Dickson, B. J. and Samakovlis, C.** (2004). Vilse, a conserved Rac/Cdc42 GAP mediating Robo repulsion in tracheal cells and axons. *Genes Dev.* **18**, 2161-2171.
**Ly, A., Nikolaev, A., Suresh, G., Zheng, Y., Tessier-Lavigne, M. and Stein, E.** (2008). DSCAM is a netrin receptor that collaborates with DCC in mediating turning responses to netrin-1. *Cell* **133**, 1241-1254.
**Madura, T., Yamashita, T., Kubo, T., Tsuji, L., Hosokawa, K. and Tohyama, M.** (2004). Changes in mRNA of Slit-Robo GTPase-activating protein 2 following facial nerve transection. *Brain Res. Mol. Brain Res.* **123**, 76-80.
**Mambetisaeva, E. T., Andrews, W., Camurri, L., Annan, A. and Sundaresan, V.** (2005). Robo family of proteins exhibit differential expression in mouse spinal cord and Robo-Slit interaction is required for midline crossing in vertebrate spinal cord. *Dev. Dyn.* **233**, 41-51.
**Marcos, S., Backer, S., Causeret, F., Tessier-Lavigne, M. and Bloch-Gallego, E.** (2009). Differential roles of Netrin-1 and its receptor DCC in inferior olivary neuron migration. *Mol. Cell Neurosci.* **41**, 429-439.
**Marillat, V., Cases, O., Nguyen-Ba-Charvet, K. T., Tessier-Lavigne, M., Sotelo, C. and Chédotal, A.** (2002). Spatiotemporal expression patterns of slit and robo genes in the rat brain. *J. Comp. Neurol.* **442**, 130-155.
**Marillat, V., Sabatier, C., Failli, V., Matsunaga, E., Sotelo, C., Tessier-Lavigne, M. and Chédotal, A.** (2004). The slit receptor Rig-1/Robo3 controls midline crossing by hindbrain precerebellar neurons and axons. *Neuron* **43**, 69-79.
**Marion, J. F., Yang, C., Caqueret, A., Boucher, F. and Michaud, J. L.** (2005). Sim1 and Sim2 are required for the correct targeting of mammillary body axons. *Development* **132**, 5527-5537.
**Mauss, A., Tripodi, M., Evers, J. F. and Landgraf, M.** (2009). Midline signalling systems direct the formation of a neural map by dendritic targeting in the Drosophila motor system. *PLoS Biol.* **7**, e1000200.
**Medioni, C., Astier, M., Zmojdzian, M., Jagla, K. and Semeriva, M.** (2008). Genetic control of cell morphogenesis during Drosophila melanogaster cardiac tube formation. *J. Cell Biol.* **182**, 249-261.
**Metin, C., Vallee, R. B., Rakic, P. and Bhide, P. G.** (2008). Modes and mishaps of neuronal migration in the mammalian brain. *J. Neurosci.* **28**, 11746-11752.
**Miyamichi, K., Serizawa, S., Kimura, H. M. and Sakano, H.** (2005). Continuous and overlapping expression domains of odorant receptor genes in the olfactory epithelium determine the dorsal/ventral positioning of glomeruli in the olfactory bulb. *J. Neurosci.* **25**, 3586-3592.
**Miyasaka, N., Sato, Y., Yeo, S. Y., Hutson, L. D., Chien, C. B., Okamoto, H. and Yoshihara, Y.** (2005). Robo2 is required for establishment of a precise glomerular map in the zebrafish olfactory system. *Development* **132**, 1283-1293.
**Morlot, C., Thielens, N. M., Ravelli, R. B., Hemrika, W., Romijn, R. A., Gros, P., Cusack, S. and McCarthy, A. A.** (2007). Structural insights into the Slit-Robo complex. *Proc. Natl. Acad. Sci. USA* **104**, 14923-14928.
**Nguyen-Ba-Charvet, K. T., Brose, K., Ma, L., Wang, K. H., Marillat, V., Sotelo, C., Tessier-Lavigne, M. and Chédotal, A.** (2001). Diversity and specificity of actions of Slit2 proteolytic fragments in axon guidance. *J. Neurosci.* **21**, 4281-4289.
**Nguyen-Ba-Charvet, K. T., Plump, A. S., Tessier-Lavigne, M. and Chédotal, A.** (2002). Slit1 and slit2 proteins control the development of the lateral olfactory tract. *J. Neurosci.* **22**, 5473-5480.
**Nguyen-Ba-Charvet, K. T., Picard-Riera, N., Tessier-Lavigne, M., Baron-Van Evercooren, A., Sotelo, C. and Chédotal, A.** (2004). Multiple roles for slits in the control of cell migration in the rostral migratory stream. *J. Neurosci.* **24**, 1497-1506.
**Nguyen-Ba-Charvet, K. T., Di Meglio, T., Fouquet, C. and Chédotal, A.** (2008). Robos and slits control the pathfinding and targeting of mouse olfactory sensory axons. *J. Neurosci.* **28**, 4244-4249.
**O'Donnell, M., Chance, R. K. and Bashaw, G. J.** (2009). Axon growth and guidance: receptor regulation and signal transduction. *Annu. Rev. Neurosci.* **32**, 383-412.

**Piper, M., Anderson, R., Dwivedy, A., Weinl, C., van Horck, F., Leung, K. M., Cogill, E. and Holt, C.** (2006). Signaling mechanisms underlying Slit2-induced collapse of Xenopus retinal growth cones. *Neuron* **49**, 215-228.
**Placzek, M. and Briscoe, J.** (2005). The floor plate: multiple cells, multiple signals. *Nat. Rev. Neurosci.* **6**, 230-240.
**Plump, A. S., Erskine, L., Sabatier, C., Brose, K., Epstein, C. J., Goodman, C. S., Mason, C. A. and Tessier-Lavigne, M.** (2002). Slit1 and Slit2 cooperate to prevent premature midline crossing of retinal axons in the mouse visual system. *Neuron* **33**, 219-232.
**Polleux, F., Ince-Dunn, G. and Ghosh, A.** (2007). Transcriptional regulation of vertebrate axon guidance and synapse formation. *Nat. Rev. Neurosci.* **8**, 331-340.
**Prasad, A., Paruchuri, V., Preet, A., Latif, F. and Ganju, R. K.** (2008). Slit-2 induces a tumor-suppressive effect by regulating beta-catenin in breast cancer cells. *J. Biol. Chem.* **283**, 26624-26633.
**Prince, J. E., Cho, J. H., Dumontier, E., Andrews, W., Cutforth, T., Tessier-Lavigne, M., Parnavelas, J. and Cloutier, J. F.** (2009). Robo-2 controls the segregation of a portion of basal vomeronasal sensory neuron axons to the posterior region of the accessory olfactory bulb. *J. Neurosci.* **29**, 14211-14222.
**Qian, L., Liu, J. and Bodmer, R.** (2005). Slit and Robo control cardiac cell polarity and morphogenesis. *Curr. Biol.* **15**, 2271-2278.
**Rajagopalan, S., Vivancos, V., Nicolas, E. and Dickson, B. J.** (2000). Selecting a longitudinal pathway: Robo receptors specify the lateral position of axons in the Drosophila CNS. *Cell* **103**, 1033-1045.
**Rajasekharan, S. and Kennedy T. E.** (2009). The netrin protein family. *Genome Biol.* **10**, 239.
**Reeber, S. L., Sakai, N., Nakada, Y., Dumas, J., Dobrenis, K., Johnson, J. E. and Kaprielian, Z.** (2008). Manipulating Robo expression in vivo perturbs commissural axon pathfinding in the chick spinal cord. *J. Neurosci.* **28**, 8698-8708.
**Renier, N., Schonewille, M., Giraudet, F., Badura, A., Tessier-Lavigne, M., Avan, P., De Zeeuw, C. I. and Chédotal, A.** (2010). Genetic dissection of the function of hindbrain axonal commissures. *PLoS Biol.* **8**, e1000325.
**Ressler, K. J., Sullivan, S. L. and Buck, L. B.** (1994). A molecular dissection of spatial patterning in the olfactory system. *Curr. Opin. Neurobiol.* **4**, 588-596.
**Rhee, J., Mahfooz, N. S., Arregui, C., Lilien, J., Balsamo, J. and VanBerkum, M. F.** (2002). Activation of the repulsive receptor Roundabout inhibits N-cadherin-mediated cell adhesion. *Nat. Cell Biol.* **4**, 798-805.
**Rhee, J., Buchan, T., Zukerberg, L., Lilien, J. and Balsamo, J.** (2007). Cables links Robo-bound Abl kinase to N-cadherin-bound beta-catenin to mediate Slit-induced modulation of adhesion and transcription. *Nat. Cell Biol.* **9**, 883-892.
**Rieger, S., Senghaas, N., Walch, A. and Koster, R. W.** (2009). Cadherin-2 controls directional chain migration of cerebellar granule neurons. *PLoS Biol.* **7**, e1000240.
**Ronca, F., Andersen, J. S., Paech, V. and Margolis, R. U.** (2001). Characterization of Slit protein interactions with glypican-1. *J. Biol. Chem.* **276**, 29141-29147.
**Rothberg, J. M., Hartley, D. A., Walther, Z. and Artavanis-Tsakonas, S.** (1988). slit: an EGF-homologous locus of D. melanogaster involved in the development of the embryonic central nervous system. *Cell* **55**, 1047-1059.
**Rothberg, J. M., Jacobs, J. R., Goodman, C. S. and Artavanis-Tsakonas, S.** (1990). slit: an extracellular protein necessary for development of midline glia and commissural axon pathways contains both EGF and LRR domains. *Genes Dev.* **4**, 2169-2187.
**Sabatier, C., Plump, A. S., Le, M., Brose, K., Tamada, A., Murakami, F., Lee, E. Y. and Tessier-Lavigne, M.** (2004). The divergent Robo family protein rig-1/Robo3 is a negative regulator of slit responsiveness required for midline crossing by commissural axons. *Cell* **117**, 157-169.
**Santiago-Martinez, E., Soplop, N. H. and Kramer, S. G.** (2006). Lateral positioning at the dorsal midline: Slit and Roundabout receptors guide Drosophila heart cell migration. *Proc. Natl. Acad. Sci. USA* **103**, 12441-12446.
**Santiago-Martinez, E., Soplop, N. H., Patel, R. and Kramer, S. G.** (2008). Repulsion by Slit and Roundabout prevents Shotgun/E-cadherin-mediated cell adhesion during Drosophila heart tube lumen formation. *J. Cell Biol.* **182**, 241-248.
**Sawamoto, K., Wichterle, H., Gonzalez-Perez, O., Cholfin, J. A., Yamada, M., Spassky, N., Murcia, N. S., Garcia-Verdugo, J. M., Marin, O., Rubenstein, J. L. et al.** (2006). New neurons follow the flow of cerebrospinal fluid in the adult brain. *Science* **311**, 629-632.
**Seeger, M., Tear, G., Ferres-Marco, D. and Goodman, C. S.** (1993). Mutations affecting growth cone guidance in Drosophila: genes necessary for guidance toward or away from the midline. *Neuron* **10**, 409-426.
**Seiradake, E., von Philipsborn, A. C., Henry, M., Fritz, M., Lortat-Jacob, H., Jamin, M., Hemrika, W., Bastmeyer, M., Cusack, S. and McCarthy, A. A.** (2009). Structure and functional relevance of the Slit2 homodimerization domain. *EMBO Rep.* **10**, 736-741.
**Shiau, C. E. and Bronner-Fraser, M.** (2009). N-cadherin acts in concert with Slit1-Robo2 signaling in regulating aggregation of placode-derived cranial sensory neurons. *Development* **136**, 4155-4164.
**Shiau, C. E., Lwigale, P. Y., Das, R. M., Wilson, S. A. and Bronner-Fraser, M.** (2008). Robo2-Slit1 dependent cell-cell interactions mediate assembly of the trigeminal ganglion. *Nat. Neurosci.* **11**, 269-276.
**Simionato, E., Barrios, N., Duloquin, L., Boissonneau, E., Lecorre, P. and Agnes, F.** (2007). The Drosophila RNA-binding protein ELAV is required for commissural axon midline crossing via control of commissureless mRNA expression in neurons. *Dev. Biol.* **301**, 166-177.
**Simpson, J. H., Kidd, T., Bland, K. S. and Goodman, C. S.** (2000). Short-range and long-range guidance by slit and its Robo receptors. Robo and Robo2 play distinct roles in midline guidance. *Neuron* **28**, 753-766.
**Soderling, S. H., Binns, K. L., Wayman, G. A., Davee, S. M., Ong, S. H., Pawson, T. and Scott, J. D.** (2002). The WRP component of the WAVE-1 complex attenuates Rac-mediated signalling. *Nat. Cell Biol.* **4**, 970-975.
**Soderling, S. H., Guire, E. S., Kaech, S., White, J., Zhang, F., Schutz, K., Langeberg, L. K., Banker, G., Raber, J. and Scott, J. D.** (2007). A WAVE-1 and WRP signaling complex regulates spine density, synaptic plasticity, and memory. *J. Neurosci.* **27**, 355-365.
**Song, M. R., Shirasaki, R., Cai, C. L., Ruiz, E. C., Evans, S. M., Lee, S. K. and Pfaff, S. L.** (2006). T-Box transcription factor Tbx20 regulates a genetic program for cranial motor neuron cell body migration. *Development* **133**, 4945-4955.
**Sotelo, C. and Chédotal, A.** (2005). Development of the olivocerebellar system: migration and formation of cerebellar maps. *Prog. Brain Res.* **148**, 1-20.
**Spitzweck, B., Brankatschk, M. and Dickson, B. J.** (2010). Distinct protein domains and expression patterns confer divergent axon guidance functions for Drosophila Robo receptors. *Cell* **140**, 409-420.
**Steigemann, P., Molitor, A., Fellert, S., Jackle, H. and Vorbruggen, G.** (2004). Heparan sulfate proteoglycan syndecan promotes axonal and myotube guidance by slit/robo signaling. *Curr. Biol.* **14**, 225-230.
**Stein, E. and Tessier-Lavigne, M.** (2001). Hierarchical organization of guidance receptors: silencing of netrin attraction by slit through a Robo/DCC receptor complex. *Science* **291**, 1928-1938.
**Stennard, F. A. and Harvey, R. P.** (2005). T-box transcription factors and their roles in regulatory hierarchies in the developing heart. *Development* **132**, 4897-4910.
**Stoller, J. Z. and Epstein, J. A.** (2005). Cardiac neural crest. *Semin. Cell Dev. Biol.* **16**, 704-715.
**Sundaresan, V., Roberts, I., Bateman, A., Bankier, A., Sheppard, M., Hobbs, C., Xiong, J., Minna, J., Latif, F., Lerman, M. et al.** (1998). The DUTT1 gene, a novel NCAM family member is expressed in developing murine neural tissues and has an unusually broad pattern of expression. *Mol. Cell Neurosci.* **11**, 29-35.
**Takeuchi, J. K., Mileikovskaia, M., Koshiba-Takeuchi, K., Heidt, A. B., Mori, A. D., Arruda, E. P., Gertsenstein, M., Georges, R., Davidson, L., Mo, R. et al.** (2005). Tbx20 dose-dependently regulates transcription factor networks required for mouse heart and motoneuron development. *Development* **132**, 2463-2474.
**Tamada, A., Kumada, T., Zhu, Y., Matsumoto, T., Hatanaka, Y., Muguruma, K., Chen, Z., Tanabe, Y., Torigoe, M., Yamauchi, K. et al.** (2008). Crucial roles of Robo proteins in midline crossing of cerebellofugal axons and lack of their up-regulation after midline crossing. *Neural Dev.* **3**, 29.
**Taniguchi, H., Kawauchi, D., Nishida, K. and Murakami, F.** (2006). Classic cadherins regulate tangential migration of precerebellar neurons in the caudal hindbrain. *Development* **133**, 1923-1931.
**Thompson, H., Camand, O., Barker, D. and Erskine, L.** (2006). Slit proteins regulate distinct aspects of retinal ganglion cell axon guidance within dorsal and ventral retina. *J. Neurosci.* **26**, 8082-8091.
**Thompson, H., Andrews, W., Parnavelas, J. G. and Erskine, L.** (2009). Robo2 is required for Slit-mediated intraretinal axon guidance. *Dev. Biol.* **335**, 418-426.
**Van Vactor, D., Wall, D. P. and Johnson, K. G.** (2006). Heparan sulfate proteoglycans and the emergence of neuronal connectivity. *Curr. Opin. Neurobiol.* **16**, 40-51.
**Vanderzalm, P. J., Pandey, A., Hurwitz, M. E., Bloom, L., Horvitz, H. R. and Garriga, G.** (2009). C. elegans CARMIL negatively regulates UNC-73/Trio function during neuronal development. *Development* **136**, 1201-1210.
**Vassar, R., Chao, S. K., Sitcheran, R., Nunez, J. M., Vosshall, L. B. and Axel, R.** (1994). Topographic organization of sensory projections to the olfactory bulb. *Cell* **79**, 981-991.
**Waltereit, R., Kautt, S. and Bartsch, D.** (2008). Expression of MEGAP mRNA during embryonic development. *Gene Expr. Patterns* **8**, 307-310.
**Walz, A., McFarlane, S., Brickman, Y. G., Nurcombe, V., Bartlett, P. F. and Holt, C. E.** (1997). Essential role of heparan sulfates in axon navigation and targeting in the developing visual system. *Development* **124**, 2421-2430.
**Wang, K. H., Brose, K., Arnott, D., Kidd, T., Goodman, C. S., Henzel, W. and Tessier-Lavigne, M.** (1999). Biochemical purification of a mammalian slit protein as a positive regulator of sensory axon elongation and branching. *Cell* **96**, 771-784.
**Watari-Goshima, N., Ogura, K., Wolf, F. W., Goshima, Y. and Garriga, G.** (2007). C. elegans VAB-8 and UNC-73 regulate the SAX-3 receptor to direct cell and growth-cone migrations. *Nat. Neurosci.* **10**, 169-176.

**Wayburn, B. and Volk, T.** (2009). LRT, a tendon-specific leucine-rich repeat protein, promotes muscle-tendon targeting through its interaction with Robo. *Development* **136**, 3607-3615.
**Wilson, S. I., Shafer, B., Lee, K. J. and Dodd, J.** (2008). A molecular program for contralateral trajectory: Rig-1 control by LIM homeodomain transcription factors. *Neuron* **59**, 413-424.
**Wong, K., Ren, X. R., Huang, Y. Z., Xie, Y., Liu, G., Saito, H., Tang, H., Wen, L., Brady-Kalnay, S. M., Mei, L. et al.** (2001). Signal transduction in neuronal migration: roles of GTPase activating proteins and the small GTPase Cdc42 in the Slit-Robo pathway. *Cell* **107**, 209-221.
**Wu, W., Wong, K., Chen, J., Jiang, Z., Dupuis, S., Wu, J. Y. and Rao, Y.** (1999). Directional guidance of neuronal migration in the olfactory system by the protein Slit. *Nature* **400**, 331-336.
**Xu, H. T., Yuan, X. B., Guan, C. B., Duan, S., Wu, C. P. and Feng, L.** (2004). Calcium signaling in chemorepellant Slit2-dependent regulation of neuronal migration. *Proc. Natl. Acad. Sci. USA* **101**, 4296-4301.
**Yang, L. and Bashaw, G. J.** (2006). Son of sevenless directly links the Robo receptor to rac activation to control axon repulsion at the midline. *Neuron* **52**, 595-607.
**Yang, L., Garbe, D. S. and Bashaw, G. J.** (2009). A Frazzled/DCC-Dependent Transcriptional Switch Regulates Midline Axon Guidance. *Science*. **324**, 944-947.
**Yang, Y., Marcello, M., Endris, V., Saffrich, R., Fischer, R., Trendelenburg, M. F., Sprengel, R. and Rappold, G.** (2006). MEGAP impedes cell migration via regulating actin and microtubule dynamics and focal complex formation. *Exp. Cell Res.* **312**, 2379-2393.
**Yao, Q., Jin, W. L., Wang, Y. and Ju, G.** (2008). Regulated shuttling of Slit-Robo-GTPase activating proteins between nucleus and cytoplasm during brain development. *Cell. Mol. Neurobiol.* **28**, 205-221.
**Yee, K. T., Simon, H. H., Tessier-Lavigne, M. and O'Leary, D. M.** (1999). Extension of long leading processes and neuronal migration in the mammalian brain directed by the chemoattractant netrin-1. *Neuron* **24**, 607-622.
**Yuan, S. S., Cox, L. A., Dasika, G. K. and Lee, E. Y.** (1999). Cloning and functional studies of a novel gene aberrantly expressed in RB-deficient embryos. *Dev. Biol.* **207**, 62-75.
**Yuan, S. S., Yeh, Y. T. and Lee, E. Y.** (2002). Pax-2 interacts with RB and reverses its repression on the promoter of Rig-1, a Robo member. *Biochem. Biophys. Res. Commun.* **296**, 1019-1025.
**Yuasa-Kawada, J., Kinoshita-Kawada, M., Rao, Y. and Wu, J. Y.** (2009a). Deubiquitinating enzyme USP33/VDU1 is required for Slit signaling in inhibiting breast cancer cell migration. *Proc. Natl. Acad. Sci. USA* **106**, 14530-14535.
**Yuasa-Kawada, J., Kinoshita-Kawada, M., Wu, G., Rao, Y. and Wu, J. Y.** (2009b). Midline crossing and Slit responsiveness of commissural axons require USP33. *Nat. Neurosci.* **12**, 1087-1089.
**Yue, Y., Grossmann, B., Galetzka, D., Zechner, U. and Haaf, T.** (2006). Isolation and differential expression of two isoforms of the ROBO2/Robo2 axon guidance receptor gene in humans and mice. *Genomics* **88**, 772-778.
**Zmojdzian, M., Da Ponte, J. P. and Jagla, K.** (2008). Cellular components and signals required for the cardiac outflow tract assembly in Drosophila. *Proc. Natl. Acad. Sci. USA* **105**, 2475-2480.

Available online at www.sciencedirect.com
ScienceDirect
Current Opinion in Cell Biology
ELSEVIER

# Born to run: creating the muscle fiber

Eyal D Schejter[1] and Mary K Baylies[2]

From the muscles that control the blink of your eye to those that allow you to walk, the basic architecture of muscle is the same: muscles consist of bundles of the unit muscle cell, the muscle fiber. The unique morphology of the individual muscle fiber is dictated by the functional demands necessary to generate and withstand the forces of contraction, which in turn leads to movement. Contractile muscle fibers are elongated, syncytial cells, which interact with both the nervous and skeletal systems to govern body motion. In this review, we focus on three key cell–cell and cell–matrix contact processes, that are necessary to create this exquisitely specialized cell: cell fusion, cell elongation, and establishment of a myotendinous junction. We address these processes by highlighting recent findings from the *Drosophila* model system.

**Addresses**
[1] Department of Molecular Genetics, Weizmann Institute of Science, Rehovot, Israel
[2] Program in Developmental Biology, Sloan-Kettering Institute, Memorial Sloan-Kettering Cancer Center, 1275 York Avenue, New York, NY, 10065, United States

Corresponding author: Schejter, Eyal D (eyal.schejter@weizmann.ac.il)

**Current Opinion in Cell Biology** 2010, **22**:566–574

This review comes from a themed issue on
Cell-to-cell contact and extracellular matrix
Edited by Peter Friedl and Jennifer Zallen

0955-0674/$ – see front matter


**DOI** 10.1016/j.ceb.2010.08.009

## Introduction

The model system, *Drosophila melanogaster*, has been used to great effect to study fundamental issues of muscle development [1–7]. This model organism offers the cell biologist an *in vivo* system, coupled to a long-established genetic tradition to study muscle morphogenesis. In addition, application of genomics and varied imaging approaches makes this model a highly tractable system for the study of the cell biology of muscle.

Body wall muscles in *Drosophila* are generated twice during the life of the fly: first, during embryogenesis to form the larval muscles [1], the process that is the main focus of this review; and subsequently during metamorphosis, in which cells set aside during embryonic myogenesis are used to generate the adult muscles [8]. In the embryo, a single fiber is considered a single muscle, whereas in the adult, multiple fibers constitute a single muscle. A similar mechanism, however, governs fiber formation in both situations: each fiber is seeded by a specialized myoblast, called a founder cell (FC), which fuses repeatedly with neighboring fusion competent myoblasts (FCMs) to generate a multi-nucleated myotube (Figure 1) [1]. Upon fusion, the newly incorporated FCM-derived nuclei adopt the transcriptional profile of the FC/myotube. By virtue of a complex developmental specification process, individual FCs/myotubes express different combinations of cell identity regulators, which endow them with unique morphological characteristics, including size (i.e. the number of fusions with FCMs), shape, and spatial orientation [9,10••].

Fusion is accompanied by elongation of the growing myofiber, which navigates towards tendon cells that arise in the overlying epidermis. Through interactions with these tendon cells, a stable attachment forms between muscle, epidermis, and cuticle (the exoskeleton) (Figure 1). These initial, crucial myogenic processes – fusion, elongation, and attachment – are at the heart of this review. Innervation of each muscle fiber occurs after fusion and tendon attachment, while the stereotypical arrangement of the fiber contractile apparatus (sarcomeres) appears late during muscle morphogenesis, just before hatching [1,10]. The contractile properties and inter-cellular associations provide body wall muscles with the capacity to execute and govern larval motility.

## Muscle fiber as syncytial cell: focus on the actin focus

A series of recent reviews provide a comprehensive, updated description of myoblast fusion in *Drosophila* and in vertebrates [11•,12,13,14•]. Here we discuss recent insights to fusion, emphasizing the remaining gaps in our knowledge, with particular emphasis on the contribution of the actin-based cytoskeleton.

Myoblast fusion, as in all cases of cell–cell fusion, requires several distinct cellular behaviors [15]. Initially, FCs/myotubes and FCMs must recognize and adhere to each other. The result of recognition and adhesion is a series of cellular events that are necessary to bring the cell membranes of the two cells in close proximity to one another. Subsequently, the tethering of the plasma membranes, the formation of pores between the membranes and the expansion of these pores leads to the merging of the two myoblasts (Figure 1d).

**Figure 1**

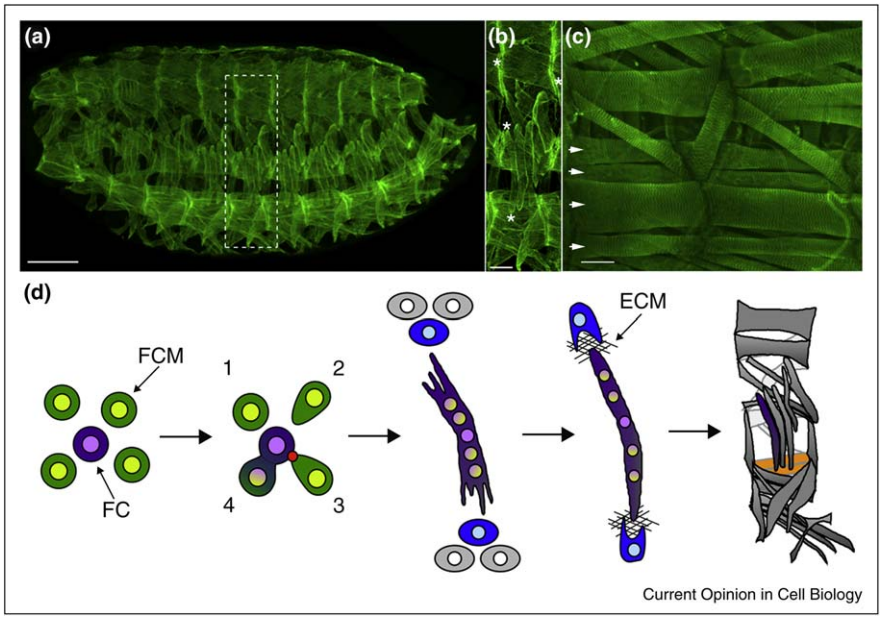


The morphogenesis of *Drosophila* larval body wall muscles. **(a)** A stage 16 *Drosophila* embryo labeled with antibodies against Tropomyosin (green), which reveal the segmentally repeated pattern of body wall muscles. Scale bar 50 μm. **(b)** A close-up of a single hemisegment from A shows that each muscle is a single fiber with unique size, shape, and attachment sites. Examples of attachment sites (*) shown for two different muscles. Scale bar 15 μm. **(c)** Subset of *Drosophila* larval muscles labeled with antibodies against Zasp (green), which labels the Z-band of the sarcomere. Scale bar 20 μm. Arrows point to the four ventral lateral (VL) muscles. **(d)** Schematic of steps leading to the development of a muscle fiber. FC, founder cell (purple); FCM, fusion-competent myoblast (green). First panel: the two types of myoblasts required to make a muscle. Second panel: Fusion. Numbers note FCMs that are in different states in the fusion cycle: 1—Rounded and not initiating fusion, 2—Cell shape change associated with orientation and migration to a FC; 3—Adhesion to a FC and formation of an actin focus (red) at the fusion site; 4—Pore formation and membrane vesiculation leading to cytoplasmic continuity. Panel 3: Both ends of an elongating myotube navigate towards a tendon cell (blue), positioned within the epidermis (gray cells). Panel 4: An attachment between muscle and tendon. ECM, extracellular matrix. Panel 5: The pattern of 30 muscles per abdominal hemisegment. Two VL muscles are highlighted in yellow.

In the *Drosophila* embryo, myoblast recognition and adhesion is mediated by a set of immunoglobulin (Ig) domain transmembrane proteins: Dumbfounded (Duf, a.k.a Kirre) and Roughest (Rst a.k.a IrreC), which are found primarily in FCs, and the FCM elements Sticks and stones (Sns) and Hibris (Hbs) [12–14,16•]. Fusion-related roles for vertebrate homologs of these proteins have been recently revealed [17,18], implying conservation of this system of cell recognition and adhesion. However, several significant issues pertaining to the underlying molecular mechanisms remain unclear, and require further investigation. Prominent among these are the initiation of contact between distant myoblasts (is a diffusible factor involved?), selection of fusion partners ('first come, first serve' vs. 'specificity of partnering'), and generation of tightly apposed myoblast membranes, primed for fusion. Recent evidence suggests that the Ig domain recognition receptors form a ring-like structure, termed the FuRMAS [13,19•] at the fusion site. These data have been used to suggest that the recognition receptors, upon engagement, are cleared from the site of actual membrane fusion. The FuRMAS, by the nature of a ring-like structure, could also limit the site of membrane fusion to within this ring. Time-lapse imaging of tagged receptors would provide a significant step forward in verifying this model.

Downstream of the receptors, genetic, cell, and biochemical approaches have implicated a set of actin regulatory proteins as crucial for myoblast fusion. Specifically, mutations in genes including Rac, Myoblast city (Dock 180), Kette (Nap1), Scar (WAVE), Vrp1 (Solitary; D-WIP), WASp, and Arp2/3, lead to defects in myoblast fusion [11•,12,13,14•]. While clarification is needed as to how particular actin regulatory proteins are recruited specifically to the recognition receptors and the fusion site [20,21•,22,23,24••,25••,26••,27,28,29••,30], it is clear that one crucial result of their function is a branched actin structure, termed the actin focus [19•,25••,29••]. Time-lapse imaging of *Drosophila* myoblasts proved conclusively that this structure marks the fusion site and revealed the dynamics of this structure. The actin focus is on average short-lived (11.9 min, range 5.7–29 min), measuring 2 $\mu m^2$ in size (range 0.7–4.5 $\mu m^2$); this structure disappears as cytoplasmic continuity between the fusing cells is achieved (Figure 2). Genetic analysis reveals that actin focus formation requires recognition receptor function for

**Figure 2**

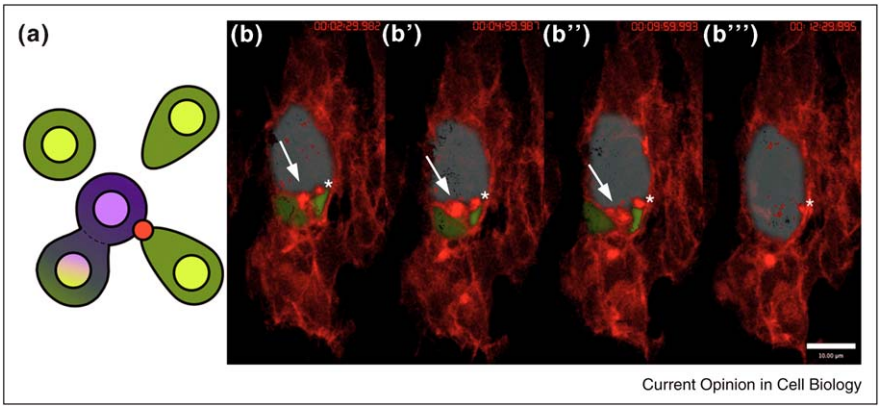


The site of myoblast fusion is marked by an actin focus. **(a)** Schematic of myoblast fusion showing fusion between a myotube (purple) and fusion competent myoblasts (green). Note shape changes in FCMs and actin focus (red dot). (**b**–**b‴**) Stills from time-lapse imaging reveal the progress of fusion events. Time stamps: **(b)** 00:02:29.982; **(b′)** 00:04:59.987; **(b″)** 00:09:59.993; **(b‴)** 00:12:29.995. An actin focus is present at each fusion site. Myotube false colored blue; FCMs false colored green. Actin (red) revealed by moesin-mcherry expressed specifically in the muscle mesoderm (using *twist-GAL4*). Stage 14 embryo, extended focus view of 10, 0.5 μm z-slices, frame rate is 2.30 min. Elapsed time shown upper right. Arrow points to one actin focus, asterisk to a second. Two others are also present below the false-colored myotube.

its formation [29••]. Consistent with these genetic experiments is the observation that the FuRMAS surrounds the actin focus [13,19•]. While double labeling experiments using actin and membrane reporter constructs suggest that the actin focus can be found on both sides of the fusion event (myotube and FCM), the distribution of actin within the focus may be biased to one cell or the other [25••,29••] (B. Richardson, I. Bothe and MKB unpub.). Whether this indicates the existence of different actin structures or reveals novel aspects of actin focus maturation remains to be investigated.

With genetics implicating SCAR/WAVE and WASp regulation of Arp2/3 as crucial to myoblast fusion, a simple model would be that these actin regulatory pathways are required for actin focus formation. However, contrary to expectation, analysis of single and double mutants between different pathway members reveals persistent and even enlarged actin foci at fusion sites [24] (B. Richardson and MKB unpub). The genetic data indicate, therefore, that these pathways are not required for formation of the foci, but may ut may influence actin rearrangements leading to dissolution of these structures. While some debate continues, these data also illustrate that the proteins required for formation of the actin focus remain to be identified. Additional Arp2/3 regulators have been uncovered in other systems [31], providing new genes to investigate for this key role in actin regulation during myoblast fusion.

An essential question arising from these studies is the function of the actin focus at the fusion site. Time-lapse imaging correlates formation and, importantly, removal of the actin focus, with cytoplasmic continuity and ultimately cell–cell fusion. With the exception of the recognition receptors and a protein implicated in receptor recycling, mutants of which do not form actin foci, all other known fusion gene mutants display actin foci that perdure at the fusion site. Of these, some mutants have enlarged foci and others have wild-type sized foci [14,29••,32]. Testing is needed to determine whether the fusion block in any of these mutants is due to the inability of the cell to remove the focus specifically, or whether the long-lived focus is just a consequence of other events gone awry. Nevertheless, several models for the cellular function of the actin focus have been put forward. These include targeting vesicles to the site of fusion [25••], supplying scaffolding to maintain cellular integrity while fusion pores are created [29••], and/or providing a force for fusion pore enlargement [26]. To provide the necessary data to evaluate these models, a combination of approaches are needed: identification of new genes and mechanisms via genetic and biochemical experiments; improved imaging, employing time-lapse videography and transmission electron microscopy; determination of composition and dynamics of cell membranes and membrane-bound vesicles associated with the fusion site; and finally, detailed description and analysis of fusion pore formation and expansion. While the *Drosophila* system has provided new views of a prominent and highly regulated form of cell–cell fusion, much remains to be investigated, particularly with regard to the cell-biological mechanism underlying the fusion process.

## Directing myotubes to their epidermal targets

In parallel to their growth via fusion with FCMs, myotubes in the *Drosophila* embryo elongate towards the

**Figure 3**

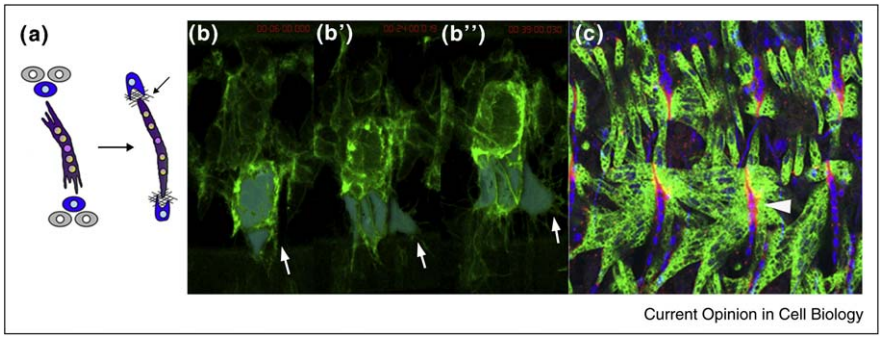


Elongation and attachment of the myotube to tendon cells. **(a)** Schematic of muscle elongation and attachment to tendon cells. (**b**–**b″**) Stills from a time-lapse movie of a late stage 15 embryo, expressing a membrane marker in the muscle mesoderm (*Twist-Gal4 > UAS-plcγPH::GFP*), and using extended focus of 28, 0.5 μm z-slices, frame rate, 3 min. Time Stamps: **(b)** 00:06:00; **(b′)** 00:24:00; **(b″)** 00:39:00. Ventral myotubes are false-colored blue to highlight elongation. Arrow in each frame points out filopodial extensions. Elapsed time shown in upper right of each frame (red). **(c)** Stage 16 embryo showing mature attachments of muscles to tendon cells (arrowhead). Tendon cell nuclei (labeled using anti-Stripe) are in blue, while muscles (labeled with anti-Myosin Heavy Chain) are in green. ECM of the myotendinous junction is visualized using anti-Thrombospondin (red). Image provided by Arul Subramanian and Talila Volk.

epidermis and attach to tendon cells at both ends (Figure 3). The highly stereotypic pattern of muscle–tendon attachments implies that regulatory mechanisms are at play, ensuring specificity and proper execution of the myotube targeting process. It is well-established that tendon cells produce spatial cues influencing the direction towards which myotubes extend. The muscles, in turn, seek out their attachment sites by sending out filopodia-like extensions that survey their environment for these instructive cues [1,33].

Perhaps the sole *bona fide* identification of a tendon-derived guidance signal has been described in the ventral-longitudinal (VL) muscles, a repeating set of four parallel fibers that stretch between epidermal attachments sites at the adjacent embryonic segment border. Segment-border tendon cells secrete the ECM glycoprotein Slit, which directs myotube targeting by binding to the Roundabout (Robo) receptor, expressed at the edges of developing VL muscle fibers [34•]. Therefore, although the Slit–Robo ligand–receptor interaction is best known as the basis for repulsion of both axons and muscle fibers away from the ventral midline of the *Drosophila* embryo [35], it also functions as an attractive cue, guiding myotubes to specific epidermal target sites. Mutations in which properly fused myotubes extend randomly and fail to connect to their epidermal target sites have recently uncovered a second myotube targeting mechanism, apparently acting in parallel to the Slit/Robo pathway [36••,37•,38••,39••]. Importantly, mutant myotubes of this class are capable of forming stable attachments, but do so with incorrect tendon target cells, or even with adjacent muscles, implying specific impairment of target recognition capacity, while other aspects of myotube differentiation remain unaffected. A key player that has emerged from this group is D-Grip, the sole fly homolog of the Grip (Glutamate receptor interacting protein) adaptor protein family. Grip proteins harbor multiple PDZ domains, and have been functionally implicated in various aspects of synaptic protein trafficking and localization [40–42]. In *Drosophila* embryos, *D-Grip* is specifically expressed in developing muscles, and the D-Grip protein accumulates within endosomes at the ends of extending myofibers [39].

While D-Grip probably acts as a mediator of intracellular trafficking, it is becoming apparent that this multi-PDZ-domain adaptor serves a key myogenic role as a common platform for multiple muscle factors contributing to myotube targeting. Prominent among these is Kon-tiki (Kon; a.k.a Perdido), a transmembrane protein and potential receptor mediating recognition of tendon-cell guidance signals by growing embryonic myotubes [36••,38••]. Kon associates with D-Grip through a C-terminal PDZ binding domain, localizes to the ends of extending VL myotubes, and is required for D-Grip localization to these sites. Kon contributes to additional aspects of muscle–tendon attachment. One of these is to regulate the extent of motile exploratory activity by myotube ends [38••]. Interestingly, a similar function has been recently proposed for the tendon cell transmembrane protein LRT [43•], which can physically associate with Robo receptors. LRT may therefore restrict myotube migratory activity by signaling through Robo, or indirectly, by competing with Slit for Robo receptor binding, thereby stifling its stimulatory effect on myotube dynamics [43,44]. Such utilization of both muscle and tendon-based programs underscores the importance of setting limits on guidance-seeking mechanisms, once initial target recognition is achieved.

An additional member of the D-Grip-based guidance machinery is the Ig superfamily transmembrane protein Echinoid (Ed) [45•]. Structurally related to the vertebrate Nectins, Ed functions as a homotypic cell adhesion molecule, mediating aspects of *Drosophila* neurogenesis and epithelial morphogenesis [46–48]. Similar to Kon, Ed associates with D-Grip PDZ domains via its extreme C-terminal region. Furthermore, Ed colocalizes with D-Grip at the ends of VL muscles, and the two elements display strong genetic interactions with respect to VL myotube extension defects [45]. Targeting and guidance errors rather than defective adhesion are the main characteristic of embryos in which the Ed/D-Grip system is impaired, implying that Ed and D-Grip influence myotube behavior by affecting cortical and cytoplasmic features of these cells. Significantly, Ed affects the outcome of cell–cell interactions through communication with cortical microfilaments [48–50], and therefore serves as a good candidate for a link between the D-Grip platform and the actin-based cytoskeleton.

This series of studies has therefore revealed a molecular complex, positioned at the tips of growing muscle fibers, which integrates a number of inputs aimed at achieving proper myotube targeting. Remarkably, a highly similar Grip-based platform mediates glia–neuron interactions during mammalian CNS development [51]. In this instance, the PDZ domains of Grip bring together several glial cell-surface proteins, including NG2, a mammalian homolog of Kon [52,53], which is thought to interact with a neuronal receptor. Cortical complexes of this type therefore represent a conserved machinery for instructive communication between distinct cell types, leading to functional maturation of a differentiating tissue.

While involvement of the Grip-based complex in myotube targeting implies functional reliance on the actin-based cytoskeleton, mutations resulting in defective muscle targeting have now revealed that growing myotubes also require properly polarized microtubule (MT) arrays, in order to reach their correct attachment sites [37•]. Key elements involved in this system are Tumbleweed (Tum) and Pavarotti (Pav), established components of the cytokinesis-mediating complex centralspindlin [54–56]. In *Drosophila* embryonic muscles, Tum and Pav are jointly responsible for localization of non-centrosomal, γ-tubulin-based microtubule organizing centers to the vicinity of myotube nuclei. These nuclei commonly cluster in the center of growing multi-nucleated fibers [37•]. The resulting microtubule array that forms extends from the myotube interior towards the periphery, and is polarized, with the microtubule plus-ends pointing towards the extending tips of the growing fibers. A similarly oriented microtubule array, nucleated from non-centrosomal organizing centers, forms in cultured mammalian myotubes [57], suggesting that reorganization of the microtubule cytoskeleton in this fashion reflects a conserved requirement during muscle differentiation. From a functional standpoint, the axial microtubule array may serve as a structural framework enabling elongation of myotube ends [37•,57], or alternatively, may provide polarized tracks for trafficking and localization of crucial guidance and targeting signals that ensure proper selection of myotube attachment sites.

## Making a strong myotendinous junction

Contact between myotubes and tendon cells is closely followed by establishment of a myotendinous junction, so that muscle and epidermis maintain a strong physical connection that will be able to withstand the considerable forces imposed on it once muscle contractions initiate [58]. Integrins play a major, conserved role in this process, and indeed, the *Drosophila* embryonic myotendinous junction now serves as a prominent example and setting for study of integrin-based adhesion between distinct cell types [59]. Both muscle and tendon cells express αβ integrin heterodimers, which fortify cell attachment to the junction by serving as transmembrane links between the ECM and the internal actin cytoskeleton. These heterodimers are composed of a common β subunit (βPS) and distinct α subunits—αPS1 for the tendon cell integrin and αPS2 in muscles. Genetic disruption of the muscle αPS2βPS integrin does not interfere with construction, elongation, and attachment of muscle fibers. However, once the muscles of such mutant embryos begin to contract, they disconnect from their attachment sites and retract into ball-shaped structures [60–63]. This classic 'myospheroid' phenotype now serves as a diagnostic tool for identification of additional elements contributing to formation and consolidation of myotendinous junctions.

Several ECM components act as ligands for the *Drosophila* αPS2βPS integrin in the context of the myotendinous junction, including the Laminin α-chain protein Wing Blister [64], and Tiggrin [65,66]. Recent studies have now identified *Drosophila* Thrombospondin (Tsp) as a major αPS2βPS integrin ligand at muscle attachment sites [67••,68••]. Vertebrate Thrombospondins comprise a family of multimeric ECM glycoproteins, which have been implicated in diverse functional settings, such as cell aggregation and attachment, angiogenesis and synaptogenesis [69–71]. *Drosophila* Tsp is produced and secreted by tendon cells at stages corresponding to establishment of muscle–tendon contacts. The muscle detachment phenotypes of *Tsp* mutant embryos, genetic interactions of *Tsp* with integrin encoding genes, and biochemical binding assays, combine to identify Tsp as a ligand for αPS2βPS. The integrin-binding capacity and localization patterns of Tsp suggest a dynamic sequence [67••,68••], in which Tsp first contributes to the initial association of myotube ends with the tendon cell and its ECM. Subsequently, muscle–tendon interactions set in

motion a general program of tendon cell differentiation [72], leading to increased expression and secretion of Tsp, which in turn fortifies the integrin-mediated myotube attachment to the myotendinous junction.

Further insight to the regulation of Tsp activity comes from the study of Slowmotion (Slow), a new player in myotendinous junction construction [73•]. Slow, the *Drosophila* homolog of vertebrate EGFL7 [74,75], is secreted from tendon cells in parallel to Tsp, and attenuates the Tsp-αPS2βPS integrin interaction by forming a complex with Tsp. Streamlining of muscle integrin activity in this manner turns out to be crucial for proper morphogenesis of the myotendinous junction into a structure capable of withstanding the wear-and-tear of intense larval muscle activity [73].

Progress in the understanding of integrin–ECM interactions in the context of myotendinous junction formation has been matched by refined characterization of the manner by which integrins are linked to cytoplasmic and cytoskeletal components. Thus the *Drosophila* homolog of ZASP (Z-band alternatively spliced PDZ-motif protein), a member of the PDZ-LIM protein family [76,77], acts as an adapter that strengthens the integrin–actin connection following its initial establishment via Talin, a ubiquitous mediator of integrin-based processes [78••]. Zasp performs this role repeatedly during myogenesis, initially to bolster the myotendinous junction, and later to mediate integrin-dependent assembly of muscle fiber sarcomeres [78].

A second adaptor of this type is Wech [79••], a well-conserved member of the growing, multi-domain TRIM protein family, the functional attributes of which are only beginning to emerge [80,81,82]. At *Drosophila* myotendinous junctions, Wech acts within tendon cells and myotubes to bridge a key interaction between Talin, which associates with the βPS integrin subunit, and the Integrin-linked Kinase (ILK) complex, a crucial mediator of the integrin-microfilament link [83]. This specific adaptor capacity of Wech appears to be conserved in mammals [79], suggesting that a fundamental aspect of integrin-mediated adhesion has now been uncovered.

## Conclusions and perspectives

In this review we have focused on a restricted set of myogenic processes, to demonstrate the power of the *Drosophila* embryo as a model system for studying muscle cell properties and behaviors. A wide variety of issues, such as cell size, shape, polarity, migration, and adhesion can all be addressed using this versatile system. The relative simplicity and segmentally repeated nature of the embryonic musculature, amenable to study via classical and modern genetic approaches coupled to imaging and biochemical analysis, provide a unique, *in vivo* experimental setting. The recent introduction of comprehensive RNAi-based genetic methods to the *Drosophila* field [84,85••], along with the application of large-scale genomic techniques [36••,86–88] now promises to significantly enhance these studies. For example, the capacity to control RNAi expression in a temporal and tissue-specific manner helps overcome a variety of obstacles confronting more conventional genetic approaches. Importantly, this tool now enables comprehensive exploration of adult fly myogenesis, and we expect that considerable insight to issues of muscle cell biology will emerge from this 'new frontier' in the years to come.

## Acknowledgements

We would like to thank members of the Baylies lab, particularly K. Dobi for critical reading, and S. Yu, I. Bothe, and T. Metzger for figures. We also thank T. Volk for kindly providing Figure 3c. We acknowledge our funding agencies: NIH (GM078318 and GM056989) and MDA to MB, ISF, and MDA to B. Shilo and EDS, and the Mary L. Ralph Fund to MB, B Shilo and EDS.

## References and recommended reading

Papers of particular interest, published within the annual period of review, have been highlighted as:

- • of special interest
- •• of outstanding interest

1. Bate M: **The embryonic development of larval muscles in Drosophila**. *Development* 1990, **110**:791-804.

2. Ciglar L, Furlong EE: **Conservation and divergence in developmental networks: a view from Drosophila myogenesis**. *Curr Opin Cell Biol* 2009, **21**:754-760.

3. Daczewska M, Picchio L, Jagla T, Figeac N, Jagla K: **Muscle development and regeneration in normal and pathological conditions: learning from Drosophila**. *Curr Pharm Des* 2010, **16**:929-941.

4. Figeac N, Daczewska M, Marcelle C, Jagla K: **Muscle stem cells and model systems for their investigation**. *Dev Dyn* 2007, **236**:3332-3342.

5. Frasch M: **Controls in patterning and diversification of somatic muscles during Drosophila embryogenesis**. *Curr Opin Genet Dev* 1999, **9**:522-529.

6. Nguyen HT, Frasch M: **MicroRNAs in muscle differentiation: lessons from Drosophila and beyond**. *Curr Opin Genet Dev* 2006, **16**:533-539.

7. Schnorrer F, Dickson BJ: **Muscle building; mechanisms of myotube guidance and attachment site selection**. *Dev Cell* 2004, **7**:9-20.

8. Bate M, Rushton E, Currie DA: **Cells with persistent twist expression are the embryonic precursors of adult muscles in Drosophila**. *Development* 1991, **113**:79-89.

9. Baylies MK, Michelson AM: **Invertebrate myogenesis: looking back to the future of muscle development**. *Curr Opin Genet Dev* 2001, **11**:431-439.

10. •• Beckett K, Baylies MK: **The development of the Drosophila larval body wall muscles**. *Int Rev Neurobiol* 2006, **75**:55-70.
This paper describes the spatial arrangement of the Founder cells and Fusion competent myoblasts during the 5.5 h period of myoblast fusion. An analysis of the timing of fusion is also investigated in wild-type and fusion mutants, leading to a reexamination of fusion models.

11. • Gildor B, Massarwa R, Shilo BZ, Schejter ED: **Making muscles: Arp, two, three**. *Fly (Austin)* 2010, **4**:145-148.
This review focuses the discussion on the requirements of the SCAR/WAVE and WASp actin nucleating factors in the cell behaviors required for myoblast fusion.

12. Haralalka S, Abmayr SM: **Myoblast fusion in Drosophila**. *Exp Cell Res* 2010 doi: 10.1016/j.yexcr.2010.05.018.

13. Onel SF, Renkawitz-Pohl R: **FuRMAS: triggering myoblast fusion in Drosophila**. *Dev Dyn* 2009, **238**:1513-1525.

14. • Rochlin K, Yu S, Roy S, Baylies MK: **Myoblast fusion: when it takes more to make one**. *Dev Biol* 2009, **341**:66-83.
This in-depth review discusses the genes and mechanisms underlying myoblast fusion in fly, zebrafish, and mouse in light of cell-biological processes required for this process: cell recognition, migration, adhesion, vesicle trafficking, and membrane breakdown.

15. Beckett K, Baylies MK: **3D analysis of founder cell and fusion competent myoblast arrangements outlines a new model of myoblast fusion**. *Dev Biol* 2007, **309**:113-125.

16. • Shelton C, Kocherlakota KS, Zhuang S, Abmayr SM: **The immunoglobulin superfamily member Hbs functions redundantly with Sns in interactions between founder and fusion-competent myoblasts**. *Development* 2009, **136**:1159-1168.
Excellent data are presented in this paper, indicating that Hbs can function redundantly with Sns to mediate cell adhesion during myoblast fusion.

17. Sohn RL, Huang P, Kawahara G, Mitchell M, Guyon J, Kalluri R, Kunkel LM, Gussoni E: **A role for nephrin, a renal protein, in vertebrate skeletal muscle cell fusion**. *Proc Natl Acad Sci USA* 2009, **106**:9274-9279.

18. Srinivas BP, Woo J, Leong WY, Roy S: **A conserved molecular pathway mediates myoblast fusion in insects and vertebrates**. *Nat Genet* 2007, **39**:781-786.

19. • Kesper DA, Stute C, Buttgereit D, Kreiskother N, Vishnu S, Fischbach KF, Renkawitz-Pohl R: **Myoblast fusion in *Drosophila melanogaster* is mediated through a fusion-restricted myogenic-adhesive structure (FuRMAS)**. *Dev Dyn* 2007, **236**:404-415.
This paper is the first to describe the organization of the recognition and adhesion receptors in a ring-like structure, designated FuRMAS, during myoblast fusion.

20. Balagopalan L, Chen MH, Geisbrecht ER, Abmayr SM: **The CDM superfamily protein MBC directs myoblast fusion through a mechanism that requires phosphatidylinositol 3,4,5-triphosphate binding but is independent of direct interaction with DCrk**. *Mol Cell Biol* 2006, **26**:9442-9455.

21. • Berger S, Schafer G, Kesper DA, Holz A, Eriksson T, Palmer RH, Beck L, Klambt C, Renkawitz-Pohl R, Onel SF: **WASP and SCAR have distinct roles in activating the Arp2/3 complex during myoblast fusion**. *J Cell Sci* 2008, **121**:1303-1313.
This paper identifies a new allele of Arp3. Through double mutant analysis the authors suggest a sequential requirement for actin nucleating factors and Arp3 at the site of fusion.

22. Chen EH, Olson EN: **Antisocial, an intracellular adaptor protein, is required for myoblast fusion in Drosophila**. *Dev Cell* 2001, **1**:705-715.

23. Chen EH, Pryce BA, Tzeng JA, Gonzalez GA, Olson EN: **Control of myoblast fusion by a guanine nucleotide exchange factor, loner, and its effector ARF6**. *Cell* 2003, **114**:751-762.

24. •• Gildor B, Massarwa R, Shilo BZ, Schejter ED: **The SCAR and WASp nucleation-promoting factors act sequentially to mediate Drosophila myoblast fusion**. *EMBO Rep* 2009, **10**:1043-1050.
This report indicates a sequential requirement of these actin nucleating factors during fusion, with SCAR required before fusion pore formation and WASp required during pore expansion. In addition, this study indicates that Scar contributes to myoblast migration by facilitating myoblast shape changes.

25. •• Kim S, Shilagardi K, Zhang S, Hong SN, Sens KL, Bo J, Gonzalez GA, Chen EH: **A critical function for the actin cytoskeleton in targeted exocytosis of prefusion vesicles during myoblast fusion**. *Dev Cell* 2007, **12**:571-586.
This paper investigates the role of the *solitary* allele of Vrp1 in myoblast fusion, and proposes a model in which filamentous actin mediates targeting of vesicles to the fusion site.

26. •• Massarwa R, Carmon S, Shilo BZ, Schejter ED: **WIP/WASp-based actin-polymerization machinery is essential for myoblast fusion in Drosophila**. *Dev Cell* 2007, **12**:557-569.
This paper identifies both Vrp1 (D-WIP) and WASp as crucial for myoblast fusion and suggests that these proteins target actin branching at the fusion site, leading to the expansion of fusion pores.

27. Menon SD, Chia W: **Drosophila rolling pebbles: a multidomain protein required for myoblast fusion that recruits D-Titin in response to the myoblast attractant Dumbfounded**. *Dev Cell* 2001, **1**:691-703.

28. Rau A, Buttgereit D, Holz A, Fetter R, Doberstein SK, Paululat A, Staudt N, Skeath J, Michelson AM, Renkawitz-Pohl R: **rolling pebbles (rols) is required in Drosophila muscle precursors for recruitment of myoblasts for fusion**. *Development* 2001, **128**:5061-5073.

29. •• Richardson BE, Beckett K, Nowak SJ, Baylies MK: **SCAR/WAVE and Arp2/3 are crucial for cytoskeletal remodeling at the site of myoblast fusion**. *Development* 2007, **134**:4357-4367.
This paper characterizes the dynamic behavior of the actin focus in wild-type and fusion mutant embryos using time-lapse videography. The paper also indicates that Scar and Arp2/3 are required for myoblast fusion in the *Drosophila* embryo.

30. Schroter RH, Lier S, Holz A, Bogdan S, Klambt C, Beck L, Renkawitz-Pohl R: **kette and blown fuse interact genetically during the second fusion step of myogenesis in Drosophila**. *Development* 2004, **131**:4501-4509.

31. Campellone KG, Welch MD: **A nucleator arms race: cellular control of actin assembly**. *Nat Rev Mol Cell Biol* 2010, **11**:237-251.

32. Richardson BE, Nowak SJ, Baylies MK: **Myoblast fusion in fly and vertebrates: new genes, new processes and new perspectives**. *Traffic* 2008, **9**:1050-1059.

33. Volk T: **Singling out Drosophila tendon cells: a dialogue between two distinct cell types**. *Trends Genet* 1999, **15**:448-453.

34. • Kramer SG, Kidd T, Simpson JH, Goodman CS: **Switching repulsion to attraction: changing responses to slit during transition in mesoderm migration**. *Science* 2001, **292**:737-740.
Identification of the Slit–Robo system as a basis for myotube attraction to tendon cells during *Drosophila* embryogenesis.

35. Kidd T, Bland KS, Goodman CS: **Slit is the midline repellent for the robo receptor in Drosophila**. *Cell* 1999, **96**:785-794.

36. •• Estrada B, Gisselbrecht SS, Michelson AM: **The transmembrane protein Perdido interacts with Grip and integrins to mediate myotube projection and attachment in the Drosophila embryo**. *Development* 2007, **134**:4469-4478.
See notes to reference [38••].

37. • Guerin CM, Kramer SG: **RacGAP50C directs perinuclear gamma-tubulin localization to organize the uniform microtubule array required for Drosophila myotube extension**. *Development* 2009, **136**:1411-1421.
This study describes and characterizes the involvement of muscle fiber microtubule arrays in myotube guidance and extension.

38. •• Schnorrer F, Kalchhauser I, Dickson BJ: **The transmembrane protein Kon-tiki couples to Dgrip to mediate myotube targeting in Drosophila**. *Dev Cell* 2007, **12**:751-766.
This paper and the study from Estrada *et al.* (reference [36]) identify the transmembrane protein Kon-tiki/Perdido as an important component of the D-Grip pathway mediating myotube guidance and extension.

39. •• Swan LE, Wichmann C, Prange U, Schmid A, Schmidt M, Schwarz T, Ponimaskin E, Madeo F, Vorbruggen G, Sigrist SJ: **A glutamate receptor-interacting protein homolog organizes muscle guidance in Drosophila**. *Genes Dev* 2004, **18**:223-237.
The initial discovery that D-Grip, a PDZ-domain adaptor, mediates myotube guidance and extension in *Drosophila* embryos.

40. Ataman B, Ashley J, Gorczyca D, Gorczyca M, Mathew D, Wichmann C, Sigrist SJ, Budnik V: **Nuclear trafficking of Drosophila Frizzled-2 during synapse development requires the PDZ protein dGRIP**. *Proc Natl Acad Sci USA* 2006, **103**:7841-7846.

41. Dong H, O'Brien RJ, Fung ET, Lanahan AA, Worley PF, Huganir RL: **GRIP: a synaptic PDZ domain-containing protein that interacts with AMPA receptors**. *Nature* 1997, **386**:279-284.

42. Hoogenraad CC, Milstein AD, Ethell IM, Henkemeyer M, Sheng M: **GRIP1 controls dendrite morphogenesis by regulating EphB receptor trafficking**. *Nat Neurosci* 2005, **8**:906-915.

43. • Wayburn B, Volk T: **LRT, a tendon-specific leucine-rich repeat protein, promotes muscle–tendon targeting through its interaction with Robo**. *Development* 2009, **136**:3607-3615.
This paper shows that LRT, expressed by tendon cells, acts to restrict migratory activity of extending myotubes by interacting with the Robo guidance receptor.

44. Gilsohn E, Volk T: **Fine tuning cellular recognition: the function of the leucine rich repeat (LRR) trans-membrane protein. LRT, in muscle targeting to tendon cells**. *Cell Adhes Migr* 2010, **4**:368-371.

45. • Swan LE, Schmidt M, Schwarz T, Ponimaskin E, Prange U, Boeckers T, Thomas U, Sigrist SJ: **Complex interaction of Drosophila GRIP PDZ domains and Echinoid during muscle morphogenesis**. *EMBO J* 2006, **25**:3640-3651.
This study suggests that the transmembrane protein Echinoid influences the D-Grip myotube guidance pathway, suggesting a link with microfilament organization and dynamics.

46. Fetting JL, Spencer SA, Wolff T: **The cell adhesion molecules Echinoid and Friend of Echinoid coordinate cell adhesion and cell signaling to regulate the fidelity of ommatidial rotation in the Drosophila eye**. *Development* 2009, **136**:3323-3333.

47. Rawlins EL, Lovegrove B, Jarman AP: **Echinoid facilitates Notch pathway signalling during Drosophila neurogenesis through functional interaction with Delta**. *Development* 2003, **130**:6475-6484.

48. Wei SY, Escudero LM, Yu F, Chang LH, Chen LY, Ho YH, Lin CM, Chou CS, Chia W, Modolell J *et al.*: **Echinoid is a component of adherens junctions that cooperates with DE-Cadherin to mediate cell adhesion**. *Dev Cell* 2005, **8**:493-504.

49. Laplante C, Nilson LA: **Differential expression of the adhesion molecule Echinoid drives epithelial morphogenesis in Drosophila**. *Development* 2006, **133**:3255-3264.

50. Lin HP, Chen HM, Wei SY, Chen LY, Chang LH, Sun YJ, Huang SY, Hsu JC: **Cell adhesion molecule Echinoid associates with unconventional myosin VI/Jaguar motor to regulate cell morphology during dorsal closure in Drosophila**. *Dev Biol* 2007, **311**:423-433.

51. Stegmuller J, Werner H, Nave KA, Trotter J: **The proteoglycan NG2 is complexed with alpha-amino-3-hydroxy-5-methyl-4-isoxazolepropionic acid (AMPA) receptors by the PDZ glutamate receptor interaction protein (GRIP) in glial progenitor cells. Implications for glial-neuronal signaling**. *J Biol Chem* 2003, **278**:3590-3598.

52. Karram K, Chatterjee N, Trotter J: **NG2-expressing cells in the nervous system: role of the proteoglycan in migration and glial-neuron interaction**. *J Anat* 2005, **207**:735-744.

53. Nishiyama A, Komitova M, Suzuki R, Zhu X: **Polydendrocytes (NG2 cells): multifunctional cells with lineage plasticity**. *Nat Rev Neurosci* 2009, **10**:9-22.

54. Mishima M, Kaitna S, Glotzer M: **Central spindle assembly and cytokinesis require a kinesin-like protein/RhoGAP complex with microtubule bundling activity**. *Dev Cell* 2002, **2**:41-54.

55. D'Avino PP: **How to scaffold the contractile ring for a safe cytokinesis—lessons from Anillin-related proteins**. *J Cell Sci* 2009, **122**:1071-1079.

56. Zavortink M, Contreras N, Addy T, Bejsovec A, Saint R: **Tum/RacGAP50C provides a critical link between anaphase microtubules and the assembly of the contractile ring in *Drosophila melanogaster***. *J Cell Sci* 2005, **118**:5381-5392.

57. Musa H, Orton C, Morrison EE, Peckham M: **Microtubule assembly in cultured myoblasts and myotubes following nocodazole induced microtubule depolymerisation**. *J Muscle Res Cell Motil* 2003, **24**:301-308.

58. Brown NH, Gregory SL, Martin-Bermudo MD: **Integrins as mediators of morphogenesis in Drosophila**. *Dev Biol* 2000, **223**:1-16.

59. Bokel C, Brown NH: **Integrins in development: moving on, responding to, and sticking to the extracellular matrix**. *Dev Cell* 2002, **3**:311-321.

60. Newman SM Jr, Wright TR: **A histological and ultrastructural analysis of developmental defects produced by the mutation, lethal(1)myospheroid, in *Drosophila melanogaster***. *Dev Biol* 1981, **86**:393-402.

61. Leptin M, Bogaert T, Lehmann R, Wilcox M: **The function of PS integrins during Drosophila embryogenesis**. *Cell* 1989, **56**:401-408.

62. Brown NH: **Null mutations in the alpha PS2 and beta PS integrin subunit genes have distinct phenotypes**. *Development* 1994, **120**:1221-1231.

63. Brabant MC, Brower DL: **PS2 integrin requirements in Drosophila embryo and wing morphogenesis**. *Dev Biol* 1993, **157**:49-59.

64. Martin D, Zusman S, Li X, Williams EL, Khare N, DaRocha S, Chiquet-Ehrismann R, Baumgartner S: **wing blister, a new Drosophila laminin alpha chain required for cell adhesion and migration during embryonic and imaginal development**. *J Cell Biol* 1999, **145**:191-201.

65. Bunch TA, Graner MW, Fessler LI, Fessler JH, Schneider KD, Kerschen A, Choy LP, Burgess BW, Brower DL: **The PS2 integrin ligand tiggrin is required for proper muscle function in Drosophila**. *Development* 1998, **125**:1679-1689.

66. Fogerty FJ, Fessler LI, Bunch TA, Yaron Y, Parker CG, Nelson RE, Brower DL, Gullberg D, Fessler JH: **Tiggrin, a novel Drosophila extracellular matrix protein that functions as a ligand for Drosophila alpha PS2 beta PS integrins**. *Development* 1994, **120**:1747-1758.

67. •• Subramanian A, Wayburn B, Bunch T, Volk T: **Thrombospondin-mediated adhesion is essential for the formation of the myotendinous junction in Drosophila**. *Development* 2007, **134**:1269-1278.
See notes to reference [68••].

68. •• Chanana B, Graf R, Koledachkina T, Pflanz R, Vorbruggen G: **AlphaPS2 integrin-mediated muscle attachment in Drosophila requires the ECM protein Thrombospondin**. *Mech Dev* 2007, **124**:463-475.
This paper, together with reference [67••], identifies and characterizes Drosophila Thrombospondin as a tendon-cell derived integrin ligand, essential for proper formation of embryonic myotendinous junctions.

69. Adams JC, Lawler J: **The thrombospondins**. *Int J Biochem Cell Biol* 2004, **36**:961-968.

70. Christopherson KS, Ullian EM, Stokes CC, Mullowney CE, Hell JW, Agah A, Lawler J, Mosher DF, Bornstein P, Barres BA: **Thrombospondins are astrocyte-secreted proteins that promote CNS synaptogenesis**. *Cell* 2005, **120**:421-433.

71. Bentley AA, Adams JC: **The evolution of thrombospondins and their ligand-binding activities**. *Mol Biol Evol* 2010, **27**:2187-2197.

72. Yarnitzky T, Min L, Volk T: **The Drosophila neuregulin homolog Vein mediates inductive interactions between myotubes and their epidermal attachment cells**. *Genes Dev* 1997, **11**:2691-2700.

73. • Gilsohn E, Volk T: **Slowdown promotes muscle integrity by modulating integrin-mediated adhesion at the myotendinous junction**. *Development* 2010, **137**:785-794.
Identification and characterization of a novel tendon-derived secreted element, which fortifies the larval myotendinous junction.

74. Bicker F, Schmidt MH: **EGFL7: a new player in homeostasis of the nervous system**. *Cell Cycle* 2010:9.

75. Schmidt MH, Bicker F, Nikolic I, Meister J, Babuke T, Picuric S, Muller-Esterl W, Plate KH, Dikic I: **Epidermal growth factor-like domain 7 (EGFL7) modulates Notch signalling and affects neural stem cell renewal**. *Nat Cell Biol* 2009, **11**:873-880.

76. Faulkner G, Pallavicini A, Formentin E, Comelli A, Ievolella C, Trevisan S, Bortoletto G, Scannapieco P, Salamon M, Mouly V *et al.*: **ZASP: a new Z-band alternatively spliced PDZ-motif protein**. *J Cell Biol* 1999, **146**:465-475.

77. Krcmery J, Camarata T, Kulisz A, Simon HG: **Nucleocytoplasmic functions of the PDZ-LIM protein family: new insights into organ development**. *Bioessays* 2010, **32**:100-108.

78. •• Jani K, Schock F: **Zasp is required for the assembly of functional integrin adhesion sites**. *J Cell Biol* 2007, **179**:1583-1597.

This paper demonstrates multiple essential roles for the Drosophila ZASP homolog in mediating integrin-based adhesions.

79. Loer B, Bauer R, Bornheim R, Grell J, Kremmer E, Kolanus W, •• Hoch M: **The NHL-domain protein Wech is crucial for the integrin-cytoskeleton link**. *Nat Cell Biol* 2008, **10**:422-428.
Identification of a novel and apparently conserved factor mediating the functional interaction of integrins with the actin cytoskeleton.

80. Lin YC, Hsieh LC, Kuo MW, Yu J, Kuo HH, Lo WL, Lin RJ, Yu AL, Li WH: **Human TRIM71 and its nematode homologue are targets of let-7 microRNA and its zebrafish orthologue is essential for development**. *Mol Biol Evol* 2007, **24**:2525-2534.

81. Maller Schulman BR, Liang X, Stahlhut C, DelConte C, Stefani G, Slack FJ: **The let-7 microRNA target gene, Mlin41/Trim71 is required for mouse embryonic survival and neural tube closure**. *Cell Cycle* 2008, **7**:3935-3942.

82. Munir M: **TRIM proteins: another class of viral victims**. *Sci Signal* 2010, **3**:jc2.

83. Zervas CG, Gregory SL, Brown NH: **Drosophila integrin-linked kinase is required at sites of integrin adhesion to link the cytoskeleton to the plasma membrane**. *J Cell Biol* 2001, **152**:1007-1018.

84. Dietzl G, Chen D, Schnorrer F, Su KC, Barinova Y, Fellner M, Gasser B, Kinsey K, Oppel S, Scheiblauer S *et al.*: **A genome-wide transgenic RNAi library for conditional gene inactivation in Drosophila**. *Nature* 2007, **448**:151-156.

85. Schnorrer F, Schonbauer C, Langer CC, Dietzl G, Novatchkova M, •• Schernhuber K, Fellner M, Azaryan A, Radolf M, Stark A *et al.*: **Systematic genetic analysis of muscle morphogenesis and function in Drosophila**. *Nature* 2010, **464**:287-291.
A *tour-de-force* application of whole-genome RNAi screens to the study of *Drosophila* myogenesis. Over 2700 genes are shown to have a role in myogenesis and are classified into functional groups.

86. Estrada B, Choe SE, Gisselbrecht SS, Michaud S, Raj L, Busser BW, Halfon MS, Church GM, Michelson AM: **An integrated strategy for analyzing the unique developmental programs of different myoblast subtypes**. *PLoS Genet* 2006, **2**:e16.

87. Sandmann T, Jensen LJ, Jakobsen JS, Karzynski MM, Eichenlaub MP, Bork P, Furlong EE: **A temporal map of transcription factor activity: mef2 directly regulates target genes at all stages of muscle development**. *Dev Cell* 2006, **10**:797-807.

88. Zinzen RP, Girardot C, Gagneur J, Braun M, Furlong EE: **Combinatorial binding predicts spatio-temporal cis-regulatory activity**. *Nature* 2009, **462**:65-70.

Developmental Cell
Article

# Radial Construction of an Arterial Wall

Daniel M. Greif,[1,2,4,5,*] Maya Kumar,[1,4] Janet K. Lighthouse,[5] Justine Hum,[1,4] Andrew An,[1,4] Ling Ding,[5] Kristy Red-Horse,[3] F. Hernan Espinoza,[1,4] Lorin Olson,[6] Stefan Offermanns,[7] and Mark A. Krasnow[1,4,*]
[1]Department of Biochemistry, School of Medicine
[2]Cardiovascular Division, Department of Medicine, School of Medicine
[3]Department of Biology
[4]Howard Hughes Medical Institute
Stanford University, Stanford, CA 94305, USA
[5]Cardiovascular Section, Department of Internal Medicine, Yale University School of Medicine, New Haven, CT 06511, USA
[6]Immunobiology and Cancer Research Program, Oklahoma Medical Research Foundation, Oklahoma City, OK 73104, USA
[7]Max-Planck-Institute for Heart and Lung Research, Department of Pharmacology, Ludwigstr. 43, 61231 Bad Nauheim, Germany
*Correspondence: daniel.greif@yale.edu (D.M.G.), krasnow@stanford.edu (M.A.K.)
http://dx.doi.org/10.1016/j.devcel.2012.07.009

## SUMMARY

**Some of the most serious diseases involve altered size and structure of the arterial wall. Elucidating how arterial walls are built could aid understanding of these diseases, but little is known about how concentric layers of muscle cells and the outer adventitial layer are assembled and patterned around endothelial tubes. Using histochemical, clonal, and genetic analysis in mice, here we show that the pulmonary artery wall is constructed radially, from the inside out, by two separate but coordinated processes. One is sequential induction of successive cell layers from surrounding mesenchyme. The other is controlled invasion of outer layers by inner layer cells through developmentally regulated cell reorientation and radial migration. We propose that a radial signal gradient controls these processes and provide evidence that PDGF-B and at least one other signal contribute. Modulation of such radial signaling pathways may underlie vessel-specific differences and pathological changes in arterial wall size and structure.**

## INTRODUCTION

Although there has been remarkable progress over the past decade elucidating the cellular and molecular mechanisms of the critical early events in blood vessel development, generation of new endothelial tubes by vasculogenesis and angiogenesis (Adams and Alitalo, 2007; Carmeliet, 2005; Jin et al., 2005; Phng and Gerhardt, 2009; Strilić et al., 2009; Weinstein and Lawson, 2002), relatively little is known about the subsequent events that create and pattern the arterial wall (Greif, 2012; Hungerford and Little, 1999; Hungerford et al., 1996; Schwartz, 1997). A mature arterial wall typically consists of an endothelial monolayer surrounded by multiple concentric rings of smooth muscle cells (SMCs), up to a few dozen or more layers, which dominate the mature arterial wall and provide it with structural integrity and contractility, plus an outer adventitial layer consisting of fibroblasts embedded in a collagen matrix. In many arteries there are also structural specializations such as an elastic layer separating the endothelial cells (ECs) from the vascular smooth muscle cells (VSMCs), and elastic fibers embedded in the smooth muscle layer and other cellular and molecular features that structurally subdivide and pattern the smooth muscle compartment (tunica media) (Frid et al., 1994, 1997; McLean et al., 2005; Wolinsky and Glagov, 1967). The size and pattern of the smooth muscle layer are carefully controlled in a vessel-specific manner during development, but are dysregulated in many prominent cardiovascular diseases such as aortic aneurysm, coronary artery atherosclerosis and pulmonary hypertension.

Current models of arterial wall development posit that nascent endothelial tubes recruit SMC progenitors, which can apparently arise from a variety of sources (DeRuiter et al., 1997; Esner et al., 2006; High et al., 2007; Jiang et al., 2000; Le Lièvre and Le Douarin, 1975; Majesky, 2007; Morimoto et al., 2010; Que et al., 2008; Wasteson et al., 2008; Wilm et al., 2005; Yamashita et al., 2000) and induce them to differentiate into VSMCs. Several signaling pathways have been implicated in VSMC migration or differentiation (Domenga et al., 2004; Gaengel et al., 2009; Hirschi et al., 1998; Lindahl et al., 1997; Mizugishi et al., 2005; Owens et al., 2004; Suri et al., 1996), but how these cells are recruited and organized into a radially patterned structure with the appropriate number and identity of layers is not well understood. Here we describe the development of the pulmonary artery (PA) wall using histochemical, clonal, and genetic analysis in mice. We show that the wall is constructed radially, from the inside out, by sequential induction and recruitment of successive cell layers from surrounding mesenchymal cells, and by developmentally regulated invasion of outer layers by inner layer cells. We also show that the endothelial-specific ligand PDGF-B can initiate wall formation but provide genetic evidence that one or more other, as yet unidentified, signals also contribute to the initiation and radial patterning of the wall.

## RESULTS AND DISCUSSION

### Pulmonary Artery Smooth Muscle Cells Arise from Lung Mesenchyme

To elucidate the cellular and molecular events of arterial wall formation, we focused on a small region of a developing mouse

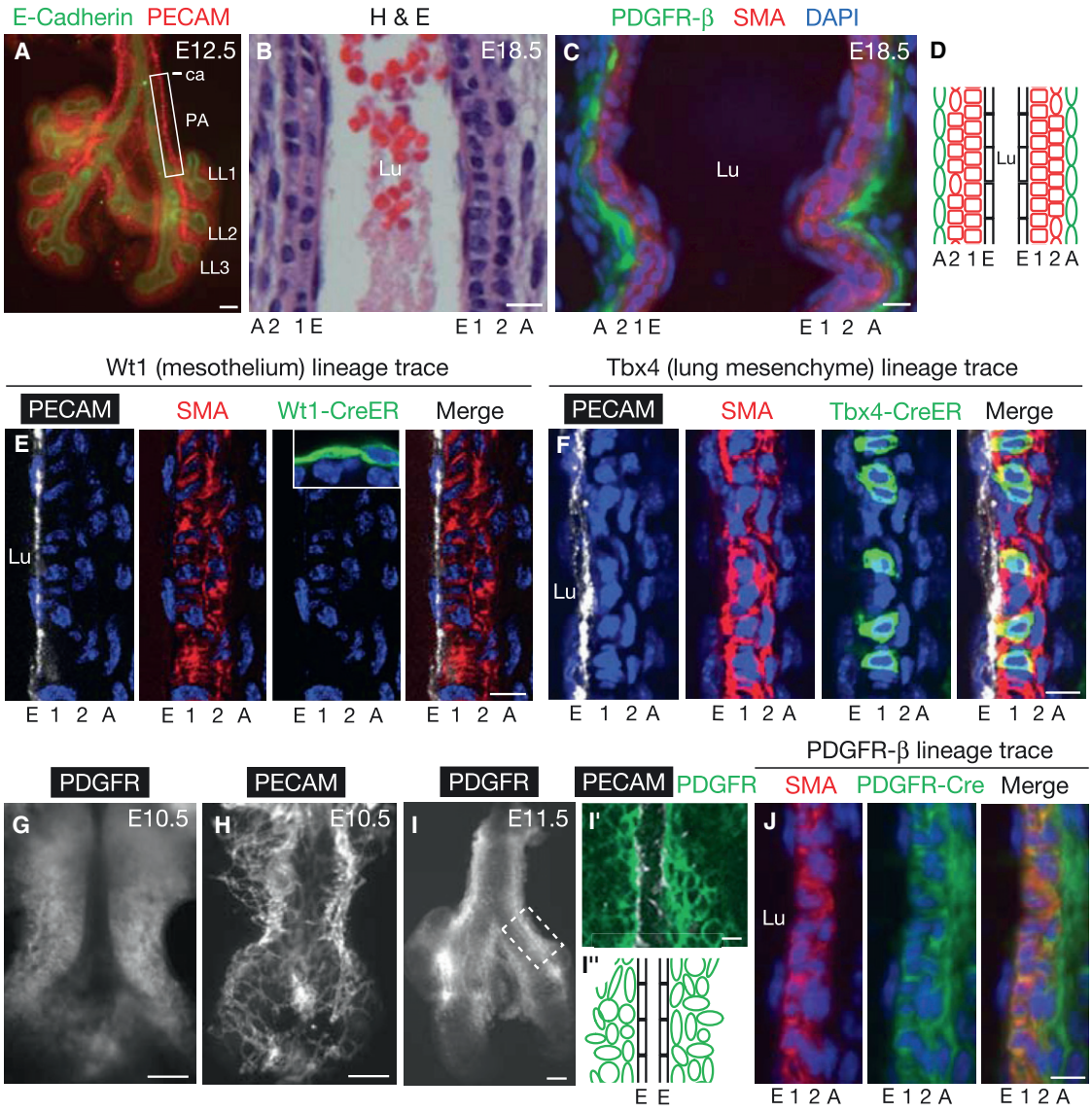


**Figure 1. Pulmonary Artery Smooth Muscle Cells Derive from Lung Mesenchyme**

(A) Ventral view of whole mount lung at embryonic day (E) 12.5 immunostained for E-cadherin (airway epithelium, green) and PECAM (endothelium, red). Box, portion of left pulmonary artery (PA) investigated here, from carina (ca) to LL1 (first lateral secondary branch off left primary bronchus) (Metzger et al., 2008). LL2 and LL3, second and third lateral secondary branches. (B and C) Longitudinal sections of left PA at E18.5 stained with hematoxylin and eosin (H&E) (B) or immunostained for α-smooth muscle actin (SMA, red), PDGFR-β (green) and counterstained with DAPI (nuclei, blue) (C). E, endothelial cell (EC) layer; 1, first (inner) smooth muscle cell (SMC) layer; 2, second SMC layer; A, adventitial cell layer. Lu, PA lumen. (D) Schematic of B and C, showing ECs (black), SMCs (red) and adventitial cells (green).

(E and F) Lineage tracing using the *Wt1-CreER*$^{T2}$ and the *Tbx4-CreER*$^{T2}$ transgenes as indicated with the mTmG Cre reporter to determine the contribution of the mesothelium and lung mesenchyme, respectively, to the PA wall. Longitudinal sections are shown of one side of the E18.5 left PA wall stained for the Cre reporter (green) and PECAM (white), SMA (red), and DAPI (blue) to visualize the PA wall. Pregnant dams were injected with a single dose of tamoxifen (3 mg at E9.5 in E; 1.5 mg at E10.5 in F) to activate the Cre(ER) recombinase. Inset in (E) shows in the same specimen lineage-labeled cells in the lung mesothelium, outside the PA. Lineage trace of lung mesenchyme (F; also see Figure S1C), but not mesothelium (E), labels PA wall cells, and the fraction of lineage labeled PA wall cells with the Tbx4-CreER$^{T2}$ in F is similar to the overall lung mesenchyme labeling efficiency (data not shown). (G–I) PDGFR-β expression around developing PA. Whole mount lungs at indicated ages immunostained for PDGFR-β (G and I) and PECAM (endothelium, H). I', Confocal optical section of boxed region of left PA in I showing both PDGFR-β and PECAM staining. I'', Schematic of I' showing zone of PDGFR-β (green) cells surrounding developing left PA ECs (black) (I''). J, Lineage trace (as in E and F) of PDGFR-β expressing cells. All cells of E18.5 PA wall are marked by lineage tag (green).

Scale bars, 100 μm (A, G–I) and 10 μm (B, C, E, F, I', J). See also Figures S1, S2A, S2C, and S2D.

artery, the left PA between the level of the carina (ca) and first branch off the left bronchus (LL1; Figure 1A). We selected this artery because of its relatively simple structure at birth, just two and occasionally three SMC layers plus an outer adventitial layer (Figures 1B–1D), the ease and precision in its identification and developmental staging provided by the adjacent bronchial

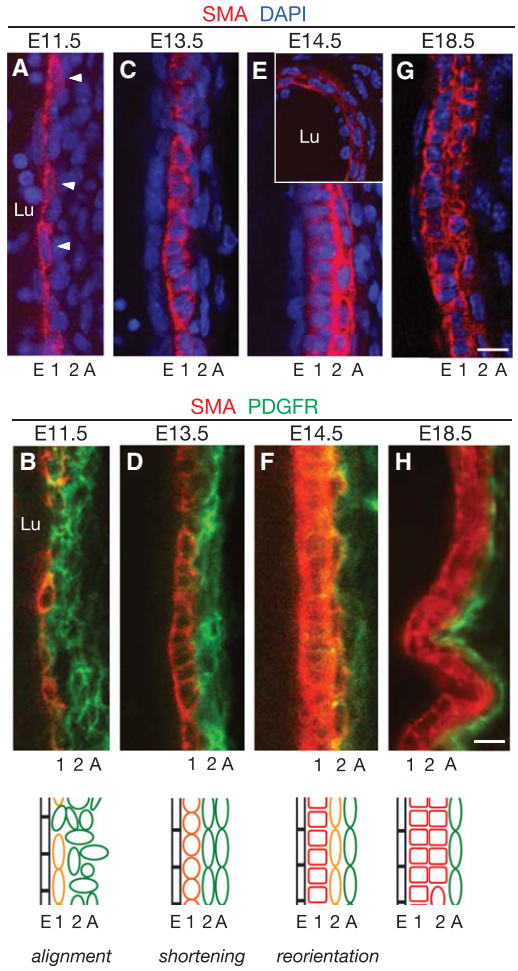


**Figure 2. Radial Development of the PA Wall**

Longitudinal sections through the left PA wall at the embryonic ages indicated, stained for SMA (red), PDGFR-β (green), and nuclei (DAPI, blue) as indicated. Arrowheads, nuclei elongated longitudinally. The inset in (E) shows a transverse section through the left PA wall. Schematics at bottom summarize SMA (red) and PDGFR-β (green) expression (orange, co-expression of SMA and PDGFR-β) and cell shape and orientation changes in the forming layers (E, 1, 2, A) of the developing PA wall. Lu, PA lumen. Square cells, circumferentially oriented cells. Scale bars, 10 μm. See also Figure S2.

airways whose full branching program is known (Metzger et al., 2008), and its involvement in devastating diseases such as pulmonary hypertension.

We carried out lineage tracing with cell- and tissue-specific Cre transgenes to investigate the developmental origin of PA SMCs. Previous studies have shown that SMCs of the outflow tract of the right heart originate at least in part from neural crest (Kirby et al., 1983; Majesky, 2007), but SMCs of more distal segments of the PA have been proposed to arise largely from lung mesothelial cells (Que et al., 2008) and ECs (Morimoto et al., 2010) by epithelial- and endothelial-to-mesenchymal transitions. However, our analysis of PA SMCs in E18.5 lungs following lineage tracing with *Wilm's tumor 1* (*Wt1)-CreER*$^{T2}$ (mesothelium), *VE-cadherin-Cre* (endothelium), *Wnt1-Cre* (neural crest), and *Sonic hedgehog-Cre* (epithelium) transgenes in conjunction with the *ROSA26R*$^{mTmG}$ Cre reporter showed that mesothelium, endothelium, neural crest, and airway epithelium are not substantial sources of SMCs of the PA during this period (Figure 1E; Figures S1A and S1B available online; data not shown). In contrast, lineage tracing with a recently generated lung mesenchyme-specific conditional transgene *Tbx4-CreER*$^{T2}$ (M.K., P. Bogard, and M.A.K., unpublished data; Menke et al., 2008), induced at E10.5, resulted in substantial labeling of E18.5 PA cells expressing the SMC marker alpha-smooth muscle actin (SMA), demonstrating that Tbx4$^{+}$ lung mesenchyme is a major, and possibly the sole source of PA SMCs at this stage (Figures 1F and S1C).

## Induction of the First Layer of Arterial Smooth Muscle

At ~E11, the first layer of the PA wall begins to form by a stereotyped sequence of molecular and cellular events that occur in the mesenchymal cells surrounding the nascent PA endothelial tube (Figure 2). Platelet-derived growth factor receptor (PDGFR)-β is initially expressed diffusely in the proximal lung mesenchyme (Figure 1G), when pulmonary ECs form a widely distributed plexus (Parera et al., 2005; P. Bogard, M.K., R. Metzger, and M.A.K., unpublished data; Figure 1H). But during the next day its expression begins to restrict to the group of mesenchymal cells surrounding the nascent PA endothelial tube, in the domain that will form the arterial wall (Figures 1I, 1I', 1I") (see below).

Beginning at ~E11.5, smooth muscle markers such as SMA are induced in the PDGFR-β$^{+}$ cells directly contacting the PA EC tube (Figures 2A and 2B). SMA is initially expressed at low levels and in a discontinuous fashion along the length of the PA, with more expressing cells on the lateral than the medial aspect of the vessel and localization of SMA protein initially polarized toward the side of the cell contacting the EC layer (Figures S2A, S2B, and S2B'). Other SMC markers also initiate expression at this time including smooth muscle myosin heavy chain (SMMHC) (Miano et al., 1994), the actin and tropomyosin binding protein SM22-alpha, and the transmembrane protein neuron glial-2 (NG2) (Figure S2F; data not shown). The expression of all four of these SMC markers increases over the next few days, forming a robustly labeled layer of smooth muscle (Figures 2C–2F and S2C; data not shown).

As SMC markers are induced in first layer cells, PDGFR-β expression is downregulated in these cells (Figure S2C) and by E18.5, expression was generally not detected in them (Figure S2D). Permanent marking of early PDGFR-β-expressing cells with a *PDGFR-β-Cre* transgene (Foo et al., 2006) (Figure S1E) labeled almost all SMA$^{+}$ PA wall cells at E18.5 (Figures 1J and S1D), including inner layer cells that do not express PDGFR-β at this time, confirming their origin from cells that initially expressed the gene.

During this period of dynamic marker expression, first layer cells reorient. Initially, at E11.5, many first layer SMA$^{+}$ cells and their nuclei were elongated longitudinally along the blood vessel (Figures 2A and 2B, "alignment"). However, over the next few days, first layer cells shortened along their longitudinal axis (Figures 2C and 2D, "shortening"), and by E14.5 they were circumferentially oriented (Figures 2E, 2F, and S2E, "reorientation"), as they are in the mature vessel. Thus, over a 3 day period (E11.5 to E14.5), the first layer of the PA wall forms by a stereotyped series of cell marker and morphogenesis events.

## Sequential Induction of the Outer Layers of the Arterial Wall

A few days after first layer cells initiate the arterial wall program, surrounding mesenchymal cells initiate a similar series of events to form the second layer of the arterial wall. At E13.5, these second layer cells express PDGFR-β and are elongated longitudinally, as first layer cells were 2 days earlier (Figures 2C and 2D). The next day smooth muscle markers begin to be expressed in these cells (Figures 2E and 2F), and as smooth muscle marker expression increases over the next several days, these cells downregulate PDGFR-β expression (Figure S2D), similar to the changes noted in first layer cells several days earlier. During this time, most of the cells shorten in the longitudinal axis and reorient to a circumferential orientation, forming the second layer of the arterial wall (Figures 1B, 1C, 2G, and 2H).

As the second layer is forming, cells surrounding this layer initiate a similar program to form the outer layer of the arterial wall. At ~E14, these outer layer cells express PDGFR-β and are elongated longitudinally along the artery (Figures 2C and 2D), like early first and second layer cells. However, the outer layer cells do not progress through the full program. By E18.5, they have not turned on SMC markers or downregulated PDGFR-β expression, and they have not undergone longitudinal shortening or reorientation (Figures 1B, 1C, 2G, and 2H). Thus, outer layer cells initiate the arterial wall program but arrest early on, forming the adventitial layer of the wall. These cells do not appear to complete the program, at least not during embryogenesis.

Taken together, the results show that the PA wall is constructed radially, from the inside-out, by sequential activation of an arterial wall program in three successive cell layers.

## Radial Patterning of Cell Division in the Arterial Wall

We next investigated cell division in the developing arterial wall by immunostaining for the mitotic marker phosphohistone H3 (pH3). There were two unexpected results. First, although undifferentiated progenitor cells are thought, in general, to become less proliferative as they differentiate into VSMCs (Owens et al., 2004), we found just the opposite in the developing PA wall. The vast majority of $pH3^+$ mitotic cells (Figure 3A) of the E11.5–14.5 PA wall are found in the inner (Figure 3B), more differentiated layers (Figure 3C), most in the innermost layer directly contacting the endothelial tube (layer 1). Cells that turn on SMA maintain their proliferative index, whereas the proliferative index of cells that do not declines (Figure 3D).

Second, we found that proliferating inner layer cells undergo a developmental shift in division plane orientation. In the early stages of PA wall development (E11.5–13.5), the axis of division of cells in the inner layer (L1) was predominately (>75%) longitudinal (Figures 3E and 3F). However, at E14.5 the axis shifts so that most (~75%) inner layer cells now divide radially (Figures 3E and 3F). This shift is specific to the innermost layer: cells in layer two (L2) and the adventitia (A) divide exclusively longitudinally at this stage (Figure 3F). Below we show by clonal analysis that this shift in division plane orientation corresponds with a transition of inner layer cells to a radially invasive mode in which they enter and help populate the surrounding cell layer.

## Clonal Analysis of Inner Layer Cells Reveals a Transition to a Radially Invasive Growth Mode

A clonal analysis was carried out in which individual first layer SMCs were genetically marked to track their proliferative potential and the final positions and pattern of the daughter cells (Figure 4A). To label first layer cells with GFP, Cre-mediated recombination was induced in transgenic *SMMHC-creER$^{T2}$*, *ROSA26R$^{mTmG/+}$* embryos using a single limiting dose (0.8–1.2 mg) of tamoxifen at E11.5, a stage at which SMMHC is expressed exclusively in the first layer of the developing PA wall. This resulted in rare or no $GFP^+$ cells within the entire visualized region of the left PA, so that labeled cells likely derived from a single recombination event. The putative PA wall clones were scored only if among *SMMHC-creER$^{T2}$*, *ROSA26R$^{mTmG/+}$* littermates, there was at least one embryo without marked cells in this region. Similar experiments using a multi-color *Rainbow Cre* reporter *ROSA26R$^{Rb/+}$* (Red-Horse et al., 2010) showed that all labeled cells in individual left PAs were almost always of a single color, confirming their clonal relationship (see Experimental Procedures). From an analysis of the size of clones between E13.5 and E18.5, we estimate the proliferation rate (doubling time) of PA SMCs as 1.0 ± 0.4 days from E12 to E14, slowing to ~3.8 ± 1.9 days from E14 to E18 (Table S1). (In comparison to these experiments with limiting doses of tamoxifen, a single high dose of tamoxifen labeled substantially more inner layer cells and formed multicolored "polyclones," as expected; Figures S3A–S3C.)

The positions of daughter cells in 32 PA wall clones derived from individual inner layer cells marked with a limiting dose of tamoxifen at E11.5 and observed at E13.5–18.5 are given in Figure S4 and Table S1. Daughter cells could potentially distribute in longitudinal, circumferential, and radial directions, and the cells could remain contiguous and form a coherent clone or intermingle with unmarked cells to form a dispersed clone (Figure 4A). At E13.5, marked cells have proliferated and many daughters have migrated extensively along the longitudinal and circumferential axes, often separating from sibling cells and intermixing with unlabeled cells (Figures 4B, 4C, 4E, and S4). All the daughter cells, however, remain within the inner, $SMA^+$ cell layer. A day later, at E14.5, this restriction to radial migration is relaxed, and daughter cells begin to invade the second layer (Figures 4E, S3D, S3E, and S4). Only a small percentage (12.5%) of marked first layer cells (n = 56) have invaded the second layer at E14.5, increasing to 32% by E17.5–18.5 with marked daughter cells found throughout the first and second layers (Figures 4D, 4E, and S4; data not shown). The relaxation of the radial restriction is only partial: although marked inner layer cells migrated extensively in the first and second layers, they did not invade the developing adventitial or intimal layers at this stage (Figure S4). Because there is a full (albeit immature) second layer at E14.5 (Figures 2E and 2F), we infer that most second layer cells arise from induction of surrounding (i.e., second layer or beyond) lung mesenchyme (see lineage analysis, Figures 1F, 1J, and S1C), rather than radial movement of inner layer cells.

A classical clonal analysis of the abdominal aortic wall in adult women using X chromosome-inactivation (analyzed by PCR) as a crude clone marker suggested limited dispersal of sibling cells in most clones (Chung et al., 1998; Schwartz and Murry, 1998), in contrast to the extensive cell migration and mixing we observe.

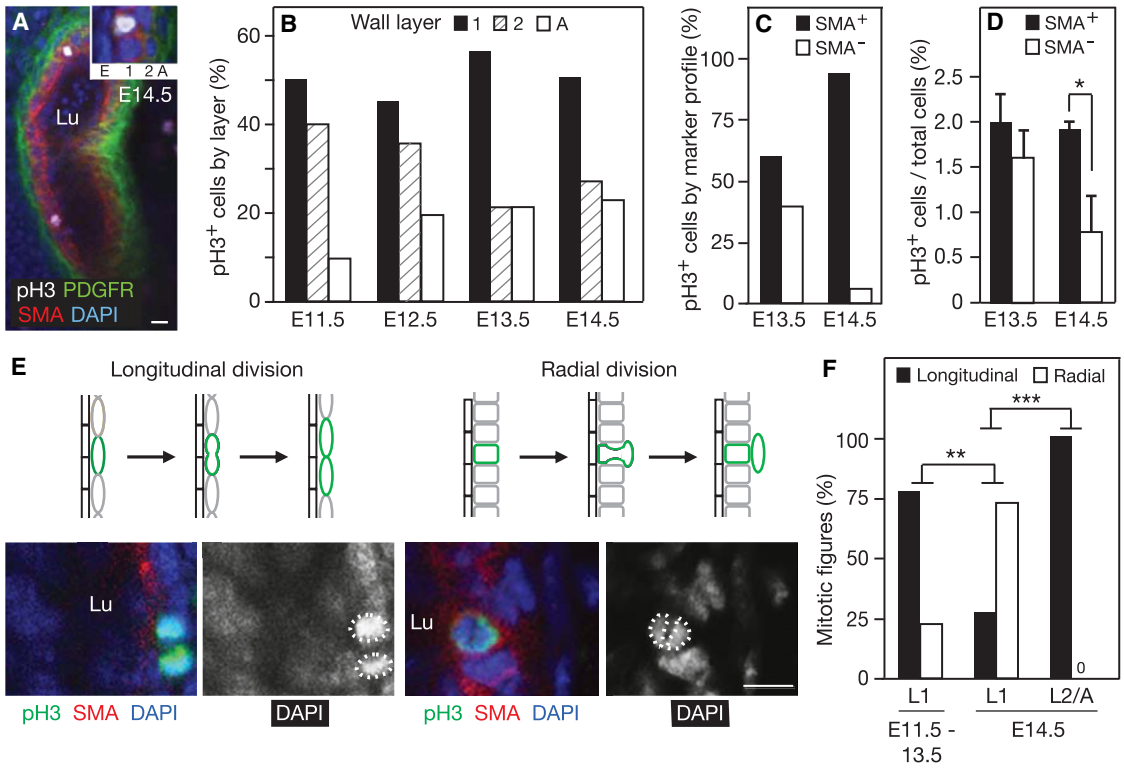


**Figure 3. Radial Patterning of Cell Division in the Developing PA Wall**

(A) Representative confocal optical section of left PA at E14.5 stained for the mitosis marker phosphohistone H3 (pH3, white) and SMA (red), PDGFR-β (green) and nuclei (DAPI, blue) to assign cell layer (1, 2, A) of each dividing cell. The inset shows a close up of a dividing cell and its assigned cell layer.

(B) Distribution of dividing cells among the three cell layers. Values shown are the fraction of all dividing ($pH3^+$) left PA wall cells located in each cell layer, for each embryonic age indicated. The total number of PA walls analyzed and dividing cells scored were: E11.5 (16 walls, 32 dividing cells), E12.5 (12, 31), E13.5 (14, 37) and E14.5 (15, 70).

(C) Marker expression pattern of dividing PA wall cells. Values shown are the fraction of all proliferating ($pH3^+$) left PA wall cells that were $SMA^+$ or PDGFR-$\beta^+$/$SMA^-$. The number of PA walls analyzed and dividing cells scored were: E13.5 (18, 48) and E14.5 (16, 80).

(D) Proliferative index of PA wall cells. Values shown are the proliferative index (fraction $pH3^+$ cells) of $SMA^+$ cells and PDGFR-$\beta^+$/$SMA^-$ cells of the PA wall at the ages indicated. The number of left PA walls analyzed and cells scored were: E13.5 (18 walls, 1286 $SMA^+$ cells, 1111 PDGFR-$\beta^+$/$SMA^-$ cells) and E14.5 (16, 3024, 519). Errors bars, s.e.m. *p = 0.019 by Student's t test.

(E) Schematic (top) and representative confocal images of stained lungs (bottom) showing longitudinal and radial axes of cell division in developing PA wall. Lungs were stained for pH3, SMA, and DAPI as indicated. Dashed circles, daughter chromosomes of dividing cell.

(F) Fraction of longitudinal versus radial cell divisions in the indicated layers of the PA wall at the indicated ages. After E13.5, layer 1 (L1) cells switch from predominantly longitudinal to predominantly radial division. The "0" in the panel indicates no detected radial cell divisions in the L2 and A layers at E14.5. The number of mitotic figures scored at E11.5–13.5 was 22 in L1 and at E14.5 was 15 in L1 and 12 in L2 and A. **p = 0.003, ***p = 0.0002 by Fisher's exact test. Scale bars, 10 μm.

It will be important to revisit this study using high-resolution clone markers to determine if this difference represents a fundamental difference between the vessels, organisms, or stages of development, or a limitation of the earlier clone marking and analysis strategy.

## A Gradient Model for Radial Patterning of the Pulmonary Artery Wall

Our results show that the PA wall is constructed radially, from the inside out (Figure 5A), by two separate but coordinated processes. One is sequential induction and recruitment of successive cell layers from surrounding mesenchymal progenitor cells. Each layer of mesenchymal cells initiates a program of gene expression and undergoes a stereotyped sequence of morphogenesis events over a 3 day period; as one muscle layer forms, the next layer initiates development. The program arrests early in the formation of the outermost layer to generate the adventitial layer. The other process is controlled invasion of the surrounding layer by inner layer cells, which initially divide and migrate extensively within the layer but later radially reorient and either migrate into the second layer or radially divide and send daughter cells into the next developing layer. Because this transition to radial invasion coincides with the switch from circumferential to primarily radial cell division, it could be that inner cells only enter an outer layer by radial cell division. Such coupling of centrifugal movement to cell division would prevent depletion of first layer cells, while supplying extra cells needed in the outer layers given their greater circumference but paradoxical dearth of proliferating cells.

We propose that a radial signaling gradient controls and coordinates the two processes (Figure 5B). The likely source of the signal is the endothelium, and the kinetics of its production

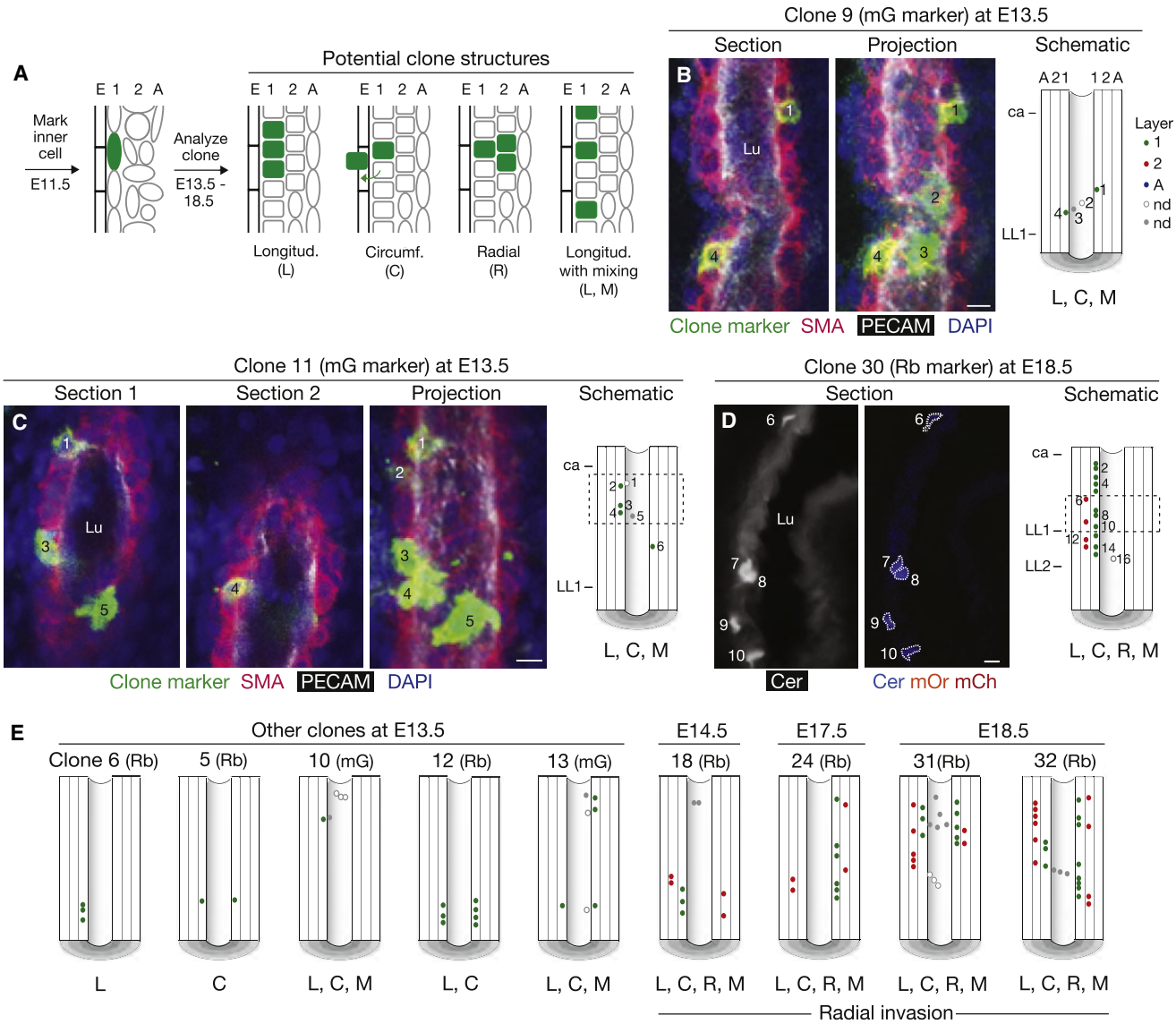


**Figure 4. Clonal Analysis of Inner Layer Cells of the PA Wall**

(A) Clonal analysis scheme showing early (E11.5) marking of an inner layer cell and four possible patterns of its proliferation and migration: longitudinal (L), circumferential (C), and radial (R) expansion, and longitudinal with mixing with unlabeled cells (L,M).

(B) A GFP-marked left PA clone (#9, Table S1) in a *SMMHC-CreER$^{T2}$, ROSA26R$^{mTmG/+}$* embryo, induced by administration of a limiting dose of tamoxifen at E11.5 and analyzed at E13.5 after staining for clone marker (membrane-localized GFP, abbreviated "mG," green) and for SMA (red), PECAM (white) and nuclei (DAPI, blue). An individual coronal confocal optical section (dorsal view, anterior up) of the four-cell clone is shown (left panel) along with a maximal projection (center panel). 1–4, cells of clone; Lu, PA lumen. In the clone schematic (right panel), the positions of marked cells are indicated by circles color coded to highlight the layer in which the cell resides: green (layer 1), red (layer 2), and blue (adventitia). For cells located superficial (gray circles) or deep (white circles) to the lumen, we were unable to determine which layer they reside in (nd, not determined). This clone expanded longitudinally (L) and circumferentially (C), with mixing (M). ca, position of carina; LL1, position of LL1 airway branch.

(C) Six cell clone (#11), induced and analyzed as in B. Two confocal optical sections are shown, along with a maximal projection and schematic. Dashed box, portion of clone shown in the confocal images.

(D) Sixteen cell clone (#30), induced and analyzed as in B, except clone marker was multicolor (Rainbow, abbreviated "Rb") ROSA26R$^{Rb}$ Cre reporter and the clone was analyzed at E18.5. Left panel, Cerulean channel of confocal image (ventral view) of coronal cryosection of the clone: bright cells are Cerulean-expressing cells of clone (numbered). Faint background staining shows the rest of the SMCs of PA wall. Center panel, Cerulean, mOrange and mCherry channels of the same cryosection. All labeled cells in left PA express Cerulean marker, confirming clonality. Clone expanded in all three axes (L, C, and R), with some cells (red in schematic) having invaded layer 2. For clarity, only every other cell in the schematic is numbered.

(E) Schematics (ventral views) of other representative clones. Although layer 1 clones can expand and mix extensively within layer 1, they do not expand radially into layer 2 until E14.5. By E18.5, they have spread extensively in layers 1 and 2, but have not invaded the adventitial layer. mG, mGFP clone marker; Rb, Rainbow (multicolor) clone marker. Scale bars, 10 μm.

See also Table S1 and Figures S3 and S4.

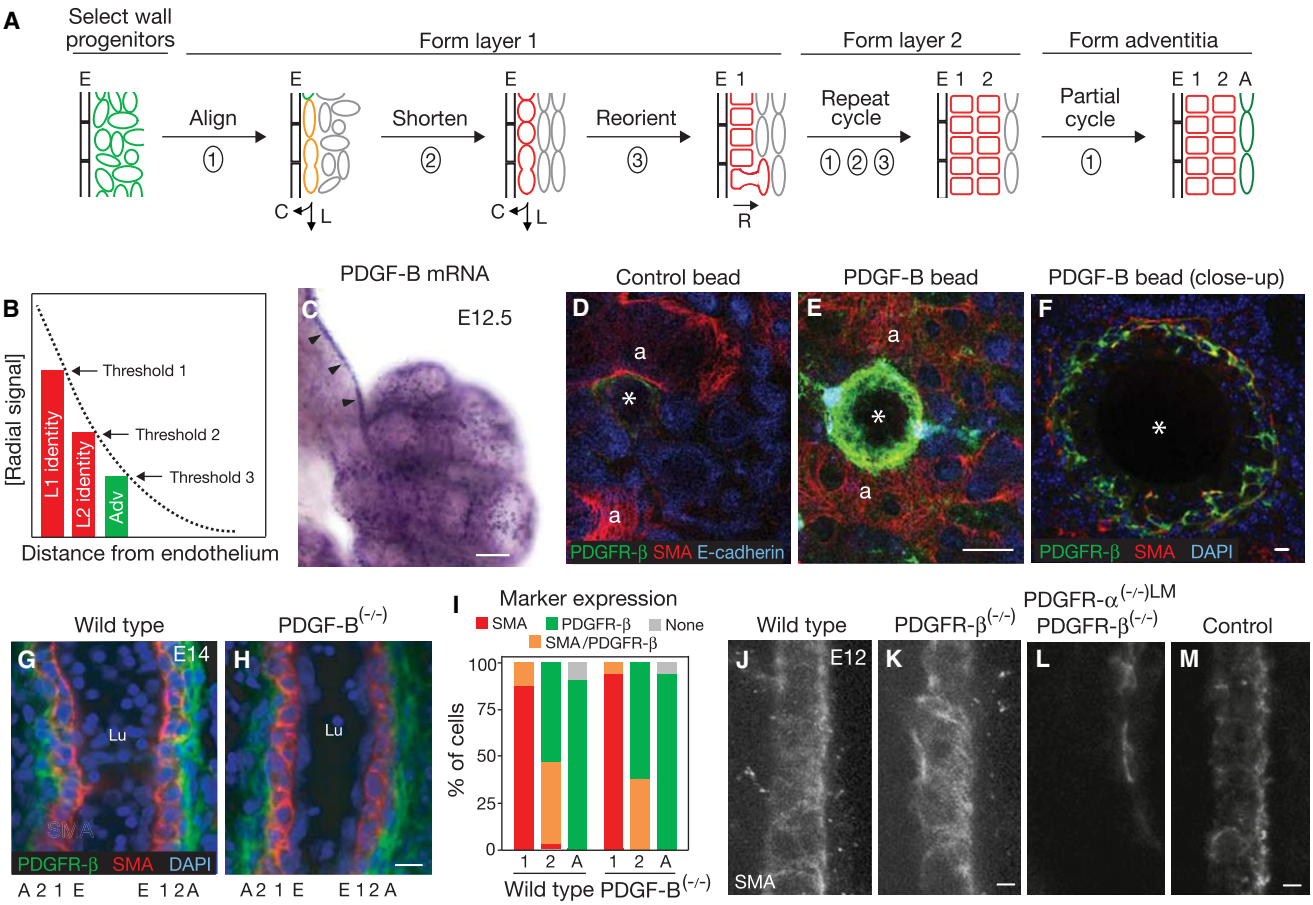


**Figure 5. Signal Gradient Model for PA Wall Patterning and Involvement of PDGF Pathway**

(A) Summary of cellular and molecular events in radial construction of PA wall. Cell wall progenitor zone surrounding PA endothelial tube is initially marked by PDGFR-β expression (green cells). Innermost cells (adjacent to endothelium, E) initiate smooth muscle marker expression and morphogenesis (orange cells) and then downregulate PDGFR-β (red cells) to form layer 1. Smooth muscle cycle repeats to form layer 2, and third cycle initiates to form adventitial (A) layer. As layer 1 cells mature, they radially reorient cell division and migration, sending daughter cells outward to supplement layer 2. R (radial), L (longitudinal), C (circumferential) cell division and migration.

(B) Gradient of a hypothetical radial signal that sequentially induces cell layers surrounding the endothelium to differentiate into the vascular wall. Different identity thresholds (1, 2, 3) result in differences among layers (e.g., smooth muscle versus adventitia, or high versus low elastin expression). The signaling gradient could also control the radial reorientation of cell division and migration.

(C) Whole mount lung in situ hybridization of the ligand PDGF-B, a candidate for the radial signal. Gene is expressed in ECs of developing PA (arrowheads).

(D and E) Confocal images of whole mount lungs from wild-type littermates implanted with a control or PDGF-B-soaked bead as indicated, cultured for 72 hr and then stained for PDGFR-β (green), SMA (red), and E-cadherin (blue) and counterstained with DAPI (not shown). a, airway with associated smooth muscle; *, bead location. Phosphohistone H3 staining (not shown) did not demonstrate any obvious differences in cell division surrounding the beads.

(F) Close up of the region in (E) around the PDGF-B bead that has initiated arterial wall formation as shown by induction of PDGFR-β and SMA expression.

(G–I) Confocal optical sections of left PAs from whole mount E14 wild-type (G) and *PDGF-B*$^{(-/-)}$ (H) littermate lungs stained for SMA, PDGFR-β and nuclei (DAPI) as indicated. Marker expression patterns are quantified in I, and values shown are fraction of cells in each layer with the indicated marker expression profile. Three wild-type PAs (n = 96 cells) and two *PDGF-B*$^{(-/-)}$ PAs (48 cells) were scored. There is no detectable phenotype in the mutant.

(J–M) Confocal images of left PAs from whole mount E12 lungs of the indicated genotypes, immunostained for SMA. Because *PDGFR-α*$^{(-/-)}$, *PDGFR-β*$^{(-/-)}$ double mutants die before the PA wall forms, double mutant shown in L is a lung-mesenchyme-specific (LM) double knock-out of genotype *PDGFR-α*$^{(flox/-)}$, *PDGFR-β*$^{(-/-)}$, *Tbx4-Cre*. Airway branching, which is stereotypically correlated with PA development, is maintained in these mutants (data not shown). Genotype of littermate control in (M) is *PDGFR-α*$^{(flox/+)}$, *PDGFR-β*$^{(+/+)}$, *Tbx4-Cre*. Compound *PDGFR-α*$^{(+/-)}$, *PDGFR-β*$^{(-/-)}$ embryos at E11.5–12.5 did not show lung developmental delay or a PA phenotype (data not shown).

Scale bars, 100 μm (C and E) and 10 μm (F, H, K, and M). See also Figure S5.

and spread, and sensitivity thresholds in the responding mesenchymal cells, would dictate arterial wall identity, the sequence in which these identities arise and the pattern of cell division. Mesenchymal cells directly adjacent to the endothelium, exposed to the highest level of signal, would be the first to induce the smooth muscle program and would proliferate most. As the signal spreads, surrounding mesenchymal cells would initiate the program and begin forming the next layer. The accumulating gradient would also polarize inner layer cells and radially reorient cell division and migration to promote invasion of the

surrounding cell layer. The low level of signal received by the outermost mesenchymal cells would be sufficient to initiate but not complete the smooth muscle program, creating the adventitial layer.

## PDGF-B Is One of Multiple Radial Patterning Signals

The ligand PDGF-B is an attractive candidate for the radial patterning signal. It has been implicated in VSMC and pericyte (vascular wall cells associated with capillaries) development (Andrae et al., 2008; Hoch and Soriano, 2003; Lindahl et al., 1997), and it is expressed in ECs of the developing PA starting at the time the arterial wall begins to form (Figure 5C and data not shown). Its receptors PDGFR-α and PDGFR-β are expressed in an overlapping pattern, complementary to that of PDGF-B, in the surrounding mesenchyme of the early lung (Figures 1G, 1I, and S5A). When PDGF-B-loaded agarose beads were implanted in E12 embryonic lung cultures, a nascent arterial wall up to two layers thick of PDGFR-$\beta^+$, $SMA^+$ cells began to form around the bead (Figures 5D–5F and S5E–S5G). Many of these cells were not in direct contact with the bead, suggesting that PDGF-B diffuses away from the bead, forming a local gradient that induces nearby mesenchymal cells to initiate arterial wall formation. Later steps in the arterial wall program, such as downregulation of PDGFR-β expression, did not occur, perhaps because of a requirement for additional signals or declining viability of the explant.

Despite the appropriate expression patterns of PDGF-B and its receptors during arterial wall formation and the ability of PDGF-B to initiate PA wall formation in explants, we found that radial patterning of the PA in mutant embryos null for *PDGF-B* was indistinguishable from that in wild-type embryos (Figures 5G–5I). Similar results were obtained for *PDGFR-*$\alpha^{(-/-)}$ or *PDGFR-*$\beta^{(-/-)}$ mutants or conditional *PDGFR-β* gain of function mutants (Figures 5J, 5K, S5B–S5D, and data not shown). However, an early step in the process was inhibited in double mutants lacking both PDGF receptors in lung mesenchyme (*PDGFR-*$\alpha^{(flox/-)}$*, PDGFR-*$\beta^{(-/-)}$*, Tbx4-Cre*) (Figures 5L and 5M). Taken together, results of these genetic experiments and the PDGF-B bead experiments implicate PDGF involvement in radial patterning but indicate redundancy among both the ligands and receptors.

Although it would be elegant if the radial patterning signal was a single diffusible factor, our results suggest it is an ensemble of factors, including PDGF-B and at least one other as yet unidentified signal. Multiple factors would provide flexibility in the control of vessel wall structure, important in generating the diversity of such structures and disease phenotypes (see below). And, although it is simplest to think of the factors as diffusible like PDGF-B from the beads, certain features of the process (e.g., the temporal aspect of radial SMC differentiation patterning) could be accounted for by membrane-bound signals transmitted radially via a sequential, contact-dependent (“bucket brigade”) signaling process (Feng et al., 2010; Hoglund and Majesky, 2012; Manderfield et al., 2012).

## Implications of the Radial Patterning Model for Arterial Diversity and Disease

Other blood vessels have different radial structures than the PA. For example, at the end of gestation, the left common carotid artery (CCA) and aorta have two or three times the number of smooth muscle layers as the PA, whereas the left anterior descending coronary artery has just a single layer (Figures 1B, 1C, and 6A–6D; data not shown). An analysis of SMA expression and fate mapping of the developing left CCA showed that, as for the PA, the CCA wall forms radially from the inside-out (Figures 6F–6J) with inner layer cells migrating radially to contribute to outer layers (Figures 6K and 6L). An initial clonal analysis of the descending thoracic aorta indicates that, here too, inner layer cells migrate radially to contribute to outer layers (A. Misra, L.D., and D.M.G., unpublished data). Thus, despite their differing radial structures, at least some of the same cellular mechanisms are used to form them.

An appealing idea is that vessel-specific modulation of the radial patterning signal(s) and response thresholds generate the observed differences in vessel wall sizes and structures (Figure 6E), and we further speculate that dysregulation of such signaling contributes to the many vascular diseases in which the radial structure of the vessel wall is altered and SMCs become highly proliferative and motile (Owens et al., 2004), resembling the developmental state (Figure 6O). Indeed, conditional activation of *PDGFR-β*, which presumably extends and levels the PDGF signaling gradient, markedly increases the thickness of the aorta (Olson and Soriano, 2011; Figures 6M and 6N), and targeted deletion of the PDGF-B matrix retention motif also alters vessel walls (Lindblom et al., 2003; Nyström et al., 2006). It must now be a priority to identify the full set of signals that control induction of cell layers and radial invasion, and how generally these pathways and cellular mechanisms operate in development and diseases of each arterial wall. Such pathways and mechanisms would be appealing therapeutic targets for arterial wall diseases and regenerative strategies.

## EXPERIMENTAL PROCEDURES

### Animals

All experiments with animals were approved by the IACUC at Stanford or Yale University School of Medicine. CD1 mice (Charles Rivers Laboratories) were used for wild-type analysis. *PDGF-*$B^{(+/-)}$ (Levéen et al., 1994), *PDGFR-*$\alpha^{GFP}$ (Hamilton et al., 2003), *PDGFR-*$\beta^{(+/-)}$ (Soriano, 1994), *PDGFR-β-Cre* (Foo et al., 2006), *SMMHC-*$CreER^{T2}$ (Wirth et al., 2008), Rainbow (Rb) Cre reporter *ROSA26*$R^{Rb}$ (Red-Horse et al., 2010), and *PDGFR-*$\beta^{J}$ (Olson and Soriano, 2011) mice have been described. *PDGFR-*$\alpha^{flox}$*, Ptch1*$^{lacZ}$*, Wt1-*$CreER^{T2}$*, VE-cadherin-Cre, Wnt1-*Cre, Shh-Cre, SM22-Cre and the Cre reporter strains *ROSA26*$R^{lacZ}$, *ROSA26*$R^{YFP}$, and *ROSA26*$R^{mTmG}$ were obtained from Jackson Laboratories. The *Tbx4-Cre* and *Tbx4-*$CreER^{T2}$ transgenes are lung mesenchyme-specific and induce expression of Cre reporters beginning at E10 and throughout the undifferentiated mesenchyme as well as in mesenchymal derivatives, including airway and vascular SMC, but not in airway epithelium (M.K., P. Bogard, and M.A.K., unpublished data; Menke et al., 2008); construction and use of the transgenes and transgenic mice will be detailed elsewhere (M.K., P. Bogard, and M.A.K., unpublished data).

### Immunohistochemistry and Histology

Embryos and lungs from timed pregnancies, in which noon of the day of vaginal plug detection was designated E0.5, were dissected and fixed in 4% paraformaldehyde (PFA) for 0.5–2 hr. For hematoxylin and eosin (H&E) staining, fixed tissue was dehydrated in methanol, and paraffin sections were prepared and stained using standard protocols. For β-galactosidase activity stains, fixed whole mount lungs were incubated with bromo-chloro-indolyl-galactopyranoside (X-gal, Sigma). For immunostains of whole mount lungs (Metzger et al., 2008), fixed lungs were dehydrated serially into 100% methanol and stored at −20°C. Lungs were rehydrated and incubated with

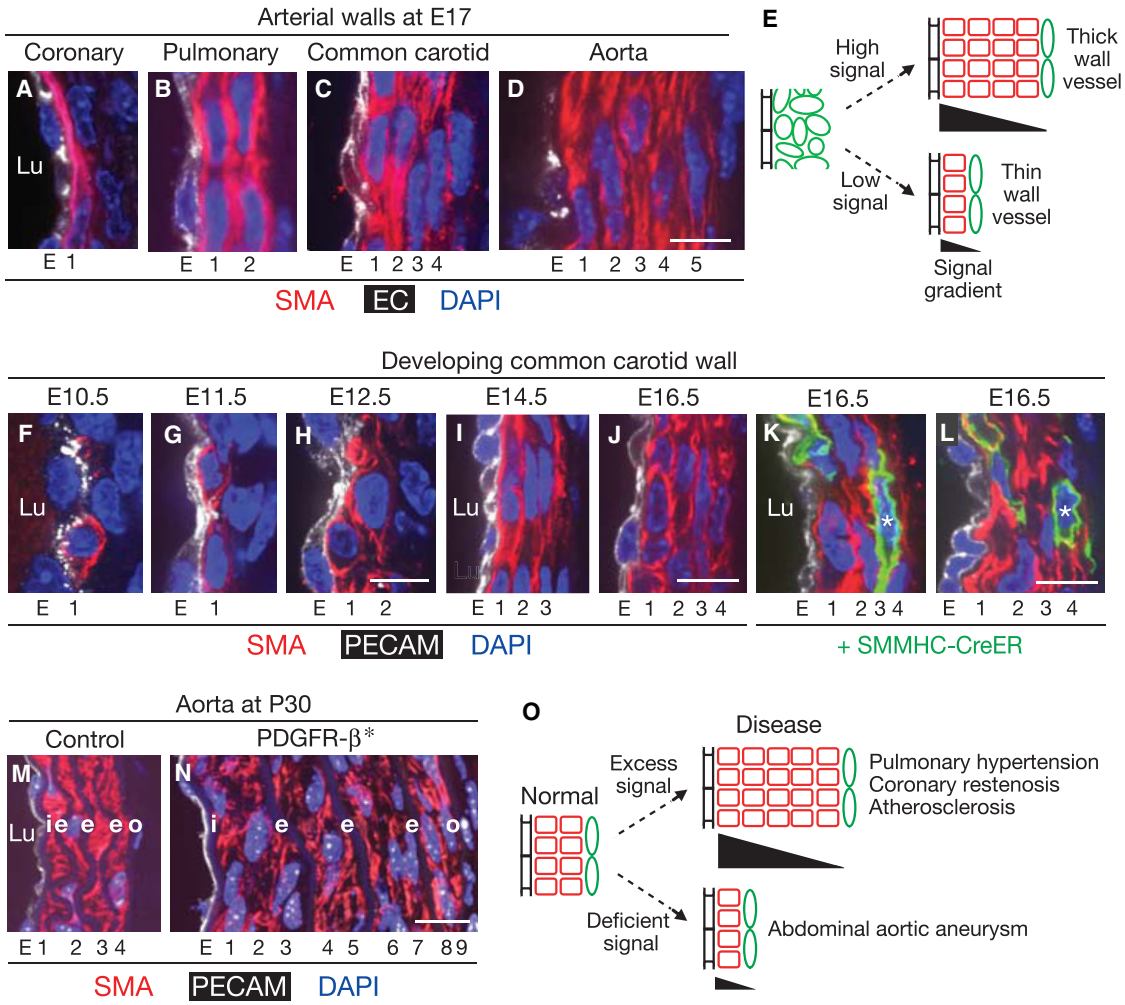


**Figure 6. Radial Patterning in Arterial Diversity and Disease**

(A–D) Transverse sections of the left anterior descending coronary artery and the left pulmonary and left common carotid arteries (CCA) and aorta at ~E17, stained for SMA (red), EC marker (VE-cadherin in A and PECAM in B–D; white) and DAPI (nuclei, blue). Walls range from one to five smooth muscle layers thick.

(E) Differences in the radial signal gradient (see Figure 5B) could determine the thickness of specific developing arteries.

(F–J) Sections through the developing left CCA (C) at the embryonic ages indicated and stained with SMA (red), PECAM (white), and DAPI (nuclei, blue). (F–H are longitudinal sections of the third aortic arch artery, which later becomes the CCA, and I, J are transverse sections of the CCA.) Note the gradual increase in $SMA^+$ cell layers from rare first layer cells at E10.5 to four continuous circumferentially elongated layers at E16.5.

(K and L) Fate mapping of CCA first layer SMC $marker^+$ cells in *SMMHC-CreER$^{T2}$, ROSA26R$^{mTmG/+}$* embryos induced with a single low dose of tamoxifen (0.5 mg) at E10.25. First layer CCA SMCs give rise to outer layer SMCs (marked by *), as for the PA (Figures 4D, 4E, S3E, S3E′, and S4). Despite the different sizes and origins of the vascular wall cells (PA from mesenchyme, see Figures 1F, 1J, and S1C; CCA from neural crest, see Jiang et al., 2000; Le Lièvre and Le Douarin, 1975), radial invasion occurs in both vessels.

(M and N) Transverse sections of descending aortic walls stained for SMA, PECAM and nuclei (DAPI) in control (M, *SM22-Cre)* and a conditional PDGFR-β gain-of-function mutation activated specifically in smooth muscle (N, *PDGFR-β$^{(+/J)}$, SM22-Cre* indicated by PDGFR-β*). (The *PDGFR-β$^J$* allele, a V536A mutation that disrupts an inhibitory juxtamembrane region and results in constitutive PDGFR-β activity, is a knock-in at the endogenous *PDGFR-β* locus; Olson and Soriano, 2011.) Note that the mutant wall has more than twice the normal number of smooth muscle layers but the normal number of elastic layers (i, e, o) (N; Olson and Soriano, 2011), whereas in the PA there was no observable phenotype (see Figure S5D).

(O) Changes in the radial signaling gradient may contribute to diseases characterized by vessel wall thickening or thinning. E, endothelial layer; 1–9, smooth muscle layers 1–9; Lu, vessel lumen; i, internal elastic lamina; e, elastic lamina; o, external elastic lamina. Scale bars, 10 μm.

blocking solution (5% rabbit or goat serum, 0.5% Triton X-100 in PBS) and then with primary antibodies diluted in blocking solution overnight at 4°C. On the next day, lungs were washed with blocking solution, followed by incubation with fluorescent-conjugated secondary antibodies overnight at 4°C. For signal amplification, a biotin-conjugated antibody was substituted, and then lungs were incubated with the ABC Elite reagent (Vector) and FITC, Cy3, or Cy5 Tyramide Reagent (Perkin Elmer). For immunostains of cryosections (Red-Horse et al., 2010), fixed tissue was cryoprotected in 30% sucrose overnight at 4°C, frozen in optical cutting temperature compound (OCT, Tissue Tek) and stored at −80°C. Tissue was sectioned (10–20 μm), washed in PBS, and immunostained as described above for whole mount lungs, except sections were incubated with secondary antibodies at room temperature for 1 hr.

Primary antibodies used were anti-CD31 (rat 1:100–200, BD PharMingen; or hamster 1:100, Serotec), anti-VE-cadherin (1:100, BD PharMingen), anti-E-cadherin (1:500–1000, Invitrogen), anti-NG2 (1:200, Millipore), anti-SMMHC

(1:100, Biomedical Technologies), anti-SM22-alpha (1:500, Abcam), anti-PDGFR-α (1:50, R&D), anti-GFP (1:500, Abcam), anti-phosphohistone H3 (pH3; 1:100–200, Millipore), anti-acetylated tubulin (1:500, Sigma), anti-Sca1 (1:100, BD PharMingen), directly conjugated FITC or Cy3 anti-alpha-SMA (1:100–1:200, Sigma), and biotinylated anti-PDGFR-β (1:50–100, R&D). Secondary antibodies were conjugated to either Alexa −488, −555, −647 (Molecular Probes), or Dylight 649 (Jackson Labs) fluorophores or to biotin (1:250). Note that mTomato fluorescence from the unrecombined *ROSA26R*$^{mTmG}$ allele is weak in lung cryosections or methanol-treated whole mount lungs, and certainly insignificant compared to the signal from immunostains with the anti-alpha-SMA antibody directly conjugated to Cy3. To mark nuclei, tissue was stained with DAPI (1:1,000).

The positions of PA wall cells were identified as located in layer 1 (L1; i.e., the cell layer adjacent to the ECs), 2 (L2; the next radial layer), or adventitia (A; the following outer layer). The identity of layer A as adventitia should be considered provisional because these cells did not detectably express Sca1 or *Ptch1*$^{lacZ}$, the extant adventitial markers that label adventitia of select regions of specific vessels starting late in embryogenesis (Majesky et al., 2011; Passman et al., 2008). For quantification of marker expression profiles in PA wall layers, longitudinal confocal sections and vascular wall cells in each section were assessed as described below for phosphohistone cell counts. L1 cells of each section were numbered sequentially around the vessel and subdivided into groups of five contiguous cells. One cell was randomly selected from each group, and the marker expression was determined for this L1 cell as well as for the adjacent cell in L2 and the successive adjacent cell in A.

### In Situ Hybridization

Dehydrated whole mount lungs were rehydrated into PBS with 0.1% Tween-20, permeabilized with proteinase K (10 mg/ml) and fixed again in 4% PFA with 0.2% glutaraldehyde (Sigma). Lungs were then hybridized at 68°C with digoxigenin (DIG)-labeled (Roche) probes overnight, washed extensively in saline sodium citrate solution, and incubated with alkaline phosphate-conjugated anti-DIG antibodies at 4°C overnight. Nitro blue tetrazolium chloride/5-bromo-4-chloro-3′-indolyphosphate p-toluidine salt (NBT-BCIP) was used to detect signal, and lungs were then washed extensively with TBS/0.1% Tween-20/10 mM EDTA. Tissue sections (10–20 μm) were hybridized and stained as described (Red-Horse et al., 2010).

### Phosphohistone Cell Counts and Mitotic Axis

Whole mount lungs stained with antibodies against pH3, SMA, and PDGFR-β and with DAPI were imaged by confocal fluorescence microscopy in the coronal plane to obtain longitudinal optical sections of the left PA extending from the carina to the first left lateral secondary airway branch (LL1). The longitudinal section of the left PA closest to the carina was the starting section and subsequent sections were collected every 12–20 μm (~1 cell length) until the vessel crossed LL1. Sections were considered adequate for analysis if the lumen and at least four cell lengths in the longitudinal axis of the vessel wall were visible. Sections containing wall cells visualized on previous sections were omitted. Vascular wall cells were identified as located in L1, L2, or A. This analysis included cells on the medial or lateral aspect of the blood vessel wall but excluded cells at the proximal or distal end of each vessel section because the layer these cells reside in could not be reliably determined. Between the carina and the LL1 airway branch, the left PA curves dorsal-ventrally, precluding definitive assignment to a specific wall layer at the proximal or distal end of each coronal section of the vessel. For mitotic axis counts, cells were only included in the analysis if they were pH3$^{+}$ and the division axis of the mitotic figure was clearly determinable. The long axis of the PA endothelium was defined as the longitudinal axis, and mitotic angles were scored relative to this axis and binned into three groups: longitudinal, radial, or 45°. However, no mitotic figures in the 45° group were observed. An analysis of pH3-stained mitotic figures co-stained for acetylated tubulin to show the mitotic spindle confirmed the fidelity of this approach for assigning axis of division (data not shown).

### Clonal Analysis

*SMMHC-CreER*$^{T2}$ mice were crossed to either *ROSA26R*$^{mTmG}$ or *ROSA26R*$^{Rb}$ ("Rainbow") mice. A single limiting dose (0.8–1.2 mg, see below) of tamoxifen (Sigma) was injected intraperitoneally into dams at E11.5 to induce recombination. Embryos were allowed to continue development and then analyzed at E13.5–18.5. For mGFP labeled clones, whole mount lungs were dissected and stained with an anti-GFP antibody in whole mount preparations for E13.5–14.5 lungs, or in cryosections for E17.5–18.5 lungs. Each GFP$^{+}$ cell was counted and its specific location and layer in the left PA wall recorded, except for cells at the proximal or distal end of each vessel section, which as described above could only be assigned to a ventral or dorsal location but not a specific layer of the PA wall. For Rainbow clones, tissue was cryosectioned and imaged using fluorescent filters for each fluorophore, and each marked cell was scored for color (i.e., Cerulean, mOrange, or mCherry), position, and specific layer of the PA wall.

To find conditions of very sparse and, ideally, single cell (i.e., clonal) marking of left PA SMCs we titrated down the dose of tamoxifen injected at E11.5 in preliminary experiments. In the range used here (0.8–1.2 mg), we found that ~48% of *SMMHC-CreER*$^{T2}$, *ROSA26R*$^{mTmG/+}$ embryos had marked cells in the PA and the rest had none. Lower doses (0.6 mg) gave no GFP$^{+}$ PA SMCs at E13.5 (n = 6), whereas higher doses (1.5 mg) yielded more embryos (83%) with marked cells and more GFP$^{+}$ cells in the marked embryos. To help ensure clonal labeling, we excluded from analysis any embryos in which there was not at least one *SMMHC-CreER*$^{T2}$, *ROSA26R*$^{mTmG/+}$ littermate lacking marked cells. At standard doses of tamoxifen (0.8–1.2 mg) in *SMMHC-CreER*$^{T2}$, *ROSA26R*$^{Rb/+}$ embryos (n = 63), the PA SMCs were almost always unlabeled (59%) or labeled with just a single color (38%), confirming clonality, and only very rarely (n = 2) were multi-color (i.e., polyclonal; 3%).

In these experiments, the labeled parent cell is always an inner layer SMC because expression of SMC markers (and presumably SMMHC-CreER$^{T2}$) is limited to this layer until three days after tamoxifen injection (i.e., E14.5; see Figures 2 and S2), and analysis of clones marked at E11.5 and analyzed at E13.5 showed labeling of only inner layer cells. In embryonic studies from other groups utilizing highly active promoters driving *CreER*, the time window for recombination of Cre reporters is 6–48 hr following a single injection of high-dose tamoxifen (1.5–3.0 mg) (Hayashi and McMahon, 2002; Nakamura et al., 2006). We found that injection of our standard dose of tamoxifen (1.2 mg) at E10.5, instead of E11.5, resulted in no marked left PA SMCs in *SMMHC-CreER*$^{T2}$, *ROSA26R*$^{mTmG/+}$ embryos at E13.5 (n = 8). Because SMMHC protein (and presumably SMMHC-CreER$^{T2}$) is expressed in the PA SMCs at E11.5 (Figure S2F), these findings suggest that the outer time limit for recombination in the left PA following a 1.2 mg injection is 1 day or less. Although there were no marked PA SMCs in these experiments, there were marked airway SMCs because expression of SMC markers, presumably including SMMHC-CreER$^{T2}$, occurs earlier in the airways than in the vessels. Similarly for *SMMHC-CreER*$^{T2}$, *ROSA26R*$^{Rb/+}$ embryos from dams injected with tamoxifen at E11.5, PA SMCs were almost always unlabeled or labeled with a single color, but airway SMCs invariably contained marked cells of all three colors (Figure S3F).

### Lung Cultures and PDGF Bead Implantation

Agarose beads (Affi-Gel Blue Gel, 100–200 mesh, Bio-Rad) were washed with sterile PBS three times for 30 min each, and then incubated for one hour with a disulfide linked homodimer of PDGF-B (R&D, 200–300 ng/ml) in PBS or with PBS alone for control beads (Furuta et al., 1997). After incubation, the beads were briefly washed and then implanted in the mesenchyme of freshly harvested E12 whole mount lungs by making a small incision in the lung mesenchyme with flame-polished tungsten needles and carefully positioning the bead. Lungs were cultured in DMEM12 with 10% FBS on 0.4 μm filters (Millipore) at the air liquid interface for 24–72 hr in a 5% CO2 incubator, then fixed with 4% PFA and immunostained as above. Lungs that did not grow normally in culture were excluded from analysis.

### Imaging

Tissue samples were imaged on a Leica MZ12 stereomicroscope (whole mounts) or on Zeiss Axiophot or Nikon Eclipse 80i fluorescence microscopes or on Leica CTR6000 or Nikon Eclipse Ti-Perkin Elmer Ultraview VoX confocal microscopes. Adobe Photoshop was used to process images and overlays.

## SUPPLEMENTAL INFORMATION

Supplemental Information includes five figures and one table and can be found with this article online at http://dx.doi.org/10.1016/j.devcel.2012.07.009.

## ACKNOWLEDGMENTS

We thank Krasnow laboratory members for input, including G. Fish for help with in situ studies, P. Bogard for help generating the *Tbx4-Cre* and *Tbx4-CreER$^{T2}$* mice, and M. Petersen for help preparing figures. We also thank R. Adams, C. Betsholtz, P. Soriano, and I. Weissman for mouse strains. D.M.G. was supported by the Sarnoff Foundation for Cardiovascular Science, Pulmonary Hypertension Association, National Institute of Health under the K08 Award (5K08HL093362), and the Stanford University School of Medicine Pediatric Research Fund. This work was supported by the National Institutes of Health (5R01HL075769 and NHLBI Progenitor Cell Biology Consortium Grant 5U01HL099995 to M.A.K.) and by the Vera M. Wall Center for Pulmonary Vascular Disease. M.A.K. is an investigator of the Howard Hughes Medical Institute. D.M.G., M.K., and M.A.K. conceived and designed the experiments; D.M.G., M.K., J.K.L., J.H., A.A., L.D., and K.R.-H. performed the experiments; S.O., L.O., and F.H.E. provided strains, reagents, and expertise; and D.M.G. and M.A.K. analyzed the results and wrote the manuscript.

Received: September 27, 2011
Revised: May 24, 2012
Accepted: July 16, 2012
Published online: September 10, 2012

## REFERENCES

Adams, R.H., and Alitalo, K. (2007). Molecular regulation of angiogenesis and lymphangiogenesis. Nat. Rev. Mol. Cell Biol. *8*, 464–478.

Andrae, J., Gallini, R., and Betsholtz, C. (2008). Role of platelet-derived growth factors in physiology and medicine. Genes Dev. *22*, 1276–1312.

Carmeliet, P. (2005). Angiogenesis in life, disease and medicine. Nature *438*, 932–936.

Chung, I.M., Schwartz, S.M., and Murry, C.E. (1998). Clonal architecture of normal and atherosclerotic aorta: implications for atherogenesis and vascular development. Am. J. Pathol. *152*, 913–923.

DeRuiter, M.C., Poelmann, R.E., VanMunsteren, J.C., Mironov, V., Markwald, R.R., and Gittenberger-de Groot, A.C. (1997). Embryonic endothelial cells transdifferentiate into mesenchymal cells expressing smooth muscle actins in vivo and in vitro. Circ. Res. *80*, 444–451.

Domenga, V., Fardoux, P., Lacombe, P., Monet, M., Maciazek, J., Krebs, L.T., Klonjkowski, B., Berrou, E., Mericskay, M., Li, Z., et al. (2004). Notch3 is required for arterial identity and maturation of vascular smooth muscle cells. Genes Dev. *18*, 2730–2735.

Esner, M., Meilhac, S.M., Relaix, F., Nicolas, J.F., Cossu, G., and Buckingham, M.E. (2006). Smooth muscle of the dorsal aorta shares a common clonal origin with skeletal muscle of the myotome. Development *133*, 737–749.

Feng, X., Krebs, L.T., and Gridley, T. (2010). Patent ductus arteriosus in mice with smooth muscle-specific Jag1 deletion. Development *137*, 4191–4199.

Foo, S.S., Turner, C.J., Adams, S., Compagni, A., Aubyn, D., Kogata, N., Lindblom, P., Shani, M., Zicha, D., and Adams, R.H. (2006). Ephrin-B2 controls cell motility and adhesion during blood-vessel-wall assembly. Cell *124*, 161–173.

Frid, M.G., Moiseeva, E.P., and Stenmark, K.R. (1994). Multiple phenotypically distinct smooth muscle cell populations exist in the adult and developing bovine pulmonary arterial media in vivo. Circ. Res. *75*, 669–681.

Frid, M.G., Dempsey, E.C., Durmowicz, A.G., and Stenmark, K.R. (1997). Smooth muscle cell heterogeneity in pulmonary and systemic vessels. Importance in vascular disease. Arterioscler. Thromb. Vasc. Biol. *17*, 1203–1209.

Furuta, Y., Piston, D.W., and Hogan, B.L. (1997). Bone morphogenetic proteins (BMPs) as regulators of dorsal forebrain development. Development *124*, 2203–2212.

Gaengel, K., Genové, G., Armulik, A., and Betsholtz, C. (2009). Endothelial-mural cell signaling in vascular development and angiogenesis. Arterioscler. Thromb. Vasc. Biol. *29*, 630–638.

Greif, D.M. (2012). Vascular embryology and angiogenesis. In Vascular Medicine, A Companion to Braunwald's Heart Disease, M. Creager, J. Beckman, and J. Loscalzo, eds. (New York: Elsevier), in press.

Hamilton, T.G., Klinghoffer, R.A., Corrin, P.D., and Soriano, P. (2003). Evolutionary divergence of platelet-derived growth factor alpha receptor signaling mechanisms. Mol. Cell. Biol. *23*, 4013–4025.

Hayashi, S., and McMahon, A.P. (2002). Efficient recombination in diverse tissues by a tamoxifen-inducible form of Cre: a tool for temporally regulated gene activation/inactivation in the mouse. Dev. Biol. *244*, 305–318.

High, F.A., Zhang, M., Proweller, A., Tu, L., Parmacek, M.S., Pear, W.S., and Epstein, J.A. (2007). An essential role for Notch in neural crest during cardiovascular development and smooth muscle differentiation. J. Clin. Invest. *117*, 353–363.

Hirschi, K.K., Rohovsky, S.A., and D'Amore, P.A. (1998). PDGF, TGF-beta, and heterotypic cell-cell interactions mediate endothelial cell-induced recruitment of 10T1/2 cells and their differentiation to a smooth muscle fate. J. Cell Biol. *141*, 805–814.

Hoch, R.V., and Soriano, P. (2003). Roles of PDGF in animal development. Development *130*, 4769–4784.

Hoglund, V.J., and Majesky, M.W. (2012). Patterning the artery wall by lateral induction of Notch signaling. Circulation *125*, 212–215.

Hungerford, J.E., and Little, C.D. (1999). Developmental biology of the vascular smooth muscle cell: building a multilayered vessel wall. J. Vasc. Res. *36*, 2–27.

Hungerford, J.E., Owens, G.K., Argraves, W.S., and Little, C.D. (1996). Development of the aortic vessel wall as defined by vascular smooth muscle and extracellular matrix markers. Dev. Biol. *178*, 375–392.

Jiang, X., Rowitch, D.H., Soriano, P., McMahon, A.P., and Sucov, H.M. (2000). Fate of the mammalian cardiac neural crest. Development *127*, 1607–1616.

Jin, S.W., Beis, D., Mitchell, T., Chen, J.N., and Stainier, D.Y. (2005). Cellular and molecular analyses of vascular tube and lumen formation in zebrafish. Development *132*, 5199–5209.

Kirby, M.L., Gale, T.F., and Stewart, D.E. (1983). Neural crest cells contribute to normal aorticopulmonary septation. Science *220*, 1059–1061.

Le Lièvre, C.S., and Le Douarin, N.M. (1975). Mesenchymal derivatives of the neural crest: analysis of chimaeric quail and chick embryos. J. Embryol. Exp. Morphol. *34*, 125–154.

Levéen, P., Pekny, M., Gebre-Medhin, S., Swolin, B., Larsson, E., and Betsholtz, C. (1994). Mice deficient for PDGF B show renal, cardiovascular, and hematological abnormalities. Genes Dev. *8*, 1875–1887.

Lindahl, P., Johansson, B.R., Levéen, P., and Betsholtz, C. (1997). Pericyte loss and microaneurysm formation in PDGF-B-deficient mice. Science *277*, 242–245.

Lindblom, P., Gerhardt, H., Liebner, S., Abramsson, A., Enge, M., Hellstrom, M., Backstrom, G., Fredriksson, S., Landegren, U., Nystrom, H.C., et al. (2003). Endothelial PDGF-B retention is required for proper investment of pericytes in the microvessel wall. Genes Dev. *17*, 1835–1840.

Majesky, M.W. (2007). Developmental basis of vascular smooth muscle diversity. Arterioscler. Thromb. Vasc. Biol. *27*, 1248–1258.

Majesky, M.W., Dong, X.R., Hoglund, V., Mahoney, W.M., Jr., and Daum, G. (2011). The adventitia: a dynamic interface containing resident progenitor cells. Arterioscler. Thromb. Vasc. Biol. *31*, 1530–1539.

Manderfield, L.J., High, F.A., Engleka, K.A., Liu, F., Li, L., Rentschler, S., and Epstein, J.A. (2012). Notch activation of Jagged1 contributes to the assembly of the arterial wall. Circulation *125*, 314–323.

McLean, S.E., Mecham, B.H., Kelleher, C.M., Mariani, T.J., and Mecham, R.P. (2005). Extracellular matrix gene expression in the developing mouse aorta. Adv. Dev. Biol. *15*, 81–128.

Menke, D.B., Guenther, C., and Kingsley, D.M. (2008). Dual hindlimb control elements in the Tbx4 gene and region-specific control of bone size in vertebrate limbs. Development *135*, 2543–2553.

Metzger, R.J., Klein, O.D., Martin, G.R., and Krasnow, M.A. (2008). The branching programme of mouse lung development. Nature *453*, 745–750.

Miano, J.M., Cserjesi, P., Ligon, K.L., Periasamy, M., and Olson, E.N. (1994). Smooth muscle myosin heavy chain exclusively marks the smooth muscle lineage during mouse embryogenesis. Circ. Res. *75*, 803–812.

Mizugishi, K., Yamashita, T., Olivera, A., Miller, G.F., Spiegel, S., and Proia, R.L. (2005). Essential role for sphingosine kinases in neural and vascular development. Mol. Cell. Biol. *25*, 11113–11121.

Morimoto, M., Liu, Z., Cheng, H.T., Winters, N., Bader, D., and Kopan, R. (2010). Canonical Notch signaling in the developing lung is required for determination of arterial smooth muscle cells and selection of Clara versus ciliated cell fate. J. Cell Sci. *123*, 213–224.

Nakamura, E., Nguyen, M.T., and Mackem, S. (2006). Kinetics of tamoxifen-regulated Cre activity in mice using a cartilage-specific CreER(T) to assay temporal activity windows along the proximodistal limb skeleton. Dev. Dyn. *235*, 2603–2612.

Nyström, H.C., Lindblom, P., Wickman, A., Andersson, I., Norlin, J., Fäldt, J., Lindahl, P., Skøtt, O., Bjarnegård, M., Fitzgerald, S.M., et al. (2006). Platelet-derived growth factor B retention is essential for development of normal structure and function of conduit vessels and capillaries. Cardiovasc. Res. *71*, 557–565.

Olson, L.E., and Soriano, P. (2011). PDGFRβ signaling regulates mural cell plasticity and inhibits fat development. Dev. Cell *20*, 815–826.

Owens, G.K., Kumar, M.S., and Wamhoff, B.R. (2004). Molecular regulation of vascular smooth muscle cell differentiation in development and disease. Physiol. Rev. *84*, 767–801.

Parera, M.C., van Dooren, M., van Kempen, M., de Krijger, R., Grosveld, F., Tibboel, D., and Rottier, R. (2005). Distal angiogenesis: a new concept for lung vascular morphogenesis. Am. J. Physiol. Lung Cell. Mol. Physiol. *288*, L141–L149.

Passman, J.N., Dong, X.R., Wu, S.P., Maguire, C.T., Hogan, K.A., Bautch, V.L., and Majesky, M.W. (2008). A sonic hedgehog signaling domain in the arterial adventitia supports resident Sca1+ smooth muscle progenitor cells. Proc. Natl. Acad. Sci. USA *105*, 9349–9354.

Phng, L.K., and Gerhardt, H. (2009). Angiogenesis: a team effort coordinated by notch. Dev. Cell *16*, 196–208.

Que, J., Wilm, B., Hasegawa, H., Wang, F., Bader, D., and Hogan, B.L. (2008). Mesothelium contributes to vascular smooth muscle and mesenchyme during lung development. Proc. Natl. Acad. Sci. USA *105*, 16626–16630.

Red-Horse, K., Ueno, H., Weissman, I.L., and Krasnow, M.A. (2010). Coronary arteries form by developmental reprogramming of venous cells. Nature *464*, 549–553.

Schwartz, S.M. (1997). Smooth muscle migration in vascular development and pathogenesis. Transpl. Immunol. *5*, 255–260.

Schwartz, S.M., and Murry, C.E. (1998). Proliferation and the monoclonal origins of atherosclerotic lesions. Annu. Rev. Med. *49*, 437–460.

Soriano, P. (1994). Abnormal kidney development and hematological disorders in PDGF beta-receptor mutant mice. Genes Dev. *8*, 1888–1896.

Strilić, B., Kucera, T., Eglinger, J., Hughes, M.R., McNagny, K.M., Tsukita, S., Dejana, E., Ferrara, N., and Lammert, E. (2009). The molecular basis of vascular lumen formation in the developing mouse aorta. Dev. Cell *17*, 505–515.

Suri, C., Jones, P.F., Patan, S., Bartunkova, S., Maisonpierre, P.C., Davis, S., Sato, T.N., and Yancopoulos, G.D. (1996). Requisite role of angiopoietin-1, a ligand for the TIE2 receptor, during embryonic angiogenesis. Cell *87*, 1171–1180.

Wasteson, P., Johansson, B.R., Jukkola, T., Breuer, S., Akyürek, L.M., Partanen, J., and Lindahl, P. (2008). Developmental origin of smooth muscle cells in the descending aorta in mice. Development *135*, 1823–1832.

Weinstein, B.M., and Lawson, N.D. (2002). Arteries, veins, Notch, and VEGF. Cold Spring Harb. Symp. Quant. Biol. *67*, 155–162.

Wilm, B., Ipenberg, A., Hastie, N.D., Burch, J.B., and Bader, D.M. (2005). The serosal mesothelium is a major source of smooth muscle cells of the gut vasculature. Development *132*, 5317–5328.

Wirth, A., Benyó, Z., Lukasova, M., Leutgeb, B., Wettschureck, N., Gorbey, S., Orsy, P., Horváth, B., Maser-Gluth, C., Greiner, E., et al. (2008). G12-G13-LARG-mediated signaling in vascular smooth muscle is required for salt-induced hypertension. Nat. Med. *14*, 64–68.

Wolinsky, H., and Glagov, S. (1967). A lamellar unit of aortic medial structure and function in mammals. Circ. Res. *20*, 99–111.

Yamashita, J., Itoh, H., Hirashima, M., Ogawa, M., Nishikawa, S., Yurugi, T., Naito, M., Nakao, K., and Nishikawa, S. (2000). Flk1-positive cells derived from embryonic stem cells serve as vascular progenitors. Nature *408*, 92–96.

Cell, Vol. 68, 201–219, January 24, 1992, 

# The Origin of Pattern and Polarity in the Drosophila Embryo

**Review**

**Daniel St Johnston* and Christiane Nüsslein-Volhard†**
*The Wellcome/CRC Institute
and Department of Genetics
Cambridge University
Cambridge CB2 1QR
England
†Max Planck Institut für Entwicklungsbiologie
D7400 Tübingen
Federal Republic of Germany

The development of a multicellular organism from a single egg cell requires both the determination of many cell types and the organization of these cells into an elaborate pattern (discussed elsewhere in this issue). In this review, we shall consider how much of the complexity of the pattern is already present at the beginning of this process in the fertilized egg? Since the early part of this century, embryologists have recognized that the eggs of many organisms contain localized regions of cytoplasm that direct the formation of specific parts of the embryonic pattern (Wilson, 1928). However, it is only in the case of Drosophila that the molecules responsible for these activities have been identified. Thanks largely to the use of genetic approaches, it is now known that four localized maternal signals define the basic organization and polarity of the two major embryonic axes. Thus, these signals not only specify cell states, but also provide a prepattern for subsequent development. Although Drosophila is probably unusual in the extent to which its pattern formation is controlled by maternal cues, many of the molecular processes involved have counterparts in other systems. More importantly, the characterization of these signals has also provided useful paradigms for the study of a variety of developmental phenomena, such as localized determinants, induction, and morphogen gradients. The purpose of this review is to describe our current understanding of how the four maternal signals establish positional information in the Drosophila embryo, and to discuss the molecular properties of each system.

The Drosophila egg is produced over a period of about 3½ days in the ovary of the female (Figure 1), and upon fertilization, develops extremely rapidly to form a larva after 24 hr. During the early stages of embryogenesis, the zygotic nuclei divide, without forming cells, to give rise to a syncytial blastoderm embryo (Figure 1). By 3 hr of development, the nuclei have been surrounded by cell membranes to form the cellular blastoderm, and gastrulation begins soon afterward. Although the organization of anterior–posterior and dorsal–ventral axes first becomes apparent in the region-specific cell movements of gastrulation, the basic prepattern of both axes has already been established in the syncytial blastoderm by the localized expression of zygotic pattern genes.

The anterior–posterior prepattern is formed by the spatially regulated transcription of the gap genes. While the identities of all of the gap genes that control head development are not yet completely clear, the embryo contains expression domains of *huckebein*, *tailless*, *giant*, *hunchback*, *Krüppel*, *knirps*, *giant*, *tailless*, and *huckebein*, as one moves from anterior to posterior (Knipple et al., 1985; Tautz, 1988; Mohler et al., 1989; Pankratz et al., 1989; Pignoni et al., 1990; Weigel et al., 1990). The first localized gene expression along the dorsal–ventral axis also occurs at this time, with the activation of *twist* and *snail* in the ventral nuclei of the embryo and *dpp* and *zen* in the dorsal regions (Rushlow et al., 1987a; St Johnston and Gelbart, 1987; Thisse et al., 1987; Leptin and Grunewald, 1990). All of these genes, with the exception of *dpp*, encode DNA-binding proteins that are believed to act as transcription factors, and it is the interactions between these factors and the genes that they regulate that lead to the subdivision of the anterior–posterior and dorsal–ventral axes into different regions (Rosenberg et al., 1986; Boulay et al., 1987; Padgett et al., 1987; Rushlow et al., 1987b; Tautz et al., 1987; Nauber et al., 1988; Thisse et al., 1988; Pignoni et al., 1990). The initial activation of these genes in their discrete spatial domains is controlled by the four localized maternal signals, and in this way these determinants establish the polarity and organization of both axes.

The genes discussed above are expressed in the zygotic nuclei of the embryo, but the maternal signals and the components required for their localization and function are synthesized during oogenesis. A number of genetic screens have been performed to isolate maternal-effect mutations that affect the embryonic pattern (Gans et al., 1975; Anderson and Nüsslein-Volhard, 1986; Schüpbach and Wieschaus, 1986; Nüsslein-Volhard et al., 1987; Schüpbach and Wieschaus, 1989). Females that carry such mutations lay normally shaped eggs that develop into embryos with cuticular pattern defects. Several important conclusions can be drawn from the results of these screens.

First, the number of genes that are specifically involved in the establishment of positional information in the egg is quite small. About 30 genes have been identified so far, and the total number is unlikely to be much higher than this. Second, the two body axes are established independently, as mutations either affect the anterior–posterior pattern or the dorsal–ventral pattern, but never both. Third, the number of embryonic phenotypes observed is much smaller than the number of genes. This means that the genes can be assigned to four classes on the basis of which parts of the embryo they affect. The common phenotype produced by mutations in the genes of one class indicates that these genes act in a common pathway to specify a discrete part of the embryonic pattern.

One class, consisting of the dorsal group genes and *cactus*, is responsible for specifying the whole of the dorsal–ventral axis of the embryo (Figure 2). Loss-of-function mutations in the ten dorsal group genes and gain-of-function *cactus* mutations result in completely dorsalized embryos, in which all cells follow a dorsal developmental pathway (Figure 3e), while loss-of-function *cactus* muta-

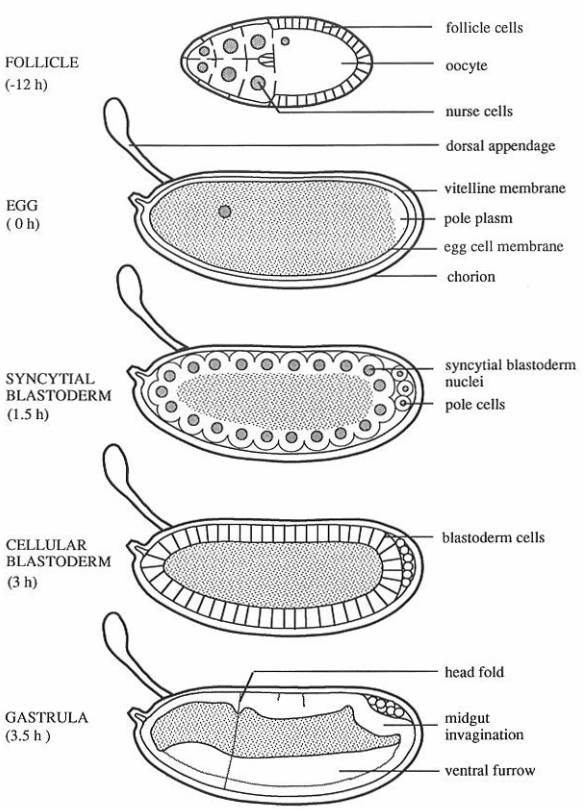


Figure 1. Oogenesis and Early Embryogenesis in Drosophila

At the beginning of oogenesis, a germline stem cell divides four times to produce 16 cells that remain connected by cytoplasmic bridges. One cell in the cluster migrates to the posterior and develops into the oocyte, while the 15 remaining cells become the anterior nurse cells. The nurse cell–oocyte complex is surrounded by somatic follicle cells, and by stage 10 of oogenesis (top panel) these cells have migrated to cover the developing oocyte. As the oocyte matures, the nurse cells contract and expel their contents into the oocyte, while the follicle cells secrete the egg coverings. Both of these cell types degenerate at the end of oogenesis. When the mature egg (second panel) is laid, it is surrounded by the vitelline membrane and the chorion, and is filled with yolky cytoplasm. The only visible specialized region of cytoplasm is the pole plasm at the posterior pole, which is yolk-free, rich in mitochondria, and contains the polar granules. After fertilization, the zygotic nuclei go through a series of rapid cleavage divisions in the interior of the egg. After nine divisions the majority of the nuclei have migrated to the cortex to form the syncytial blastoderm (middle panel). At this stage, the 3–4 nuclei that have entered the pole plasm at the posterior pole form polar buds, which will give rise to the pole cells, the precursors of the germline. The rest of the nuclei divide four more times at the surface of the egg before being surrounded by cell membranes to give rise to the ~6000 cells of the cellular blastoderm (fourth panel). Soon after cellularization is complete, gastrulation (bottom panel) begins with the invagination of the presumptive mesoderm through the ventral furrow, the formation of the posterior midgut invagination that contains the pole cells, and the appearance of the head fold.

tions and some gain-of-function dorsal group alleles lead to the development of ventralized embryos (Figure 3f) (Nüsslein-Volhard et al., 1980; Anderson et al., 1985a; Anderson and Nüsslein-Volhard, 1986; Chasan and Anderson, 1989; Schüpbach and Wieschaus, 1989; Roth et al., 1991). The specification of the anterior–posterior axis requires three classes of maternal genes: the anterior, posterior, and terminal genes (see Figure 2) (Nüsslein-Volhard et al., 1987). Mutations in the anterior class lead to a reduction or loss of head and thoracic structures, posterior group mutations cause abdominal deletions, and the terminal class (*torso* group) is required for the development of the unsegmented ends of the embryo, the acron and telson (Figures 3b–3d). To a first approximation, these three gene systems act independently and additively to define discrete parts of the pattern; the parts of the pattern removed by mutations in one system are the only regions that are unaffected when both of the other two systems are absent (Figure 4). This complementarity between the regions defined by each of the maternal signals only breaks down in the most anterior region of the embryo, the acron, which requires both the terminal and anterior systems. In the absence of the anterior signal, the terminal system directs the formation of an anterior telson, usually the posterior-most structure of the embryo.

## Localized Cytoplasmic Determinants

The first demonstration that the Drosophila egg contains

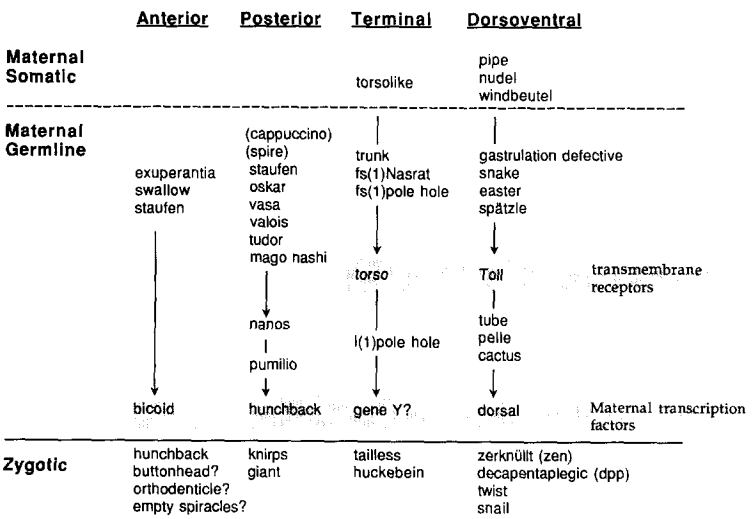


Figure 2. The Genes of the Four Maternal Systems in Drosophila

Where possible, the genes of each maternal class are shown in the order in which they are believed to act, while the lower section of the figure lists the zygotic genes that are regulated by each maternal system. Note that *staufen* is the only maternal gene that participates in two of these systems (anterior and posterior). The parentheses around *cappuccino* and *spire* indicate that these genes do not fall into the category of strict maternal-effect genes that we have used. In addition to a posterior group phenotype, mutations in these loci also affect the shape of the egg.

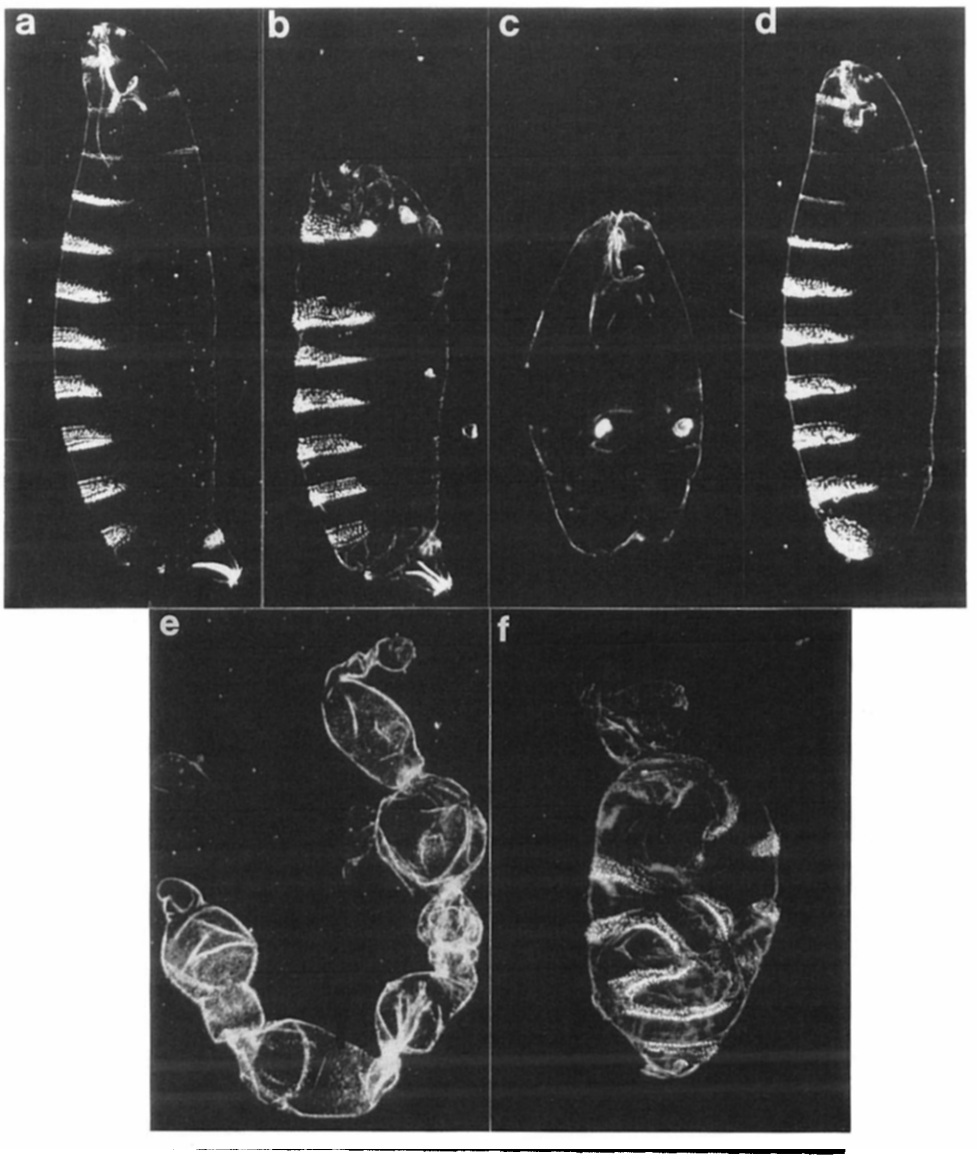


Figure 3. The Cuticular Patterns of Wild-Type and Mutant Embryos
(a) wild-type, (b) anterior (*bicoid*), (c) posterior (*oskar*), (d) terminal (*torso-like*), (e) dorsalized (*dorsal*), (f) ventralized (*cactus*).

localized cytoplasmic determinants comes from experiments in which the egg is pricked and a small amount of cytoplasm is allowed to leak out (Frohnhöfer et al., 1986; Sugiyama and Okada, 1990). Pricking at the anterior pole leads to the development of larvae with head and thoracic defects that closely resemble those produced by mutations in the anterior gene *bicoid*. When the pole plasm is removed from the posterior pole, the telson, the most posterior region of the embryo is not affected, but the resulting larvae show abdominal deletions that are very similar to those produced by posterior group mutations. These results indicate that the anterior and posterior systems produce localized signals that reside at the corresponding poles of the egg. This conclusion is supported by the results of transplantation experiments; defects produced by *bicoid* mutations can be rescued by transplanting anterior cytoplasm into the anterior pole of mutant eggs (Frohnhöfer and Nüsslein-Volhard, 1986). In a similar fashion, the transplantation of wild-type pole plasm can rescue the defects caused by posterior group mutations (Lehmann and Nüsslein-Volhard, 1986, 1987a; Manseau and Schüpbach, 1989; Lehmann and Nüsslein-Volhard, 1991). However, in this case, although the donor cytoplasm must be taken from the posterior pole, the best rescue is observed when this cytoplasm is injected into the presumptive abdominal region. Thus, the pole plasm contains a localized posterior determinant that acts more anteriorly to determine the formation of the abdomen. The pole plasm also contains a second determinant, which directs the formation of the pole cells (Illmensee and Mahowald, 1974), but

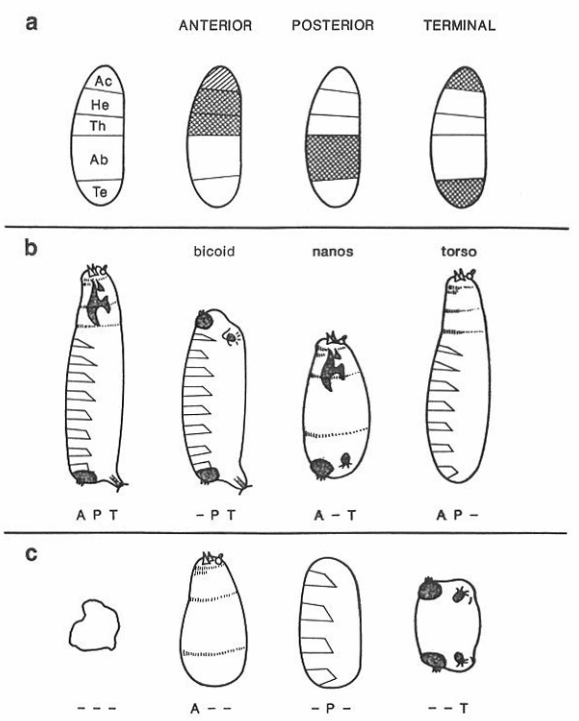


Figure 4. The Complementarity between the Parts of the Pattern Specified by the Anterior, Posterior, and Terminal Systems

(a) The wild-type blastoderm fate map and mutant fate maps showing the parts of the pattern that are absent in mutants of each class (cross-hatched). The hatched shading indicates the anterior region in *bicoid* mutants that develops into telson instead of acron. The five marked areas of the fate map show the regions of the blastoderm that will give rise to the acron (Ac), the head (He), the thorax (Th), the abdomen (Ab), and the telson (Te).

(b) A schematic representation of the final cuticle phenotypes of wild-type embryos and single mutants in each of the three systems. A, P, and T refer to the presence of the anterior, posterior, or terminal systems, respectively, while dashes indicate that this system is mutant.

(c) Final cuticular phenotypes of a triple mutant and the three possible double mutant combinations.

this signal has not yet been identified. The removal of cytoplasm from other regions of the egg does not cause specific pattern defects, nor is it possible to mimic the phenotypes engendered by mutations in the dorsal or terminal systems in this way. As described below, these maternal systems do not produce localized cytoplasmic determinants, but instead act through signals that are localized outside the egg cell.

A combination of genetic and classical embryological experiments have defined the basic properties of the four Drosophila maternal systems. One surprising aspect of these four systems is that, although they all serve to control the localized activation of zygotic pattern gene expression, at a molecular level they act through very different pathways. This is reflected in the fact that with one exception, the genes involved in the production of one maternal signal are not involved in any of the other systems (see Figure 2).

### The Anterior Determinant, *bicoid*

For a maternal system to act to specify part of the embryonic pattern it needs to have two properties. First, some component of the system must be localized to provide the initial asymmetric signal. Second, this signal must directly or indirectly lead to the production of an active transcription factor that regulates zygotic target genes. In the case of the anterior system, both of these roles are performed by the products of the gene *bicoid*.

*bicoid* RNA is localized in the cytoplasm at the anterior pole of the egg (Figure 5A), and is translated after fertilization to produce an anterior to posterior concentration gradient of bicoid protein that extends over the anterior two-thirds of the embryo (Figure 5B) (Frigerio et al., 1986; Berleth et al., 1988; Driever and Nüsslein-Volhard, 1988a; St Johnston et al., 1989). This gradient is believed to arise from diffusion from the anterior source coupled to a uniform rate of degradation. Two lines of evidence demonstrate that the bicoid protein gradient is sufficient to determine the polarity and pattern of the anterior half of the embryo. As the number of maternal copies of *bicoid* is increased, more RNA and protein are produced, resulting in an expansion of the bicoid protein gradient toward the posterior. This change in the shape of the gradient produces a corresponding change in the anterior fate map, as monitored by the positions of gap and pair-rule gene expression domains at the blastoderm stage and the position of the head fold at gastrulation (Driever and Nüsslein-Volhard, 1988b; Struhl et al., 1989). A more dramatic demonstration is provided by RNA injection experiments (Figure 6) (Driever et al., 1990). Injection of in vitro synthesized RNA into other positions in the embryo results in a protein gradient that directs the formation of ectopic head and thoracic structures, with the most anterior pattern elements forming closest to the site of injection. These results show that anterior structures form in regions with high concentrations of bicoid, while lower concentrations lead to the development of more posterior pattern elements. In this way the shape of the gradient defines the polarity of the anterior pattern.

The presence of a homeodomain within the bicoid protein suggests that bicoid is a sequence-specific DNA-binding protein that determines the anterior pattern by directly regulating zygotic target genes (Frigerio et al., 1986; Berleth et al., 1988). One target is the gap gene *hunchback*, which is required for the development of the thorax and part of the head, and is first transcribed at the syncytial blastoderm stage in a large anterior domain that extends to about 50% egg length (see Figure 5C) (Bender et al., 1987; Lehmann and Nüsslein-Volhard, 1987b; Tautz et al., 1987). This early expression is dependent on the bicoid protein gradient, as it does not form in *bicoid* mutant embryos and it expands posteriorly when the *bicoid* gene dosage is increased (Figures 7a–7d) (Schröder et al., 1988; Tautz, 1988; Struhl et al., 1989). There are a number of bicoid-binding sites in the *hunchback* upstream region, including three strong and three weak sites in the 300 bp immediately 5′ to the major start site of zygotic transcription (Driever and Nüsslein-Volhard, 1989a). This region of *hunchback* can direct the bicoid-dependent expression of a reporter gene in the anterior half of the embryo, indicating that bicoid acts as a transcriptional activator of *hunchback* (Schröder et al., 1988; Struhl et al., 1989; Driever and

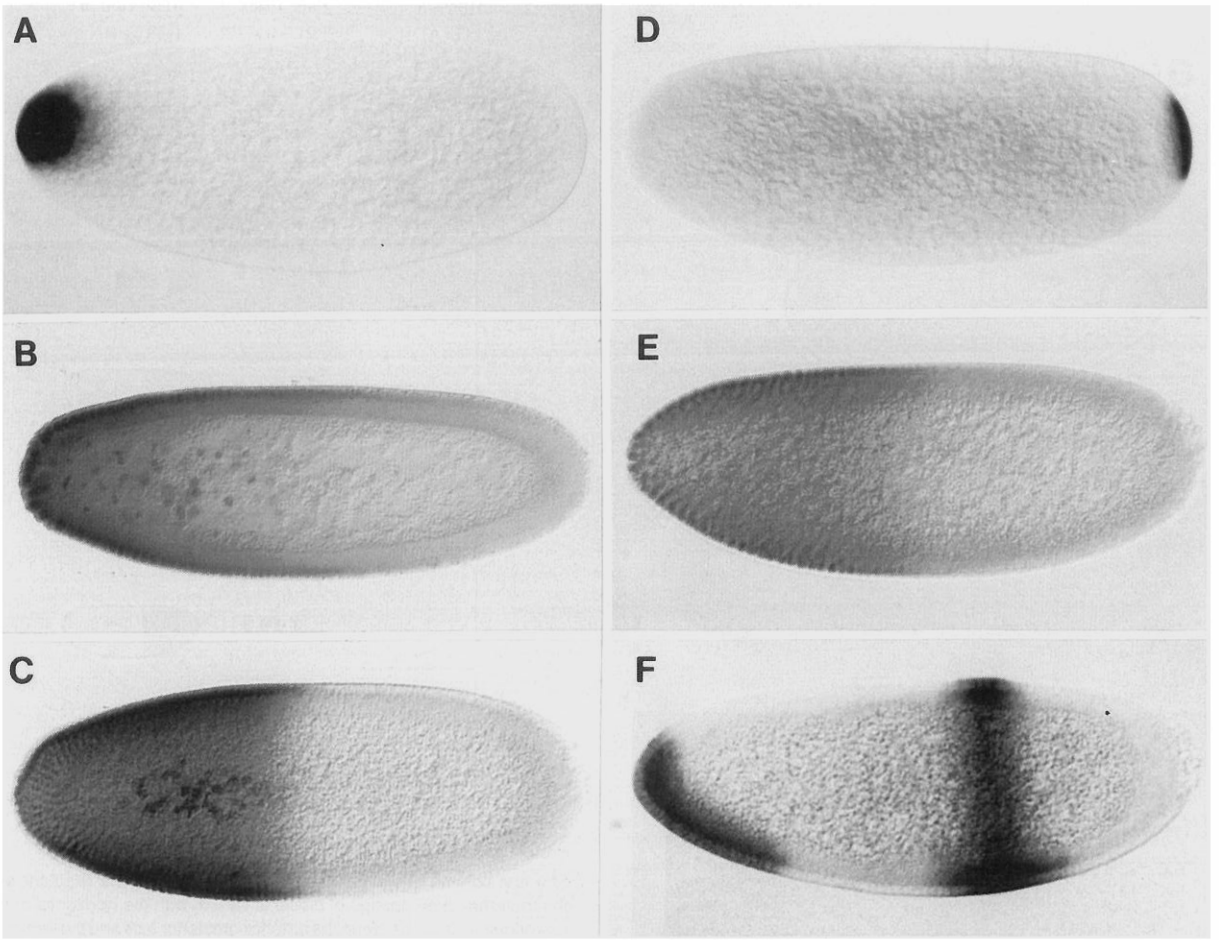


Figure 5. The Distribution of the Localized Maternal RNAs, Transcription Factors, and Target Gene Expression in the Anterior and Posterior Systems
(A–C) The anterior system. (A) *bicoid* RNA. (B) The bicoid protein gradient. (C) The zygotic *hunchback* expression domain.
(D–E) The posterior system. (D) *nanos* RNA. (E) hunchback protein translated from maternal *hunchback* RNA. (F) *knirps* expression (only the posterior domain of *knirps* expression is dependent upon the posterior system).

Nüsslein-Volhard, 1989b). It is unlikely that bicoid requires any specific cofactors to activate transcription, since these *hunchback* sequences are also able to mediate the bicoid-dependent activation of reporter genes in both yeast and Drosophila tissue culture cells (Driever and Nüsslein-Volhard, 1989a; Struhl et al., 1989).

Since *hunchback* is only required for the development of part of the region defined by the anterior system, the bicoid protein gradient must also regulate other zygotic target genes. Indeed, the dependence of the anterior fate map upon the shape of the protein gradient indicates that bicoid acts as a morphogen, with different threshold concentrations defining a number of anterior positions. A model for how this may occur is suggested by analysis of the ability of different bicoid-binding sites to direct the embryonic activation of a basic promoter (Driever and Nüsslein-Volhard, 1989b). Four tandem copies of a high affinity bicoid-binding site direct expression in a large anterior domain that is approximately the same size as the wild-type *hunchback* domain (Figure 7e). In contrast, four low affinity sites direct expression in a much smaller anterior region (Figure 7f). Adding extra binding sites to either construct leads to a large increase in the level of expression, but only causes a slight posterior shift in the extent of the domain. Thus, promoters with low affinity bicoid-binding sites require high concentrations of protein to be activated and are therefore expressed in small anterior regions, while high affinity sites can bind bicoid at lower concentrations and direct expression in larger domains. Although there is still some doubt whether the threshold concentration for activation by bicoid depends solely on the affinity of the bicoid-binding sites in the genes that it normally regulates (Struhl et al., 1989), it is clear that the bicoid gradient can activate target genes in anterior domains of various sizes. In this manner, the smooth protein gradient can be converted into a number of discrete domains of zygotic gene expression, which define several anterior positional values.

The model proposed above requires the existence of at least one additional zygotic gap gene (gene X in Figure 9; Driever and Nüsslein-Volhard, 1989a), which is directly regulated by bicoid and which is expressed in a smaller

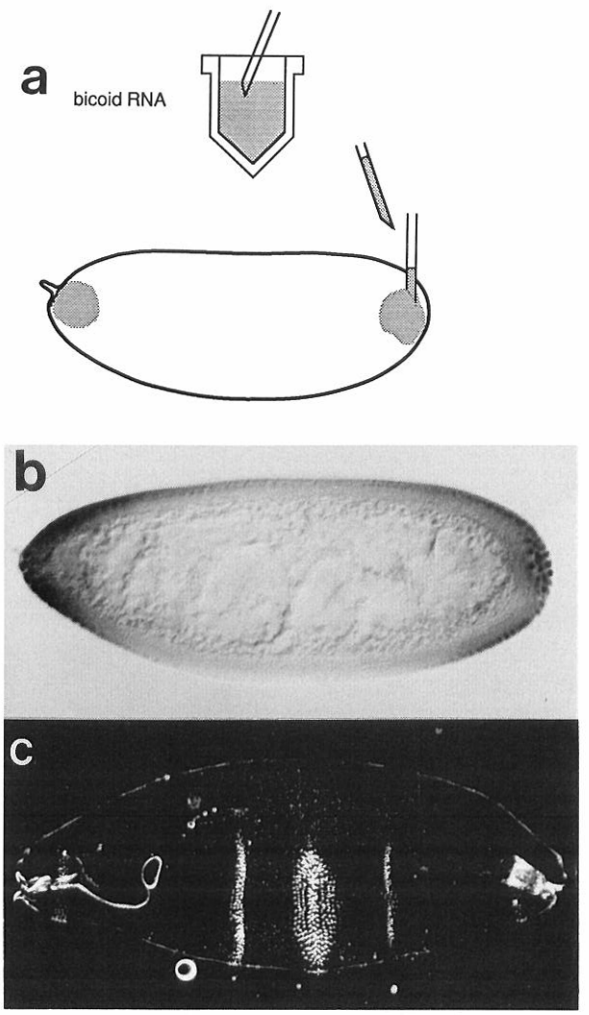


Figure 6. Injected *bicoid* RNA Can Induce a Second Anterior Pattern
(a) Experimental design. In vitro transcribed *bicoid* RNA is injected into the posterior end of wild-type embryos.
(b) The resulting double gradient of bicoid protein.
(c) The cuticular pattern of the dicephalic embryos that develop.

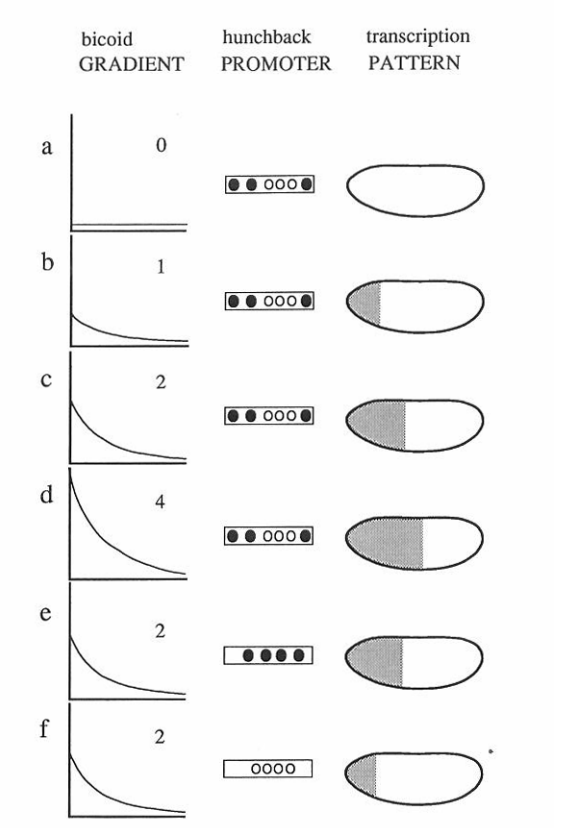


Figure 7. The Spatial Regulation of Zygotic Transcription by the bicoid Protein Gradient

The first column shows the shape of the bicoid protein gradient as the maternal gene dosage of *bicoid* is varied, with the horizontal axis representing distance along the anterior–posterior axis and the vertical axis showing the concentration of bicoid protein. The second column shows the bicoid-binding sites in the regulatory region of *hunchback* (a–d) or two reporter gene constructs (e–f). The closed circles indicate high affinity binding sites, and the open circles, low affinity sites. The third column shows the size of the anterior expression domain of a gene with the bicoid-binding sites shown in column 2, in the presence of the gradient shown in column 1. (a) No maternal copies of *bicoid*, wild-type *hunchback*. (b) One maternal copy of *bicoid*, wild-type *hunchback*. (c) Two maternal copies of *bicoid* (normal) wild-type *hunchback*. (d) Four maternal copies of *bicoid*, wild-type *hunchback*. (e) Two maternal copies of *bicoid*, reporter gene construct containing four high affinity bicoid-binding sites. (f) Two maternal copies of *bicoid*, reporter gene construct containing four low affinity bicoid-binding sites.

anterior domain than *hunchback*. No gene has been proven to fulfil both these criteria, but there are several promising candidates. Mutations in *orthodenticle*, *empty spiracles*, and *buttonhead* delete partially overlapping, adjacent regions of the head, just anterior to the region affected by *hunchback* (Dalton et al., 1989; Cohen and Jurgens, 1990; Finkelstein and Perrimon, 1990). Each of these genes is required very early in development, as the mutants alter the expression patterns of other zygotic pattern genes at the cellular blastoderm stage. Thus, in terms of their phenotypes and their positions in the zygotic hierarchy, these loci behave like gap genes. *empty spiracles* and *orthodenticle* encode homeodomain proteins that are first expressed in a single stripe near the anterior end of the syncytial blastoderm embryo (Dalton et al., 1989; Finkelstein and Perrimon, 1990). Furthermore, the positions of these stripes depend upon the bicoid gradient, since both shift posteriorly when extra maternal copies of *bicoid* are present. Another possible target for *bicoid* regulation is the anterior domain of *giant* expression, whose position is also dependent on the shape of the bicoid protein gradient (Eldon and Pirrotta, 1991; Kraut and Levine, 1991a). However, it still remains to be shown that bicoid protein binds to the regulatory regions of any of these genes to activate their transcription directly. Without knowing how many genes are regulated by the bicoid gradient, it is not possible at present to determine how many different threshold concentrations of bicoid are used to determine the anterior pattern.

**The Posterior Determinant**

Although superficially similar, the posterior system differs in several major respects from the anterior. First, while the

initial localized signal at the posterior pole is a maternal RNA, the product of this RNA does not regulate zygotic gene expression directly. Instead, the posterior determinant acts by preventing the translation of a transcription factor encoded by an ubiquitous maternal RNA. Second, unlike bicoid, which plays an instructive role in anterior pattern formation, the posterior signal only plays a permissive role.

The pole plasm at the posterior pole contains two localized signals: the posterior determinant, which controls the development of the abdomen, and a second signal that directs the formation of the pole cells. Mutations in all posterior group genes result in abdominal deletions, but the majority of these genes (*cappuccino*, *spire*, *staufen*, *oskar*, *vasa*, *valois*, *tudor*, and *mago nashi*) are also required for the formation of the pole plasm, with its characteristic polar granules, and for pole cell development (Mahowald, 1968; Boswell and Mahowald, 1985; Lehmann and Nüsslein-Volhard, 1986; Schüpbach and Wieschaus, 1986; Lehmann and Nüsslein-Volhard, 1987a; Manseau and Schüpbach, 1989; Boswell et al., 1991). Mutations in this class of posterior group gene cause their abdominal phenotype not by preventing the production of the posterior determinant, but by failing to localize this signal to the posterior pole (Sander and Lehmann, 1988; Lehmann and Nüsslein-Volhard, 1991). These genes are all required for the localization and stepwise assembly of the polar granules during oogenesis, and the formation of these granules seems to be a prerequisite for the localization of the posterior determinant.

The two remaining posterior group genes, *nanos* and *pumilio*, are specifically involved in the determination of the abdomen and are not required for the formation of polar granules or pole cells (Lehmann and Nüsslein-Volhard, 1987a, 1991). No posterior determinant activity is detectable at any stage in *nanos* mutant ovaries or eggs, indicating that *nanos* is required for the synthesis of this signal (Lehmann and Nüsslein-Volhard, 1991). In fact, *nanos* actually encodes the posterior determinant, and *nanos* RNA is highly concentrated in the pole plasm of the freshly laid egg (see Figure 5D) (Wang and Lehmann, 1991). Injection of in vitro synthesized *nanos* RNA into the abdominal region of mutant embryos restores normal abdomen development, while the injection of a control RNA containing a frame shift mutation has no effect on the phenotype. Furthermore, the wild-type RNA can also rescue the abdominal deletions produced by all other posterior group mutations. Since *nanos* activity is required in the region where the abdomen will form, while the RNA is localized at the posterior pole, either nanos protein, or some activity dependent on nanos, must move to this more anterior region. The distribution of the *nanos* product is not yet known, but the simplest model would be that the protein diffuses from its posterior source to form a posterior–anterior gradient in a similar way to that in which the bicoid gradient forms. *pumilio* mutations seem to prevent sufficient nanos activity from reaching the presumptive abdominal region, as mutant embryos do not form complete abdomens, although they have posterior determinant activity in their pole plasm (Lehmann and Nüsslein-Volhard, 1987a). It is possible that the *pumilio* product facilitates the anterior movement of nanos. Alternatively, pumilio could enhance the amount of nanos activity produced at the posterior pole.

The gap genes *knirps* and *giant* are both required for the formation of the abdominal pattern and are expressed in adjacent domains in the syncytial blastoderm embryo, in the region where the abdomen will develop (Mohler et al., 1989; Pankratz et al., 1989). This expression is dependent on *nanos*, since neither domain is formed in posterior group mutant embryos (Rothe et al., 1989; Eldon and Pirrotta, 1991; Kraut and Levine, 1991a). However, although *nanos* provides the localized signal that initiates abdomen formation, it does not directly regulate these zygotic gap genes. Instead, *nanos* appears to prevent the expression of a transcriptional repressor encoded by maternal *hunchback* RNA. We have already described how the bicoid gradient activates zygotic *hunchback* expression in the anterior of the embryo. *hunchback* is also transcribed during oogenesis to give rise to a maternal transcript that is uniformly distributed in the mature egg (Schröder et al., 1988; Tautz, 1988; Tautz and Pfeifle, 1989). During the cleavage stages of embryogenesis, this maternal RNA is degraded in the posterior half of the embryo, and hunchback protein, which is first synthesized during this period, shows a similar distribution (see Figure 5E) (Tautz, 1988; Tautz and Pfeifle, 1989). In *nanos* mutants, both the RNA and the protein are present throughout the embryo, indicating that an early function of *nanos* is to repress maternal hunchback expression in posterior regions. Using two different experimental approaches, Hülskamp et al. (1989) and Struhl (1989) have caused the ectopic expression of hunchback protein in the posterior half of the embryo, in the presence of wild-type *nanos* activity. In both cases, this posterior hunchback protein blocks the formation of the abdomen and results in a phenotype that is very similar to that produced by *nanos* mutations (Hülskamp et al., 1989; Struhl, 1989). Since hunchback contains six zinc finger domains and binds DNA, it is likely that it prevents abdomen formation by directly repressing the expression of *knirps* and *giant* (Tautz et al., 1987; Stanojević et al., 1989; Treisman and Desplan, 1989). These results indicate that an essential role of *nanos* is to prevent the posterior expression of *hunchback*. In fact, this is the only role that *nanos* plays in the determination of the abdomen. Using mitotic recombination to generate *hunchback* mutant germline clones, it has been possible to produce embryos that lack both maternal *hunchback* activity and *nanos* activity (Hülskamp et al., 1989; Irish et al., 1989; Struhl, 1989). These embryos develop normal abdomens and give rise to fertile adults. Thus, in the absence of maternal *hunchback*, *nanos* is not required for normal development.

The protein sequence of *nanos* shows no strong similarities with other known proteins and therefore does not suggest how the nanos product might regulate the expression of *hunchback*. However, since *nanos* activity affects the distribution of both maternal *hunchback* RNA and hunchback protein, it probably acts at the level of the RNA (Tautz, 1988; Tautz and Pfeifle, 1989). This has now been confirmed by the identification of a short sequence that occurs

twice in the 3′ untranslated region (3′UTR) of the *hunchback* transcript that is required for nanos regulation (Wharton and Struhl, 1991). The presence of both copies of this sequence is sufficient to confer *nanos*-dependent posterior repression on a heterologous transcript. Ectopic *nanos* activity seems to suppress anterior development by a similar mechanism. When *nanos* RNA is injected into the anterior of the egg, or is mislocalized there genetically by *Bicaudal-D* mutations, the bicoid protein gradient never forms (Wharton and Struhl, 1989; Wang and Lehmann, 1991). *bicoid* RNA is degraded prematurely in these eggs, but it is still present at the time that the protein would normally be translated. The 3′UTR of *bicoid* RNA contains a similar sequence to the two found in *hunchback* RNA, and this suggests that *nanos* regulates the expression of both of these transcripts by preventing their translation, and that the degradation of these RNAs is probably a consequence of this translational control (Wharton and Struhl, 1991).

The surprising result that *nanos* is not required in the absence of maternal *hunchback* raises several important questions. First, if *nanos* is not supplying an instructive signal, how is the abdominal pattern generated? The answer to this question lies in the long-range interactions between the gap genes. In maternal *hunchback nanos* double mutant eggs, the anterior and terminal signals are still present and lead to the activation of zygotic *hunchback* in the anterior of the embryo and the terminal gap genes at both ends. hunchback protein is distributed in a gradient extending into the posterior half of the embryo that can specify the anterior and posterior borders of *Krüppel* expression and the anterior border of the *knirps* domain (Gaul and Jäckle, 1989; Stanojević et al., 1989; Hülskamp et al., 1990). It is likely that the protein product of the terminal gap gene *tailless* also forms a gradient from the posterior of the embryo that specifies the posterior borders of *knirps* and *giant* expression (Pankratz et al., 1989; Pignoni et al., 1990; Eldon and Pirrotta, 1991; Kraut and Levine, 1991a). The correct positioning of the gap gene expression domains is further refined by regulatory interactions between *Krüppel*, *knirps*, and *giant* (Pankratz et al., 1989; Eldon and Pirrotta, 1991; Kraut and Levine, 1991a, 1991b). In this way, the initial asymmetric signals produced by the anterior and terminal systems, the secondary gradients of gap gene products and the interactions between the gap genes are sufficient to define the order of expression of the abdominal genes *Krüppel*, *knirps*, and *giant*, without an instructive signal from the posterior determinant.

Since the abdomen forms normally in the absence of maternal *hunchback* and *nanos*, it is hard to imagine why this system has evolved. Although it acts by a very different mechanism, the posterior determinant restricts maternal *hunchback* expression to the same anterior region as that in which bicoid activates zygotic *hunchback* (see Figures 5C and 5E). Thus, the anterior and posterior determinants both define the anterior region of the embryo in the same way. It is possible that the posterior system is the more primitive of the two and originally subdivided the anterior–posterior axis on its own, while *bicoid* evolved more recently and took over this role. This does not explain why a functional posterior system has survived, despite the presence of *bicoid*. One possibility is that the existence of maternal *hunchback* and *nanos* allows the anterior expression of hunchback protein to begin slightly earlier and increases the amount of protein produced; these two effects may help to speed up embryogenesis and make pattern formation a more error-free process. *nanos* has also evolved the ability to regulate bicoid translation, which is more difficult to explain, as nanos is restricted to the posterior half of the wild-type embryo, while *bicoid* RNA is localized to the anterior pole.

### The Terminal System

As is the case for the anterior and posterior systems, the defects produced by several terminal and dorsal group mutations can be rescued by cytoplasmic transplantations or RNA injections (Santamaria and Nüsslein-Volhard, 1983; Anderson and Nüsslein-Volhard, 1984; Anderson et al., 1985b; Müller-Holtkamp et al., 1985; Seifert et al., 1987; Klingler et al., 1988; Strecker et al., 1989). However, these results differ in two important respects. In general, the rescuing activities are not localized within the donor eggs, and the polarity of the resulting patterns is not affected by the site of transplantation into the recipient embryos. There are two partial exceptions to these generalizations (see below), but they do not alter the basic conclusion that the terminal and dorsoventral systems do not produce cytoplasmic determinants that are localized in the unfertilized egg. Instead these two systems share a number of features that indicate that they provide positional information to the egg by a quite different mechanism. In both the terminal and dorsal groups, at least one gene is required in the somatic cells of the female, and not in the germline (Stevens et al., 1990; Stein et al., 1991). These genes are most probably expressed in the somatic follicle cells that surround the developing oocyte. In addition, one of the germline genes in each system encodes a transmembrane protein that is uniformly distributed in the egg membrane and that shows homology to other cell surface receptor proteins (Hashimoto et al., 1988; Sprenger et al., 1989). Gain-of-function alleles have been recovered in both of these putative receptor genes and result in the opposite phenotype to loss-of-function mutations (Anderson et al., 1985a; Klingler et al., 1988). These alleles are believed to produce mutant receptors that are constitutively active everywhere in the egg.

Although our information on the pathway for either system is incomplete, drawing on data from each, one can propose the following scheme. In each system, one of the genes that is required in the soma is active in a subpopulation of the somatic follicle cells, leading to the production of a localized signal that is deposited outside the egg in the vitelline membrane or in the perivitelline space, a fluid-filled region between this membrane and the egg membrane. After fertilization, the asymmetric signal provided by the follicle cells causes the release of a localized ligand that binds to the receptors in the egg membrane. The receptors then transmit this signal to the inside of the egg, activating a signal transduction pathway that results in

the local activation of a transcription factor that regulates zygotic pattern gene expression.

In the terminal system, the product of the gene *torso* probably acts as a receptor for an extracellular signal that is produced at the two poles of the egg. The *torso* protein sequence contains an N-terminal signal peptide, a putative transmembrane domain, and a C-terminal region that show significant homology to the tyrosine kinase domains of other receptors (Sprenger et al., 1989). This structure strongly suggests that *torso* encodes a transmembrane receptor tyrosine kinase. Although *torso* RNA is synthesized during oogenesis, the protein is not translated until after fertilization, when it localizes to the egg membrane (Casanova and Struhl, 1989). As predicted by experiments showing that *torso*-rescuing activity is not localized along the anterior–posterior axis, both the RNA and protein show a uniform distribution (Klingler et al., 1988; Casanova and Struhl, 1989; Strecker et al., 1989).

In addition to loss-of-function *torso* mutations, which cause a typical terminal group phenotype (see Figure 3d), there exist three gain-of-function alleles that have the opposite effect (Klingler et al., 1988; Strecker et al., 1988). Embryos laid by mutant females develop normal terminal structures but have defects in the segmented regions of the pattern (Klingler et al., 1988). The gain-of-function segmentation defects are suppressed in embryos that are also mutant for the terminal gap genes, *tailless* and *huckebein*, the zygotic targets for the terminal system (Klingler et al., 1988; Strecker et al., 1988; Weigel et al., 1990). This indicates that these phenotypes are most probably due to the ectopic expression of *tailless* and *huckebein* in the middle of the embryo, which leads to the repression of central gap genes such as *Krüppel*. It is believed that the gain-of-function *torso* alleles encode mutant receptors with constitutive tyrosine kinase activity independent of the binding of ligand.

The existence of *torso* gain-of-function mutations has made it possible to determine which of the other maternal *torso* group genes act upstream of *torso* in the production of the ligand and which act downstream in the signal transduction pathway inside the egg. In double mutant combinations, mutations in the upstream genes should have no effect upon the ligand-independent gain-of-function phenotype, but those in downstream genes should suppress this phenotype and should instead cause the loss of terminal structures. These experiments have placed *torso-like*, *trunk*, *fs(1)Nasrat*, and *fs(1)pole hole* upstream of *torso* and *l(1)pole hole* downstream (Ambrosio et al., 1989; Stevens et al., 1990). *l(1)pole hole* is the Drosophila homolog (*D-raf*) of the vertebrate proto-oncogene *c-raf*, which encodes a serine/threonine kinase (Nishida et al., 1988; Ambrosio et al., 1989). *c-raf* has been implicated in the signal transduction pathways of a number of vertebrate receptor tyrosine kinases, but its exact role is unclear (reviewed by Li et al., 1991; Rapp, 1991). The demonstration that mutations in *D-raf* cause terminal pattern deletions and suppress the *torso* gain-of-function phenotype indicates that the raf kinase is an essential component of the *torso* signal transduction pathway. It is likely that there are still several genes that act downstream of *torso* that have not yet been identified, including the transcription factor at the end of this pathway (gene Y in Figures 2 and 9) that activates *tailless* and *huckebein* in the terminal regions of the embryo.

The genes upstream from *torso* are responsible for the production of the localized extracellular ligand at the two ends of the egg. Since the developing oocyte is surrounded by about 1000 somatic follicle cells, the simplest way that such a ligand might be localized is if it is produced by terminal subpopulations of these cells. Germline clones of *trunk*, *fs(1)Nasrat*, and *fs(1)pole hole* give rise to embryos that display a typical *torso* group phenotype, indicating that these genes are required in the nurse cell–oocyte complex (Perrimon and Gans, 1983; Schüpbach and Wieschaus, 1986). In contrast, *torso-like* is required in the soma and not in the germline (Stevens et al., 1990). Stevens et al. (1990) have produced follicle cell mosaics that are mutant for *torso-like* and have found that *torso-like* clones of only 6–30 cells surrounding the posterior pole of the egg can produce a terminal phenotype at just the posterior end of the resulting embryo. Thus, *torso-like* is specifically required in the terminal follicle cells, strongly suggesting that these cells produce the localized terminal signal. It is not known whether *torso-like* or the three germline-dependent upstream genes actually encode the ligand for *torso*. *torso-like* may produce an inactive ligand that is anchored in the vitelline membrane until after fertilization when it is released by the activities of the germline genes. Alternatively, the follicle cell signal may lead to the local activation of one of the germline products, which then acts as a ligand for *torso*.

### The Dorsoventral System

The dorsoventral pathway is the most complex of the four maternal systems in Drosophila, since it requires the largest number of genes and specifies positional information along the whole of the dorsoventral axis. However, the basic features of this pathway are very similar to those of the terminal system. An initial ventral signal outside the egg leads to the production of a localized ligand for a receptor in the egg membrane. The localized activation of the receptor then initiates a signal transduction pathway inside the egg that culminates in the spatial regulation of zygotic gene expression. Like *torso*, the dorsal group gene *Toll* encodes a transmembrane protein that is believed to act as the receptor for a localized external signal (Hashimoto et al., 1988, 1991). The Toll protein sequence contains an N-terminal signal peptide, a putative transmembrane domain, and two distinct regions of homology to other genes. The extracellular portion of the protein contains two blocks of leucine-rich repeats followed by cysteine-containing domains that are similar to those found in a number of other receptors, including both the α and β chains of the human platelet glycoprotein Ib (a receptor for von-Willebrand factor and thrombin), while a stretch of 217 amino acids in the intracellular domain of Toll shares 26% amino acid identity with the intracellular portion of the interleukin-1 receptor (Lopez et al., 1988; McFarland et al., 1989; Keith and Gay, 1990; Vicente et al., 1990; Soppet et al., 1991; Squinto et al., 1991; Gay and Keith, 1991; Schneider et al., 1991). These homologies strongly support a model in which Toll acts as a receptor

for a localized external ligand, and transduces this signal to the interior of the egg. Consistent with this view, Toll is expressed everywhere in the egg membrane at the syncytial blastoderm stage, the time at which the upstream signal is known to be active (Hashimoto et al., 1991).

While *Toll* loss-of-function mutations produce a dorsalized phenotype, dominant gain-of-function alleles result in the development of embryos that are ventralized (Anderson et al., 1985a; Schneider et al., 1991). Several of these mutations are believed to produce Toll protein with constitutive activity that is partially independent of the extracellular signal (Schneider et al., 1991). Using the same approach described for the terminal system, these gain-of-function alleles can be used to position the other dorsal group genes relative to *Toll* in the pathway: *gastrulation-defective*, *pipe*, *nudel*, *windbeutel*, *snake*, *easter*, and *spätzle* all function upstream of *Toll* in the production of the localized signal; *tube*, *pelle*, and *dorsal* (*dl*) act downstream, in the signal transduction pathway inside the egg (Anderson et al., 1985a; K. V. Anderson, personal communication).

Genetic experiments have suggested that the product of the gene *dorsal* lies at the end of the signal transduction pathway that begins when *Toll* is activated on the ventral side of the embryo. Only *dorsal* mutations produce a dorsalized phenotype in double mutants with loss-of-function, ventralizing *cactus* alleles (Roth et al., 1991). Thus, *dorsal* functions downstream of *cactus*, while all other dorsal group genes do not. Second, only in the case of *dorsal* can a localized rescuing activity be found in transplantation experiments, although this localization only appears at the syncytial blastoderm stage (Santamaria and Nüsslein-Volhard, 1983). Finally, unlike all other dorsal group genes, loss-of-function *dorsal* mutations show a dominant effect (Nüsslein-Volhard et al., 1980). At 29°C, *dl*/+ females produce embryos that do not develop mesoderm, showing that the determination of the most ventral cell fates in the embryo requires higher levels of *dorsal* activity than the lateral and dorsal regions.

The exact role of *dorsal* has only become evident as a result of molecular experiments. These show that the ventral signal transmitted by *Toll* regulates the differential nuclear localization of dorsal protein. The resulting gradient of dorsal protein in the nuclei then controls zygotic gene expression in a concentration-dependent manner. Both *dorsal* RNA and protein are synthesized during oogenesis and are uniformly distributed in the cytoplasm of the freshly laid egg (Steward et al., 1988; Roth et al., 1989; Rushlow et al., 1989; Steward, 1989). When the zygotic nuclei reach the cortex of the egg after the ninth cleavage division, the protein becomes highly concentrated in the nuclei on the ventral side of the embryo and is depleted from the ventral cytoplasm (Roth et al., 1989; Rushlow et al., 1989; Steward, 1989). At more lateral levels, the nuclear and cytoplasmic concentrations of dorsal are approximately equal, while the protein is excluded from the nuclei on the dorsal side. The formation of the concentration gradient of dorsal in the syncytial blastoderm nuclei seems to be entirely regulated at the level of nuclear localization, since a uniform distribution of protein is observed when the nuclear membranes break down during mitosis (Roth et al., 1989).

Using different combinations of mutants in the genes that act upstream of *dorsal*, it is possible to produce a wide range of dorsalized, lateralized, and ventralized phenotypes. In all cases, the distribution of dorsal in the nuclei correlates perfectly with the expression patterns of the zygotic dorsoventral genes and the final cuticular phenotype (Roth et al., 1989). For example, in loss-of-function dorsal group mutations, dorsal protein is excluded from the nuclei at all positions around the dorsoventral axis, the dorsal zygotic genes *zen* and *dpp* are expressed everywhere while the ventral genes *twist* and *snail* are not expressed, and all the cells adopt a dorsal fate (Figures 8i–8m). In the strongest ventralizing mutants, the converse is seen. dorsal protein localizes to all of the nuclei, which leads to the repression of *zen* and *dpp* and the activation of *twist* and *snail* all around the circumference of the embryo, and all cells follow a ventral pathway of development (Figures 8a–8d). Finally, in mutant combinations that produce a lateralized phenotype, dorsal protein is evenly distributed between the nuclei and the cytoplasm, and neither the dorsal nor ventral zygotic genes are expressed in the main part of the embryo (Figures 8e–8h). These observations provide strong evidence that the nuclear concentration of dorsal determines the dorsoventral pattern by controlling the expression of the zygotic genes.

The sequence of *dorsal* indicates that it is likely to encode a transcription factor. The N-terminal half of the protein shares approximately 50% amino acid identity with the N-terminal portions of the proto-oncogene *c-rel* and the p50 and p65 subunits of the transcription factor, NF-κB, and this region of similarity includes both the DNA-binding and dimerization domains of these proteins (Steward, 1987; Ghosh et al., 1990; Kieran et al., 1990; Nolan et al., 1991; Ruben et al., 1991). More direct evidence that dorsal acts as a transcription factor comes from studies on the zygotic genes that are regulated by the dorsal protein gradient. The dorsal-dependent repression of *zen* expression in the ventral and lateral regions of the embryo requires a repression element in the *zen* promoter that contains a number of dorsal-binding sites (Doyle et al., 1989; Ip et al., 1991). The upstream sequences that control the ventral expression of *twist* also contain two clusters of dorsal-binding sites, and these regions can mediate the dorsal-dependent activation of transcription in tissue culture cells (Thisse et al., 1991; Jiang et al., 1991; Pan et al., 1991). Interestingly, dorsal protein binds more strongly to the sites in the *zen* repression element in vitro than it does to sites in the *twist* upstream region (Thisse et al., 1991; Jiang et al., 1991). Therefore, dorsal may control the spatial domains of zygotic gene expression in a similar way to that proposed for bicoid. Genes like *zen* with high affinity dorsal-binding sites can bind dorsal protein when it is present at the low concentrations found in lateral nuclei, while higher concentrations are needed to bind to the lower affinity sites of genes such as *twist*, and this will restrict the binding to the ventral nuclei of the embryo. One important additional property of dorsal is that it seems to function as both a transcriptional activator and repressor, activating

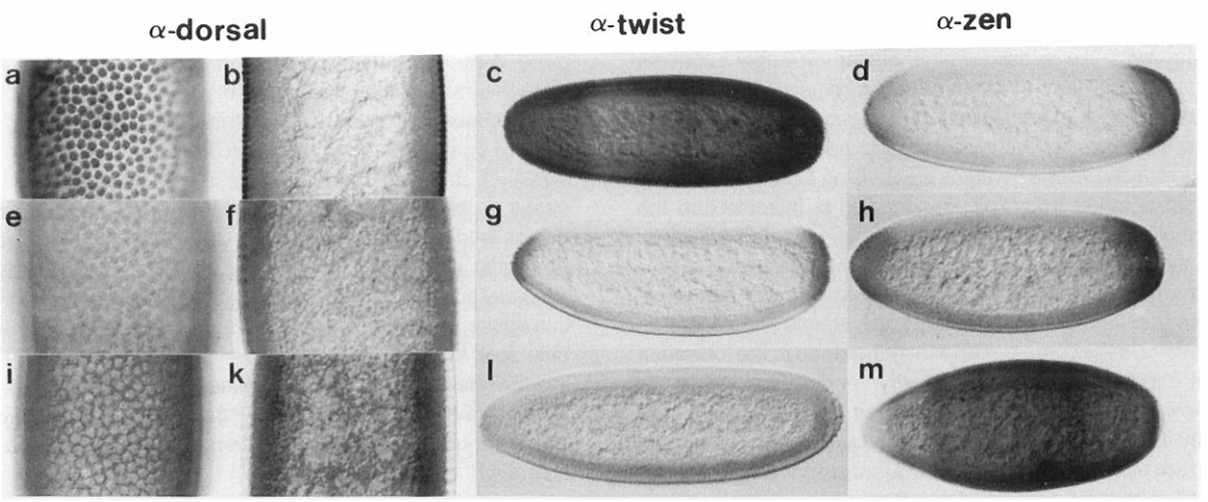


Figure 8. The Regulation of Zygotic Transcription by the Nuclear Concentration of dorsal Protein

The uniform distribution of dorsal protein and the resulting expression of the zygotic target genes, *twist* and *zen*, are shown for three apolar phenotypes.

(a–d) V0, completely ventralized embryos (*cactus*$^{A2}$; *Toll*$^{rm9}$). dorsal protein is localized to all of the nuclei, resulting in the expression of twist and the repression of zen protein, all around the egg circumference. (Note that the poles of the egg behave differently in several of these stainings, because of the influence of the terminal system.)

(e–h) L1, lateralized at a ventrolateral level (*Toll*$^{rm9}$). dorsal protein is present at equal concentrations in the nuclei and the cytoplasm, and neither twist nor zen is expressed.

(i–m) D0, completely dorsalized (*Toll*$^{5BRE}$/Deletion). dorsal protein is excluded from all of the nuclei, twist is not activated, and zen is expressed everywhere.

(a), (e), and (i) show surface views of the middle part of syncytial blastoderm embryos stained with an antibody against dorsal protein; (b), (f), and (k) show optical midsections of the same embryos; (c), (g), and (l) show optical midsections of cellular blastoderm embryos stained with an anti-twist antibody; (d), (h), and (m) show optical midsections of cellular blastoderm embryos stained with an anti-zen antibody. Data from Roth et al. (1989).

*twist* ventrally and repressing *zen* in the ventral and lateral nuclei. At present, we have no information on why the binding of dorsal can have these two opposite effects, but this probably depends on the context of the binding sites and on the other factors that bind in the region (Pan et al., 1991).

The homology between *dorsal* and the p50 and p65 subunits of NF-κB is especially intriguing since the activity of NF-κB is also regulated at the level of nuclear localization. In several cell types NF-κB is found in the cytoplasm in an inactive form in which p65 is bound to IκB (Baeuerle and Baltimore, 1988a, 1988b; Nolan et al., 1991). Upon activation of the cells by a number of signals, IκB is released from the complex, allowing the active NF-κB to translocate to the nucleus. There is strong evidence that *cactus* performs a homologous function to IκB in the Drosophila dorsoventral system (Roth et al., 1991). The sequence of *cactus* is actually very similar to that of IκB (R. Geisler and C. N.-V., unpublished data), and *cactus* loss-of-function mutations produce an increase in dorsal nuclear localization, resulting in a ventralized phenotype, which one would expect if *cactus* encodes a cytoplasmic anchor for dorsal protein. In vitro experiments have shown that the phosphorylation of IκB by cellular kinases can activate NF-κB (Ghosh and Baltimore, 1990). While a similar process may occur in the dorsoventral pathway, it is unlikely that the ventral activation of dorsal nuclear localization occurs solely through the modification of cactus. The ventralized embryos produced by even the strongest *cactus* mutations are still polar, and although more dorsal protein localizes to the nuclei, the ventral nuclei still contain higher levels of protein than those on the dorsal side (Roth et al., 1991). It is possible that none of these mutations completely abolishes *cactus* activity, but it seems more likely that the release of dorsal protein from cactus inhibition is insufficient to produce the highest levels of dorsal nuclear localization. This suggests a model in which the dorsal group genes activate dorsal nuclear localization independently of *cactus*, perhaps by modifying dorsal directly. It is interesting to note that one of the signals that can lead to the activation of NF-κB is interleukin-1 (Shirakawa and Mizel, 1989; Shirakawa et al., 1989). As mentioned above, the interleukin-1 receptor is homologous to Toll, raising the possibility that both receptors use similar intracellular signaling pathways to regulate nuclear localization. The two dorsal group genes *tube* and *pelle* are required for the transmission of this activating signal in Drosophila, but although *tube* has been cloned, its sequence does not suggest what role it may play (Letsou et al., 1991).

The discovery that *Toll* encodes a transmembrane receptor that is localized in the egg membrane has led to the hypothesis that dorsoventral polarity is induced from outside the egg by a localized ligand for Toll, and that the production of this external signal depends upon the seven dorsal group genes that act upstream from *Toll* in the hierarchy. Two recent results have provided strong support for this model (Stein et al., 1991). First, three of the upstream dorsal group genes—*pipe*, *nudel*, and *windbeutel*—are re-

quired in the soma and not in the germline. The similarity with *torso-like* in the terminal system strongly suggests that at least one of these genes is required in a specific population of ventral follicle cells. Second, transplantation experiments have shown that the perivitelline fluid that surrounds the egg contains a polarizing activity. When this fluid is taken from *Toll*⁻ donors and is injected into the perivitelline space of *pipe*, *nudel*, or *windbeutel* recipients, it induces the formation of ventral pattern elements. Furthermore, the site of injection determines the polarity of the resulting embryos. These experiments show that mutations in the soma-dependent genes lead to the formation of eggs with no intrinsic polarity, lending support to the view that these genes are required for the production of the initial asymmetric signal. No polarizing activity is found in the perivitelline fluid of donors that carry a wild-type copy of *Toll*, but wild-type *Toll* is required in the recipients. These observations suggest that the rescuing activity corresponds to the Toll ligand. In the presence of wild-type *Toll*, the ligand will bind to the Toll protein in the egg membrane of the donors and will therefore no longer be free in the perivitelline fluid for transplantation.

The four other genes upstream of *Toll* are germline dependent (Seifert et al., 1987; Konrad et al., 1988; Stein et al., 1991). While *gastrulation-defective* cannot be rescued by cytoplasmic transplantation and has a temperature-sensitive period that begins during oogenesis, *easter*, *snake*, and *spätzle* can be rescued by the injection of RNA or cytoplasm into mutant embryos (Anderson and Nüsslein-Volhard, 1984; Seifert et al., 1987). This indicates that the activities of these genes are not required until after fertilization. *snake* and *easter* have been cloned and their sequences indicate that they both encode serine proteases that are probably secreted as inactive precursors (DeLotto and Spierer, 1986; Chasan and Anderson, 1989). It is likely that *spätzle* also encodes a product that is secreted into the perivitelline space, since the dorsalization produced by mutants in any of these three genes can be rescued by the transplantation of perivitelline fluid (Stein and Nüsslein-Volhard, 1992). Similar transplantation experiments have shown that *easter*, *snake*, and *spätzle* are required for the production of the polarizing activity that is believed to correspond to the ligand for Toll. For example, perivitelline fluid from *easter Toll* donors cannot generate polarity in *pipe* recipients, even though there is no Toll protein present in the donors to sequester any ligand produced.

While all the evidence so far supports the idea that the ventral follicle cells provide the initial asymmetric signal in the dorsoventral pathway, the relationship between this signal, the germline-dependent activities, and the Toll ligand remains unclear. The expression of the somatic genes in the ventral follicle cells could result in the synthesis of a localized inactive ligand for Toll that is released after fertilization as a result of the activities of the germline-dependent genes, perhaps by proteolysis. Alternatively, the follicle cell signal may lie upstream of the germline-dependent activities. For example, this signal might actually be in the form of a ventral site that stimulates the local activation of one of the serine proteases, which then acts through a protease cascade to generate the ligand. A number of gain-of-function *easter* mutations produce ventralized or lateralized embryos, and these phenotypes presumably arise because the spatial distribution of the Toll ligand has been altered (Chasan and Anderson, 1989; Jin and Anderson, 1990). It is hard to explain how *easter* mutations can alter the localization of this ligand unless wild-type easter activity is also localized. Thus, it has been suggested that the easter serine protease is normally activated only in the ventral region of the perivitelline space, while the gain-of-function alleles encode products that are released from this spatial regulation. Although there are other possibilities, this interpretation strongly favors the second model, in which the follicle cell signal controls the ventral activation of the germline products such as easter.

**Delayed Induction and Limited Diffusible Ligands**

Although the components of the dorsoventral and terminal systems are different, the basic features of the two pathways are quite similar. One particularly striking aspect of both is that the initial asymmetric signals seem to originate from the follicle cells that surround the developing egg. Thus, the formation of ventral and terminal pattern can be seen as an inductive process, in which the follicle cells provide an inducing signal to specific regions of the egg. Unlike classical inductive events, there is a large temporal delay between the production of the inducing signal and the response. In fact, the inducing cells have degenerated long before the fertilized egg responds to the localized signals. Several lines of evidence indicate that the egg does not receive the ventral or terminal signals until after fertilization. For example, mutations in many of the germline-dependent terminal and dorsal group genes can be rescued by cytoplasmic transplantation or RNA injection into the syncytial blastoderm embryo (e.g., Anderson and Nüsslein-Volhard, 1984; Klingler et al., 1988). Furthermore, torso, the receptor for the terminal signal, is not translated during oogenesis, demonstrating that the egg is not competent to respond until after egg deposition (Casanova and Struhl, 1989). In contrast, the contribution of the follicle cells must occur during oogenesis, as these cells die at the end of this process. Since mature eggs can be held in the female for up to 15 days before being fertilized, the localization and activity of the follicle cell signals must remain stable for long periods of time between their synthesis during oogenesis and their activation after the egg has been laid.

After fertilization, the localized follicle cell signals result in the production of ligands for the two receptors in the egg membrane. Unlike their precursors during oogenesis, these ligands appear to be freely diffusible in the perivitelline space. For example, perivitelline fluid taken from the dorsal side of *Toll*⁻ embryos contains the same amount of polarizing activity as fluid taken from the ventral side (Stein et al., 1991). These results create an apparent paradox. It is clearly important that the receptor, Toll, is only activated on the ventral side of the embryo, yet the polarizing activity seems not to be localized. The most likely solution to this problem is that Toll limits the diffusion of its own ligand. In

wild-type embryos all of the ligand probably binds to Toll on the ventral side of the egg, but the ligand cannot be sequestered in the absence of Toll and remains free to diffuse into the dorsal perivitelline fluid. This model requires that the amount of ligand is limited, and that Toll is present in excess. In situations where the amount of Toll is reduced, the polarity of the embryo can be determined by the localization of Toll rather than the external signal. When *Toll*$^{+}$ cytoplasm or *Toll* RNA is injected into the dorsal side of *Toll*$^{-}$ embryos, the site of injection determines where ventral structures will form (Anderson et al., 1985b). Since there is no Toll protein on the ventral side of these eggs, the ligand can diffuse in the perivitelline space until it binds to the dorsal patch of Toll that is synthesized from the injected RNA. This leads to the activation of dorsal protein nuclear localization on the dorsal rather than ventral side, and results in the development of embryos with reversed polarity.

A similar phenomenon has also been observed in the terminal system. The injection of *torso* RNA into the middle of *torso*$^{-}$ recipients leads to the suppression of segmentation, and sometimes causes the development of telson structures in the middle of the embryo (F. Sprenger and C. N.-V., unpublished data). The induction of this phenotype depends upon the presence of ligand and the absence of endogenous torso with a wild-type extracellular domain. These results indicate that when there is no torso at the poles to bind the ligand, this activity can diffuse to the middle of the egg and activate any wild-type torso protein that is expressed there. For an inductive process to be spatially controlled, either the inducer or the competence to respond must be localized. In the dorsoventral and terminal pathways, it is normally the inducing activity that is localized, but in the exceptional cases described above this situation is reversed and it is the distribution of responsiveness that determines the final pattern.

### Morphogen Gradients

Both bicoid and dorsal proteins form gradients in the nuclei of the syncytial blastoderm embryo, and the shapes of these gradients correspond well with the resulting patterns. However, to prove that either molecule functions as a morphogen, a third criterion must be satisfied. A morphogen has been defined as a "factor which can evoke more than one positive response from the responding tissue" (Slack, 1991). Thus, the presence of the morphogen alone must be sufficient to generate at least two different responses or cell states with different threshold concentrations. In general, it is hard to be certain that all of the observed cell states are determined directly by the absolute concentration of the morphogen, and that they do not arise as a result of secondary interactions. For example, even though retinoic acid behaves as a morphogen when applied to the chick limb bud, one cannot rule out that it acts as a local inducer of one cell state and that the pattern is actually formed by a series of cell–cell interactions or by a gradient of a second molecule (Brockes, 1991; Noji et al., 1991; Wanek et al., 1991). One way to exclude the possibility that different cell states are being generated by subsequent cell–cell interactions or secondary gradients is to expose single cells to various concentrations of the factor in question (Green and Smith, 1990; Simeone et al., 1990). Since the maternal signals in Drosophila act before cellularization has occurred, this approach cannot be used for bicoid and dorsal. Instead, it is possible to generate a uniform concentration of either protein across the whole axis. Since all the nuclei will therefore be exposed to the same concentration of morphogen, they should all respond in the same way, thereby eliminating any effects of secondary interactions between different regions. In the dorsoventral system, a number of different mutant combinations give rise to apolar phenotypes in which all nuclei contain the same concentration of dorsal protein (Roth et al., 1989). At a molecular level, two different thresholds can be distinguished for the response to the dorsal protein concentration, leading to the specification of three cell states (Figure 8). When no dorsal is present in the nuclei, *zen* and *dpp* are expressed everywhere. Above the first threshold, *zen* and *dpp* are repressed, but *twist* and *snail* are not activated; above the second threshold, *zen* and *dpp* remain repressed, and *twist* and *snail* are turned on. Using various combinations of dorsal group and *cactus* alleles, it is possible to generate two additional apolar lateralized phenotypes (Roth et al., 1991). This suggests that the dorsal nuclear concentration gradient actually defines five different positional values. At present, the three apolar lateralized phenotypes cannot be distinguished by their patterns of zygotic gene expression, and it is possible that there is another zygotic target of dorsal regulation that has not yet been identified.

To create a uniform distribution of bicoid protein, it is necessary to prevent the localization of both *bicoid* and *nanos* RNAs, since localized nanos activity will inhibit the translation of bicoid in the posterior of the embryo. This can be done by using *exuperantia staufen* double mutant embryos and varying the number of maternal copies of *bicoid*. In this way, it has been possible to show that bicoid also acts as a morphogen, with at least two threshold concentrations (W. Driever and C. N.-V., unpublished data).

### The Localization of the Maternal Signals

Although the way that the four maternal signals generate polarity in the embryo is quite well understood, much less is known about how this asymmetry initially arises during oogenesis, when the maternal signals themselves are localized. In the case of the terminal and dorsoventral systems, this seems to be a question of how different follicle cell populations are defined, and most probably involves cell–cell interactions. The determination of follicle cell states along the dorsoventral axis also seems to require signaling between the oocyte and the follicle cells. The soma-dependent *torpedo* mutations in the Drosophila epidermal growth factor receptor homolog cause all of the follicle cells to adopt a ventral fate, leading to the production of ventralized egg coverings and embryos (Schüpbach, 1987; Price et al., 1989; Schejter and Shilo, 1989). Two other genes involved in this signaling, *K10* and *gurken*, are required in the germline, and *K10* RNA accumulates specifically around the oocyte nucleus, which lies on the dorsal side of the cell (Wieschaus et al., 1978; Haenlin

et al., 1987; Schüpbach, 1987). These observations have led to a model in which the oocyte nucleus produces a signal that diffuses to the nearby follicle cells and binds to the Drosophila epidermal growth factor receptor homolog, thereby inducing the cells to adopt a dorsal fate.

The anterior and posterior determinants must be localized by quite a different mechanism, since these are both maternal RNAs that reside in the cytoplasm at opposite ends of the oocyte. The localization of *bicoid* RNA is mediated through the 3′ untranslated region of the transcript and occurs in several steps, in which the RNA first localizes to the apical regions of the nurse cells before being transported into the oocyte and binding to the cortex at the anterior pole (Macdonald and Struhl, 1988; St Johnston et al., 1989). The initial phase of this process is disrupted by *exuperantia* mutations, while *swallow* mutations cause the RNA to fall off the cortex in the middle of oogenesis (Berleth et al., 1988; Stephenson et al., 1988). Before the egg is laid, *bicoid* RNA is released from the cortex into the anterior cytoplasm, where the product of the *staufen* gene seems to be required to hold the RNA in position (St Johnston et al., 1989). staufen protein is concentrated in the anterior cytoplasm in the same region as *bicoid* RNA, suggesting that staufen may bind to the RNA to prevent its diffusion (St Johnston et al., 1991). While almost nothing is known about the mechanisms that direct the localization of *bicoid* RNA, this process does require microtubules, and this raises the possibility that the RNA is transported along the microtubule network (Pokrywka and Stephenson, 1991).

Localization to the posterior pole seems to be an even more complicated process. One reason for this is that it is not just *nanos* RNA that is localized, but all the components of the pole plasm as well. The first identified molecules to reach the posterior pole are staufen protein and *oskar* RNA (Ephrussi et al., 1991; Kim-Ha et al., 1991; St Johnston et al., 1991). These are followed by vasa protein, cyclin B RNA, and toward the end of oogenesis, *nanos* RNA and pole cell–determining activity (Illmensee et al., 1976; Hay et al., 1988; Whitfield et al., 1989; Lasko and Ashburner, 1990; Wang and Lehmann, 1991). The pole plasm forms in a stepwise manner, in which the components that localize early are required for the subsequent localization of those that arrive later in oogenesis (Whitfield et al., 1989; Hay et al., 1990; Lasko and Ashburner, 1990). Although the majority of these molecules may accumulate in the pole plasm by binding to other components that have already been localized, this model cannot account for the localization of the first molecules to reach the posterior pole, most probably staufen protein and *oskar* RNA. Several lines of evidence suggest that staufen protein associates with *oskar* RNA at the anterior of the oocyte and the two are then transported around the cortex to the posterior pole as a complex, in a process that requires the activities of two other posterior group genes, *cappuccino* and *spire* (Manseau and Schüpbach, 1989; Ephrussi et al., 1991; Kim-Ha et al., 1991; St Johnston et al., 1991). Thus, staufen protein seems to associate with both *oskar* and *bicoid* RNAs, mediating the transport of the former to the posterior end of the egg and anchoring the latter at the anterior end.

Although many of the genes that are involved in localization in the oocyte have now been identified, the cell biology of these processes is not well understood, nor is it known how the anterior and posterior ends of the egg are first defined as the sites for localization. The polarity of the oocyte probably depends upon the geometry of the nurse cell–oocyte complex, which is initially established near the beginning of oogenesis when the oocyte migrates to the posterior of the follicle. However, recent results suggest that the follicle cells are also involved in defining the two ends of the oocyte, since the reduction of the activities of the neurogenic genes *Notch* and *Delta* in these cells frequently results in the localization of *bicoid* RNA to the posterior as well as the anterior pole (Ruohola et al., 1991).

**Conclusions**

The results described in this review show that we now have a fairly clear picture of the elegant way that the four maternal signals generate asymmetry in the Drosophila embryo (Figure 9). However, our understanding of the process by which positional information is transmitted from one generation to the next is still incomplete, as so little is known about the origin of asymmetry in the oocyte. While the general organization of each pathway is probably correct, there are still many steps that are poorly characterized. It is also likely that several genes that play a part in these pathways have not yet been identified, and we have already mentioned a couple of examples where the existence of an additional gene has been proposed. Although a few maternal-specific genes may have been missed in the screens for maternal-effect mutations, a potentially much larger class of unidentified genes are those that are required in the zygote as well as in the mother, since mutations in these genes cannot be tested for maternal-effect phenotypes if the mutants die before adulthood. One such gene is *l(1)pole hole*, the Drosophila *raf* homolog. This gene is required at several developmental stages, and its maternal role was only discovered by making germline clones (Perrimon et al., 1985; Ambrosio et al., 1989). *pumilio*, *cactus*, and *torpedo* also mutate to zygotic lethality, but some alleles of these genes are viable, allowing their identification in maternal screens. Since it is possible to make sense of each maternal system without invoking more than a few additional components, it is unlikely that there are a large number of unknown zygotic lethal genes that play a specific role in these processes.

Although there are still many unsolved questions, the early development of Drosophila is probably better understood than that of any other organism. In this context it is worth considering how relevant the information gained in Drosophila is to other developmental systems. It is clear that many of the later developmental processes in flies have counterparts in vertebrates (see the reviews by Ingham and Martinez Arias, 1992; McGinnis and Krumlauf, 1992, this issue), but the early events that we have described are probably less general. Drosophila is unusual in that both major body axes are already defined in the

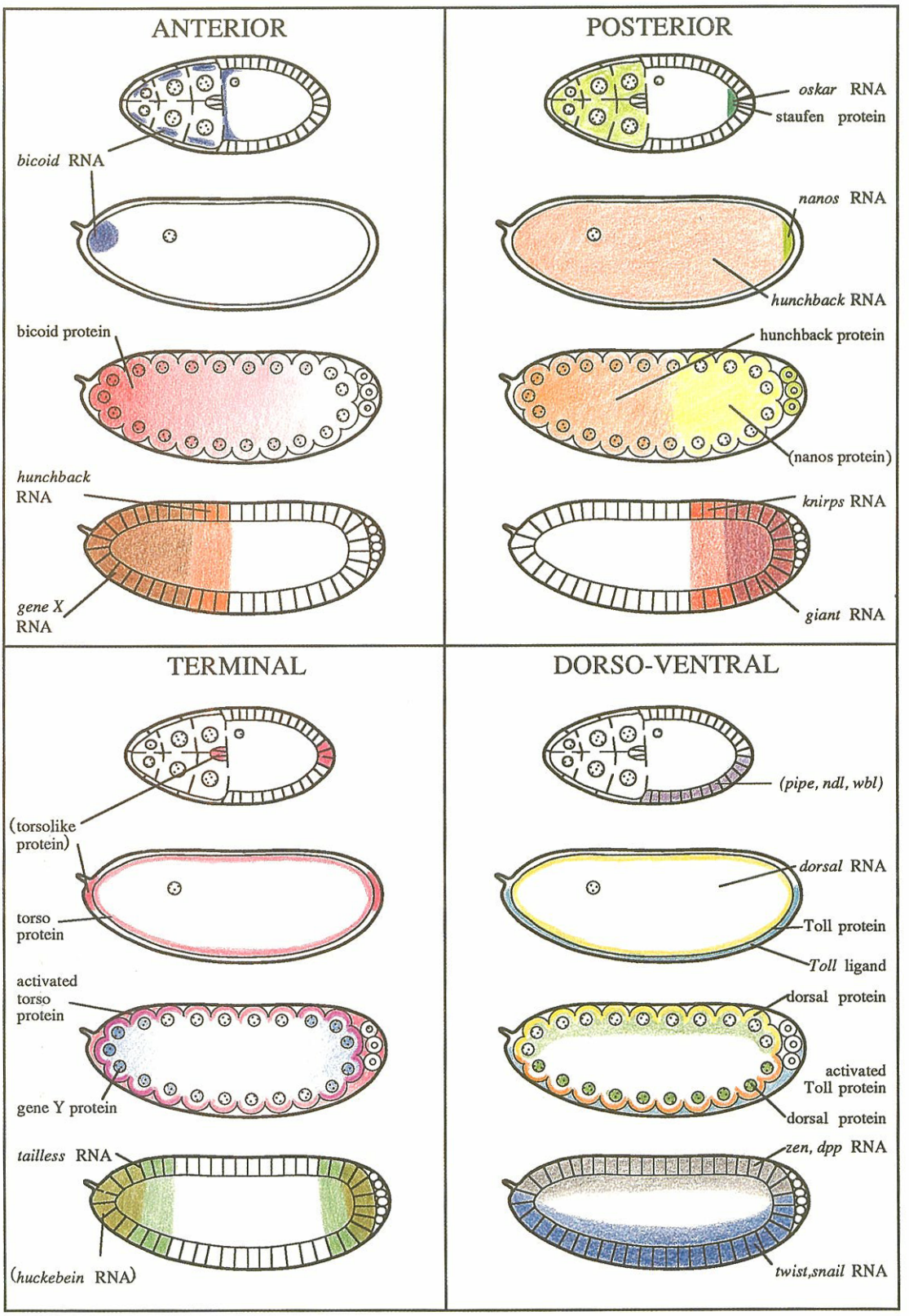


Figure 9. A Summary of the Major Steps in Each of the Four Maternal Pathways

The distributions of gene products shown in parentheses are hypothetical, as are gene X in the anterior system and gene Y in the terminal system.

unfertilized egg, and the first steps of pattern formation occur in a syncytium. However, many of the individual steps in these maternal pathways do resemble processes that occur during the development of other organisms and are therefore of more general relevance, such as RNA localization, signal transduction, induction, and the regulation of nuclear localization.

Drosophila axis formation also provides an excellent model for studying several important pattern-forming mechanisms. For instance, bicoid and dorsal provide the best-characterized examples of morphogen gradients. The gradient of bicoid protein forms by diffusion in a syncytium from a localized RNA source. This is unlikely to be a common mechanism for setting up morphogen gradients, since in most other developmental systems pattern formation takes place after cells have formed, and cell membranes will limit the movement of intracellular factors. The dorsoventral system may provide a more useful paradigm. In this case, the first gradient probably forms outside the egg in the extracellular space, and this leads via a signal transduction pathway to a graded intracellular response, the formation of the dorsal nuclear gradient.

One of the most surprising aspects of axis formation in Drosophila is that although all four maternal systems result in the region-specific activation of zygotic pattern genes, each achieves this by a unique pathway. While two of the initial asymmetric signals are localized outside the egg, the other two are found in the egg cytoplasm as localized RNAs. Furthermore, the spatial control of transcription arises in a number of different ways. The bicoid protein gradient regulates zygotic gene expression directly, nanos seems to function as a repressor of a repressor, and dorsoventral polarity is generated by the control of nuclear localization. It is known that localized maternal determinants play a role in the development of many organisms, but it is only in Drosophila that such molecules have been identified and characterized. The variety of mechanisms found in this one system suggests that maternal determinants may turn out to constitute a diverse collection of molecules that can regulate embryonic development in very different ways.

**Acknowledgments**

We are grateful to all of the members of the Tübingen fly group, past and present, for their contributions to the figures in this review, and for permission to present unpublished results. We would also like to thank Diethard Tautz for providing photographs, and Maria Leptin, Nick Brown, and Lisa Elphick for their comments on this manuscript.

**References**

Ambrosio, L., Mahowald, A. P., and Perrimon, N. (1989). Requirement of the *Drosophila raf* homolog for *torso* function. Nature *342*, 288–291.

Anderson, K. V., and Nüsslein-Volhard, C. (1984). Information for the dorsal-ventral pattern of the *Drosophila* embryo is stored as maternal mRNA. Nature *311*, 223–227.

Anderson, K., and Nüsslein-Volhard, C. (1986). Dorsal-group genes of *Drosophila*. In Gametogenesis and the Early Embryo, J. Gall, ed. (New York: Alan R. Liss, Inc.), pp. 177–194.

Anderson, K. V., Jürgens, G., and Nüsslein-Volhard, C. (1985a). Establishment of dorsal-ventral polarity in the Drosophila embryo: genetic studies on the role of the *Toll* gene product. Cell *42*, 779–789.

Anderson, K. V., Bokla, L., and Nüsslein-Volhard, C. (1985b). Establishment of dorsal-ventral polarity in the Drosophila embryo: the induction of polarity by the *Toll* gene product. Cell *42*, 791–798.

Baeuerle, P. A., and Baltimore, D. (1988a). Activation of DNA-binding activity in an apparently cytoplasmic precursor of the NF-κB transcription factor. Cell *53*, 211–217.

Baeuerle, P. A., and Baltimore, D. (1988b). IκB: a specific inhibitor of the NF-κB transcription factor. Science *242*, 540–546.

Bender, M., Turner, F. R., and Kaufman, T. C. (1987). A developmental genetic analysis of the gene *Regulator of postbithorax* in *Drosophila melanogaster*. Dev. Biol. *119*, 418–432.

Berleth, T., Burri, M., Thoma, G., Bopp, D., Richstein, S., Frigerio, G., Noll, M., and Nüsslein-Volhard, C. (1988). The role of localization of *bicoid* RNA in organizing the anterior pattern of the *Drosophila* embryo. EMBO J. *7*, 1749–1756.

Boswell, R. E., and Mahowald, A. P. (1985). *tudor*, a gene required for assembly of the germ plasm in Drosophila melanogaster. Cell *43*, 97–104.

Boswell, R. E., Prout, M. E., and Steichen, J. C. (1991). Mutations in a newly-identified *Drosophila melanogaster* gene, *mago nashi*, disrupt germ cell formation and result in the formation of mirror-image, symmetrical double abdomen embryos. Development *113*, 373–384.

Boulay, J. L., Dennefeld, C., and Alberga, A. (1987). The *Drosophila* developmental gene *snail* encodes a protein with nucleic acid binding fingers. Nature *330*, 395–398.

Brockes, J. (1991). Developmental biology. We may not have a morphogen. Nature *350*, 15.

Casanova, J., and Struhl, G. (1989). Localized surface activity of *torso*, a receptor tyrosine kinase, specifies terminal body pattern in *Drosophila*. Genes Dev. *3*, 2025–2038.

Chasan, R., and Anderson, K. V. (1989). The role of *easter*, an apparent serine protease, in organizing the dorsal–ventral pattern of the Drosophila embryo. Cell *56*, 391–400.

Cohen, S. M., and Jurgens, G. (1990). Mediation of *Drosophila* head development by gap-like segmentation genes. Nature *346*, 482–485.

Dalton, D., Chadwick, R., and McGinnis, W. (1989). Expression and embryonic function of *empty spiracles*: a *Drosophila* homeo box gene with two patterning functions on the anterior-posterior axis of the embryo. Genes Dev. *3*, 1940–1956.

DeLotto, R., and Spierer, P. (1986). A gene required for the specification of dorsal-ventral pattern in *Drosophila* appears to encode a serine protease. Nature *323*, 688–692.

Doyle, H., Kraut, R., and Levine, M. (1989). Spatial regulation of *zerknüllt*: a dorsal-ventral patterning gene in *Drosophila*. Genes Dev. *3*, 1518–1533.

Driever, W., and Nüsslein-Volhard, C. (1988a). A gradient of *bicoid* protein in Drosophila embryos. Cell *54*, 83–93.

Driever, W., and Nüsslein-Volhard, C. (1988b). The *bicoid* protein determines position in the Drosophila embryo in a concentration-dependent manner. Cell *54*, 95–104.

Driever, W., and Nüsslein-Volhard, C. (1989a). The bicoid protein is a positive regulator of hunchback transcription in the early *Drosophila* embryo. Nature *337*, 138–143.

Driever, W., and Nüsslein-Volhard, C. (1989b). Determination of spatial domains of zygotic gene expression in the *Drosophila* embryo by the affinity of binding sites for the bicoid morphogen. Nature *340*, 363–367.

Driever, W., Siegel, V., and Nüsslein-Volhard, C. (1990). Autonomous determination of anterior structures in the early *Drosophila* embryo by the *bicoid* morphogen. Development *109*, 811–820.

Eldon, E. D., and Pirrotta, V. (1991). Interactions of the *Drosophila* gap gene *giant* with maternal and zygotic pattern-forming genes. Development *111*, 367–378.

Ephrussi, A., Dickinson, L. K., and Lehmann, R. (1991). *oskar* organizes the germ plasm and directs localization of the posterior determinant *nanos*. Cell *66*, 37–50.

Finkelstein, R., and Perrimon, N. (1990). The orthodenticle gene is

regulated by bicoid and torso and specifies *Drosophila* head development. Nature *346*, 485–488.

Frigerio, G., Burri, M., Bopp, D., Baumgartner, S., and Noll, M. (1986). Structure of the segmentation gene *paired* and the Drosophila PRD gene set as part of a gene network. Cell *47*, 735–746.

Frohnhöfer, H. G., and Nüsslein-Volhard, C. (1986). Organization of anterior pattern in the *Drosophila* embryo by the maternal gene *bicoid*. Nature *324*, 120–125.

Frohnhöfer, H. G., Lehmann, R., and Nüsslein-Volhard, C. (1986). Manipulating the anteroposterior pattern of the *Drosophila* embryo. J. Embryol. Exp. Morphol. *97*, 169–179.

Gans, M., Audit, C., and Masson, M. (1975). Isolation and characterization of sex-linked female-sterile mutants in *Drosophila melanogaster*. Genetics *81*, 683–704.

Gaul, U., and Jäckle, H. (1989). Analysis of maternal effect mutant combinations elucidates regulation and function of the overlap of *hunchback* and *Krüppel* gene expression in the *Drosophila* blastoderm embryo. Development *107*, 651–663.

Gay, N. J., and Keith, F. J. (1991). *Drosophila* Toll and IL-1 receptor. Nature *351*, 355–356.

Ghosh, S., and Baltimore, D. (1990). Activation in vitro of NF-κB by phosphorylation of its inhibitor IκB. Nature *344*, 678–682.

Ghosh, S., Gifford, A. M., Riviere, L. R., Tempst, P., Nolan, G. P., and Baltimore, D. (1990). Cloning of the p50 DNA binding subunit of NF-κB: homology to *rel* and *dorsal*. Cell *62*, 1019–1029.

Green, J. B., and Smith, J. C. (1990). Graded changes in dose of a *Xenopus* activin A homologue elicit stepwise transitions in embryonic cell fate. Nature *347*, 391–394.

Haenlin, M., Roos, C., Cassab, A., and Mohier, E. (1987). Oocyte-specific transcription of fs(1)K10: a *Drosophila* gene affecting dorsal-ventral developmental polarity. EMBO J. *6*, 801–807.

Hashimoto, C., Hudson, K. L., and Anderson, K. V. (1988). The *Toll* gene of Drosophila, required for dorsal-ventral embryonic polarity, appears to encode a transmembrane protein. Cell *52*, 269–279.

Hashimoto, C., Gerttula, S., and Anderson, K. V. (1991). Plasma membrane localization of the *Toll* protein in the syncytial *Drosophila* embryo: importance of transmembrane signaling for dorsal-ventral pattern formation. Development *111*, 1021–1028.

Hay, B., Ackerman, L., Barbel, S., Jan, L. Y., and Jan, Y. N. (1988). Identification of a component of *Drosophila* polar granules. Development *103*, 625–640.

Hay, B., Jan, L. Y., and Jan, Y. N. (1990). Localization of vasa, a component of *Drosophila* polar granules, in maternal-effect mutants that alter embryonic anteroposterior polarity. Development *109*, 425–433.

Hülskamp, M., Schroeder, C., Pfeifle, C., Jaeckle, H., and Tautz, D. (1989). Posterior segmentation of the *Drosophila* embryo in the absence of a maternal posterior organizer gene. Nature *338*, 629–632.

Hülskamp, M., Pfeifle, C., and Tautz, D. (1990). A morphogenetic gradient of *hunchback* protein organizes the expression of the gap genes *Krüppel* and *knirps* in the early *Drosophila* embryo. Nature *346*, 577–580.

Illmensee, K., and Mahowald, A. P. (1974). Transplantation of posterior pole plasm in *Drosophila*: induction of germ cells at the anterior pole of the egg. Proc. Natl. Acad. Sci. USA *71*, 1016–1020.

Illmensee, K., Mahowald, A. P., and Loomis, M. R. (1976). The ontogeny of germ plasm during oogenesis in *Drosophila*. Dev. Biol. *49*, 40–65.

Ingham, P. W., and Martinez Arias, A. (1991). Developmental fields and polarity in early embryos. Cell *68*, this issue.

Ip, Y. T., Kraut, R., Levine, M., and Rushlow, C. A. (1991). The *dorsal* morphogen is a sequence-specific DNA-binding protein that interacts with a long-range repression element in Drosophila. Cell *64*, 439–446.

Irish, V., Lehmann, R., and Akam, M. (1989). The *Drosophila* posterior-group gene nanos functions by repressing hunchback activity. Nature *338*, 646–648.

Jiang, J., Kosman, D., Ip, Y. T., and Levine, M. (1991). The *dorsal* morphogen gradient regulates the mesoderm determinant *twist* in early *Drosophila* embryos. Genes Dev. *5*, 1881–1891.

Jin, Y., and Anderson, K. V. (1990). Dominant and recessive alleles of the Drosophila easter gene are point mutations at conserved sites in the serine protease catalytic domain. Cell *60*, 873–881.

Keith, F. J., and Gay, N. J. (1990). The Drosophila membrane receptor Toll can function to promote cellular adhesion. EMBO J. *9*, 4299–4306.

Kieran, M., Blank, V., Logeat, F., Vandekerckhove, J., Lottspeich, F., Le Bail, O., Urban, M. B., Kourilsky, P., Baeuerle, P. A., and Israël, A. (1990). The DNA binding subunit of NF-κB is identical to factor KBF1 and homologous to the *rel* oncogene product. Cell *62*, 1007–1018.

Kim-Ha, J., Smith, J. L., and Macdonald, P. M. (1991). *oskar* mRNA is localized to the posterior pole of the Drosophila oocyte. Cell *66*, 23–35.

Klingler, M., Erdelyi, M., Szabad, J., and Nüsslein-Volhard, C. (1988). Function of torso in determining the terminal anlagen of the *Drosophila* embryo. Nature *335*, 275–277.

Knipple, D. C., Seifert, E., Rosenberg, U. B., Preiss, A., and Jäckle, H. (1985). Spatial and temporal patterns of Krüppel gene expression in early *Drosophila* embryos. Nature *317*, 40–45.

Konrad, K. D., Goralski, T. J., and Mahowald, A. P. (1988). Developmental genetics of the *gastrulation defective* locus in *Drosophila melanogaster*. Dev. Biol. *127*, 133–142.

Kraut, R., and Levine, M. (1991a). Spatial regulation of the gap gene *giant* during *Drosophila* development. Development *111*, 601–609.

Kraut, R., and Levine, M. (1991b). Mutually repressive interactions between the gap genes *giant* and *Krüppel* define middle body regions of the *Drosophila* embryo. Development *111*, 611–621.

Lasko, P. F., and Ashburner, M. (1990). Posterior localization of *vasa* protein correlates with, but is not sufficient for, pole cell development. Genes Dev. *4*, 905–921.

Lehmann, R., and Nüsslein-Volhard, C. (1986). Abdominal segmentation, pole cell formation, and embryonic polarity require the localized activity of *oskar*, a maternal gene in Drosophila. Cell *47*, 141–152.

Lehmann, R., and Nüsslein-Volhard, C. (1987a). Involvement of the *pumilio* gene in the transport of an abdominal signal in the *Drosophila* embryo. Nature *329*, 167–170.

Lehmann, R., and Nüsslein-Volhard, C. (1987b). *hunchback*, a gene required for segmentation of an anterior and posterior region of the *Drosophila* embryo. Dev. Biol. *119*, 402–417.

Lehmann, R., and Nüsslein-Volhard, C. (1991). The maternal gene *nanos* has a central role in posterior pattern formation in the *Drosophila* embryo. Development *112*, 679–691.

Leptin, M., and Grunewald, B. (1990). Cell shape changes during gastrulation in *Drosophila*. Development *110*, 73–84.

Letsou, A., Alexander, S., Orth, K., and Wasserman, S. A. (1991). Genetic and molecular characterization of tube, a *Drosophila* gene maternally required for embryonic dorsoventral polarity. Proc. Natl. Acad. Sci. USA *88*, 810–814.

Li, P., Wood, K., Mamon, H., Haser, W., and Roberts, T. (1991). Raf-1: a kinase currently without a cause but not lacking in effects. Cell *64*, 479–482.

Lopez, J. A., Chung, D. W., Fujikawa, K., Hagen, F. S., Davie, E. W., and Roth, G. J. (1988). The α and β chains of human platelet glycoprotein Ib are both transmembrane proteins containing a leucine-rich amino acid sequence. Proc. Natl. Acad. Sci. USA *85*, 2135–2139.

Macdonald, P. M., and Struhl, G. (1988). Cis-acting sequences responsible for anterior localization of *bicoid* mRNA in *Drosophila* embryos. Nature *336*, 595–598.

Mahowald, A. P. (1968). Polar granules of *Drosophila*. II. Ultrastructural changes during early embryogenesis. J. Exp. Zool. *167*, 237–262.

Manseau, L. J., and Schüpbach, T. (1989). *cappuccino* and *spire*: two unique maternal-effect loci required for both the anteroposterior and dorsoventral patterns of the *Drosophila* embryo. Genes Dev. *3*, 1437–1452.

McFarland, K. C., Sprengel, R., Phillips, H. S., Kohler, M., Rosemblit, N., Nikolics, K., Segaloff, D. L., and Seeburg, P. H. (1989). Lutropin-choriogonadotropin receptor: an unusual member of the G protein-coupled receptor family. Science *245*, 494–499.

McGinnis, W., and Krumlauf, R. (1992). Homeobox genes and axial patterning. Cell *68*, this issue.

Mohler, J., Eldon, E. D., and Pirrotta, V. (1989). A novel spatial transcription pattern associated with the segmentation gene, *giant*, of *Drosophila*. EMBO J. *8*, 1539–1548.

Müller-Holtkamp, F., Knipple, D. C., Seifert, E., and Jäckle, H. (1985). An early role of maternal mRNA in establishing the dorsoventral pattern in pelle mutant *Drosophila* embryos. Dev. Biol. *110*, 238–246.

Nauber, U., Pankratz, M. J., Kienlin, A., Seifert, E., Klemm, U., and Jäckle, H. (1988). Abdominal segmentation of the *Drosophila* embryo requires a hormone receptor-like protein encoded by the gap gene *knirps*. Nature *336*, 489–492.

Nishida, Y., Hata, M., Ayaki, T., Ryo, H., Yamagata, M., Shimizu, K., and Nishizuka, Y. (1988). Proliferation of both somatic and germ cells is affected in the *Drosophila* mutants of raf proto-oncogene. EMBO J. *7*, 775–781.

Noji, S., Nohno, T., Koyama, E., Muto, K., Ohyama, K., Aoki, Y., Tamura, K., Ohsugi, K., Ide, H., Taniguchi, S., and Saito, T. (1991). Retinoic acid induces polarizing activity but is unlikely to be a morphogen in the chick limb bud. Nature *350*, 83–86.

Nolan, G. P., Ghosh, S., Liou, H.-C., Tempst, P., and Baltimore, D. (1991). DNA binding and IκB inhibition of the cloned p65 subunit of NF-κB, a *rel*-related polypeptide. Cell *64*, 961–969.

Nüsslein-Volhard, C., Lohs-Schardin, M., Sander, K., and Cremer, C. (1980). A dorsoventral shift of embryonic primordia in a new maternal-effect mutant of *Drosophila*. Nature *283*, 474–476.

Nüsslein-Volhard, C., Frohnhöfer, H. G., and Lehmann, R. (1987). Determination of anteroposterior polarity in *Drosophila*. Science *238*, 1675–1681.

Padgett, R. W., St Johnston, D., and Gelbart, W. M. (1987). A transcript from a *Drosophila* pattern gene predicts a protein homologous to the transforming growth factor-beta family. Nature *325*, 81–84.

Pan, D., Huang, J.-D., and Courey, A. J. (1991). Functional analysis of the *Drosophila twist* promoter reveals a *dorsal*-binding ventral activator region. Genes Dev. *5*, 1892–1901.

Pankratz, M. J., Hoch, M., Seifert, E., and Jaeckle, H. (1989). Krüppel requirement for knirps enhancement reflects overlapping gap gene activities in the *Drosophila* embryo. Nature *341*, 337–340.

Perrimon, N., and Gans, M. (1983). Clonal analysis of the tissue specificity of recessive female-sterile mutations of *Drosophila melanogaster* using a dominant female-sterile mutation Fs(1)K1237. Dev. Biol. *100*, 365–373.

Perrimon, N., Engstrom, L., and Mahowald, A. P. (1985). A pupal lethal mutation with a paternally influenced maternal effect on embryonic development in *Drosophila melanogaster*. Dev. Biol. *110*, 480–491.

Pignoni, F., Baldarelli, R. M., Steingrimsson, E., Diaz, R. J., Patapoutian, A., Merriam, J. R., and Lengyel, J. A. (1990). The Drosophila gene *tailless* is expressed at the embryonic termini and is a member of the steroid receptor superfamily. Cell *62*, 151–163.

Pokrywka, N. J., and Stephenson, E. C. (1991). Microtubules mediate the localization of *bicoid* RNA during *Drosophila* oogenesis. Development *113*, 55–66.

Price, J. V., Clifford, R. J., and Schüpbach, T. (1989). The maternal ventralizing locus *torpedo* is allelic to *faint little ball*, an embryonic lethal, and encodes the Drosophila EGF receptor homolog. Cell *56*, 1085–1092.

Rapp, U. R. (1991). Role of Raf-1 serine/threonine protein kinase in growth factor signal transduction. Oncogene *6*, 495–500.

Rosenberg, U. B., Schröder, C., Preiss, A., Kienlin, A., Cote, S., Riede, I., and Jäckle, H. (1986). Structural homology of the product of the *Drosophila Krüppel* gene with *Xenopus* transcription factor IIA. Nature *319*, 336–339.

Roth, S., Stein, D., and Nüsslein-Volhard, C. (1989). A gradient of nuclear localization of the *dorsal* protein determines dorsoventral pattern in the Drosophila embryo. Cell *59*, 1189–1202.

Roth, S., Hiromi, Y., Godt, D., and Nüsslein-Volhard, C. (1991). *cactus*, a maternal gene required for proper formation of the dorsoventral morphogen gradient in *Drosophila* embryos. Development *112*, 371–388.

Rothe, M., Naubler, U., and Jäckle, H. (1989). Three hormone receptor-like *Drosophila* genes encode an identical DNA-binding finger. EMBO J. *8*, 3087–3094.

Ruben, S. M., Dillon, P. J., Schreck, R., Henkel, T., Chen, C. H., Maher, M., Baeuerle, P. A., and Rosen, C. A. (1991). Isolation of a rel-related human cDNA that potentially encodes the 65-kD subunit of NF-κB. Science *251*, 1490–1493.

Ruohola, H., Bremer, K. A., Baker, D., Swedlow, J. R., Jan, L. Y., and Jan, Y. N. (1991). Role of neurogenic genes in establishment of follicle cell fate and oocyte polarity during oogenesis in Drosophila. Cell *66*, 433–449.

Rushlow, C., Doyle, H., Hoey, T., and Levine, M. (1987a). Molecular characterization of the zerknüllt region of the *Antennapedia* gene complex in *Drosophila*. Genes Dev. *1*, 1268–1279.

Rushlow, C., Frasch, M., Doyle, H., and Levine, M. (1987b). Maternal regulation of zerknüllt: a homeobox gene controlling differentiation of dorsal tissues in *Drosophila*. Nature *330*, 583–586.

Rushlow, C. A., Han, K., Manley, J. L., and Levine, M. (1989). The graded distribution of the *dorsal* morphogen is initiated by selective nuclear transport in Drosophila. Cell *59*, 1165–1177.

St Johnston, R. D., and Gelbart, W. M. (1987). Decapentaplegic transcripts are localized along the dorsal-ventral axis of the *Drosophila* embryo. EMBO J. *6*, 2785–2791.

St Johnston, D., Driever, W., Berleth, T., Richstein, S., and Nüsslein-Volhard, C. (1989). Multiple steps in the localization of *bicoid* RNA to the anterior pole of the *Drosophila* oocyte. Development (Suppl.) *107*, 13–19.

St Johnston, D., Beuchle, D., and Nüsslein-Volhard, C. (1991). *staufen*, a gene required to localize maternal RNAs in the Drosophila egg. Cell *66*, 51–63.

Sander, K., and Lehmann, R. (1988). *Drosophila* nurse cells produce a posterior signal required for embryonic segmentation and polarity. Nature *335*, 68–70.

Santamaria, P., and Nüsslein-Volhard, C. (1983). Partial rescue of dorsal, a maternal effect mutation affecting the dorsoventral pattern of the *Drosophila* embryo, by the injection of wild-type cytoplasm. EMBO J. *2*, 1695–1699.

Schejter, E. D., and Shilo, B.-Z. (1989). The Drosophila EGF receptor homolog (DER) gene is allelic to *faint little ball*, a locus essential for embryonic development. Cell *56*, 1093–1104.

Schneider, D. S., Hudson, K. L., Lin, T. Y., and Anderson, K. V. (1991). Dominant and recessive mutations define functional domains of Toll, a transmembrane protein required for dorsal-ventral polarity in the *Drosophila* embryo. Genes Dev. *5*, 797–807.

Schröder, C., Tautz, D., Seifert, E., and Jäckle, H. (1988). Differential regulation of the two transcripts from the *Drosophila* gap segmentation gene *hunchback*. EMBO J. *7*, 2881–2887.

Schüpbach, T. (1987). Germ line and soma cooperate during oogenesis to establish the dorsoventral pattern of egg shell and embryo in Drosophila melanogaster. Cell *49*, 699–707.

Schüpbach, T., and Wieschaus, E. (1986). Germline autonomy of maternal-effect mutations altering the embryonic body plan of *Drosophila*. Dev. Biol. *113*, 443–448.

Schüpbach, T., and Wieschaus, E. (1989). Female sterile mutations on the second chromosome of *Drosophila melanogaster*. I. Maternal effect mutations. Genetics *121*, 101–117.

Seifert, E., Müller-Holtkamp, F., Marcey, D., and Jäckle, H. (1987). Injection of wild-type cytoplasm and poly(A)$^+$ RNA provokes phenotype rescue in *spätzle* mutant *Drosophila* embryos. Roux's Arch. Dev. Biol. *196*, 78–82.

Shirakawa, F., and Mizel, S. B. (1989). In vitro activation and nuclear translocation of NF-κB catalyzed by cyclic AMP-dependent protein kinase and protein kinase C. Mol. Cell. Biol. *9*, 2424–2430.

Shirakawa, F., Chedid, M., Suttles, J., Pollok, B. A., and Mizel, S. B. (1989). Interleukin 1 and cyclic AMP induce kappa immunoglobulin light-chain expression via activation of an NF-κB-like DNA-binding protein. Mol. Cell. Biol. *9*, 959–964.

Simeone, A., Acampora, D., Arcioni, L., Andrews, P. W., Boncinelli,

E., and Mavilio, F. (1990). Sequential activation of HOX2 homeobox genes by retinoic acid in human embryonal carcinoma cells. Nature *346*, 763–766.

Slack, J. (1991). From Egg to Embryo, 2nd edition (Cambridge, England: Cambridge University Press).

Soppet, D., Escandon, E., Maragos, J., Middlemas, D. S., Reid, S. W., Blair, J., Burton, L. E., Stanton, B. R., Kaplan, D. R., Hunter, T., Nikolics, K., and Parada, L. F. (1991). The neurotrophic factors brain-derived neurotrophic factor and neurotrophin-3 are ligands for the *trk*B tyrosine kinase receptor. Cell *65*, 895–903.

Sprenger, F., Stevens, L. M., and Nüsslein-Volhard, C. (1989). The *Drosophila* gene *torso* encodes a putative receptor tyrosine kinase. Nature *338*, 478–483.

Squinto, S. P., Stitt, T. N., Aldrich, T. H., Davis, S., Bianco, S. M., Radziejewski, C., Glass, D. J., Masiakowski, P., Furth, M. E., Valenzuela, D. M., DiStefano, P. S., and Yancopoulos, G. D. (1991). *trk*B encodes a functional receptor for brain-derived neurotrophic factor and neurotrophin-3 but not nerve growth factor. Cell *65*, 885–893.

Stanojević, D., Hoey, T., and Levine, M. (1989). Sequence-specific DNA-binding activities of gap proteins encoded by *hunchback* and *Krüppel* in *Drosophila*. Nature *341*, 331–335.

Stein, D., and Nüsslein-Volhard, C. (1992). Multiple extracellular activities in Drosophila egg perivitelline fluid are required for establishment of embryonic dorsal–ventral polarity. Cell *68*, in press.

Stein, D., Roth, S., Vogelsang, E., and Nüsslein-Volhard, C. (1991). The polarity of the dorsoventral axis in the Drosophila embryo is defined by an extracellular signal. Cell *65*, 725–735.

Stephenson, E. C., Chao, Y. C., and Fackenthal, J. D. (1988). Molecular analysis of the swallow gene of *Drosophila melanogaster*. Genes Dev. *2*, 1655–1665.

Stevens, L. M., Frohnhöfer, H. G., Klingler, M., and Nüsslein-Volhard, C. (1990). Localized requirement for *torso-like* expression in follicle cells for development of terminal anlagen of the *Drosophila* embryo. Nature *346*, 660–663.

Steward, R. (1987). *Dorsal*, an embryonic polarity gene in *Drosophila*, is homologous to the vertebrate proto-oncogene, c-rel. Science *238*, 692–694.

Steward, R. (1989). Relocalization of the *dorsal* protein from the cytoplasm to the nucleus correlates with its function. Cell *59*, 1179–1188.

Steward, R., Zusman, S. B., Huang, L. H., and Schedl, P. (1988). The *dorsal* protein is distributed in a gradient in early Drosophila embryos. Cell *55*, 487–495.

Strecker, T. R., Merriam, J. R., and Lengyel, J. A. (1988). Graded requirement for the zygotic terminal gene, *tailless*, in the brain and tail region of the *Drosophila* embryo. Development *102*, 721–734.

Strecker, T. R., Halsell, S. R., Fisher, W. W., and Lipshitz, H. D. (1989). Reciprocal effects of hyper- and hypoactivity mutations in the *Drosophila* pattern gene *torso*. Science *243*, 1062–1066.

Struhl, G. (1989). Differing strategies for organizing anterior and posterior body pattern in *Drosophila* embryos. Nature *338*, 741–744.

Struhl, G., Struhl, K., and Macdonald, P. M. (1989). The gradient morphogen *bicoid* is a concentration-dependent transcriptional activator. Cell *57*, 1259–1273.

Sugiyama, S., and Okada, M. (1990). Cytoplasmic factors determining anteroposterior polarity in *Drosophila* embryos. Roux's Arch. Dev. Biol. *198*, 402–410.

Tautz, D. (1988). Regulation of the *Drosophila* segmentation gene *hunchback* by two maternal morphogenetic centres. Nature *332*, 281–284.

Tautz, D., and Pfeifle, C. (1989). A non-radioactive in situ hybridization method for the localization of specific RNAs in *Drosophila* embryos reveals translational control of the segmentation gene *hunchback*. Chromosoma *98*, 81–85.

Tautz, D., Lehmann, R., Schnürch, H., Schuh, R., Seifert, E., Kienlin, A., Jones, K., and Jäckle, H. (1987). Finger protein of novel structure encoded by *hunchback*, a second member of the gap class of *Drosophila* segmentation genes. Nature *327*, 383–389.

Thisse, B., Stoetzel, C., Messal, M. E., and Perrin-Schmitt, F. (1987). Genes of the drosophila maternal dorsal group control the specific expression of the zygotic gene *twist* in presumptive mesodermal cells. Genes Dev. *1*, 709–715.

Thisse, B., Stoetzel, C., Gorostiza-Thisse, C., and Perrin-Schmitt, F. (1988). Sequence of the *twist* gene and nuclear localization of its endomesodermal cells of early *Drosophila* embryos. EMBO J. *7*, 2175–2183.

Thisse, C., Perrin-Schmitt, F., Stoetzel, C., and Thisse, B. (1991). Sequence-specific transactivation of the Drosophila *twist* gene by the *dorsal* gene product. Cell *65*, 1191–1201.

Treisman, J., and Desplan, C. (1989). The products of the *Drosophila* gap genes *hunchback* and *Krueppel* bind to the hunchback promoters. Nature *341*, 335–337.

Vicente, V., Houghten, R. A., and Ruggeri, Z. M. (1990). Identification of a site in the alpha chain of platelet glycoprotein Ib that participates in von Willebrand factor binding. J. Biol. Chem. *265*, 274–280.

Wanek, N., Gardiner, D. M., Muneoka, K., and Bryant, S. V. (1991). Conversion by retinoic acid of anterior cells into ZPA cells in the chick wing bud. Nature *350*, 81–83.

Wang, C., and Lehmann, R. (1991). Nanos is the localized posterior determinant in Drosophila. Cell *66*, 637–647.

Weigel, D., Jürgens, G., Klingler, M., and Jäckle, H. (1990). Two gap genes mediate maternal terminal pattern information in *Drosophila*. Science *248*, 495–498.

Wharton, R. P., and Struhl, G. (1989). Structure of the Drosophila *BicaudalD* protein and its role in localizing the posterior determinant *nanos*. Cell *59*, 881–892.

Wharton, R. P., and Struhl, G. (1991). RNA regulatory elements mediate control of Drosophila body pattern by the posterior morphogen *nanos*. Cell *67*, 955–967.

Whitfield, W. G. F., Gonzalez, C., Sanchez-Herrero, E., and Glover, D. M. (1989). Transcripts of one of two *Drosophila* cyclin genes become localized in pole cells during embryogenesis. Nature *338*, 334–337.

Wieschaus, E., Marsh, J. L., and Gehring, W. (1978). fs(1)K10, a germline-dependent female sterile mutation causing abnormal chorion morphology in *Drosophila melanogaster*. Roux's Arch. Dev. Biol. *184*, 75–82.

Wilson, E. B. (1928). The Cell in Development and Heredity, 3rd edition (New York: Macmillan Publishing).

45 Mayeda, A. and Krainer, A.R. (1992) *Cell* 68, 365–375
46 Yang, X. *et al.* (1994) *Proc. Natl. Acad. Sci. U. S. A.* 91, 6924–6928
47 Mayeda, A., Helfman, D.M. and Krainer, A.R. (1993) *Mol. Cell. Biol.* 13, 2993–3001
48 Mayeda, A., Munroe, S.M., Cáceres, J.F. and Krainer, A.R. (1994) *EMBO J.* 13, 5483–5495
49 Himmelspach, M. *et al.* (1995) *RNA* 1, 794–806
50 Roche, S.E., Schiff, M. and Rio, D.C. (1995) *Genes Dev.* 9, 1278–1288
51 Eperon, I.P., Graham, I.R., Griffiths, A.D. and Eperon, I.C. (1988) *Cell* 54, 393–401
52 Cobianchi, F. *et al.* (1993) *Nucleic Acids Res.* 21, 949–955
53 Gui, J-F., Lane, W.S. and Fu, X-D. (1994) *Nature* 369, 678–682
54 Colwill, K. *et al.* (1996) *EMBO J.* 15, 265–275
55 Dreyfuss, G., Matunis, M.J., Piñol-Roma, S. and Burd, C.G. (1993) *Annu. Rev. Biochem.* 62, 289–321
56 Gontarek, R.R. and Derse, D. (1996) *Mol. Cell. Biol.* 16, 2325–2331
57 Burd, C.G. and Dreyfuss, G. (1994) *Science* 265, 615–621
58 Cavaloc, Y. *et al.* (1994) *EMBO J.* 13, 2639–2649
59 Singh, R., Valcárcel, J. and Green, M.R. (1995) *Science* 268, 1173–1176
60 Tacke, R. and Manley, J.L. (1995) *EMBO J.* 14, 3540–3551
61 Amrein, H., Hedley, M.L. and Maniatis, T. (1994) *Cell* 76, 735–746
62 Burd, C.G. and Dreyfuss, G. (1994) *EMBO J.* 13, 1197–1204
63 Zuo, P. and Maniatis, T. (1996) *Genes Dev.* 10, 1356–1368

*B. Chabot (b.chabot@courrier.usherb.ca) is in the Département de Microbiologie et Infectiologie, Faculté de Médecine, Université de Sherbrooke, 3001, 12th Avenue North, Sherbrooke, Québec, Canada J1H 5N4.*

# From gradients to stripes in *Drosophila* embryogenesis: filling in the gaps

**ROLANDO RIVERA-POMAR AND HERBERT JÄCKLE**

***Pattern formation along the anterior–posterior axis of the Drosophila embryo is organized by asymmetrically distributed maternal transcription factors. They initiate a cascade of spatially restricted and interacting zygotic gene activities that provide a molecular blueprint of the larval body at blastoderm stage. The key players in the pattern forming process have been identified. Recent progress has begun to reveal the mechanisms by which coherent positional information of maternal origin becomes transferred into serially repeated zygotic gene expression domains reflecting the metameric body plan of the larva.***

*Drosophila* pattern formation along the anterior–posterior axis involves three maternal genetic pathways: the anterior, the posterior and the terminal organizer systems. Key components of the systems are *bicoid*, *nanos* and *torso*, respectively, which set in motion an elaborate cascade of zygotically expressed transcription factors (reviewed in Refs 1, 2). In effect, this gives a prepattern of the segmented larval body at the blastoderm stage by establishing a series of repetitive domains of pair-rule gene expression (reviewed in Refs 1, 2). Up to this stage, the embryo develops in a syncytium where the nuclei divide without being separated by cellular membranes. This mode of development facilitates the diffusion of morphoregulatory factors of maternal and early zygotic origin, and allows them to instruct single-layered preblastoderm nuclei according to their position in the embryo.

Anterior–posterior polarity is initiated by cell communication events between the oocyte and the surrounding epithelium of somatic follicle cells, which depend on the *gurken–torpedo* signalling pathway (Fig. 1a; reviewed in Ref. 3). This results in the microtubule-dependent localization of *bicoid* mRNA to the anterior pole of the oocyte and *oskar* mRNA to the posterior. *oskar* organizes the assembly of the pole plasm required for the co-localization of *nanos* mRNA needed for the establishment of the abdominal segments (reviewed in Ref. 3). In addition, components of the terminal organizer system generate a follicle-cell-dependent signal, which is deposited between the egg membrane and the surrounding vitelline membrane (Fig. 1b; reviewed in Ref. 4). This signal activates the *torso*-dependent RAF–RAS signalling pathway[5], which overrules the activity of the anterior and posterior maternal systems to establish the terminal regions.

## Asymmetry by diffusion and translational repression

Translation of the localized *bicoid* mRNA occurs after egg deposition. This is regulated, in part, by cytoplasmic polyadenylation[6], a process disrupted in the maternal mutants *grauzone* and *cortex*[7]. BICOID diffuses from the anterior pole and thereby forms a concentration gradient extending posteriorly[1] (Fig. 2a). It is a homeodomain transcription factor required for the activation of zygotic genes that establish the head and thoracic segments[1].

NANOS, which is required for abdomen formation[1,3], forms a posterior-to-anterior concentration gradient. It acts along with uniformly distributed PUMILIO, which binds a *nanos* response element within the 3′ untranslated region (3′ UTR) of evenly distributed maternal *hunchback* mRNA. This leads to translational repression of *hunchback* mRNA in the posterior half of the embryo[8]. The zinc-finger-type transcription factor HUNCHBACK is a repressor of the posteriorly expressed gap genes *knirps* and *giant* (Ref. 2; Fig. 2b, 2c). Thus, *nanos*-dependent repression of *hunchback* serves to derepress activation of posterior segmentation genes[1,2] by an activator for which the search took almost a decade.




PII: S0168-9525(96)10044-5

## BICOID and CAUDAL are redundant posterior activators

The identity of the activator of posterior segmentation genes emerged recently through the analysis of the *cis*-acting control region of the posterior gap gene *knirps* (Refs 9, 10). This control element contains a number of separate modules including a small activator element for ubiquitous gene expression and several repressor elements mediating either *hunchback*-dependent repression from anterior or *tailless*-dependent repression from posterior[9] (Figs 2, 3; see below). Furthermore, binding sites were found for the gap gene proteins KRÜPPEL and GIANT, which enhance and repress *knirps* expression, respectively[9,10].

The activator element of *knirps* was found to bind BICOID and a second homeodomain protein, CAUDAL (Ref. 10). BICOID binds to multiple sites within a 60 bp DNA fragment, while CAUDAL binds to clustered sites within an adjacent fragment. CAUDAL forms a concentration gradient with reversed polarity to BICOID (Refs 11, 12; Fig. 2a). It was noted, however, that embryos lacking both maternal and zygotic *caudal* activity develop abdominal segments, although their pattern was characterized by deletions and fusions of segments[11]. Based on this observation, *caudal* was not considered as the posterior equivalent of *bicoid* that activates posterior segmentation genes. However, the expression patterns of *knirps*, *giant* and the pair-rule gene *hairy* in the blastoderm embryo and the resulting larval phenotype show that the absence of CAUDAL affects posterior segmentation and that the effect is enhanced in embryos lacking both CAUDAL and BICOID (Fig. 3). This argues that BICOID and CAUDAL combine their activating functions to generate the segments along the entire axis. Binding-site deletion studies with the activator element of *knirps* combined with reporter gene expression in mutant embryos revealed that CAUDAL is indeed an activator of posterior *knirps* expression and that BICOID can compensate for the lack of CAUDAL in the posterior region of the blastoderm embryo[10]. This finding explains why the absence of *caudal* activity does not cause the absence of posterior segmentation: BICOID has the ability to substitute, at least partially, for the lack of *caudal* activity in the posterior region of the embryo, indicating that BICOID does not act as a determinant in the anterior region of the embryo exclusively[1].

## BICOID controls CAUDAL gradient formation

CAUDAL and HUNCHBACK gradient formation have two features in common. *caudal* and *hunchback* are maternally and zygotically expressed. Their maternal mRNAs remain evenly distributed in the egg whereas the proteins form gradients[1,11–13]. Also, HUNCHBACK is evenly distributed in embryos lacking NANOS (Refs 1, 13) as CAUDAL is in embryos lacking BICOID (Ref. 14). The latter observation indicates that CAUDAL gradient formation involves *bicoid* activity. Recent evidence has shown that the BICOID homeodomain, which was known to act as a DNA-binding motif, can also bind RNA. In fact, BICOID binds via its homeodomain to regulatory sequences present in the 3′ UTR of *caudal* mRNA, blocks cap-dependent translation initiation and thereby prevents CAUDAL synthesis in response to the BICOID gradient[15,16]. This surprising result shows that

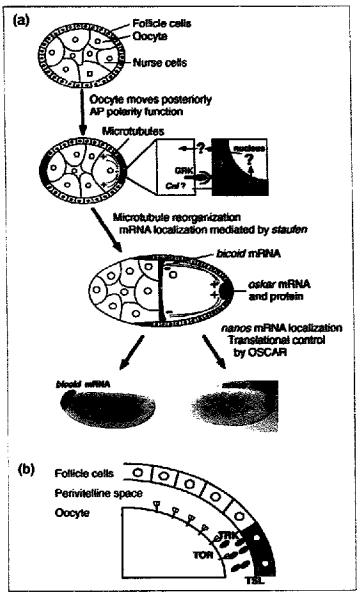


FIGURE 1. Generation of anterior–posterior (AP) polarity and non-segmented regions of the embryo involves two signal transduction pathways. In all figures, anterior is to the left and dorsal to the top. (a) The *Drosophila* egg develops in an egg chamber consisting of an oocyte and 15 siblings, the nurse cells[43]. It gains its polarity by intercellular communication events involving the surrounding epithelium of follicle cells. After an initial move of the oocyte, a signal involving the *gurken–torpedo* signalling pathway, involving cornichon (*cni*), reaches the adjacent posterior follicle cells (reviewed in Ref. 5). *gurken* (*grk*) encodes a transforming growth factor α-like molecule produced in the oocyte, while *torpedo* (*top*) encodes an epidermal growth-factor-receptor-like molecule present in the follicle cells. Due to the position of the oocyte, the *gurken* signal is limited to the posterior-most epithelial cells, which respond by a signal that causes re-orientation of the microtubule cytoskeleton (red) in the oocyte, which allows for *bicoid* mRNA localization at the anterior end and the transport of *oskar* mRNA to the posterior pole. This process also involves the activity of *staufen*, which codes for an RNA-binding microtubule-associated protein that mediates the transport of the mRNAs in a microtubule-dependent manner (reviewed in Refs 3, 44). (b) The 'terminal maternal system', required to establish the terminal pattern elements in the embryo, involves a signal transduction cascade active between the follicle cells and the oocyte. The genes *torso-like* (*tsl*) and *trunk* (*trk*), which are active in the follicle cells[45–47], generate an extraembryonic signal, a putative ligand molecule likely to be the *trunk* gene product, which is stored as a signal in the perivitelline space[47]. After egg deposition, it locally activates the TOR5O (TOR) tyrosine receptor kinase at both ends of the embryo[46], which, in turn, activates a cascade of serine/threonine kinases of the RAF–RAS signal transduction pathway (reviewed in Refs 5, 48).

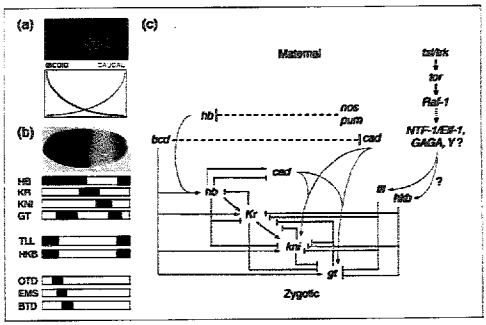


**FIGURE 2.** Maternal and first zygotic transcription factors, their expression domains and genetic interactions in the pre-blastoderm embryo. (a) BICOID (red) and CAUDAL (green) form opposing concentration gradients along the anterior–posterior axis. (b) Blastoderm expression domain of zygotic *hunchback* (*hb*), and schematic representation of the gap gene expression domains. Note the zygotic *hb* expression in the anterior half, the central domains of *Krüppel* (*Kr*), *knirps* (*kni*) and *giant* (*gt*), the terminal gap genes *tailless* (*tll*) and *huckebein* (*hkb*) at both ends of the embryo, and the domains of the gap-like head genes *orthodenticle* (*otd*), *empty spiracles* (*ems*) and *buttonhead* (*btd*). (For details on the expression domains and the molecular nature of the gap gene proteins, see Ref. 2.) (c) Genetic circuitry establishing the localized expression domains of the gap genes. Red lines represent negative interactions, green arrows represent activating interactions. Note that the maternal terminal pathway, which involves *torso-like* (*tsl*)[35], *trunk* (*trk*)[47] and *torso* (*tor*)[46] activities, the RAS–RAF transduction pathway[5,48], the transcription factors NTF-1/Elf-1 (Ref. 31), GAGA (Ref. 31) and possibly an unknown transcription factor Y (Ref. 1) causes the activation of *tll* and *hkb*. The *tll* and *hkb* activities provide repression of the central gap genes and, thereby, delimit the region of the embryo where segmentation occurs. Note that this pathway acts on both ends of the embryo (only posterior shown). For details of the interactions, see text. Abbreviations other than in (b) are *bicoid* (*bcd*), *caudal* (*cad*), *nanos* (*nos*) and *pumilio* (*pum*).

BICOID functions at different regulatory levels and, thereby, combines the two separate functions provided in the posterior region by NANOS (translational control) and CAUDAL (transcriptional control). Also, the anterior and posterior systems, previously thought to act independently, are linked through the BICOID-dependent spatial control of CAUDAL (Refs 15, 16), which generates a second, complementing, homeodomain protein gradient (Fig. 2a).

### First subdivisions by gap gene activities

The first zygotically expressed segmentation genes are the gap genes. Their activities are found in specific regions of the preblastoderm that fail to develop in the respective mutants (reviewed in Refs 1, 2). This class of genes includes the terminal gap genes *tailless* and *huckebein*, the gap-like head genes *orthodenticle*, *empty spiracles* and *buttonhead*, and the central gap genes *hunchback*, *Krüppel*, *knirps* and *giant* (Fig. 2b). Gene expression studies in mutant embryos revealed an elaborate genetic network (Fig. 2c), which established that: (1) terminal gap genes are activated by the maternal terminal system; (2) gap-like head genes are activated by *bicoid*; (3) central gap genes are activated either by a synergistic interaction of *bicoid* and *hunchback* (in the case of zygotic *hunchback*) or by *bicoid* and *hunchback* independently (in the case of *Krüppel*) or by *bicoid* and *caudal* (in the case of *knirps* and *giant*); and (4) the setting of the spatial limits of the central gap gene expression domains involves repression activities by adjacent gap gene expression domains (reviewed in Ref. 2). Only the terminal gap gene activities are controlled independently of the other gap gene activities. However, *tailless* and *huckebein* repress the activity of other zygotic segmentation genes that otherwise would be activated at both ends of the embryo[2,3]. Also, activated *torso* is thought to interfere directly with BICOID and prevent its function in the anterior-most position[17]. Finally, the genetic interactions suggest that gap genes control target gene expression in several different ways. For example, *hunchback* helps *bicoid* to control spatially zygotic *hunchback* expression, and it acts as an activator of *Krüppel* and as a repressor of *knirps* (Ref. 2; Fig. 2c).

### Generating adjacent gap gene domains

Molecular dissection of zygotic *hunchback* activation provides a mechanistic model of how the BICOID gradient controls position-dependent target gene expression[18,19]. High-affinity BICOID binding sites within an enhancer cause gene expression at low BICOID concentrations, while low-affinity binding sites cause gene expression at correspondingly higher concentrations within the gradient[18]. This observation implies that binding sites of the highest affinity within a promoter/enhancer define the posterior-most position to which gene activation extends in the BICOID gradient (reviewed in Ref. 1). This would elegantly explain how BICOID defines different posterior limits of gene expression, but more-recent results reach a different conclusion.

BICOID is necessary and sufficient for the activation of zygotic *hunchback* expression. However, it lacks the ability to regulate spatially the expression domain in HUNCHBACK-depleted embryos[20], suggesting that the spatial control by BICOID requires a synergistic interaction with maternal HUNCHBACK in wild-type embryos (Fig. 4a). Cell-free transcription reactions were described that recapitulate transcriptional synergism directed by BICOID and HUNCHBACK (Refs 21, 22). Two specific coactivator subunits ($TAF_H110$ and $TAF_H60$) of the basal transcription factor IID (TFIID; reviewed in Ref. 25) served as targets to mediate transcriptional activation by BICOID and HUNCHBACK activities. Quadruple complexes containing the TATA binding protein (TBP) and three coactivator subunits ($TAF_H250$, $TAF_H110$ and $TAF_H60$)

mediated transcriptional synergism in response to BICOID and HUNCHBACK, while complexes lacking $TAF_{II}110$ or $TAF_{II}60$ resulted in non-synergistic activation[21,22]. This finding provides a model of how the concerted action of BICOID and HUNCHBACK with different coactivators establishes the pattern of zygotic *hunchback* expression: BICOID is necessary and sufficient for the activation but does not provide the spatial information for the limits of the expression domain directly. Instead, spatial information is generated by a synergistic interaction between BICOID and maternal HUNCHBACK, causing the efficient recruitment of the $TBP–TAF_{II}$ complexes to the promoter (Fig. 4a).

It is conceivable that *Krüppel* expression is activated in a similar manner and that a repressor prevents activation in the region occupied by zygotic *hunchback*. However, regulation of *Krüppel* expression is more complex: both BICOID and HUNCHBACK act as independent activators and the gap genes expressed adjacent to the *Krüppel* domain restrict activation by repression[24] (Fig. 2b, 2c). In fact, when *knirps*, *giant* or *tailless* expression was ubiquitously induced, their activities were found either to reduce or to abolish *Krüppel* expression[24]. The current data suggest that HUNCHBACK and BICOID activate *Krüppel* broadly, and refined spatial restriction is brought about by redundant repression by the other gap gene activities which antagonize the activation[24] (Fig. 4b).

The enhancer that is necessary and sufficient for *Krüppel* expression contains multiple overlapping binding sites for repressors and activators[25]. *In vitro* studies combined with cell culture experiments have shown that the binding of activators and repressors are mutually exclusive and that high repressor concentrations prevent activators from functioning[25]. This would explain why activation of *Krüppel* occurs in the central region of the embryo where repressor concentrations are too low to compete for the binding of the activators (Fig. 4b). However, *knirps* expression, which is posteriorly adjacent to the *Krüppel* domain, is mediated by a modular array of non-overlapping elements where activators and repressors can bind in parallel (Fig. 4c). Furthermore, repressors in the *Krüppel* control region do not only compete for activator binding, but extinguish activation over short distances by a phenomenon termed 'quenching'[26]: repressors interfere with activators through protein–protein interactions and thereby prevent transcription (reviewed in Ref. 27).

The mechanisms establishing the expression domains of the gap-like head genes and the patterns of *giant* expression (Fig. 2c) are not yet studied beyond genetic analysis[28–30]. The collection of players and their impact on gene expression domains make it likely that activation and spatial control of these genes employ similar mechanisms as seen with *hunchback*, *Krüppel* or *knirps*. Activation of the terminal gap genes *huckebein* and *tailless* is also not yet fully understood. Studies on *tailless* regulation, however, suggest that *torso*-dependent activation depends on derepression involving the transcription factors GAGA and NTF-1/Elf-1 (Ref. 31; Fig. 2b).

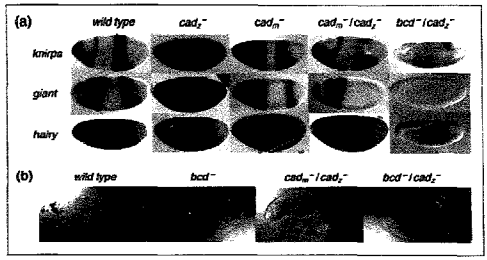


**FIGURE 3.** Gap and pair-rule gene expression patterns in wild type and *caudal* mutant embryos and phenotypes of the larvae. (a) Blastoderm expression of *knirps*, *giant* and the pair-rule gene *hairy* in wild type, in embryos lacking zygotic ($cad_z^-$) or maternal ($cad_m^-$) *caudal* activity, in embryos lacking maternal and zygotic *caudal* activities ($cad_m^-/cad_z^-$) and in embryos lacking *bicoid* and zygotic *caudal* activities ($bcd^-/cad_z^-$). Note the low level of *knirps* expression, the absence of *giant* expression and the low level of ubiquitous pair-rule gene *hairy* expression (except for the ends) in $bcd^-/cad_z^-$ embryos, probably due to maternal *caudal* activity (*knirps* expression is absent in $bcd^-/cad_m^-/cad_z^-$ embryos). The anterior expression domain seen in $cad_z^-$ embryos corresponds to β-galactosidase, a genetic marker used to distinguish them from embryos that lack zygotic *caudal* gene expression in addition (for details, see Ref. 10). (b) Cuticle preparations of a wild-type larva showing the normal segment pattern and patterns of various mutants [abbreviations as in (a)]. A low level of ubiquitous pair-rule gene expression [see (a)] is not sufficient to generate any segments in the larva.

Taken together, the available evidence suggests that the gap gene expression domains are mainly controlled by mutual repression. One mechanism defining the region of gene expression involves competitive binding of repressors and activators to overlapping sites within the enhancer. Different affinities of corresponding binding sites within the enhancer sense local combinations and concentrations of the relevant factors and, thereby, determine the spatial limits of the expression domain. Although such a mechanism is intuitively easy to understand, it would not explain the sharp on/off borders of gene expression, which argue for cooperative interactions between the factors that bind. Quenching as an additional mode of repression implies that enhancer-bound factors are able to interact before or while they communicate with the basal transcription machinery. Such interactions have been observed in cell culture and *in vitro* by showing the binding of KRÜPPEL to HUNCHBACK, and of KRÜPPEL to KNIRPS (reviewed in Ref. 32). The results suggested that KNIRPS and HUNCHBACK can interact with KRÜPPEL, which serves as their DNA-bound tether. Furthermore, the phenomenon that HUNCHBACK acts as a synergistic partner of BICOID, as an activator and as a repressor, has an interesting parallel in the finding that KRÜPPEL can also act two ways, at least in cell culture. In this system the KRÜPPEL monomer is able to cause transcriptional

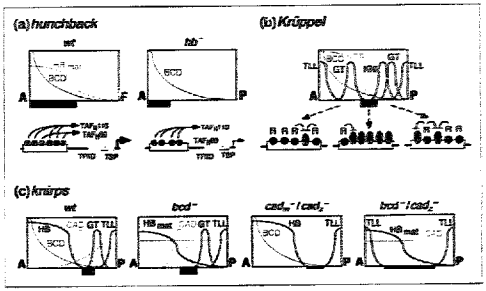


**FIGURE 4.** Schematic representation of *hunchback*, *Krüppel* and *knirps* expression in response to maternal activators and gap-gene-dependent repression. (a) *hunchback* expression (blue bar) is regulated in response to the graded distribution of BICOID and HUNCHBACK in the egg. The synergism between the two factors required to establish the spatial limit is due to their different contacts with different components of the basal transcription machinery (details in the text). Note that in the absence of maternal *hunchback* activity, BICOID is able to activate zygotic *hunchback* expression (diagram on the right) leading to simple activation at high concentrations of BICOID through limited contacts ($TAF_II110$) with the basal transcription machinery. (b) *Krüppel* activation is mediated through BICOID and HUNCHBACK independently and spatial restriction (blue bar) is brought about by repression through the adjacently expressed gap genes (see distribution in the diagram on top). In the anterior region (left side), filling of the enhancer involves competition between repressors (R) and activators (A). The central region of the embryo contains low levels of repressors (top diagram) so that activators can bind to the enhancer and, thereby, cause *Krüppel* activation. In the posterior region (right side), activation does not occur due to either a low concentration of the activators or high concentrations of the multiple repressors. (c) The mechanisms involved in *knirps* expression are still elusive. However, the expression patterns of *knirps* in wild-type embryos in response to the activator and repressor distributions suggest that CAUDAL and BICOID cause ubiquitous activation and that the spatial restriction is brought about by repression (see text). Note the expanded *knirps* expression domain in embryos lacking *bicoid* activity (*bcd*⁻) and weak expression in embryos lacking both maternal and zygotic *caudal* (*cad*⁻). In the absence of *bicoid* and zygotic *caudal* activities (*bcd*⁻/*cad*⁻), *knirps* is ubiquitously expressed (in response to maternal *caudal* activity) except at the ends. Abbreviations: BCD, BICOID; GT, GIANT; HB, maternal and zygotic HUNCHBACK; $HB_{mat}$, maternal HUNCHBACK; TLL, TAILLESS; wt, wild type.

activation when acting from a single binding site in front of a heterologous promotor, while the KRÜPPEL dimer functions as a repressor. The two opposite actions of KRÜPPEL are provided through different interactions with components of the basal transcription machinery involving TFIIB for activation and TFIIE for repression[32]. These results point out that although the functional binding sites and players for most enhancers are known, the mechanism of how spatial control is brought about in the embryo is still elusive.

## Gradients turn into stripes

How does the distribution of maternal activators and gap-gene-encoded transcription factors regulate the expression of pair-rule genes in a pattern of seven repetitive stripes? The ten pair-rule genes that encode transcription factors act at two different levels. Accordingly, they were grouped as primary and secondary pair-rule genes[33] (reviewed in Refs 2, 34). The *cis*-acting control of the primary pair-rule genes *even-skipped* and *hairy* depends on a modular array of distinct 'stripe elements'. This phenomenon emerged from altered expression patterns of the pair-rule gene *hairy* in various *hairy* mutant embryos[35]. Subsequent molecular analysis revealed that each stripe element contains a specific set of activator and repressor binding sites[36–38]; maternal transcription factors appear to be activators, the gap-gene-encoded transcription factors act mainly as repressors (reviewed in Refs 2, 34).

Expression of *even-skipped* in stripe two (second stripe from the anterior; anterior to the *Krüppel* expression domain) is activated in response to BICOID and HUNCHBACK, while repression is provided by GIANT and KRÜPPEL (Refs 36, 39). As seen with the *Krüppel* enhancer region, overlapping binding sites for activators and repressors were found, and much of the repressor action is provided through quenching[39]. Conversely, *hairy* stripe six expression (second stripe from the posterior; posterior to the *Krüppel* expression domain) is activated in response to *knirps* (Refs 37, 40) and also by *caudal* (T. Häder and R. Rivera-Pomar, unpublished; Fig. 3). Repression is brought about by *Krüppel*, *hunchback* (the posterior expression domain) and *tailless* (Refs 37, 40). This scenario suggests that the control of the primary pair-rule genes involves the combined activities of maternal and gap genes employing the mechanisms established for gap gene regulation. In addition, stripe expression involves cross-regulatory interactions among the pair-rule genes (reviewed in Refs 2, 34). Thus, the spatial control of pair-rule gene expression is not exclusively dependent on pre-existing transcription factors but also on other pair-rule genes. The initial question of how repetitive stripes are generated has been partially answered by the finding that the composition and concentration of transcription factors is sensed and mediated by separate *cis*-acting stripe elements. The more interesting part of the question – how these elements were generated during evolution and coordinated to result in a metameric pattern – is still open.

## Conclusions and perspectives

Pre-embryonic determination of anterior–posterior polarity results in the asymmetric distribution of three maternal transcription factors. Their activities and distributions are linked: BICOID controls the formation of the CAUDAL gradient by translational suppression; it also synergistically interacts with NANOS-controlled maternal HUNCHBACK to define the spatial limit of zygotic HUNCHBACK expression. These findings were

as unexpected as the result that the anterior determinant BICOID substitutes CAUDAL-dependent gene activation in the posterior region of the embryo, including *knirps* and *giant*. Furthermore, the posterior stripes of the secondary pair-rule gene *fushi tarazu* were shown to be CAUDAL dependent[11,51]. Thus, the three maternal transcription factor gradients might not only initiate the segmentation gene cascade but also represent a general activator system that, with the exception of the *torso*-controlled terminal regions, is likely to act at each level of the segmentation gene cascade and possibly also on homeotic genes. The latter proposal is consistent with the finding that the disruption of one of the murine *caudal* homologues affects axial skeletal identities by altering mesodermal expression of *hox* genes in the mouse embryo[42].

Ultimately, activation or repression is achieved through contacts established between the enhancer-bound factors and components of the basal transcription machinery. Such contacts have been unravelled *in vitro*, but it is not yet established whether they are also relevant for the embryo, which of the contacts of enhancer-bound factors will be decisive in driving or preventing transcription and how they do it. Mutually exclusive binding of factors might limit the number of actual players present on the enhancer, but most aspects of the repression involve quenching. This type of repression is likely to involve protein–protein interactions that prevent, for example, contacts of activators with the basal transcription machinery. Thus, although the transcription factors and the arrangement and affinities of their binding sites within the relevant enhancer elements are identified, the mechanism leading to restricted gene expression is still not transparent enough to reveal how the molecular blueprint of the embryonic body pattern is drawn. Future efforts will undoubtedly focus more deeply on how the factors work, how they interact and how they control transcription as well as translation mechanistically. Given the advantage of *Drosophila* for genetic and molecular studies, those basic questions relevant to cell determination and differentiation in general might soon be answered.

**Acknowledgements**

We thank our colleagues, in particular Beverly Purnell, Michael J. Pankratz, Julia P. Forjanic, Gerd Vorbrüggen and Felix Loosli, for critical comments on the manuscript. We apologize to colleagues whose work is not cited due to the size restraints of the review. Our work on segmentation is supported by the Max Planck Gesellschaft. R.R-P. was an A. von Humboldt fellow.

**References**

1 St Johnston, D. and Nüsslein-Volhard, C. (1992) *Cell* 68, 201–211
2 Pankratz, M. and Jäckle, H. (1993) in *The Development of Drosophila melanogaster* (Vol. 1), (Bate, M. and Martínez Arias, A., eds), pp. 467–516, Cold Spring Harbor Laboratory Press
3 Rongo, C. and Lehmann, R. (1996) *Trends Genet.* 12, 102–110
4 Sprenger, F. and Nüsslein-Volhard, C. (1993) in *The Development of Drosophila melanogaster* (Vol. 1), (Bate, M. and Martínez Arias, A., eds), pp. 365–385, Cold Spring Harbor Laboratory Press
5 Perrimon, N. and Desplan, C. (1994) *Trends Biochem. Sci.* 19, 509–513
6 Sallés, F.J. *et al.* (1994) *Science* 266, 1996–1999
7 Lieberfarb, M.E. *et al.* (1996) *Development* 122, 579–588
8 Murata, Y. and Wharton, R. (1995) *Cell* 80, 747–756
9 Pankratz, M.J. *et al.* (1992) *Science* 255, 986–989
10 Rivera-Pomar, R. *et al.* (1995) *Nature* 376, 253–256
11 Macdonald, P.M. and Struhl, G. (1986) *Nature* 324, 537–545
12 Mlodzik, M. and Gehring, W.J. (1987) *Cell* 48, 465–478
13 Tautz, D. (1988) *Nature* 332, 281–284
14 Mlodzik, M. and Gehring, W.J. (1987) *Development* 101, 421–430
15 Dubnau, J. and Struhl, G. (1996) *Nature* 379, 694–699
16 Rivera-Pomar, R. *et al.* (1996) *Nature* 379, 746–749
17 Ronchi, E. *et al.* (1993) *Cell* 74, 347–355
18 Driever, W., Thoma, G. and Nüsslein-Volhard, C. (1989) *Nature* 340, 363–367
19 Struhl, G. *et al.* (1989) *Cell* 57, 1259–1273
20 Simpson-Brose, M., Treisman, J. and Desplan, C. (1994) *Cell* 78, 855–865
21 Sauer, F., Hansen, S. and Tjian, R. (1995) *Science* 270, 1783–1788
22 Sauer, F., Hansen, S. and Tjian, R (1995) *Science* 270, 1825–1828
23 Tjian, R. and Maniatis, T. (1994) *Cell* 77, 5–9
24 Hoch, M., Seifert, E. and Jäckle, H. (1991) *EMBO J.* 10, 2267–2278
25 Hoch, M. *et al.* (1992) *Science* 256, 94–97
26 Levine, M. and Manley, J.L. (1989) *Cell* 59, 405–408
27 Gray, S. *et al.* (1995) *Philos. Trans. R. Soc. London Ser. B* 349, 257–262
28 Kraut, R. and Levine, M. (1991) *Development* 3, 601–609
29 Wimmer, E.A. *et al.* (1995) *Mech. Dev.* 53, 235–245
30 Gao, Q., Wang, Y. and Finkelstein, R. (1996) *Mech. Dev.* 56, 3–16.
31 Liaw, G-J. *et al.* (1995) *Genes Dev.* 9, 3163–3176
32 Sauer, F. *et al.* (1996) *Philos. Trans. R. Soc. London Ser. B* 351, 579–587
33 Howard, K. and Ingham, P. (1986) *Cell* 44, 949–957
34 Carroll, S. (1990) *Cell* 60, 9–16
35 Howard, K., Ingham, P. and Rushlow, C. (1988) *Genes Dev.* 2, 1037–1046
36 Harding, K. *et al.* (1989) *EMBO J.* 8, 1205–1212
37 Pankratz, M.J. *et al.* (1990) *Cell* 61, 309–317
38 Riddihough, G. and Ish-Horowicz, D. (1991) *Genes Dev.* 5, 840–854
39 Small, S., Blair, A. and Levine, M. (1992) *EMBO J.* 11, 4047–4057
40 Lengeland, J. *et al.* (1994) *Development* 120, 2945–2955
41 Dearolf, C., Topol, J. and Parker, C. (1989) *Nature* 341, 340–343
42 Subramanian, V., Meyer, B. and Gruss, P. (1995) *Cell* 83, 641–653
43 Spradling, A. (1993) in *The Development of Drosophila melanogaster* (Vol. 1), (Bate, M. and Martínez Arias, A., eds), pp. 1–70, Cold Spring Harbor Laboratory Press
44 St Johnston, D. (1995) *Cell* 81, 161–170
45 Martin, J-R., Raibaud, A. and Ollo, R. (1994) *Nature* 367, 741–745
46 Casanova, J. and Struhl, G. (1993) *Nature* 362, 152–155
47 Casanova, J. *et al.* (1995) *Genes Dev.* 9, 2539–2544
48 Hill, C.S. and Treisman, R. (1995) *Cell* 80, 199–211

*R. Rivera-Pomar (rrivera@gwdg.de) and H. Jäckle (hjaeckl@gwdg01.dnet.gwdg.de) are in the Max-Planck-Institut für Biophysikalische Chemie, Postfach 2841, D-37018 Göttingen, Germany.*

CHAPTER THREE

# Groucho: A Corepressor with Instructive Roles in Development

Wiam Turki-Judeh *and* Albert J. Courey

## Contents



## Abstract

*Drosophila* Groucho (Gro) is the founding member of a family of metazoan corepressors. Gro mediates repression through interactions with a myriad of DNA-binding repressor proteins to direct the silencing of genes involved

Department of Chemistry & Biochemistry and Molecular Biology Institute, University of California, Los Angeles, California, USA

*Current Topics in Developmental Biology*, Volume 98
ISSN 0070-2153, DOI: 10.1016/B978-0-12-386499-4.00003-3

in many developmental processes, including neurogenesis and patterning of the main body axis, as well as receptor tyrosine kinase/Ras/MAPK, Notch, Wingless (Wg)/Wnt, and Decapentaplegic (Dpp) signaling. Gro mediates repression by multiple molecular mechanisms, depending on the regulatory context. Because Gro is a broadly expressed nuclear factor, whereas its repressor partners display restricted temporal and spatial distribution, it was presumed that this corepressor played permissive rather than instructive roles in development. However, a wide range of studies demonstrates that this is not the case. Gro can sense and integrate many cellular inputs to modulate the expression of variety of genes, making it a versatile corepressor with crucial instructive roles in development and signaling.

## Abbreviations

| | |
|---|---|
| AES | amino-terminal enhancer of split |
| AH1 and AH2 | amphipathic α-helices 1 and 2 |
| CRM | *cis*-regulatory module |
| CtBP | C-terminal binding protein |
| EGFR | epidermal growth factor receptor |
| Grg | Groucho-related gene |
| Gro | Groucho |
| HDAC1 | histone deacetylase 1 |
| HES | Hairy/Enhancer of split |
| HIPK2 | homeodomain-interacting protein kinase 2 |
| MAPK | mitogen-activated protein kinase |
| RTK | receptor tyrosine kinase |
| TLE | transducin-like enhancer of split |
| TSA | Trichostatin A |

## 1. The Gro/TLE Family

### 1.1. Initial characterization of Gro

The *Drosophila gro* gene was initially identified through a weak hypomorphic allele ($gro^1$) that results in thick tufts of sensory bristles over the eyes, bearing resemblance to the bushy eyebrows of Groucho Marx (Lindsley and Grell, 1968). While $gro^1$ is viable, stronger mutations in *gro* are lethal and reveal essential maternal and zygotic requirements for Gro in a wide variety of developmental processes.

Proof that Gro is a regulator of transcription came from the finding of a functional interaction with the *Drosophila* Hairy protein, a bHLH protein that represses transcription (Paroush *et al.*, 1994). *hairy*, many of the genes of the E(spl) complex, and *deadpan (dpn)* encode structurally related proteins that together comprise the Hairy/E(spl) (HES) family of transcription factors. HES family factors, which are also found in vertebrates, are characterized by a bHLH DNA-binding domain and a C-terminal WRPW motif (Dawson *et al.*, 1995). Gro interacts directly with HES proteins via the WRPW motif (Fisher *et al.*, 1996; Grbavec and Stifani, 1996; Paroush *et al.*, 1994). The functional relevance of the interaction between Gro and HES family factors was demonstrated by experiments showing that *Drosophila* embryos lacking maternally deposited Gro display misregulation of neurogenesis, sex determination, and embryonic segmentation, that is, many of the processes known to be regulated by HES family factors (Delidakis *et al.*, 1991; Paroush *et al.*, 1994).

Subsequent studies have shown that Gro interacts with a wide variety of repressor partners in addition to HES family proteins, including Dorsal, Runt, Huckebein, Goosecoid, and Brinker (Aronson *et al.*, 1997; Dubnicoff *et al.*, 1997; Fisher *et al.*, 1996; Flores-Saaib *et al.*, 2001; Goldstein *et al.*, 1999; Hasson *et al.*, 2001; Jimenez *et al.*, 1997, 1999; Paroush *et al.*, 1994). While some of these repressors contain a WRPW motif, others contain a different peptide motif mediating the interaction with Gro known as the engrailed homology 1 (eh1) motif, and still others lack a recognizable Gro interaction motif.

## 1.2. Gro homologs

Members of the Gro family are present in all or almost all metazoans (Choudhury *et al.*, 1997; Mallo *et al.*, 1993; Miyasaka *et al.*, 1993; Pflugrad *et al.*, 1997; Schmidt and Sladek, 1993; Sharief *et al.*, 1997; Stifani *et al.*, 1992). A comparison of the predicted protein sequences reveals that most of the family members share a conserved structural organization consisting of five domains, which, from N- to C-terminus, are termed the Q, GP, CcN, SP, and WD-repeat domains (Fig. 3.1). The Q and WD-repeat domains are highly conserved, suggesting a highly conserved function (Chen and Courey, 2000; Jennings and Ish-Horowicz, 2008; Stifani *et al.*, 1992). As will be discussed in subsequent sections, the Q domain mediates self-association and repressor binding, while the WD-repeat domain mediates interactions with repressor proteins. The three central domains (the GP, CcN, and SP domains) are much more weakly conserved. However, as will become clear in later sections, these domains nonetheless have multiple vital functions in repression and its regulation.

While the *Drosophila* genome encodes a single Gro family member, the mouse and human genomes encode four family members each, termed transducin-like Enhancer of Split 1–4 (TLE1–4) in humans (Stifani *et al.*, 1992)

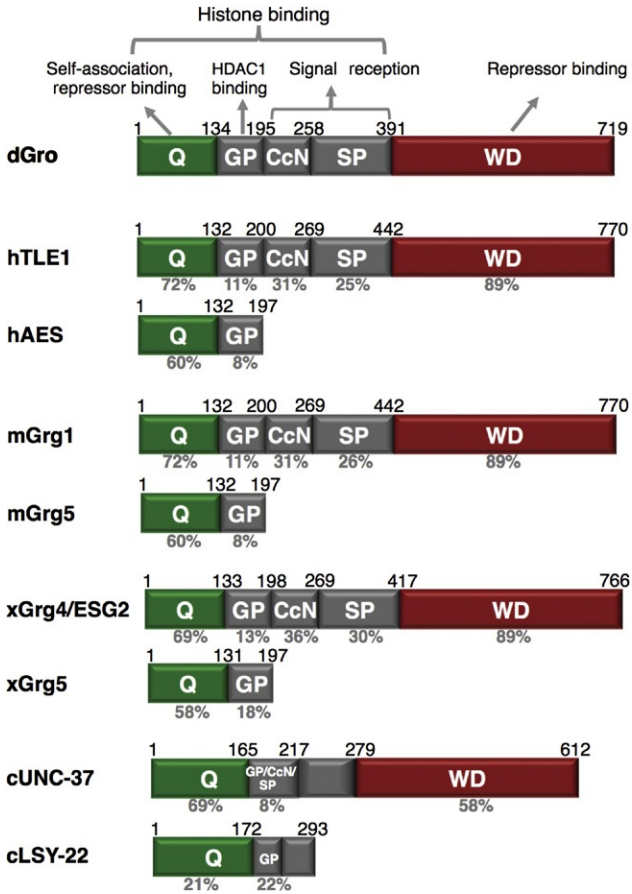


**Figure 3.1** Structural organization and sequence conservation in the Gro/TLE family. A comparison of the amino acid sequence of *Drosophila* Gro (dGro) with those of the human protein hTLE1 and hAES, the mouse proteins mGrg1 and mGrg5, the *Xenopus* proteins xGrg4/ESG2 and xGrg5, and the *C. elegans* proteins cUNC-37 and cLSY-22 reveals that most Gro/TLE family members share a conserved structural organization, which consists of a glutamine-rich (Q) domain, followed by a glycine/proline-rich (GP) domain, a so-called CcN domain, a serine/proline-rich (SP) domain, and a WD-repeat domain. A few of the suspected functions of these domains are indicated above the diagram of dGro. The percentages below the domains indicate sequence identity to the corresponding domains in *Drosophila* Gro. Percent identity was determined from proteins alignments calculated using the ClustalW BLOSUM scoring matrix. The Q and WD-repeat domains are highly conserved, while the central region consisting of GP, CcN, and SP domains is much less well conserved among Gro/TLE family members. The proteins shown have the following NCBI accession numbers: dGro (P16371); hTLE1 (NP_005068); hAES (NP_001121.2), mGrg1 (Q62440), mGrg5 (NP_034477.1), xGrg4/ESG2 (CAA12236), xGrg5 (NP_001083532.1), cUNC-37 (O02482), and cLSY-22 (CAB01968.3).

and Gro-related genes 1–4 (Grg1–4) in mouse (Mallo *et al.*, 1993; Miyasaka *et al.*, 1993). The human and mouse family members are broadly, but specifically, expressed in various developing tissues and are not functionally redundant (Gasperowicz and Otto, 2005; Stifani *et al.*, 1992; Yao *et al.*, 1998). TLE1/Grg1 is involved in myogenesis, hematogenesis, apoptosis, neurogenesis, and eye development (Gao *et al.*, 2001; Imai *et al.*, 1998; Jan *et al.*, 2004; Swingler *et al.*, 2004; Yao *et al.*, 2000; Zhu *et al.*, 2002); TLE2/Grg2 in neural tube formation and osteogenesis (Grbavec *et al.*, 1998; Thirunavukkarasu *et al.*, 1998); TLE3/Grg3 in placental and adipose development (Nakayama *et al.*, 1997; Villanueva *et al.*, 2011); and TLE4/Grg4 in regulating the B cell lineage and heart development (Bajoghli *et al.*, 2007; Eberhard *et al.*, 2000; Linderson *et al.*, 2004). Gro homologs have also been found in frogs (Choudhury *et al.*, 1997; Sharief *et al.*, 1997) and roundworms (Pflugrad *et al.*, 1997).

Although clear Gro/TLE orthologs have not been found outside the metazoans, corepressors exhibiting homology to Gro/TLE proteins have been found in diverse eukaryotic taxa, such as fungi (Treitel and Carlson, 1995) and plants (Liu and Karmarkar, 2008). For example, Tup1, a yeast corepressor, contains a conserved C-terminal WD-repeat domain and this domain is more closely related to the Gro/TLE WD-repeat domain than to WD-repeat domains in other proteins (Flores-Saaib and Courey, 2000). Outside the WD-repeat region, there is no recognizable homology between Tup1 and Gro/TLE proteins, but there is functional conservation (Courey and Jia, 2001). For example, Tup1 contains an N-terminal domain in the same position as the Gro/TLE Q domain that, like the Q domain, mediates essential corepressor self-association (Chen *et al.*, 1998; Flores-Saaib and Courey, 2000; Malave and Dent, 2006; Redd *et al.*, 1997; Tzamarias and Struhl, 1995). Further, as will be discussed later, Gro/TLE binds to hypoacetylated histone tails and the same is true for Tup1 (Edmondson and Roth, 1998; Edmondson *et al.*, 1996; Flores-Saaib and Courey, 2000). As will also be discussed later, Gro/TLE interacts with the histone deacetylase Rpd3/HDAC1, and once again, the same is true for Tup1 (Edmondson *et al.*, 1998; Flores-Saaib and Courey, 2000; Malave and Dent, 2006; Redd *et al.*, 1997). These functional parallels suggest that, despite the poor structural conservation between Gro/TLE and Tup1, the molecular mechanisms used by Gro/TLE to regulate transcription may be similar to those used by Tup1.

## 1.3. An instructional role for Gro/TLE during development

Gro/TLE family proteins have diverse developmental roles mediated by interactions with repressors that regulate embryonic patterning, the transition from proliferation to differentiation, specification of cell identity, and apoptosis (Buscarlet and Stifani, 2007; Chen and Courey, 2000; Fisher and Caudy, 1998; Gasperowicz and Otto, 2005). This is supported by many

studies in *Drosophila* that have demonstrated essential roles for Gro in a wide array of developmental processes, including embryonic patterning, sex determination, neuronal development, and imaginal disc patterning (Buscarlet and Stifani, 2007; Chen and Courey, 2000). Gro also plays equally important, although less well understood, roles in vertebrate development (Buscarlet and Stifani, 2007; Fisher and Caudy, 1998; Gasperowicz and Otto, 2005).

As will be repeatedly emphasized in this review, the role of Gro in development is not merely permissive. That is, Gro is not simply a constitutive component of the repression machinery that must be present to allow repression to occur. Rather, it plays many instructive roles in development, by doing such things as converting activators into repressors and dictating the threshold responses to repressor gradients in ways that are highly sensitive to Gro activity levels and that are intensively regulated by signaling pathways.

## 2. Mechanisms of Gro/TLE-Mediated Repression

Despite the widespread importance of Gro/TLE-mediated repression in development and signal transduction, relatively little is known about the mechanisms by which Gro/TLE proteins mediate transcriptional repression. Genetic, molecular, and biochemical data suggest that Gro/TLE proteins direct repression through a variety of mechanisms, depending on the developmental context and the target gene. Biochemical activities of Gro that may underlie many examples of Gro-mediated repression include (1) self-association (oligomerization), (2) direct interaction with histone deacetylase, (3) binding to histones leading to changes in chromatin structure such as increased nucleosome density or chromatin condensation, (4) interactions with the core transcriptional machinery, and (5) masking of activation domains (Fig. 3.2).

### 2.1. Self-association

The highly conserved Gro Q domain mediates homo-oligomerization via two coiled-coil motifs termed amphipathic α-helices 1 and 2 (AH1 and AH2) (Chen *et al.*, 1998; Miyasaka *et al.*, 1993; Pinto and Lobe, 1996). The Q domain forms a predominant homo-tetramer, although other size oligomers are also observed including dimers and larger species that appear to be mulitmers of the tetramer (Chen *et al.*, 1998; Jimenez *et al.*, 1999; Kuo *et al.*, 2011; Palaparti *et al.*, 1997; Pinto and Lobe, 1996; Song *et al.*, 2004). Point mutations that disrupt the hydrophobic faces of AH1 and AH2 eliminate these multimers, converting Gro into a monomer (Chen *et al.*, 1998; Pinto and Lobe, 1996; Song *et al.*, 2004).

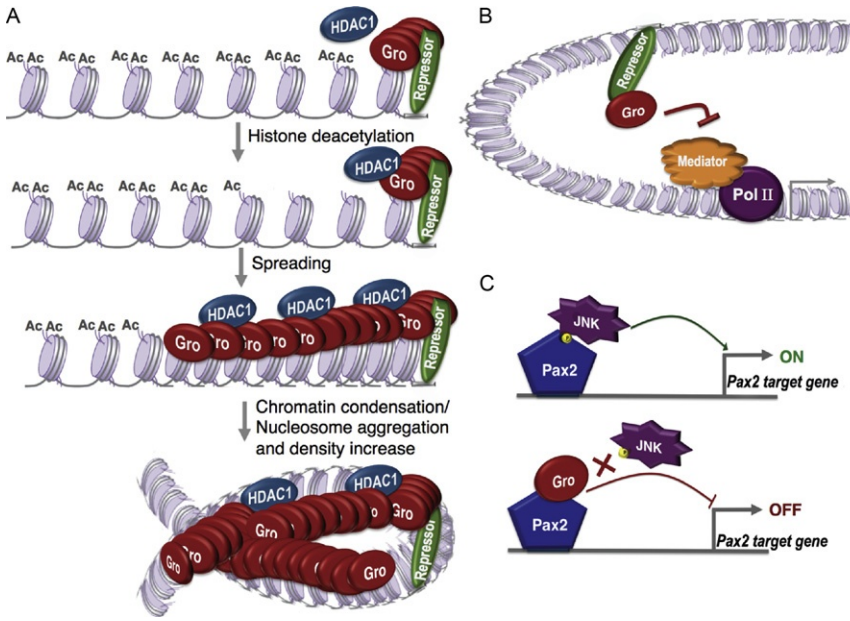


**Figure 3.2** Models for Gro/TLE-mediated repression. Gro/TLE appears to direct repression by multiple mechanisms. (A) A variety of studies indicate that the ability of Gro/TLE proteins to self-associate, recruit histone deacetylase, bind to deacetylated histones, and direct chromatin condensation (or increased nucleosome density) are required for Gro-mediated repression. This multistep model accounts for all of these biochemical functions. (B) Gro/TLE may interact with the Mediator, a component of the basal transcriptional machinery, thereby interfering with the formation or function of the preinitiation complex. (C) Gro/TLE may mask the activation domains of transcriptional activators. In the example shown here, Gro binding prevents phosphorylation of the activation domain in Pax2, thereby preventing Pax2 activation. Additional details regarding these three models and references are given in the text.

A number of lines of evidence indicate that Q domain-mediated Gro self-association makes a significant contribution to Gro-mediated repression. First, repression in both *Drosophila* wing discs and cultured cells is inhibited by point mutations in AH1 and AH2 that prevent self-association. Second, swapping of the Q domain with the heterologous tetramerization domain from the tumor suppressor p53 allows repression in S2 cells, implying that the primary function of the Q domain is to facilitate oligomerization (Chen *et al.*, 1998). Finally, forms of Gro with an intact Q domain, but with mutations in other domains that prevent repression, behave as dominant negatives to prevent repression by endogenous wild-type Gro strongly supporting the idea that Gro oligomerizes *in vivo*. However, oligomerization may not be uniformly required for repression since a

mutant *gro* allele encoding an oligomerization deficient form Gro, while lethal, is not a genetic null (Jennings *et al.*, 2008). Thus, Gro/TLE oligomerization may be required for repression of some but not all Gro/TLE target genes, suggesting diverse modes of transcriptional regulation (Jennings and Ish-Horowicz, 2008).

Although it seems clear that self-association is required for many although perhaps not all instances of Gro/TLE-mediated repression, the mechanisms linking homo-oligomerization to repression are still unclear. The self-association properties of Gro/TLE could perhaps allow a silent chromatin structure to spread over large areas of the genome, as proposed for heterochromatic silencing by SIR proteins in budding yeast (Buchberger *et al.*, 2008; Hecht *et al.*, 1995; Hoppe *et al.*, 2002; Huang, 2002; Radman-Livaja *et al.*, 2011; Rusche *et al.*, 2002). In support of this idea, Gro/TLE family proteins bind to chromosomal domains that extend beyond the sites to which Gro/TLE is initially recruited by DNA-bound repressors (Martinez and Arnosti, 2008; Sekiya and Zaret, 2007; Winkler *et al.*, 2010).

## 2.2. Interaction with histone deacetylase

Although the GP domain is poorly conserved, both mammalian and *Drosophila* Gro/TLE make a conserved interaction with the class I histone deacetylase Rpd3/HDAC1 via this domain (Brantjes *et al.*, 2001; Chen *et al.*, 1999). Evidence that this interaction is functional comes from *Drosophila* cell culture studies in which wild-type Rpd3, but not a catalytically inactive mutant, was found to stimulate repression of a Gal4-responsive reporter by a Gal4-Gro fusion protein (Chen *et al.*, 1998). Further, treatment with the histone deacetylase inhibitor trichostatin A (TSA) in both mammalian and *Drosophila* cell culture (Chen *et al.*, 1999; Choi *et al.*, 1999) or RNAi knockdown of *rpd3* in *Drosophila* cell culture (Chen *et al.*, 1999; Winkler *et al.*, 2010) significantly decreases this repression, although neither treatment eliminated Gal4-Gro-mediated repression completely. Thus, in addition to histone deacetylase-dependent mechanisms, Gro may utilize histone deacetylase-independent mechanisms for transcriptional repression. The conclusion that histone deacetylation contributes to Gro-mediated repression is reinforced by chromatin immunoprecipitation (ChIP) assays showing that Gro colocalizes with Rpd3 to the chromatin of target genes, leading to the deacetylation of specific lysine residues in histones H3 and H4, including H3K9, H3K14, H4K5, H4K8, and H4K12 (Winkler *et al.*, 2010).

*In vivo* studies in flies also demonstrate the functional relevance of the interaction between Gro and histone deacetylase. First, a simultaneous twofold reduction in the *gro* and *rpd3* gene dosage leads to synergistic effects on embryonic lethality and pattern formation (Chen *et al.*, 1999). Second, a hypomorphic mutation in *rpd3* disrupts repression by Even-skipped, a Gro-dependent repressor (Mannervik and Levine, 1999). Third, the

wing-patterning defects and ectopic repression of Gro target genes caused by overexpression of Gro in the wing disc were significantly reduced when flies were fed either of two different histone deacetylase inhibitors, TSA (which is specific for class I and II histone deacetylases) and HC-toxin (which is specific for the class I enzymes), and this effect was enhanced when the *rpd3* gene dosage was reduced (Winkler *et al.*, 2010).

## 2.3. Chromatin condensation

Gro and related proteins are able to bind to histones, an activity that could contribute to Gro-mediated repression. Such an interaction was first demonstrated for yeast Tup1 (Edmondson and Roth, 1998; Edmondson *et al.*, 1996) and later extended to mammalian and *Drosophila* Gro/TLE (Flores-Saaib and Courey, 2000; Palaparti *et al.*, 1997). Gro binds all four core histones, with highest affinity for histone H3. The interaction is mediated by the N-terminal tail of this histone and is significantly enhanced when the tail is deacetylated.

The notion that histone binding and oligomerization are functionally relevant is supported by a study showing that Gro/TLE binds nucleosomal arrays *in vitro* and condenses the chromatin, thereby reducing the accessibility of the template to the transcriptional machinery (Sekiya and Zaret, 2007). Binding of Gro/TLE to the nucleosomal arrays is dependent on histone tails and nucleosome aggregation requires the Q domain, which, as mentioned above, mediates self-association. Interestingly, binding of Gro to the nucleosomes is not, by itself, sufficient for complete protection of the DNA from DNase I digestion or complete exclusion from the template of activators and components of the general transcriptional. This requires the additional binding of Gro/TLE to a template-bound repressor, which, in turn, leads to the formation of a closed chromatin region spanning three to four nucleosomes and the exclusion of factors such as TBP and RNA polymerase II (Pol II) from the template.

Further evidence that repression might involve significant alterations in chromatin structure is provided by histone H3 ChIP assays on a Gro target in *Drosophila* wing discs. These studies showed that Gro mediated an increase in nucleosomal density, which was reversed in the presence of TSA. This suggests a model in which Gro/TLE directs the formation of a chromatin environment characterized by high-density deacetylated nucleosomes that may block activators and the transcriptional machinery (Winkler *et al.*, 2010).

Putting together the data on Gro self-association, histone deacetylation, and chromatin condensation or increased nucleosome density leads to the following multistep model for Gro-mediated repression (Fig. 3.2A). First, Gro is recruited to the template via an interaction with a DNA-bound repressor. Second, Gro recruits an Rpd3/HDAC1-containing histone

deacetylase complex, which catalyzes local histone deacetylation. Third, the ability of Gro to interact both with itself and with deacetylated histones leads to the recruitment of additional Gro. Fourth, Gro association leads to nucleosome aggregation creating a condensed form of chromatin with reduced accessibility to the transcriptional machinery. While this model may explain many instances of Gro-mediated repression, it is important to note that there is at least one documented case in which Gro-mediated repression is not accompanied by a decrease in the accessibility of the template to nucleases (Li and Arnosti, 2011).

## 2.4. Core transcriptional machinery interactions

In addition to chromatin-mediated mechanisms, Gro is likely to repress by other mechanisms as well. For example, Gro may directly interact with the core machinery to inhibit some step in the transcription cycle such as preinitiation complex assembly, promoter release, or elongation (Fig. 3.2B). Along these lines, genetic and biochemical studies in yeast have linked the activity of the Gro-related corepressor Tup1 to several components of the Mediator complex (Gromoller and Lehming, 2000; Kuchin and Carlson, 1998; Papamichos-Chronakis *et al.*, 2000). This complex interacts with the C-terminal domain (CTD) of the largest subunit of RNA Pol II and also makes extensive contact with the core domain (Berk, 1999; Kornberg, 2005; Malik and Roeder, 2010). The Mediator functions as a bridge to relay information from gene-specific regulatory proteins to the basal Pol II transcription machinery and serves as a scaffold for the assembly of a functional preinitiation complex including Pol II and the general transcription factors (Kornberg, 2005).

Evidence that metazoan Gro/TLE homologs may also interact with the Mediator comes from studies of the *Caenorhabditis elegans* Gro/TLE homolog encoded by *unc-37*. In *C. elegans*, the nine pairs of rays in the adult male tail develop from three pairs of embryonic seam cells, V5, V6, and T. Male-specific postembryonic proliferation of V6 begins with the expression of *pal-1* (a homolog of *Drosophila caudal*). Expression of *pal-1* in V6 is partly dependent on a pathway that is repressed normally by the two essential Mediator subunits MED1 and MED12 (also known as SOP3 and SOP1 in *C. elegans*) (Zhang and Emmons, 2002). A mutation in *unc-37* alone has little effect on activation of *pal-1* in V6, thus leading to very few missing V6 rays. The effect is greatly increased, however, when the *unc-37* mutation is combined with mutations in MED1 and MED12 (Zhang and Emmons, 2002). At this point, however, it is not clear if the interaction between the *unc-37* gene product and Mediator subunits is direct or indirect since a physical interaction between these proteins has not been established. For example, it is possible that Gro and the Mediator have separate parallel inputs into *C. elegans* tail development.

## 2.5. Masking of activation domains

Another mechanism of Gro-mediated repression is masking of the activation domains of transcriptional activators (Fig. 3.2C). In general, this involves the binding of Gro to an activator to block coactivator binding or to induce a conformational change in an activation domain that renders it inactive (Arnosti, 2004). The paired domain protein, Pax2, a DNA-binding transcriptional activator that is conserved across eukaryotes, provides a particularly interesting example of masking. Phosphorylation of the Pax2 activation domain by c-jun N-terminal kinase (JNK) potentiates Pax2 activation of target genes (Cai *et al.*, 2003). Gro/TLE binds directly to Pax2 and this interaction inhibits Pax2 phosphorylation by JNK, resulting in a decrease in its transactivation potential (Cai *et al.*, 2003).

## 2.6. Long- versus short-range transcriptional repression

Transcriptional repressors are thought to work via two different mechanisms depending on how far their binding sites are located from the activator sites and/or the core promoter. The two general modes of repression are known as short- and long-range repression (Courey and Jia, 2001; Gray and Levine, 1996b; Mannervik *et al.*, 1999). In short-range repression, the repressors inhibit activators bound within ~100bp of the repressor binding site. Spatially regulated genes, such as segmentation genes often contain multiple *cis*-regulatory modules (CRMs), each of which directs the formation of a different portion of the transcriptional pattern through combinatorial interactions between multiple activators and repressors, which are, themselves, expressed in spatially restricted patterns. It is critical that repressors bound to one CRM not interfere with the function of another CRM and short-range repression helps to ensure this so-called enhancer autonomy (Gray and Levine, 1996a). Long-range repression, in contrast, involves repressors that are able to render a promoter resistant to the influence of all enhancers including those that are located thousands (or hundreds of thousands) of base pairs away from the binding site of the repressor (Cai *et al.*, 1996; Courey and Jia, 2001; Mannervik *et al.*, 1999).

While we do not understand what determines the distinction between long- and short-range repression, a clue may come from the observation that long-range repressors (e.g., Dorsal, HES family factors) often utilize Gro/TLE as a corepressor, while short-range repressors (e.g., Snail, Knirps) often utilize an alternative corepressor termed C-terminal binding protein (CtBP). However, recent studies on Gro are breaking down this distinction. In particular, these studies suggest that Gro can, in some cases, mediate short-range repression, depending on the DNA-binding repressor and the context of the *cis*-regulatory element. For example, Gro is an essential corepressor for the short-range repressors Sloppy-paired 1 (Slp1) and Knirps (Andrioli *et al.*, 2004; Payankaulam and Arnosti, 2009).

Gro interacts with Slp1 via an eh1 motif and this interaction is functionally relevant because deletion of this region inhibits Slp1 mediated repression of a subset of its target genes (Andrioli *et al.*, 2004). One such target, *runt*, is a pair rule gene expressed in a seven-stripe pattern. These various stripes are under the control of different CRMs. The CRMs that direct formation of stripes 1, 3, and 5 are located near each other, yet the Gro/TLE-Slp1 complex is only able to repress the stripe 1 CRM, allowing for enhancer autonomy (Andrioli *et al.*, 2004).

Additional evidence contravening the idea that Gro is strictly a long-range corepressor is provided by a study showing that Gro physically interacts with the classical short-range repressor Knirps via two N-terminal eh1-like motifs (Payankaulam and Arnosti, 2009). This interaction is functionally relevant because deletions of the two eh1-like motifs not only prevent the Knirps-Gro interaction but also result in very weak repressor activity (Payankaulam and Arnosti, 2009).

At this point, we can only speculate about how it is that Gro can act as a short-range corepressor when it interacts with some targets and a long-range corepressor when it interacts with others. One possibility is that short-range repressors like Knirps and Slp1 induce conformational changes in Gro that inhibit its ability to self-associate and spread, while recruitment by long-range repressors allow such spreading to occur (Payankaulam *et al.*, 2010). Another possibility is that the ability to spread depends on *cis*-regulatory elements that either block or allow spreading. Finally, we note that that long- and short-range repression may be associated with different chromatin modifications (Burks *et al.*, 2009). Perhaps other coregulators interact with Gro in a gene-specific manner to determine the chromatin modification state and thereby determine the range of repression.

In conclusion, Gro/TLE family proteins appear to utilize multiple mechanisms to repress transcription, depending on the regulatory context. The long- and short-range repression categories probably represent an oversimplification. An understanding of the true complexities that determine what mechanism predominates at any given target will require greater knowledge of factors that interact with Gro to modulate its function.

## 2.7. Gro/TLE central domains may be intrinsically disordered regions

As mentioned previously, Gro/TLE family members have a five-domain structure including conserved N- and C-terminal domains (the Q and WD-repeat domains, respectively) and three weakly conserved internal regions (GP, CcN, and SP domains; Fig. 3.1). Sequencing of a large set of lethal Gro/TLE point mutant alleles revealed a large number of mutations that map to the WD-repeat domain and a smaller number that map to the Q domain, demonstrating the functional importance of these two domains

(Jennings *et al.*, 2006, 2008). However, none of the lethal point mutations map to the GP, CcN, or SP domains, an observation that, along with the lack of conservation of these domains, suggests that these internal domains might be dispensable for function (Jennings *et al.*, 2008). Contrary to this suggestion, however, a recent analysis of a series of Gro internal deletion variants suggests that these regions are absolutely critical for repression by Gro and for the regulation of this repression (Turki-Judeh and Courey, unpublished observations).

Rather than reflecting a lack of function, the lack of conservation in the central region could reflect a disordered structure. Like the Gro central domains, regions of intrinsic disorder are typically characterized by a high content of polar and charged amino acids and a low content of bulky hydrophobic amino acids (Chouard, 2011; Dunker *et al.*, 2005). To determine whether the Gro central region is likely to be intrinsically disordered, we applied several protein disorder predictors to the *Drosophila* Gro amino acid sequence (Fig. 3.3) (Li *et al.*, 1999; Radivojac *et al.*, 2003; Romero *et al.*, 1997; Romero *et al.*, 2001; Xue *et al.*, 2010). The predictors produce disorder scores by calculating such parameters as hydropathy and amino acid composition and then comparing these parameters to those calculated from a database of disordered proteins (Dunker *et al.*, 2005; Xue *et al.*, 2010). Essentially, the entire Gro central region displays high

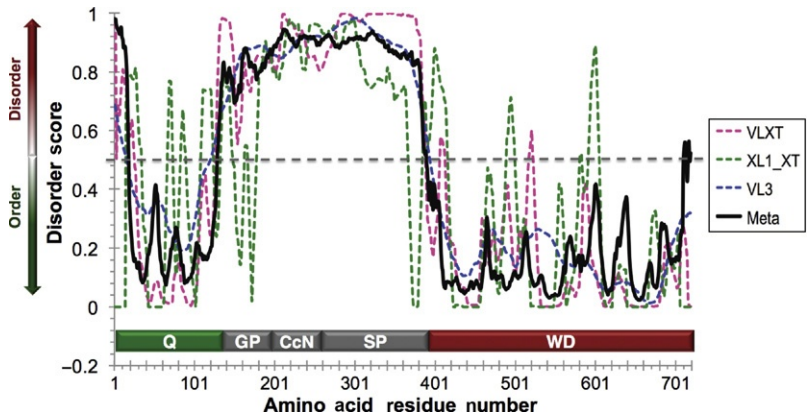


**Figure 3.3** The Gro/TLE central region appears to be intrinsically disordered. Prediction of disorder in *Drosophila* Gro using four disorder prediction algorithms: PONDR-FIT™ (Meta, black solid line) (Xue *et al.*, 2010); PONDR®VLXT (pink dashed line) (Li *et al.*, 1999; Romero *et al.*, 2001); PONDR®XL1_XT (green dashed line) (Romero *et al.*, 1997); and PONDR®VL3 (blue dashed line) (Radivojac *et al.*, 2003). Amino acid residues with scores exceeding 0.5 are likely to be disordered. All four prediction tools strongly suggest that the central region of Gro is disordered, while the Q and WD-repeat domains are ordered.

disorder scores, while the Q and WD-repeat domains appear to be largely ordered. The same is true for all the mammalian Gro family proteins (data not shown). Thus, it seems that the absence of a well-ordered structure in the Gro central domains could lead to a high tolerance of single amino acid changes, thus explaining why lethal point mutations mapping to the GP, CcN, or SP domains have not been identified.

Proteins with regions of intrinsic disorder are not a rare phenomenon (Dunker *et al.*, 2005). In higher eukaryotes, the majority of proteins contain such domains. Many such proteins exist in dynamic ensembles of structural states, thus making structure determination difficult or impossible. Further, such domains often assume extended structures allowing them to contact their binding partners over a large binding surface thereby increasing binding specificity (Dunker *et al.*, 2005). Thus, instead of using large but compactly folded domains that bind only to a few targets, it may sometimes be more efficient to use unstructured domains that can bind to a multitude of proteins, and thereby function as hubs of large regulatory networks (Chouard, 2011; Dunker *et al.*, 2005). In the case of Gro, a disordered central region could account for the position of this protein as a "champion corepressor" (Shilo, 1998) by facilitating a large number of interactions.

While interactions involving disordered domains can be of high specificity, they are generally of low affinity. Such binding may be easily reversed upon posttranslational modification (Dunker *et al.*, 2005). This is in accord with findings showing that the Gro central region is a frequent target for regulation via covalent modification (see below).

## 3. The Regulation of Gro/TLE-Mediated Repression

Gro is not simply a static component of the nuclear machinery that must be present to allow repressors to function. Rather, it is intensively regulated and thus plays an important role in the interpretation of positional and temporal information during development. Mechanisms for regulating Gro function include (1) variation in the strength of the repressor/corepressor interaction; (2) interaction with naturally occurring truncated Gro family proteins; and (3) posttranslational modification of Gro/TLE (Fig. 3.4).

### 3.1. Affinity of the interaction between Gro/TLE and repressors

Gro/TLE function depends on the strength of the Gro/TLE-interaction motif in the repressor protein (Fig. 3.4A). The WD-repeat domain is the primary domain in Gro with responsibility for binding to DNA-bound

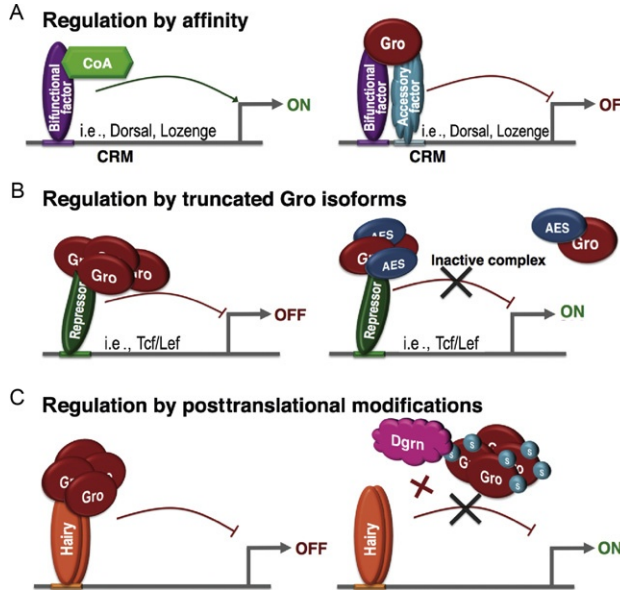


**Figure 3.4** The regulation of Gro/TLE-mediated repression. Gro/TLE function is regulated in a variety of ways. (A) Gro/TLE function depends on the affinity of the Gro/TLE-interaction motif in the repressor protein for Gro. The dual functionality of Lozenge and Dorsal relies on the fact that these two factors have an intrinsically low affinity for Gro. They therefore require assistance from accessory proteins to create a high-affinity platform for Gro/TLE recruitment. (B) The AES proteins, which consist only of the Q and GP domains, inhibit Gro/TLE-mediated transcriptional repression in a dominant negative manner perhaps by forming mixed oligomers with full-length Gro/TLE proteins through the Q domain, resulting in an inactive complex. (C) Gro/TLE is also regulated by posttranslational modification. For example, sumoylated Gro/TLE is targeted by the ubiquitin ligase Degringloade (Dgrn) for inactivation, thereby antagonizing Gro/TLE function. See text for references and details.

repressors. The high-resolution X-ray structure of the WD-repeat domain shows that it assumes a toroidal shape in which each repeat forms a four-stranded antiparallel β-sheet (Pickles *et al.*, 2002). Thus, the structure resembles a seven-bladed propeller, sometimes termed a β-propeller, a structure known to mediate many protein–protein interactions (Li and Roberts, 2001; Pickles *et al.*, 2002).

The β-propeller provides the binding site for two distinct short peptide sequences that, as mentioned previously, are often found in Gro-interacting repressors. These are the WRPW motif and the Engrailed homology-1 (eh1) motif (consensus sequence = FxIxxIL), found in a wide variety of Gro-dependent repressor proteins. Repressors that contain WRPW or its

variants include HES, Runt, Ripply1, Bowline, Huckebein, and Brinker, while proteins that contain eh1 motifs include Engrailed, Goosecoid, Pax, Six, Dorsal, Knirps, Slp1, and Hex (Andrioli *et al.*, 2004; Fisher *et al.*, 1996; Flores-Saaib *et al.*, 2001; Goldstein *et al.*, 1999; Jimenez *et al.*, 1997, 1999; Kawamura *et al.*, 2005; Kondow *et al.*, 2006; Paroush *et al.*, 1994; Payankaulam and Arnosti, 2009; Swingler *et al.*, 2004; Tolkunova *et al.*, 1998). Insight into the basis for the interaction between the β-propeller and these short motifs is provided by genetic and structural analysis of the WD-repeat domain bound to the peptides (Jennings *et al.*, 2006). Although the two motifs occupy overlapping sites across the β-propeller central pore, they bind in different conformations. The WRPW motif adopts a β-strand conformation that forms a tight hydrophobic plug, whereas the eh1 motif forms a short α helix (Jennings *et al.*, 2006).

Runt family members, which are involved in embryonic pattern formation, sex determination, eye patterning, and hematopoiesis, contain a motif similar to the WRPW sequence in which the C-terminal Trp is replaced with a Tyr (Aronson *et al.*, 1997; Canon and Banerjee, 2003). This change weakens binding, and as a result, the Runt family protein Lozenge can function as an activator or a repressor and repression depends on additional accessory proteins, such as Cut to assist with Gro recruitment (Fig. 3.4A) (Canon and Banerjee, 2003). In support of these ideas, replacing the C-terminal Tyr with Trp converted Lozenge into a dedicated repressor independent of the presence or absence of Cut (Canon and Banerjee, 2003).

How can a Trp to Tyr conversion lead to such a dramatic change in affinity for Gro/TLE? According to the crystal structure, all four residues of the WRPW motif are fully engaged by the WD-repeat domain, resulting in a strong hydrophobic interaction (Jennings *et al.*, 2006). This suggests that the phenolic hydroxyl group of a C-terminal tyrosine would be buried in the binding pocket, resulting in a loss of a hydrogen bond, consistent with decreased affinity of this motif (Jennings *et al.*, 2006).

The Rel family transcription factor, Dorsal, which directs dorsoventral embryonic patterning, provides another example of a factor in which the regulation of Gro affinity by accessory factors plays a critical role in repression. Dorsal lacks high-affinity Gro/TLE recruitment motifs but contains a highly degenerate and therefore weak eh1-like motif in its CTD that is required for Dorsal-mediated repression (Flores-Saaib *et al.*, 2001). The low-affinity nature of this motif seems to be essential for the ability of Dorsal to function as an activator of some targets and a repressor of others as Dorsal becomes a dedicated repressor when its eh1-like motif is replaced with a WRPW motif (Ratnaparkhi *et al.*, 2006).

The mechanism by which Gro converts Dorsal from an activator to a repressor has been characterized through studies of the *zen* gene. The *zen* locus harbors a CRM termed the ventral repression region, which contains multiple Dorsal binding sites, several of which are closely juxtaposed to sites

for the ARID-domain containing transcription factor Dead ringer (Dri) (Valentine *et al.*, 1998). Individually, Dorsal and Dri bind weakly to Gro but together form a high-affinity platform for Gro/TLE recruitment (Fig. 3.4A). Thus, if the Dri sites are mutated, Gro fails to bind and Dorsal functions as an activator rather than as a repressor.

## 3.2. Interactions with truncated Gro family proteins

In addition to full-length Gro/TLE family proteins, truncated members of this family termed amino-terminal enhancer of split (AES) family proteins are often found in vertebrate proteomes and also in the *C. elegans* proteome (Bajoghli, 2007; Beagle and Johnson, 2010; Flowers *et al.*, 2010; Li, 2000). Interactions between full-length Gro/TLE family proteins and their shorter relatives from the AES family may be another way to regulate Gro/TLE-mediated repression (Fig. 3.4B). The AES proteins, which consist only of the Q and GP region, were postulated to inhibit Gro/TLE-mediated transcriptional repression in a dominant negative manner by binding to Gro/TLE through the Q domain. Support for this idea comes from experiments in which coexpression of AES and Gro/TLE resulted in a four- to fivefold reduction of Gro/TLE-mediated repression by the Nkx repressor in COS-7 cells (Muhr *et al.*, 2001). Similarly, AES relieves repression by the Gro/TLE-dependent factor proline-rich homeodomain (PRH). Thus, the balance between full-length Gro/TLE family proteins and AES family proteins seems to be crucial for the proper developmental regulation of transcription (Swingler *et al.*, 2004).

How does this naturally occurring truncated form of Gro modulate Gro/TLE mediate repression? A possible answer to this question is suggested by a study showing that AES cannot bind to Rpd3/HDAC1 even though a truncated form of Gro/TLE containing just the Q and GP domains is able to bind this histone deacetylase. This suggests that the GP domain in AES may lack full functionality, and therefore, the Q domain-mediated interaction between Gro/TLE and AES could disrupt the function of the Gro/TLE oligomer (Brantjes *et al.*, 2001). In addition, since the Q domain of Gro/TLE interacts with some repressor proteins, including Tcf/Lef, AES may antagonize Gro/TLE-mediated repression by interacting directly with repressors (Brantjes *et al.*, 2001; Mallo *et al.*, 1993).

## 3.3. Regulation of Gro/TLE function by posttranslational modification

Posttranslational modification of transcription factors is an effective means by which developmental, metabolic, and mitogenic cues can modify gene expression in a rapid and reversible manner. Given that Gro/TLE functions in conjunction with many repressors in a myriad of developmental processes,

it represents an ideal candidate for achieving a coordinated transcriptional response. In accord with this view, many studies have demonstrated that Gro/TLE proteins are substrates for posttranslational modification, including phosphorylation, sumoylation, and poly(ADP-ribosyl)ation.

### 3.3.1. Gro/TLE phosphorylation

The Gro/TLE CcN and SP domains appear to be important targets for phosphorylation by a variety of Ser/Thr kinases. While phosphorylation of the CcN domain can be associated with either enhancement or inhibition of Gro-mediated repression, phosphorylation of the SP domain generally inhibits repression.

The CcN domain contains phosphoacceptor sites for casein kinase II (CK II) and the cyclin-dependent kinase family member cdc2 (Stifani *et al.*, 1992), and phosphorylation by both of these kinases modulates Gro/TLE function. For instance, pharmacological inhibition of cdc2 enhances Gro/TLE-mediated repression (Nuthall *et al.*, 2002b). In addition, the phosphorylation of Ser 239 in the CcN domain enhances Gro/TLE activity by increasing the affinity of Gro for HES family factors and chromatin (Nuthall *et al.*, 2002a, 2004). Further, this phosphorylation event is necessary for cofactor-activated phosphorylation in which Gro/TLE undergoes further phosphorylation as a consequence of its interaction with HES family factors (Buscarlet *et al.*, 2009; Nuthall *et al.*, 2002a, 2004).

The SP domain may function as a negative regulatory domain because phosphorylation of residues in this domain results in decreased Gro/TLE repression activity. For example, phosphorylation of a serine in the SP domain by homeodomain-interacting protein kinase 2 (HIPK2) decreases Gro/TLE-mediated repression by attenuating its binding to a DNA-bound repressor partner and by weakening the interaction between Gro/TLE and Rpd3/HDAC1 (Choi *et al.*, 1999, 2005; Lee *et al.*, 2009). However, these experiments were performed using triple point mutations, only two of which mapped to the SP region, and thus it is not clear from these studies if phosphorylation of any single residue in the SP domain modulates Gro-mediated repression.

The SP domain also contains one of two residues that are phosphorylated by mitogen-activated protein kinase (MAPK) in response to activation of the receptor tyrosine kinase (RTK)/Ras/MAPK signaling pathway, resulting in a decrease of Gro/TLE repressive activity (Cinnamon *et al.*, 2008; Hasson *et al.*, 2005). Although the mechanism by which phosphorylation of the SP domain reduces Gro activity is not clear, a clue may be provided by a study showing that mutation of a phosphoacceptor residue in the SP domain inhibited phosphorylation of Ser 239 in the CcN domain, indirectly resulting in weakened Gro/TLE chromatin association (Buscarlet *et al.*, 2009; Nuthall *et al.*, 2004). This suggests cross talk between the posttranslational modifications much like what is observed for histone tails (Berger, 2007).

It is becoming increasingly clear that downregulation of Gro by RTK/Ras/MAPK signaling plays critical roles in many aspects of development, including patterning of the nonsegmental termini in *Drosophila* embryos. Terminal patterning is directed by the gap genes *huckebein* (*hkb)* and *tailless* (*tll*), the expression of which is restricted to the embryonic termini by Gro through its interactions with the repressor Capicua (Cic) (Jimenez *et al.*, 2000; Paroush *et al.*, 1997). Terminal expression of *hkb* and *tll* depends on the Torso RTK, which works through the RTK/Ras/MAPK signal transduction pathway to alleviate Gro-mediated repression at the embryonic termini. While this depends in part on the signal-induced degradation of Cic, it also appears that direct phosphorylation of Gro itself attenuates Gro function thereby allowing terminal-specific expression of *hkb* and *tll*. Thus, once again Gro appears to have an active and instructional role in pattern formation (Astigarraga *et al.*, 2007; Cinnamon *et al.*, 2008).

It also appears that phosphorylation of Gro in response to RTK/Ras/MAPK signaling may provide a cellular memory of the RTK signal (Ajuria *et al.*, 2011; Cinnamon *et al.*, 2008; Helman *et al.*, 2011). While the phosphorylated (and therefore activated) state of MAPK can be short-lived, the phosphorylated form of Gro that results from the action of activated MAPK can be relatively stable. For example, the gene *intermediate neuroblasts defective* (*ind*) is initially activated in a portion of the presumptive ventral nerve cord by the epidermal growth factor receptor (EGFR), an RTK that signals via Ras and MAPK. This activation occurs, at least part, by the phosphorylation and resulting inactivation of Gro, which serves to keep *ind* off in the absence of the EGFR signal. Gro phosphorylation and therefore *ind* derepression are maintained for several hours after the end of EGFR signaling and resulting dephosphorylation of MAPK. Similar mechanisms appear to allow Gro phosphorylation to function as a memory for signaling via other RTKs, including Torso and fibroblast growth factor receptor (Helman *et al.*, 2011).

### 3.3.2. Other posttranslational modifications

Gro/TLE is also poly(ADP-ribosy)lated. This covalent modification, in which the enzyme poly(ADP-ribose) polymerase1 (PARP-1) transfers ADP-ribose units from $NAD^+$ onto glutamic acid residues of acceptor proteins, is involved in chromatin decondensation, DNA replication, and repair (Ju *et al.*, 2004). A study in rat neural stem cells not only revealed that Gro/TLE is in a protein complex consisting of PARP-1, nucleophosmin, nucleolin, topoisomerase IIb, and Rad50 but also that activation of PARP-1 by $Ca^{2+}$/calmodulin-dependent kinase II (CaMKIIδ) leads to poly(ADP-ribosy)lation of Gro/TLE, resulting in Gro/TLE dissociation from its repressor partner HES and the relief of repression of its target genes (Ju *et al.*, 2004).

Finally, Gro/TLE is also known to be sumoylated. A study in early fly embryos using mass spectrometry-based proteomics identified Gro/TLE as a conjugation target of the ubiquitin-like protein SUMO, but the biological relevance of this modification was unknown (Nie *et al.*, 2009). Since sumoylation often leads to downregulation of targets, this modification might inhibit Gro/TLE-mediated repression. Support for this idea comes from a recent study showing that sumoylated Gro/TLE is specifically inactivated by the ubiquitin ligase Degringloade (Dgrn) thereby antagonizing Gro/TLE function (Fig. 3.4C). Thus, Gro/TLE sumoylation followed by Dgrn-mediated inactivation may also serve as a molecular switch that regulates Gro recruitment in development (Abed *et al.*, 2011).

## 3.4. Gro as a mediator of interplay between signal transduction pathways

Gro/TLE proteins have roles in many signal transduction pathways in addition to the RTK/Ras/MAPK pathway discussed above (Cinnamon and Paroush, 2008). These include the Notch, decapentaplegic (Dpp), and Wnt/Wingless (Wg) pathways and thus Gro has the potential to mediate cross talk between the RTK/Ras/MAPK signal and these other pathways. Perhaps the best evidence for such interplay comes from studies of the Notch pathway.

Gro plays both negative and positive roles in transducing the Notch signal (Fig. 3.5A). In the absence of Notch signaling, Gro is recruited by the DNA-binding transcription factor Suppressor of Hairless (Su(H)) to Notch target genes such as the genes of the E(spl) complex. This recruitment is mediated by the adapter protein Hairless (H) and the resulting complex additionally includes the corepressor CtBP and leads to silencing of the Notch targets including E(spl) complex genes (Nagel *et al.*, 2005). Upon Notch activation, Notch is cleaved, and the Notch intracellular domain translocates to the nucleus and binds to Su(H). This interaction displaces the Gro/TLE-H-CtBP corepressor complex, resulting in the activation of E(spl) genes. As we have seen, these E(spl) factors are members of the HES family of bHLH domain-containing factors. They contain C-terminal WRPW motifs, by which they recruit Gro to repress proneural genes (Barolo *et al.*, 2002; Hasson and Paroush, 2006; Nagel *et al.*, 2005). Thus, in addition to antagonizing Notch signaling via interactions with Su(H), Gro cooperates with Notch signaling via interactions with E(spl) complex-encoded transcriptional repressors. As mentioned above, activation of RTK/Ras/MAPK signaling results in phosphorylated Gro, inhibiting its function as a repressor. As a result, Gro can mediate cross talk between the Notch and RTK/Ras/MAPK signaling pathways.

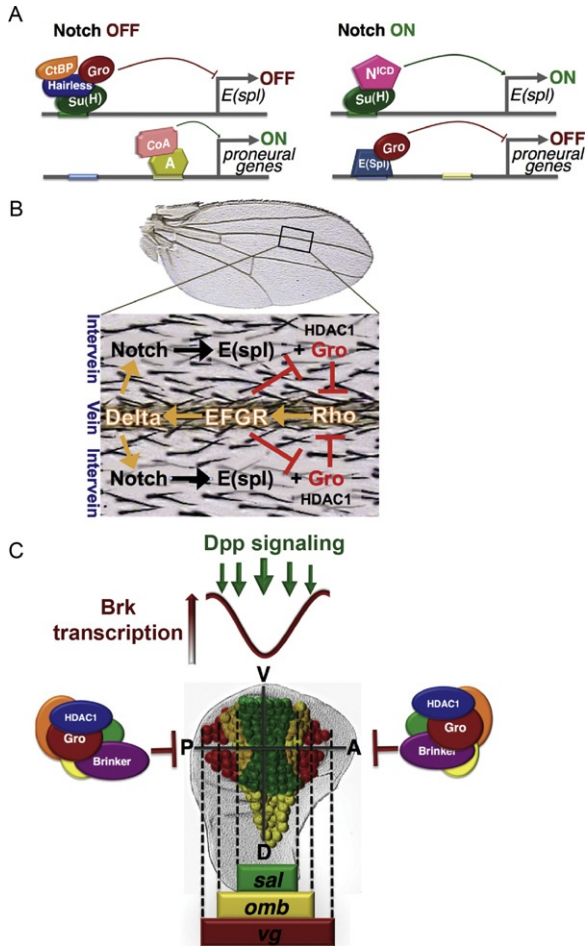


**Figure 3.5** Roles for Gro/TLE family proteins in signaling. (A) Gro plays multiple roles in Notch signaling, working both cooperatively and antagonistically with Notch. In the absence of Notch signaling, Gro is recruited by Suppressor of Hairless (Su(H)) to a corepressor complex at Notch target genes such as the genes of the E(spl) complex. Upon activation of Notch signaling, the Notch intracellular domain translocates to the nucleus displacing the Gro-containing complex from Su(H) and resulting in the activation of E(spl) complex genes. bHLH factors encoded by E(spl) then employ Gro as a corepressor to silence proneural genes. (B) Gro/Notch antagonism is required for wing veination. Wing vein specification is initiated by the activation of *rhomboid* (*rho*) in the wing disc in territories where the veins will develop (the provein region). This leads to activation of EGFR and therefore of the RTK/Ras/MAPK signaling pathway triggering expression of genes that lead to vein formation. (These so-called provein genes have been omitted from the diagram for simplicity). RTK/Ras/MAPK signaling also leads to expression of the Notch ligand Delta in the provein region, which signals to adjacent intervein cells. Notch signaling in the intervein region antagonizes wing veination via the Gro-dependent repression of *rho*, thereby preventing inappropriate expansion of

A good example of the interplay between RTK/Ras/MAPK and Notch signaling may be provided by the events that lead to formation of the *Drosophila* wing veins (Fig. 3.5B). Wing vein specification is initiated by the activation of *rhomboid* (*rho*) in the wing disc in territories where the veins will develop (Guichard *et al.*, 1999). The intramembrane protease encoded by *rho* is then responsible for the processing and activation of the EGFR ligand Spitz leading to the activation of the RTK/Ras/MAPK signaling pathway and the expression of provein genes. EGFR signaling within the provein region leads to expression of the Notch ligand Delta, which in turn results in Notch signaling in cells flanking the provein region (de Celis *et al.*, 1997). Notch signaling in the intervein region serves to antagonize wing veination and prevent inappropriate expansion of veins into the intervein region. As discussed above, Notch signaling requires Gro. Thus, by inactivating Gro, the RTK/Ras/MAPK signal in the provein region serves to prevent the Notch signal from spreading into the provein region, which would block normal wing vein formation. In support of this notion, mutations that convert the MAPK phosphoacceptor residues in Gro to Ala lead to vein loss, while mutation of these residues to phosphomimetic Asp residues leads to excess vein development (Hasson *et al.*, 2005). Finally, the ability of Gro to interfere with wing vein formation is blocked by histone deacetylase inhibitors reinforcing the notion that Gro functions via histone deacetylation (Winkler *et al.*, 2010).

Antagonism between Notch and RTK/Ras/MAPK signaling is not just limited to wing veination but is found in many other developmental contexts, and it is highly likely that Gro will play a role in mediating additional examples of such antagonism (Hasson and Paroush, 2006). Further, as mentioned above, Gro also plays roles in many other signaling pathways including the Wnt/Wg and Dpp pathways where it plays a negative role (Brantjes *et al.*, 2001; Cavallo *et al.*, 1998; Hasson *et al.*, 2001; Roose *et al.*, 1998). Thus, it is very likely that Gro is at the nexus of many signaling pathways thereby playing multiple essential roles in the coordination of signaling during development.

**veins into the intervein region. Gro phosphorylation by RTK/Ras/MAPK signaling in the provein region leads to Gro inactivation. Thus, the RTK/Ras/MAPK signal in the provein region prevents the Notch signal from spreading into the provein region and blocking normal wing vein formation. (C) Anteroposterior patterning in the developing wing results in large part from the repression of *brk* in response to the Dpp signal in the region surrounding the anteroposterior midline. Brk protein acts, in turn, as a Gro-dependent repressor to turn off the expression of genes such as *vg*, *omb*, and *sal* at the anterior and posterior edges of the developing wing. These Brk targets are responsive to different concentrations of Brk, thus leading to different size expression domains.**

## 4. A Final Example of Gro's Instructive Role in Development—Anteroposterior Patterning of the Wing

As the foregoing discussion has made clear, Gro has multiple instructive roles in development: It is actively involved in the interpretation of morphogen gradients and in the reception and interpretation of developmental signals. One final example of a developmental process in which Gro is intimately involved and which illustrates the role of this corepressor in signaling and in determining spatial and temporal boundaries of gene activity is the anteroposterior patterning of the wing imaginal disc as mediated by Dpp signaling (Fig. 3.5C).

*dpp* is expressed in a narrow band along the anteroposterior compartment boundary in the wing disc, from which its secreted protein product spreads toward the anterior and posterior edges of the disc (Muller *et al.*, 2003; Nellen *et al.*, 1996). The resulting Dpp morphogen gradient patterns the wing disc, in large part because the Dpp signal represses *brk* transcription in the region surrounding the midline. Brk acts, in turn, as a Gro-dependent repressor to silence the expression of genes, such as *spalt* (*sal*), *vestigial* (*vg*), and *optomotor blind* (*omb*), at the anterior and posterior edges of the developing wing (Hasson *et al.*, 2001; Sivasankaran *et al.*, 2000). The anteroposterior borders of these target gene expression domains vary since each target is sensitive to a different threshold concentration of Brk.

Once again, as is the case for interpretation of the Cic and Dorsal morphogen gradients, the evidence suggests that the threshold responses to Brk are critically dependent upon levels of Gro activity. At high enough concentrations of Gro, Brk will repress its targets all the way to the midline of the disc where Brk activity is extremely low (Fig. 3.6). Thus, regulatory processes that modulate Gro activity such as Gro phosphorylation and sumoylation could play critical roles in wing patterning by modulating threshold responses to Brk.

At this point, we can only speculate about how the activity of graded transcription factors such as Brk can be so sensitive to Gro concentration and activity levels. One possibility is suggested by the model discussed in the section on the mechanism of Gro-mediated repression in which it was proposed that Gro spreads along chromatin to establish large transcriptionally silent domains. Perhaps these large domains represent cooperative units, the stability of which could be exquisitely sensitive to Gro concentration, thus accounting for the ability of Gro to play an important instructive role in development.

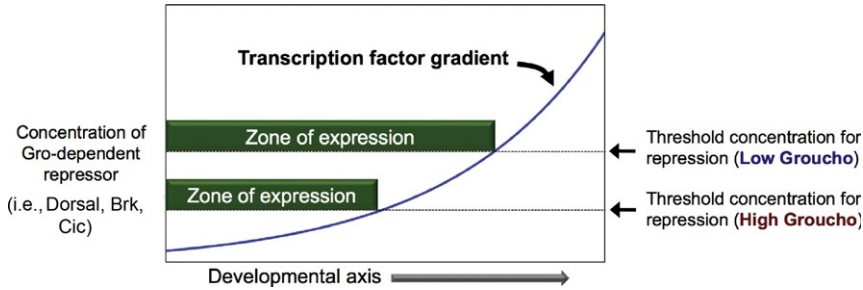


**Figure 3.6** Gro/TLE plays an active role in transcription factor gradient interpretation. Gro/TLE plays a critical role in determining the threshold response of genes to transcription factor gradients. Affinity of a repressor for its binding site along with Gro/TLE activity levels determines the height of a threshold response. When Gro/TLE activity levels are low, higher expression levels of the graded transcription factor is needed to generate repression, whereas when Gro/TLE levels are high, the threshold transcription factor concentration required for repression is lower.

## 5. Concluding Remarks

In conclusion, while early studies on Gro focused on its role as a "universal corepressor" that simply had to be present to allow repression to occur, it now appears that Gro plays an extremely active role in development. Its levels and activity are precisely regulated by multiple mechanisms and such recognition is critical in development. In accord with these conclusions, misregulation of Gro/TLE family members in humans is often linked to cancer, including cervical, colon, lung, brain, pituitary gland, and skin cancers (Allander *et al.*, 2002; Allen *et al.*, 2006; Buscarlet and Stifani, 2007; Rorive *et al.*, 2006; Ruebel *et al.*, 2006; Terry *et al.*, 2007). Moreover, *in vivo* studies show that overexpression of Gro/TLE in transgenic mice induces lung adenocarcinoma (Allen *et al.*, 2006). This is likely because many of the pathways and factors that interact with Gro/TLE have oncogenic properties, including the Wg/Wnt pathway (colorectal cancer), the Notch pathway (acute lymphocytic leukemia), and Runt (acute myeloid leukemia) (Bienz and Clevers, 2000; Lund and van Lohuizen, 2002; Lutterbach *et al.*, 2000; Morin, 1999; Weng *et al.*, 2004; Yamagata *et al.*, 2005). As a result, precisely regulated levels of Gro/TLE activity are essential for normal growth and development, and the illumination of the mechanisms of repression by Gro/TLE may lead to a better understanding of the events in tumorigenesis.

## ACKNOWLEDGMENTS

We thank our colleagues in the Courey lab and in the field for many stimulating discussions regarding the mechanisms and regulation of developmental control by Groucho. This work was partially supported by NIH grant GM44522 to A. J. C. and National Research Service Award GM86122 to W. T. J.

## REFERENCES


Abed, M., Barry, K. C., Kenyagin, D., *et al.* (2011). Degringolade, a SUMO-targeted ubiquitin ligase, inhibits Hairy/Groucho-mediated repression. *EMBO J.* **30,** 1289–1301.

Ajuria, L., Nieva, C., Winkler, C., *et al.* (2011). Capicua DNA-binding sites are general response elements for RTK signaling in Drosophila. *Development* **138,** 915–924.

Allander, S. V., Illei, P. B., Chen, Y., *et al.* (2002). Expression profiling of synovial sarcoma by cDNA microarrays: Association of ERBB2, IGFBP2, and ELF3 with epithelial differentiation. *Am. J. Pathol.* **161,** 1587–1595.

Allen, T., van Tuyl, M., Iyengar, P., *et al.* (2006). Grg1 acts as a lung-specific oncogene in a transgenic mouse model. *Cancer Res.* **66,** 1294–1301.

Andrioli, L. P., Oberstein, A. L., Corado, M. S., *et al.* (2004). Groucho-dependent repression by sloppy-paired 1 differentially positions anterior pair-rule stripes in the Drosophila embryo. *Dev. Biol.* **276,** 541–551.

Arnosti, D. N. (2004). Multiple mechanisms of transcriptional repression in eukaryotes. *Handb. Exp. Pharmacol.* **66,** 33–67.

Aronson, B. D., Fisher, A. L., Blechman, K., *et al.* (1997). Groucho-dependent and -independent repression activities of Runt domain proteins. *Mol. Cell. Biol.* **17,** 5581–5587.

Astigarraga, S., Grossman, R., Diaz-Delfin, J., *et al.* (2007). A MAPK docking site is critical for downregulation of Capicua by Torso and EGFR RTK signaling. *EMBO J.* **26,** 668–677.

Bajoghli, B. (2007). Evolution of the Groucho/Tle gene family: Gene organization and duplication events. *Dev. Genes Evol.* **217,** 613–618.

Bajoghli, B., Aghaallaei, N., Soroldoni, D., *et al.* (2007). The roles of Groucho/Tle in left-right asymmetry and Kupffer's vesicle organogenesis. *Dev. Biol.* **303,** 347–361.

Barolo, S., Stone, T., Bang, A. G., *et al.* (2002). Default repression and Notch signaling: Hairless acts as an adaptor to recruit the corepressors Groucho and dCtBP to Suppressor of Hairless. *Genes Dev.* **16,** 1964–1976.

Beagle, B., and Johnson, G. V. (2010). AES/GRG5: More than just a dominant-negative TLE/GRG family member. *Dev. Dyn.* **239,** 2795–2805.

Berger, S. L. (2007). The complex language of chromatin regulation during transcription. *Nature* **447,** 407–412.

Berk, A. J. (1999). Activation of RNA polymerase II transcription. *Curr. Opin. Cell Biol.* **11,** 330–335.

Bienz, M., and Clevers, H. (2000). Linking colorectal cancer to Wnt signaling. *Cell* **103,** 311–320.

Brantjes, H., Roose, J., van De Wetering, M., *et al.* (2001). All Tcf HMG box transcription factors interact with Groucho-related co-repressors. *Nucleic Acids Res.* **29,** 1410–1419.

Buchberger, J. R., Onishi, M., Li, G., *et al.* (2008). Sir3-nucleosome interactions in spreading of silent chromatin in Saccharomyces cerevisiae. *Mol. Cell. Biol.* **28,** 6903–6918.

Burks, P. J., Isaacs, H. V., and Pownall, M. E. (2009). FGF signalling modulates transcriptional repression by Xenopus groucho-related-4. *Biol. Cell* **101,** 301–308.

Buscarlet, M., and Stifani, S. (2007). The 'Marx' of Groucho on development and disease. *Trends Cell Biol.* **17,** 353–361.

Buscarlet, M., Hermann, R., Lo, R., *et al.* (2009). Cofactor-activated phosphorylation is required for inhibition of cortical neuron differentiation by Groucho/TLE1. *PLoS One* **4,** e8107.

Cai, H. N., Arnosti, D. N., and Levine, M. (1996). Long-range repression in the Drosophila embryo. *Proc. Natl. Acad. Sci. USA* **93,** 9309–9314.

Cai, Y., Brophy, P. D., Levitan, I., *et al.* (2003). Groucho suppresses Pax2 transactivation by inhibition of JNK-mediated phosphorylation. *EMBO J.* **22,** 5522–5529.

Canon, J., and Banerjee, U. (2003). In vivo analysis of a developmental circuit for direct transcriptional activation and repression in the same cell by a Runx protein. *Genes Dev.* **17,** 838–843.

Cavallo, R. A., Cox, R. T., Moline, M. M., *et al.* (1998). Drosophila Tcf and Groucho interact to repress Wingless signalling activity. *Nature* **395,** 604–608.
Chen, G., and Courey, A. J. (2000). Groucho/TLE family proteins and transcriptional repression. *Gene* **249,** 1–16.
Chen, G., Nguyen, P. H., and Courey, A. J. (1998). A role for Groucho tetramerization in transcriptional repression. *Mol. Cell. Biol.* **18,** 7259–7268.
Chen, G., Fernandez, J., Mische, S., *et al.* (1999). A functional interaction between the histone deacetylase Rpd3 and the corepressor groucho in Drosophila development. *Genes Dev.* **13,** 2218–2230.
Choi, C. Y., Kim, Y. H., Kwon, H. J., *et al.* (1999). The homeodomain protein NK-3 recruits Groucho and a histone deacetylase complex to repress transcription. *J. Biol. Chem.* **274,** 33194–33197.
Choi, C. Y., Kim, Y. H., Kim, Y. O., *et al.* (2005). Phosphorylation by the DHIPK2 protein kinase modulates the corepressor activity of Groucho. *J. Biol. Chem.* **280,** 21427–21436.
Chouard, T. (2011). Structural biology: Breaking the protein rules. *Nature* **471,** 151–153.
Choudhury, B. K., Kim, J., Kung, H. F., *et al.* (1997). Cloning and developmental expression of Xenopus cDNAs encoding the Enhancer of split groucho and related proteins. *Gene* **195,** 41–48.
Cinnamon, E., and Paroush, Z. (2008). Context-dependent regulation of Groucho/TLE-mediated repression. *Curr. Opin. Genet. Dev.* **18,** 435–440.
Cinnamon, E., Helman, A., Ben-Haroush Schyr, R., *et al.* (2008). Multiple RTK pathways downregulate Groucho-mediated repression in Drosophila embryogenesis. *Development* **135,** 829–837.
Courey, A. J., and Jia, S. (2001). Transcriptional repression: The long and the short of it. *Genes Dev.* **15,** 2786–2796.
Dawson, S. R., Turner, D. L., Weintraub, H., *et al.* (1995). Specificity for the hairy/enhancer of split basic helix-loop-helix (bHLH) proteins maps outside the bHLH domain and suggests two separable modes of transcriptional repression. *Mol. Cell. Biol.* **15,** 6923–6931.
de Celis, J. F., Bray, S., and Garcia-Bellido, A. (1997). Notch signalling regulates veinlet expression and establishes boundaries between veins and interveins in the Drosophila wing. *Development* **124,** 1919–1928.
Delidakis, C., Preiss, A., Hartley, D. A., *et al.* (1991). Two genetically and molecularly distinct functions involved in early neurogenesis reside within the Enhancer of split locus of Drosophila melanogaster. *Genetics* **129,** 803–823.
Dubnicoff, T., Valentine, S. A., Chen, G., *et al.* (1997). Conversion of dorsal from an activator to a repressor by the global corepressor Groucho. *Genes Dev.* **11,** 2952–2957.
Dunker, A. K., Cortese, M. S., Romero, P., *et al.* (2005). Flexible nets. The roles of intrinsic disorder in protein interaction networks. *FEBS J.* **272,** 5129–5148.
Eberhard, D., Jimenez, G., Heavey, B., *et al.* (2000). Transcriptional repression by Pax5 (BSAP) through interaction with corepressors of the Groucho family. *EMBO J.* **19,** 2292–2303.
Edmondson, D. G., and Roth, S. Y. (1998). Interactions of transcriptional regulators with histones. *Methods* **15,** 355–364.
Edmondson, D. G., Smith, M. M., and Roth, S. Y. (1996). Repression domain of the yeast global repressor Tup1 interacts directly with histones H3 and H4. *Genes Dev.* **10,** 1247–1259.
Edmondson, D. G., Zhang, W., Watson, A., *et al.* (1998). In vivo functions of histone acetylation/deacetylation in Tup1p repression and Gcn5p activation. *Cold Spring Harb. Symp. Quant. Biol.* **63,** 459–468.
Fisher, A. L., and Caudy, M. (1998). Groucho proteins: Transcriptional corepressors for specific subsets of DNA-binding transcription factors in vertebrates and invertebrates. *Genes Dev.* **12,** 1931–1940.

Fisher, A. L., Ohsako, S., and Caudy, M. (1996). The WRPW motif of the hairy-related basic helix-loop-helix repressor proteins acts as a 4-amino-acid transcription repression and protein-protein interaction domain. *Mol. Cell. Biol.* **16,** 2670–2677.

Flores-Saaib, R. D., and Courey, A. J. (2000). Analysis of Groucho-histone interactions suggests mechanistic similarities between Groucho- and Tup1-mediated repression. *Nucleic Acids Res.* **28,** 4189–4196.

Flores-Saaib, R. D., Jia, S., and Courey, A. J. (2001). Activation and repression by the C-terminal domain of Dorsal. *Development* **128,** 1869–1879.

Flowers, E. B., Poole, R. J., Tursun, B., *et al.* (2010). The Groucho ortholog UNC-37 interacts with the short Groucho-like protein LSY-22 to control developmental decisions in C. elegans. *Development* **137,** 1799–1805.

Gao, X., Chandra, T., Gratton, M. O., *et al.* (2001). HES6 acts as a transcriptional repressor in myoblasts and can induce the myogenic differentiation program. *J. Cell Biol.* **154,** 1161–1171.

Gasperowicz, M., and Otto, F. (2005). Mammalian Groucho homologs: Redundancy or specificity? *J. Cell. Biochem.* **95,** 670–687.

Goldstein, R. E., Jimenez, G., Cook, O., *et al.* (1999). Huckebein repressor activity in Drosophila terminal patterning is mediated by Groucho. *Development* **126,** 3747–3755.

Gray, S., and Levine, M. (1996a). Short-range transcriptional repressors mediate both quenching and direct repression within complex loci in Drosophila. *Genes Dev.* **10,** 700–710.

Gray, S., and Levine, M. (1996b). Transcriptional repression in development. *Curr. Opin. Cell Biol.* **8,** 358–364.

Grbavec, D., and Stifani, S. (1996). Molecular interaction between TLE1 and the carboxyl-terminal domain of HES-1 containing the WRPW motif. *Biochem. Biophys. Res. Commun.* **223,** 701–705.

Grbavec, D., Lo, R., Liu, Y., *et al.* (1998). Transducin-like Enhancer of split 2, a mammalian homologue of Drosophila Groucho, acts as a transcriptional repressor, interacts with Hairy/Enhancer of split proteins, and is expressed during neuronal development. *Eur. J. Biochem.* **258,** 339–349.

Gromoller, A., and Lehming, N. (2000). Srb7p is a physical and physiological target of Tup1p. *EMBO J.* **19,** 6845–6852.

Guichard, A., Biehs, B., Sturtevant, M. A., *et al.* (1999). rhomboid and Star interact synergistically to promote EGFR/MAPK signaling during Drosophila wing vein development. *Development* **126,** 2663–2676.

Hasson, P., and Paroush, Z. (2006). Crosstalk between the EGFR and other signalling pathways at the level of the global transcriptional corepressor Groucho/TLE. *Br. J. Cancer* **94,** 771–775.

Hasson, P., Muller, B., Basler, K., *et al.* (2001). Brinker requires two corepressors for maximal and versatile repression in Dpp signalling. *EMBO J.* **20,** 5725–5736.

Hasson, P., Egoz, N., Winkler, C., *et al.* (2005). EGFR signaling attenuates Groucho-dependent repression to antagonize Notch transcriptional output. *Nat. Genet.* **37,** 101–105.

Hecht, A., Laroche, T., Strahl-Bolsinger, S., *et al.* (1995). Histone H3 and H4 N-termini interact with SIR3 and SIR4 proteins: A molecular model for the formation of heterochromatin in yeast. *Cell* **80,** 583–592.

Helman, A., Cinnamon, E., Mezuman, S., *et al.* (2011). Phosphorylation of Groucho mediates RTK feedback inhibition and prolonged pathway target gene expression. *Curr. Biol.* **21,** 1102–1110.

Hoppe, G. J., Tanny, J. C., Rudner, A. D., *et al.* (2002). Steps in assembly of silent chromatin in yeast: Sir3-independent binding of a Sir2/Sir4 complex to silencers and role for Sir2-dependent deacetylation. *Mol. Cell. Biol.* **22,** 4167–4180.

Huang, Y. (2002). Transcriptional silencing in Saccharomyces cerevisiae and Schizosaccharomyces pombe. *Nucleic Acids Res.* **30,** 1465–1482.

Imai, Y., Kurokawa, M., Tanaka, K., *et al.* (1998). TLE, the human homolog of groucho, interacts with AML1 and acts as a repressor of AML1-induced transactivation. *Biochem. Biophys. Res. Commun.* **252,** 582–589.

Jan, Y., Matter, M., Pai, J. T., *et al.* (2004). A mitochondrial protein, Bit1, mediates apoptosis regulated by integrins and Groucho/TLE corepressors. *Cell* **116,** 751–762.

Jennings, B. H., and Ish-Horowicz, D. (2008). The Groucho/TLE/Grg family of transcriptional co-repressors. *Genome Biol.* **9,** 205.

Jennings, B. H., Pickles, L. M., Wainwright, S. M., *et al.* (2006). Molecular recognition of transcriptional repressor motifs by the WD domain of the Groucho/TLE corepressor. *Mol. Cell* **22,** 645–655.

Jennings, B. H., Wainwright, S. M., and Ish-Horowicz, D. (2008). Differential in vivo requirements for oligomerization during Groucho-mediated repression. *EMBO Rep.* **9,** 76–83.

Jimenez, G., Paroush, Z., and Ish-Horowicz, D. (1997). Groucho acts as a corepressor for a subset of negative regulators, including Hairy and Engrailed. *Genes Dev.* **11,** 3072–3082.

Jimenez, G., Verrijzer, C. P., and Ish-Horowicz, D. (1999). A conserved motif in goosecoid mediates groucho-dependent repression in Drosophila embryos. *Mol. Cell. Biol.* **19,** 2080–2087.

Jimenez, G., Guichet, A., Ephrussi, A., *et al.* (2000). Relief of gene repression by torso RTK signaling: Role of capicua in Drosophila terminal and dorsoventral patterning. *Genes Dev.* **14,** 224–231.

Ju, B. G., Solum, D., Song, E. J., *et al.* (2004). Activating the PARP-1 sensor component of the groucho/TLE1 corepressor complex mediates a CaMKinase IIdelta-dependent neurogenic gene activation pathway. *Cell* **119,** 815–829.

Kawamura, A., Koshida, S., Hijikata, H., *et al.* (2005). Groucho-associated transcriptional repressor ripply1 is required for proper transition from the presomitic mesoderm to somites. *Dev. Cell* **9,** 735–744.

Kondow, A., Hitachi, K., Ikegame, T., *et al.* (2006). Bowline, a novel protein localized to the presomitic mesoderm, interacts with Groucho/TLE in Xenopus. *Int. J. Dev. Biol.* **50,** 473–479.

Kornberg, R. D. (2005). Mediator and the mechanism of transcriptional activation. *Trends Biochem. Sci.* **30,** 235–239.

Kuchin, S., and Carlson, M. (1998). Functional relationships of Srb10-Srb11 kinase, carboxy-terminal domain kinase CTDK-I, and transcriptional corepressor Ssn6-Tup1. *Mol. Cell. Biol.* **18,** 1163–1171.

Kuo, D., Nie, M., De Hoff, P., *et al.* (2011). A SUMO-Groucho Q domain fusion protein: Characterization and in vivo Ulp1-mediated cleavage. *Protein Expr. Purif.* **76,** 65–71.

Lee, W., Andrews, B. C., Faust, M., *et al.* (2009). Hipk is an essential protein that promotes Notch signal transduction in the Drosophila eye by inhibition of the global co-repressor Groucho. *Dev. Biol.* **325,** 263–272.

Li, S. S. (2000). Structure and function of the Groucho gene family and encoded transcriptional corepressor proteins from human, mouse, rat, Xenopus, Drosophila and nematode. *Proc. Natl. Sci. Counc. Republ. Chin. B* **24,** 47–55.

Li, L. M., and Arnosti, D. N. (2011). Long- and short-range transcriptional repressors induce distinct chromatin states on repressed genes. *Curr. Biol.* **21,** 406–412.

Li, D., and Roberts, R. (2001). WD-repeat proteins: Structure characteristics, biological function, and their involvement in human diseases. *Cell. Mol. Life Sci.* **58,** 2085–2097.

Li, X., Romero, P., Rani, M., *et al.* (1999). Predicting protein disorder for N-, C-, and internal regions. *Genome Inform. Ser. Workshop Genome Inform.* **10,** 30–40.

Linderson, Y., Eberhard, D., Malin, S., *et al.* (2004). Corecruitment of the Grg4 repressor by PU.1 is critical for Pax5-mediated repression of B-cell-specific genes. *EMBO Rep.* **5,** 291–296.

Lindsley, D. L., and Grell, E. H. (1968). Genetic Variations of *Drosophila melanogaster. Carnegie Institution of Washington Publication* **627**.

Liu, Z., and Karmarkar, V. (2008). Groucho/Tup1 family co-repressors in plant development. *Trends Plant Sci.* **13,** 137–144.

Lund, A. H., and van Lohuizen, M. (2002). RUNX: A trilogy of cancer genes. *Cancer Cell* **1,** 213–215.

Lutterbach, B., Westendorf, J. J., Linggi, B., *et al.* (2000). A mechanism of repression by acute myeloid leukemia-1, the target of multiple chromosomal translocations in acute leukemia. *J. Biol. Chem.* **275,** 651–656.

Malave, T. M., and Dent, S. Y. (2006). Transcriptional repression by Tup1-Ssn6. *Biochem. Cell Biol.* **84,** 437–443.

Malik, S., and Roeder, R. G. (2010). The metazoan Mediator co-activator complex as an integrative hub for transcriptional regulation. *Nat. Rev. Genet.* **11,** 761–772.

Mallo, M., Franco del Amo, F., and Gridley, T. (1993). Cloning and developmental expression of Grg, a mouse gene related to the groucho transcript of the Drosophila Enhancer of split complex. *Mech. Dev.* **42,** 67–76.

Mannervik, M., and Levine, M. (1999). The Rpd3 histone deacetylase is required for segmentation of the Drosophila embryo. *Proc. Natl. Acad. Sci. USA* **96,** 6797–6801.

Mannervik, M., Nibu, Y., Zhang, H., *et al.* (1999). Transcriptional coregulators in development. *Science* **284,** 606–609.

Martinez, C. A., and Arnosti, D. N. (2008). Spreading of a corepressor linked to action of long-range repressor hairy. *Mol. Cell. Biol.* **28,** 2792–2802.

Miyasaka, H., Choudhury, B. K., Hou, E. W., *et al.* (1993). Molecular cloning and expression of mouse and human cDNA encoding AES and ESG proteins with strong similarity to Drosophila enhancer of split groucho protein. *Eur. J. Biochem.* **216,** 343–352.

Morin, P. J. (1999). Beta-catenin signaling and cancer. *Bioessays* **21,** 1021–1030.

Muhr, J., Andersson, E., Persson, M., *et al.* (2001). Groucho-mediated transcriptional repression establishes progenitor cell pattern and neuronal fate in the ventral neural tube. *Cell* **104,** 861–873.

Muller, B., Hartmann, B., Pyrowolakis, G., *et al.* (2003). Conversion of an extracellular Dpp/BMP morphogen gradient into an inverse transcriptional gradient. *Cell* **113,** 221–233.

Nagel, A. C., Krejci, A., Tenin, G., *et al.* (2005). Hairless-mediated repression of notch target genes requires the combined activity of Groucho and CtBP corepressors. *Mol. Cell. Biol.* **25,** 10433–10441.

Nakayama, H., Liu, Y., Stifani, S., *et al.* (1997). Developmental restriction of Mash-2 expression in trophoblast correlates with potential activation of the notch-2 pathway. *Dev. Genet.* **21,** 21–30.

Nellen, D., Burke, R., Struhl, G., *et al.* (1996). Direct and long-range action of a DPP morphogen gradient. *Cell* **85,** 357–368.

Nie, M., Xie, Y., Loo, J. A., *et al.* (2009). Genetic and proteomic evidence for roles of Drosophila SUMO in cell cycle control, Ras signaling, and early pattern formation. *PLoS One* **4,** e5905.

Nuthall, H. N., Husain, J., McLarren, K. W., *et al.* (2002a). Role for Hes1-induced phosphorylation in Groucho-mediated transcriptional repression. *Mol. Cell. Biol.* **22,** 389–399.

Nuthall, H. N., Joachim, K., Palaparti, A., *et al.* (2002b). A role for cell cycle-regulated phosphorylation in Groucho-mediated transcriptional repression. *J. Biol. Chem.* **277,** 51049–51057.

Nuthall, H. N., Joachim, K., and Stifani, S. (2004). Phosphorylation of serine 239 of Groucho/TLE1 by protein kinase CK2 is important for inhibition of neuronal differentiation. *Mol. Cell. Biol.* **24,** 8395–8407.

Palaparti, A., Baratz, A., and Stifani, S. (1997). The Groucho/transducin-like enhancer of split transcriptional repressors interact with the genetically defined amino-terminal silencing domain of histone H3. *J. Biol. Chem.* **272,** 26604–26610.

Papamichos-Chronakis, M., Conlan, R. S., Gounalaki, N., *et al.* (2000). Hrs1/Med3 is a Cyc8-Tup1 corepressor target in the RNA polymerase II holoenzyme. *J. Biol. Chem.* **275,** 8397–8403.

Paroush, Z., Finley, R. L., Jr., Kidd, T., *et al.* (1994). Groucho is required for Drosophila neurogenesis, segmentation, and sex determination and interacts directly with hairy-related bHLH proteins. *Cell* **79,** 805–815.

Paroush, Z., Wainwright, S. M., and Ish-Horowicz, D. (1997). Torso signalling regulates terminal patterning in Drosophila by antagonising Groucho-mediated repression. *Development* **124,** 3827–3834.

Payankaulam, S., and Arnosti, D. N. (2009). Groucho corepressor functions as a cofactor for the Knirps short-range transcriptional repressor. *Proc. Natl. Acad. Sci. USA* **106,** 17314–17319.

Payankaulam, S., Li, L. M., and Arnosti, D. N. (2010). Transcriptional repression: Conserved and evolved features. *Curr. Biol.* **20,** R764–R771.

Pflugrad, A., Meir, J. Y., Barnes, T. M., *et al.* (1997). The Groucho-like transcription factor UNC-37 functions with the neural specificity gene unc-4 to govern motor neuron identity in C. elegans. *Development* **124,** 1699–1709.

Pickles, L. M., Roe, S. M., Hemingway, E. J., *et al.* (2002). Crystal structure of the C-terminal WD40 repeat domain of the human Groucho/TLE1 transcriptional corepressor. *Structure* **10,** 751–761.

Pinto, M., and Lobe, C. G. (1996). Products of the grg (Groucho-related gene) family can dimerize through the amino-terminal Q domain. *J. Biol. Chem.* **271,** 33026–33031.

Radivojac, P., Obradovic, Z., Brown, C. J., *et al.* (2003). Prediction of boundaries between intrinsically ordered and disordered protein regions. *Pac. Symp. Biocomput.* **8,** 216–227.

Radman-Livaja, M., Ruben, G., Weiner, A., *et al.* (2011). Dynamics of Sir3 spreading in budding yeast: Secondary recruitment sites and euchromatic localization. *EMBO J.* **30,** 1012–1026.

Ratnaparkhi, G. S., Jia, S., and Courey, A. J. (2006). Uncoupling dorsal-mediated activation from dorsal-mediated repression in the Drosophila embryo. *Development* **133,** 4409–4414.

Redd, M. J., Arnaud, M. B., and Johnson, A. D. (1997). A complex composed of tup1 and ssn6 represses transcription in vitro. *J. Biol. Chem.* **272,** 11193–11197.

Romero, P., Obradovic, Z., and Dunker, K. (1997). Sequence data analysis for long disordered regions prediction in the calcineurin family. *Genome Inform. Ser. Workshop Genome Inform.* **8,** 110–124.

Romero, P., Obradovic, Z., Li, X., *et al.* (2001). Sequence complexity of disordered protein. *Proteins* **42,** 38–48.

Roose, J., Molenaar, M., Peterson, J., *et al.* (1998). The Xenopus Wnt effector XTcf-3 interacts with Groucho-related transcriptional repressors. *Nature* **395,** 608–612.

Rorive, S., Maris, C., Debeir, O., *et al.* (2006). Exploring the distinctive biological characteristics of pilocytic and low-grade diffuse astrocytomas using microarray gene expression profiles. *J. Neuropathol. Exp. Neurol.* **65,** 794–807.

Ruebel, K. H., Leontovich, A. A., Jin, L., *et al.* (2006). Patterns of gene expression in pituitary carcinomas and adenomas analyzed by high-density oligonucleotide arrays, reverse transcriptase-quantitative PCR, and protein expression. *Endocrine* **29,** 435–444.

Rusche, L. N., Kirchmaier, A. L., and Rine, J. (2002). Ordered nucleation and spreading of silenced chromatin in Saccharomyces cerevisiae. *Mol. Biol. Cell* **13,** 2207–2222.

Schmidt, C. J., and Sladek, T. E. (1993). A rat homolog of the Drosophila enhancer of split (groucho) locus lacking WD-40 repeats. *J. Biol. Chem.* **268,** 25681–25686.

Sekiya, T., and Zaret, K. S. (2007). Repression by Groucho/TLE/Grg proteins: Genomic site recruitment generates compacted chromatin in vitro and impairs activator binding in vivo. *Mol. Cell* **28,** 291–303.

Sharief, F. S., Tsoi, S. C., and Li, S. S. (1997). cDNA cloning and genomic organization of enhancer of split groucho gene from nematode Caenorhabditis elegans. *Biochem. Mol. Biol. Int.* **43,** 327–337.

Shilo, B. Z. (1998). Flies over Crete: Drosophila molecular biology. Kolymbari, Crete, July 12–18, 1998. *EMBO J.* **17,** 6769–6771.

Sivasankaran, R., Vigano, M. A., Muller, B., *et al.* (2000). Direct transcriptional control of the Dpp target omb by the DNA binding protein Brinker. *EMBO J.* **19,** 6162–6172.

Song, H., Hasson, P., Paroush, Z., *et al.* (2004). Groucho oligomerization is required for repression in vivo. *Mol. Cell. Biol.* **24,** 4341–4350.

Stifani, S., Blaumueller, C. M., Redhead, N. J., *et al.* (1992). Human homologs of a Drosophila Enhancer of split gene product define a novel family of nuclear proteins. *Nat. Genet.* **2,** 119–127.

Swingler, T. E., Bess, K. L., Yao, J., *et al.* (2004). The proline-rich homeodomain protein recruits members of the Groucho/Transducin-like enhancer of split protein family to co-repress transcription in hematopoietic cells. *J. Biol. Chem.* **279,** 34938–34947.

Terry, J., Saito, T., Subramanian, S., *et al.* (2007). TLE1 as a diagnostic immunohistochemical marker for synovial sarcoma emerging from gene expression profiling studies. *Am. J. Surg. Pathol.* **31,** 240–246.

Thirunavukkarasu, K., Mahajan, M., McLarren, K. W., *et al.* (1998). Two domains unique to osteoblast-specific transcription factor Osf2/Cbfa1 contribute to its transactivation function and its inability to heterodimerize with Cbfbeta. *Mol. Cell. Biol.* **18,** 4197–4208.

Tolkunova, E. N., Fujioka, M., Kobayashi, M., *et al.* (1998). Two distinct types of repression domain in engrailed: One interacts with the groucho corepressor and is preferentially active on integrated target genes. *Mol. Cell. Biol.* **18,** 2804–2814.

Treitel, M. A., and Carlson, M. (1995). Repression by SSN6-TUP1 is directed by MIG1, a repressor/activator protein. *Proc. Natl. Acad. Sci. USA* **92,** 3132–3136.

Tzamarias, D., and Struhl, K. (1995). Distinct TPR motifs of Cyc8 are involved in recruiting the Cyc8-Tup1 corepressor complex to differentially regulated promoters. *Genes Dev.* **9,** 821–831.

Valentine, S. A., Chen, G., Shandala, T., *et al.* (1998). Dorsal-mediated repression requires the formation of a multiprotein repression complex at the ventral silencer. *Mol. Cell. Biol.* **18,** 6584–6594.

Villanueva, C. J., Waki, H., Godio, C., *et al.* (2011). TLE3 is a dual-function transcriptional coregulator of adipogenesis. *Cell Metab.* **13,** 413–427.

Weng, A. P., Ferrando, A. A., Lee, W., *et al.* (2004). Activating mutations of NOTCH1 in human T cell acute lymphoblastic leukemia. *Science* **306,** 269–271.

Winkler, C. J., Ponce, A., and Courey, A. J. (2010). Groucho-mediated repression may result from a histone deacetylase-dependent increase in nucleosome density. *PLoS One* **5,** e10166.

Xue, B., Dunbrack, R. L., Williams, R. W., *et al.* (2010). PONDR-FIT: A meta-predictor of intrinsically disordered amino acids. *Biochim. Biophys. Acta* **1804,** 996–1010.

Yamagata, T., Maki, K., and Mitani, K. (2005). Runx1/AML1 in normal and abnormal hematopoiesis. *Int. J. Hematol.* **82,** 1–8.

Yao, J., Liu, Y., Husain, J., *et al.* (1998). Combinatorial expression patterns of individual TLE proteins during cell determination and differentiation suggest non-redundant functions for mammalian homologs of Drosophila Groucho. *Dev. Growth Differ.* **40,** 133–146.

Yao, J., Liu, Y., Lo, R., *et al.* (2000). Disrupted development of the cerebral hemispheres in transgenic mice expressing the mammalian Groucho homologue transducin-like-enhancer of split 1 in postmitotic neurons. *Mech. Dev.* **93,** 105–115.

Zhang, H., and Emmons, S. W. (2002). Caenorhabditis elegans unc-37/groucho interacts genetically with components of the transcriptional mediator complex. *Genetics* **160,** 799–803.

Zhu, C. C., Dyer, M. A., Uchikawa, M., *et al.* (2002). Six3-mediated auto repression and eye development requires its interaction with members of the Groucho-related family of co-repressors. *Development* **129,** 2835–2849.